frontiers | Research Topics

Research on Brassicaceae crops genomics and breeding, volume II

Edited by
Xiangshu Dong, Xiaodong Yang and Yoonkang Hur

Published in
Frontiers in Plant Science

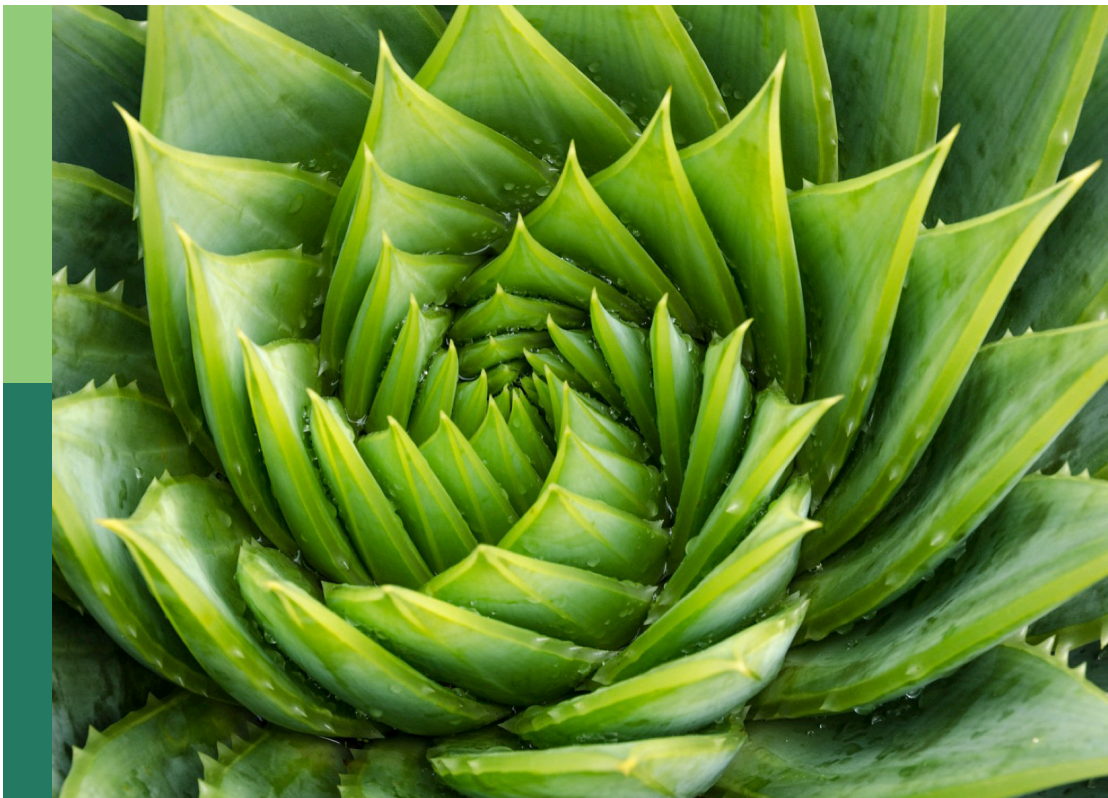

ISSN 1664-8714
ISBN 978-2-8325-6549-0
DOI 10.3389/978-2-8325-6549-0

Generative AI statement
Any alternative text (Alt text) provided alongside figures in the articles in this ebook has been generated by Frontiers with the support of artificial intelligence and reasonable efforts have been made to ensure accuracy, including review by the authors wherever possible. If you identify any issues, please contact us.

About Frontiers

Frontiers is more than just an open access publisher of scholarly articles: it is a pioneering approach to the world of academia, radically improving the way scholarly research is managed. The grand vision of Frontiers is a world where all people have an equal opportunity to seek, share and generate knowledge. Frontiers provides immediate and permanent online open access to all its publications, but this alone is not enough to realize our grand goals.

Frontiers journal series

The Frontiers journal series is a multi-tier and interdisciplinary set of open-access, online journals, promising a paradigm shift from the current review, selection and dissemination processes in academic publishing. All Frontiers journals are driven by researchers for researchers; therefore, they constitute a service to the scholarly community. At the same time, the *Frontiers journal series* operates on a revolutionary invention, the tiered publishing system, initially addressing specific communities of scholars, and gradually climbing up to broader public understanding, thus serving the interests of the lay society, too.

Dedication to quality

Each Frontiers article is a landmark of the highest quality, thanks to genuinely collaborative interactions between authors and review editors, who include some of the world's best academicians. Research must be certified by peers before entering a stream of knowledge that may eventually reach the public - and shape society; therefore, Frontiers only applies the most rigorous and unbiased reviews. Frontiers revolutionizes research publishing by freely delivering the most outstanding research, evaluated with no bias from both the academic and social point of view. By applying the most advanced information technologies, Frontiers is catapulting scholarly publishing into a new generation.

What are Frontiers Research Topics?

Frontiers Research Topics are very popular trademarks of the *Frontiers journals series*: they are collections of at least ten articles, all centered on a particular subject. With their unique mix of varied contributions from Original Research to Review Articles, Frontiers Research Topics unify the most influential researchers, the latest key findings and historical advances in a hot research area.

Find out more on how to host your own Frontiers Research Topic or contribute to one as an author by contacting the Frontiers editorial office: frontiersin.org/about/contact

Research on Brassicaceae crops genomics and breeding, volume II

Topic editors

Xiangshu Dong — Yunnan University, China

Xiaodong Yang — Yangzhou University, China

Yoonkang Hur — Chungnam National University, Republic of Korea

Citation

Dong, X., Yang, X., Hur, Y., eds. (2025). *Research on Brassicaceae crops genomics and breeding, volume II*. Lausanne: Frontiers Media SA.

doi: 10.3389/978-2-8325-6549-0

Table of contents

frontiers | Frontiers in Plant Science

TYPE Original Research
PUBLISHED 16 April 2024
DOI 10.3389/fpls.2024.1371451

OPEN ACCESS

EDITED BY
Xiangshu Dong,
Yunnan University, China

REVIEWED BY
Yinbo Ma,
Yangzhou University, China
Mingliang Jiang,
Jilin Agricultural Science and Technology University, China

*CORRESPONDENCE
Shanshan Nie
niess@nwafu.edu.cn
Lugang Zhang
lugangzh@163.com

RECEIVED 16 January 2024
ACCEPTED 03 April 2024
PUBLISHED 16 April 2024

CITATION
Huo J, Zhang N, Gong Y, Bao Y, Li Y, Zhang L and Nie S (2024) Effects of different light intensity on leaf color changes in a Chinese cabbage yellow cotyledon mutant. *Front. Plant Sci.* 15:1371451. doi: 10.3389/fpls.2024.1371451

Effects of different light intensity on leaf color changes in a Chinese cabbage yellow cotyledon mutant

Jianyu Huo, Ninan Zhang, Ying Gong, Yongrong Bao, Yinyin Li, Lugang Zhang* and Shanshan Nie*

State Key Laboratory of Crop Stress Resistance and High-Efficiency Production, College of Horticulture, Northwest A&F University, Yangling, Shaanxi, China

Leaf color is one of the most important phenotypic features in horticultural crops and directly related to the contents of photosynthetic pigments. Most leaf color mutants are determined by the altered chlorophyll or carotenoid, which can be affected by light quality and intensity. Our previous study obtained a Chinese cabbage yellow cotyledon mutant that exhibited obvious yellow phenotypes in the cotyledons and the new leaves. However, the underlying mechanisms in the formation of yellow cotyledons and leaves remain unclear. In this study, the Chinese cabbage yellow cotyledon mutant 19YC-2 exhibited obvious difference in leaf color and abnormal chloroplast ultrastructure compared to the normal green cotyledon line 19GC-2. Remarkably, low-intensity light treatment caused turn-green leaves and a significant decrease in carotenoid content in 19YC-2. RNA-seq analysis revealed that the pathways of photosynthesis antenna proteins and carotenoid biosynthesis were significantly enriched during the process of leaf color changes, and many differentially expressed genes related to the two pathways were identified to respond to different light intensities. Remarkably, *BrPDS* and *BrLCYE* genes related to carotenoid biosynthesis showed significantly higher expression in 19YC-2 than that in 19GC-2, which was positively related to the higher carotenoid content in 19YC-2. In addition, several differentially expressed transcription factors were also identified and highly correlated to the changes in carotenoid content, suggesting that they may participate in the regulatory pathway of carotenoid biosynthesis. These findings provide insights into the molecular mechanisms of leaf color changes in yellow cotyledon mutant 19YC-2 of Chinese cabbage.

KEYWORDS

Chinese cabbage, yellow cotyledon mutant, leaf color, light intensity, carotenoid, RNA-seq

1 Introduction

Leaf is an important source of plant photosynthesis which is critical for plant growth and development (Brodribb et al., 2007). Various leaf color is significant for enhancing the ornamental effect of plant species and is an important quality trait for fruits and vegetables (Zhao et al., 2020). Leaf color is mainly determined by the types and contents of pigments, such as chlorophyll and carotenoid, which are two major photosynthetic pigments (Markwell and Namuth, 2003). Chlorophyll is the most important pigment in photosynthesis and responsible for capturing light energy and energy conversion (Fromme et al., 2003; Eckhardt et al., 2004). Carotenoid is natural light capture pigment and transfers absorbed light to chlorophyll, and it also plays vital roles in photoprotection against oxidative damage (Frank and Cogdell, 1996; Hashimoto et al., 2016). Leaf color mutants are widespread in plants, and one of the widely available mutation types is leaf yellowing. Numerous yellow leaf mutants have been identified and reported in many vegetable crops, such as pepper (Yang et al., 2023), watermelon (Xu et al., 2023), cucumber (Zhang et al., 2022a), wucai (Nie et al., 2021), and Chinese cabbage (Zhang et al., 2017; Zhao et al., 2021). Studies have demonstrated that yellow leaf phenotype of mutant is usually caused by the disrupted biosynthesis and degradation of chlorophyll and carotenoid (Zhao et al., 2020), and thus it is commonly used for studying the photosynthetic system, pigment biosynthetic pathway, and genetic regulatory mechanism.

The inhibition of chlorophyll photosynthesis or chlorophyll deficiencies caused leaf color changes involve a series of genes that regulate the complex chlorophyll biosynthetic pathway (Zhao et al., 2020). The first committed step of chlorophyll synthesis is mediated by magnesium chelatase (MgCh), which is a key enzyme in chlorophyll biosynthesis and catalyzes the insertion of Mg^{2+} into protoporphyrin IX (Masuda, 2008). Plant MgCh consists of three subunits, MgCh I (CHLI), MgCh D (CHLD), and MgCh H (CHLH), whose mutations have been extensively characterized in many plant mutants (Masuda, 2008). A yellow-green leaf mutant of strawberry (*Fragaria pentaphylla*) was reported to be attributed to the gene mutation of *CHLI*, which resulted in lower chlorophyll level in mutant (Ma et al., 2023). The mutation of *CHLH* in zucchini (*Cucurbita pepo*) caused the decrease in chlorophyll content and exhibited yellow peel phenotype (Niu et al., 2023). Virus-induced gene silencing of *CHLI* and *CHLD* in pea (*Pisum sativum*) led to the decrease in chlorophyll content and abnormal chloroplast structure and showed yellow leaf phenotype (Luo et al., 2013). With the roles of chlorophyll in leaf color changes being well studied, the effects of carotenoid biosynthesis on the genetic diversity of plant colors also receive the increasing research attention. Carotenoid biosynthetic pathway is highly regulated by the coordinated expression of many carotenogenic genes, which mediate the accumulation and degradation of different components of carotenoids (Cazzonelli and Pogson, 2010; Yuan et al., 2015). Studies in red or yellow tomato fruits and citrus showed that the increases in phytoene synthase gene (*PSY*) and phytoene desaturase gene (*PDS*) expressions contributed to the elevated carotenoid content (Kato et al., 2004; Cao et al., 2019; Chen et al., 2023a). The decreased expressions of downstream lycopene β-carotene (*LCYB*) and lycopene ϵ-cyclase (*LCYE*) genes in strawberry were reported to be related to the changes in β-carotene and lutein (Zhu et al., 2015). Moreover, a yellow-fleshed fruit tomato mutant was a consequence of the deletion of *PSY1* gene region and showed a reduction in carotenoid accumulation (Gady et al., 2012). In addition, previous studies had revealed that orange head Chinese cabbage accumulated significant higher amounts of carotenoids in leaves in comparison with white head Chinese cabbage (Watanabe et al., 2011; Zhang et al., 2015). Although many studies have explored the roles of carotenoid in determining fruit colors and leaf coloration, whether carotenoid metabolism is associated with yellow leaf mutation in leafy vegetables requires in-depth research.

Carotenoid metabolism is affected by various environmental stimuli (Yuan et al., 2015; Sun et al., 2018). Different light quality has been documented to affect the content and compound of carotenoid in many studies (Stanley and Yuan, 2019). For instance, blue light treatment can promote the synthesis and accumulation of lutein in strawberry and citrus (Chen et al., 2023b; Ma et al., 2021). Moreover, different light intensity or the presence of light has a significant impact on carotenoid production (Grumbach and Lichtenthaler, 1982; Stanley and Yuan, 2019). In bagged fruits of apple, light exclusion reduced the content of carotenoid, but it was alleviated by *PSY* overexpression in fruits (Ampomah-Dwamena et al., 2022). In green leaves of chili pepper, the absence of light was related to the low expressions of *PSY* and *PDS* genes and led to the low carotenoid content (Simkin et al., 2003). In white mustard (*Sinapis alba*), the upregulated expression of *PSY* gene resulted in an increase in carotenoid content under light conditions (Lintig et al., 1997). Notably, in the yellowing leaf mutant of pepper, high-intensity light was required to regulate the transition of leaves from green to yellow, which was positively related to the increased carotenoid pigments (Liu et al., 2023). Therefore, to investigate the light intensity induced changes in carotenoid content is necessary for understanding the underlying mechanisms of leaf color changes in yellow leaf mutants.

In this study, a yellow cotyledon mutant of Chinese cabbage (*Brassica rapa* L. ssp. *Pekinensis*) was used, and it was obtained through a natural mutation in the hybrid progenies of Chinese cabbage. To study the effects of different light intensity on leaf color changes in Chinese cabbage yellow cotyledon mutant, physiological characteristics and changes in chlorophyll and carotenoid contents were analyzed both in the cotyledons and leaves of mutant in the current study. Furthermore, RNA-seq analysis was performed to identify the critical differentially expressed genes (DEGs) involved in the leaf color changes in response to different light intensity. These results facilitate uncovering the regulatory mechanisms of leaf color changes in Chinese cabbage yellow cotyledon mutant.

2 Materials and methods

2.1 Plant materials and different light intensity treatments

Two genetically stable pure lines of Chinese cabbage yellow cotyledon mutant 19YC-2 and normal green cotyledon near

isogenic line (wild type) 19GC-2 were used and provided by Cruciferae Research Group of Northwest A&F University (Yangling, China). The seedlings were grown in Caoxinzhuang vegetable experimental farm (Yangling, China). Five individual seedlings were selected for phenotype statistics at the cotyledon stage, the two-leaf stage, the four-leaf stage, the six-leaf stage, the rosette stage, and the heading stage, respectively. The shoots were harvested to measure the fresh weight at different stages and then dried at 65°C with 12 h for measuring the dry weight. Three independent replicates were performed for each sample at every stage.

For different light intensity treatments, the germinated seeds of 19YC-2 and 19GC-2 were sowed in plant growth chamber with 16 h light (24°C, 216 μmol·m^{-2}·s^{-1}), 8 h dark (16°C), and 55% relative humidity. After the cotyledon of seedlings were fully expanded, the seedlings were separately subjected to the conditions under low-intensity light (72 μmol·m^{-2}·s^{-1}) and normal intensity light (216 μmol·m^{-2}·s^{-1}) conditions, with the same other conditions. The leaf color observation and sampling were performed at the cotyledon stage, the first-leaf stage, the two-leaf stage, the three-leaf stage, and the four-leaf stage, respectively. The cotyledons and leaves for RNA extraction were collected, immediately frozen in liquid nitrogen and stored at −80°C.

2.2 Ultrastructural observation of chloroplast

Transmission electron microscopy (TEM) was performed to observe the chloroplast ultrastructure of the cotyledons and leaves of 19YC-2 and 19GC-2. The cotyledons were used from 19YC-2 and 19GC-2 at the cotyledon stage. The 1st leaves of 19YC-2 and 19GC-2 were separately collected at the two-leaf stage and the four-leaf stage. The samples in size with 1 mm^2 were fixed in a mixture of 2% glutaraldehyde fixative in 0.2 M phosphate buffered saline (PBS). The fixed samples were then dehydrated and embedded in resin as previously decreased (Nie et al., 2023). Ultrathin sections were obtained and examined using a transmission electron microscopy (Hitachi HT7800, Japan).

2.3 Measurement of color difference parameters

The color difference parameters of cotyledons and leaves were measured by a colorimeter (Konica Minolta CR-400, Japan). A CIE Lab color system was used to examine the L*, A* and B* values. The L* value represents leaf brightness. The A* value represents the red and green, where a positive value indicates red and a negative value indicates green. The B* value represents the yellow and blue, where a positive value indicates yellow and a negative value indicates blue.

2.4 Measurement of photosynthetic pigment and chlorophyll fluorescence

The contents of photosynthetic pigments were determined as previously reported methods (Lichtenthaler, 1987; Yang et al., 2023). The fresh leaves with 0.3 g were cut and mixed in a 50 mL tube containing 10 mL 95% ethanol in the dark for 24 h. The absorbance was measured by a M200pro microplate reader (Tecan, Switzerland) at wavelengths of 665 nm, 649 nm, and 470 nm, respectively. The contents of carotenoid, chlorophyll a, and chlorophyll b were calculated according to the reported formula by Yang et al. (2023). A Dual-PAM-100 Chlorophyll Fluorometer (Walz, Germany) was used to monitor the chlorophyll fluorescence parameters, including maximum quantum efficiency of photosystem II (Fv/Fm), effective quantum efficiency of photosystem II (Fv'/Fm'), and electron transport in photosystem II [ETR(II)] and nonphotochemical quenching (NPQ). Three individual seedlings were used in each replicate, and three independent replicates were performed for each sample.

2.5 RNA-seq analysis

A total of 18 cDNA libraries were constructed using six samples from 19GC-2 and 19YC-2, including the cotyledons (CK0 and T0) at the cotyledon stage, and the 4th leaves after 72 μmol·m^{-2}·s^{-1} (CK1 and T1) and 216 μmol·m^{-2}·s^{-1} (CK2 and T2) light treatments at the four-leaf stage, with three independent biological replicates. The library construction and sequencing for RNA-seq analysis were completed on Illumina sequencing platform by Genedenovo Biotechnology Co., Ltd (Guangzhou, China). Clean reads were mapped to the reference genome of Chinese cabbage V3.0 (http://brassicadb.cn). Pearson correlation coefficients (PCC) and principal component analysis (PCA) were used to evaluate the correlation between samples and repeatability. The abundance of gene expression was quantified as fragments per kilobase of transcript sequence per millions (FPKM) value. The differentially expressed genes (DEGs) were identified using the DEseq 2 R package with the absolute value of log2 fold change ≥ 1 and FDR < 0.05 (Love et al., 2014). TB tools software was used to draw heat maps and Venn diagram. Functional annotation of gene was performed according to Gene Ontology (GO) and Kyoto Encyclopedia of Genes and Genomes (KEGG) databases, and enrichment analysis was performed at *P*-value ≤ 0.05. The data of RNA-seq were deposited in NCBI Sequence Read Archive (SRA; http://www.ncbi.nlm.nih.gov/Traces/sra/) database under the accession number: BioProject PRJNA1005457.

2.6 Quantitative real-time PCR

Total RNA extraction, cDNA synthesis, and qRT-PCR analysis were performed as previously reported methods (Nie et al., 2019). The qRT-PCR analysis was conducted on an iCycler iQ5 Real-Time PCR Detection System (Bio-Rad, USA). Three biological replicates were performed for each sample. The specific primer sequences were designed using Beacon Designer 8.0 software (Supplementary Table S1). The *BrEF-1α* gene (*Bra031602*) was selected as the internal control. The relative expression level of gene was calculated using $2^{-\Delta\Delta CT}$ method.

2.7 Weighted gene co-expression network analysis

To construct a co-expression network and identify the modules of highly correlated DEGs based on the gene expression profiles and pigment contents, weighted gene co-expression network analysis (WGCNA) was performed using the R package with the soft threshold of 8 and the minimum module size of 50 (Langfelder and Horvath, 2008). Correlation analysis between the identified modules and the contents of photosynthetic pigments were determined by Pearson correlation coefficients (PCC).

2.8 Statistical analysis

All the data were analyzed using SPSS Statistics 24.0. The expression data were presented as the means ± SEM. Independent samples t-test was used to determine statistically significant difference.

3 Results

3.1 Phenotype characteristic and chloroplast ultrastructure of Chinese cabbage yellow cotyledon mutant

The leaf phenotypes of Chinese cabbage yellow cotyledon mutant 19YC-2 and green cotyledon line 19GC-2 were observed at different growth stages. The cotyledons and leaves of 19GC-2 were normal green from the cotyledon stage to the heading stage. The cotyledons of 19YC-2 were obvious yellow at the cotyledon stage (Figure 1A) and began to turn green at the two-leaf stage (Figure 1B). The 1st leaves of 19YC-2 also exhibited yellow at the two-leaf stage (Figure 1B), while it gradually turned green at the four-leaf stage (Figure 1C). Interestingly, the newly unfolded leaves of 19YC-2 were still yellow from the four-leaf stage until the rosette stage (Figures 1C-E). At the heading stage, all the outer leaves of 19YC-2 were close to green (Figure 1F). In addition, the fresh weight and dry weight of shoots in 19YC-2 were significantly lower than that in 19GC-2 at each stage (Figures 1G, H).

Observation of chloroplast ultrastructure by TEM showed that there were fewer chloroplasts per cell in the cotyledons of 19YC-2 (approximately 11 chloroplasts) than that in 19GC-2 (approximately 20 chloroplasts) (Figures 2A, B). The chloroplasts in 19GC-2 were regular and oval in shape, and the obvious grana lamellae and starch grains were observed (Figure 2C). However, the chloroplasts in 19YC-2 were irregular and shrunken in shape and exhibited the lack of grana lamellae and starch grains (Figure 2D). Moreover, at the two-leaf stage, the chloroplasts in the 1st leaves of 19GC-2 were normal in shape and structure (Figure 2E), while the 1st leaves of 19YC-2 were still yellow and exhibited abnormal chloroplasts and a lower number of grana lamellae and starch grains (Figure 2F). Remarkably, at four-leaf stage, the 1st leaves of 19YC-2 had gradually turned green, and the chloroplasts exhibited the normal structures with obvious grana lamellae and increased starch grains (Figure 2H), which was almost similar to the normal chloroplasts in 19GC-2 (Figure 2G).

3.2 Leaf color changes of Chinese cabbage yellow cotyledon mutant under different light intensity

To explore the effects of different light intensities on leaf color changes in Chinese cabbage yellow cotyledon mutant 19YC-2, the two light intensities of 72 μmol·m^{-2}·s^{-1} and 216 μmol·m^{-2}·s^{-1} were separately used to treat the seedlings from fully expanded cotyledons (Figure 3A). Under 72 μmol·m^{-2}·s^{-1} light condition, both 19YC-2 and 19GC-2 displayed thinner leaves. All the leaves of 19YC-2 gradually turned green until the four-leaf stage, which had few differences with the leaf color in 19GC-2 (Figure 3B). Under 216 μmol·m^{-2}·s^{-1} light condition, the heart leaves of 19YC-2 remained yellow at the four-leaf stage (Figure 3B). Further analysis of color difference showed that the values of L *, A *, and B * in 19YC-2 cotyledons were significantly higher than that in 19GC-2 at the cotyledon stage (Figure 3C). After the treatment under 72 μmol·m^{-2}·s^{-1} light, there was no significant difference in color difference parameters in the 4th leaves between 19YC-2 and 19GC-2 at the four-leaf stage (Figure 3D). However, under 216 μmol·m^{-2}·s^{-1} light condition, the significant differences in color difference parameters in the 4th leaves between 19YC-2 and 19GC-2 were found at the four-leaf stage (Figure 3E). The results of color difference analyses were consistent with the observation of leaf color in 19YC-2 and 19GC-2 after different light intensity treatments.

3.3 Effects of different light intensity on pigment contents in Chinese cabbage yellow cotyledon mutant

Analyses of pigment contents showed that the chlorophyll content in 19YC-2 cotyledons was significantly lower than that in 19GC-2 (Figure 4A), and the carotenoid content in 19YC-2 cotyledons was significantly higher than that in 19GC-2 (Figure 4B). Furthermore, after the treatment using 72 μmol·m^{-2}·s^{-1} light, the chlorophyll and carotenoid contents in the 4th leaves of 19YC-2 had no significant difference compared to that in 19GC-2 at the four-leaf stage (Figures 4A, B). Under 216 μmol·m^{-2}·s^{-1} light condition, the chlorophyll content was significantly lower, and the carotenoid content was significantly higher in the 4th leaves of 19YC-2 than that in 19GC-2 at the four-leaf stage, which was consistent with the changes in pigment contents at the cotyledon stage (Figures 4A, B). Additionally, the ratio of chlorophyll/carotenoid in the 4th leaves of 19YC-2 under 72 μmol·m^{-2}·s^{-1} light was nearly equal to that in 19GC-2, while the significant lower ratio was found in the 4th leaves of 19YC-2 under 216 μmol·m^{-2}·s^{-1} light than that in 19GC-2 (Figure 4C), which may be responsible for the leaf color differences in 19YC-2 exposed to different light intensities. More importantly, the carotenoid content in the heart leaves of 19YC-2 was gradually decreased with the growth of seedlings (Figure 4D). The decrease trend of the level of carotenoid in 19YC-2 after 72 μmol·m^{-2}·s^{-1} light treatment was more rapid, resulting in the nearly equal level of carotenoid with the 4th leaves of 19YC-2 to that in 19GC-2. The results indicated that low-intensity light treatment caused the rapid decrease in

10.3389/fpls.2024.1371451

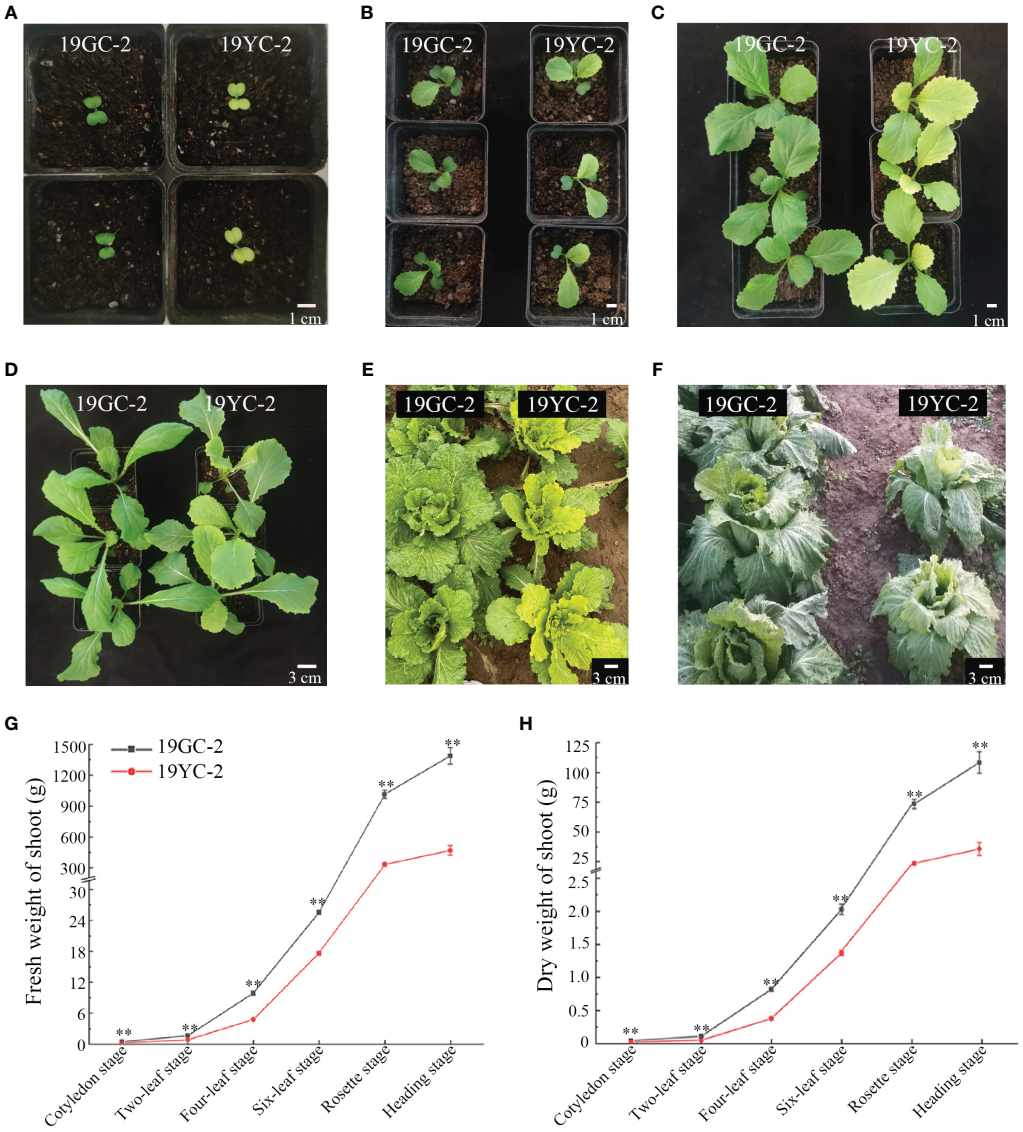

FIGURE 1
Leaf phenotypes in green cotyledon line 19GC-2 and yellow cotyledon mutant 19YC-2 of Chinese cabbage. **(A)** Cotyledon stage. **(B)** Two-leaf stage. **(C)** Four-leaf stage. **(D)** Six-leaf stage. **(E)** Rosette stage. **(F)** Heading stage. **(G)** Statistic of fresh weight of shoots in 19GC-2 and 19YC-2. **(H)** Statistic of dry weight of shoots in 19GC-2 and 19YC-2. Scale bar = 1 cm **(A–C)** and 3 cm **(D–F)**. $^{**}P < 0.01$.

carotenoid content in 19YC-2 may be one of the major reasons for the leaf color changes from yellow to green.

3.4 Effects of different light intensity on chlorophyll fluorescence parameters in Chinese cabbage yellow cotyledon mutant

Analyses of chlorophyll fluorescence parameters in Chinese cabbage yellow cotyledon mutant 19YC-2 showed that at the cotyledon stage, the values of Fv/Fm, Fv'/Fm', and ETR (II) were significantly lower in 19YC-2 cotyledons than that in 19GC-2 (Figure 4E-G), while the NPQ had no difference between 19YC-2 and 19GC-2 (Figure 4H). The observation revealed that the yellow cotyledons in 19YC-2 exhibited obvious photoinhibition, which may be related to the abnormal chloroplasts and lower chlorophyll content in 19YC-2 cotyledons. After 72 $\mu mol \cdot m^{-2} \cdot s^{-1}$ light treatment, there was no significant difference in the values of Fv/Fm, Fv'/Fm', and ETR (II) in the 4th leaves between 19YC-2 and 19GC-2 at the four-leaf stage (Figures 4E-G), while the NPQ was significantly higher in 19YC-2 (Figure 4H), indicating that low-intensity light activated the NPQ and induced the raised energy dissipation to defense photodamage in 19YC-2. After 216 $\mu mol \cdot m^{-2} \cdot s^{-1}$ light treatment, the values of Fv/Fm, Fv'/Fm', and ETR (II) were also significantly lower in the 4th leaves of 19YC-2 at the four-leaf stage (Figures 4E-G), and the NPQ had no difference between 19YC-2 and 19GC-2 (Figure 4H), which was consistent with the results at the cotyledon stage.

10.3389/fpls.2024.1371451

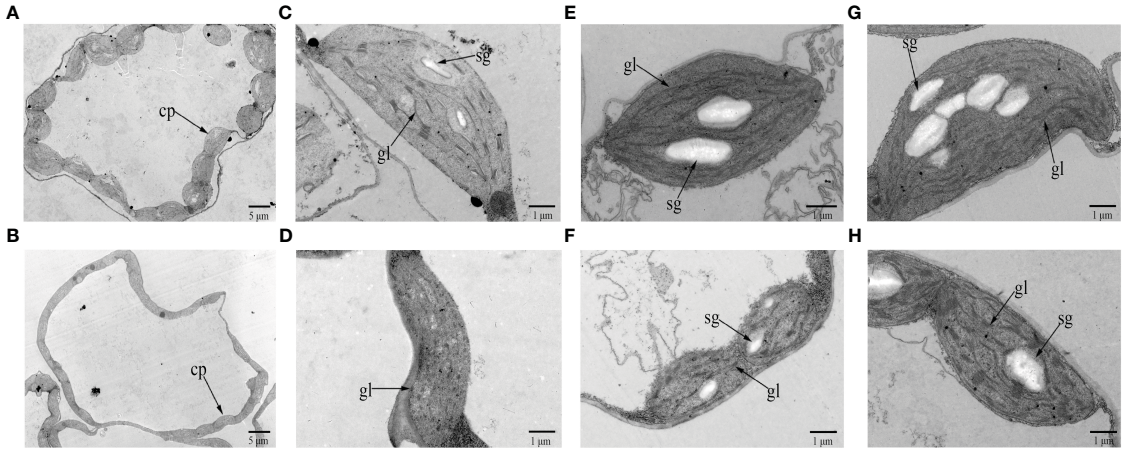

FIGURE 2
Chloroplast ultrastructure in the cotyledons and leaves of 19GC-2 **(A, C, E, G)** and 19YC-2 **(B, D, F, H)**. Observation of the number of chloroplasts per cell **(A, B)** and the chloroplast structure **(C, D)** at the cotyledon stage. The chloroplast structure in the 1st leaves of 19GC-2 and 19YC-2 at the two-leaf stage **(E, F)** and at the four-leaf stage **(G, H)**. cp, chloroplast; gl, grana lamellae; sg, starch grain. Scale bar = 5 μm **(A, B)** and 1 μm **(C-H)**.

3.5 RNA-seq analysis of Chinese cabbage yellow cotyledon mutant under different light intensity

The cotyledons of 19GC-2 (CK0) and 19YC-2 (T0) and the 4th leaves of 19GC-2 (CK1 and CK2) and 19YC-2 (T1 and T2) after 72 and 216 μmol·m^{-2}·s^{-1} light treatment were used for constructing six cDNA libraries and RNA-seq analysis (Figures 5A, B). After filtering the original data, the average clean data ranged from 38.84 to 44.02 million were obtained in six cDNA libraries, the average GC contents were ranged from 47.17% to 48.46%, and the average Q30 values were ranged from 92.85% to 93.46% (Supplementary Table S2). These obtained reads were mapped to the reference genome of Chinese cabbage with the average

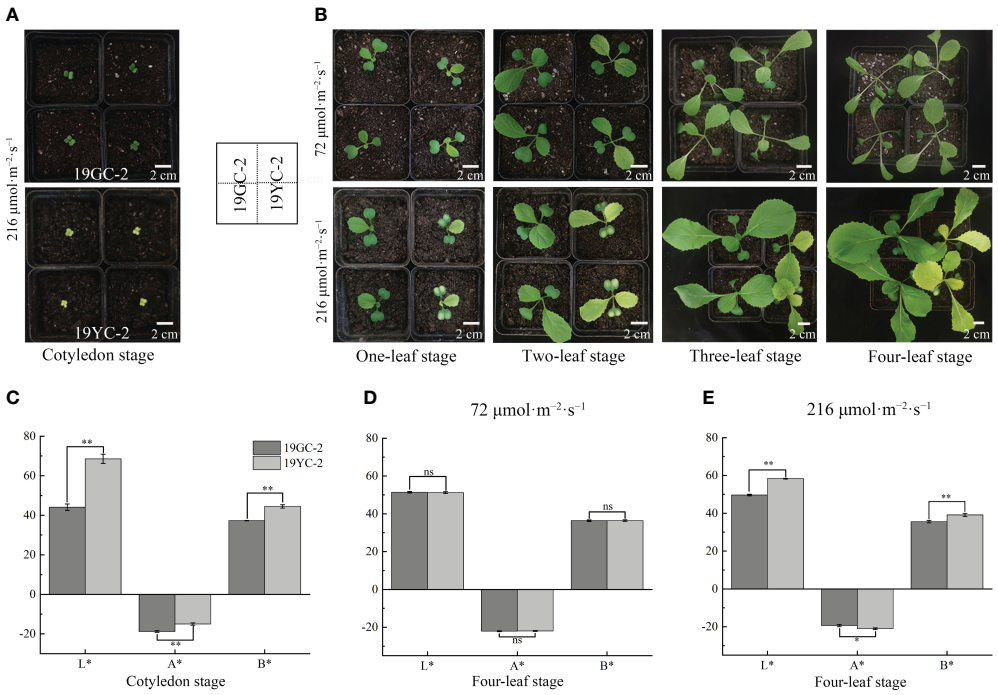

FIGURE 3
Effects of different light intensities on leaf colors in 19GC-2 and 19YC-2. **(A)** The cotyledons of 19GC-2 and 19YC-2 before treatment. **(B)** Leaf phenotypes of 19GC-2 and 19YC-2 at different growth stages after 72 μmol·m^{-2}·s^{-1} and 216 μmol·m^{-2}·s^{-1} light treatment. Color difference parameters of the cotyledons **(C)** at the cotyledon stage and the 4th leaves at the four-leaf stage after 72 μmol·m^{-2}·s^{-1} **(D)** and 216 μmol·m^{-2}·s^{-1} **(E)** light treatments. The L*, A* and B* values represent the color difference parameters. The L* value represents leaf brightness. The A* value represents the red and green. The B* value represents the yellow and blue. Scale bar = 2 cm **(A, B)**. ns, no significant; *P < 0.05; **P < 0.01.

10.3389/fpls.2024.1371451

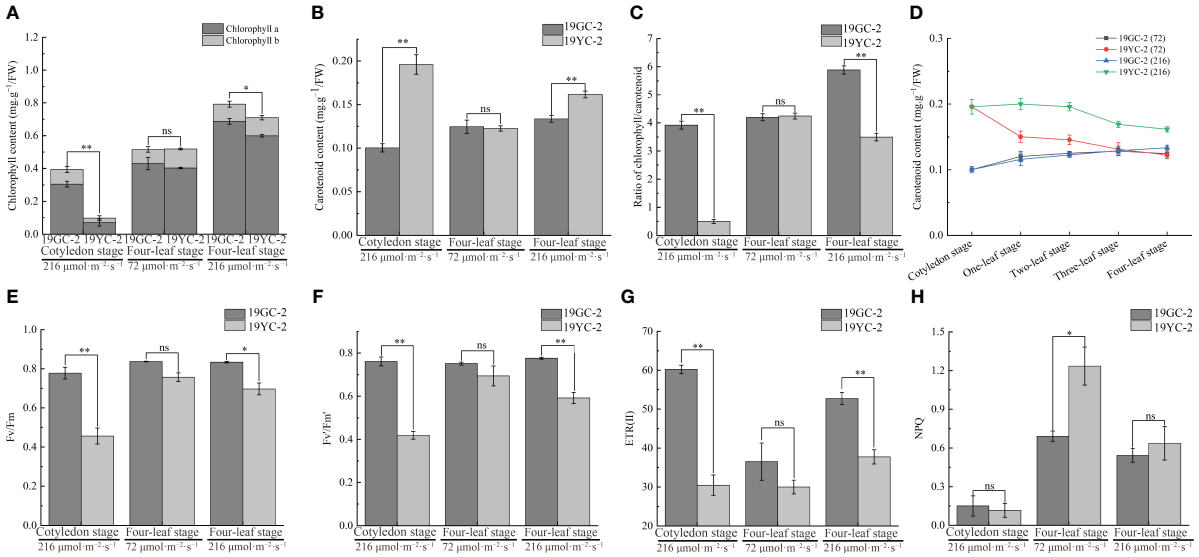

FIGURE 4
Effects of different light intensities on pigment contents and chlorophyll fluorescence parameters in 19GC-2 and 19YC-2. **(A)** Chlorophyll content. **(B)** Carotenoid content. **(C)** The ratio of chlorophyll/carotenoid content. **(D)** Changes in carotenoid content in the heart leaves of 19GC-2 and 19YC-2 at different stages. **(E)** Fv/Fm: The maximum quantum efficiency of photosystem II. **(F)** Fv'/Fm': The effective quantum efficiency of photosystem II. **(G)** ETR(II): The electron transport in photosystem II. **(H)** NPQ: The non-photochemical quenching. ns, no significant; *$P < 0.05$; **$P < 0.01$.

comparison efficiency ranged from 91.75% to 92.78% (Supplementary Table S3). PCA analysis validated the high reliability among three biological replications in the six sample groups (Figure 5C). Statistics of the number of DEGs showed that 3015 DEGs were identified in the comparison group of CK0 vs T0 (1376 upregulated and 1639 downregulated DEGs), 1084 DEGs were identified in the comparison group of CK1 vs T1 (391 upregulated and 693 downregulated DEGs), and 817 DEGs were identified in the comparison group of CK2 vs T2 (427 upregulated and 390 downregulated DEGs) (Figure 5D). Additionally, 169 common DEGs were obtained among three comparison groups of CK0 vs T0, CK1 vs T1, and CK2 vs T2, 345 common DEGs were obtained among the comparison groups of CK0 vs T0 and CK1 vs T1, 314 common DEGs were obtained among the comparison groups of CK0 vs T0 and CK2 vs T2, and 290 common DEGs were obtained among the comparison groups of CK1 vs T1 and CK2 vs T2 (Figure 5E).

Functional annotation and enrichment analysis showed that these DEGs were classified into 48 (CK0 vs T0), 45 (CK1 vs T1), and 43 (CK2 vs T2) GO subcategories (Supplementary Figure S1). Moreover, 662 (CK0 vs T0), 224 (CK1 vs T1) and 171 (CK2 vs T2) DEGs were annotated on 119, 94, and 89 KEGG pathways (Supplementary Figure S2), respectively. Among these pathways, the metabolic pathway (ko01100) and biosynthesis of secondary metabolites (ko01110) showed significant enrichment in all the three comparison groups. Importantly, the pathways of photosynthesis antenna proteins (ko00196) and carotenoid biosynthesis (ko00906) showed significant enrichment in the comparison groups of CK0 vs T0 and CK2 vs T2, while the two pathways were not found in the comparison group of CK1 vs T1. In addition, DEGs related to porphyrin and chlorophyll metabolism (ko00860) was enriched only in the comparison group of CK0 vs T0, while no DEGs were found in CK1 vs T1 and CK2 vs T2. Furthermore, gene set enrichment analysis (GSEA) also showed that the pathways of photosynthesis antenna proteins (ko00196) and carotenoid biosynthesis (ko00906) exhibited striking enrichment in the comparison groups of CK0 vs T0 and CK2 vs T2, while not in CK1 vs T1 (Supplementary Figure S3). The results of enrichment analyses suggested that DEGs encoding photosynthesis antenna proteins and the differential expressed carotenoid biosynthesis genes may be directly related to the leaf color difference between 19YC-2 and 19GC-2 under different light intensity.

3.6 Identification of DEGs related to photosynthesis antenna proteins

Photosynthetic antenna proteins had been documented to be capable of binding pigments, turning their excitation energies, and directing energy transfer to the reaction center of photosystem (Ruban, 2015). In this study, a total of 17 DEGs were identified and enriched in the pathway of photosynthesis antenna proteins (Supplementary Table S4). Expression analysis showed that 15 DEGs exhibited downregulated expression in the comparison group of CK0 vs T0, and 8 DEGs exhibited downregulated expression in the comparison group of CK2 vs T2, while no DEGs were identified in the comparison group of CK1 vs T1. Remarkably, the expression levels of six transcripts, including *BrCAB1* (*BraA03g018080.3C*), *BrCAB13* (*BraA10g012410.3C*), *BrCAB36* (*BraA02g037860.3C*), *BrLHCB1.3* (*BraA07g010770.3C*, *BraA07g010780.3C*), and *BrLHCB4.2* (*BraA05g037360.3C*), were significantly downregulated in both CK0 vs T0 and CK2 vs T2. To validate the differential expression of these DEGs, 5 genes were

10.3389/fpls.2024.1371451

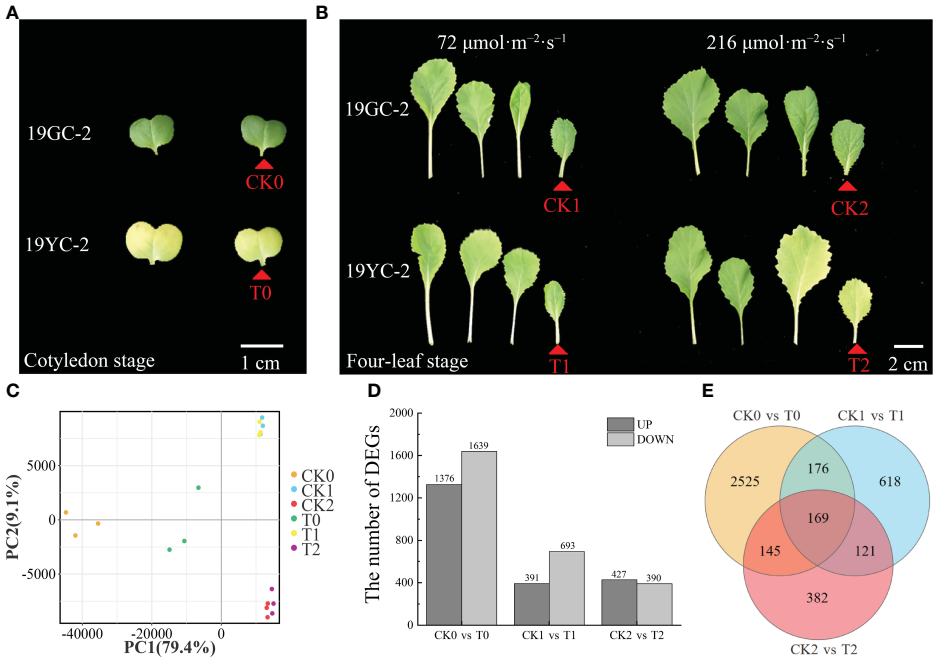

FIGURE 5
RNA-seq analysis of DEGs in 19GC-2 and 19YC-2. **(A)** The cotyledons of 19GC-2 and 19YC-2 at the cotyledon stage were used for constructing the cDNA libraries of CK0 and T0 (red arrowhead marked). **(B)** The leaves of 19GC-2 and 19YC-2 at the four-leaf stage after 72 and 216 μmol·m^{-2}·s^{-1} light treatment. The 4th leaves were used for constructing the cDNA libraries of CK1, CK2, T1, and T2 (red arrowhead marked). **(C)** Principal component analysis (PCA). **(D)** The number of DEGs. **(E)** Venn diagram of the unique and common DEGs among different libraries. Scale bar = 1 cm **(A)** and 2 cm **(B)**.

selected for qRT-PCR analysis. The results showed that all the selected genes were significantly decreased in T0 compared with CK0 and in T2 compared with CK2 (Figure 6), which was consistent with the results from RNA-seq analysis.

3.7 Identification of DEGs involved in carotenoid biosynthesis pathway

The pathway enrichment analysis of DEGs indicated that carotenoid metabolic pathway may be associated with the leaf color differences in 19GC-2 and 19YC-2 under different light intensity treatment. As expected, a total of 25 DEGs were identified and involved in carotenoid biosynthesis (Figure 7; Supplementary Table S5). Among these DEGs, six upregulated and 16 downregulated genes were found in the comparison group of CK0 vs T0, nine upregulated genes were found in the comparison group of CK1 vs T1, and five upregulated and three downregulated genes were found in the comparison group of CK2 vs T2 (Supplementary Table S5). Moreover, two genes of *BrPDS* (*BraA08g023090.3C*) and *BrLCYE* (*BraA01g034180.3C*) were significant upregulated expression in the comparison groups of CK0 vs T0 and CK2 vs T2, and three genes of *BrAAO3* (*BraA04g019480.3C*), *BrCCD4* (*BraA01g010560.3C*), and *BrNCED3* (*BraA05g032610.3C*) were significant downregulated expression in the comparison groups of CK0 vs T0 and CK2 vs T2.

Further qRT-PCR analysis showed that the expression levels of *BrPDS* and *BrLCYE* genes that were the upstream genes of carotenoid biosynthesis, were increased in the three comparison groups and showed significant increases in CK0 vs T0 and CK2 vs T2 (Figures 8A, B). The expression levels of *BrAAO3*, *BrCCD4*, and *BrNCED3* genes that were the downstream genes of carotenoid biosynthesis, were significantly decreased in CK0 vs T0 and CK2 vs T2 (Figures 8C-E). The results indicated that the upregulation of upstream genes and the downregulation of downstream genes were accordant with the changes in carotenoid contents. In addition, the results of qRT-PCR analysis in gene expressions were almost identical to the results of RNA-seq analysis (R^2 = 0.7784) (Figure 8F), demonstrating the reliability of RNA-seq data.

3.8 Analysis of co-expression network of DEGs and identification of transcription factors involved in carotenoid metabolism

To further investigate the relationships of gene differential expression and carotenoid content, WGCNA was performed to identify the highly correlated modules of DEGs. As a result, 19 modules named from A to S and labeled by different colors were identified (Figure 9). The A (r = 0.666), J (r = 0.714), and K (r = 0.728) modules containing 97, 1371, and 1828 DEGs, respectively, were highly positively related to the changes in carotenoid content, and the D (r = 0.597) module containing 175 DEGs was highly negatively related to the changes in carotenoid content. In addition, the upregulated expressed *BrPDS* and *BrLCYE* genes were assigned to the positively related J module, which was

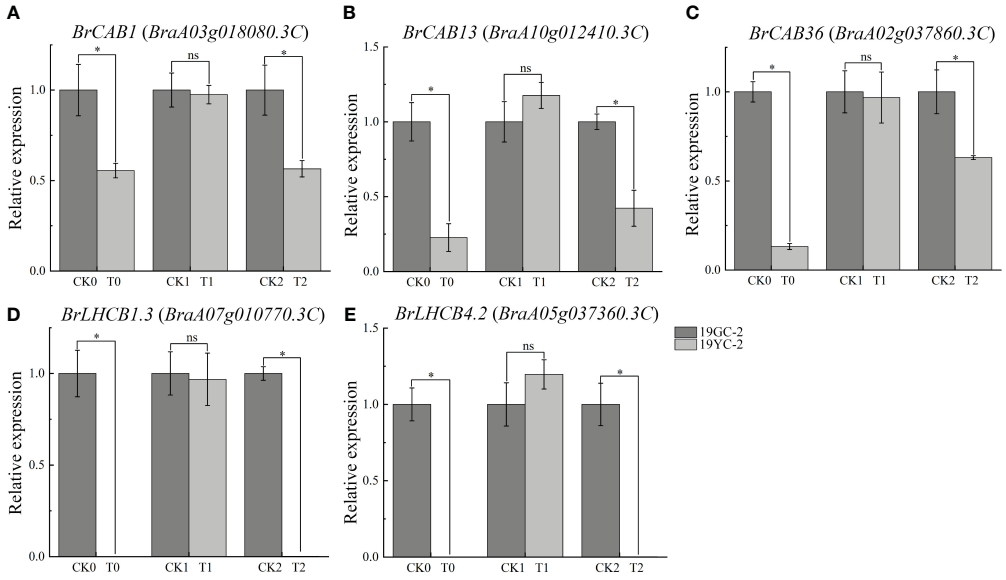

FIGURE 6
Expression analysis of DEGs related to photosynthetic antenna proteins by qRT-PCR in 19GC-2 and 19YC-2. **(A)** *BrCAB1* gene. **(B)** *BrCAB13* gene. **(C)** *BrCAB36* gene. **(D)** *BrLHCB1.3* gene. **(E)** *BrLHCB4.2* gene. CK0, T0, CK1, T1, CK2, and T2 represent the six cDNA libraries from 19GC-2 and 19YC-2. ns, no significant; *$P < 0.05$.

consistent with the positive regulation of the two genes in carotenoid synthesis. The downregulated expressed *BrAAO3* and *BrCCD4* were assigned to the negatively related F (r=−0.307) module, and the downregulated expressed *BrNCED3* was assigned to the negatively related M (r=−0.393) module. The downregulated expressed *BrCAB1* was assigned to the negatively related F (r=−0.307) module, and the downregulated expressed *BrCAB13*, *BrCAB36*, *BrLHCB1.3* and *BrLHCB4.2* were assigned to the negatively related M (r=−0.393) module. The results suggest that these DEGs identified in these highly correlated modules may play potential roles in regulating the pathway of carotenoid biosynthesis and metabolism.

Furthermore, a total of 56 DEGs belonging to transcription factors (TFs) were identified in these highly correlated modules by WGCNA (Figure 10). Among these differentially expressed TFs, most of these TFs were upregulated expression in the comparison group of CK0 vs T0, and seven genes were downregulated expression. Correlation analysis showed that the differential expressions of 17 TFs were strongly correlated with the changes in carotenoid contents (Figure 10B; Supplementary Table S6). For instance, the gene expression of *BraA08g033820.3C* (*BrRF2b*), *BraA08g001340.3C* (*BrRAP2-12*), *BraA04g017150.3C* (*BrERF008*), and *BraA06g042530.3C* (*BrR2R3-MYB*) had highly positive correlation (r > 0.91) to the changes in carotenoid contents, and the gene expression of *BraA08g003010.3C* (*BrSCL3*) and *BraA07g009390.3C* (*BrbHLH77*) had highly negative correlation (r < −0.9) to the changes in carotenoid contents. Moreover, many genes were identified as the transcription factor families of *BrERF/AP2* (*BraA08g001340.3C*, *BraA04g017150.3C*, *BraA10g029700.3C*, *BraA09g009130.3C*, and *BraA09g040790.3C*), *BrR2R3-MYB* (*BraA06g042530.3C*), *BrbHLH* (*BraA10g001670.3C*, *BraA09g011350.3C*, and *BraA07g009390.3C*), and *BrWRKY* (*BraA04g018060.3C* and *BraA02g028540.3C*) (Supplementary Table S6). In general, these identified DEGs and TFs that highly related to carotenoid biosynthesis and metabolism may play important roles in regulating leaf color changes in Chinese cabbage yellow cotyledon mutant 19YC-2.

4 Discussion

4.1 Changes in carotenoid content may determine the leaf color changes in Chinese cabbage yellow cotyledon mutant in response to different light intensities

Leaf color formation is closely related to the contents of photosynthetic pigments (Terry et al., 2001). Leaf color mutants are easy to recognize in leaf phenotypes and often used as valuable materials for investigating pigment biosynthesis and enriching the germplasms in genetic breeding (Deng et al., 2012). Various leaf color mutants usually impact the accumulation and metabolism of photosynthetic pigments and have been characterized in many horticultural crops (Wang et al., 2004; Zhao et al., 2020). In this study, the Chinese cabbage yellow cotyledon mutant 19YC-2 is a distinctive mutant that displays obvious yellow phenotype in the cotyledons. Like the other reported yellow leaf mutants, the Chinese cabbage yellow cotyledon mutant has special excellent characters and can be used as a selective biomarker for hybrid breeding. More importantly, yellow cotyledon phenotype can be directly selected at the earlier cotyledon stage for hybrid purity identification, which shortens the breeding time and improves the breeding efficiency.

Most yellow leaf phenotype of mutant is mainly determined by the changed contents in chlorophyll and carotenoid and the

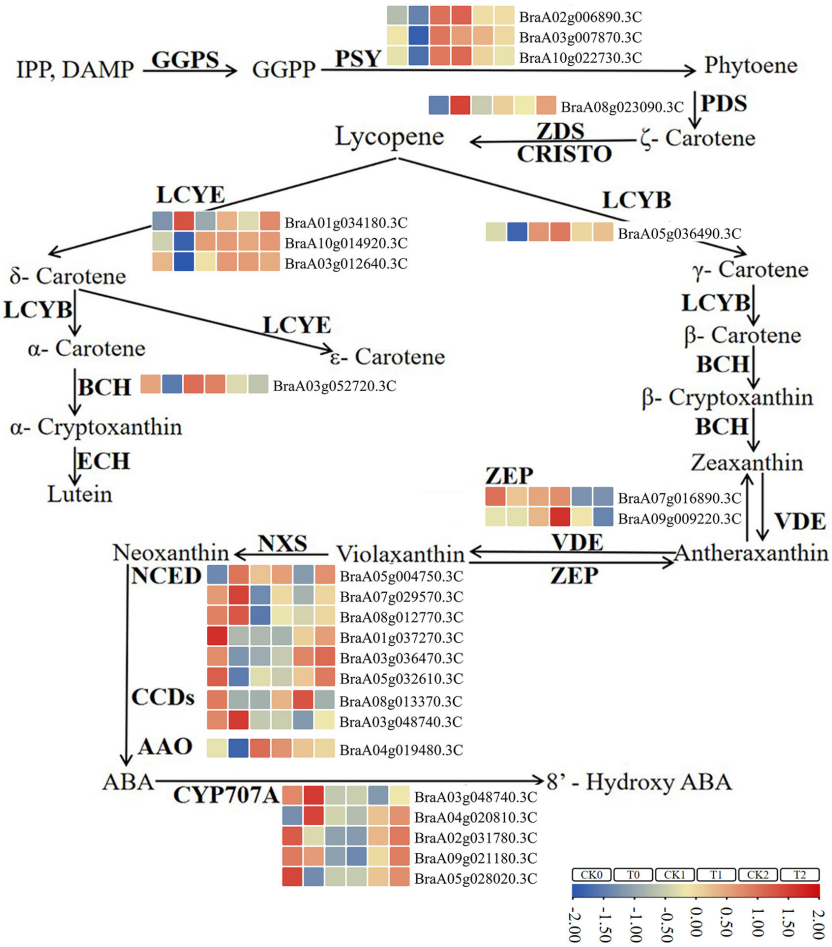

FIGURE 7
The identified DEGs involved in the pathway of carotenoid biosynthesis in 19GC-2 and 19YC-2. CK0, T0, CK1, T1, CK2, and T2 represent the six cDNA libraries. The boxes in different colors indicate gene expression in corresponding library. Gene expression levels are based on log2 FPKM values.

disrupted chloroplast development (Sakamoto, 2003; Cheng et al., 2022). Previous study reported the reduced chlorophyll content in the yellow leaf mutant of ginkgo (*Ginkgo biloba*) (Sun et al., 2022). In the green leaf mutant of *Populus deltoides* Marsh, the leaf color was associated with the lower levels of chlorophyll and carotenoid (Zhang et al., 2019). The yellow-green leaf color in wheat (*Triticum aestivum L.*) was consequence of the decreased chlorophyll content and abnormal chloroplast development (Wu et al., 2018). In addition, chlorophyll deficient was also showed to cause yellow leaf phenotypes in watermelon (Xu et al., 2023), and the chlorophyll deficient mutant in Pak-choi exhibited the obvious yellow leaves and the reduced total chlorophyll content (Zhang et al., 2017). As expected, our studies also showed the changes in chlorophyll and carotenoid contents in Chinese cabbage yellow cotyledon mutant 19YC-2. The significantly higher carotenoid content and lower chlorophyll content were found in the cotyledons of 19YC-2, which may be responsible for the yellow cotyledon phenotypes and was similar to the previous reports (Zhang et al., 2015; Sun et al., 2022; Xu et al., 2023). It is known that chloroplast development also affects the accumulation of chlorophyll and carotenoid and leaf color changes (Pogson and Albrecht, 2011; Zhao et al., 2020). The thylakoid is an important part of chloroplast structures and essential for chloroplast function (Allen and Forsberg, 2001; Pogson and Albrecht, 2011). Many studies in leaf color mutants demonstrated that the variations in thylakoid structure caused the decreases in grana numbers and thylakoid lamella, resulting in the damaged chloroplast ultrastructure (Nie et al., 2021; Wang et al., 2022; Zhang et al., 2022b). In the current study, observation of leaf color found that the 1st leaves of 19YC-2 gradually turned green with the growth of seedlings. Observation of chloroplast ultrastructure showed that the cotyledons and the yellow 1st leaves of 19YC-2 exhibited the abnormal chloroplast and thylakoid structures with the absence of grana lamellae and starch grains, while the normal chloroplast in shape and structure were observed in the turn-green 1st leaves of 19YC-2 at the four-leaf stage. The abnormal chloroplast ultrastructure may contribute to the yellow phenotypes in cotyledons and leaves of 19YC-2 mutant, which was consistent with many other reports (Nie et al., 2021; Wang et al., 2022; Zhang et al., 2022b). The results suggest that the changes in the contents of photosynthetic pigments in yellow cotyledon mutant 19YC-2 may be attributed to the abnormal chloroplast development, which can impair photosynthetic efficiency (Pogson and Albrecht, 2011).

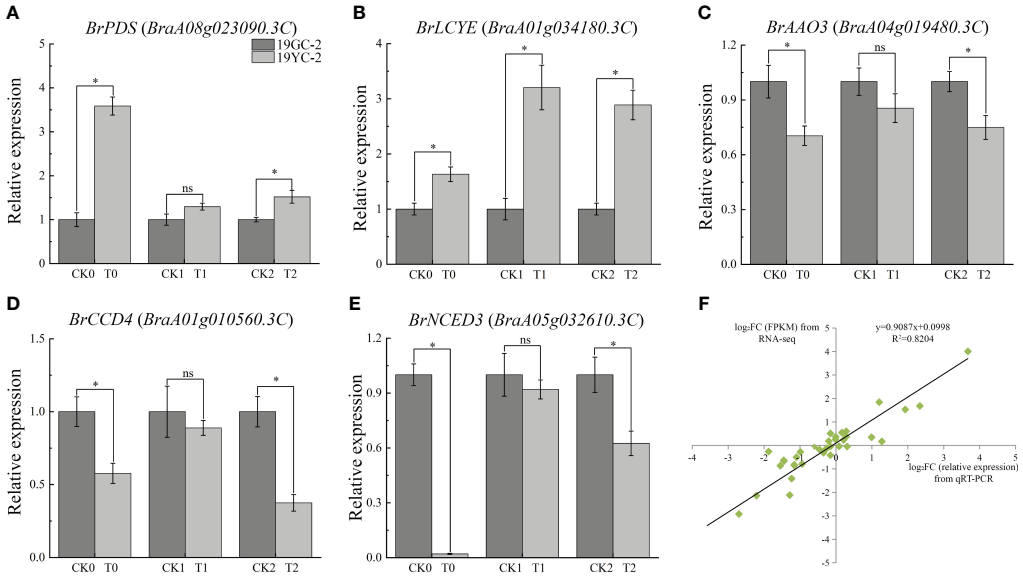

FIGURE 8
Expression analysis of critical carotenoid biosynthetic DEGs by qRT-PCR in 19GC-2 and 19YC-2. **(A)** *BrPDS* gene. **(B)** *BrLCYE* gene. **(C)** *BrAAO3* gene. **(D)** *BrCCD4* gene. **(E)** *BrNCED3* gene. **(F)** Correlation between qRT-PCR and RNA-seq analysis. CK0, T0, CK1, T1, CK2, and T2 represent the six cDNA libraries from 19GC-2 and 19YC-2. ns, no significant; *$P < 0.05$.

Numerous environmental factors, such as light, have been described to affect the development and biogenesis of chloroplast *via* photomorphogenic pathways (Xu et al., 2021; Chen et al., 2023b). Long-term deficient light can lead to degradation of chlorophyll and leaf yellowing (Lee et al., 2014). Different light intensities can affect the chloroplast formation and the synthesis and degradation of photosynthetic pigments (Kong et al., 2016). The mutants of lacking photosynthetic electron transport in *Arabidopsis* exhibited a variegated phenotype under high light intensity and a green phenotype under low light intensity (Rosso et al., 2009). The yellow leaf mutant in pepper showed the increase in carotenoid content under high light intensity (Liu et al., 2023). Our previous study also found that low-intensity light treatment caused the turn-green leaves in Chinese cabbage yellow cotyledon mutant 19YC-2. Therefore, to investigate the underlying physiological mechanism of leaf color change in 19YC-2 under low-intensity light treatment is significant in this study. We found that the leaves of 19YC-2 showed higher carotenoid and lower chlorophyll contents under normal light condition than that under low-intensity light condition. The observation was coincident with that the leaves of 19YC-2 exhibited yellow exposed to normal light but turned green under low-intensity light. These results indicated

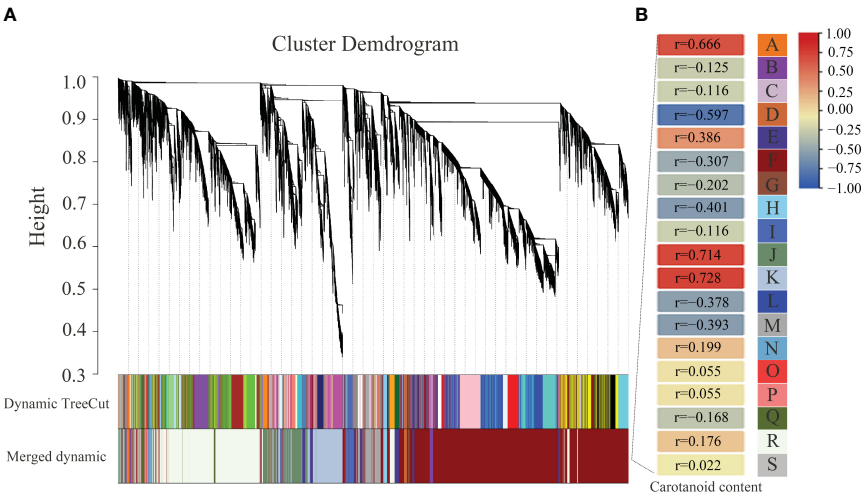

FIGURE 9
Association analysis between DEGs and carotenoid contents by weighted gene co-expression network analysis (WGCNA) in 19GC-2 and 19YC-2. **(A)** The hierarchical cluster tree of correlated modules. **(B)** The identified highly correlated modules represented by different letters from A to S.

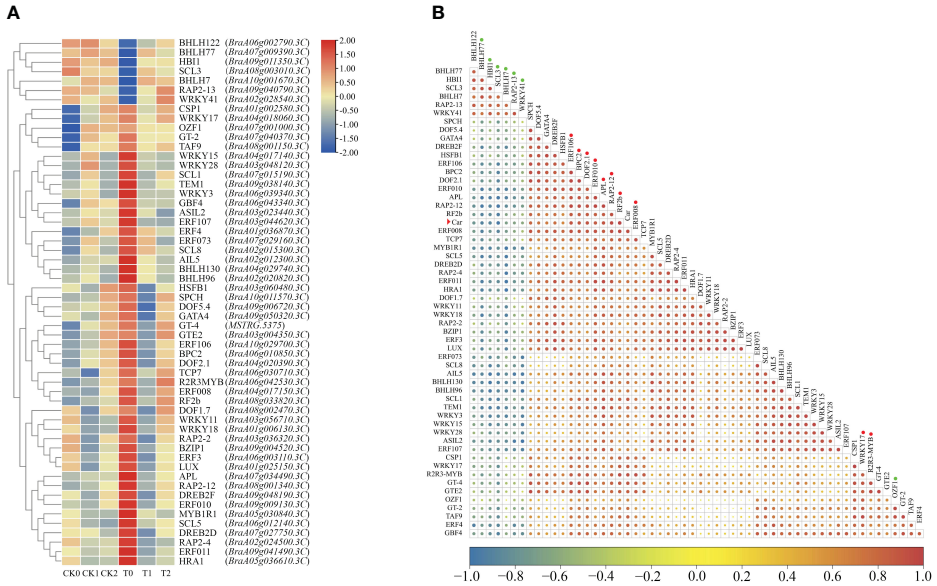

FIGURE 10
Identification of differentially expressed TFs related to carotenoid metabolism by WGCNA. **(A)** Heat map of differentially expressed TFs. **(B)** Correlation of TFs and carotenoid content. The red arrowhead indicates the carotenoid (car). The circles after gene names indicate the strongly positively (in red) and negatively (in green) correlated TFs.

that low-intensity light treatment primarily changed the carotenoid and chlorophyll contents and then induced the transition from yellow to green in the new leaves of 19YC-2. Meanwhile, RNA-seq analysis and KEGG pathway enrichment revealed that many DEGs were identified in the significantly enriched pathway of carotenoid biosynthesis in CK0 vs T0 (the cotyledon stage) and CK2 vs T2 (normal light treatment), but not in CK1 vs T1 (low-intensity light treatment), which indicated that the carotenoid biosynthesis and metabolism may be closely related to leaf color changes in 19YC-2. However, the pathway related to porphyrin and chlorophyll metabolism was enriched only in CK0 vs T0, but not in CK1 vs T1 and CK2 vs T2, implying that different light intensity treatments may have no significant effects on the DEGs related to chlorophyll biosynthesis in yellow cotyledon mutant 19YC-2. In addition, the existence of photosynthetic antenna proteins can increase the rate of energy delivery and photosynthetic efficiency (Pogson and Albrecht, 2011; Ruban, 2015). In the current study, the expression levels of DEGs encoding photosynthesis antenna proteins, such as *BrCAB1*, *BrCAB13*, *BrCAB36*, *BrLHCB1.3*, and *BrLHCB4.2*, were significantly decreased in CK0 vs T0 and CK2 vs T2, suggesting the suppressed photosynthesis in the yellow cotyledons and yellow leaves in 19YC-2.

4.2 The putative regulatory pathway of carotenoid biosynthesis in Chinese cabbage yellow cotyledon mutant

Carotenoid biosynthesis is documented to be influenced by the changes in light and is stalled in darkness (Yuan et al., 2015; Xu et al., 2021). Carotenoids are synthesized in plastids, which is regulated by the complex and highly conserved biosynthetic pathway that has been well established and involves the transcription of many biosynthetic genes (Nisar et al., 2015; Yuan et al., 2015). Among these key genes that encode carotenogenic enzymes, *PDS* and *ζ*-carotene desaturase (*ZDS*) genes are responsible for the conversion of uncolored phytoene to red-colored lycopene and have been identified and studied in many colored fruits and crops (Fanciullino et al., 2007; Yuan et al., 2015). The high expression of *PDS* gene had been found to be correlated with the accumulation of carotenoid during tomato fruit ripening and citrus fruit development (Pecker et al., 1992; Kato et al., 2004; Rodrigo et al., 2004). The subsequent two biochemical pathways, lycopene converted to lutein and zeaxanthin, were mediated by *LCYE* and *LCYB* genes (Nisar et al., 2015). These carotenoid pigments are abundant not only in the yellow fruits and flowers, but also in leafy vegetables exposed to light (Yuan et al., 2015). Studies showed that *LCYE* mutation caused lutein deficiency and higher *β*-carotene accumulation (Pogson et al., 1996), and the high expression of *LCYE* gene promoted lutein accumulation in tomato and strawberry (Zhu et al., 2015; Yuan et al., 2022). Exploring the expression changes of these carotenoid biosynthesis related genes and their potential function can contribute to further understand the mechanism of leaf color changes in Chinese cabbage yellow cotyledon mutant 19YC-2. In this study, RNA-seq analysis showed that *BrPDS* (*BraA08g023090.3C*) and *BrLCYE* (*BraA01g034180.3C*) genes were upregulated expression in the yellow leaves of yellow cotyledon mutant 19YC-2, indicating the putative regulatory roles of *BrPDS* and *BrLCYE* in leaf color changes in 19YC-2.

Furthermore, the downstream genes in the pathway of carotenoid metabolism, such as *BrAAO3* (*BraA04g019480.3C*), *BrCCD4* (*BraA01g010560.3C*), and *BrNCED3* (*BraA05g032610.3C*), were found to be downregulated expression in the cotyledons and leaves of 19YC-2 when displayed yellow. In the downstream process of

carotenoid metabolism, a list of enzymes can cleave carotenoid to produce phytohormone abscisic acid (ABA) and strigolactones, and the downregulated expression of these downstream genes had been extensively demonstrated to be involved in the catabolism of carotenoid (Nisar et al., 2015; Yuan et al., 2015). The expression of *NCED* gene in ginkgo was increased in yellow leaves in autumn, while decreased in green leaves in summer (Sun et al., 2022). Previous studies in zucchini reported that *NCED* and *CCD* genes were downregulated in yellow and orange peels, which was agreement with the accumulation of yellow lutein (Obrero et al., 2013; Niu et al., 2023). These evidences suggest that the differential expression of carotenoid-related genes combining the alteration of carotenoid content favor the leaf color changes in yellow cotyledon mutant 19YC-2.

Many putative regulators have been identified to function in transcriptional regulation of carotenoid biosynthetic genes in photosynthetic tissues, which is highly influenced by various environmental factors (Stanley and Yuan, 2019). In the current study, many differentially expressed TFs were identified to be highly correlated with the changes in carotenoid contents by WGCNA, and belonged to the families of *BrERF/AP2*, *BrR2R3-MYB*, *BrbHLH*, and *BrWRKY*. The *BrERF/AP2* family contains many TFs that had been characterized to participate in regulating the process of carotenoid metabolism (Yuan et al., 2015; Stanley and Yuan, 2019). In *Arabidopsis* leaves, *RAP2.2* (a member of *ERF/AP2* family) was reported to interact with *SINAT2* and positively regulate *PSY* and *PDS* during carotenoid biosynthesis (Welsch et al., 2007). In tomato, an *AP2a* gene was found to be a major regulator of the upstream genes of carotenoid biosynthesis, mediating fruit ripening (Chung et al., 2010; Karlova et al., 2011). We also found that two DEGs, *BraA08g001340.3C* and *BraA04g017150.3C*, were identified to *BrERF/AP2* family and highly positively related to the changes in carotenoid contents, which provide important references for exploring the functions of the two TFs. Meanwhile, the TFs of *MYB* family had been demonstrated to involve in the transcriptional regulation of leaf-color mutation in ginkgo (Wu et al., 2019). In kiwifruit, *MYB7* gene was found to activate the promoter of *LCYB* gene that modulates carotenoid accumulation (Ampomah-Dwamena et al., 2019). In the current study, a *BrMYB* gene (*BraA06g042530.3C*) was upregulated expressed in the cotyledons and leaves of yellow cotyledon mutant 19YC-2 and highly positively related to carotenoid accumulation. Overall, these differentially expressed TF genes may play potential important roles in regulating carotenoid biosynthesis mediating leaf color change in yellow cotyledon mutant 19YC-2.

5 Conclusion

Chinese cabbage yellow cotyledon mutant 19YC-2 has obvious yellow phenotypes in the cotyledons and the new leaves, which is valuable for hybrid breeding. In this study, we found that low-intensity light treatment induced an obvious change from yellow to green in the new leaves of 19YC-2. The decreased carotenoid content may be the major reason of leaf color change in 19YC-2 under low-intensity light treatment. RNA-seq analysis identified that the expression changes of many DEGs encoding photosynthesis antenna proteins and related to carotenoid biosynthesis were consistent with the changes in carotenoid content, indicating the putative important roles of these DEGs in regulating leaf color changes of 19YC-2. Based on the above results, we drew a schematic diagram on the regulatory network of leaf color changes of Chinese cabbage yellow cotyledon mutants exposed to different light intensity (Figure 11). These results facilitate understanding the effects of photosynthetic pigments on leaf color changes and provide insights into the formation

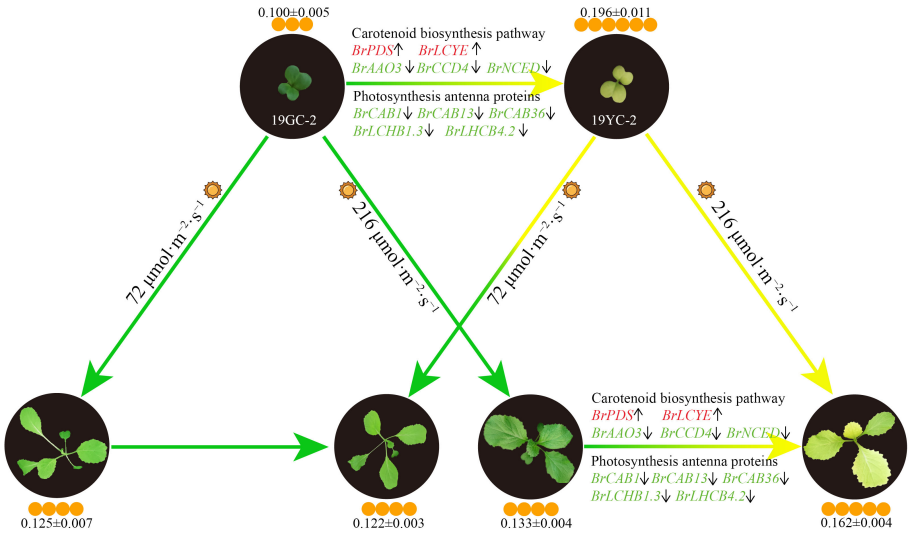

FIGURE 11
Schematic diagram of the regulatory network of leaf color changes of Chinese cabbage yellow cotyledon mutants under different light intensity. The color of gene name indicates the upregulation (red) or downregulation (green) of gene expression, and the arrows after gene names indicate increases (upward) or decreases (downward) in gene expression levels. The sun represents light conditions. The number of orange circles indicates the relative content of carotenoids (± SEM; mg·g^{-1}/FW).

mechanisms of yellow cotyledons and yellow leaves in Chinese cabbage 19YC-2.

Data availability statement

The datasets presented in this study can be found in online repositories. The names of the repository/repositories and accession number(s) can be found in the article/Supplementary Material.

Author contributions

JH: Data curation, Formal analysis, Investigation, Methodology, Software, Validation, Writing – original draft. NZ: Data curation, Formal analysis, Investigation, Validation, Writing – original draft. YG: Investigation, Validation, Writing – original draft. YB: Investigation, Validation, Writing – original draft. YL: Investigation, Validation, Writing – original draft. LZ: Conceptualization, Funding acquisition, Methodology, Resources, Supervision, Writing – review & editing. SN: Conceptualization, Data curation, Funding acquisition, Methodology, Supervision, Writing – original draft, Writing – review & editing.

Funding

The author(s) declare financial support was received for the research, authorship, and/or publication of this article. This work was supported by the National Natural Science Foundation of China (31801869), and the Natural Science Basic Research Program in Shaanxi Province of China (2023-JC-YB-184), the Key Research and Development Program of Yangling Seed Innovative Center (Ylzy-sc-04).

Conflict of interest

The authors declare that the research was conducted in the absence of any commercial or financial relationships that could be construed as a potential conflict of interest.

Publisher's note

Supplementary material

The Supplementary Material for this article can be found online at: https://www.frontiersin.org/articles/10.3389/fpls.2024.1371451/full#supplementary-material

SUPPLEMENTARY FIGURE 1
Enrichment analysis of the identified DEGs based on GO terms. CK0, T0, CK1, T1, CK2, and T2 represent the six cDNA libraries from 19GC-2 and 19YC-2.

SUPPLEMENTARY FIGURE 2
Top 30 enriched KEGG pathways of the identified DEGs. CK0, T0, CK1, T1, CK2, and T2 represent the six cDNA libraries from 19GC-2 and 19YC-2. Red circles indicate the critical pathways.

SUPPLEMENTARY FIGURE 3
GSEA analysis of the pathways of photosynthesis antenna proteins **(A)** and carotenoid biosynthesis **(B)**. CK0, T0, CK1, T1, CK2, and T2 represent the six cDNA libraries from 19GC-2 and 19YC-2.

References

Allen, J. F., and Forsberg, J. (2001). Molecular recognition in thylakoid structure and function. *Trends Plant Sci.* 6, 317–326. doi: 10.1016/S1360-1385(01)02010-6

Ampomah-Dwamena, C., Thrimawithana, A. H., Dejnoprat, S., Lewis, D., Espley, R. V., and Allan, A. C. (2019). A kiwifruit (*Actinidia deliciosa*) R2R3-MYB transcription factor modulates chlorophyll and carotenoid accumulation. *New Phytol.* 221, 309–325. doi: 10.1111/nph.15362

Ampomah-Dwamena, C., Tomes, S., Thrimawithana, A. H., Elborough, C., Bhargava, N., Rebstock, R., et al. (2022). Overexpression of PSY1 increases fruit skin and flesh carotenoid content and reveals associated transcription factors in apple (*Malus×domestica*). *Front. Plant Sci.* 13. doi: 10.3389/fpls.2022.967143

Brodribb, T. J., Feild, T. S., and Jordan, G. J. (2007). Leaf maximum photosynthetic rate and venation are linked by hydraulics. *Plant Physiol.* 144, 1890–1898. doi: 10.1104/pp.107.101352

Cao, H. B., Luo, H. M., Yuan, H., Eissa, M. A., Thannhauser, T. W., Welsch, R., et al. (2019). A neighboring aromatic-aromatic amino acid combination governs activity divergence between tomato phytoene synthases. *Plant Physiol.* 180, 1988–2003. doi: 10.1104/pp.19.00384

Cazzonelli, C. I., and Pogson, B. J. (2010). Source to sink: regulation of carotenoid biosynthesis in plants. *Trends Plant Sci.* 15, 266–274. doi: 10.1016/j.tplants.2010.02.003

Chen, H. Y., Ji, H. Y., Zhu, S. P., Zhu, K. J., Ye, J. L., and Deng, X. X. (2023a). Carotenoid and transcriptome profiles of a novel citrus cultivar 'Jinlegan' reveal mechanisms of yellowish fruit formation. *Hortic. Adv.* 1, 5. doi: 10.1007/s44281-023-00005-4

Chen, X. D., Cai, W. J., Xia, J., Yuan, H. Z., Wang, Q. L., Pang, F. H., et al. (2023b). Metabolomic and transcriptomic analysis reveals the molecular mechanism by which blue light promotes lutein synthesis in strawberry. *J. Integr. Agr.* 22, 1695–1703. doi: 10.1016/j.jia.2023.04.002

Cheng, M. Z., Meng, F. Y., Mo, F. L., Chen, X. L., Zhang, H., and Wang, A. X. (2022). Insights into the molecular basis of a yellow leaf color mutant (ym) in tomato (*Solanum lycopersicum*). *Sci. Hortic.* 293, 110743. doi: 10.1016/j.scienta.2021.110743

Chung, M. Y., Vrebalov, J., Alba, R., Lee, J., McQuinn, R., Chung, J. D., et al. (2010). A tomato (*Solanum lycopersicum*) APETALA2/ERF gene, *SlAP2a*, is a negative regulator of fruit ripening. *Plant J.* 64, 936–947. doi: 10.1111/tpj.2010.64.issue-6

Deng, X. J., Zhang, H. Q., Wang, Y., Shu, Z. F., Wang, G. H., and Wang, G. L. (2012). Research advances on rice leaf-color mutant genes. *Hybr. Rice* 27, 9–14. doi: 10.1007/s11032-019-1003-6

Eckhardt, U., Grimm, B., and Hortensteiner, S. (2004). Recent advances in chlorophyll biosynthesis and breakdown in higher plants. *Plant Mol. Biol.* 56, 1–14. doi: 10.1007/s11103-004-2331-3

Fanciullino, A. L., Dhuique-Mayer, C., Luro, F., Morillon, R., and Ollitrault, P. (2007). Carotenoid biosynthetic pathway in the *Citrus* genus: number of copies and phylogenetic diversity of seven genes. *J. Agric. Food Chem.* 55, 7405–7417. doi: 10.1021/jf070711h

Frank, H. A., and Cogdell, R. J. (1996). Carotenoids in photosynthesis. *Photochem. Photobiol.* 63, 257–264. doi: 10.1111/j.1751-1097.1996.tb03022.x

Fromme, P., Melkozernov, A., Jordan, P., and Krauss, N. (2003). Structure and function of photosystem I: Interaction with its soluble electron carriers and external antenna systems. *FEBS Lett.* 555, 40–44. doi: 10.1016/S0014-5793(03)01124-4

Gady, A. L. F., Vriezen, W. H., Van de Wal, M. H. B. J., Huang, P. P., Bovy, A. G., Visser, R. G. F., et al. (2012). Induced point mutations in the phytoene synthase 1 gene cause differences in carotenoid content during tomato fruit ripening. *Mol. Breed.* 29, 801–812. doi: 10.1007/s11032-011-9591-9

Grumbach, K. H., and Lichtenthaler, H. K. (1982). Chloroplast pigments and their biosynthesis in relation to light intensity. *Photochem. Photobiol.* 35, 209–212. doi: 10.1111/j.1751-1097.1982.tb03833.x

Hashimoto, H., Uragami, C., and Cogdell, R. J. (2016). Carotenoids and photosynthesis. *Carotenoids nature: Biosynthes. Regul. Funct.* 79, 111–139. doi: 10.1007/978-3-319-39126-7_4

Karlova, R., Rosin, F. M., Busscher-Lange, J., Parapunova, V., Do, P. T., Fernie, A. R., et al. (2011). Transcriptome and metabolite profiling show that APETALA2a is a major regulator of tomato fruit ripening. *Plant Cell* 23, 923–941. doi: 10.1105/tpc.110.081273

Kato, M., Ikoma, Y., Matsumoto, H., Sugiura, M., Hyodo, H., and Yano, M. (2004). Accumulation of carotenoids and expression of carotenoid biosynthetic genes during maturation in citrus fruit. *Plant Physiol.* 134, 824–837. doi: 10.1104/pp.103.031104

Kong, D. X., Li, Y. Q., Wang, M. L., Bai, M., Zou, R., Tang, H., et al. (2016). Effects of light intensity on leaf photosynthetic characteristics, chloroplast structure, and alkaloid content of *Mahonia bodinieri* (Gagnep.) Laferr. *Acta Physiol. Plant* 38, 1–15. doi: 10.1007/s11738-016-2147-1

Langfelder, P., and Horvath, S. (2008). WGCNA: an R package for weighted correlation network analysis. *BMC Bioinf.* 9, 1–13. doi: 10.1186/1471-2105-9-559

Lee, E., Ahn, H., and Choe, E. (2014). Effects of light and lipids on chlorophyll degradation. *Food Sci. Biotechnol.* 23, 1061–1065. doi: 10.1007/s10068-014-0145-x

Lichtenthaler, H. K. (1987). Chlorophylls and carotenoids: pigments of photosynthetic biomembranes. *Methods Enzymol.* 148, 350–382. doi: 10.1016/0076-6879(87)48036-1

Lintig, J., Welsch, R., Bonk, M., Giuliano, G., Batschauer, A., and Kleinig, H. (1997). Light-dependent regulation of carotenoid biosynthesis occurs at the level of phytoene synthase expression and is mediated by phytochrome in *Sinapis alba* and *Arabidopsis thaliana* seedlings. *Plant J.* 12, 625–634. doi: 10.1046/j.1365-313X.1997.d01-16.x

Liu, Z. B., Mao, L. Z., Yang, B. Z., Cui, Q. Z., Dai, Y. H., Li, X. Q., et al. (2023). A multi-omics approach identifies bHLH71-like as a positive regulator of yellowing leaf pepper mutants exposed to high-intensity light. *Hortic. Res.* 10, uhad098. doi: 10.1093/hr/uhad098

Love, M. I., Huber, W., and Anders, S. (2014). Moderated estimation of fold change and dispersion for RNA-seq data with DESeq2. *Genome Biol.* 15, 1–21. doi: 10.1186/s13059-014-0550-8

Luo, T., Luo, S., Araújo, W. L., Schlicke, H., Rothbart, M., Yu, J., et al. (2013). Virus-induced gene silencing of pea CHLI and CHLD affects tetrapyrrole biosynthesis, chloroplast development and the primary metabolic network. *Plant Physiol. Biochem.* 65, 17–26. doi: 10.1016/j.plaphy.2013.01.006

Ma, Y. Y., Shi, J. C., Wang, D. J., Liang, X., Wei, F., Gong, C. M., et al. (2023). A point mutation in the gene encoding magnesium chelatase I subunit influences strawberry leaf color and metabolism. *Plant Physiol.* 192, kiad247. doi: 10.1093/plphys/kiad247

Ma, G., Zhang, L. C., Kitaya, Y., Seoka, M., Kudaka, R., Yahata, M., et al. (2021). Blue LED light induces regreening in the flavedo of Valencia orange in *vitro*. *Food Chem.* 335, 127621. doi: 10.1016/j.foodchem.2020.127621

Markwell, J., and Namuth, D. (2003). Plant pigments and photosynthesis. *J. Nat. Resour. Life Sci. Educ.* 32, 137–137. doi: 10.2134/jnrlse.2003.0137a

Masuda, T. (2008). Recent overview of the Mg branch of the tetrapyrrole biosynthesis leading to chlorophylls. *Photosynth. Res.* 96, 121–143. doi: 10.1007/s11120-008-9291-4

Nie, S. S., Wang, R. F., Li, R., Zhang, M. J., and Zhang, L. G. (2019). Transcriptomic analysis identifies critical signaling components involved in the self-incompatibility response in Chinese cabbage. *Sci. Hortic.* 248, 189–199. doi: 10.1016/j.scienta.2019.01.022

Nie, S. S., Zheng, S. J., Lyu, C. S., Cui, S. N., Huo, J. Y., and Zhang, L. G. (2023). Calcium/calmodulin modulates pollen germination and pollen tube growth and self-incompatibility response in Chinese cabbage (*Brassica rapa* L.). *Sci. Hortic.* 308, 111607. doi: 10.1016/j.scienta.2022.111607

Nie, L. B., Zheng, Y. S., Zhang, L. T., Wu, Y., Zhu, S. D., Hou, J. F., et al. (2021). Characterization and transcriptomic analysis of a novel yellow-green leaf wucai (*Brassica campestris* L.) germplasm. *BMC Genomics* 22, 1–15. doi: 10.1186/s12864-021-07573-7

Nisar, N., Li, L., Lu, S., Khin, N. C., and Pogson, B. J. (2015). Carotenoid metabolism in plants. *Mol. Plant* 8, 68–82. doi: 10.1016/j.molp.2014.12.007

Niu, J. Q., Chen, Q., Lu, X. A., Wang, X. Q., Tang, Z. L., Liu, Q. H., et al. (2023). Fine mapping and identifying candidate gene of Y underlying yellow peel in *Cucurbita pepo*. *Front. Plant Sci.* 14. doi: 10.3389/fpls.2023.1159937

Obrero, Á., González-Verdejo, C. I., Die, J. V., Gómez, P., Del Río-Celestino, M., and Román, B. (2013). Carotenogenic gene expression and carotenoid accumulation in three varieties of *Cucurbita pepo* during fruit development. *J. Agric. Food Chem.* 61, 6393–6403. doi: 10.1021/jf4004576

Pecker, I., Chamovitz, D., Linden, H., Sandmann, G., and Hirschberg, J. (1992). A single polypeptide catalyzing the conversion of phytoene to zeta-carotene is transcriptionally regulated during tomato fruit ripening. *Proc. Natl. Acad. Sci. U.S.A.* 89, 4962–4966. doi: 10.1073/pnas.89.11.4962

Pogson, B. J., and Albrecht, V. (2011). Genetic dissection of chloroplast biogenesis and development: an overview. *Plant Physiol.* 155, 1545–1551. doi: 10.1104/pp.110.170365

Pogson, B., McDonald, K. A., Truong, M., Britton, G., and DellaPenna, D. (1996). *Arabidopsis* carotenoid mutants demonstrate that lutein is not essential for photosynthesis in higher plants. *Plant Cell* 8, 1627–1639. doi: 10.1105/tpc.8.9.1627

Rodrigo, M. J., Marcos, J. F., and Zacarías, L. (2004). Biochemical and molecular analysis of carotenoid biosynthesis in flavedo of orange (*Citrus sinensis* L.) during fruit development and maturation. *J. Agric. Food Chem.* 52, 6724–6731. doi: 10.1021/jf049607f

Rosso, D., Bode, R., Li, W. Z., Krol, M., Saccon, D., Wang, S., et al. (2009). Photosynthetic redox imbalance governs leaf sectoring in the *Arabidopsis thaliana* variegation mutants *immutans*, *spotty*, *var1*, and *var2*. *Plant Cell* 21, 3473–3492. doi: 10.1105/tpc.108.062752

Ruban, A. V. (2015). Evolution under the sun: optimizing light harvesting in photosynthesis. *J. Exp. Bot.* 66, 7–23. doi: 10.1093/jxb/eru400

Sakamoto, W. (2003). Leaf-variegated mutations and their responsible genes in *Arabidopsis thaliana*. *Genes Genet. Syst.* 78, 1–9. doi: 10.1266/ggs.78.1

Simkin, A. J., Zhu, C., Kuntz, M., and Sandmann, G. (2003). Light-dark regulation of carotenoid biosynthesis in pepper (*Capsicum annuum*) leaves. *J. Plant Physiol.* 160, 439–443. doi: 10.1078/0176-1617-00871

Stanley, L., and Yuan, Y. W. (2019). Transcriptional regulation of carotenoid biosynthesis in plants: So many regulators, so little consensus. *Front. Plant Sci.* 10. doi: 10.3389/fpls.2019.01017

Sun, Y., Bai, P. P., Gu, K. J., Yang, S. Z., Lin, H. Y., Shi, C. G., et al. (2022). Dynamic transcriptome and network-based analysis of yellow leaf mutant *Ginkgo biloba*. *BMC Plant Biol.* 22, 465. doi: 10.1186/s12870-022-03854-9

Sun, T. H., Yuan, H., Cao, H. B., Yazdani, M., Tadmor, Y., and Li, L. (2018). Carotenoid metabolism in plants: the role of plastids. *Mol. Plant* 11, 58–74. doi: 10.1016/j.molp.2017.09.010

Terry, M. J., Ryberg, M., Raitt, C. E., and Page, A. M. (2001). Altered etioplast development in phytochrome chromophore-deficient mutants. *Planta* 214, 314–325. doi: 10.1007/s004250100624

Wang, Q., Sullivan, R. W., Kight, A., Henry, R. L., Huang, J., Jones, A. M., et al. (2004). Deletion of the chloroplast-localized Thylakoid formation1 gene product in *Arabidopsis* leads to deficient thylakoid formation and variegated leaves. *Plant Physiol.* 136, 3594–3604. doi: 10.1104/pp.104.049841

Wang, Y. S., Wang, J. J., Chen, L. Q., Meng, X. W., Zhen, X. X., Liang, Y. P., et al. (2022). Identification and function analysis of yellow-leaf mutant (YX-yl) of broomcorn millet. *BMC Plant Biol.* 22, 1–15. doi: 10.1186/s12870-022-03843-y

Watanabe, M., Musumi, K., and Ayugase, J. (2011). Carotenoid pigment composition, polyphenol content, and antioxidant activities of extracts from orange-colored Chinese cabbage. *LWT-Food Sci. Technol.* 44, 1971–1975. doi: 10.1016/j.lwt.2011.04.010

Welsch, R., Maass, D., Voegel, T., Dellapenna, D., and Beyer, P. (2007). Transcription factor RAP2.2 and its interacting partner SINAT2: stable elements in the carotenogenesis of *Arabidopsis* leaves. *Plant Physiol.* 145, 1073–1085. doi: 10.1104/pp.107.104828

Wu, Y. Q., Guo, J., Wang, T. L., Cao, F. L., and Wang, G. B. (2019). Transcriptional profiling of long noncoding RNAs associated with leaf-color mutation in *Ginkgo biloba* L. *BMC Plant Biol.* 19, 1–13. doi: 10.1186/s12870-019-2141-z

Wu, H. Y., Shi, N. R., An, X. Y., Liu, C., Fu, H. F., Cao, L., et al. (2018). Candidate genes for yellow leaf color in common wheat (*Triticum aestivum* L.) and major related metabolic pathways according to transcriptome profiling. *Int. J. Mol. Sci.* 19, 1594. doi: 10.3390/ijms19061594

Xu, J., Guo, Z. X., Jiang, X. C., Ahammed, G. J., and Zhou, Y. H. (2021). Light regulation of horticultural crop nutrient uptake and utilization. *Hortic. Plant J.* 7, 367–379. doi: 10.1016/j.hpj.2021.01.005

Xu, B. H., Zhang, C. Y., Gu, Y., Cheng, R., Huang, D. Y., Liu, X., et al. (2023). Physiological and transcriptomic analysis of a yellow leaf mutant in watermelon. *Sci. Rep.* 13, 9647. doi: 10.1038/s41598-023-36656-6

Yang, S., Zhang, Z. Q., Chen, W. C., Liang, C. L., Li, X. F., Liu, Z. B., et al. (2023). Fine-mapping and transcriptome analysis of the photosensitive leaf-yellowing gene *CaLY1* in pepper (*Capsicum annuum* L.). *Hortic. Plant J.* 9, 122–132. doi: 10.1016/j.hpj.2022.06.007

Yuan, Y., Ren, S. Y., Liu, X. F., Su, L. Y., Wu, Y., Zhang, W., et al. (2022). *SlWRKY35* positively regulates carotenoid biosynthesis by activating the MEP pathway in tomato fruit. *New Phytol.* 234, 164–178. doi: 10.1111/nph.17977

Yuan, H., Zhang, J. X., Nageswaran, D., and Li, L. (2015). Carotenoid metabolism and regulation in horticultural crops. *Hortic. Res.* 2, 15036. doi: 10.1038/hortres.2015.36

Zhang, T. T., Dong, X. Y., Yuan, X., Hong, Y. Y., Zhang, L. L., Zhang, X., et al. (2022a). Identification and characterization of *CsSRP43*, a major gene controlling leaf yellowing in cucumber. *Hortic. Res.* 9, uhac212. doi: 10.1093/hr/uhac212

Zhang, K., Liu, Z. Y., Shan, X. F., Li, C. Y., Tang, X. Y., Chi, M. Y., et al. (2017). Physiological properties and chlorophyll biosynthesis in a Pak-choi (*Brassica rapa* L. ssp. *chinensis*) yellow leaf mutant, pylm. *Acta Physiol. Plant* 39, 1–10. doi: 10.1007/s11738-016-2321-5

Zhang, S. Z., Wu, X. L., Cui, J., Zhang, F., Wan, X. Q., Liu, Q. L., et al. (2019). Physiological and transcriptomic analysis of yellow leaf coloration in *Populus deltoides Marsh*. *PloS One* 14, e0216879. doi: 10.1371/journal.pone.0216879

Zhang, J. X., Yuan, H., Fei, Z. J., Pogson, B. J., Zhang, L. G., and Li, L. (2015). Molecular characterization and transcriptome analysis of orange head Chinese cabbage (*Brassica rapa* L. ssp. *pekinensis*). *Planta* 241, 1381–1394. doi: 10.1007/s00425-015-2262-z

Zhang, L. L., Zhang, J. X., Mao, Y. F., Yin, Y. J., and Shen, X. (2022b). Physiological analysis and transcriptome sequencing of a delayed-green leaf mutant 'Duojiao'of ornamental crabapple (*Malus* sp.). *Physiol. Mol. Biol. Plants* 28, 1833–1848. doi: 10.1007/s12298-022-01248-7

Zhao, Y. H., Huang, S. N., Zhang, M. D., Zhang, Y., and Feng, H. (2021). Mapping of a pale green mutant gene and its functional verification by allelic mutations in Chinese cabbage (*Brassica rapa* L. ssp. *pekinensis*). *Front. Plant Sci.* 12. doi: 10.3389/fpls.2021.699308

Zhao, M. H., Li, X., Zhang, X. X., Zhang, H., and Zhao, X. Y. (2020). Mutation mechanism of leaf color in plants: A review. *Forests* 11, 851. doi: 10.3390/f11080851

Zhu, H. S., Chen, M. D., Wen, Q. F., and Li, Y. P. (2015). Isolation and characterization of the carotenoid biosynthetic genes LCYB, LCYE and CHXB from strawberry and their relation to carotenoid accumulation. *Sci. Hortic.* 182, 134–144. doi: 10.1016/j.scienta.2014.12.007

frontiers | Frontiers in Plant Science

TYPE Original Research
PUBLISHED 17 May 2024
DOI 10.3389/fpls.2024.1355090

OPEN ACCESS

EDITED BY
Xiangshu Dong,
Yunnan University, China

REVIEWED BY
Wenxing Pang,
Shenyang Agricultural University, China
Zhansheng Li,
Chinese Academy of Agricultural Sciences, China
Chunyu Zhang,
Huazhong Agricultural University, China

*CORRESPONDENCE
Yuxiang Yuan
yuxiangyuan126@126.com
Xiaowei Zhang
xiaowei5737@163.com

†These authors have contributed equally to this work

RECEIVED 13 December 2023
ACCEPTED 21 March 2024
PUBLISHED 17 May 2024

CITATION
Wei X, Xiao S, Zhao Y, Zhang L, Nath UK, Yang S, Su H, Zhang W, Wang Z, Tian B, Wei F, Yuan Y and Zhang X (2024) Fine mapping and candidate gene analysis of *CRA8.1.6*, which confers clubroot resistance in turnip (*Brassica rapa* ssp. *rapa*). *Front. Plant Sci.* 15:1355090. doi: 10.3389/fpls.2024.1355090

Fine mapping and candidate gene analysis of *CRA8.1.6*, which confers clubroot resistance in turnip (*Brassica rapa* ssp. *rapa*)

Xiaochun Wei[1,2†], Shixiong Xiao[1,2†], Yanyan Zhao[1], Luyue Zhang[2], Ujjal Kumar Nath[3], Shuangjuan Yang[1], Henan Su[1], Wenjing Zhang[1], Zhiyong Wang[1], Baoming Tian[2], Fang Wei[2], Yuxiang Yuan[1*] and Xiaowei Zhang[1*]

[1]Institute of Vegetables, Henan Academy of Agricultural Sciences, Graduate T&R Base of Zhengzhou University, Zhengzhou, Henan, China, [2]School of Agricultural Sciences, Zhengzhou University, Zhengzhou, Henan, China, [3]Department of Genetics and Plant Breeding, Bangladesh Agricultural University, Mymensingh, Bangladesh

Clubroot disease poses a significant threat to *Brassica* crops, necessitating ongoing updates on resistance gene sources. In F_2 segregants of the clubroot-resistant inbred line BrT18-6-4-3 and susceptible DH line Y510, the genetic analysis identified a single dominant gene responsible for clubroot resistance. Through bulk segregant sequencing analysis and kompetitive allele-specific polymerase chain reaction assays, *CRA8.1.6* was mapped within 110 kb (12,255–12,365 Mb) between markers L-CR11 and L-CR12 on chromosome A08. We identified *BraA08g015220.3.5C* as the candidate gene of *CRA8.1.6*. Upon comparison with the sequence of disease-resistant material BrT18-6-4-3, we found 249 single-nucleotide polymorphisms, seven insertions, six deletions, and a long terminal repeat (LTR) retrotransposon (5,310 bp) at 909 bp of the first intron. However, the LTR retrotransposon was absent in the coding sequence of the susceptible DH line Y510. Given the presence of a non-functional LTR insertion in other materials, it showed that the LTR insertion might not be associated with susceptibility. Sequence alignment analysis revealed that the fourth exon of the susceptible line harbored two deletions and an insertion, resulting in a frameshift mutation at 8,551 bp, leading to translation termination at the leucine-rich repeat domain's C-terminal in susceptible material. Sequence alignment of the CDS revealed a 99.4% similarity to *Crr1a*, which indicate that *CRA8.1.6* is likely an allele of the *Crr1a* gene. Two functional markers, CRA08-InDel and CRA08-KASP1, have been developed for marker-assisted selection in CR turnip cultivars. Our findings could facilitate the development of clubroot-resistance turnip cultivars through marker-assisted selection.

KEYWORDS

turnip, clubroot, fine mapping, C-terminal, CRA08-InDel

1 Introduction

Turnip (*Brassica rapa* L. spp. *rapifera*) is a vegetable belonging to the genus *Brassica*. It originated in Afghanistan, Pakistan, Transcaucasia (part of Asia), and the Mediterranean. The Asian turnip variety is predominantly distributed in China and western Japan (Pu et al., 2018). Clubroot disease is caused by *Plasmodiophora brassicae* (*P. brassicae*) and has been reported in numerous countries (Chai et al., 2014). It affects plants in the *Brassicaceae* family, such as Chinese cabbage, turnips, radish, cauliflower, and mustard (Howard et al., 2010). *P. brassicae* first infects root hairs by free primary spores and then releases secondary zoospores to invade the cortex (Kageyama and Asano, 2009). This results in gradual swelling of the roots in affected plants, hindering nutrient absorption and ultimately leading to wilting and death of the entire plant. Dormant spores of *P. brassicae* can remain active in the soil for up to 20 years, posing a long-term threat to cruciferous plants (Dixon, 2009). Clubroot diseases tend to exacerbate annually, making control challenging through chemical, biological, and agricultural means. From an ecological standpoint, developing resistant varieties through breeding is a promising solution (Piao et al., 2009). Zhang et al. (2024) successfully identified a CR gene, facilitating CR-resistant breeding in *B. oleracea*.

Single-nucleotide polymorphisms (SNPs) represent a prevalent form of DNA variation across the genome, offering advantages such as high throughput and seamless integration. Consequently, they find wide applications in various fields, such as disease treatment, drug development, and plant breeding. The kompetitive allele-specific polymerase chain reaction (PCR) (KASP) technique is a precise allele-specific PCR method capable of accurately identifying SNPs by matching terminal primer bases. KASP technology is renowned for its time efficiency, reduced error rates, and cost-effectiveness in genotyping, providing flexibility for genotyping multiple samples with minimal SNP loci (Gouda et al., 2021).

Significant progress has been made in developing clubroot-resistant genotypes. European fodder turnips (*Brassica rapa* L. spp. *rapifera*) (AA, 2n = 20) 'ECD01-04,' 'Gelria R,' 'Siloga,' 'Debra,' and 'Milan White' (Eckholm, 1993; Elke et al., 2009) have emerged as a widely utilized resistant source, successfully integrated into CR breeding programs in Chinese cabbage and canola (Piao et al., 2009). To date, 36 clubroot-resistant loci have been identified across *Brassica* species, including *B. rapa*, *B. oleracea*, *B. napus*, and *B. nigra* (Hasan et al., 2021; Pang et al., 2022). Among these loci, the majority are found on chromosomes A03 and A08. Chromosome A03 harbors 19 resistance loci, encompassing *CRa*, *CRb*, *CRd*, *CRq*, *CRk*, *Rcr1*, *Rcr2*, *Rcr4*, *Rcr5*, *pbBa3.1*, *pbBa3.2*, *pbBa3.3*, *CR6b*, CRb^{kato}, *BraA.CRa*, *BraA.CRc*, $BraA3PSX.CRa/b^{kato}1.1$, $BraA3PSX.CRa/b^{kato}1.2$, and *Crr3* (Etsuo et al., 1998; Hirai et al., 2004; Piao et al., 2004; Ueno et al., 2012; Chen et al., 2013; Chu et al., 2014; Sun et al., 2016; Yu et al., 2017; Pang et al., 2018; Huang et al., 2019). On chromosome A08, nine resistance loci are identified, namely, *CRs*, *Crr1*, *Rcr3*, *Rcr9*, *PbBa8.1*, *qBrCR38-2*, $RCr9^{wa}$, $PbBrA08^{Banglim}$, and *BraACRb* (Hirani et al., 2018; Laila et al., 2019; Md. Masud et al., 2020; Yu et al., 2022). Additionally, chromosome A01 hosts three loci, namely, *CR6a*, *Crr2*, and *PbBa1.1* (Suwabe et al., 2006). Chromosome A02 carries two loci, namely, *CRc* and *Rcr8* (Yu et al., 2017), whereas resistance loci *CrrA5*, *Crr4*, and q*BrCR38-1* are located on chromosomes A05, A06, and A07, respectively (Suwabe et al., 2006; Nguyen et al., 2018; Zhu et al., 2019). The collection of resistance loci appears to be extensive; however, only *Crr1a*, *CRa*, and their alleles have been cloned (Ueno et al., 2012; Hatakeyama et al., 2013; Yang et al., 2022). These cloned genes have been found to contain important components of effector-induced immunity, TIR-NBS-LRR [Toll/interleukin-1 (IL-1) receptor–like nucleotide binding site, leucine-rich repeat] protein domain family (Mariana et al., 2002).

CRA8.1.6 was finely mapped and cloned from the F_2 population, resulting from a cross between the resistant inbred line BrT18-6-4-3 and the susceptible DH line Y510. Our investigation aimed to elucidate the mechanisms underlying the loss of resistance by analyzing the structure of candidate genes in the susceptible line. Gene sequence alignment revealed a frameshift mutation in the susceptible line Y510, resulting in translation termination at 8,551 bp. This mutation altered the C-terminal leucine-rich repeat (LRR) domain, leading to a loss of resistance. The disease index survey demonstrated a significantly lower disease index in overexpression transgenic *Arabidopsis* than in wild-type *Arabidopsis*. The results of the target gene expression revealed a significant increase in the relative expression of *CRA8.1.6* in the T_2 generation of *Arabidopsis* compared to the wild-type. This indicates that the conferred *CRA8.1.6* gene is indeed a clubroot-resistant gene. Functional markers, CRA08-InDel and CRA08-KASP1, linked to *CRA8.1.6* were successfully developed and validated. These markers represent valuable resources for marker-assisted selection in breeding CR cultivars against *P. brassicae*.

2 Materials and methods

2.1 Plant materials

In the current study, F_1 and F_2 populations were developed by crossing the clubroot-resistant turnip inbred line BrT18-6-4-3 (P_1) with the susceptible Chinese cabbage DH line Y510 (P_2) followed by the selfing of F_1. Parental lines, F_1, and F_2 populations, were inoculated with *P. brassicae* race four isolate 'XY-2' (Yuan et al., 2017). The F_2 population was cultivated between September 2021 and November 2021, and the inheritance pattern of the resistant gene was determined using a Chi-square test (χ^2). Furthermore, 26 disease-resistant and 29 susceptible lines were used to analyze mutations in the candidate gene (Supplementary Table 1). All materials used in this study were provided by the Institute of Vegetables, Henan Academy of Agricultural Sciences.

2.2 Estimation of disease index

The disease index was assessed by inoculating the plants on the 20th day after sowing using a root irrigation method with a concentration of 10^7 spores/mL of *P. brassicae* suspension (Luo et al., 2014). AKIMEKI and ECD05 were utilized for disease index estimation as controls for disease resistance and susceptibility,

respectively (Matsumoto et al., 2012). The inoculated plants were maintained at 22°C ± 2°C and 16-h/8-h (light/dark) photoperiod (Yuan et al., 2021). Samples were collected and immediately frozen in liquid nitrogen and then stored at −80°C for subsequent use. Root samples from resistant and susceptible materials were collected at different time points: 0 days after inoculation (DAI; indicating no infection), 3 DAI (representing cortical infection), 9 DAI (indicating early onset of disease), and 20 DAI (indicating late onset of disease). One-centimeter-long root segments were cut from the junction of the rhizome and fixed with Formalin-Aceto-Alcohol (FAA) solution (containing 5 mL of acetic acid + 5 mL of formalin + 50 mL of 95% alcohol + 35 mL of sterile water) for 24 h. After fixation with FAA, the roots were rinsed with sterile water, dried with absorbent paper, and stained with 0.5% fluorescent pink for 3 h. The infected roots were observed under a light microscope (Li et al., 2022).

2.3 Bulked segregant analysis by resequencing

DNA was extracted from resistant and susceptible parents, along with 30 highly resistant (DI = 0; R-pool) and susceptible F_2 plants (DI = 5–7; S-pool) (Supplementary Table 1) following the cetyl trimethyl ammonium bromide method. Bulked segregant analysis (BSA) sequencing (BSA-seq) was performed on four DNA pools (Huang et al., 2017), and sequencing was conducted using the Illumina HiSeq platform, with analysis carried out using NovoGene (http://www.novogene.com). The raw reads underwent quality control trimming to remove low-quality paired reads with the adapter and retained clean reads. The clean reads from the four DNA bulks were combined using BWA software (V0.7.17) and compared with *B. rapa* (Chiifu-401) genome version 3.0 (http://brassicadb.org/brad/index.phpM) (Kathiresan et al., 2014). SAMtools software (V1.3.1) was employed to identify SNPs and insertion/deletion (InDel) variations between the R and S pools. The ΔSNP index for all genomic positions in the R and S libraries was calculated (Supplementary Table 2) using a sliding window analysis with a window width of 1 Mb and a sliding window step size of 10 kb.

2.4 Marker analysis and linkage map construction

Sequences of the genes were downloaded from the *Brassica* database (http://brassicadb.org/brad/downloadOverview.php), and the SNPs of candidate genes were validated. Thirty-five pairs of primers for KASP markers were designed using DNAMAN software (V6.0) to verify the parents and F_2 population (Supplementary Table 3), and, ultimately, 21 pairs of polymorphic primers were selected (Xiang et al., 2007).

The KASP markers were utilized for genotyping the F_2 population consisting of 98 individuals. Linked loci were identified using JoinMap4.0 to form linkage groups (Voorrips, 2002), and a genetic linkage map was constructed according to the Kosambi mapping function (Kosambi, 1944).

An additional large F_2 population of 1,489 individuals was planted for recombination selection, from which 438 susceptible individuals were selected and used to map candidate genes.

2.5 Cloning and sequencing of the *CRA8.1.6* gene

DNA and cDNA sequences of *CRA8.1.6* candidate genes were cloned from the parents using Phanta Super-Fidelity DNA polymerase Mix (Vazyme, Nanjing, China) (Supplementary Table 4). Standard PCR was conducted with 30-s denaturation at 98°C followed by 35 cycles of 98°C for 10 s, 58°C for 5 s, and 72°C for 60 s.

PCR products were sequenced by Sangon Biotech Co., Ltd. (Zhengzhou, China) and analyzed using DNAMAN software (V6.0). The complete coding sequence (CDS) of the *CRA8.1.6* gene from BrT18-6-4-3 and Y510 has been submitted to GenBank under the accession number AB605024.1. Protein's physical and chemical properties were determined with Expasy (http://web.expasy.org/protparam/).

2.6 Quantitative real-time PCR and semi-quantitative RT-PCR analyses

Total RNA was extracted from root samples collected at 0 DAI, 3 DAI, 9 DAI, and 20 DAI of BrT18-6-4-3 and Y510 lines using the RNA Prep Pure Plant Kit (Beijing Day, China) (Wei et al., 2021). Single-stranded cDNA was synthesized using Trans-script after a two-step removal of genomic DNA (gDNA) (Trans, Beijing, China).

The quantitative real-time PCR (qRT-PCR) was performed in a Roche Light Cycler 480-II system (Roche Applied Sciences, Beijing, China). *GAPDH* was used as an internal reference gene to calculate relative expression levels using the $2^{-\Delta\Delta Ct}$ method (Livak and Schmittgen, 2001). *B. rapa* sequence information was utilized to design RT-PCR primers. Standard PCR was conducted by denaturing for 5 min at 94°C, followed by 30 s at 94°C, 30 s at 55°C, and 60 s at 72°C for 25 cycles. PCR products were visualized after electrophoresis on a 1% agarose gel (Supplementary Table 4).

2.7 Vector construction and transformation

Specific full-length primers were designed to incorporate restriction sites and protective bases. This was achieved using the plasmid DNA of the target gene as a template. The PCR amplification procedure was conducted as follows: 95°C for 5 min; 30 cycles of 95°C for 30 s, 50°C for 45 s, and 72°C for 258 s; followed by 72°C for 10 min; and 16°C for 30 min.

The purified PCR product was digested with pBWA (V) HS expression vector (Bio Run, Hu Bei, China), and the digested product was further purified and ligated with the vector using T4 ligase to obtain the recombinant plasmid pBWA (V) HS-BrT18-6. The ligation product was then transformed into competent DH5α cells and PCR-screened positive clones. After sequencing and

verification, *Arabidopsis thaliana* was transformed using dip method (Hamann et al., 2002). The resulting T_0 transgenic *A. thaliana* was identified (Pang et al., 2022), and positive plants were selected for future planting to obtain T_2 generation seeds.

2.8 Inoculation of overexpression transgenic *A. thaliana* and identification of candidate gene

The T_2 generation seeds of *A. thaliana* were sown on a medium containing hygromycin to select homozygous strains based on positive reactions on specific media (Tang, 2007). T_2 generation *A. thaliana* seeds were planted (Suwabe et al., 2006). The *P. brassicae* strain used in this study was obtained from a clubroot-infected Chinese cabbage field (*B. rapa*) in Xinye County, Henan Province, China (113.97°E, 35.05°N), and the Williams system was used to confirm the *P. brassicae* strain as race 4 (Yuan et al., 2017).

Twenty-five-day-old transgenic and wild-type *A. thaliana* were inoculated with *P. brassicae*. Similarly, another set was inoculated with fresh water without any *P. brassicae* spores, which served as the control group. After 30 days of inoculation, the wild-type and transgenic *A. thaliana* were examined in control and experimental groups. The frequency of clubroot disease and expression of candidate genes were observed (Keita et al., 2012).

3 Results

3.1 Phenotypic and genetic analyses and cytological observation

After 30 days of infection with *P. brassicae*, all F_1 individuals resisted clubroot disease. We inoculated two fractions of the F_2 population with *P. brassicae* to account for the nature of disease-resistance gene action. In a small fraction of the F_2 population, 341 plants were resistant and 132 were susceptible, whereas, in a large fraction, 1,134 plants were resistant and 335 were susceptible. Both F_2 populations exhibited a 3:1 segregation, indicating Mendelian genetics for a single dominant gene (Table 1).

Microscopic examination revealed abundant spores attached to root hairs in all test plants at 1 DAI, indicating sufficient spores to initiate root infection. However, no cortical infection was detected in the resistant line (BrT18-6-4-3) at 1 DAI, 2 DAI, and 3 DAI or in the control group. In contrast, root hair infection was observed in the susceptible line (Y510) at 1 DAI, with cortical infection and free spores in epidermal cells observed at 3 DAI. No such symptoms were observed in the susceptible lines of the control group.

At 9 DAI, the roots of the resistant line appeared normal, whereas the roots of the susceptible line were slightly swollen. Numerous spores were found in the swollen root cortical cells of the susceptible line. In contrast, only a few spores were observed in the cortical cells of the resistant line (Figure 1), indicating cortical infection occurred between 3 DAI and 9 DAI.

3.2 Mapping of *CRA8.1.6* QTL

BSA-seq analysis generated 36,416,118 and 38,958,860 clean reads from the R and S pools, respectively (Supplementary Table 2). These reads were aligned to the *B. rapa* genome, identifying 218,150 SNPs and 53,040 InDels between the R and S pools. $\triangle$ (SNP index) for each locus was calculated using sliding window analysis. Subsequently, a new quantitative trait locus (QTL) called *CRA8.1.6* was identified on chromosome A08, likely between 11.04 Mb and 16.10 Mb (Supplementary Figure 1).

Thirty-five KASP markers were created on the basis of SNP variants within the candidate interval and polymorphism between the resistant (BrT18-6-4-3) and susceptible (Y510) lines, with 21 markers selected for genotyping of 98 F_2 plants to develop markers for chromosome A08. Within the reported *CRA8.1.6* QTL, one recombinant individual was found each for markers L-CR10 and L-CA01 with a genetic distance of 0.9 cM and 1.2 cM, respectively (Figure 2A). The order of markers on the genetic map was consistent with the physical map.

To refine the *CRA8.1.6* QTL, 438 susceptible homozygous F_2 individuals were screened for polymorphisms between markers L-CR03 and L-CA22, identifying 36 recombinants. All 51 recombinants were further genotyped using markers L-CR10 and L-CA01, identifying nine recombinants. Five KASP markers were developed, two of which showed polymorphism. Ultimately, a candidate gene for the *CRA8.1.6* QTL was determined at a position (12,255–12,365 Mb) on chromosome A08 marked by markers L-CR11 and L-CR12 (Figure 2B).

3.3 Candidate gene analysis

Detailed mapping of the *CRA8.1.6* QTL region revealed 15 genes, with *BraA08g015220.3.5C* being the sole gene encoding the

TABLE 1 Genetic analysis of clubroot resistance and susceptibility in F_2 populations of the cross between BrT18-6-4-3 and Y510.

Experiment	Population size	Resistant plants	Susceptible plants	Segregation	χ^2	$\chi^2_{(0.05)}$
P_1 (BrT18-6-4-3)	12	12	0	–	–	–
P_2 (Y510)	12	0	12	–	–	–
F_1	48	48	0	–	–	–
F_2-small	473	341	132	3:1	2.13	3.84
F_2-large	1,489	1,134	355	3:1	1.07	3.84

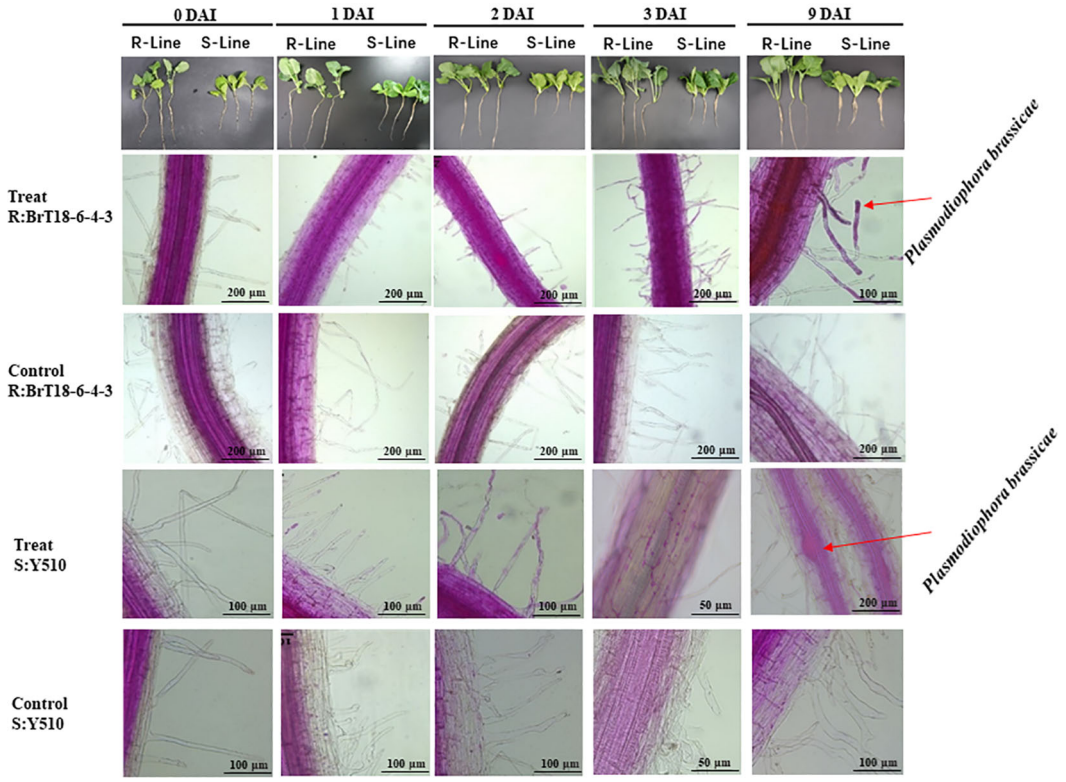

FIGURE 1
Comparison of root infection status between R-line (BrT18-6-4-3) and S-line (Y510) of control and *P. brassicae* inoculated groups. BrT18-6-4-3 initiated root hair infection at 1 DAI, and few spores were present in cortical cells at 9 DAI. Y510 showed root hair infection at 1 DAI and cortical infection at 3 DAI to 9 DAI, with many spores in cortical cells at 9 DAI. Bar = 200 µm, 100 µm, and 50 µm.

TIR-NBS-LRR domains (Table 2). We utilized qRT-PCR to examine the expression of the hypothesized candidate gene. Among the 15 genes, only *BraA08g015220.3.5C* exhibited differential expression between the parental lines (Figure 3A). The expression of the *BraA08g015220.3.5C* gene was analyzed across various periods. The *BraA08g015220.3.5C* gene exhibited a four-fold increase in expression in the inoculated resistant line (BrT18-6-4-3) compared to the non-inoculated resistant line and both the inoculated and non-inoculated susceptible (Y510) lines at 3 DAI. Similarly, at 9 DAI, there was a two-fold increase in expression in the inoculated resistant line compared to the other lines (Figure 3B). The trend of gene expression analyzed by RT-PCR was consistent with that of qPCR (Figure 3C). Hence, the *BraA08g015220.3.5C* gene was identified as a potential candidate gene responsible for imparting resistance against clubroot disease.

3.4 Sequence variation of candidate genes between resistant and susceptible lines

PCR products of the *BraA08g015220.3.5C* gene were utilized to determine gDNA and CDS. Specific primers amplify disease-resistant (BrT18-6-4-3) and susceptible (Y510) lines. In the resistant line, the genome and CDS sequences of *BraA08g015220.3.5C* were 4295 bp and 3675 bp, respectively. Conversely, in the susceptible parent, the genome and CDS sequences were 9586 bp and 3644 bp, respectively (Supplementary Figure 2). Conserved domain analysis unveiled several domains within the *BraA08g015220.3.5C* gene, including a Toll and IL-1 domain (TIR, amino acids 70–235), a nucleotide binding site (NBS-ARC, amino acids 260–484), and an LRR (amino acids 701–908). Compared to disease-resistant and susceptible materials, we identified 249 SNPs, seven insertions, and six deletions in the susceptible line. Among these mutations, the insertion of the long terminal repeat (LTR) retrotransposon does not influence the *CRA8.1.6* function, as it does not alter the CDS sequence (Figure 4A, Supplementary Figure 2). The sequencing results revealed six non-synonymous mutations that did not influence the resistance of the wild, because these mutations were contained in both resistant and susceptible materials (Supplementary Figures 3, 4). Furthermore, sequence alignment analysis revealed that the fourth exon of the susceptible line harbored two deletions and an insertion, leading to premature termination of the C-terminus and destruction of the LRR domain (Figure 4B). This premature termination consequently led to the loss of *CRA8.1.6* function, rendering Y510 susceptible to clubroot disease.

Using the sequence variation observed in the fourth exon between the parental lines, we designed upstream and downstream primers for 2,855 bp and 3,395 bp, respectively. Functional markers, including CRA08-InDeL (Supplementary Table 4), were also developed to distinguish individuals of BrT18-6-4-3, Y510, and F_2 populations. The amplified fragment size was 541 bp in the resistant materials and 447 bp in the susceptible materials. The results

10.3389/fpls.2024.1355090

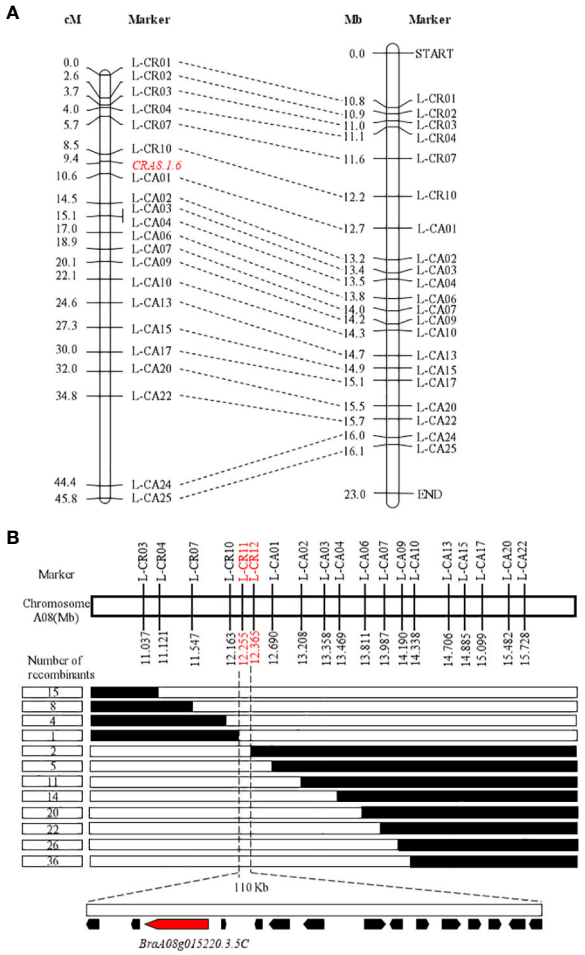

FIGURE 2
Initial and fine mapping of the *CRA8.1.6* in Chinese Turnip. **(A)** Preliminary mapping of the area *CRA8.1.6*. The left side depicts the *CRA8.1.6* genetic map, with marker distance indicated in cM. The corresponding physical map is also shown on the right, with units in megabases (Mb). **(B)** The *CRA8.1.6* gene was delineated between markers L-CR11 and L-CR12, spanning an estimated length of 110 kb. Fifteen genes were annotated on the basis of the reference genome sequence (Chiifu-401-42). Each genotype is represented, with white indicating the homozygote and black representing the heterozygote. The number of recombinants is displayed in the boxes to the left of the map.

indicated complete concordance between the phenotypes of resistant, susceptible, and heterozygous F_2 plants with their respective genotypes. This suggests that CRA08-InDel is a functional marker capable of accurately distinguishing clubroot-resistance phenotypes within segregating populations (Figure 5A). Within a natural population, the genotypes of disease-resistant materials consistently matched their phenotypes. However, the identification of susceptible materials was not sufficiently consistent. Hence, we sequenced materials that did not match this marker and identified a trait-associated SNP at 3,209 bp. Subsequently, we developed the KASP functional marker CRA08-KASP1 (Supplementary Table 4). Upon screening F_2 populations with this marker, we observed that the expected amplified products for resistant, susceptible, and heterozygous F_2 individuals perfectly matched the anticipated

TABLE 2 Annotated genes in the candidate region of *CRA8.1.6*.

Gene name	Gene position	Homolog gene	Gene function
BraA08g015200.3.5C	12,252,676–12,258,432	*AT4G21910*	MATE efflux family protein
BraA08g015210.3.5C	12,269,419–12,271,510	Unknown	Gag-polypeptide of long terminal repeat (LTR) copia-type
BraA08g015220.3.5C	12,271,230–12,287,495	*AT3G25510*	Disease-resistance protein (TIR-NBS-LRR class) family protein
BraA08g015230.3.5C	12,289,217–12,290,401	*AT4G22030*	F-box protein with a domain protein
BraA08g015240.3.5C	12,298,469–12,300,228	*AT4G22080*	Root hair–specific 14
BraA08g015250.3.5C	12,302,519–12,306,933	*AT4G22100*	Beta glucosidase 2
BraA08g015260.3.5C	12,310,890–12,314,574	*AT4G22120*	Calcium-permeable stretch-activated cation channel
BraA08g015270.3.5C	12,326,130–12,329,824	*AT4G22130*	STRUBBELIG-receptor family 8
BraA08g015280.3.5C	12,329,820–12,332,255	*AT4G22140*	Encodes a chromatin remodeling factor that regulates flowering time
BraA08g015290.3.5C	12,334,419–12,335,973	*AT4G22220*	Encodes a mitochondrial protein accepting sulfur and iron to build a transient Fe-S cluster
BraA08g015300.3.5C	12,336,747–12,338,591	*AT4G05530*	Encodes a peroxisomal member of the short-chain dehydrogenase/reductase family of enzymes
BraA08g015310.3.5C	12,344,064–12,346,459	*AT4G22360*	SWIB complex BAF60b domain-containing protein
BraA08g015320.3.5C	12,347,226–12,348,876	*AT4G12590*	ER membrane protein complex subunit-like protein
BraA08g015330.3.5C	12,356,313–12,357,823	*AT4G11580*	Methylesterase PCR A
BraA08g015340.3.5C	12,358,221–12,360,158	LOC103834248	Pectinesterase

results. This suggests that the marker CRA08-KASP1 segregated in the F_2 population with a clubroot-resistant phenotype (Figure 5B). The CRA08-KASP1 markers were also screened for 24 disease-resistant and 26 disease-susceptible materials. Among these, the phenotype and genotype of all 23 resistant materials were matched entirely, whereas the phenotype and genotype of 22 susceptible materials were matched. However, only five materials (DH40,

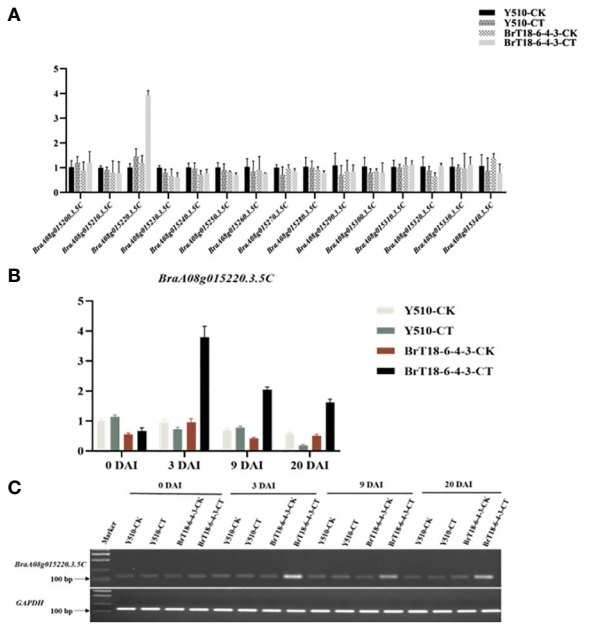

FIGURE 3
Gene expression of two parents in experimental and control groups at different periods. **(A)** qRT-PCR analysis of 15 candidate genes. **(B)** The expression of *BraA08g015220.3.5c* across different periods. **(C)** Semi-quantitative RT-PCR of *CRA8.1.6* (*BraA08g015220.3.5c*), with *GAPDH* served as the internal control.

BrT127, BrT47-1-1-1, BrT133, and BrT71-1-1-4-3) did not correspond with the genotype (Figure 5C). In our future research, we will clone the genes of these five non-matching materials identified by the CRA08-KASP1 marker to explore other variations that might cause clubroot disease.

3.5 Construction of an overexpression vector and the development of transgenic *Arabidopsis*

PCR was conducted using specific full-length primers to amplify the target gene from the subclone vector, which has a length of 4,000 bp. The correct cloning vector was digested using *Xho*I + *Eco*RI. Subsequently, the exogenous fragment was ligated into the pBWA (V) HS vector using T4 DNA ligase to obtain the recombinant plasmid (Supplementary Figure 4). The recombinant plasmid was confirmed to be correct, and the overexpression vector was successfully constructed. Overexpression *Arabidopsis* lines were identified in hygromycin-resistant medium, and homozygous lines were obtained through consecutive selfing over two generations. DNA extracted from T_1 transgenic *A. thaliana* was identified (Supplementary Figure 5). The recombinant plasmid was the positive control, whereas water was the negative control. The PCR bands observed in the eight transgenic plants were consistent with the bands of the positive control. Consequently, eight T_2 lines (CR-1, CR-2, CR-3, CR-6, CR-7, CR-8, CR-11, and CR-12) were identified as overexpressing the target gene (Figures 6A, B).

3.6 Identification of transgenic *Arabidopsis* with target gene expression

Transgenic lines CR-6, CR-7, and CR-12, along with wild-type *Arabidopsis*, were chosen for clubroot phenotypic identification. One set of 25-day-old *Arabidopsis* plants was inoculated with *P. brassicae* spores, whereas the other set was inoculated with water only as an experimental control. The experiments were performed with three biological replicates.

After 30 days of inoculation, the control wild-type and transgenic *Arabidopsis* plants displayed no disease symptoms. In the experimental group, within the overexpression line, CR-6, 22, 5,

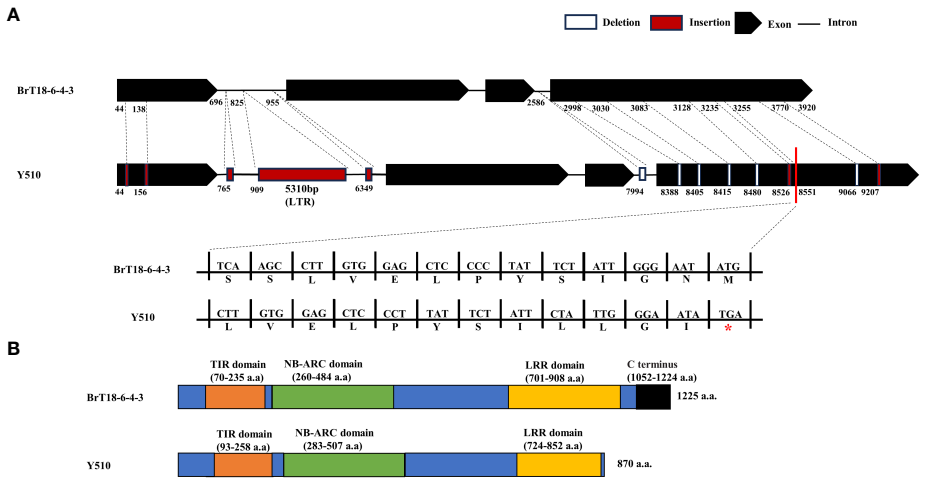

FIGURE 4
CRA8.1.6 gene structure, amino acid analysis, and protein structure prediction. **(A)** *CRA8.1.6* comprises four exons and three introns. Gene sequences in the disease-susceptible material exhibited 249 SNPs, seven insertions, and six deletions, including 5,310 bp insertions at 909 bp. INS, insertion; DEL, deletion. **(B)** A frameshift mutation caused premature termination at 870 amino acids of exon four, disrupting the LRR domain in the C-terminal region.

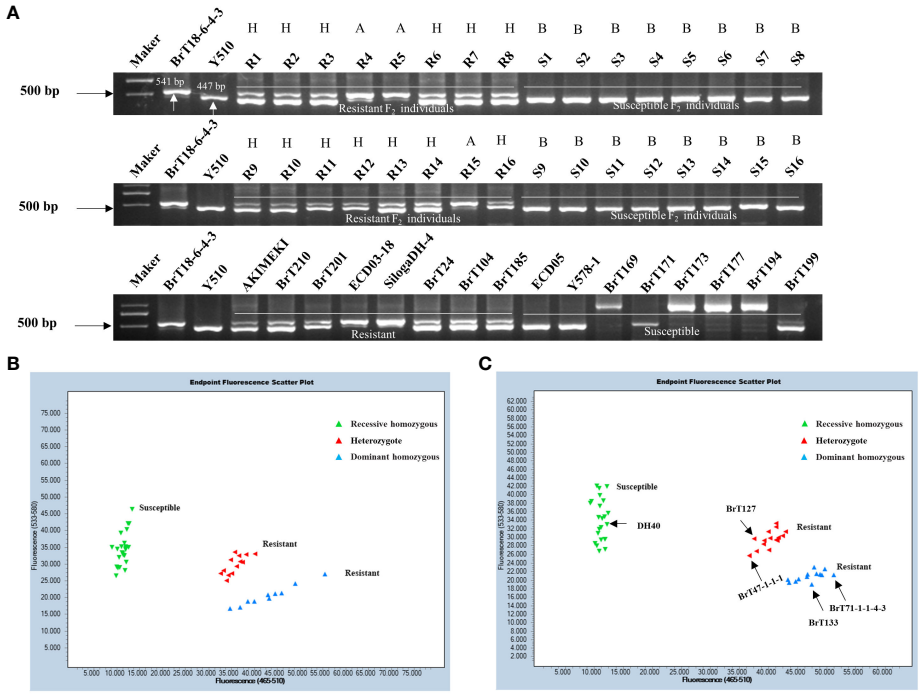

FIGURE 5
Validation of functional markers. **(A)** Validation of the CRA08-Indel marker in F_2 individuals and natural populations. **(B)** Validation of the CRA08-KASP1 marker in F_2 individuals. **(C)** Validation of the CRA08-KASP1 marker in 24 disease-resistant (AKIMEKI, ECD03-18, ECD04-1, ECD04-15, SilogaDH-4, SilogaDH-5, BrT22, BrT24, BrT25, BrT30-2-1-3, BrT81, BrT104, BrT114DH-1, BrT114DH-2, BrT114DH-3, BrT185, BrT201, BrT210, BrT238, BrT242, BrT243, WJ2-5-1, and DH40) and 26 disease-susceptible materials (ECD05, R16, BrT121, BrT127, BrT47-1-1-1, BrT130, BrT131, BrT133, BrT165, BrT169, BrT171, BrT71-1-1-4-3, BrT177, BrT193, BrT194, BrT199, BrT221, BrT222, BrT223, BrT224, BrT225, BrT226, BrT228, BrT229, BrT232, and Y578-1). Note: A, dominant homozygous; B, recessive homozygous; and H, heterozygote.

and 7 out of the 34 plants displayed disease grades 0, 1, and 3, respectively, resulting in a disease index of 10.92%. For the CR-7 line, 19, 5, and 6 out of the 30 plants exhibited disease grades 0, 1, and 3, respectively, with a disease index of 10.95%. Regarding the CR-12 overexpression line, 20, 3, and 9 out of the 32 plants showed disease grades 0, 1, and 3, respectively, yielding a disease index of 13.39% (Supplementary Table 6). In wild-type *Arabidopsis*, the frequency of disease stages in CR-6, CR-7, and CR-12 was 5 or 7, with disease rates of 85.71%, 89.01%, and 79.59%, respectively (Figure 6C).

The disease index in the overexpression transgenic *Arabidopsis* was significantly lower than that of the wild-type *Arabidopsis* in the experimental group (Figure 6D). RNA was extracted from transgenic *Arabidopsis* plants and reverse transcribed into cDNA to analyze the expression of candidate genes. Criterion 1 was used to evaluate the expression level of the candidate genes in transgenic *Arabidopsis* based on their expression levels in the control group. The relative expression of the candidate gene in the wild *A. thaliana* from the experimental and control groups was only 0.04. In contrast, gene expression levels were over 40 in transgenic lines, significantly higher than those in the control (Figure 6E).

4 Discussion

This study analyzed the clubroot resistance of the inbred line BrT18-6-4-3 and the susceptible DH line Y510. Microscopic observation and qRT-PCR verification of gene expression led us to speculate that the stages between 3 DAI and 9 DAI are crucial for cortical infection and clubroot formation in turnip. The infection cycle of *P. brassicae* typically involves primary infection of the root epidermis followed by secondary infection of cortex tissue. Root hair and cortex infections are thought to occur in host and non-host organisms. We proceeded to morphologically characterize the polymorphic developmental structures of *P. brassicae* during the primary infection in root hairs and epidermal cells, a process that concluded within 7 days of inoculation (Liu et al., 2020a). In this study, we observed that root hair infection occurred in parents at 1 DAI, and swelling of the root of the susceptible parent commenced at 9 DAI. The cortical cells of the susceptible parent harbored numerous spores, whereas those of the resistant parent contained only a few spores. We hypothesize that cortical infection is inhibited in the resistant parent, which is consistent with the study by Liu et al. (2020b).

The *CRA8.1.6* QTL was successfully mapped to a physical interval between 12.255 Mb and 12.365 Mb. Functional annotation of the genes within the QTL suggests that the *BraA08g015220.3.5C* gene is a potential candidate for clubroot resistance. Analysis of gene sequence alignment between lines BrT18-6-4-3 and Y510 revealed 249 SNPs, seven insertions, and six deletions. Among these variations, an LTR retrotransposon (5,310 bp) was identified as an insertion at 909 bp within the first intron. This LTR retrotransposon was not detected in the resistant

10.3389/fpls.2024.1355090

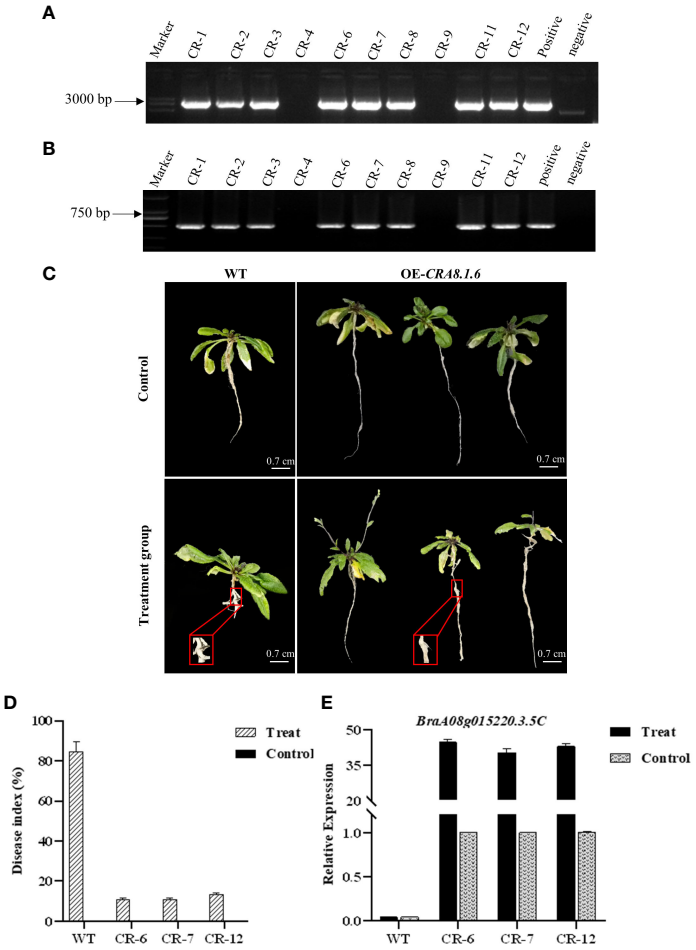

FIGURE 6
Detection map of genomic primers and hygromycin primers of T_2 transgenic *Arabidopsis* lines, phenotypic characteristics of overexpressed *Arabidopsis thaliana*, disease index investigation, and qPCR analysis. **(A)** Primer CRA8-full-F/R; **(B)** primer Hyg-F/R. CR1-12: T_1 lines; positive control: recombinant plasmid; and negative control: H_2O. **(C)** Disease incidence in wild-type roots and overexpression transgenic *Arabidopsis* following infection with *P. brassicae*. WT, wild-type *Arabidopsis*; OE-*CRA8.1.6*, overexpression *Arabidopsis*. Bar = 0.7 cm, 0.7 cm, 0.7 cm, and 0.7 cm. **(D)** Disease index comparison between wild-type and overexpression transgenic *Arabidopsis* CR-6, CR-7, and CR-12. **(E)** Analysis of candidate gene expression levels in wild-type and overexpression transgenic *Arabidopsis* CR-6, CR-7, and CR-12.

line; however, another non-functional LTR insertion was detected in our other materials. Therefore, we concluded that LTR insertion may not be responsible for susceptibility.

Additionally, amino acid sequence alignment indicated six non-synonymous SNPs in the TIR domain but had no effect on clubroot resistance. Because these six non-synonymous mutations are present in both resistant and susceptible materials of natural populations. The frameshift mutation that we identified led to early translation termination at 8,551 bp in the susceptible line Y510. This premature termination in the C-terminal LRR domain resulted in a complete loss of function, leading to the loss of clubroot resistance. Recently, the clubroot-resistant genes *Crr1a*, *CRa*, and their alleles have been cloned (Ueno et al., 2012; Hatakeyama et al., 2013, Hatakeyama et al., 2017, Hatakeyama et al., 2022). All of these genes encode nucleotide-binding LRR receptors and feature a TIR domain at the N-terminus. Wang et al. (2023) identified a broad-spectrum clubroot-resistance gene, *WeiTsing*, in *A. thaliana*, which was induced in the pericycle to hinder the colonization of *P. brassicae* in the stele. Moreover, *WeiTsing's* channel activity is essential for increasing $[Ca^{2+}]_{cyt}$ and enhancing plant defense. *WeiTsing* is situated in the endoplasmic reticulum and functions as a calcium-permeable cation-selective channel. However, no *WeiTsing* homologs have been discovered in *B. rapa* or *B. oleracea* (Ochoa et al., 2023). Consequently, current breeding efforts for clubroot resistance in *Brassica* primarily rely on NBS-LRR genes. Hatakeyama et al. (2013) discovered an LTR retrotransposon inserted into the first exon of the susceptible $Crr1a^{A9709}$ allele, with a similar result observed in Chiifu-401. However, this insertion is not prevalent in CR-resistant Chinese cabbage varieties. Two susceptible *CR* alleles lacking 172 amino acids in the C-terminal region were identified in *A. thaliana*. A chimeric *Crr1a* transgene restored resistance in susceptible *A. thaliana* (Hatakeyama et al., 2022), suggesting that susceptibility is attributed to the absence of the C-terminus.

The candidate gene of *CRA8.1.6* QTL was located in the same region as previously reported *CR* genes: $Crr1^{G004}$, $Crr1a^{Kinami90\text{-}a}$, $Crr1a^{Kiko85\text{-}a}$, and $Crr1a^{Hiroki\text{-}b}$. Gene sequencing revealed a candidate *CRA8.1.6* with a genomic length of 4,295 bp and a CDS length of 3,675 bp in the resistant line BrT18-6-4-3. In contrast, in the

susceptible line Y510, the genome sequence was 9,586 bp, with a CDS length of 3,644 bp. Sequence alignment of the CDS revealed a 99.4% similarity to *Crr1*^{G004} (Supplementary Table 5, Supplementary Figure 4). We hypothesize that *CRA8.1.6* is likely an allele of the *Crr1*^{G004} gene.

The *RPS4*, *RPP1*, and *RPP5* genes in tobacco belonging to the TIR-NB-LRR class R genes are functionally impaired by TIR domain deletion or point mutation. In this study, we aligned the TIR region of the susceptible lines Y510, Crr1a^{Kiko85_a}, and Crr1a^{Hiroki_b} with the disease-resistant lines Crr1^{G004} and Crr1a^{Kinami90_a}. Six non-synonymous SNPs were identified through amino acid sequence alignment and confirmed to be unrelated to the trait in natural populations. In the susceptible Y510 line, we observed premature translation termination at 8,551 bp and alterations in the LRR domain. The underlying cause could be the insertion and deletion of large fragments in the LRR region, resulting in structural damage to this domain. This mutation results in losing resistance in clubroot (Hatakeyama et al., 2022). We developed two variant-based functional markers, CRA08-InDel and CRA08-KASP1, compatible with genotypes and phenotypes. They showed >90% concordance with the clubroot-resistant phenotype.

5 Conclusion

The fine localization distance of *CRA8.1.6* was 110 kb. *BraA08g0152203.5C* is likely the candidate gene for *CRA8.1.6*, encoding a TIR-NBS-LRR protein. Compared to disease-resistant and susceptible materials, we identified 249 SNPs, seven insertions, and six deletions in *CRA8.1.6* (*BraA08g015220.3.5C*). We discovered premature translation termination at 8,551 bp, leading to the loss of the LRR domain at the C-terminus and ultimately resulting in the loss of clubroot resistance. Furthermore, we developed and validated two functional markers for *CRA8.1.6*. This accomplishment represents a significant advancement in molecular research on turnip clubroot resistance.

Data availability statement

The original contributions presented in the study are included in the article/Supplementary Material. Further inquiries can be directed to the corresponding authors.

Author contributions

XW: Writing – original draft, Writing – review & editing. SX: Writing – original draft, Writing – review & editing. YZ: Data curation, Writing – review & editing. LZ: Data curation, Writing – review & editing. UN: Writing – review & editing. SY: Methodology, Data curation, Writing – review & editing. HS: Project administration, Software, Supervision, Writing – review & editing. WZ: Resources, Writing – review & editing. ZW: Investigation, Writing – review & editing. BT: Formal Analysis, Writing – review & editing. FW: Investigation, Writing – review & editing. YY: Conceptualization, Supervision, Writing – review & editing. XZ: Supervision, Writing – review & editing.

Funding

The author(s) declare financial support was received for the research, authorship, and/or publication of this article. This work was supported by the National Science Foundation of China (Grant No. 31801874, 31872945), Science and Technology R & D Joint Fund of Henan Province (232301420024), Young Elite Scientists Sponsorship Program by Henan Association for Science and Technology (Grant No. 2023HYTP022) and Sci-Tech Innovation Team of Henan Academy Agricultural Sciences (2023TD06).

Conflict of interest

The authors declare that the research was conducted in the absence of any commercial or financial relationships that could be construed as a potential conflict of interest.

Publisher's note

Supplementary material

The Supplementary Material for this article can be found online at: https://www.frontiersin.org/articles/10.3389/fpls.2024.1355090/full#supplementary-material

References

Chai, A. L., X.-w., X., Shi, Y. X., and Li, B. J. (2014). Research status of clubroot (*Plasmodiophora brassicae*) on cruciferous crops in China. *Can. J. Plant Pathology*. 36, 142–153. doi: 10.1080/07060661.2013.868829

Chen, J., Jing, J., Zhan, Z., Zhang, T., Zhang, C., and Piao, Z. (2013). Identification of novel QTLs for isolate-specific partial resistance to *Plasmodiophora brassicae* in *Brassica rapa*. *PloS One* 8, e85307. doi: 10.1371/journal.pone.0085307

Chu, M., Song, T., Falk, K. C., Zhang, X., Liu, X., Chang, A., et al. (2014). Fine mapping of *Rcr1* and analyses of its effect on transcriptome patterns during infection by *Plasmodiophora brassicae*. *BMC Genomics* 15, 1166. doi: 10.1186/1471-2164-15-1166

Dixon, G. R. (2009). The occurrence and economic impact of plasmodiophora brassicae and clubroot disease. *J. Plant Growth Regulation.* 28, 194–202. doi: 10.1007/s00344-009-9090-y

Eckholm, E. (1993). Studies on breeding of clubroot resistance in cole Cruciferae crops. *Bull. Natl. Res. Inst Veg Ornam Plants Tea Jpn Ser. A* 7.

Elke, D., Martin, F., Enrico, G. A. L., Katsunori, H., and Masashi, H. (2009). Status and perspectives of clubroot resistance breeding in crucifer crops. *J. Plant Growth Regul.* 28, 265–281. doi: 10.1007/s00344-009-9100-0

Etsuo, M., Chika, Y., Michio, O., and Motohisa, T. (1998). Linkage analysis of RFLP markers for clubroot resistance and pigmentation in Chinese cabbage (*Brassica rapa ssp. pekinensis*). *Euphytica* 104, 79–86. doi: 10.1023/A:1018370418201

Gouda, A. C., Warburton, M. L., Djedatin, G. L., Kpeki, S. B., Wambugu, P. W., Gnikoua, K., et al. (2021). Development and validation of diagnostic SNP markers for quality control genotyping in a collection of four rice (Oryza) species. *Sci. Rep.* 11, 18617. doi: 10.1038/s41598-021-97689-3

Hamann, T., Benkova, E., Bäurle, I., Kientz, M., and Jürgens, G. (2002). The *Arabidopsis* BODENLOS gene encodes an auxin response protein inhibiting MONOPTEROS-mediated embryo patterning. *Genes Dev.* 16, 1610–1615. doi: 10.1101/gad.229402

Hasan, J., Megha, S., and Rahman, H. (2021). Clubroot in *Brassica*: recent advances in genomics, breeding, and disease management. *Genome.* 64, 735–760. doi: 10.1139/gen-2020-0089

Hatakeyama, K., Niwa, T., Kato, T., Ohara, T., Kakizaki, T., and Matsumoto, S. (2017). The tandem repeated organization of NB-LRR genes in the clubroot-resistant *CRb* locus in *Brassica rapa* L. *Mol. Genet. genomics: MGG.* 292, 397–405. doi: 10.1007/s00438-016-1281-1

Hatakeyama, K., Suwabe, K., Tomita, R. N., Kato, T., Nunome, T., Fukuoka, H., et al. (2013). Identification and characterization of *Crr1a*, a gene for resistance to clubroot disease (*Plasmodiophora brassicae* Woronin) in *Brassica rapa* L. *PloS One* 8, e54745. doi: 10.1371/journal.pone.0054745

Hatakeyama, K., Yuzawa, S., Tonosaki, K., Takahata, Y., and Matsumoto, S. (2022). Allelic variation of a clubroot resistance gene (*Crr1a*) in Japanese cultivars of Chinese cabbage (*Brassica rapa* L). *Breed. Science.* 72, 115–123. doi: 10.1270/jsbbs.21040

Hirai, M., Harada, T., Kubo, N., Tsukada, M., Suwabe, K., and Matsumoto, S. (2004). A novel locus for clubroot resistance in *Brassica rapa* and its linkage markers. *TAG.* 108, 639–643. doi: 10.1007/s00122-003-1475-x

Hirani, A. H., Gao, F., Liu, J., Fu, G., Wu, C., McVetty, P. B. E., et al. (2018). Combinations of independent dominant loci conferring clubroot resistance in all four Turnip Accessions (*Brassica rapa*) from the European clubroot differential set. *Front. Plant science.* 9, 1628. doi: 10.3389/fpls.2018.01628

Howard, R. J., Strelkov, S. E., and Harding, M. W. (2010). Clubroot of cruciferous crops - new perspectives on an old disease. *Can. J. Plant Pathology: Rev. Can. phytopathologie* (1), 32. doi: 10.1080/07060661003621761

Huang, Z., Peng, G., Gossen, B. D., and Yu, F. (2019). Fine mapping of a clubroot resistance gene from turnip using SNP markers identified from bulked segregant RNA-Seq. *Mol. Breeding.* 39, 131. doi: 10.1007/s11032-019-1038-8

Huang, Z., Peng, G., Liu, X., Deora, A., Falk, K. C., Gossen, B. D., et al. (2017). Fine mapping of a clubroot resistance gene in Chinese Cabbage using SNP markers identified from Bulked Segregant RNA Sequencing. *Front. Plant Sci.* 8. doi: 10.3389/fpls.2017.01448

Kageyama, K., and Asano, T. (2009). Life cycle of *Plasmodiophora brassicae*. *J. Plant Growth Regulation.* 28, 203–211. doi: 10.1007/s00344-009-9101-z

Kathiresan, N., Temanni, M. R., and Al-Ali, R. (2014). Performance improvement of BWA MEM algorithm using data-parallel with concurrent parallelization. *Int. Conf. Parallel Distributed Grid Computing.* 406–411. doi: 10.1109/PDGC.2014.7030780

Keita, S., Go, S., Tsukasa, N., Katsunori, H., Yasuhiko, M., Hiroyuki, F., et al. (2012). Microstructure of a *Brassica rapa* genome segment homoeologous to the resistance gene cluster on *Arabidopsis* chromosome 4. *Breed. Science.* 62, 170–177. doi: 10.1270/jsbbs.62.170

Kosambi, D. D. (1944). The estimation of map distance from recombination values. *Ann. Eugen.* 12, 172–175. doi: 10.1111/j.1469-1809.1943.tb02321.x

Laila, R., Park, J.-I., Robin, A. H. K., Natarajan, S., Vijayakumar, H., Shirasawa, K., et al. (2019). Mapping of a novel clubroot resistance QTL using ddRAD-seq in Chinese cabbage (*Brassica rapa* L). *BMC Plant Biol.* 19, 13. doi: 10.1186/s12870-018-1615-8

Li, S., Yang, N., and Chen, L. (2022). Paraffin section observation of flower bud differentiation of Chimonanthus praecox in Kunming and comparison of the differentiation processes in different regions, China. *Hortic. Plant J.* 8, 221–229. doi: 10.1016/j.hpj.2021.11.001

Liu, L., Qin, L., Cheng, X., Zhang, Y., and Wei, Y. (2020a). Comparing the infection biology of *Plasmodiophora brassicae* in clubroot susceptible and resistant hosts and non-hosts. *Front. Microbiol.* 11, 507036. doi: 10.3389/fmicb.2020.507036

Liu, L., Qin, L., Zhou, Z., Hendriks, W., Liu, S., and Wei, Y. (2020b). Refining the life cycle of *Plasmodiophora brassicae*. *Phytopathology.* 110, 1704–1712. doi: 10.1094/PHYTO-02-20-0029-R

Livak, K. J., and Schmittgen, T. D. (2001). Analysis of relative gene expression data using real-time quantitative PCR and the 2(-Delta Delta C(T)) Method. *Methods: A Companion to Methods Enzymology* 25 (4), 402–408. doi: 10.1006/meth.2001.1262

Luo, H., Chen, G., Liu, C., and Yun, H. (2014). An improved culture solution technique for *Plasmodiophora brassicae* infection and the dynamic infection in the root hair. *Australas. Plant Pathology.* 43, 53–60. doi: 10.1007/s13313-013-0240-0

Mariana, M.-P., Meyers, B. C., Michelmore, R. W., and Gaut, B. S. (2002). Patterns of positive selection in the complete NBS-LRR gene family of *Arabidopsis thaliana*. *Genome Res.* 12, 1305–1315. doi: 10.1101/gr.159402

Matsumoto, S., Hatakeyama, K., Takashita, S., Miyazaki, T., and Kondo, T. (2012). Clubroot and verticillium-resistant Chinese cabbage F_1 cultivar, 'Akimeki', developed by DNA marker-assisted selection. *Agriculture forestry fisheries Technol. Res. J.* 35, 1–7.

Md. Masud, K., Abdulsalam, D., Zhang, Y., Chen, Q., Peng, G., Stephen, E. S., et al. (2020). Two clubroot-resistance genes, *Rcr3* and *Rcr9*^{wa}, mapped in *Brassica rapa* using Bulk Segregant RNA Sequencing. *Int. J. Mol. Sci.* 21, 5033. doi: 10.3390/ijms21145033

Nguyen, M. L., Monakhos, G. F., Komakhin, R. A., and Monakhos, S. G. (2018). The new clubroot resistance locus is located on Chromosome A05 in Chinese Cabbage (*Brassica rapa* L). *Russian J. Genet.* 54, 296–304. doi: 10.1134/S1022795418030080

Ochoa, J. C., Mukhopadhyay, S., Bieluszewski, T., Jędryczka, M., Malinowski, R., and Truman, W. (2023). Natural variation in *Arabidopsis* responses to *Plasmodiophora brassicae* reveals an essential role for resistance to *Plasmodiophora brasssicae 1* (RPB1). *Plant journal: Cell Mol. Biol.* 6, 511079. doi: 10.1111/tpj.16438

Pang, W., Fu, P., Li, X., Zhan, Z., Yu, S., and Piao, Z. (2018). Identification and mapping of the clubroot resistance gene *CRd* in Chinese Cabbage (*Brassica rapa* ssp. *pekinensis*). *Front. Plant science.* 9, 653. doi: 10.3389/fpls.2018.00653

Pang, W., Zhang, X., Ma, Y., Wang, Y., Zhan, Z., and Piao, Z. (2022). Fine mapping and candidate gene analysis of *CRA3.7* conferring clubroot resistance in *Brassica rapa*. *TAG.* 135, 4541–4548. doi: 10.1007/s00122-022-04237-2

Piao, Z., Ramchiary, N., and Lim, Y. P. (2009). Genetics of clubroot resistance in *Brassica* species. *J. Plant Growth Regulation.* 28, 252–264. doi: 10.1007/s00344-009-9093-8

Piao, Z. Y., Deng, Y. Q., Choi, S. R., Park, Y. J., and Lim, Y. P. (2004). SCAR and CAPS mapping of *CRb*, a gene conferring resistance to *Plasmodiophora brassicae* in Chinese cabbage (Brassica rapa ssp. pekinensis). *TAG.* 108, 1458–1465. doi: 10.1007/s00122-003-1577-5

Pu, Y., Yang, D., Yin, X., Wang, Q., Chen, Q., Yang, Y., et al. (2018). Genome-wide analysis indicates diverse physiological roles of the turnip (*Brassica rapa* var. *rapa*) oligopeptide transporters gene family. *Plant Diversity.* 40, 57–67. doi: 10.1016/j.pld.2018.03.001

Sun, Z., Anfeng, M. A., Fei, C., Dandan, C., Pingping, R., and Jianwei, G. (2016). Rapid detection of *Crr3* gene against clubroot disease by PCR and selection of corresponding germplasm in Chinese Cabbage(*Brassica pekinensis* L). *Northern Horticulture*. (22), 120–123. doi: 10.11937/bfyy.201622030

Suwabe, K., Tsukazaki, H., Iketani, H., Hatakeyama, K., Kondo, M., Fujimura, M., et al. (2006). Simple sequence repeat-based comparative genomics between *Brassica rapa* and *Arabidopsis thaliana*: the genetic origin of clubroot resistance. *Genetics.* 173, 309–319. doi: 10.1534/genetics.104.038968

Tang, W. (2007). Genetic analysis of several transgenic plant progenies. *Anhui Agric. Sci.* (31), 9867–9868. doi: 10.13989/j.cnki.0517-6611.2007.31.020

Ueno, H., Matsumoto, E., Aruga, D., Kitagawa, S., Matsumura, H., and Hayashida, N. (2012). Molecular characterization of the *CRa* gene conferring clubroot resistance in *Brassica rapa*. *Plant Mol. Biol. Reporter.* 80, 621–629. doi: 10.1007/s11103-012-9971-5

Voorrips, R. E. (2002). MapChart: software for the graphical presentation of linkage maps and QTLs. *J. Hered.* 93, 77–78. doi: 10.1093/jhered/93.1.77

Wang, W., Qin, L., Zhang, W., Tang, L., Zhang, C., Dong, X., et al. (2023). WeiTsing, a pericycle-expressed ion channel, safeguards the stele to confer clubroot resistance. *Cell* 186, 2656–2671.e2618. doi: 10.1016/j.cell.2023.05.023

Wei, X., Zhang, Y., Zhao, Y., Xie, Z., Hossain, M. R., Yang, S., et al. (2021). Root transcriptome and metabolome profiling reveal key phytohormone-related genes and pathways involved clubroot resistance in *Brassica rapa* L. *Front. Plant Science.* 12, 759623. doi: 10.3389/fpls.2021.759623

Xiang, Y., Huang, X., Wang, T., Zhang, Y., Liu, Q., Hussey, P. J., et al. (2007). ACTIN BINDING PROTEIN 29 from Lilium pollen plays an important role in dynamic actin remodeling. *Plant Cell.* 19, 1930–1946. doi: 10.1105/tpc.106.048413

Yang, Z., Jiang, Y., Gong, J., Li, Q., Dun, B., Liu, D., et al. (2022). R gene triplication confers European fodder turnip with improved clubroot resistance. *Plant Biotechnol. J.* 20, 1502–1517. doi: 10.1111/pbi.13827

Yu, F., Zhang, X., Peng, G., Falk, K. C., Strelkov, S. E., and Gossen, B. D. (2017). Genotyping-by-sequencing reveals three QTL for clubroot resistance to six pathotypes of *Plasmodiophora brassicae* in *Brassica rapa*. *Sci. Rep.* 7, 4516. doi: 10.1038/s41598-017-04903-2

Yu, F., Zhang, Y., Wang, J., Chen, Q., Karim, M. M., Gossen, B. D., et al. (2022). Identification of two major QTLs in *Brassica napus* lines with introgressed clubroot resistance from Turnip Cultivar ECD01. *Front. Plant Science.* 12, 785989. doi: 10.3389/fpls.2021.785989

Yuan, Y., Qin, L., Su, H., Yang, S., Wei, X., Wang, Z., et al. (2021). Transcriptome and coexpression network analyses reveal hub genes in Chinese Cabbage (*Brassica rapa* L. ssp. *pekinensis*) during different stages of *Plasmodiophora brassicae* Infection. *Front. Plant Science.* 12, 650252. doi: 10.3389/fpls.2021.650252

Yuan, Y., Zhao, Y., Wei, X., Yao, Q., Jiang, W., Wang, Z., et al. (2017). Pathotype identification of *Plasmodiophora brassicae* woron. collected from Chinese Cabbage in Henan Province. *J. Henan Agric. Sci.* 46 (7), 71–76. doi: 10.15933/j.cnki.1004-3268

Zhang, X., Han, F., Li, Z., Wen, Z., Cheng, W., Shan, X., et al. (2024). Map-based cloning and functional analysis of a major quantitative trait locus, BolC.Pb9.1, controlling clubroot resistance in a wild Brassica relative (Brassica macrocarpa). *Theor. Appl. Genet.* 137 (2), 41. doi: 10.1007/s00122-024-04543-x

Zhu, H., Zhai, W., Li, X., and Zhu, Y. (2019). Two QTLs controlling clubroot resistance identified from Bulked Segregant Sequencing in Pakchoi (*Brassica campestris* ssp. *chinensis* Makino). *Sci. Rep.* 9, 9228. doi: 10.1038/s41598-019-44724-z

frontiers | Frontiers in Plant Science

TYPE Original Research
PUBLISHED 06 June 2024
DOI 10.3389/fpls.2024.1391173

OPEN ACCESS

EDITED BY
Xiangshu Dong,
Yunnan University, China

REVIEWED BY
Su Ryun Choi,
Seeders, Daejeon, Republic of Korea
Jie Feng,
Alberta Plant Health Lab, Alberta Agriculture and Irrigation, Canada

*CORRESPONDENCE
Wenxing Pang
pwxsyau@syau.edu.cn

†These authors have contributed equally to this work

RECEIVED 25 February 2024
ACCEPTED 20 May 2024
PUBLISHED 06 June 2024

CITATION
Meng S, Yan X, Piao Y, Li S, Wang X, Jiang J, Liang Y and Pang W (2024) Multiple transcription factors involved in the response of Chinese cabbage against *Plasmodiophora brassicae*. *Front. Plant Sci.* 15:1391173. doi: 10.3389/fpls.2024.1391173

Multiple transcription factors involved in the response of Chinese cabbage against *Plasmodiophora brassicae*

Sida Meng[1†], Xinyu Yan[1†], Yinglan Piao[2], Shizhen Li[3], Xin Wang[4], Jing Jiang[1], Yue Liang[5] and Wenxing Pang[1*]

[1]College of Horticulture, Shenyang Agricultural University, Shenyang, China, [2]State Key Laboratory of Vegetable Biobreeding, Institute of Vegetables and Flowers, Chinese Academy of Agricultural Sciences, Beijing, China, [3]State Key Laboratory of Plant Cell and Chromosome Engineering, Institute of Genetics and Developmental Biology, Chinese Academy of Sciences, Beijing, China, [4]Institute of Vegetable Research, Liaoning Academy of Agricultural Sciences, Shenyang, China, [5]College of Plant Protection, Shenyang Agricultural University, Shenyang, China

Clubroot disease, which is caused by the obligate biotrophic protist *Plasmodiophora brassicae*, leads to the formation of galls, commonly known as pathogen-induced tumors, on the roots of infected plants. The identification of crucial regulators of host tumor formation is essential to unravel the mechanisms underlying the proliferation and differentiation of *P. brassicae* within plant cells. To gain insight into this process, transcriptomic analysis was conducted to identify key genes associated with both primary and secondary infection of *P. brassicae* in Chinese cabbage. Our results demonstrate that the k-means clustering of subclass 1, which exhibited specific trends, was closely linked to the infection process of *P. brassicae*. Of the 1610 differentially expressed genes (DEGs) annotated in subclass 1, 782 were identified as transcription factors belonging to 49 transcription factor families, including bHLH, B3, NAC, MYB_related, WRKY, bZIP, C2H2, and ERF. In the primary infection, several genes, including the predicted *Brassica rapa* probable pectate lyase, RPM1-interacting protein 4-like, L-type lectin-domain-containing receptor kinase, G-type lectin S-receptor-like serine, *B. rapa* photosystem II 22 kDa protein, and MLP-like protein, showed significant upregulation. In the secondary infection stage, 45 of 50 overlapping DEGs were upregulated. These upregulated DEGs included the predicted *B. rapa* endoglucanase, long-chain acyl-CoA synthetase, WRKY transcription factor, NAC domain-containing protein, cell division control protein, auxin-induced protein, and protein variation in compound-triggered root growth response-like and xyloglucan glycosyltransferases. In both the primary and secondary infection stages, the DEGs were predicted to be *Brassica rapa* putative disease resistance proteins, L-type lectin domain-containing receptor kinases, ferredoxin-NADP reductases, 1-aminocyclopropane-1-carboxylate synthases, histone deacetylases, UDP-glycosyltransferases, putative glycerol-3-phosphate transporters, and chlorophyll a-binding proteins, which are closely associated with plant defense responses, biosynthetic processes, carbohydrate transport, and photosynthesis. This study

revealed the pivotal role of transcription factors in the initiation of infection and establishment of intracellular parasitic relationships during the primary infection stage, as well as the proliferation and differentiation of the pathogen within the host cell during the secondary infection stage.

KEYWORDS

Plasmodiophora brassicae, Chinese cabbage, clubroot, transcription factor, intracellular

Introduction

Clubroot disease, which is caused by the obligate biotrophic protist *Plasmodiophora brassicae*, affect the roots of cruciferous plants, leading to the formation of root galls that disrupt water and nutrient uptake (Voorrips et al., 2003). It is considered one of the most damaging diseases affecting crucifer crops worldwide, and can cause total yield loss under conducive conditions (Dixon, 2009a). The disease affects all cultivated Brassica species, including important vegetables and oilseed crops such as Chinese cabbage, cauliflower, cabbage, turnip, oilseed rape, and the model plant *Arabidopsis thaliana* (Dixon, 2009b).

A significant breakthrough in clubroot research was the unraveling of the pathogen life cycle and infection processes. Scientists have successfully identified the crucial stages in the development of this disease, including spore germination, primary infection, secondary infection, and gall formation. It is difficult to observe the clear time point between primary infection and secondary infection cause of the primary and secondary zoospores cannot be differentiated based on morphology (Kageyama and Asano, 2009). Feng et al. (2013a) reported that primary infections began to be noticed as early as 12 hours after inoculation (hai) with resting spores and secondary infections were observed at 72 hai. In recently, Liu et al. (2020) reported that the primary infection stage from 0 to 7 days post inoculation (DPI)and the secondary infection stage from 7 to the resting spore formation. Starch accumulation in infected hosts provides *P. brassicae* with carbon and energy during infection (Ikegami et al., 1984; Schuller et al., 2016; Ma et al., 2022). This understanding has paved the way for targeted interventions to disrupt these processes and reduce the disease severity.

Genetic studies have also played a crucial role in clubroot research, as researchers have identified and characterized multiple resistance genes in cruciferous crops that confer resistance to specific pathotypes of *P. brassicae* (Pang et al., 2020). Advancements in molecular techniques have facilitated the identification and characterization of genes involved in clubroot susceptibility and resistance (Ueno et al., 2012; Hatakeyama et al., 2013; Pang et al., 2022; Wang et al., 2023). Effective clubroot management relies heavily on the use of resistant cultivars because chemical and cultural controls have limited effectiveness against this soil-borne disease. However, the resistance conferred by major clubroot resistance (CR) genes is often quickly overcome by the prevalence of pathogenic strains of *P. brassicae* as a result of selection pressure (Kuginuki et al., 1999; Strelkov et al., 2016; Struck et al., 2022). Therefore, it is crucial to make efforts to understand the molecular mechanisms underlying clubroot pathogenesis and CR in order to develop durable clubroot resistance and improve management strategies.

Over the past decade, transcriptomic studies utilizing microarrays and RNA sequencing have generated extensive datasets that offer novel insights into the molecular basis of clubroot infection and defense responses in cruciferous hosts (Ciaghi et al., 2019; Zhou et al., 2020). Extensive transcriptomic reprogramming occurred during the secondary phase of clubroot development and coincided with gall formation. Galls develop abnormally enlarged cells with thin cell walls, large vacuoles, dense cytoplasmic bodies, and highly proliferating mitochondria and plastids (Ludwig-Müller et al., 2009; Dodueva et al., 2020). Feng et al. (2013b) reported that the differentially expressed gene expression patterns in primary and secondary zoospores investigated by dot-blot and qPCR. Microarray analysis of Arabidopsis has identified over 3,900 differentially expressed genes (>2-fold change) in infected gall tissues, whereas RNA-seq has identified over 4,500 differentially expressed transcripts (Agarwal et al., 2011; Jubault et al., 2013). The upregulated pathways in galls included JA, ET, auxin, CK, and brassinosteroid (BR) hormone signaling, which stimulate cell enlargement and division. Genes involved in cell wall modification, cytochrome P450s, transporters, and DNA replication/repair were also upregulated. Conversely, the genes associated with photosynthesis, sulfur/glucosinolate metabolism, defense responses, and cell death were strongly downregulated, indicating extensive metabolic reprogramming. Comparative analysis of Arabidopsis transcriptomes at 10, 14, 21, and 28 DPI revealed dynamic temporal changes, with the most significant alteration occurring at 21 DPI, coinciding with extensive gall formation (Agarwal et al., 2011). In late-stage infection (35 DPI), Shi et al. (2014) identified 515 *Arabidopsis* genes that were differentially expressed and shared between *B. napus* and *B. rapa*. These included genes involved in cell wall modification, hormone signaling, and secondary metabolism. Phenylpropanoid biosynthesis is exclusively induced in Brassica species, whereas photosynthetic genes are repressed solely in Arabidopsis. These analyses revealed the common induction of

certain cellular processes, such as cell wall remodeling and hormone signaling, but also indicated divergence in specific responsive genes during clubroot infection across crucifer hosts. Additionally, they demonstrated a stronger correlation between transcriptional changes during the latter stages of disease progression than during the early stages.

Comparative transcriptomics of clubroot-resistant and clubroot-susceptible genotypes have facilitated the identification of candidate resistance genes and pathways. Chu et al. (2014) observed a higher upregulation of genes associated with ET signaling, glutathione-S-transferases, and trehalose biosynthesis in resistant *B. rapa* lines than in susceptible lines at 10 DPI. Hosts of crucifers and *P. brassicae* interactions in clubroot has been reviewed in which clubroot pathogenesis and host resistance were well discussed (Feng et al., 2014). Furthermore, RNA-seq analysis of two *B. napus* lines with varying resistance revealed 618 differentially expressed genes at 21 DPI, which were related to cell organization, biotic stress response, hormone signaling, and glucosinolate biosynthesis (Zhang et al., 2016). The more resistant line exhibited increased expression of the camalexin biosynthesis genes PAD3 and CYP71A13, which corresponded to higher levels of camalexin.

These findings contribute to a better understanding of the mechanisms involved in plant defense responses and susceptibility to clubroot. Over the past ten years, research on clubroot disease has made noteworthy progress in various areas, such as pathogen biology, genetics, and management strategies (Zhang et al., 2023). These advancements have not only improved our comprehension of the disease, but have also provided valuable tools and techniques for effective disease control. However, continuous research efforts are required to advance our understanding of pathogen evolution and adaptation, thereby ensuring sustainable management options for cruciferous crop production.

Materials and methods

Plant materials and *P. brassica* inoculation

In this study, a highly susceptible Chinese cabbage inbred line '325' was used. The '325' line was inoculated with P. brassicae isolate 'SCDY-57,' identified as pathotype Pb1 according to the Sinitic clubroot differential set (Pang et al., 2020). The P. brassicae resting spore preparation and inoculation processes followed the methodology described by Pang et al. (2020). Briefly, the galls were ground in sterile distilled water using a homogenizer, and the resulting mixtures were filtered through eight layers of cheesecloth. Resting spores were collected by centrifugation at 2,500g and quantified using a hemocytometer (Neubauer improved, Marienfeld, Germany). The concentration of the resting spores was adjusted to 1×10^7/ml, and 1 ml of the suspension was inoculated into 10-day-old seedlings of each plant. Plants treated with 1 ml distilled water were used as mock controls.

Transcriptome sample preparation, total RNA isolation, and transcriptome sequencing

Tissue sampling was performed at 3, 7, 14, 21, 28, and 35 DPI with P. brassicae isolate 'SCDY-57' or distilled water according to Ma et al. (2022). Roots of 20 individual plants were sampled at each time point and used for RNA isolation. Total RNA was extracted from infected and mock control root samples using TRIzol™ reagent (Invitrogen, Carlsbad, USA). Additional RNA quality was determined using a NanoDrop spectrophotometer (Thermo Scientific, Waltham, MA, USA). Sequencing libraries were generated using the NEBNext UltraTM RNA Library Prep Kit for Illumina [New England Biolabs (NEB), Ipswich, MA, USA], following the manufacturer's recommendations, and index codes were added to attribute sequences for each sample. Sequencing was performed on an Illumina HiSeq 2500 platform (Illumina, San Diego, CA, USA) by Annoroad Gene Technology Co., Ltd. (Beijing, China).

Preprocessing and *de novo* assembly

Raw data were cleaned by removing adapter sequences, N-sequences, and low-quality reads. Reference genomes of Brassica rapa (Brapa_genome_v3.0) and P. brassicae downloaded from the Brassicaceae Database and NCBI were used in this study (Stjelja et al., 2019; Chen et al., 2022). Bowtie2 v2.2.3 was used to build the genome index, and Clean Data were aligned to the reference genome using HISAT2 v2.1.0. The read Count for each gene in each sample was determined using HTSeq v0.6.0, and fragments per kilobase million mapped reads (FPKM) were calculated to estimate the expression level of genes in each sample. DEGseq was used for differential gene expression analysis. Genes with $q \leq 0.05$ and $|\log2\_ratio| \geq 1$ are identified as differentially expressed genes (DEGs). The TBtools software (Chen et al., 2020) was used for the Venn map and heat map analysis according to the RNA-Seq data in this study.

Unigene annotation and classification

Functional and pathway enrichment of proteins encoded by the candidate genes was analyzed. Gene Ontology (GO, http://geneontology.org/) enrichment of DEGs was implemented using the hypergeometric test, in which the p-value was calculated and adjusted as a q-value, and the data background was genes in the whole genome. GO terms with $q<0.05$ were considered to be significantly enriched. GO enrichment analysis revealed the biological functions of DEGs. The KEGG enrichment of DEGs was implemented using the hypergeometric test, in which the p-value was adjusted by multiple comparisons as q-values. KEGG terms with $q<0.05$ were considered to be significantly enriched.

Quantification of gene expression levels and differential expression analysis

PrimeScript™ RT Reagent Kit (TaKaRa, Beijing, China) was used for cDNA synthesis according to the manufacturer's instructions. The Primer 3.0 online program was used to design the primers for qRT–PCR; the primer information is listed in Supplementary Table 5. The qRT–PCR was conducted in TB Green® Premix Ex Taq™ II FAST qPCR (TaKaRa, Beijing, China) with the CFX96™ Real-Time System. All experiments were performed in triplicate. The relative expression levels of the genes were determined by the $2^{-\Delta\Delta CT}$ method (Livak and Schmittgen, 2001), and the sample from each time point for distilled water treatment was used as the control.

Data analysis

Data analyses were performed using the SPSS statistical package (SPSS, Chicago, IL, USA). Analysis of variance (ANOVA) was conducted to evaluate the treatments. If a significant treatment effect was identified (P = 0.05), Duncan's Multiple Range Test was used to determine significant differences at $P < 0.05$.

Results

Transcriptome analyses

A total of 12 root samples were collected from Chinese cabbage inbred line '325' at 3, 7, 14, 21, 28, and 35 days post-treatment with P. brassicae isolate 'SCDY-57' as well as distilled water. The samples were named D3Pb, W1Pb, W2Pb, W3Pb, W4Pb, and W5Pb, and D3CK, W1CK, W2CK, W3CK, W4CK, and W5CK for 3, 7, 14, 21, 28, and 35 days after treated with P. brassicae and distilled water, respectively. Twelve libraries were constructed and analyzed, resulting in clean Q30 base-rate values ranging from 93.77%–94.31%. Overall, 516 million good-quality reads were obtained, with mapping rates to the B. rapa genome ranging from 35.61% to 90.51% (Table 1). The mapping rate greatly increased from 0.0078% to 58.37% in P. brassicae genome from 3 to 35 days after P. brassicae inoculation. In total, 30495 and 10518 genes were predicted from W5Pb for B. rapa and P. brassicae, respectively.

The sample cluster revealed that 12 samples were grouped into three distinct clusters (Figure 1). Samples D3CK and D3Pb formed a separate cluster that was distinct from that of the other samples. Furthermore, the remaining 10 samples were divided into two groups, with W1Pb, W2Pb, W3Pb, W4Pb, and W5Pb representing the samples treated with P. brassicae, and W1CK, W2CK, W3CK, W4CK, and W5CK representing the samples treated with distilled water.

Differently expressed genes (DEGs)

A total of 9025, 10997, 9620, 8999, 10658, and 10333 DEGs were identified in response to P. brassicae inoculation compared to distilled water at 3, 7, 14, 21, 28, and 35 days post-treatment (Figure 2). The downregulated genes were upregulated more in all P. brassicae treatments than in distilled water, except at 3 and 28 d after treatment.

K-means clustering analysis of the DEGs revealed that these genes were related to processes associated with the infection of P. brassicae (Figure 3). The results showed that the k-means clustering of sub-classes 1 and 3 with certain trends were associated with the infection of P. brassicae. However, sub-class 1 had a much closer

TABLE 1 The clean reads mapping rate and annotated gene number of the RNA-Seq data were compared to the reference genome of *Brassica rapa* and *Plasmodiophora brassicae*.

NO.	Sample name	Total clean reads	*Brassica rapa*		*Plasmodiophora brassicae*	
			Mapping rate[A]	Total gene number	Mapping rate[B]	Total gene number
1	D3CK	40,145,846	0.8936	31001	–	–
2	D3Pb	44,413,690	0.9004	32156	7.77E-05	180
3	W1CK	45,020,494	0.9051	32164	–	–
4	W1Pb	40,464,846	0.9031	31981	0.0004	2238
5	W2CK	40,308,672	0.8781	31730	–	–
6	W2Pb	42,711,550	0.8900	32198	0.0197	8071
7	W3CK	44,778,000	0.8986	32277	–	–
8	W3Pb	43,520,202	0.7752	31959	0.1387	9280
9	W4CK	44,358,100	0.8723	31202	–	–
10	W4Pb	43,316,456	0.5481	31127	0.3601	10416
11	W5CK	41,024,024	0.8988	31511	–	–
12	W5Pb	45,517,750	0.3561	30495	0.5837	10518

D3Pb, W1Pb, W2Pb, W3Pb, W4Pb, W5Pb, and D3CK, W1CK, W2CK, W3CK, W4CK, and W5CK indicate *P. brassicae* and distilled water treatments at 3, 7, 14, 21, 28, and 35 days, respectively.
[A]Mapping rate indicated the total clean reads map to the *Brassica rapa* (Brapa_genome_v3.0) genome; [B]Mapping rate indicated the total clean reads map to the Plasmodiophora brassicae genome.
-, indicated that no data generated.

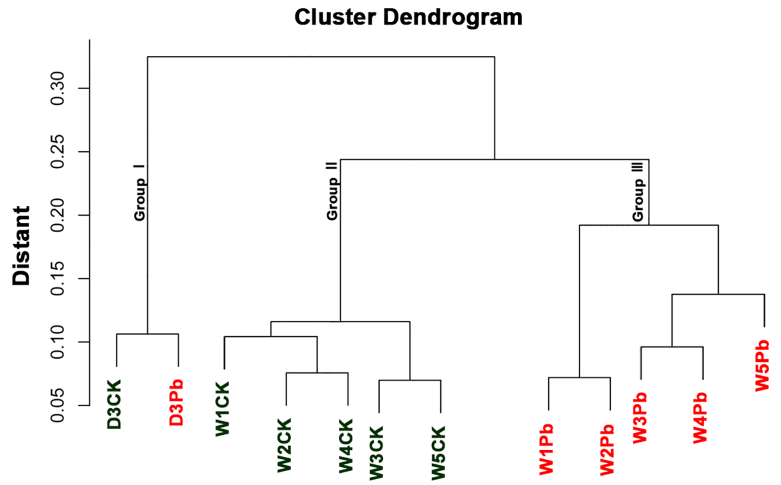

FIGURE 1
Cluster dendrogram and grouping information of 12 samples.

relationship with the process of P. brassicae infection than sub-class 3. Of the 1610 DEGs annotated in subclass 1, 782 were characterized as transcription factors. These 782 genes belonged to 49 transcription factor families, including basic helix-loop-helix (bHLH), B3, NAC (no apical meristem (NAC), MYB_related, WRKY, bZIP (basic region/leucine zipper motif (bZIP), C2H2, and ERF(Ethylene response factors) etc. (Figure 4). Most genes were annotated to the transcription factor family bHLH, and 79 genes were detected.

Functional annotation of sub class 1

To explore the functional genes involved in P. brassicae infection, DEGs in subclass 1 were chosen for further analysis. Figure 5 shows the Venn map of the DEGs obtained from subclass 1. There were 29 overlapping genes at all-time points. Moreover, 17 and 50 genes overlapped at the primary (3 and 7 DAI, respectively) and secondary (14, 21, 28, and 35 DAI) infection stages (Figure 5).

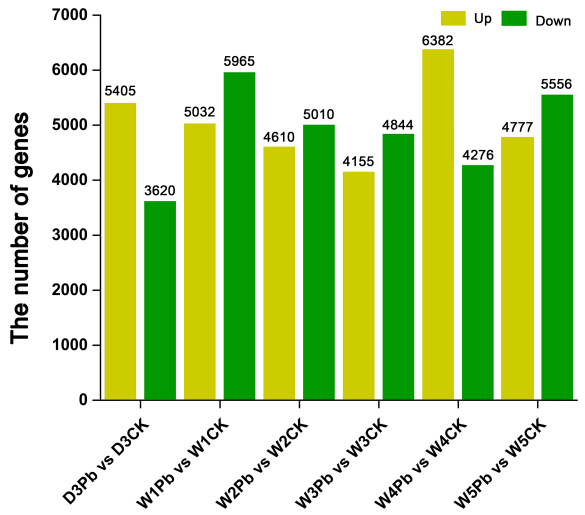

FIGURE 2
Numbers of differentially expressed genes (DEGs) obtained from *P. brassicae* inoculation compared to distilled water at 3, 7, 14, 21, 28, and 35 days after treatment.

In both the primary and secondary infection stages, the 29 overlapping DEGs were predicted to be Brassica rapa putative disease resistance proteins, L-type lectin-domain-containing receptor kinases, ferredoxin–NADP reductases, 1-aminocyclopropane-1-carboxylate synthases, histone deacetylases, UDP-glycosyltransferases, putative glycerol-3-phosphate transporters, and chlorophyll a-b binding proteins, which are closely related to plant defense responses, biosynthetic processes, carbohydrate transport, and photosynthesis (Figure 6A; Supplementary Table 1).

The predicted Brassica rapa probable pectate lyase, RPM1-interacting protein 4-like, L-type lectin-domain-containing receptor kinase, Brassica napus G-type lectin S-receptor-like serine, Brassica rapa photosystem II 22 kDa protein and MLP-like protein were all upregulated during primary infection (Figure 6B; Supplementary Table 2). Meanwhile, the predicted Brassica rapa cation/H(+) antiporter and Brassica napus uncharacterized LOC106429977 were downregulated during primary infection (Figure 6B; Supplementary Table 2).

In the secondary infection stage, 45 out of 50 overlapping DEGs were upregulated, including predicted as Brassica rapa endoglucanase, long-chain acyl-CoA synthetase, probable WRKY transcription factor, NAC domain-containing protein, cell division control protein, auxin-induced protein, protein variation in compound triggered root growth response-like, and Brassica napus xyloglucan glycosyltransferase (Figure 6C; Supplementary Table 3). Only 5 DEGs BraA02g029820.3C, BraA07g021130.3C, BraA09g063110.3C, BraA04g025820.3C and BraAnng005450.3C, identified as Brassica rapa kinesin-like protein NACK1, cell division control protein, and uncharacterized, were downregulated at certain time points (Figure 6C; Supplementary Table 3).

KEGG analysis of identified DEGs

Kyoto Encyclopedia of Genes and Genomes (KEGG) pathway enrichment analysis, 131, 131, 132, 131, 132, and 133 KEGG

10.3389/fpls.2024.1391173

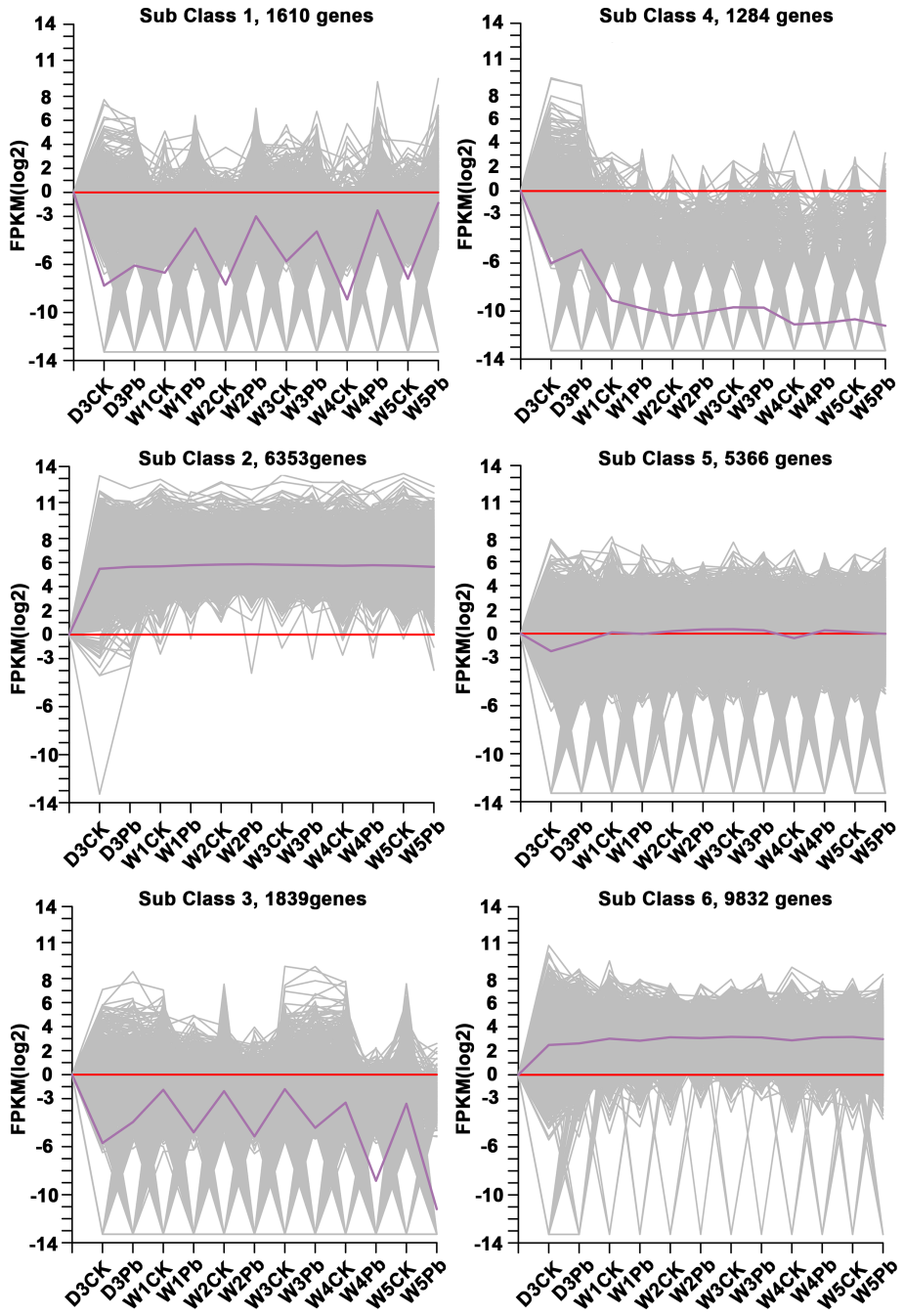

FIGURE 3
Clusters obtained by k-means cluster analysis.

pathways were associated with the infection of P. brassicae at 3, 7, 14, 21, 28, and 35 days after treatment. The top 10 enriched pathways are shown in Figure 7; Supplementary Table 4. KEGG analysis revealed significant enrichment in plant hormone signal transduction, plant-pathogen interactions, starch and sucrose metabolism, MAPK signaling, cysteine and methionine metabolism, carbon metabolism, and phenylpropanoid biosynthesis pathways, all of which are related to the infection process of P. brassicae.

Verification of DEGs involved in different *P. brassicae* infection stages

Differentially expressed transcription factors were selected from primary, secondary, and primary and secondary infection stages. Three genes were selected at each stage for quantitative real-time PCR analysis. The primers used for qRT-PCR are listed in Supplementary Table 5. The qRT-PCR results showed the same expression pattern as the RNA-Seq data (Figure 8). During the

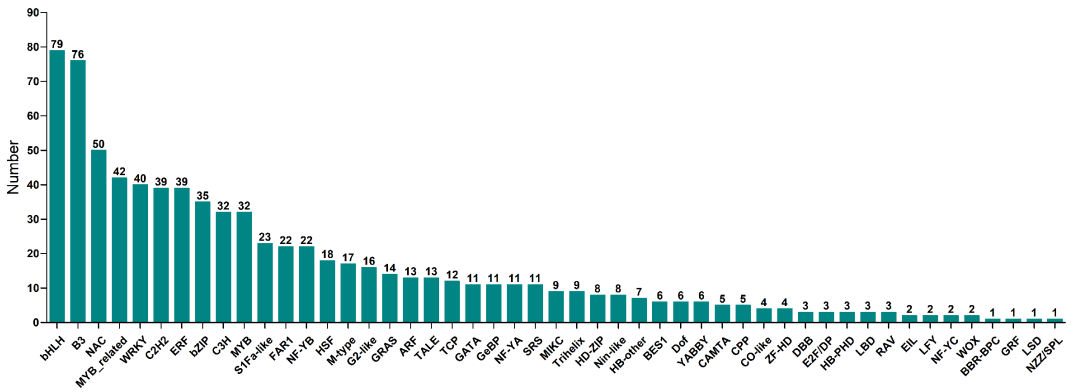

FIGURE 4
Transcription factors number of 49 transcription factor family annotated in sub class 1.

primary infection stage, *BraA01g012740.3C* (*Brassica rapa* probable pectate lyase 16) and *BraA03g053610.3C* (*Brassica napus* G-type lectin S-receptor-like serine/threonine-protein kinase) were significantly upregulated at 3 and 7 DPI. However, *BraA03g010470.3C* (*Brassica rapa* cation/H(+) antiporter 9-like) was significantly downregulated at 3 and 7 DPI (Figure 8A). During the secondary infection stage, the WRKY transcription factor BraA02g028550.3C (*Brassica rapa* long-chain acyl-CoA synthetase 5-like) and *BraA02g042810.3C* (Brassica rapa histone deacetylase 5-like) were significantly upregulated (Figure 8B). Both *BraA01g012860.3C* (*Brassica rapa* putative cysteine-rich receptor-like protein kinase) and *BraA02g008010.3C* (*Brassica rapa* putative disease resistance protein) were downregulated at 3DPI and then, upregulated, 7,14,21,28 and 35 DPI (Figure 8C).

Discussion

Infection with P. brassicae leads to increased cell division in both the cambium and the phloem parenchyma of Arabidopsis (Kobelt et al., 2000). Tumors in higher plants are abnormal tissue outgrowths resulting from the uncontrolled proliferation of a group of cells (Dodueva et al., 2020). Therefore, clubs that form on the roots of infected plants caused by the obligate biotrophic protist P. brassicae also called tumors, were described by Dodueva et al. (2020) in a review. Clubroot causes considerable economic damage owing to reduced crop yields in cultivated cruciferous crops. The prevention and management of clubroots has become a global challenge. Transcriptomic and genomic studies of the interactions between P. brassicae and cruciferous plants have provided valuable insights into the molecular mechanisms underlying these interactions (Zhao et al., 2017; Irani et al., 2018; Li et al., 2023). Studies have identified differentially expressed genes and signaling pathways associated with the response of cruciferous plants to P. brassicae infection (Grsic-Rausch et al., 2000; Devos et al., 2005; Ma et al., 2022).

The cell wall provides the first line of defense in plants and plays an important role in disease resistance (Wan et al., 2021). Microorganisms have evolved various strategies to break down cell walls. Pectin is a major component of primary cell walls and plays an important role in cell wall formation in higher plants. During the primary infection, the predicted *B. rapa* probable pectate lyase gene *BraA01g012740.3C* was upregulated by infection with *P. brassicae* (Figure 6B). *BraA01g012740.3C*

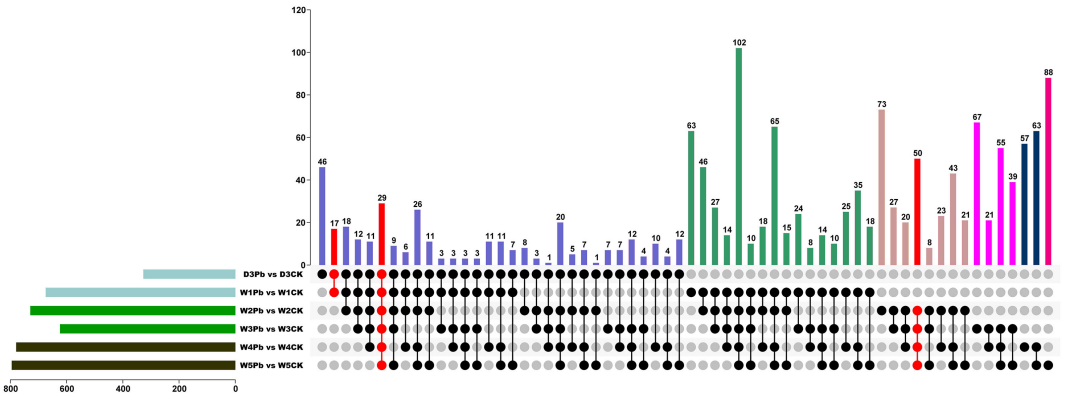

FIGURE 5
Venn diagram of differentially expressed genes (DEGs) from *P. brassicae* inoculation compared to distilled water at 3, 7, 14, 21, 28, and 35 days after treatment.

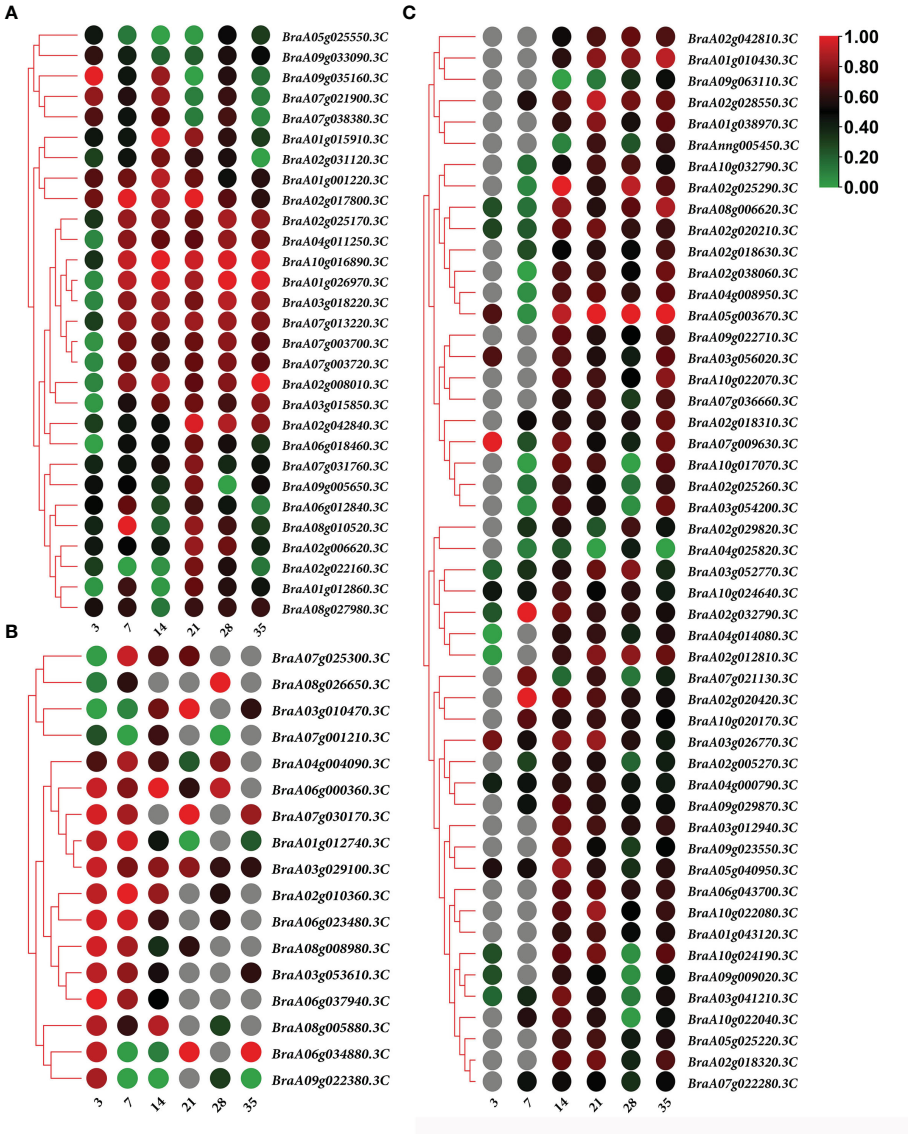

FIGURE 6
Heatmap of gene expression. **(A)** 29 overlapping differentially expressed genes (DEGs) expression heatmap in both of the primary and secondary infection stages. **(B)** 17 overlapping DEGs expression heatmap in primary infection stage. **(C)** 50 overlapping DEGs expression heatmap in the secondary infection stage. Notes: Numbers 3, 7, 14, 21, 28, and 35 indicate the different stages at 3, 7, 14, 21, 28, and 35 days after treatment, respectively.

encodes an HD-ZIP family protein that activates Poly(1,4-alpha-D-galacturonate)(n) via the unsaturated D-galacturonate pathway. A series of pectin enzymes are secreted by microorganisms to directly break down de-esterified HG, and infection attempts have been reported (Lionetti et al., 2012). Moreover, Pst DC3000 hijacks the host signaling pathway, which induces cell wall remodeling during plant development in *Arabidopsis* (Wang et al., 2017). IDL6 is upregulated upon infection with Pst DC3000, which then activates the HAE/HSL2 pathway, thereby promoting pectin degradation. These results indicated that Pst DC3000 can enhance infection by hijacking the IDL6-HAE/HSL2-ADPG2 signaling pathway (Wang et al., 2017). RPM1-interacting protein 4 (RIN4) is a conserved plant immunity regulator that can be modified by pathogenic effector proteins that plays an important role in both PAMP-triggered (PTI) and effector-triggered immunity (ETI) (Zhao et al., 2021). Kim et al. (2005) showed that RIN4 is a negative regulator of regulator of PAMP signaling, as the overexpression of RIN4 results in reduced defense responses. *BraA02g010360.3C*, predicted to be *B. rapa* RPM1-interacting protein 4-like, was highly upregulated by infection with *P. brassicae* during primary infection (Figure 6B). Moreover, L-type lectin domain-containing receptor kinase (*BraA03g029100.3C*, S1Fa-like), *B. napus* G-type lectin S-receptor-like serine (*BraA03g053610.3C*,TALE), and *B. rapa* photosystem II 22 kDa protein (*BraA08g005880.3C*) were upregulated at the primary infection stage. L-type lectin receptor kinases (LecRKs) recognize a variety of invasion patterns because of their large diversity. LecRKs are key players in plant immunity; however, their functions in plant defense are not well understood

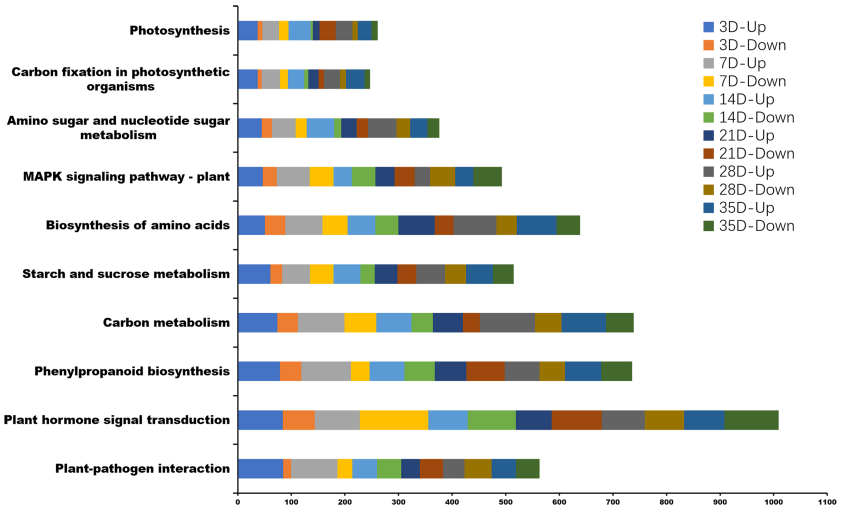

FIGURE 7
The top 10 Kyoto Encyclopedia of Genes and Genomes (KEGG) pathway enrichment analysis between *P. brassicae* inoculation compared to distilled water at 3, 7, 14, 21, 28, and 35 days after treatment.

(Wang and Bouwmeester, 2017). The G-type lectin S-receptor-like serine/threonine protein kinase has been identified as a positive regulator of salt stress (Sun et al., 2013). Major latex-like proteins (MLP) confer resistance to pathogens by inducing pathogenesis-related protein genes. The MLP-like protein (*BraA08g026650.3C*) was downregulated at 3 DPI in *P. brassicae*. All of these DEGs were closely related to pathogen invasion induced by the infection of *P. brassicae*, offering insights for future investigations.

P. brassicae can manipulate Brassicaceae hosts by hijacking plant carbohydrate metabolism pathways to generate a strong physiological sink, such as accumulating abundant starch grains in infected roots (Malinowski et al., 2012; Ma et al., 2022). Our study showed that

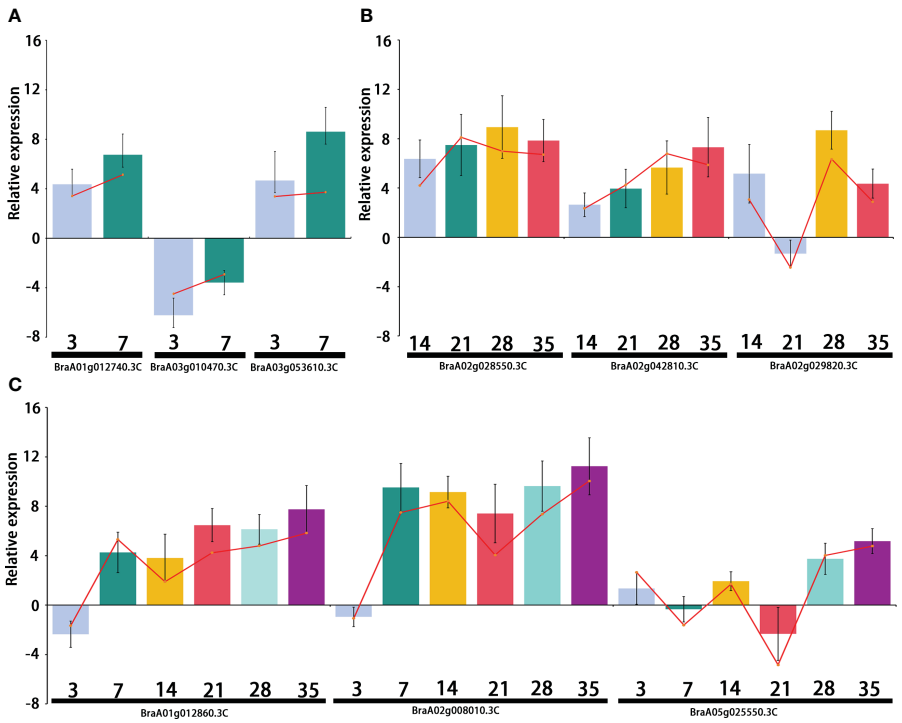

FIGURE 8
Relative expression of the differentially expressed genes (DEGs) selected from the primary infection, secondary infection, and primary and secondary infection stages, respectively. **(A)** Relative expression of DEGs from the primary infection stage; **(B)** Relative expression of DEGs from the secondary infection stage; **(C)** Relative expression of DEGs from the primary and secondary infection stages. Bar chat graph represents the gene expression by comparing *P. brassicae* inoculation to distilled water treatment from qRT-PCR at different stages, and the red line represents the gene expression from RNA-seq.

putative glycerol-3-phosphate transporter (*BraA08g010520.3C*), *B. rapa* endoglucanase 9-like (*BraA02g020420.3C*, WRKY), and long-chain acyl-CoA synthetase *(BraA02g028550.3C*, WRKY) were upregulated during *P. brassicae* secondary infection stage. A recent study reported that glucose transporters and glucose content significantly increase during the late stages of root infection (Kong et al., 2022). Moreover, previous studies have shown that the upregulation of the MEX1 maltose transporter and starch synthesis pathway (BrAGPS2 and BrISA2b) is activated by the growing *P. brassicae* plasmodia to mediate the energy supply from the host to the pathogen (Badstöber et al., 2020; Ma et al., 2022).

In the present study, transcription factors related to carbohydrate synthesis and transportation were found to play important roles in the invasion and proliferation of *P. brassicae.* Transcription factors such as *BraA02g018320.3C*, *BraA03g056020.3C*, *BraA07g022280.3C*, *BraA10g022040.3C*, *BraA10g022070.3C*, *BraA10g022080.3C*, *BraA10g024190.3C* and *BraA10g024640.3C* all belong to the bHLH family. These genes annotated as *B. rapa* protein variation in compound-triggered root growth response-like, *B. rapa* lectin domain-containing receptor kinase VI.3-like, *B. rapa* auxin-induced protein 15A-like, *B. rapa* transcription factor PRE2, *B. rapa* cytochrome P450 were upregulated during the secondary infection stage. Lectins serve as sugar code readers and reversibly bind to specific carbohydrates (Naithani et al., 2021). Evidence has shown that L-type lectin receptor kinase is involved in the resistance response to *the pathogenic oomycetes P. infestans and P. capsici and fungus A. brassicicola (*Wang et al., 2014). Auxins are also involved in invasion and gall formation during *P. brassicae* infection (Malinowski et al., 2016), and the auxin-induced protein-encoding gene 15A-like (*BraA10g022040.3C*, *BraA10g022070.3C*, *BraA10g022080.3C*) was upregulated, strengthening the result that auxin and cytokines play a key role during gall formation (Devos et al., 2006). The cytochrome P450 (CYP) superfamily catalyzes a wide range of reactions and plays important roles in several fundamental biological processes, such as steroid synthesis, fatty acid metabolism, and chemical defense (Pankov et al., 2021). A total of 258 non-redundant P450 genes have been identified, and P450 genes may play essential roles in pathogen-triggered immunity (PTI) in Chinese cabbage (Zhang et al., 2021).

In the context of *Plasmodiophora brassicae* infection, transcription factor families including bHLH, B3, NAC, MYB_related, WRKY, bZIP, C2H2, and ERF regulate the expression of genes related to defense responses, cell wall modifications, hormone signaling, and other processes involved in the plant's defense mechanisms against the pathogen. Their coordination is essential for orchestrating an effective response to the infection and is likely crucial for the plant's ability to combat the pathogen. Overall, transcript and genomic studies have provided valuable insights into the molecular mechanisms underlying interactions between P. brassicae and cruciferous plants. Understanding these molecular mechanisms can help to develop strategies for the management and control of clubroot diseases. In summary, this interaction involves complex changes in gene expression in both organisms, with the pathogen actively modulating plant defense and development through the secretion of effector proteins. Further research on the transcription factors related to carbohydrate metabolism pathways will provide more evidence for P. brassicae host manipulation in cruciferous crops.

Data availability statement

The datasets generated and analyzed during this study are available on reasonable requests from the corresponding authors. The RNA-Seq data of this study has been deposited at NCBI under the BioProject ID PRJNA1060352.

Author contributions

SM: Data curation, Formal Analysis, Writing – original draft. XY: Data curation, Formal Analysis, Writing – original draft. YP: Data curation, Writing – review & editing. SL: Data curation, Writing – review & editing. XW: Data curation, Writing – review & editing. JJ: Data curation, Writing – review & editing. YL: Data curation, Writing – review & editing. WP: Data curation, Funding acquisition, Project administration, Resources, Writing – review & editing.

Funding

The author(s) declare financial support was received for the research, authorship, and/or publication of this article. This study was supported by grants from the National Natural Science Foundation of China (Project No. 32272720); the Liaoning Natural Science Foundation (2021-MS-229); the Fundamental Research Program for Liaoning Higher Education Institution (LJKMZ20221046) and the Shenyang Science and Technology Project (23–410-2–10).

Conflict of interest

The authors declare that the research was conducted in the absence of any commercial or financial relationships that could be construed as a potential conflict of interest.

Publisher's note

Supplementary material

The Supplementary Material for this article can be found online at: https://www.frontiersin.org/articles/10.3389/fpls.2024.1391173/full#supplementary-material

References

Agarwal, A., Kaul, V., Faggian, R., Rookes, J. E., Ludwig-Müller, J., and Cahill, D. M. (2011). Analysis of global host gene expression during the primary phase of the *Arabidopsis thaliana-Plasmodiophora brassicae* interaction. *Funct. Plant Biol.* 38, 462–475. doi: 10.1071/FP11026

Badstöber, J., Gachon, C. M.M., Ludwig-Müller, J., Sandbichler, A. M., and Neuhauser, S. (2020). Demystifying biotrophs: FISHing for mRNAs to decipher plant and algal pathogen–host interaction at the single cell level. *Scientific Reports* 10.

Chen, C., Chen, H., Zhang, Y., Thomas, H. R., Frank, M. H., He, Y., et al. (2020). TBtools: an integrative toolkit developed for interactive analyses of big biological data. *Mol. Plant* 13, 1194–1202. doi: 10.1016/j.molp.2020.06.009

Chen, H., Wang, T., He, X., Cai, X., Lin, R., Liang, J., et al. (2022). Brad v3.0: an upgraded brassicaceae database. *Nucleic Acids Res.* 50 (D1), D1432–D1441. doi: 10.1093/nar/gkab1057

Chu, M., Song, T., Falk, K. C., Zhang, X., and Liu, X. (2014). Fine mapping of *Rcr1* and analyses of its effect on transcriptome patterns during infection by *Plasmodiophora brassicae*. *BMC Genomics* 15, 1166. doi: 10.1186/1471-2164-15-1166

Ciaghi, S., Schwelm, A., and Neuhauser, S. (2019). Transcriptomic response in symptomless roots of clubroot infected kohlrabi (*Brassica oleracea* var. *gongylodes*) mirrors resistant plants. *BMC Plant Biol.* 19. doi: 10.1186/s12870-019-1902-z

Devos, S., Laukens, K., Deckers, P., Van Der Straeten, D., Beeckman, T., Inzé, D., et al. (2006). A hormone and proteome approach to picturing the initial metabolic events during. *Mol. Plant Microbe Interact.* 19, 1431–1443. doi: 10.1094/MPMI-19-1431

Devos, S., Vissenberg, K., Verbelen, J.-P., and Prinsen, E. (2005). Infection of Chinese cabbage by *Plasmodiophora brassicae* leads to a stimulation of plant growth: impacts on cell wall metabolism and hormone balance. *New Phytol.* 166, 241–250. doi: 10.1111/j.1469-8137.2004.01304.x

Dixon, G. R. (2009a). *Plasmodiophora brassicae* (Clubroot): A plant pathogen that alters host growth and productivity. *J. Plant Growth Regul.* 28, 193. doi: 10.1007/s00344-009-9087-6

Dixon, G. R. (2009b). The occurrence and economic impact of *Plasmodiophora brassicae* and clubroot disease. *J. Plant Growth Regul.* 28, 194–202. doi: 10.1007/s00344-009-9090-y

Dodueva, I. E., Lebedeva, M. A., Kuznetsova, K. A., Gancheva, M. S., Paponova, S. S, and Lutova, L. L. (2020). Plant tumors: a hundred years of study. *Planta* 251, 82. doi: 10.1007/s00425-020-03375-5

Feng, J., Cao, T., Rennie, D. C., Strelkov, S. E., and Hwang, S. F. (2014). Host-parasite interactions in clubroot of crucifers, Canadian. *J. Plant Pathol.* 36:sup1, 113–121. doi: 10.1080/07060661.2013.860192

Feng, J., Hwang, S. F., and Strelkov, S. E. (2013a). Studies into primary and secondary infection processes by Plasmodiophora brassicae on canola. *Plant Pathol.* 62, 177–183. doi: 10.1111/j.1365-3059.2012.02612.x

Feng, J., Hwang, S. F., and Strelkov, S. E. (2013b). Assessment of gene expression profiles in primary and secondary zoospores of Plasmodiophora brassicae by dot blot and real-time PCR. *Microbiol. Res.* 168, 518–524. doi: 10.1016/j.micres.2013.02.011

Grsic-Rausch, S., Kobelt, P., Siemens, J. M., Bischof, M., and Ludwig-Müller, J. (2000). Expression and localization of nitrilase during symptom development of the clubroot disease in Arabidopsis. *Plant Physiol.* 122, 369–378. doi: 10.1104/pp.122.2.369

Hatakeyama, K., Suwabe, K., Tomita, R. N., Kato, T., Nunome, T., Fukuoka, H., et al. (2013). Identification and characterization of *Crr1a*, a gene for resistance to clubroot disease (*Plasmodiophora brassicae* Woronin) in *Brassica rapa* L. *PloS One* 8, e54745. doi: 10.1371/journal.pone.0054745

Ikegami, H., Watanabe, Y., Ito, T., and Imuro, Y. (1984). Ultrastructures of starch grains in Chinese cabbage and turnip root cells infected with *Plasmodiophora brassicae* (Studies on the Clubroot of Cruciferous Plants 6). *Res. Bull. Fac. Agr. Gifu. Univ.* 49, 37–48.

Irani, S., Trost, B., Waldner, M., Nayidu, N., Tu, J., Kusalik, A. J., et al. (2018). Transcriptome analysis of response to *Plasmodiophora brassicae* infection in the Arabidopsis shoot and root. *BMC Genomics* 19, 23. doi: 10.1186/s12864-017-4426-7

Jubault, M., Hamon, C., Gravot, A., Lariagon, C., Delourme, R., Bouchereau, A., et al. (2013). Differential regulation of root arginine catabolism and polyamine metabolism in clubroot-susceptible and partially resistant Arabidopsis genotypes. *Plant Physiol. Biochem.* 70, 195–203. doi: 10.1104/pp.108.117432

Kageyama, K., and Asano, T. (2009). Life cycle of *Plasmodiophora brassicae*. *J. Plant Growth Regul.* 28, 203–211. doi: 10.1007/s00344-009-9101-z

Kim, M. G., da Cunha, L., McFall, A. J., Belkhadir, Y., DebRoy, S., Dangl, J. L., et al. (2005). Two *Pseudomonas syringae* type III effectors inhibit RIN4-regulated basal defense in Arabidopsis. *Cell* 121, 749–759. doi: 10.1016/j.cell.2005.03.025

Kobelt, P., Siemens, J., and Sacristan, M. D. (2000). Histological characterization of the incompatible interaction between Arabidopsis thaliana and the obligate biotrophic pathogen Plasmodiophora brassicae. *Mycol. Res.* 2, 220–225. doi: 10.1017/S0953756299001781

Kong, L., Li, X., Zhan, Z., and Piao, Z. (2022). Sugar transporters in *Plasmodiophora brassicae*: genome-wide identification and functional verification. *Int. J. Mol. Sci.* 23, 5264. doi: 10.3390/ijms23095264

Kuginuki, Y., Yoshigawa, H., and Hirai, M. (1999). Variation in virulence of *Plasmodiophora brassicae* in Japan tested with clubroot resistant cultivars of Chinese cabbage. *Eur. J. Plant Pathol.* 105, 327–332. doi: 10.1023/A:1008705413127

Li, P., Lv, S., Zhang, Z., Su, T., Wang, W., Xin, X., et al. (2023). Genome assembly of the plant pathogen *Plasmodiophora brassicae* reveals novel secreted proteins contributing to the infection of *Brassica rapa*. *Hortic. Plant J.* doi: 10.1016/j.hpj.2023.09.001

Lionetti, V., Cervone, F., and Bellincampi, D. (2012). Methyl esterification of pectin plays a role during plant-pathogen interactions and affects plant resistance to diseases. *J. Plant Physiol.* 169, 1623–1630. doi: 10.1016/j.jplph.2012.05.006

Liu, L., Qin, L., Zhou, Z., Hendriks, W. G. H. M., Liu, S., and Wei, Y. (2020). Refining the life cycle of Plasmodiophora brassicae. *Phytopathology* 110, 1704–1712. doi: 10.1094/PHYTO-02-20-0029-R

Livak, K. J., and Schmittgen, T. D. (2001). Analysis of relative gene expression data using real-time quantitative PCR and the 2(-Delta Delta C(T)) Method. *Methods* 25, 402–408. doi: 10.1006/meth.2001.1262

Ludwig-Müller, J., Prinsen, E., Rolfe, S. A., and Scholes, J. D. (2009). Metabolism and plant hormone action during clubroot disease. *J. Plant Growth Regul.* 28, 229–244. doi: 10.1007/s00344-009-9089-4

Ma, Y., Choi, S. R., Wang, Y., Chhapekar, S. S., Zhang, X., Wang, Y., et al. (2022). Starch content changes and metabolism related gene regulation of Chinese cabbage synergistically induced by *plasmodiophora brassicae* infection. *Hortic. Res.* 9. doi: 10.1093/hr/uhab071

Malinowski, R., Novák, O., Borhan, M. H., Spíchal, L., Strnad, M., and Rolfe, S. A. (2016). The role of cytokinins in clubroot disease. *Eur. J. Plant Pathol.* 145, 543–557. doi: 10.1007/s10658-015-0845-y

Malinowski, R., Smith, J. A., Fleming, A. J., Scholes, J. D., and Rolfe, S. A. (2012). Gall formation in clubroot-infected Arabidopsis results from an increase in existing meristematic activities of the host but is not essential for the completion of the pathogen life cycle. *Plant J.* 71, 226–238. doi: 10.1111/j.1365-313X.2012.04983.x

Naithani, S., Komath, S. S., Nonomura, A., and Govindjee, G. (2021). Plant lectins and their many roles: Carbohydrate-binding and beyond. *J. Plant Physiol.* 266, Article 153531. doi: 10.1016/j.jplph.2021.153531

Pang, W., Liang, Y., Zhan, Z., Li, X., and Piao, Z. (2020). Development of a sinitic clubroot diferential set for the pathotype classifcation of *Plasmodiophora brassicae*. *Front. Plant Sci.* 11, 568771. doi: 10.3389/fpls.2020.568771

Pang, W., Zhang, X., Ma, Y., Wang, Y., Zhan, Z., and Piao, Z. (2022). Fine mapping and candidate gene analysis of *CRA3.7* conferring clubroot resistance in *Brassica rapa*. *Theor. Appl. Genet.* 135, 4541–4548. doi: 10.1007/s00122-022-04237-2

Pankov, K. V., McArthur, A. G., Gold, D. A., Nelson, D. R., Goldstone, J. V., and Wilson, J. Y. (2021). The cytochrome P450 (CYP) superfamily in cnidarians. *Sci. Rep.* 11, 9834. doi: 10.1038/s41598–021-88700-y

Schuller, A., and Ludwig-Müller, J. (2016). Histological methods to detect the clubroot pathogen *Plasmodiophora brassicae* during its complex life cycle. *Plant Pathol.* 65, 1223–1237. doi: 10.1111/ppa.12520

Shi, Z., Liu, Y., Noor, N., Bao, Y., Ming, R., Liu, T., et al. (2014). Gene expression profiles deciphering clubroot infection and defense mechanisms in Brassica genomes. *PloS One* 9, e98660. doi: 10.1007/s10142-013-0312-9

Stjelja, S., Fogelqvist, J., Tellgren-Roth, C., and Dixelius, C. (2019). The architecture of the *Plasmodiophora brassicae* nuclear and mitochondrial genomes. *Sci. Rep.* 9, 15753. doi: 10.1038/s41598-019-52274-7

Strelkov, S. E., Hwang, S., Manolii, V. P., Cao, T., and Feindel, D. (2016). Emergence of new virulence phenotypes of *Plasmodiophora brassicae* on canola (*Brassica napus*) in Alberta. *Can. Eur. J. Plant Pathol.* 145, 517–529. doi: 10.1007/s10658-016-0888-8

Struck, C., Rüsch, S., and Strehlow, B. (2022). Control strategies of clubroot disease caused by *Plasmodiophora brassicae*. *Microorganisms* 10, Art. 3. doi: 10.3390/microorganisms10030620

Sun, X. L., Yu, Q. Y., Tang, L. L., Ji, W., Bai, X., Cai, H., et al. (2013). GsSRK, a G-type lectin S-receptor-like serine/threonine protein kinase, is a positive regulator of plant tolerance to salt stress. *J. Plant Physiol.* 170, 505–515. doi: 10.1016/j.jplph.2012.11.017

Ueno, H., Matsumoto, E., Aruga, D., Kitagawa, S., Matsumura, H., and Hayashida, N. (2012). Molecular characterization of the CRa gene conferring clubroot resistance in Brassica rapa. *Plant Mol. Biol.* 80, 621–629.

Voorrips, R. E., Jongerius, M. C., and Kanne, H. J. (2003). Quantitative trait loci for clubroot resistance in *Brassica oleracea*. *Biotechnol. Agric. For.* 52, 87–104. doi: 10.1094/MPMI-06-14-0191-R

Wan, J., He, M., Hou, Q., Zou, L., Yang, Y., Wei, Y., et al. (2021). Cell wall associated immunity in plants. *Stress Biol.* 1, 3. doi: 10.1007/s44154-021-00003-4

Wang, Y., and Bouwmeester, K. (2017). L-type lectin receptor kinases: New forces in plant immunity. *PloS Pathog.* 13, e1006433. doi: 10.1371/journal.ppat.1006433

Wang, Y., Bouwmeester, K., Beseh, P., Shan, W., and Govers, F. (2014). Phenotypic analyses of Arabidopsis T-DNA insertion lines and expression profiling reveal that multiple L-type lectin receptor kinases are involved in plant immunity. *Mol. Plant-Microbe Interactions.: MPMI.* 27, 1390. doi: 10.1094/MPMI-06-14-0191-R

Wang, W., Qin, L., Zhang, W., Tang, L., Zhang, C., Dong, X., et al. (2023). WeiTsing, a pericycle-expressed ion channel, safeguards the stele to confer clubroot resistance. *Cell* 186, 2656–2671 e2618. doi: 10.1016/j.cell.2023.05.023

Wang, X., Hou, S., Wu, Q., Lin, M., Acharya, B. R., Wu, D., et al. (2017). IDL6-HAE/HSL2 impacts pectin degradation and resistance to Pseudomonas syringae pv tomato DC3000 in Arabidopsis leaves. *Plant J. Cell Mol. Biol.* 89, 250–263. doi: 10.1111/tpj.13380

Zhang, C., Du, C., Li, Y., Wang, H., Zhang, C., and Chen, P. (2023). Advances in biological control and resistance genes of brassicaceae clubroot disease-the study case of China. *Int. J. Mol. Sci.* 24, 785. doi: 10.3390/ijms24010785

Zhang, S., Wu, Q. R., Zhang, H. M., Pei, Z. M., and Gao, J. W. (2021). Genome-wide identification and transcriptomic data exploring of the cytochrome P450 family in Chinese cabbage (*Brassica rapa* L. ssp. *pekinensis*). *J. Plant Interact.* 16, 136–155. doi: 10.1080/17429145.2021.1909761

Zhang, F., Yu, J., Cui, X., Shen, X., and Dong, X. (2016). Transcriptomic analysis of Brassica napus the highly resistant genotype infected with *Plasmodiophora brassicae*. *BMC Genomics* 17, 836.

Zhao, Y., Bi, K., Gao, Z., Chen, T., Liu, H., Xie, J., et al. (2017). Transcriptome Analysis of *Arabidopsis thaliana* in Response to *Plasmodiophora brassicae* during Early Infection. *Front. Microbiol.* 8, 673. doi: 10.3389/fmicb.2017.00673

Zhao, G., Guo, D., Wang, L., Li, H., Wang, C., and Guo, X. (2021). Functions of RPM1-interacting protein 4 in plant immunity. *Planta* 253, 11. doi: 10.1007/s00425-020-03527-7

Zhou, Q., Galindo-Gonzalez, L., Hwang, S.-F., and Strelkov, S. E. (2020). Application of genomics and transcriptomics to accelerate development of clubroot resistant canola. *Can. J. Plant Pathol.* 43, 189–208. doi: 10.1080/07060661.2020.1794541

frontiers | Frontiers in Plant Science

TYPE Original Research
PUBLISHED 12 July 2024
DOI 10.3389/fpls.2024.1418319

OPEN ACCESS

EDITED BY
Xiangshu Dong,
Yunnan University, China

REVIEWED BY
Sandip Das,
University of Delhi, India
Dierk Wanke,
University of Tübingen, Germany

*CORRESPONDENCE
Chunguo Wang
wangcg@nankai.edu.cn

RECEIVED 19 April 2024
ACCEPTED 25 June 2024
PUBLISHED 12 July 2024

CITATION
Zhu Y, Liu C, Zhao M, Duan Y, Xie J and Wang C (2024) Transcriptome profiling reveals key regulatory factors and metabolic pathways associated with curd formation and development in broccoli.
Front. Plant Sci. 15:1418319.
doi: 10.3389/fpls.2024.1418319

Transcriptome profiling reveals key regulatory factors and metabolic pathways associated with curd formation and development in broccoli

Yinxia Zhu[1], Ce Liu[2,3], Mengyao Zhao[1], Yuxuan Duan[1], Jingjing Xie[1] and Chunguo Wang[1]*

[1]College of Life Sciences, Nankai University, Tianjin, China, [2]Cucumber Research Institute, Tianjin Academy of Agricultural Sciences, Tianjin, China, [3]State Key Laboratory of Vegetable Biobreeding, Tianjin, China

Broccoli, a cruciferous vegetable, has a unique indeterminate inflorescence structure known as curds. It is the main edible organ of broccoli and has a rich nutritional value and health benefits. However, the formation and development mechanism of the curd is still not well understood. In the present study, the shoot apical meristem (SAM) stage and three different development stages of curd (formation stage (FS), expansion stage (ES), and maturation stage (MS)) were identified and subjected to transcriptome sequencing to uncover the potential genes and regulatory networks involved in curd formation and development. The results indicated that the genes associated with the development of SAM such as *BolAP1A*, *BolAP1C*, *BolCAL*, and *BolAGL6* play an important role in the abnormal differentiation of the curd apical buds. The genes, *BolFRI*, *BolbHLH89*, *BolKAN4*, *BolAGL12*, and *BolAGL24*, displayed significantly differential expression patterns in curd development may function in the regulation of the transition from inflorescence meristem (IM) to floral meristem (FM). Moreover, gene ontology (GO) and Kyoto Encyclopedia of Genes and Genomes (KEGG) enrichment analysis of the differentially expressed genes (DEGs) indicate that phytohormones, such as auxin (AUX), gibberellins (GA), and abscisic acid (ABA) also play an important role in SAM proliferation and the transition from SAM to IM. In addition, the genes regulating photosynthetic reaction (*BolLHCA1*, *BolLHCB1*, *BolPsbO*, etc.) have a key involvement in the differentiation of secondary IMs during curd expansion. The genes associated with the metabolism of starch and sucrose (e.g., *BolSPS4*, *BolBAM4*) were significantly upregulated at the MS should contribute to the maturation of the curd. These findings provide new insights into the potential key regulatory factors and metabolic pathways involved in the formation and development of broccoli curds.

KEYWORDS

broccoli, curd, phytohormones, photosynthesis, starch metabolism

1 Introduction

Broccoli (*Brassica oleracea* var. *Italica*) belongs to the cruciferous family, is characterized by its unique indeterminate inflorescence structure, composing numerous short branches known as curds (Kieffer et al., 1998; Cao et al., 2020). Curd is the main edible organ of broccoli and is rich in various active ingredients and nutrients like phenolic compounds, glucosinolates, vitamins and minerals (Li et al., 2022). Several researches have explored the formation and development mechanism of the curd (Smyth, 1995; Kieffer et al., 1996). However, due to its complex regulatory relationships and the influence of environmental factors, understanding in curd formation and development is still relatively limited (Rosen et al., 2018). As the reproductive developmental organs of broccoli, the formation and development of the curd are primarily categorized into shoot apical meristem (SAM) and three curd development stages, 1) formation stage (FS), where SAM differentiates to the inflorescence meristem (IM). 2) expansion stage (ES), the generation of secondary IMs (each secondary IM becomes a second-order SAM and starts differentiating into new secondary IMs, with the curd diameter increases rapidly). 3) maturation stage (MS), where the IM resumes the ability to differentiate into FM and continues flower development (Sadik, 1962, 1968; Kieffer et al., 1998). Compared with the reproductive development process of other *Brassica* species, such as cabbage, oilseed rape and radish, the differentiation and development of broccoli and cauliflower curds is a flowering reversal phenomenon caused by abnormal differentiation of terminal buds (Zhao et al., 2020a). The apical meristem temporarily loses the ability to differentiate into FM, but the secondary IM continues to differentiate, and the pedicel becomes thicker and the elongation of internodes is inhibited. The curd in cauliflower is caused by the repeated proliferation of the inflorescence or FM development cessation, which has the characteristics of vegetative and reproductive apices (Anthony et al., 1996). However in broccoli, this differentiation cessation occurs before flowering, resulting in a dense collection of small buds on the curd surface (Fujime and Hirose, 1980).

Early studies attempt to elucidate the genetic control of curd development by identifying and characterizing homologous genes in *Arabidopsis thaliana*. An increase in the expression of *LEAFY* (*LFY*) subsequently suppresses *TERMINAL FLOWER 1* (*TFL1*) expression, which initiates flowering by upregulating *APETALA 1* (*AP1*) and *CAULIFLOWER* (*CAL*) in *Arabidopsis* (Goslin et al., 2017; Serrano-Mislata et al., 2017). Studies indicate that the *cal ap1* double mutant in *Arabidopsis* results in the cauliflower phenotype (Bowman et al., 1993). Subsequent research indicates that *BobAP1* and *BobCAL* are the dominant regulatory factors for the curd development cessation (Goslin et al., 2017). In addition, the genomic comparisons between the cauliflower and cabbage have been identified several structural variants crucial for the unique cauliflower phenotype, implicating genes such as *BobFLC* and *BobFRI* in curd initiation, *BobWUS* and *BobMP* in inflorescence proliferation, *BobCAL*, *BobAP1* and *BobSEP3* in floral development cessation and the potential negative regulatory genes in FM, such as *BobAGL14*, *BobSVP* and *BobCCE1* (Guo et al., 2021). Similarly, a total of 86 quantitative trait loci (QTL) were identified which were associated with the agronomic traits of curds in *Brassica oleracea*, such as germination time, and days from germination to flowering (Lan and Paterson, 2000). Furthermore, a total of 20 QTLs were detected in association with the basal diameter, stalk length, stalk angle, and curd solidity of the cauliflower (Zhao et al., 2020b). Additionally, a high-density genetic map including 2741 SNPs was constructed to uncover the cessation of floral development, which further indicates that the formation and development of curd in cauliflower is subjected to multi-gene regulations having a complex regulatory mechanism (Irwin et al., 2016). However, the cessation of cauliflower curd development occurs earlier compared to broccoli curd development. Therefore, the molecular mechanisms and the regulatory network that leads to the special structure of broccoli curd remain unrevealed.

Plant phytohormones play pivotal regulatory roles in the growth, development, and physiological processes, including the flowering process (Liu et al., 2022; Xu et al., 2022). Auxin (AUX) has a critical role in determining the number and identity of floral organs (Cheng and Zhao, 2007). Research indicates that AtAG regulates *AtCRC* and inhibits the expression of *AtTRN2* to modulate AUX homeostasis, thereby controlling the determinacy of the FM (Yamaguchi et al., 2017). The gene *WUSCHEL* (WUS) responds to AUX to maintain the proliferation and differentiation of apical stem cells in *Arabidopsis* (Mayer et al., 1998). At stage 6 of the flower development, the AG-WUS-KNU module precisely controls the maintenance program of FM stem cells (Lenhard et al., 2001; Payne et al., 2004; Prunet et al., 2008; Kwaniewska et al., 2021). Similarly, the expression of *BobLFY* is also influenced by the maximum concentration of AUX, which marks the initiation sites of FMs (Azpeitia et al., 2021). Several studies offer insights into the potential hormonal influences on the unique meristem formation in broccoli curds. However, the specific molecular mechanisms underpinning broccoli curd formation and development remain largely unexplored. Therefore, the objective of this study was to further understand the formation and development of curds in broccoli. The curds with four different development stages were sampled and subjected to transcriptome sequencing. The genes expression profiles and the regulatory networks and metabolic pathways in which the identified DEGs participate should be analyzed in each development stage.

2 Materials and methods

2.1 Plant materials

The KRJ-012 homozygous broccoli seeds used in this study were provided by associate professor Hanmin Jiang of the Tianjin Kernel Vegetable Research Institute, Tianjin, China. The seeds were

Abbreviations: SAM, shoot apical meristem; FS, formation stage; ES, expansion stage; MS, maturation stage; IM, inflorescence meristem; FM, floral meristem; GO, gene ontology; KEGG, Kyoto Encyclopedia of Genes and Genomes; DEGs, differentially expressed genes; AUX, Auxin; GA, gibberellins; ABA, abscisic acid; JA, jasmonic acid; CTK, cytokinin; ET, ethylene; BR, brassinosteroid; qRT-PCR, quantitative reverse-transcription PCR.

cultivated in pots in a greenhouse with a photoperiod of 16 hours light/8 hours dark and temperatures varying between 15°C and 28°C. Thirty days old seedlings were transplanted to the field. Seventy days after transplantation, starting from the appearance of the meristem in the broccoli curd, samples were taken from the apex of the curd every seven days (Figure 1A). The stages included: (1) SAM (0 days); (2) FS (7 days); (3) ES (14 days); (4) MS (21 days). The samples from two biological replicates were immediately stored in liquid nitrogen and later kept at -80°C for subsequent RNA extraction and sequencing analysis.

2.2 Paraffin embedding, sectioning, and staining

Fresh tissues were immediately fixed using a fixative solution (70% (v/v) ethanol, 5% (v/v) formalin and 5% (v/v) glacial acetic acid) for 48 hours. The trimmed tissues were then dehydrated using a gradient alcohol and embedded in melted paraffin wax. After solidification, the paraffin slicer were sliced with a thickness of 4 μm. The tissue is flattened when the slice floats on the 40 °C warm water of the spreading machine, and then picked up by the glass slides and baked in the oven at 60 °C. The tissue sections were stained with safranin O staining solution and plant solid green staining solution, then scanned and imaged using the Pannoramic MIDI scanner (3DHISTECH, Hungary).

2.3 RNA library construction and high-throughput sequencing

Total RNA of the samples was extracted using the RNeasy Kit (Qiagen, China), followed by mRNA enrichment using oligo (dT). The enriched mRNA was subjected to fragmentation, reverse transcription, and PCR amplification for RNA-seq libraries preparation. RNA-seq libraries in this study were sequenced on the BGISEQ-500 platform (Beijing Genomics Institute, China). The analyses were conducted with two biological replicates.

2.4 Transcriptome data analysis

The raw sequencing reads were subjected to filtering using SOAPnuke software (https://github.com/BGI-flexlab/SOAPnuke) with the following criteria: 1) removal of reads containing adapters (adapter contamination); 2) removal of reads with unknown base content exceeding 5%; 3) removal of low-quality reads (reads with a proportion of bases with quality values less than 15 and greater than 20% of the total bases were considered low-quality reads). For each sample, a minimum of 4 Gb of raw data, including over 50 million clean reads were required to obtain sufficient transcriptional information. Clean reads were aligned and classified against the reference genome and transcript sequences of *Brassica oleracea* var.

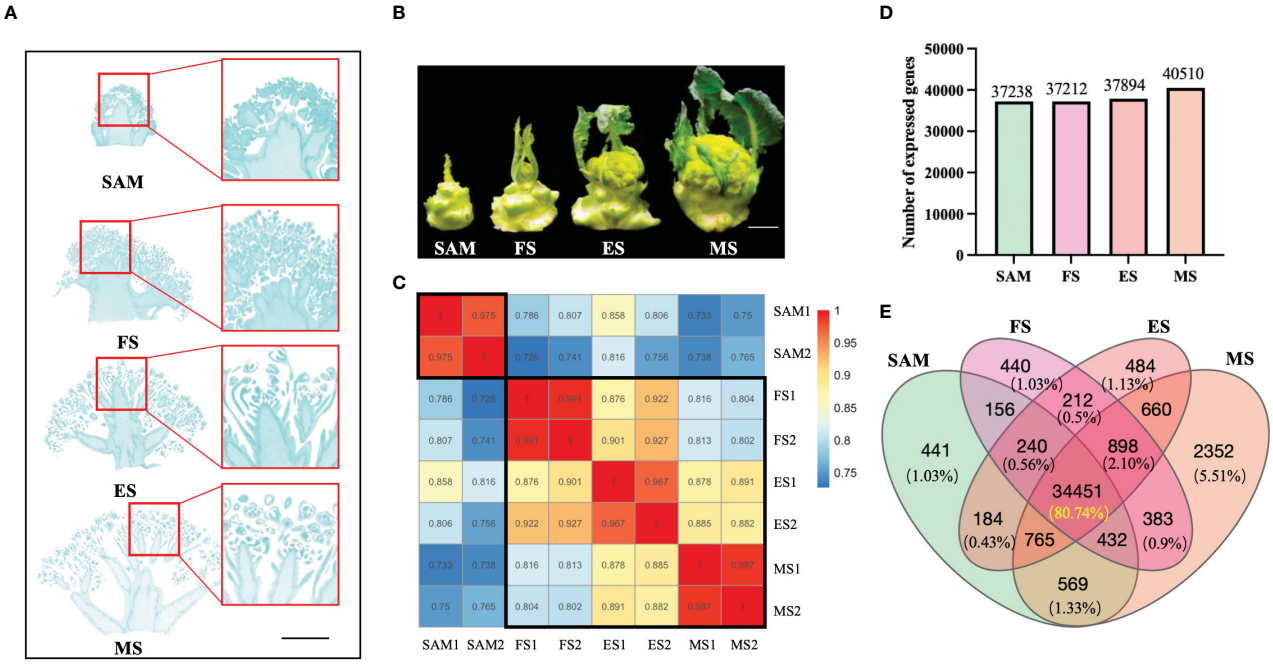

FIGURE 1
Phenotypes and overall gene expression profiles at four stages of curd development. **(A)** Specific tissues used for constructing RNA libraries at different stages of curd development (shoot apical meristem (SAM), formation stage (FS), expansion stage (ES), maturation stage (MS)), Scale bars=1 cm; **(B)** Phenotypes of broccoli curd formation and development at four stages (SAM, FS, ES, MS), Scale bars=5 cm); **(C)** Samples correlation of four development stages; **(D)** Number of expressed genes at each curd development stage; **(E)** Venn diagram showing the number of commonly or uniquely expressed genes.

oleracea (https://www.ncbi.nlm.nih.gov/datasets/genome/GCF_000695525.1/, Parkin et al., 2014) using Bowtie2 (v2.3.4.3) (http://bowtie-bio.sourceforge.net/Bowtie2/index.shtml). Transcript abundances were calculated using StringTie software (Shumate et al., 2022), and normalization was performed using the DESeq2 package in *R* software (Love et al., 2014).

2.5 Identification of DEGs

RSEM (v1.3.1) (http://deweylab.biostat.wisc.edu/rsem/rsem-calculate-expression.html) was used for gene expression quantification, $|\log_2(A/B)| > 1$ and q value <0.01 were used as standards to identify DEGs, where A and B represent FPKM value of two groups respectively.

2.6 GO and KEGG and genomes analysis of DEGs

GO analysis of DEGs was performed using the agriGO platform (http://bioinfo.cau.edu.cn/agriGO/), with a hypergeometric test was performed to identify significantly enriched GO terms (corrected p value <0.05). To further visualize statistically significant overexpressed GO terms, GO and KEGG enrichment analysis of DEGs was performed using the enrichGO and enrichKEGG functions in the clusterProfiler (Wu et al., 2021).

2.7 Gene expression pattern analysis of DEGs

Pearson correlation coefficient and hierarchical clustering for all samples were analyzed using the "cor" and "hclust" functions in *R* software (version 3.0.1) with default values. Hierarchical clustering and Heatmap cluster analysis of DEGs was performed using the *R* package "gplots" and "pheatmap", respectively.

2.8 Validation of gene expression levels by qRT-PCR

Differential expression patterns of representative genes detected by transcriptome data were validated by qRT-PCR analysis. To detect the corresponding genes, specific primer pairs were designed (Supplementary Table 6). The *Bolactin* gene from broccoli was selected as an internal reference. Faststart Universal SYBR Green Master (Roche, Germany) was used in all experiments. Relative expression levels of genes were calculated by the comparative $2^{-\Delta\Delta CT}$ method based on the manufacturer's recommendations. Three batches of RNA independently isolated from each sample were used, and three technical replicates were performed to ensure the reliability of the quantitative analysis.

3 Results

3.1 Overview of transcriptome data

The samples of curds at four different stages were conducted to transcriptome sequencing (Figures 1A, B). Results showed that a total of 350,731,464 clean reads were filtered from 371,602,504 raw reads. The alignment rates of these clean reads to the reference genome were 83.64% for SAM, 84.04% for the FS, 84.67% for the ES, and 83.95% for the MS (Supplementary Table 1). The correlation analysis of these sequencing samples indicates that the correlation was higher between the samples within a group ($r > 0.96$) (Figure 1C). Besides, the FS, ES, and MS groups exhibited higher correlations ($r > 0.87$) compared to the SAM group. These results indicate that the sequencing quality is satisfied and the clean reads are suitable for further analysis. Based on the function annotation of these clean reads detected in each sample, a total of 42,667 genes were identified (Supplementary Table 2), with 37,238, 37,212, 37,894, and 40,510 genes showing transcriptional expression at SAM, FS, ES, and MS, respectively (Figure 1D). Among these expressed genes, 441 genes showed uniquely expression at the SAM stage. 440, 484 and 2352 genes were exclusively expressed at the FS, ES, and MS, respectively (Figure 1E). Furthermore, 34,451 genes, constituting 80.74% of the total detected genes, were commonly expressed at all four stages of curd development (Figure 1E).

3.2 DEGs between SAM and three stages of curd development were identified

To investigate candidate genes functioning in the transition from SAM to curd formation, the transcriptional expression levels of genes were compared between SAM and three curd development stages, FS, ES, and MS, respectively. A total of 10,652 genes exhibited differential expression levels. Specifically, in the comparison between SAM and FS, there were 1,624 DEGs upregulated and 2,162 DEGs downregulated. In the SAM vs. ES comparison, 1,410 DEGs were upregulated and 1,274 were downregulated. In the SAM vs. MS comparison, 2,326 DEGs were upregulated and 1,856 were downregulated. (Figure 2A). Among them, 965 genes displayed significantly differential expression levels in SAM vs. FS and SAM vs. ES, 559 genes displayed significantly differential expression levels in SAM vs. FS and SAM vs. MS, and 965 genes displayed significantly differential expression levels in SAM vs. FS and SAM vs. ES (Figure 2B). A total of 1,399 genes showed significantly differential expression patterns at SAM stage compared with each of the three curd development stages (Figure 2B; Supplementary Table 3).

These overlapping DEGs between the SAM and three curd development stages likely play crucial role in regulating curd formation and development. Subsequently, the possible genetic regulatory networks and pathways enriched by these 1,399 overlapping DEGs were explored by GO and KEGG analysis. The GO enrichment assay indicates that among the GO terms targeted by

10.3389/fpls.2024.1418319

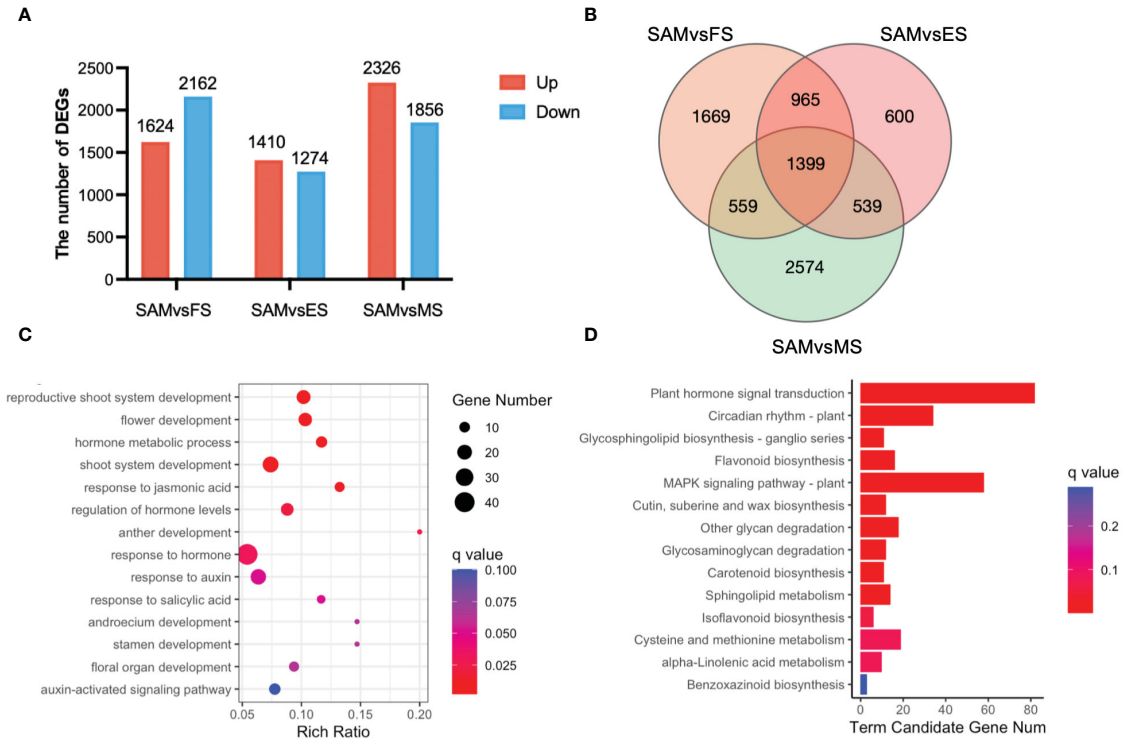

FIGURE 2
DEGs identified in three pairwise comparisons (SAM vs. FS, SAM vs. ES, and SAM vs. MS). **(A)** The number of DEGs between each two groups (red represents upregulation, blue represents downregulation); **(B)** Venn diagram of DEGs; **(C)** GO functional enrichment of DEGs between SAM and the curd development stages (FS, ES, MS); **(D)** KEGG enrichment of DEGs between the SAM and the curd development stages (FS, ES, MS). DEGs were identified based on the criteria of $|\log_2(\text{fold change})| > 1$ and q value < 0.01.

these overlapping DEGs, the reproductive-associated terms, such as reproductive shoot system development (GO:0090567), flower development (GO:0009908), anther development (GO:0048653), stamen development (GO:0048443), and floral organ development (GO:0048437); phytohormones, especially AUX, JA and SA-associated terms, such as hormone metabolic processes (GO:0042445), response to jasmonic acid (GO:0009753), regulation of hormone levels (GO:0010817) and response to AUX (GO:0009733), were significantly enriched. Moreover, KEGG pathway assay also indicates that plant hormone signal transduction (ko04075) and circadian rhythm (ko04712) were significantly enriched by these overlapping DEGs, suggesting their pivotal roles in the complex regulation of the transition from SAM to curd formation.

In addition, DEGs in temporal stages specific manner (SAM vs. FS, FS vs. ES, and ES vs. MS) were identified. GO term enrichment analysis revealed that DEGs in SAM vs. FS were predominantly involved in auxin-activated signaling pathway (GO:0009734), photosystem I (GO:0009522) and shoot system development (GO:0048367) (Supplementary Figure 3). KEGG pathway analysis revealed that DEGs in SAM vs. FS were predominantly annotated in the plant hormone signal transduction (ko04075) and circadian rhythm (ko04712) pathways (Supplementary Figure 3), which are consistent across the SAM and the later three developmental stages. However, during the transition from SAM to FS, the pentose phosphate pathway (ko00030) was also identified, indicating that this pathway may also be involved in the curd formation. In the FS vs. ES comparison, significant annotation of photosystem (GO:0009521) in the GO terms and photosynthesis-antenna proteins (ko00196) in the KEGG pathway suggests the crucial role of photosynthesis in the transition from curd formation to enlargement. In the ES vs. MS comparisons, DEGs were significantly annotated in floral organ development-related GO categories, including pollen wall assembly (GO:0010208), flower development (GO:0009908) and anther development (GO:0048653). Moreover, DEGs in the ES vs. MS comparisons were predominantly annotated in the starch and sucrose metabolism (ko00500) KEGG pathway (Supplementary Figure 3). These analysis results were consistent with the following comparison results of the three stages of curd development.

3.3 DEGs associated with AUX, GA and ABA signal pathways were highly expressed at SAM stage

GO term annotation and KEGG pathway enrichment analyses revealed that phytohormones may play a key regulatory role in the formation of curd (Figures 2C, D). Among the DEGs involved in phytohormone signal transduction pathways, 27 genes were significantly enriched in AUX signal pathway (Figure 3A), 18 in

10.3389/fpls.2024.1418319

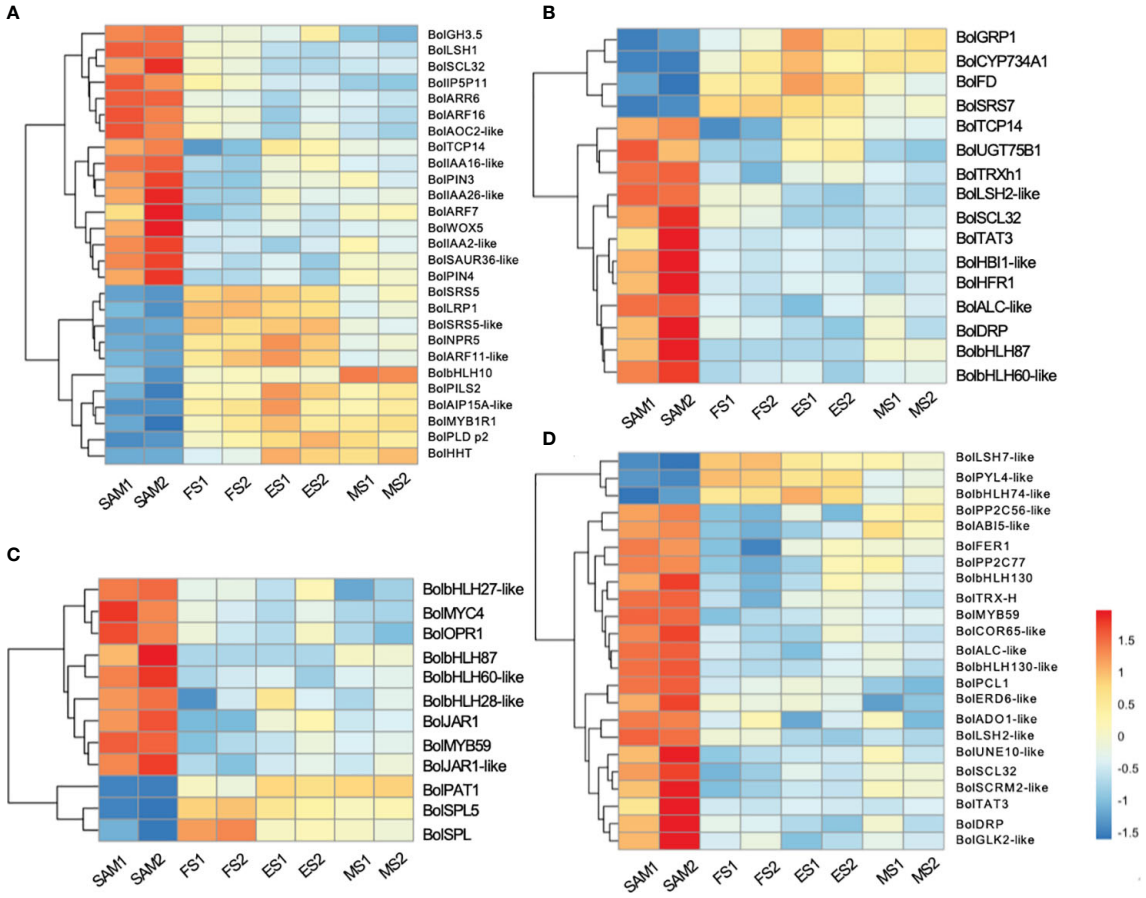

FIGURE 3
Transcriptional expression profiles of DEGs involved in the phytohormone signal transduction pathways. The DEGs were identified in three pairwise comparisons (SAM vs. FS, SAM vs. ES, and SAM vs. MS). **(A)** DEGs related to AUX; **(B)** DEGs related to GA; **(C)** DEGs related to JA; **(D)** DEGs related to ABA. DEGs were identified based on the criteria of $|\log_2(\text{fold change})| > 1$ and q value < 0.01.

the GA signal pathway (Figure 3B), 12 in the JA signal pathway (Figure 3C), and 23 in the ABA signal pathway (Figure 3D).

AUX, GA, and ABA are known for their roles in organ identity and development (Wei et al., 2021). Gene expression profile assay indicates that genes involved in AUX signal pathways, such as *BolAUX/IAA*, *BolGH3*, *BolSAUR*, *BolARF16*, *BolARF7*, *BolARR6*, *BolIAA16-like*, *BolSAUR36-like* and *BolWOX5*, were highly expressed at the SAM stage, and then downregulated at the subsequent stages of curd development (Figures 3A, 4). Notably, the AUX transduction negative regulator *BolNPR5* was upregulated at FS, ES and MS compared to SAM (Figure 3A).

GA plays a crucial role in regulating the proliferation and differentiation of the SAM and the formation of buds and floral buds. Among the 22 DEGs related to the GA signal pathway, the majority of genes were highly expressed at SAM stage, but showed lower expressions during the subsequent development stages, including four negative regulators: *BolUGT75B1*, *BolTAT3*, *BolGLK2-like*, and *BolLDSH2-like*. Notably, the expression of *Gibberellin-Regulated Protein 1* (*BolGRP1*) was low at SAM stage but upregulated at the development stages (Figure 3B). In the ABA signal pathway, ABA negative regulatory protein coding genes *BolABI5-like*, *BolPP2C56-like* and *BolPP2C77* were highly expressed at SAM stage, but significantly downregulated at the development stages, while the positive regulator *BolPYL4* was upregulated at FS, ES and MS compared to SAM (Figure 3D). The upregulation of *BolPYL4* may directly affect the transcription levels of downstream gene *BolABF*, thereby positively regulating the differentiation process of SAM (Figure 4).

Among the 12 DEGs related to the JA signal pathway, 9 genes were highly expressed at SAM stage and significantly downregulated during the subsequent development stages, including the JA signaling activator *BolJAR1*, *BolbHLH27-like*, *BolMYC4*, *BolMYB59*, *BolTAT3* and *BolbHLH87*. Notably, the negative regulator *BolSPL5* and *BolSPL10* were highly expressed at FS, ES and MS (Figure 3C), suggesting that genes related to JA negatively regulate the development of SAM, promoting the transition from SAM to IM. In the cytokinin (CTK) pathway, *BolA-ARR*, which positively regulates cell division, was highly expressed at SAM, FS and ES, but its expression decreased at MS (Figure 4).

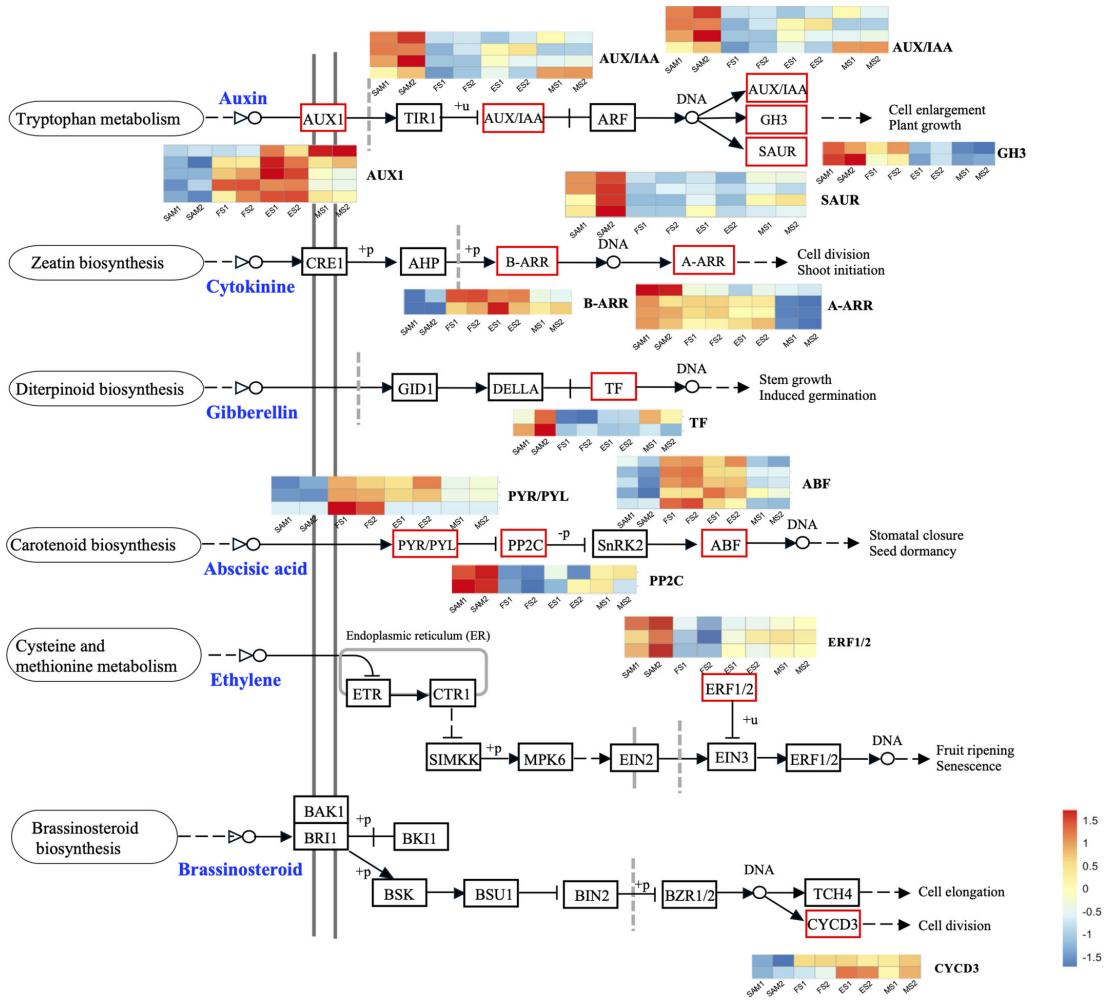

FIGURE 4
Plant hormone signal transduction pathway components and the expression profiles of DEGs. The DEGs were identified in three pairwise comparisons (SAM vs. FS, SAM vs. ES, and SAM vs. MS), based on the criteria of $|\log_2(\text{fold change})| > 1$ and q value < 0.01.

3.4 DEGs related to shoot apical and flower development were identified in comparison between SAM and curd development stages

The formation of curds is a flowering reversal phenomenon caused by abnormal differentiation of terminal buds. During the FS, the apical IM temporarily loses its capacity to differentiate into floral organs but continues to differentiate into secondary IMs. In this study, reproductive shoot system development took the first place in GO terms in the SAM vs. FS, SAM vs. ES, and SAM vs. MS (Figure 2C). Therefore, it is speculated that genes involved in the reproductive shoot system development may play a crucial role in the floral development cessations, and significantly influence the unique structure of the curd. Among the 22 genes associated with the reproductive shoot system development (Figure 5A), 13 of them exhibited low expression levels at the SAM stage but were significantly upregulated at the development stages (FS, ES, MS), such as *BolLRP1*, *BolFAS1*, *BolEMS1*, *BolFRI*, *BolAP1A*, *BolAP1C*, *BolAGL6*, and *BolCAL*. On the contrary, 9 genes were highly expressed at the SAM stage, such as sucrose transporter *BolSWEET13*, *BolTT12-like*, *BolTCP14*, and *BolAP2-like*. Additionally, a part of the DEGs associated with the reproductive shoot system development were also involved in the flower development process (Figure 5B), indicating that these genes are involved in the transformation from IM to FM and the development of floral organs.

3.5 Transcription factors with MADS and bHLH domain were extensively involved in the transition of SAM

Following the functional enrichment and pathway analysis of DEGs from overlapping genes in three pairwise comparisons (FS vs. SAM, ES vs. SAM, MS vs. SAM), it became evident that multiple transcription factors (TFs) likely play a pivotal role at the SAM stage. Given the significant role of TFs in regulating plant morphology, growth, and development (Wang et al., 2019; Jiang et al., 2022), the TF families among the DEGs shared in SAM vs. FS,

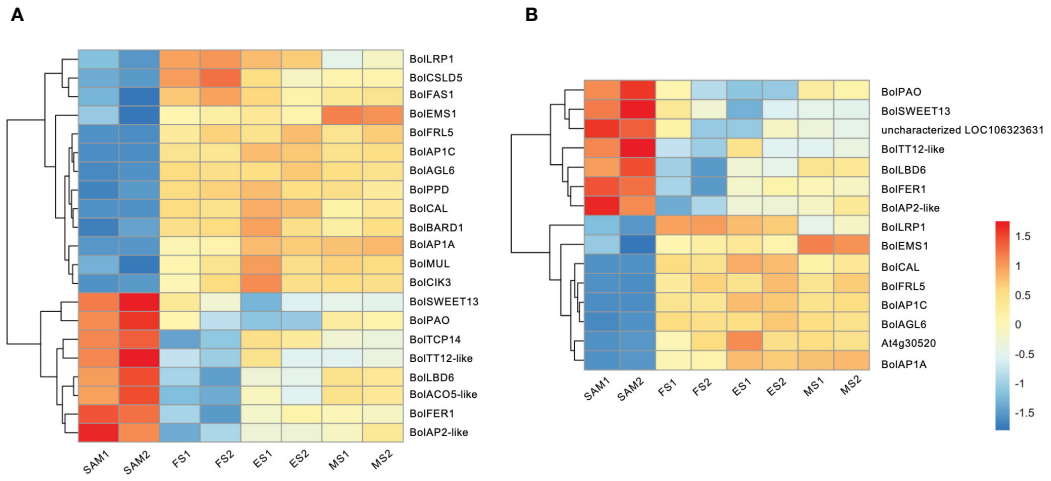

FIGURE 5
Transcriptional expression profiles of DEGs identified in three pairwise comparisons (SAM vs. FS, SAM vs. ES, and SAM vs. MS). **(A)** DEGs involved in reproductive shoot system development; **(B)** DEGs involved in flower development. The DEGs were identified based on the criteria of $|\log_2(\text{fold change})| > 1$ and q value < 0.01.

SAM vs. ES, and SAM vs. MS were classified. In this comparison, 152 DEGs were identified, belonging to 31 TF families. The top six families, based on percentage representation, included MADS (14.47%), bHLH (11.84%), AP2-EREBP (9.87%), MYB (8.55%), C2H2 (5.92%), and ABI3VP1 (5.26%) (Figure 6A). Notably, the MADS-box gene family, a large and crucial group in plants, especially for flower development, was prominently featured. Within this family, 6 DEGs, such as *BolAGL16*, *BolAGL19*, *BolAGL21*, were observed to be downregulated (Figure 6B), while the majority of the DEGs belonging to the MADS family were significantly upregulated during curd development (Figure 6B), such as *BolAGL3*, *BolAP1-A*, *BolAP3*, *BolPISTILLATA*, *BolSEP2* and *BolSEP1*. This pattern indicates that the MADS-box TF family plays a critical role in the transition from SAM to IMs.

3.6 DEGs associated with photosynthesis were highly expressed at the ES and MS

The overlapping DEGs in the FS vs. ES, FS vs. MS and ES vs. MS were analyzed to investigate the flowering reversal phenomenon in broccoli curds (Supplementary Table 4). The results showed that there were 853 upregulated and 459 downregulated genes in FS vs. ES, 3,235 upregulated and 1,267 downregulated genes in FS vs. MS, 1,853 upregulated and 835 downregulated genes in ES vs. MS (Figure 7A). Additionally, 1,085 DEGs shared in the FS vs. ES and FS vs. MS were identified (Figure 7B).

Twenty-three significantly enriched GO terms and KEGG pathways were identified based on the DEGs shared in FS vs. ES and FS vs. MS (Figure 7). Specifically, GO term enrichment was linked to photosystems (I, II), photosynthesis membrane, thylakoid part, thylakoid membranes and chloroplasts (Figure 7C). The transcriptional expression level analysis of DEGs involved in the photosystem (GO:0009521) revealed that 33 photosynthesis-related genes were significantly upregulated at FS and ES (Supplementary Figure 1), which may contribute to the formation of the FM. Additionally, carbon metabolism, amino acid metabolism and signal transduction pathways were enriched in both pairwise comparisons (FS vs. ES and FS vs. MS). The detailed metabolic pathways included photosynthesis-antenna protein (ko00196), photosynthesis (ko00195), tryptophan metabolism (ko00380), and plant cycle rhythm (ko04712) (Figure 7D). DEGs related to photosynthesis-antenna protein (ko00196) and photosynthesis (ko00195) were also highly expressed at ES and MS (Figure 8). The joint analysis of GO and KEGG revealed that photosynthesis-related DEGs, such as *BolLhca1*, *BolLhcb1* and *BolPsbO*, play a pivotal regulatory role in curd expansion and maturation.

3.7 A series of genes related to flower and pollen development were highly expressed at MS

A total of 2,170 overlapping DEGs were identified in the comparison of MS vs. SAM, MS vs. ES and MS vs. FS (Supplementary Figure 2, Supplementary Table 5). GO term enrichment analysis revealed that these DEGs predominantly involved in biological processes such as pollen development (GO:0009555), anther development (GO:0048653), and flower development (GO:0009908) (Figure 9A). This finding reveals that at the curd development stages, the IM regains the capacity to differentiate FM and resume the flower development process, involving the formation of floral organs like pollen tubes, anthers, and stamens. Specifically, the expression profile of genes related to flower development shows that the expression level of *BolFRI-like5*, *BolKAN4*, *BolbHLH89* and *BolTT12-like* were significantly upregulated at MS (Figure 9B), indicating their vital role in flower organ formation. Furthermore, a consistent pattern of significant upregulation at the MS was observed among 18 DEGs related to pollen development (Figure 9C). Additionally, two AG-like family genes, *BolAGL12* and

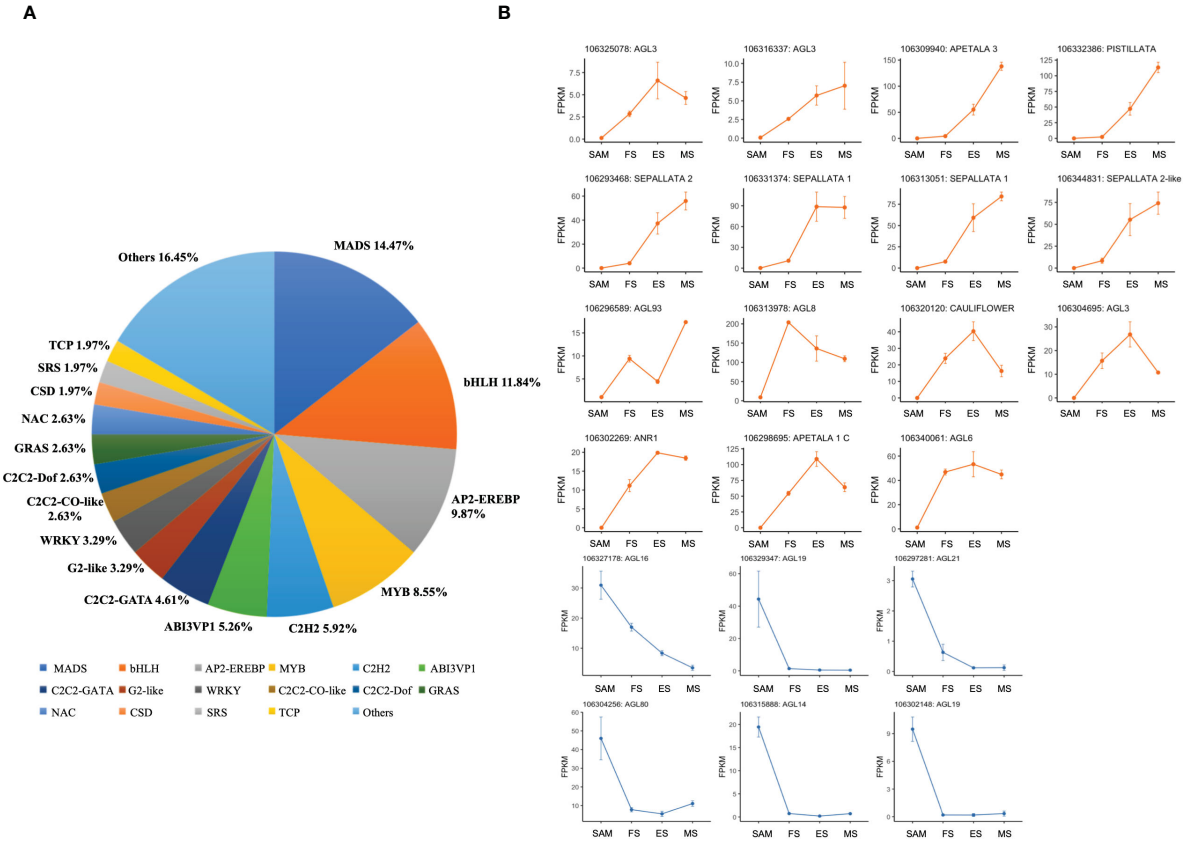

FIGURE 6
Statistics analysis of transcription factor families enriched in DEGs detected in three pairwise comparisons (SAM vs. FS, SAM vs. ES, and SAM vs. MS). **(A)** Proportion of each transcription factor family; **(B)** Transcriptional expression profiles of transcription factor with MADS domain at SAM stage and three development stages of curd (orange and blue line respectively represents upregulation and downregulation during the curd development stages compared to SAM).

BolAGL24 were observed, exhibited a high expression level at ES and FS, but significantly decreased at MS. Therefore, it is speculated that *BolAGL12* and *BolAGL24* may negatively regulate the differentiation process of FM in broccoli curd. Similarly, *BolLRP1* exhibited a high expression level at ES and FS, followed by a significant reduction at MS, suggesting its positive influence on the development of lateral IMs in the broccoli curds.

3.8 Genes involved in starch and sucrose metabolic pathways accumulate highly at the transcriptional level at MS

KEGG pathway enrichment analysis revealed that 87 overlapping DEGs in MS vs. SAM, MS vs. FS and MS vs. ES were predominantly annotated in the starch and sucrose metabolism (ko00500) pathway and the plant hormone signal transduction (ko04075) pathway (Figure 10A), suggesting a potential connection of these pathways with the regulation of the curd maturation. The expression profile of genes involved in the starch and sucrose metabolism pathway showed that 39 genes, including 16 from the GELP gene family, maintained low expression levels at the SAM stage, ES and FS, but significantly increased at the MS (Figure 10B). These processes are essential for sustaining the cellular energy supply and the growth and development of organisms.

3.9 Validation of DEGs expression patterns by qRT-PCR

In order to validate the RNA-seq quality, quantitative reverse-transcription PCR (qRT-PCR) analysis was performed on the 9 representative DEGs identified in the SAM and curd development stages, including *BolARF7*, *BolAP1A*, *BolCAL*, *BolAGL6*, *BolAGL12*, *BolTCP14*, *BolAGL24*, *BolFRI* and *BolFLC*. The selection of these genes was based on their prominent roles in the development processes as identified in the RNA-seq data. The results of the qRT-PCR analysis showed a high degree of consistency with the expression patterns obtained from the high-throughput sequencing data (Figure 11). This consistency reinforced the reliability of the RNA-seq in capturing the gene expression dynamics across the various stages of the curd development.

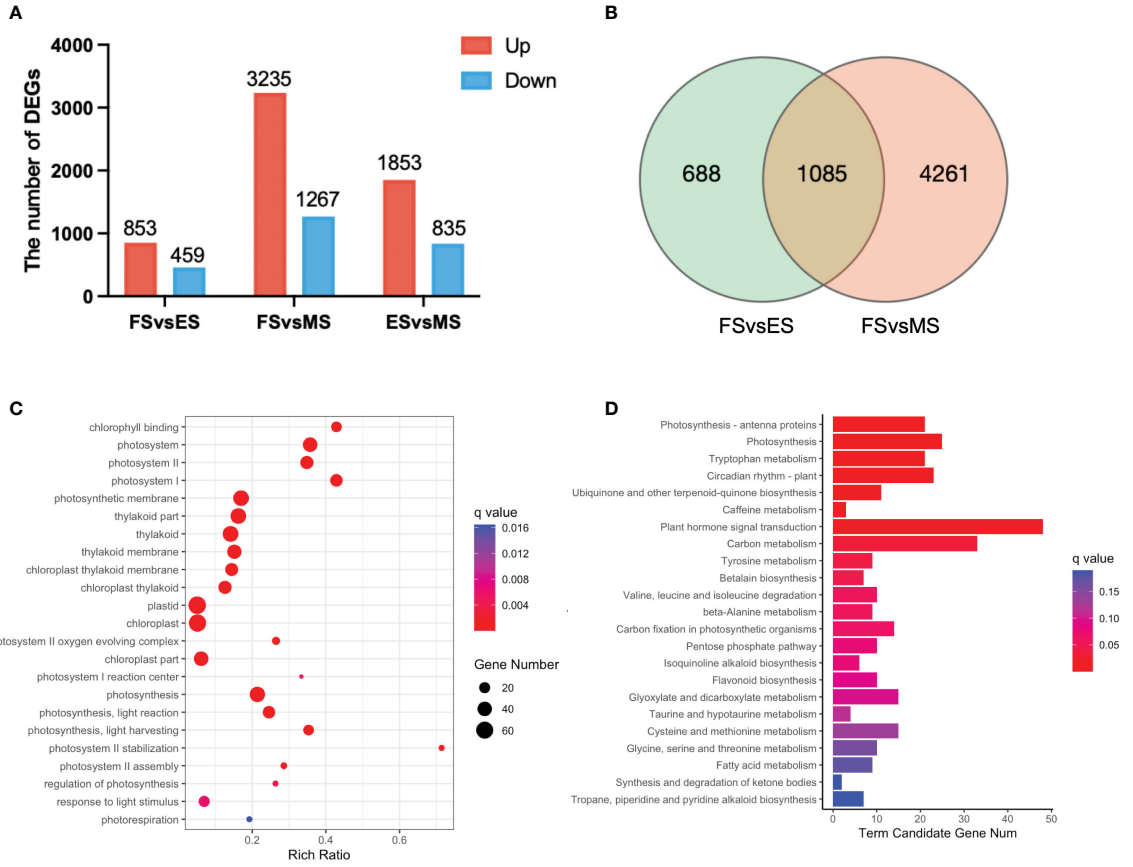

FIGURE 7
DEGs between the three stages of curd development (ES, FS, MS). **(A)** The number of upregulated and downregulated DEGs between each group; **(B)** Venn diagram of DEGs between the two groups (FS vs. ES, FS vs. MS); **(C)** GO term enrichment of overlapping DEGs in two pairwise comparisons (FS vs. ES, FS vs. MS); **(D)** KEGG enrichment of overlapping DEGs in two pairwise comparisons (FS vs. ES, FS vs. MS). DEGs were identified based on the criteria of $|\log_2$ (fold change)| >1 and q value < 0.01.

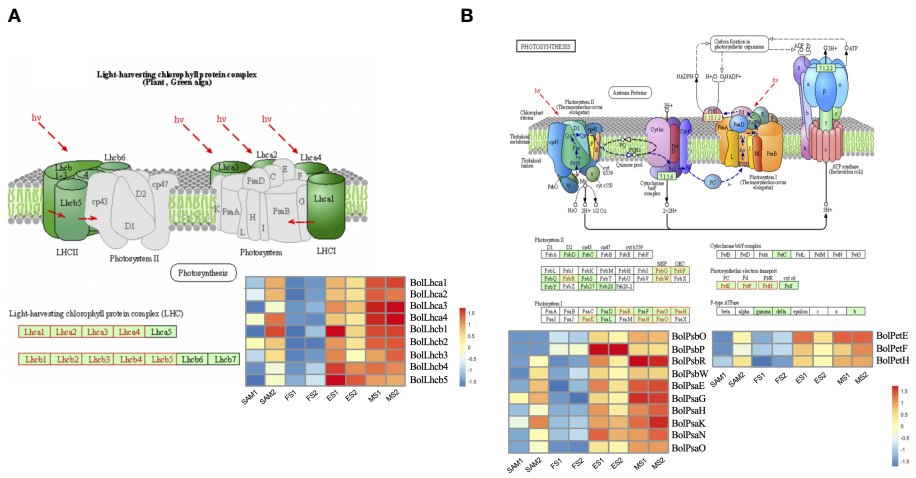

FIGURE 8
Transcriptional expression profile of genes involved in photosynthesis. **(A)** Transcriptional expression profile of genes which match Photosynthesis-antenna protein pathway (ko00196). These genes showed significant expression levels in in two pairwise comparisons (FS vs. ES, FS vs. MS). **(B)** Transcriptional expression profile of genes which match Photosynthesis pathway (ko00195). These genes showed significant expression levels in two pairwise comparisons (FS vs. ES, FS vs. MS). DEGs were identified based on the criteria of $|\log_2$(fold change)| >1 and q value < 0.01.

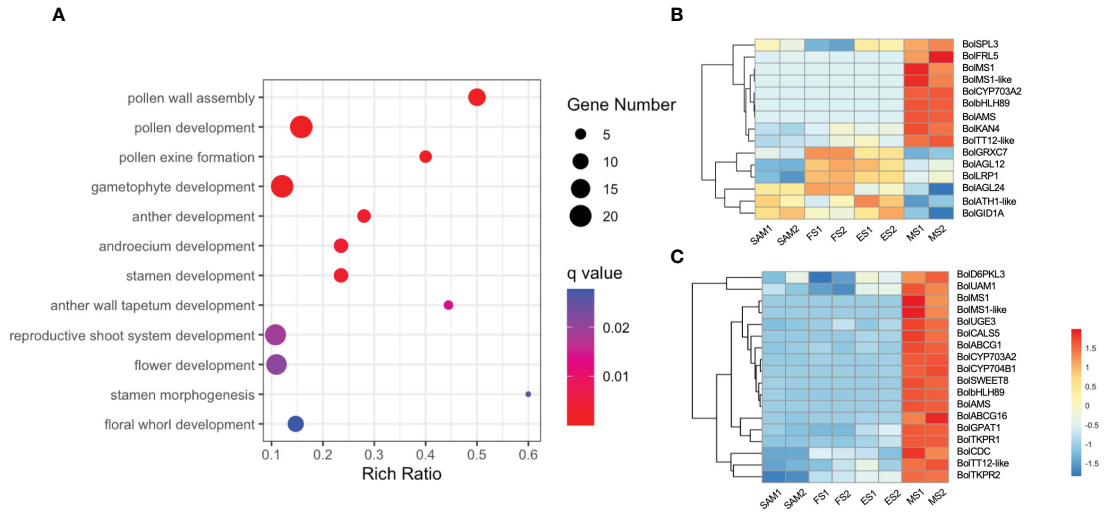

FIGURE 9
Analysis of DEGs identified in three pairwise comparisons (MS vs. SAM, MS vs. FS, and MS vs. ES). **(A)** GO term enrichment related to flower development; **(B)** Expression profile of DEGs involved in flower development (GO:0009908); **(C)** Expression profile of DEGs involved in pollen development (GO:0009555). DEGs were identified based on the criteria of $|\log_2$ (fold change)| >1 and q value < 0.01.

4 Discussion

4.1 Endogenous hormones are closely related to the proliferation and differentiation of the SAM

The role of endogenous hormones in the floral transition has been extensively studied in model plants (Davis, 2009), but their function in the formation of curd in broccoli remains largely unknown. This study proposes that AUX, GA, ABA signaling pathways are involved in regulating the formation and development of broccoli curd, forming a complex and interconnected hormone signaling network to coordinate the proliferation and differentiation of meristem at different stages (Figures 3, 4). It has been reported that AUX gradually accumulates in the SAM during the flowering transition in strawberries, indicating a crucial role of AUX in flowering transition (Hou and Huang, 2005). *AUX/IAA* and *SAUR*, play crucial roles in AUX signaling, affecting root, shoot and flower development (Guilfoyle, 2015; Luo et al., 2018). AUX/IAA always

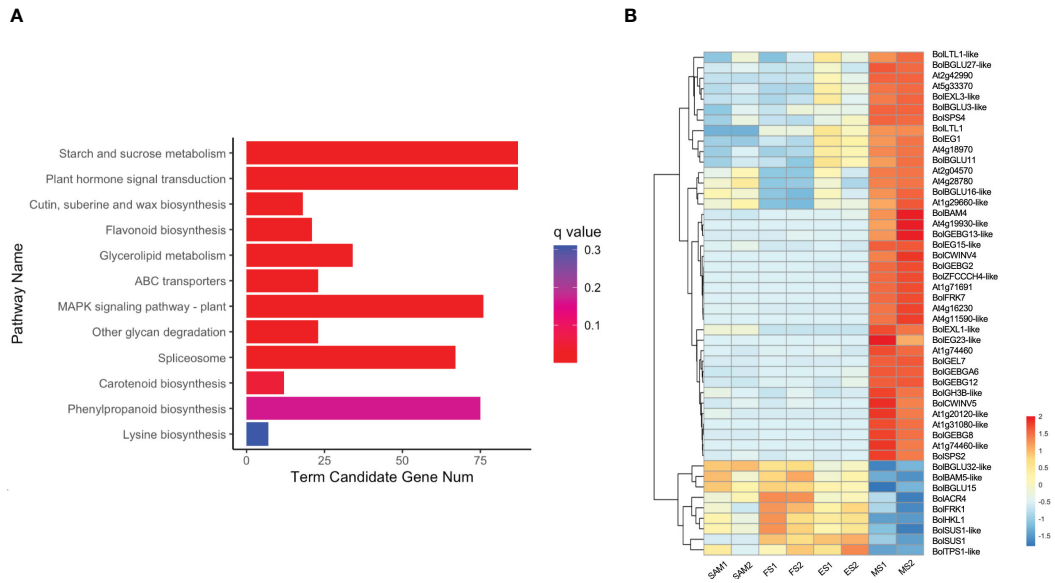

FIGURE 10
Analysis of DEGs identified in three pairwise comparisons (MS vs. SAM, MS vs. FS, and MS vs. ES). **(A)** KEGG enrichment analysis of DEGs; **(B)** Transcriptional expression profile of DEGs involved in starch and sucrose metabolism (ko00500). DEGs were identified based on the criteria of $|\log_2$ (fold change)| >1 and q value < 0.01.

10.3389/fpls.2024.1418319

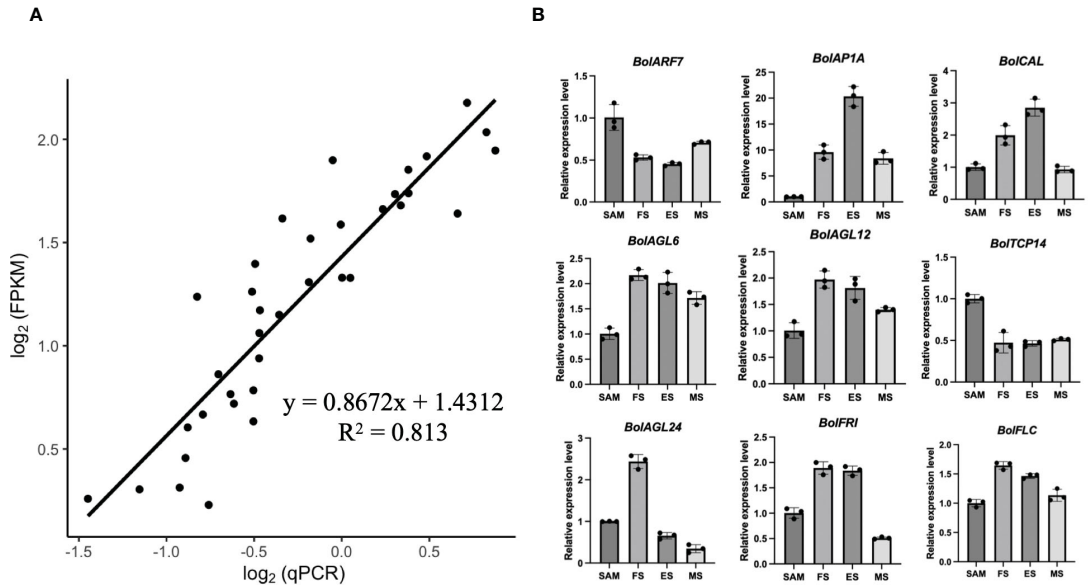

FIGURE 11
Validation of transcriptional expression levels of the representative DEGs by qRT-PCR. **(A)** The correlation between transcriptional data and qRT-PCR mean values for the nine DEGs; **(B)** qRT-PCR analysis of the representative DEGs (Bar graphs with error bars depict the mean and standard deviation values).

act as transcriptional repressors (Cheng et al., 2021), inhibiting *BolARF* activity and the transcription of AUX-responsive genes by competing with ARF proteins to bind to the SCFTIR1/AFB complex (Figueiredo and Strader, 2022). The high expression of *BolAUX/IAA* in SAM may be one of the main reasons for the abnormal differentiation of the SAM of the curd (Figure 12). Conversely, *BolNPR5*, a negative regulator of the AUX signal transduction pathway, upregulated at the development stage (Figure 12),

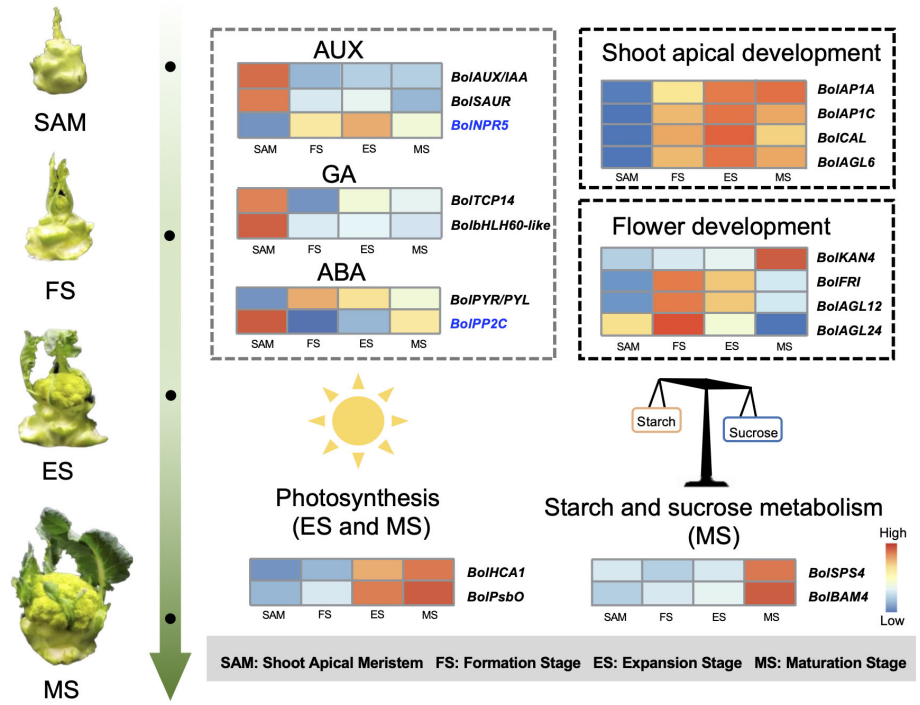

FIGURE 12
Pattern diagram of key regulatory factors at SAM stage and curd development stages (The genes marked in blue represent negative regulatory factors related to specific hormones.).

appears to fine-tune the AUX signal transduction, balancing growth-promoting and inhibitory processes (Wang et al., 2015).

GA is known to regulate the SAM proliferation and differentiation (Song et al., 2022). GA-regulated class I TCP-DELLA interactions regulate the development of inflorescence stem apex (Davière et al., 2014). Low expression of *BolTCP14* at curd development stages suggests the accumulation of DELLA proteins, which could be a primary reason for inhibiting the elongation of inflorescence stems and internodes (Figure 3C). bHLH60 could interact with DELLA and positively regulate GA-mediated flowering by upregulating *FT* in *Arabidopsis* (Li et al., 2017). The sustained low expression of the *BolbHLH60* during the three stages of curd development may be one of the main reasons for the abnormal differentiation of the apical meristem. In the ABA signal pathway, ABA negative regulatory protein coding gene *BolPP2C* were highly expressed at SAM stage, but significantly downregulated at curd development stages (Figure 12), while the positive regulator *BolPYR/PYL* was upregulated (Figure 12), which means genes associated with ABA positively regulate the formation and development of the curd. Therefore, the high expression of AUX and GA-related DEGs at the SAM stage may primarily contribute to the regulation of SAM proliferation, the subsequent sustained low expression during development stages may be one of the main reasons for abnormal differentiation of apical meristem. DEGs related to ABA are closely associated with the differentiation of SAM into IM in the curd.

4.2 Several genes play key regulatory roles in curd development

In this study, most of the genes related to the reproductive shoot system development and flower development was significantly upregulated at the FS, ES and MS, including key genes like *BolLRP1*, *BolFAS1*, *BolEMS1*, *BolFRI*, *BolAP1A*, *BolAP1C*, *BolCAL* and *BolAGL6* (Figures 5A, B). Studies have shown that *BobAP1* and *BobCAL* are the dominant regulators of the floral development cessation of cauliflower (Bowman et al., 1993; Kempin et al., 1995). *BobCAL*-transformed cauliflowers were unable to form curds, but instead produced green, loose inflorescences composed of flower buds (Zhao et al., 2003). Subsequent studies further confirmed that *BobCAL* plays a key regulatory role in the curd formation of cauliflower (Goslin et al., 2017; Azpeitia et al., 2021). In this study, *BolAP1* and *BolCAL* were significantly upregulated at the FS, ES and MS compared to SAM (Figure 12), indicating their potential role in the curd formation and expansion. AGL6, along with AP1 and CAL, belongs to the MADS-box family, plays a role in lateral and floral organ development in *Arabidopsis*, interacting with proteins like SEP1, SEP3, SHP2, AP1, FUL, SVP, AGL24, and AGL42 (Koo et al., 2010). However, the function of *BolAGL6* in broccoli curd development is not yet clear. In this study, the high expression of *BolAGL6* during the three stages of curd development suggests that *BolAGL6* may be involved in the proliferation and differentiation processes of the IM in the curd (Figure 6B).

Analysis in this study revealed differential expression of genes like *BolFRI*, *BolAGL12*, *BolAGL24*, and *BolLRP1* in the flower development (Figure 9B). Among them, *BolFRI* was significantly upregulated at the MS, potentially influencing the expression of *BolFLC* to inhibit flowering. Conversely, *BolAGL12* and *BolAGL24* regulate the development of FM were significantly downregulated at the MS, likely contributing to the developmental cessation of broccoli curds during the formation of immature buds. The synergistic/antagonistic regulatory effects between these DEGs provide crucial insights into the establishment of broccoli curd morphology.

4.3 Expression patterns of representative genes in the meristem of the curd

In *Arabidopsis*, the SAM transitions from the juvenile vegetative meristem (JVM) to the adult vegetative meristem (AVM), and then develops into the inflorescence meristem (IM) and the lateral floral meristems (FM) (Kaufmann et al., 2010; Huijser and Schmid, 2011). We found significant differences in the expression patterns of key genes in the meristems at different stages of broccoli compared to *Arabidopsis*. For instance, *AtAP2L* shows upregulation during the transition from IM to FM in *Arabidopsis* (Chávez-Hernández et al., 2022), whereas its expression starts to decline at the FS in broccoli (Supplementary Figure 4). Conversely, *AtTFL1* is significantly downregulated at the FM stage in *Arabidopsis*, but the expression of *BolTFL1* in broccoli begins to increase significantly when the curd begins to form, possibly contributing to the abnormal IM differentiation (Supplementary Figure 4). Additionally, *AtAGL24* and *AtFLC* do not show significant changes at the FM stage compared to the IM stage in *Arabidopsis*, but *BolAGL24* and *BolFLC* start to show significant upregulation at FS (Supplementary Figure 4), possibly supporting the dense formation of small flower buds in broccoli. In addition, we analyzed the expression patterns of some homolog-specific genes, and found that there were some small changes in the expression patterns of homologous genes, but the overall expression patterns were similar (Supplementary Figure 5).

4.4 Photosynthesis and Starch and sucrose metabolism facilitating the enlargement and maturation of the curd

Photosynthesis, a crucial chemical reaction in plants, enables the conversion of carbon dioxide and water into energy-rich organic compounds and oxygen through the utilization of light energy by chloroplasts (Kaiser et al., 2019). At the FS, the inflorescence apical meristem of the curd temporarily loses the ability to differentiate into floral organs, but continues to differentiate into secondary IMs. During the subsequent development of the curd, the IM regains the ability to differentiate into FMs. The ongoing photosynthetic activity during this period accumulates energy necessary for the continuous differentiation of floral organs, contributing to the curd's enlargement.

From the curd enlargement stage, photosynthesis emerges as a key process, capturing sunlight energy and converting it into chemical energy, and then through the action of a series of enzymes, excess glucose is converted into starch and stored in chloroplasts and plastids (Lebon et al., 2005; Ning et al., 2020). At night or when photosynthesis is limited, plants break down starch back into glucose and then further synthesize into sucrose to meet their energy and carbon needs (Delatte et al., 2006). The activity and expression level of *BolSPS4* and *BolBAM4* are closely related to the relative ratio of starch and sucrose. Increased activity of SPS4 enzyme may lead to higher sucrose accumulation and lower starch accumulation (Li et al., 2018), and BAM4 is a starch-degrading factor, *bam4* mutants display a starch-excess phenotype (David et al., 2022). Notably, the expression of *BolSPS4* and *BolBAM4* were significantly higher at the MS compared to earlier stages (Figure 10B), suggesting that broccoli may shift towards decomposing starch into small carbon metabolites to provide energy. It is speculated that in the curd development stage, starch and sucrose metabolism supplies energy for the differentiation of FMs, thus promoting curd maturation. This interplay of photosynthesis and carbohydrate metabolism underscores their pivotal roles in the complex process of broccoli curd development.

5 Conclusion

This study obtained 350,731,464 clean reads through transcriptome sequencing of broccoli curd at different stages. It is suggested that the roles of *BolAP1A*, *BolAP1C*, *BolCAL*, and *BolAGL6* in the abnormal differentiation of SAM, as well as the involvement of *BolKAN4*, *BolFRI, BolAGL12*, and *BolAGL24* in the development of FM in the broccoli curd. Additionally, the study emphasizes the importance of phytohormones such as AUX, GA, and ABA in SAM proliferation and differentiation, as well as the significant roles of photosynthesis and starch and sucrose metabolism related genes in curd expansion and maturation (Figure 12). These insights significantly contribute to understanding the molecular basis of broccoli curd formation and the unique reproductive development of cruciferous plants.

Data availability statement

The data presented in the study are deposited in the NCBI repository, accession number PRJNA1087260.

Author contributions

YZ: Conceptualization, Writing – original draft, Data curation. CL: Software, Writing – review & editing. MZ: Methodology, Writing – review & editing. YD: Investigation, Writing – review & editing. JX: Investigation, Methodology, Writing – review & editing. CW: Conceptualization, Funding acquisition, Resources, Supervision, Writing – review & editing.

Funding

The author(s) declare financial support was received for the research, authorship, and/or publication of this article. This work was supported by the Sci-Tech Innovation 2030 Agenda (No. 2023ZD040590301), the Science and Technology Foundation of Tianjin, China (No. 23YFZCSN00190) and the Natural Science Foundation of China (No. 31872115).

Acknowledgments

We are grateful to Hanmin Jiang of Tianjin Kernel Vegetable Research Institute, Tianjin, China, for kindly providing the homozygous broccoli seeds. Furthermore, we thank Dr. Husain Ahmad for editing this manuscript.

Conflict of interest

The authors declare that the research was conducted in the absence of any commercial or financial relationships that could be construed as a potential conflict of interest.

Publisher's note

Supplementary material

The Supplementary Material for this article can be found online at: https://www.frontiersin.org/articles/10.3389/fpls.2024.1418319/full#supplementary-material.

References

Anthony, R. G., James, P. E., and Jordan, B. R. (1996). Cauliflower (*Brassica oleracea* var. *Botrytis* L.) curd development: The expression of meristem identity genes. *J. Exp. Bot.* 47, 181–188. doi: 10.1093/jxb/47.2.181

Azpeitia, E., Tichtinsky, G., Masson, M. L., Serrano-Mislata, A., and Parcy, F. (2021). Cauliflower fractal forms arise from perturbations of floral gene networks. *Science* 373, 192–197. doi: 10.1126/science.abg5999

Bowman, J. L., Alvarez, J., Weigel, D., Meyerowitz, E. M., and Smyth, D. R. (1993). Control of flower development in *Arabidopsis thaliana* by *APETALA1* and interacting genes. *Development* 119, 721–743. doi: 10.1242/dev.119.3.721

Cao, W., Cao, B., Wang, X., Bai, J., Xu, Y. Z., Zhao, J., et al. (2020). Alternatively spliced *BobCAL* transcripts alter curd morphotypes in a collection of Chinese cauliflower accessions. *Hortic. Res.* 7, 160. doi: 10.1038/s41438-020-00378-x

Chávez-Hernández, E. C., Quiroz, S., García-Ponce, B., and Álvarez-Buylla, E. R. (2022). The flowering transition pathways converge into a complex gene regulatory network that underlies the phase changes of the shoot apical meristem in *Arabidopsis thaliana*. *Front. Plant Sci.* 13. doi: 10.3389/fpls.2022.852047

Cheng, W., Zhang, M., Cheng, T., Wang, J., and Zhang, Q. (2021). Genome-wide identification of AUX/IAA gene family and their expression analysis in *prunus mume*. *Front. Genet.* 13. doi: 10.3389/fgene.2022.1013822

Cheng, Y. F., and Zhao, Y. D. (2007). A role for auxin in flower development. *J. Integr. Plant Biol.* 49, 99–104. doi: 10.1111/j.1672-9072.2007.00412.x

David, L. C., Lee, S. K., Bruderer, E., Abt, M. R., Fischer-Stettler, M., Tschopp, M. A., et al. (2022). BETA-AMYLASE9 is a plastidial nonenzymatic regulator of leaf starch degradation. *Plant Physiol.* 188, 191–207. doi: 10.1093/plphys/kiab468

Davière, J.-M., Wild, M., Regnault, T., Baumberger, N., Eisler, H., Genschik, P., et al. (2014). Class I TCP-DELLA interactions in inflorescence shoot apex determine plant height. *Curr. Biol.* 24, 1923–1928. doi: 10.1016/j.cub.2014.07.012

Davis, S. J. (2009). Integrating hormones into the floral-transition pathway of *Arabidopsis thaliana*. *Plant Cell Environ.* 32, 1201–1210. doi: 10.1111/j.1365-3040.2009.01968.x

Delatte, T., Umhang, M., Trevisan, M., Eicke, S., Thorneycroft, D., Smith, S. M., et al. (2006). Evidence for distinct mechanisms of starch granule breakdown in plants. *J. Biol. Chem.* 281, 12050–12059. doi: 10.1074/jbc.M513661200

Figueiredo, M.R.A. d., and Strader, L. C. (2022). Intrinsic and extrinsic regulators of AUX/IAA protein degradation dynamics. *Trends Biochem. Sci.* 47, 865–874. doi: 10.1016/j.tibs.2022.06.004

Fujime, Y., and Hirose, T. (1980). Studies on thermal conditions of curd formation and development in cauliflower and broccoli. II. Effects of diurnal variation of temperature on curd formation. *J. Jpn. Soc Hortic. Sci.* 49, 217–227. doi: 10.2503/jjshs.49.217

Goslin, K., Zheng, B., Serrano-Mislata, A., Rae, L., Ryan, P. T., Kwaniewska, K., et al. (2017). Transcription factor interplay between LEAFY and APETALA1/CAULIFLOWER during floral initiation. *Plant Physiol.* 174, 1097–1109. doi: 10.1104/pp.17.00098

Guilfoyle, T. J. (2015). The PB1 domain in auxin response factor and Aux/IAA proteins: a versatile protein interaction module in the auxin response. *Plant Cell.* 27, 33–43. doi: 10.1105/tpc.114.132753

Guo, N., Wang, S., Gao, L., Liu, Y., Duan, M., Wang, G., et al. (2021). Genome sequencing sheds light on the contribution of structural variants to *Brassica oleracea* diversification. *Cold Sbpring Harbor La.* 19, 93. doi: 10.1186/s12915-021-01031-2

Hou, Z. X., and Huang, W. D. (2005). Immunohistochemical localization of IAA and ABP1 in strawberry shoot apexes during floral induction. *Planta* 222, 678–687. doi: 10.1007/s00425-005-0014-1

Huijser, P., and Schmid, M. (2011). The control of developmental phase transitions in plants. *Development* 138, 4117–4129. doi: 10.1242/dev.063511

Irwin, J. A., Soumpourou, E., Lister, C., Ligthart, J.-D., Kennedy, S., and Dean, C. (2016). Nucleotide polymorphism affecting *FLC* expression underpins heading date variation in horticultural brassicas. *Plant J.* 87, 597–605. doi: 10.1111/tpj.13221

Jiang, H., Liu, L., Shan, X., Wen, Z., Zhang, X., Yao, X., et al. (2022). Genome-wide identification and expression analysis of the bHLH gene family in cauliflower (*Brassica oleracea L.*). *Physiol. Mol. Biol. Plants* 28, 1737–1751. doi: 10.1007/s12298-022-01238-9

Kaiser, E., Galvis, V. C., and Armbruster, U. (2019). Efficient photosynthesis in dynamic light environments: A chloroplast's perspective. *Biochem. J.* 476, 2725–2741. doi: 10.1042/BCJ20190134

Kaufmann, K., Pajoro, A., and Angenent, G. C. (2010). Regulation of transcription in plants: mechanisms controlling developmental switches. *Nat. Rev. Genet.* 11, 830–842. doi: 10.1038/nrg2885

Kempin, S. A., Savidge, B., and Yanofsky, M. F. (1995). Molecular basis of the *cauliflower* phenotype in *Arabidopsis*. *Science* 267, 522–525. doi: 10.1126/science.7824951

Kieffer, M., Fuller, M. P., and Jellings, A. J. (1996). Mathematical model of cauliflower curd architecture based on biometrical analysis. *Acta Hortic.* 407, 361–368. doi: 10.17660/ActaHortic.1996.407.46

Kieffer, M., Fuller, M., and Jellings, A. (1998). Explaining curd and spear geometry in broccoli, cauliflower and 'romanesco': Quantitative variation in activity of primary meristems. *Planta* 206, 34–43. doi: 10.1007/s004250050371

Koo, S. C., Bracko, O., Park, M. S., Schwab, R., and Kim, M. C. (2010). Control of lateral organ development and flowering time by the *Arabidopsis thaliana* MADs-box gene AGAMOUS-LIKE6. *Plant J. Cell Mol. Biol.* 62, 807–816. doi: 10.1111/tpj.2010.62.issue-5

Kwaniewska, K., Breathnach, C., Fitzsimons, C., Goslin, K., and Wellmer, F. (2021). Expression of *KNUCKLES* in the stem cell domain is required for its function in the control of floral meristem activity in *Arabidopsis*. *Front. Plant Sci.* 23. doi: 10.3389/fpls.2021.704351

Lan, T. H., and Paterson, A. H. (2000). Comparative mapping of quantitative trait loci sculpting the curd of Brassica oleracea. *Genetics* 155, 1927. doi: 10.1017/S0016672300004560

Lebon, G., Brun, O., Magné, C., and Clément, C. (2005). Photosynthesis of the grapevine (*Vitis vinifera*) inflorescence. *Tree Physiol.* 25, 633–639. doi: 10.1093/treephys/25.5.633

Lenhard, M., Bohnert, A., Jürgens, G., and Laux, T. (2001). Termination of stem cell maintenance in *Arabidopsis* floral meristems by interactions between WUSCHEL and AGAMOUS. *Cell* 105, 805–814. doi: 10.1016/S0092-8674(01)00390-7

Li, X., Du, J., Guo, J., Wang, H., Ma, S., Lü, J., et al. (2018). The functions of *cucumber sucrose phosphate synthases 4* (*CsSPS4*) in carbon metabolism and transport in sucrose- and stachyose-transporting plants. *J. Plant Physiol.* 228, 150–157. doi: 10.1016/j.jplph.2018.05.013

Li, Y., Wang, H., Li, X., Liang, G., and Yu., D. (2017). Two della-interacting proteins bhlh48 and bhlh60 regulate flowering under long-day conditions in *arabidopsis thaliana*. *J. Exp. Bot.* 68, 2757–2767. doi: 10.1093/jxb/erx143

Li, H., Xia, Y., Liu, H. Y., Guo, H., He, X. Q., Liu, Y., et al. (2022). Nutritional values, beneficial effects, and food applications of broccoli (*Brassica oleracea* var. *Italica plenck*). *Trends Food Sci. Technol.* 119, 288–308. doi: 10.1016/j.tifs.2021.12.015

Liu, X., Wu, J., Ji, F., Cao, X., Zhao, Q., Cheng, C., et al. (2022). Transcriptomic profiling of rose flower under treatment of various phytohormones and plant growth regulators. *Sci. Data* 9, 669. doi: 10.1038/s41597-022-01800-w

Love, M. I., Huber, W., and Anders, S. (2014). Moderated estimation of fold change and dispersion for rna-seq data with deseq2. *Genome Biol.* 15, 550. doi: 10.1186/s13059-014-0550-8

Luo, J., Zhou, J. J., and Zhang, J. Z. (2018). *Aux/IAA* gene family in plants: Molecular structure, regulation, and function. *Int. J. Mol. Sci.* 19, 259. doi: 10.3390/ijms19010259

Mayer, K. F. X., Schoof, H., Haecker, A., Lenhard, M., Jürgens, G., and Laux, T. (1998). Role of *WUSCHEL* in regulating stem cell fate in the *Arabidopsis* shoot meristem. *Cell* 95, 805–815. doi: 10.1016/S0092-8674(00)81703-1

Ning, G., Yan, X., Chen, H., Dong, R., and Jin, S. (2020). Genetic manipulation of *SOC1*-like genes promotes photosynthesis in flowers and leaves and enhances plant tolerance to high temperature. *Plant Biotechnol. J.* 19, 8–10. doi: 10.1111/pbi.13432

Parkin, I. A., Koh, C., Tang, H., Robinson, S. J., Kagale, S., Clarke, W. E., et al. (2014). Transcriptome and methylome profiling reveals relics of genome dominance in the mesopolyploid *Brassica oleracea*. *Genome Biol.* 15, R77. doi: 10.1186/gb-2014-15-6-r77

Payne, T., Johnson, S. D., and Koltunow, A. M. (2004). *KNUCKLES* (*KNU*) encodes a C_2H_2 zinc-finger protein that regulates development of basal pattern elements of the Arabidopsis gynoecium. *Development* 131, 3737–3749. doi: 10.1242/dev.01216

Prunet, N., Morel, P., Thierry, A. M., Eshed, Y., Bowman, J. L., Negrutiu, I., et al. (2008). *REBELOTE*, *SQUINT*, and *ULTRAPETALA1* function redundantly in the temporal regulation of floral meristem termination in *Arabidopsis thaliana*. *Plant Cell* 95, 805–815. doi: 10.1105/tpc.107.053306

Rosen, A., Hasan, Y., Briggs, W., and Uptmoor, R. (2018). Genome-based prediction of time to curd induction in cauliflower. *Front. Plant Sci.* 9. doi: 10.3389/fpls.2018.00078

Sadik, S. (1962). Morphology of the curd of cauliflower. *Am. J. Bot.* 49, 290–297. doi: 10.1002/j.1537-2197.1962.tb14940.x

Sadik, S. (1968). Development of vegetative and reproductive apices of cauliflower (*Brassica oleracea* var. *Botrytis.*). *Bot. Gaz.* 129, 365–370. doi: 10.1086/336458

Serrano-Mislata, A., Goslin, K., Zheng, B., Rae, L., Wellmer, F., Graciet, E., et al. (2017). Regulatory interplay between LEAFY, APETALA1/CAULIFLOWER and TERMINAL FLOWER1: New insights into an old relationship. *Plant Signal Behav.* 12, e1370164. doi: 10.1080/15592324.2017.1370164

Shumate, A., Wong, B., Pertea, G., and Pertea, M. (2022). Improved transcriptome assembly using a hybrid of long and short reads with stringtie. *PloS Comp. Biol.* 18, e1009730. doi: 10.1371/journal.pcbi.1009730

Smyth, D. R. (1995). Flower development: Origin of the cauliflower. *Curr. Biol.* 5, 361–363. doi: 10.1016/S0960-9822(95)00072-8

Song, S., Huang, B., Pan, Z., Zhong, Q., Yang, Y., Chen, D., et al. (2022). The SlTPL3–SlWUS module regulates multi-locule formation in tomato by modulating auxin and gibberellin levels in the shoot apical meristem. *J. Integr. Plant Biol.* 64, 18. doi: 10.1111/jipb.13347

Wang, T., Li, R., Wen, L., Fu, D., Zhu, B., Luo, Y., et al. (2015). Functional analysis and RNA sequencing indicate the regulatory role of *Argonaute1* in tomato compound leaf development. *PloS One* 10, e0140756. doi: 10.1371/journal.pone.0140756

Wang, Y., Zhang, J., Hu, Z., Guo, X., and Chen, G. (2019). Genome-Wide analysis of the MADS-Box transcription factor family in *Solanum lycopersicum*. *Int. J. Mol. Sci.* 20, 2961. doi: 10.3390/ijms20122961

Wei, S., Chen, Y., Hou, J., Yang, Y., and Yin, T. (2021). Aux/IAA and ARF Gene Families in *Salix suchowensis*: Identification, evolution, and dynamic transcriptome profiling during the plant growth process. *Front. Plant Sci.* 12. doi: 10.3389/fpls.2021.666310

Wu, T., Hu, E., Xu, S., Chen, M., and Yu, G. (2021). clusterProfiler 4.0: A universal enrichment tool for interpreting omics data. *Innovation (Camb)* 2, 11. doi: 10.1016/j.xinn.2021.100141

Xu, X., Tao, J., Xing, A., Wu, Z., Xu, Y., Sun, Y., et al. (2022). Transcriptome analysis reveals the roles of phytohormone signaling in tea plant (*Camellia sinensis* L.) flower development. *BMC Plant Biol.* 22, 471. doi: 10.1186/s12870-022-03853-w

Yamaguchi, N., Huang, J., Xu, Y., Tanoi, K., and Ito, T. (2017). Fine-tuning of auxin homeostasis governs the transition from floral stem cell maintenance to gynoecium formation. *Nat. Commun. Nat. Commun.* 8, 1125. doi: 10.1038/s41467-017-01252-6

Zhao, S., Cao, W. G., Liu, P. L., Gong, Z. H., and He, Y. K. (2003). Regulation to curd morphogenesis and genetics of exogenous bocal gene in cauliflower. *Acta Biol. Exp. Sin.* 36, 259–263.

Zhao, Z., Sheng, X., Yu, H., Wang, J., and Gu, H. (2020a). Identification of candidate genes involved in curd riceyness in cauliflower. *Int. J. Mol. Sci.* 21, 1999. doi: 10.3390/ijms21061999

Zhao, Z. Q., Sheng, X. G., Yu, H. F., Wang, J. S., Shen, Y. S., and Gu, H. H. (2020b). Identification of QTLs associated with curd architecture in cauliflower. *BMC Plant Biol.* 20, 177. doi: 10.1186/s12870-020-02377-5

frontiers | Frontiers in Plant Science

TYPE Original Research
PUBLISHED 30 August 2024
DOI 10.3389/fpls.2024.1450242

OPEN ACCESS

EDITED BY
Xiaodong Yang,
Yangzhou University, China

REVIEWED BY
Yuxiang Yuan,
Henan Academy of Sciences, China
Kengo Kanamaru,
Kobe University, Japan

*CORRESPONDENCE
Yun Zhang
zhangyun511@syau.edu.cn
Zhiyong Liu
liuzhiyong99@syau.edu.cn

RECEIVED 17 June 2024
ACCEPTED 13 August 2024
PUBLISHED 30 August 2024

CITATION
Liu C, Chai Y, Tan C, Shi F, Zhang Y and Liu Z (2024) *Brchli1* mutation induces bright yellow leaves by disrupting magnesium chelatase I subunit function in Chinese cabbage (*Brassica rapa* L. ssp. *pekinensis*). *Front. Plant Sci.* 15:1450242. doi: 10.3389/fpls.2024.1450242

Brchli1 mutation induces bright yellow leaves by disrupting magnesium chelatase I subunit function in Chinese cabbage (*Brassica rapa* L. ssp. *pekinensis*)

Chuanhong Liu[1], Yi Chai[1], Chong Tan[1], Fengyan Shi[2], Yun Zhang[1]* and Zhiyong Liu[1]*

[1]Laboratory of Vegetable Genetics Breeding and Biotechnology, Department of Horticulture, Shenyang Agricultural University, Shenyang, China, [2]Vegetable Research Institute, Liaoning Academy of Agricultural Sciences, Shenyang, China

Magnesium chelatase (MgCh) plays a pivotal role in photosynthesis, catalyzing the insertion of magnesium into protoporphyrin IX (Proto IX), a key intermediate in chlorophyll (Chl) biosynthesis. MgCh is a heteromeric complex composed of the MgCh D subunit (CHLD), the MgCh H subunit (CHLH), and the MgCh I subunit (CHLI). The *bright yellow leaves* (*byl*) mutant was obtained through ethyl methanesulfonate (EMS) mutagenesis of the 'FT' Chinese cabbage (*Brassica rapa* L. ssp. *pekinensis*) doubled haploid line, whose Chl content, net photosynthetic rate (*Pn*), and non-photochemical quenching coefficient (NPQ) were decreased, and whose chloroplast development was incomplete. *byl* recovered to a light green phenotype under weak light conditions. Genetic analysis revealed that the bright yellow leaves phenotype of *byl* was caused by a single recessive nuclear gene. Using Mutmap sequencing and Kompetitive allele-specific PCR (KASP) identification, *BraA01g010040.3.5C*, encoding the CHLI subunit of MgCh, was identified as the candidate gene and named *Brchli1*. A nonsynonymous G-to-A mutation in the *Brchli1* exon resulted in the substitution of aspartic acid with asparagine. *Brchli1*-silenced Chinese cabbage displayed bright yellow leaves with decreased *Brchli1* expression. Transiently overexpressed *Brchli1* in the *byl* mutant restored the green leaf phenotype and significantly increased relative *Brchli1* expression levels. Both BrCHLI1 and its mutated variant were localized in chloroplasts. Yeast two-hybrid and luciferase complementation imaging assays demonstrated that BrCHLI1 interacted with both BrCHLD and itself. BrCHLI1 mutations did not affect its interaction with BrCHLD. Together, *Brchli1* mutations impaired the function of MgCh, providing insights into the molecular mechanism of leaf coloration.

KEYWORDS

***Brassica rapa*, bright yellow leaves, MutMap, magnesium chelatase, CHLI, protoporphyrin, chlorophyll biosynthesis**

Introduction

Chlorophyll (Chl) is a photosynthetic pigment present in plants, algae, and certain bacteria, that plays a pivotal role in photosynthesis (Kunugi et al., 2013). Leaf color is linked to the biosynthesis of heme and Chl, both situated downstream in the tetrapyrrole degradation metabolic pathway. The biosynthetic pathways of Chl and heme both proceed from 5-aminolevulinic acid (ALA) to protoporphyrin IX (Proto IX). The divergence lies in the synthesis of Mg-Proto IX under Mg^{2+} involvement (Brzezowski et al., 2015), leading to Chl production, while heme synthesis occurs with the participation of Fe^{2+} (Masuda, 2008).

Magnesium chelatase (MgCh), a heterotrimer consisting of D, H, and I subunits, is a key enzyme in Chl synthesis found ubiquitously in photosynthetic bacteria and plants (Masuda, 2008). It catalyzes Mg^{2+} insertion into Proto IX, leading to the final synthesis of Chl (Masuda, 2008). MgCh was first discovered to possess catalytic activity in pea (Sirijovski, 2006). Enzyme-catalyzed reactions requiring ATP hydrolysis involve two steps: activation and insertion. The CHLI subunit catalyzes ATP hydrolysis (Reid et al., 2003) and stabilizes the CHLI-CHLD-Mg-ATP complex in the enzymatic reaction (Lake et al., 2004a). Glutamic acid 660 (E660) in the CHLH subunit is crucial for magnesium insertion because it binds the porphyrin in MgCh (Adams et al., 2020). The I and D subunits are members of the AAA+ family of ATPases associated with various cellular activities. They readily form hexamers or heptamers, but notably, the D subunit lacks ATPase activity, whereas the I subunit possesses it (Vale, 2000). The CHLI and CHLD subunits form an AAA+ complex in the presence of Mg^{2+} and ATP, which then interacts with the CHLH-chelating subunit to form an active chelatase (Farmer et al., 2019).

CHLI is the smallest subunit of MgCh, with a molecular weight of 38–45 kDa. It contains the structural domains Sensor I, Sensor II, Walker A, Walker B, and I Rfinger, which are involved in ATP hydrolysis. Walker A stabilizes the binding of ATP, whereas Walker B facilitates ATP hydrolysis by binding to Mg^{2+} (Jessop et al., 2021). In *Arabidopsis* and pea, the semidehydroascorbate in CHLI's C-terminal helix is easily oxidized, leading to undetectable ATPase activity in oxidizing environments. However, its interaction with thioredoxin (TRX) reductase can restore activity upon adding TRX reducing agents to oxidized CHLI (Kobayashi et al., 2008).

Numerous *CHLI* mutants have been identified that induce changes in leaf coloration. In *Arabidopsis*, insertion of a T nucleotide in *AtCHLI1* resulted in a pale green color mutation (Koncz et al., 1990); the *CHLI2* T-DNA knockout mutant was still able to accumulate a certain amount of Chl (Rissler et al., 2002); *CHLI2* aided in the construction of MgCh complexes (Kobayashi et al., 2008); double knockout mutants of *chli1* and *chli2* exhibited albino leaves (Huang and Li, 2009). In barley, ATPase activity of CHLI was essential for maintaining functionality of the D-subunit (Lake et al., 2004b). Ethyl methanesulfonate (EMS) mutagenesis in cucumber identified a mutant with yellow leaves caused by a *CsChlI* point mutation (Gao et al., 2016). Amino acid missense mutations in *ChlI* resulted in a yellow-green phenotype in rice (Zhang et al., 2006). *TaCHLI* single-nucleotide mutations in wheat were responsible for pale green leaves caused by impaired Chl synthesis (Wang et al., 2020). A mutant variant of *CHLI* with yellow-green leaves was identified in strawberries (Ma et al., 2023). However, the *CHLI* gene has not yet been studied in Chinese cabbage.

Reports indicate that certain plant phenotypes can change in response to variations in light intensity. The *immutans* mutant of *Arabidopsis* showed green leaves under low light conditions, but variegated leaves under high light conditions (Rosso et al., 2009). The Chl-less barley mutant NYB exhibited a yellower leaf color under higher light intensities (Yuan et al., 2010b). In a study on *Acer palmatum*, the 'Jingling Huangfeng' mutant displayed a yellow leaf phenotype, with leaves turning green under low light intensity conditions (Li et al., 2015). The R24 photosensitive chlorotic mutant was isolated in pepper, and under shaded low light intensity conditions the Chl content of tea was increased (Liu et al., 2018). The R24 mutant had yellow leaves under low light conditions, but the leaf color turned green and the Chl content increased with increasing light intensity (Yang et al., 2023).

The candidate gene for the golden inner leaf mutant has been identified as *BraA09g007080.3C* in Chinese cabbage (Zhang et al., 2022). Studies on the CHLI subunit in Chinese cabbage have not been reported. Here, we isolated *bright yellow leaves* (*byl*) mutant from an EMS-mutagenized population, which showed impaired chloroplast development and decreased Chl, photosynthetic rate (*Pn*), and non-photochemical quenching (NPQ). Under conditions of low light intensity, the *byl* mutant reverted to a light green phenotype. MutMap and Kompetitive Allele-Specific PCR (KASP) analyses identified *BraA01g010040.3.5C* as the candidate gene, which harbors a non-synonymous point mutation and encodes the CHLI subunit of MgCh. Silencing of *Brchli1* in Chinese cabbage plants resulted in a bright yellow leaves phenotype. Transiently overexpressed *Brchli1* in the *byl* mutant restored the green leaf phenotype and significantly increased relative *Brchli1* expression levels. Both BrCHLI1 and its mutated variant were localized in chloroplasts. Yeast two-hybrid and luciferase complementation imaging assays demonstrated that BrCHLI1 interacted with both BrCHLD and itself. BrCHLI1 mutations did not affect its interaction with BrCHLD, but impaired its interaction with itself. This study is the first to clone the *BrChli1* gene in Chinese cabbage, and the results provide insights into the molecular mechanism of leaf color formation.

Materials and methods

Plant materials

Wild-type 'FT' Chinese cabbage (*Brassica rapa* L. ssp. *pekinensis*) was obtained from microspore culture as a DH line (Huang et al., 2016). The *bright yellow leaves* (*byl*) mutant was obtained by immersing germinated seeds of 'FT' in EMS. Hybridization of *byl* with 'FT' resulted in the F_1, F_2, and BC_1 generations for genetic analysis, with the F_2 population also utilized for phenotypic identification, gene mapping, and KASP analysis.

Determination of photosynthetic pigment content

Leaves of *byl* and 'FT' at 20 days after seeding (DAS) were individually sliced into small pieces weighing 0.1 g and placed into 10 mL of 80% (v/v) acetone for dark treatment until the leaves turned white. The absorbance values of the samples at wavelengths of 663 nm, 645 nm, and 470 nm were measured using a spectrophotometer. Levels of Chl a, Chl b, and carotenoids were calculated following previously reported methods (Holm, 1954).

Measurement of photosynthesis and Chl fluorescence parameters

Ten plants each of *byl* and 'FT' (40 DAS) were selected on a sunny morning for photosynthetic parameter measurements. The sixth true leaf from each plant was used to measure photosynthetic characteristics using a Li-6800 instrument (LI-COR Biotechnology, USA). Light intensity was set to 1500 μmol m^{-2} s^{-1}. After achieving a stable net photosynthetic rate, readings for net photosynthetic rate (*Pn*), transpiration rate (*Ts*), stomatal conductance (*Ls*), and intercellular CO_2 concentration (*Ci*) were recorded.

Ten plants each of *byl* and 'FT' (40 DAS) were selected for Chl fluorescence parameter measurements as described previously (Zhao et al., 2022).

Ultrastructural observation of chloroplast

Leaves of *byl* and 'FT' plants (40DAS) were sliced into 1 mm × 2 mm pieces. Sample handling was performed as described previously (Zhao et al., 2014). The ultrastructure of chloroplasts was observed using an H-7700 TEM instrument (Hitachi, Japan).

Identification of the candidate gene

Identification of the candidate gene *Brchli1* was performed using an improved MutMap approach (Abe et al., 2012). The bright yellow leaves mutant pool was generated by pooling DNA from 70 F_2 plants displaying the bright yellow leaves phenotype. DNA extraction was performed using a DNAsecure Plant Kit (Tiangen Biotech Ltd., Beijing, China) for 'FT' and the bright yellow leaves mutant pool. Subsequent resequencing was conducted using a NovaSeq 6000 sequencer (Illumina, San Diego, California, USA). High-quality data were obtained by filtering raw data using the sliding window method with fastp (v0.20.0) (Gao et al., 2020). High-quality filtered data were aligned to the reference genome using bwa (0.7.12-r1039) (Li and Durbin, 2010). GATK (McKenna et al., 2010) was utilized for the detection of SNPs and insertions and deletions (INDELs). Functional annotation was performed using ANNOVAR (Wang et al., 2010), and Circos (Krzywinski et al., 2009) was employed to map mutation information onto the genome.

SNP genotyping by KASP

Genotype analysis was conducted using KASP to detect the co-segregation of SNPs, identifying candidate genes for *Brchli1*. The KASP experiment was conducted on 157 F_2 individuals with the bright yellow leaves phenotype and two 'FT' plants. The KASP thermal cycling conditions were set as previously described (Xi et al., 2018).

Cloning and sequencing of *Brchli1*

The DNA and coding sequences of the *Brchli1* gene from *byl* and 'FT' were amplified. The specific operational procedures were performed as described previously (Liu et al., 2021). Sequencing was performed at Sangon Biotech (Shanghai, China) using the Sanger method.

Protein characterization and phylogenetic analysis of BrCHLI1

A phylogenetic tree was constructed using the neighbor-joining method with 1000 bootstrap replicates in MEGA6.0. Multiple sequence alignment of amino acid sequences was performed using DNAMAN v6.0. Protein structural domains of BrCHLI1 were predicted using SMART (https://smart.embl-Heidelberg.de/).

VIGS analysis

To further investigate the function of *Brchli1* in response to golden Chinese cabbage leaves, a 300 bp Brchli1-specific segment was cloned into the viral vector pTRV2 following a previously described procedure (Pflieger et al., 2010). Next, pTRV2-*Brchli1*, pTRV2, and pTRV1 were individually transformed into *A. tumefaciens* GV3101 using the freeze-thaw method (Zhou et al., 2021). The GV3101 suspension containing pTRV1 was mixed in a 1:1 ratio with GV3101 suspensions containing pTRV2-*0* (empty vector) or pTRV2-*Brchli1*, and used to infect newly germinated 'FT' seeds. Each group infected 90 seeds (three replicates). Seeds were then sown in a greenhouse, and silencing efficiency was assessed 10, 20, and 30 days post-infection.

Functional validation of transient overexpression

The coding sequence of *Brchli1* lacking the stop codon was inserted into the pSuper1300-GFP (pSuper::GFP) vector, and transformed into the *byl* mutant alongside the control group pSuper::GFP using the VIGS method. Each group of 90 seeds (three replicates), which were subsequently planted in a greenhouse. Transient overexpression efficiency was evaluated at 10, 20, and 30 days after infection.

Subcellular localization of BrCHLI1 and *Brchli1*

The coding regions of the BrCHLI1 and Brchli1 sequences, excluding the stop codons, were cloned into the ProCAMV35S: BrCHLI1:GFP and ProCAMV35S:Brchli1:GFP vectors to determine the subcellular localization of the BrCHLI1 and Brchli1 proteins. After sequencing validation, vectors were transferred into *Agrobacterium tumefaciens* GV3101, and injected into tobacco leaf mesophyll cells at an OD_{600} of 0.6–0.8, followed by a 24 h dark treatment then a 24 h light treatment. The 35S-driven GFP vector served as a negative control. Fluorescence signals were observed using a confocal laser scanning microscope (Leica Microsystems, Wetzlar, Germany). The GFP fluorescence and emission signals of Chl autofluorescence were detected at wavelengths of 496–540 nm and 643–730 nm, respectively.

Y2H assays

Y2H assays were conducted following the manufacturer's instructions (Coolaber, Beijing, China). The full-length CDS of *Brchli1* was cloned into the pGBKT7 and pGADT7 vectors to obtain pGBKT7-BrCHLI1 and pGADT7-BrCHLI1. Point-mutated *Brmchli1* was cloned into the pGBKT7 vector to obtain pGBKT7-Brchli1. The full-length CDS of *Brchld* was cloned into the pGADT7 vector to obtain pGADT7-BrCHLD. pGBKT7-53 + pGADT7-T served as the positive control, while pGBKT7-Lam + pGADT7-T served as the negative control. pGBKT7-BrCHLI1 + pGADT7-BrCHLI1, pGBKT7-Brchli1 + pGADT7-BrCHLI1, pGBKT7-BrCHLI1 + pGADT7-BrMCHLD, and pGBKT7-Brchli1 + pGADT7-BrMCHLD were co-transformed into yeast competent cells (Y2HGold strain) and plated on SD/-Leu-Trp (DDO) solid medium. Positive clones were picked and transferred to SD/-Leu-Trp-His-Ade + 30 mg L^{-1} X-α-gal (QDO/X) solid medium.

Luciferase complementation imaging assays

The full-length CDS of BrCHLI1 was incorporated into the N-terminal luciferase (pCAMBIA1300-nLUC) and C-terminal luciferase (pCAMBIA1300-cLUC) vectors. Full-length CDS of BrCHLD and Brchli1 were also incorporated into the N-terminal luciferase vector. nLUC and cLUC were co-injected into tobacco leaves, followed by dark treatment for 24 h and light treatment for another 24 h at 25°C. The leaves were coated with a solution of potassium luciferin and observed using a Night Shade LB 985 system (Berthold, Bad Wildbad, Germany).

qRT-PCR

RNA extracted from the leaves of 'FT' was subsequently reverse-transcribed into cDNA. qRT-PCR was conducted using Ultra SYBR Green Mix (Kangwei Century, Beijing, China) and a QuantStudio 6 PCR system. *ACTIN* was employed as an internal control. Relative expression levels were calculated using the $2^{-\Delta\Delta Ct}$ method.

Results

Bright yellow leaves and impaired chloroplast development in *byl*

The *bright yellow leaves* (*byl*) mutant was obtained by EMS mutagenesis of DH line 'FT' seeds. Compared with the green leaves of 'FT', *byl* leaves were golden, with no impact on growth and development (Figure 1A). To investigate the effect of *byl* on chloroplast development, transmission electron microscopy (TEM) was used to observe chloroplasts in 'FT' and *byl* leaves, revealing fewer and sparser stacked layers of thylakoid grana in *byl* compared to the well-organized grana observed in 'FT' (Figure 1B). Levels of Chl*a*, Chl*b*, and Car in *byl* were significantly lower than in 'FT', suggesting a potential association between the bright yellow leaves phenotype of *byl* and insufficient Chl accumulation (Figure 1C). The *byl* mutant had a significantly lower net photosynthetic rate (*Pn*), stomatal conductance (*Gs*), and transpiration rate (*Ts*) than 'FT'. In addition, the intercellular CO_2 concentration (*Ci*) was higher in *byl* than in 'FT'. These results suggest that the reduced photosynthetic pigment content in *byl* may have impaired *Pn*. The higher *Ci* in *byl* indicated a lower CO_2 utilization efficiency, leading to a reduction in *Pn* (Supplementary Table 1). The values of minimum fluorescence under dark adaptation (F_0), maximum fluorescence under dark adaptation (Fm), minimum fluorescence under light adaptation (F_0'), maximum fluorescence under light adaptation (Fm'), actual photochemical efficiency of PSII (Φ_{PSII}), photochemical quenching (Qp), and non-photochemical quenching (NPQ) in *byl* were significantly lower than in 'FT', consistent with the reduction in Chl content in *byl* leaves (Figure 1D).

Genetic analysis of the offspring of *byl* and 'FT' showed that leaves of the F_1 generation plants were all green. In the F_2 generation population, there were 571 green-leaved plants and 201 golden-leaved plants, conforming to a 3:1 ratio ($\chi^2 = 0.44$). This implies that the bright yellow leaves mutation trait in *byl* is controlled by a pair of recessive nuclear genes (Supplementary Table 2).

byl turned light green in low light intensity

The *byl* mutant displayed distinct phenotypes under different light intensities, exhibiting bright yellow leaves in high light intensity (320 μmol m^{-2} s^{-1}) and lighter green in low light intensity (40 μmol m^{-2} s^{-1}). 'FT' and *byl* were cultured for 10 days under light intensities of 320 μmol m^{-2} s^{-1} and 40 μmol m^{-2} s^{-1}, respectively; *byl* exhibited a change in leaf color, while 'FT' remained unaffected (Figure 1E). TEM revealed *byl* chloroplasts returning to normal under low light intensity (Figure 1F). At 40 μmol m^{-2} s^{-1} light intensity, there was a significant increase in levels of Chl*a*, Chl*b*, and Car in *byl* (Figure 1G), indicating an enhancement in photosynthetic pigment content under low light conditions. Moreover, *byl* exhibited significant increases in *Pn*, *Gs*, and *E* (Supplementary Table 3), along with significant elevations in F_0, Fm, F_0', Fm', Φ_{PSII}, Qp, and NPQ (Figure 1H). The increase in photosynthetic pigment content under 40 μmol m^{-2} s^{-1} light intensity also enhanced the photosynthetic rate of *byl*.

10.3389/fpls.2024.1450242

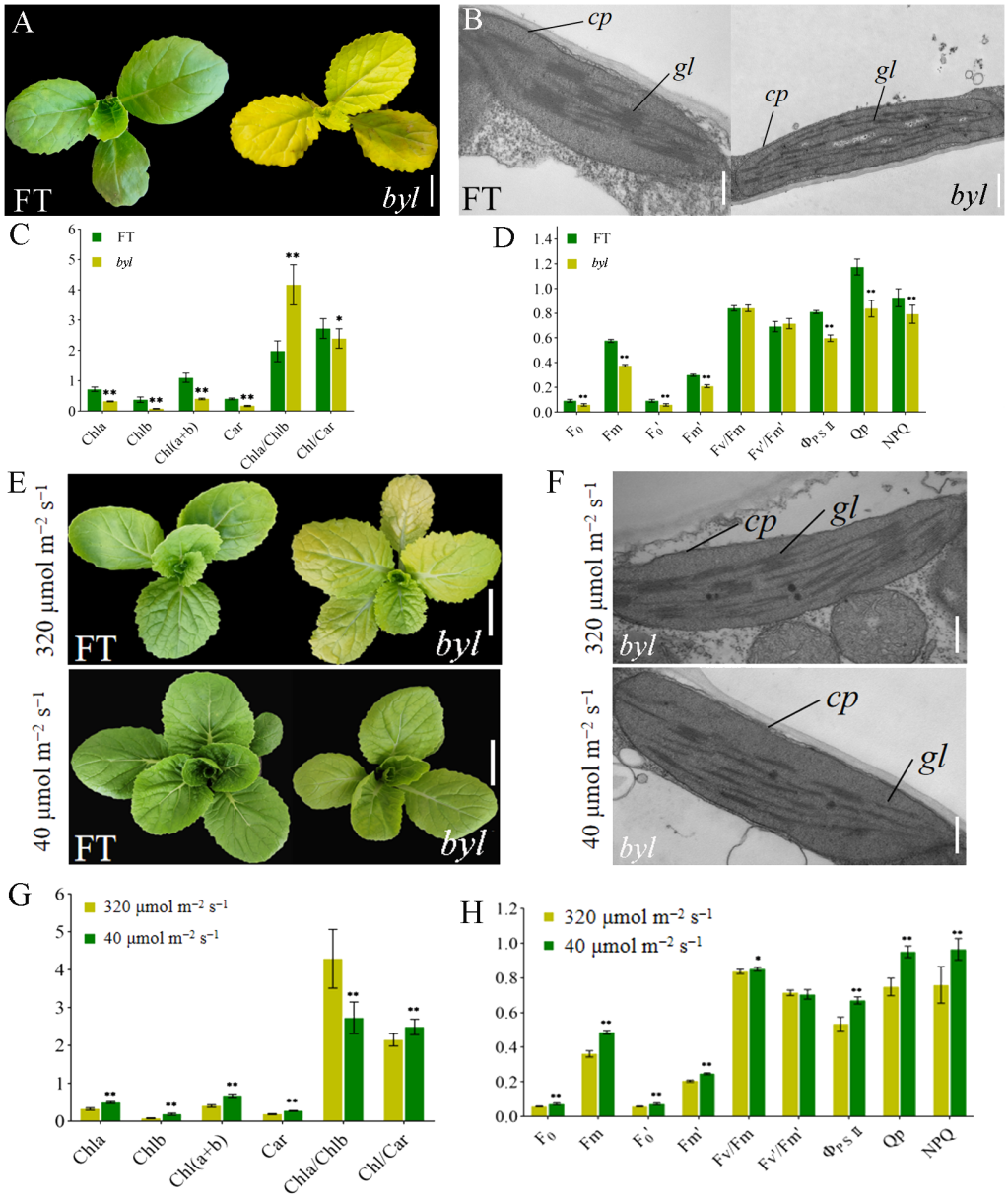

FIGURE 1
Morphological characteristics of 'FT' and *byl*. **(A)** Phenotypic observations of 'FT' and *byl* 20 days after sowing. Scale bar = 1 cm. **(B)** TEM observations of 'FT' and *byl*. Scale bar = 200 nm. Note: *cp* chloroplast, *gl* grana lamella. **(C)** Photosynthetic pigment content in 'FT' and *byl*. * represents significant differences at $p < 0.05$ (Student's t-test), ** represents significant differences at $p < 0.01$. **(D)** Fluorescence dynamics parameters of 'FT' and *byl*. ** represents significant differences at $p < 0.01$. **(E)** Phenotypic observations of 'FT' and *byl* under varying light intensities. Scale bar = 1 cm. **(F)** TEM observations of 'FT' and *byl* under varying light intensities. Scale bar = 200 nm. *cp*, chloroplast; *gl*, grana lamella. * represents significant differences at $p < 0.05$ (Student's t-test), **(G)** Photosynthetic pigment content in *byl* under varying light intensities. ** represents significant differences at $p < 0.01$. **(H)** Fluorescence dynamics parameters of *byl* under varying light intensities. * represents significant differences at $p < 0.05$ (Student's t-test), ** represents significant differences at $p < 0.01$.

Identification of the candidate gene for *Brchli1*

We employed a modified MutMap method to identify the candidate gene. Via resequencing we obtained 175,935,758 (95.25%) and 162,498,262 (96.23%) HQ_Reads for 'FT' and the mutant pool, respectively, of which 93.06% and 93.07% were aligned to the Brara_Chiifu_V3.5 reference genome. Single-nucleotide polymorphisms (SNPs) between 'FT' and the mutant pool were detected and filtered, resulting in 366,300 SNPs located in exons. SNP-index was computed and filtered, followed by plotting its distribution across the chromosome (Figure 2A). Using a 0.95 SNP index as the threshold, we identified a candidate region of 5.6 Mb (2,000,000 –7,600,000) on chromosome A01. Within the candidate interval, there were 58 SNPs, 12 of which were located in exonic regions, including three non-synonymous mutations (Supplementary Table 4).

To further validate the candidate SNPs, we conducted KASP genotyping on three non-synonymous mutation SNPs using a

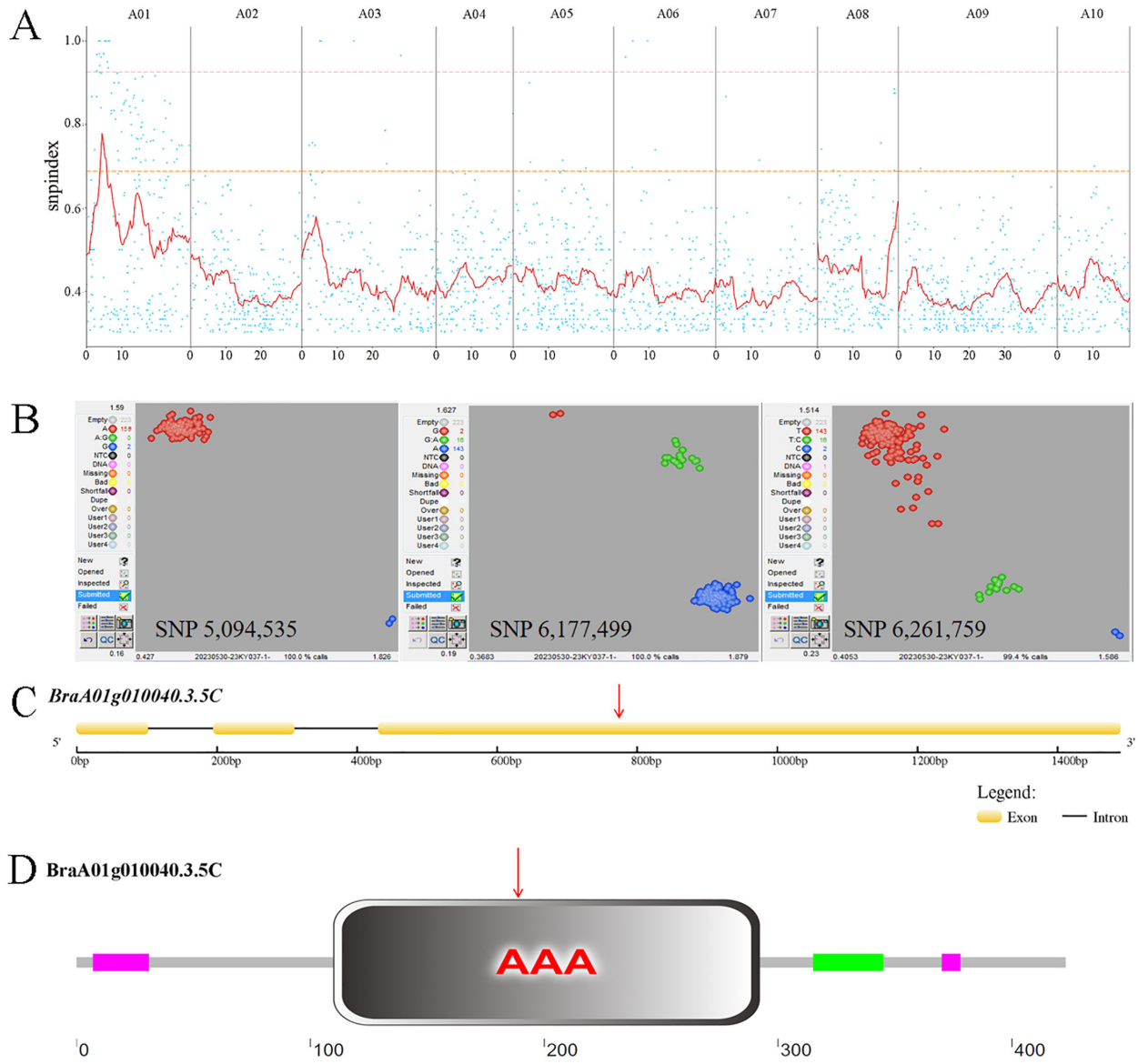

FIGURE 2
MutMap SNP index plot and KASP genotyping. **(A)** MutMap SNP index plot. Dots represent SNP-index values, the red line represents the mean SNP-index within the window, the pink line corresponds to the threshold line at the 99th percentile, and the orange line corresponds to the threshold line at the 95th percentile. **(B)** KASP genotyping of three candidate SNPs. In SNP 5,094,535, red dots represent the A:A genotype and blue dots represent the G:G genotype. In SNP 6,177,499, red dots represent the G:G genotype, green dots represent the G:A genotype, and blue dots represent the A:A genotype. In SNP 6,261,759, red dots represent the T:T genotype, green dots represent the T:C genotype, and blue dots represent the C:C genotype. **(C)** *Brchli1* gene structure. Red arrows indicate the mutation sites. **(D)** Domain distribution of BrCHLI1. Red arrows indicate the mutation sites.

population of two 'FT' and 159 F_2 generation individuals with the mutant phenotype. The results indicated that only SNP 5,094,535 within *BraA01g010040.3.5C* co-segregates with the mutant phenotype, with all mutants being A:A and both wild-type 'FT' plants being G:G. By contrast, both SNP 6,177,499 and SNP 6,261,759 exhibited recombinants, with both showing 16 G:A genotypes in mutant phenotype plants (Figure 2B). The homologous gene of *BraA01g010040.3.5C* in *Arabidopsis*, *AT4G18480*, encodes the CHLI subunit of Mgch, which is required for Chl biosynthesis. Therefore, we hypothesized that *BraA01g010040.3.5C* was a candidate gene for *Brchli1*.

Cloning and sequence analysis of *Brchli1*

The full-length and coding sequence (CDS) of *BraA01g010040.3.5C* were cloned from 'FT' and *byl*, revealing that *BraA01g010040.3.5C* spans 1666 bp with a CDS of 1272 bp encoding 424 amino acids (Figure 2C). This gene consisted of three exons and two introns, with a G to A mutation at position 783 (Supplementary Figure S1) that changes the GAT codon to AAT (Figure 2D), causing substitution of aspartic acid (Asp) with asparagine (Asn). The mutation site of *Brchli1* is located on the conserved domain AAA of BrCHLI1.

Functional verification of *Brchli1*

To further confirm whether *Brchli1* was responsible for the bright yellow leaves phenotype of the *byl* mutant, a pTRV2-*Brchli1* recombinant vector was constructed (Figure 3A). We assessed gene silencing efficiency at 10, 20, and 30 days following virus-induced gene silencing (VIGS) treatment. Unlike the TRV::*0* group, the TRV::*Brchli1* silencing group displayed bright yellow leaves (Figure 3B). At 10 days post-treatment, there was no significant difference in *Brchli1* expression between TRV::*0* and TRV::*Brchli1*. By day 20, *Brchli1* expression was significantly decreased in TRV::*Brchli1* compared to the blank control, with the most pronounced decrease observed after 30 days (Figure 3C).

Additionally, we transiently overexpressed the vector pSuper::*Brchli1-GFP* in the mutant *byl* (Figure 3D). The results indicated that *byl* plant containing pSuper::*Brchli1-GFP* exhibited restored green leaf phenotype (Figure 3E), accompanied by a significant increase in relative expression levels of *Brchli1* (Figure 3F). These results implied that *Brchli1* is the causative factor for the bright yellow leaves of the *byl* mutant.

Phylogenetic and structural analysis of BrCHLI1

The BrCHLI1 protein comprises 423 amino acids with a molecular weight of 45.9 kDa and a theoretical isoelectric point of 6.41. A phylogenetic tree was constructed to elucidate the evolutionary relationships between BrCHLI1 homologous sequences in different species, revealing high homology among various crops of the *Brassicaceae* family (Figure 4A). The AAA domain of the BrCHLI1 protein is highly conserved across *Cruciferae* species (Figure 4B).

Brchli1 exhibits high expression in leaves

We quantified the relative transcription levels of *Brchli1* across diverse plant organs using quantitative reverse transcription PCR (qRT-PCR) to explore its physiological functionality. In 'FT', expression of *Brchli1* was highest in leaves, followed sequentially by stems, buds, flowers, and siliques, with lowest expression in roots (Figure 4C). Hence, *Brchli1* plays a significant role in Chinese cabbage leaves.

Subcellular localization of BrCHLI1 and *Brchli1* within chloroplasts

To ascertain whether the mutation in BrCHLI1 affected its expression localization, BrCHLI1-green fluorescent protein (GFP) and the mutated Brchli1-GFP were introduced into tobacco, and their co-localization with chloroplast autofluorescence was assessed. The results demonstrated that the GFP fluorescence of both BrCHLI1 and Brchli1 was localized within chloroplasts (Figure 5), with the mutation in BrCHLI1 having no effect on the localization.

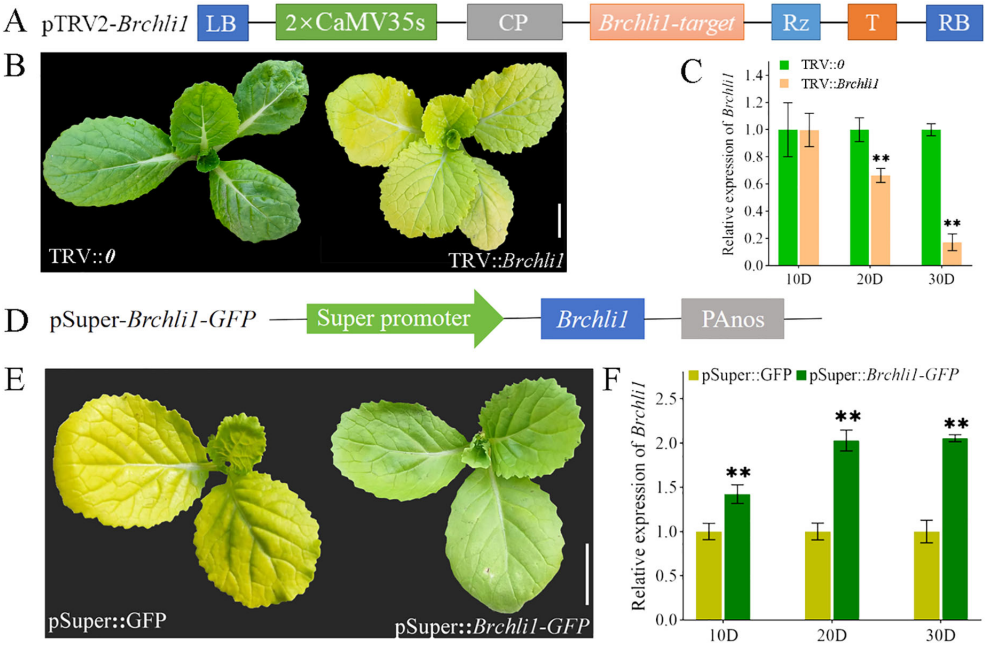

FIGURE 3
Silencing and transient overexpression of the *Brchli*. **(A)** Schematic diagram of carrier construction used in VIGS analysis. **(B)** Plant phenotypes of TRV::*0* and TRV::*Brchli1* at 30D. Scale bar = 1 cm. **(C)** Relative expression levels of *Brchli1* in TRV::*0* and TRV::*Brchli1* at 10, 20, and 30 days. ** represents significant differences at $p < 0.01$. **(D)** Schematic diagram of transient overexpression vector structure. **(E)** Plant phenotypes of pSuper: GFP and pSuper::*Brchli1-GFP* at 20D. Scale bar = 1 cm. **(F)** Relative expression levels of *Brchli1* in pSuper: GFP and pSuper::*Brchli1-GFP* at 10, 20, and 30 days. ** represents significant differences at $p < 0.01$.

10.3389/fpls.2024.1450242

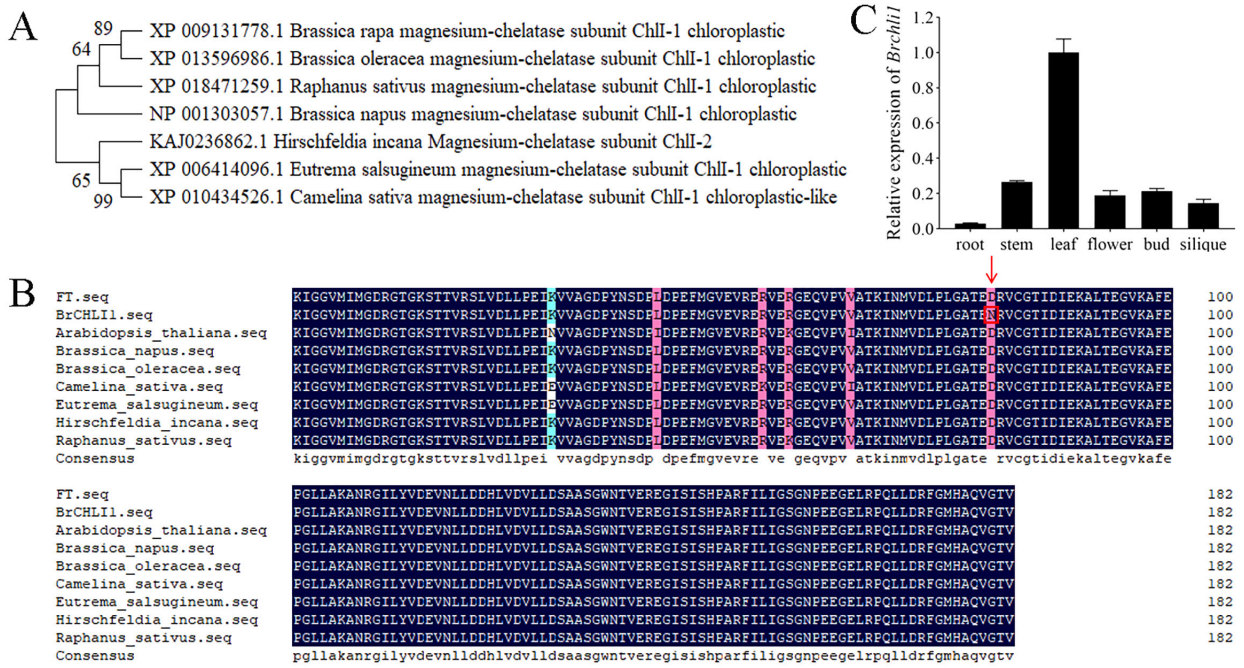

FIGURE 4
Phylogenetic tree of BrCHLI1, alignment of the AAA domain in BrCHLI1, and expression levels of *Brchli1*. **(A)** Phylogenetic analysis of BrCHLI1. **(B)** AAA sequence alignment. Black shaded regions represent 100% similarity, while pink shaded regions represent >75% similarity. Red arrows and red boxes denote the mutation sites. **(C)** Relative expression levels of *Brchli1* in different organs of 'FT'.

The mutation in BrCHLI1 does not affect interaction with BrCHLD

To investigate the role of BrCHLI1 in Chinese cabbage leaf coloration and assess its interaction with BrCHLD, we co-transformed recombinant vectors pGBKT7-BrCHLI1 and pGADT7-BrCHLD into yeast cells using the yeast 2-hybrid (Y2H) system for interaction analysis. On the SD/−Trp/−Leu (DDO) plate, yeast colonies for pGBKT7-BrCHLI1 + pGADT7-BrCHLD, pGADT7-T + pGBKT7-53 (positive control), and pGADT7-T + pGBKT7-Lam (negative control) exhibited normal growth, confirming successful yeast transformation. PGBKT7-BrCHLI1 + PGADT7-BrCHLD, as well as the positive control, showed normal yeast growth on SD/-Leu-Trp-His-Ade-X-α-gal

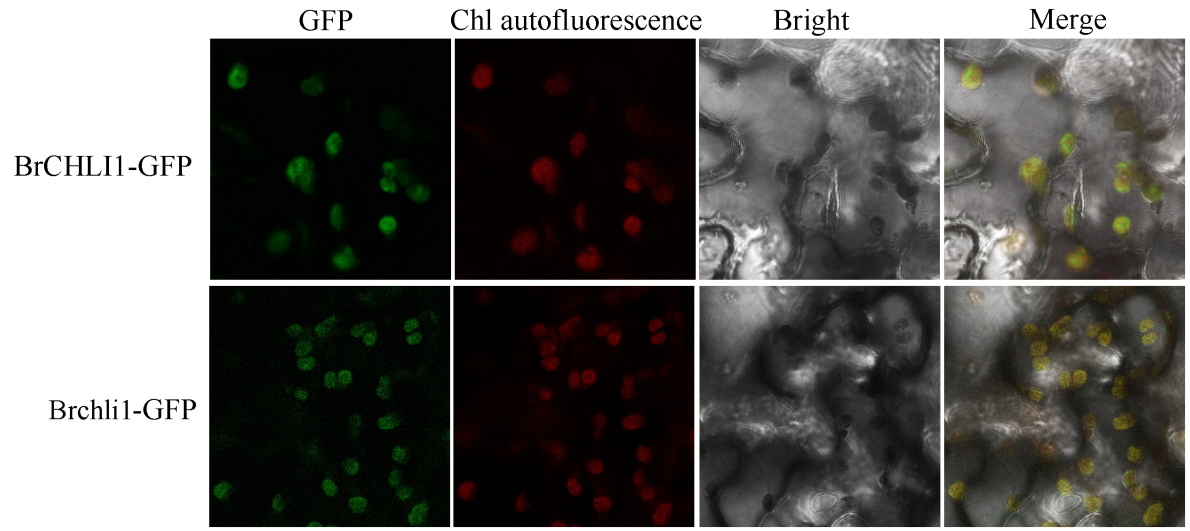

FIGURE 5
Subcellular localization of BrCHLI1 and Brchli1.

(QDO/X) plates, while the negative control did not exhibit any growth, indicating that BrCHLI1 interacted with BrCHLD (Figure 6A). To confirm this interaction *in vivo*, we conducted luciferase complementation imaging (LCI) analysis in tobacco. When co-expressing cLUC-BrCHLI1 and BrCHLD-nLUC, a strong luminescence signal was observed in leaves, while the control group containing empty vectors showed no luminescence signal, indicating that BrCHLI1 interacts with BrCHLD (Figure 6B). These results suggest that BrCHLI1 and BrCHLD interact both *in vivo* and *in vitro*.

To ascertain if the mutation in BrCHLI1 affected its interaction with BrCHLD, we employed Y2H assay to determine the relationship between Brchli1 and BrCHLD. Yeast cells co-transformed with pGBKT7-Brchli1 + pGADT7-BrCHLD grew on QDO/X plates, demonstrating that Brchli1 interacted with BrCHLD (Figure 6A). Co-transformation of cLUC-Brchli1 and BrCHLD-nLUC into tobacco leaves resulted in a strong fluorescence signal, confirming that Brchli1 interacted with BrCHLD *in vivo* (Figure 6B). Thus, the mutation in BrCHLI1 did not affect its interaction with BrCHLD.

The BrCHLI1 mutation weakens self-interaction

To further explore the potential self-interaction of BrCHLI1, we conducted Y2H analysis and LCI assays. Yeast cells co-transformed with pGBKT7-BrCHLI1 and pGADT7-BrCHLI1 displayed normal growth on QDO/X plates, confirming that BrCHLI1 can bind by themselves (Figure 6A), and the LCI assay further validated this interaction. Bioluminescence signals were detected in plant cells co-expressing cLUC-BrCHLI1 and BrCHLI1-nLUC fusion proteins (Figure 6B), indicating successful reconstitution of luciferase activity due to their physical interaction. Control experiments with non-interacting protein pairs did not exhibit any significant bioluminescence, confirming the specificity of the observed signal.

Subsequently, the interaction between BrCHLI1 and Brchli1 was further determined. Y2H assays revealed a reduced yeast colony viability in co-expressing colonies of BrCHLI1 and Brchli1 (Figure 6A), indicating a weakened physical interaction between the proteins. This observation was further substantiated by LCI, in which only faint bioluminescence signals were detected in cells expressing BrCHLI1 and Brchli1 fusion proteins (Figure 6B). These results demonstrated a diminished self-interaction capability of BrCHLI1 following mutation.

Discussion

In this study, we identified the *bright yellow leaves* (*byl*) mutant in Chinese cabbage, and cloned the mutant gene *BraA01g010140.3.5C*. Silencing of *BraA01g010140.3.5C* in plants resulted in a bright yellow leaves phenotype. Transiently overexpressed *Brchli1* in the *byl* mutant restored the green leaf phenotype. Chloroplast development of *byl* was impaired, with decreased Chl content, *Pn*, and NPQ. The *byl* mutant displayed photosensitive phenotypes under variable light intensities. Mutation in BrCHLI1 weakened its self-interaction.

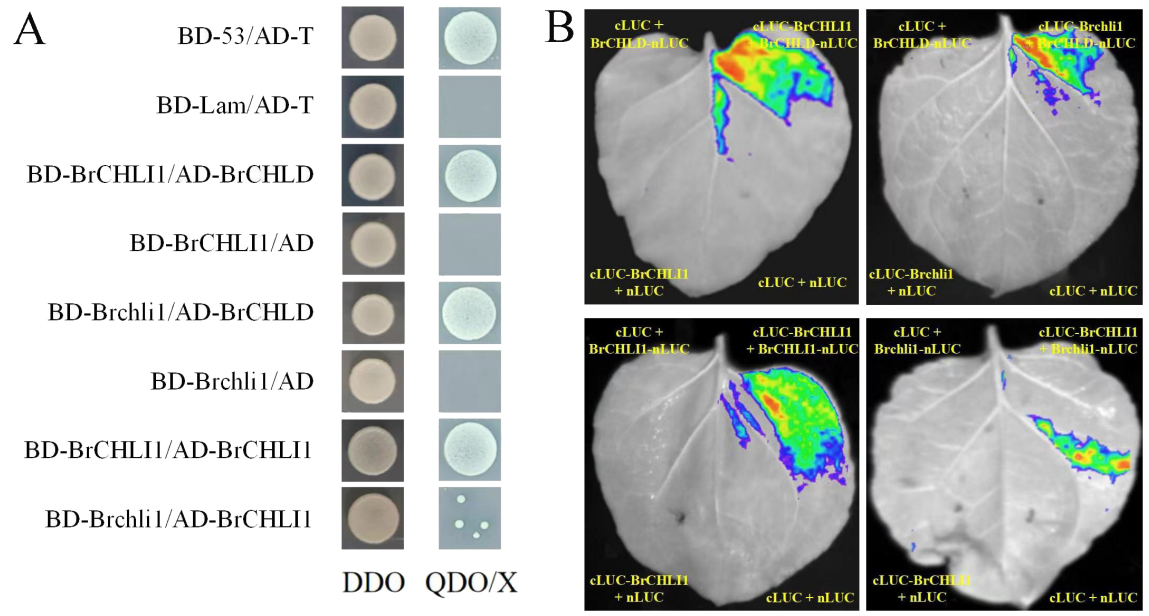

FIGURE 6
Interaction relationships between BrCHLI1 and Brchli1 with BrCHLD and BrCHLI1. **(A)** Interaction relationships analyzed by Y2H. DDO, SD/-Leu-Trp. QDO/X, SD/-Leu-Trp. **(B)** Analysis of interplay/interaction using LCI in tobacco leaves.

The CHLI subunit is essential for catalytic activity of MgCh. CHLI is a member of the AAA+ protein family possessing ATP hydrolysis activity (Fodje et al., 2001). The chelation reaction catalyzed by MgCh is a highly ATP-dependent process (Palmer and Mascia, 1980). Chelation of Mg^{2+} and Proto IX catalyzed by MgCh is an important regulatory step in the Chl biosynthesis pathway (Jensen et al., 1996). Previous studies demonstrated that mutations in subunit I can impact Chl synthesis within plant leaves. Mutations in the *OsCHLI* gene of rice led to yellow leaves and a significant decrease in Chl content (Zhang et al., 2015). Mutations in the *AtCHLI1* (Koncz et al., 1990) and *CHLI2* genes in *Arabidopsis* both resulted in a pale green leaf phenotype (Kobayashi et al., 2008). Amino acid missense mutations in *ChlI* resulted in a yellow-green phenotype in rice (Zhang et al., 2006). *TaCHLI* single-nucleotide mutations in wheat were responsible for pale green leaves caused by impaired Chl synthesis (Wang et al., 2020). We identified a point mutation in *Brchli1* at position 783 in the *byl* mutant of Chinese cabbage, resulting in the substitution of Asp to Asn, which in turn resulted in bright yellow leaves phenotype. Phylogenetic analysis of the *CHLI* gene indicated a high degree of conservation across different species. The *Brchli1* gene was cloned from Chinese cabbage for the first time in this study.

In the Chl synthesis pathway, Mgch catalyzes the reaction of Proto IX to form Mg-proto IX, a critical regulatory point in the process (Masuda, 2008). In the rice yellow leaf mutant *ell*, loss of function of Mgch prevents the conversion of Proto IX to Mg-proto IX, leading to accumulation of Proto IX, and levels of Proto IX in the mutant were significantly increased (Zhang et al., 2015). In the wheat pale green leaf mutant *byl*, levels of Proto IX and Mg-proto IX were significantly lower than those in wild-type plants (Wang et al., 2020). In the strawberry pale green leaf mutant *CHLI*, the content of Mg-proto IX was significantly lower than that in wild-type plants (Ma et al., 2023).

In the presence of Mg^{2+} and ATP, the CHLI and CHLD subunits formed an AAA+ complex which subsequently interacted with the CHLH chelating subunit, resulting in the formation of an active chelatase (Farmer et al., 2019). ChlI protein complexes that self-assemble are known to contain 6–8 ChlI subunits (Jensen et al., 1998). A single-nucleotide mutation in subunit I of the rice yellow leaf mutant *ell* disrupted its interaction with the H subunit, leading to the loss of MgCh catalytic activity and appearance of the yellow leaf phenotype (Zhang et al., 2015). In the wheat yellow leaf mutant *chli*, the mutant protein Tachli-7A was unable to interact with TaCHLI-7A in yeast, but showed weak interaction in bimolecular fluorescence complementation assays (Wang et al., 2020). In the present study, Y2H and LCI assays showed that BrCHLI1 mutations did not affect its interaction with BrCHLD, but impaired its interaction with itself. An amino acid mutation in the conserved structural domain of subunit I in the *byl* mutant compromised the activity of the BrCHLI protein, and disrupted its protein-protein interaction with itself. As a result, the synthesis of Chl was impaired, resulting in the yellow leaf phenotype.

The *byl* mutant could convert from bright yellow leaves to light green leaves in low light intensity, and chloroplasts recovered to normal, suggesting that *byl* may be better adapted to low light conditions. Under low light conditions, the *Arabidopsis immutans* mutant retained green leaves, while it displayed variegated leaves under high light conditions (Rosso et al., 2009). Compared with lower light conditions, the Chl-less barley mutant NYB displayed a more evident yellow leaf color under high light intensities (Yuan et al., 2010b). The same phenotype has been reported for the *Petunia hybrida* yellow-green leaf mutant (Colijn et al., 1983), golden-leaf privet (Yuan et al., 2010a), and *Acer palmatum* 'Jingling Huangfeng' (Li et al., 2015). Therefore, the Chinese cabbage *byl* mutant provides a useful material for studying the potential molecular mechanisms underlying the relationship between light conditions, leaf color, and photosynthetic capacity.

Our study demonstrated that mutation in *Brchli1* led to disrupted chloroplast development and a reduction in Brchli1 self-interaction, ultimately resulting in the manifestation of a golden yellow leaf phenotype. The *chli1* mutant exhibited a transformation of leaf color to pale green under weak light conditions. These findings provide insights into the leaf color formation mechanism in Chinese cabbage.

Data availability statement

The original data generated in the study are included in the article/Supplementary Material. The MutMap sequencing datasets are available in the Sequence Read Archives (SRA) of the NCBI under BioProject ID: PRJNA1074262. Genomic sequences and gene annotation information of B.rapa are downloaded online at http://brassicadb.cn.

Author contributions

CL: Writing – original draft. YC: Data curation, Writing – review & editing. CT: Methodology, Writing – review & editing. FS: Methodology, Writing – review & editing. YZ: Writing – review & editing. ZL: Writing – review & editing.

Funding

The author(s) declare that financial support was received for the research, authorship, and/or publication of this article. This work was supported by the Earmarked Fund for CARS-23-A02, the National Natural Science Foundation of China (32272736 and 31972406) and the Key Research and Development Program of Liaoning (2021JH2/10200003).

Conflict of interest

The authors declare that the research was conducted in the absence of any commercial or financial relationships that could be construed as a potential conflict of interest.

Publisher's note

Supplementary material

The Supplementary Material for this article can be found online at: https://www.frontiersin.org/articles/10.3389/fpls.2024.1450242/full#supplementary-material.

SUPPLEMENTARY FIGURE 1
Cloning of the *Brchli1* gene from 'FT' and *byl*. The mutation site is located in the red box.

References

Abe, A., Kosugi, S., Yoshida, K., Natsume, S., Takagi, H., Kanzaki, H., et al. (2012). Genome sequencing reveals agronomically important loci in rice using MutMap. *Nat. Biotechnol.* 30, 174–178. doi: 10.1038/nbt.2095

Adams, N. B., Bisson, C., Brindley, A. A., Farmer, D. A., Davison, P. A., Reid, J. D., et al. (2020). The active site of magnesium chelatase. *Nat. Plants* 6, 1491–1502. doi: 10.1038/s41477-020-00806-9

Brzezowski,, Richter, A. S., and Grimm, (2015). Regulation and function of tetrapyrrole biosynthesis in plants and algae. *BBA-BIOENERGETICS* 1847, 968–985. doi: 10.1016/j.bbabio.2015.05.007

Colijn, C., Mol, J., Kool, A., and Nijkamp, H. (1983). Plastid gene expression in a yellow-green leaf mutant of Petunia hybrida. *Planta* 157, 209–217. doi: 10.1007/BF00405184

Farmer, D. A., Brindley, A. A., Hitchcock, A., Jackson, P. J., Johnson, B., Dickman, M. J., et al. (2019). The ChlD subunit links the motor and porphyrin binding subunits of magnesium chelatase. *Biochem. J.* 476, 1875–1887. doi: 10.1042/BCJ20190095

Fodje, M., Hansson, A., Hansson, M., Olsen, J., Gough, S., Willows, R., et al. (2001). Interplay between an AAA module and an integrin I domain may regulate the function of magnesium chelatase. *J. Mol. Biol.* 311, 111–122. doi: 10.1006/jmbi.2001.4834

Gao, M., Hu, L., Li, Y., and Weng, Y. (2016). The chlorophyll-deficient golden leaf mutation in cucumber is due to a single nucleotide substitution in CsChlI for magnesium chelatase I subunit. *Theor. Appl. Genet.* 129, 1961–1973. doi: 10.1007/s00122-016-2752-9

Gao, Y., Huang, S., Qu, G., Fu, W., and Feng, H. (2020). The mutation of ent-kaurene synthase, a key enzyme involved in gibberellin biosynthesis, confers a non-heading phenotype to Chinese cabbage (Brassica rapa L. ssp. pekinensis). *Horticulture Res.* 7, 10. doi: 10.1038/s41438-020-00399-6

Holm, G. (1954). Chlorophyll mutations in barley. *Acta Agriculturae Scandinavica* 4, 457–471. doi: 10.1080/00015125409439955

Huang, Y.-S., and Li, H.-M. (2009). Arabidopsis CHLI2 can substitute for CHLI1. *Plant Physiol.* 150, 636–645. doi: 10.1104/pp.109.135368

Huang, S., Liu, Z., Li, D., Yao, R., and Feng, H. (2016). A new method for generation and screening of Chinese cabbage mutants using isolated microspore culturing and EMS mutagenesis. *Euphytica* 207, 23–33. doi: 10.1007/s10681-015-1473-5

Jensen, P. E., Gibson, L. C., Henningsen, K. W., and Hunter, C. N. (1996). Expression of the chlI, chlD, and chlH genes from the cyanobacterium Synechocystis PCC6803 in Escherichia coli and demonstration that the three cognate proteins are required for magnesium-protoporphyrin chelatase activity. *J. Biol. Chem.* 271, 16662–16667. doi: 10.1074/jbc.271.28.16662

Jensen, P. E., Gibson, L. C., and Hunter, C. N. (1998). Determinants of catalytic activity with the use of purified I, D and H subunits of the magnesium protoporphyrin IX chelatase from Synechocystis PCC6803. *Biochem. J.* 334, 335–344. doi: 10.1042/bj3340335

Jessop, M., Felix, J., and Gutsche, I. (2021). AAA+ ATPases: structural insertions under the magnifying glass. *Curr. Opin. Struct. Biol.* 66, 119–128. doi: 10.1016/j.sbi.2020.10.027

Kobayashi, K., Mochizuki, N., Yoshimura, N., Motohashi, K., Hisabori, T., and Masuda, T. (2008). Functional analysis of Arabidopsis thaliana isoforms of the Mg-chelatase CHLI subunit. *Photochemical Photobiological Sci.* 7, 1188–1195. doi: 10.1039/b802604c

Koncz, C., Mayerhofer, R., Koncz-Kalman, Z., Nawrath, C., Reiss, B., Redei, G., et al. (1990). Isolation of a gene encoding a novel chloroplast protein by T-DNA tagging in Arabidopsis thaliana. *EMBO journa* 9, 1337–1346. doi: 10.1002/embj.1990.9.issue-5

Krzywinski, M., Schein, J., Birol, I., Connors, J., Gascoyne, R., Horsman, D., et al. (2009). Circos: An information aesthetic for comparative genomics. *Genome Res.* 19, 1639–1645. doi: 10.1101/gr.092759.109

Kunugi, M., Takabayashi, A., and Tanaka, A. (2013). Evolutionary changes in Chlorophyllide a Oxygenase (CAO) structure contribute to the acquisition of a new light-harvesting complex in micromonas. *J. Biol. Chem.* 288, 19330-19341. doi: 10.1074/jbc.M113.462663

Lake, V., Olsson, U., Willows, R. D., and Hansson, M. (2004a). ATPase activity of magnesium chelatase subunit I is required to maintain subunit D *in vivo*. *FEBS J.* doi: 10.1111/j.1432-1033.2004.04143.x

Lake, V., Olsson, U., Willows, R. D., and Hansson, M. (2004b). ATPase activity of magnesium chelatase subunit I is required to maintain subunit D *in vivo*. *Eur. J. Biochem.* 271, 2182–2188. doi: 10.1111/j.1432-1033.2004.04143.x

Li, H., and Durbin, R. (2010). Fast and accurate long-read alignment with Burrows–Wheeler transform. *Bioinformatics* 26 (5), 589-595. doi: 10.1093/bioinformatics/btp698

Li, S.-S., Li, Q.-Z., Rong, L.-P., Tang, L., and Zhang, B. (2015). Gene expressing and sRNA sequencing show that gene differentiation associates with a yellow Acer palmatum mutant leaf in different light conditions. *BioMed. Res. Int.* 1, 843470. doi: 10.1155/2015/843470

Liu, L., Li, Y., She, G., Zhang, X., Jordan, B., Chen, Q., et al. (2018). Metabolite profiling and transcriptomic analyses reveal an essential role of UVR8-mediated signal transduction pathway in regulating flavonoid biosynthesis in tea plants (Camellia sinensis) in response to shading. *BMC Plant Biol.* 18, 1–18. doi: 10.1186/s12870-018-1440-0

Liu, C., Song, G., Wang, N., Huang, S., Gao, Y., Fu, W., et al. (2021). A single SNP in Brcer1 results in wax deficiency in Chinese cabbage (Brassica campestris L. ssp. pekinensis). *Scientia Hortic.* 282, 110019. doi: 10.1016/j.scienta.2021.110019

Ma, Y.-Y., Shi, J.-C., Wang, D.-J., Liang, X., Wei, F., Gong, C.-M., et al. (2023). A point mutation in the gene encoding magnesium chelatase I subunit influences strawberry leaf color and metabolism. *Plant Physiol.* 192 (4), 2737-2755. doi: 10.1093/plphys/kiad247

Masuda, T. (2008). Recent overview of the Mg branch of the tetrapyrrole biosynthesis leading to chlorophylls. *Photosynthesis Res.* 96, 121-143. doi: 10.1007/s11120-008-9291-4

McKenna, A., Hanna, M., Banks, E., Sivachenko, A., Cibulskis, K., Kernytsky, A., et al. (2010). The Genome Analysis Toolkit: a MapReduce framework for analyzing next-generation DNA sequencing data. *Genome Res.* 20, 1297–1303. doi: 10.1101/gr.107524.110

Palmer, R. G., and Mascia, P. N. (1980). Genetics and ultrastructure of a cytoplasmically inherited yellow mutant in soybeans. *Genetics* 95, 985–1000. doi: 10.1093/genetics/95.4.985

Pflieger, S., Blanchet, S., Camborde, L., Drugeon, G., and Jupin, I. (2010). Efficient virus-induced gene silencing in Arabidopsis using a 'one-step' TYMV-derived vector. *Plant J.* 56, 678–690. doi: 10.1111/j.1365-313X.2008.03620.x

Reid, J. D., Siebert, C. A., Bullough, P. A., and Hunter, C. N. (2003). The ATPase activity of the chlI subunit of magnesium chelatase and formation of a heptameric AAA + Ring. *Biochemistry* 42, 6912–6920. doi: 10.1021/bi034082q

Rissler, H. M., Collakova, E., DellaPenna, D., Whelan, J., and Pogson, B. J. (2002). Chlorophyll biosynthesis. Expression of a second chl I gene of magnesium chelatase in Arabidopsis supports only limited chlorophyll synthesis. *Plant Physiol.* 128, 770–779. doi: 10.1104/pp.010625

Rosso, D., Bode, R., Li, W., Krol, M., Saccon, D., Wang, S., et al. (2009). Photosynthetic redox imbalance governs leaf sectoring in the Arabidopsis thaliana variegation mutants immutans, spotty, var1, and var2. *Plant Cell* 21, 3473–3492. doi: 10.1105/tpc.108.062752

Sirijovski, N. (2006). Magnesium Chelatase: Insights into the first Step of Chlorophyll Biosynthesis. *Kfs Ab*.

Vale, R. D. (2000). AAA proteins: lords of the ring. *J. Cell Biol.* 150, F13–F20. doi: 10.1083/jcb.150.1.f13

Wang, K., Li, M., and Hakonarson, H. (2010). ANNOVAR: functional annotation of genetic variants from high-throughput sequencing data. *Nucleic Acids Res.* 38(16), e164-e164. doi: 10.1093/nar/gkq603

Wang, C., Zhang, L., Li, Y., Ali Buttar, Z., Wang, N., Xie, Y., et al. (2020). Single nucleotide mutagenesis of the TaCHLI gene suppressed chlorophyll and fatty acid

biosynthesis in common wheat seedlings. *Front. Plant Sci.* 11, 97. doi: 10.3389/fpls.2020.00097

Xi, X., Wei, K., Gao, B., Liu, J., Liang, J., Cheng, F., et al. (2018). BrFLC5: a weak regulator of flowering time in Brassica rapa. *Theor. Appl. Genet.* 131, 2107–2116. doi: 10.1007/s00122-018-3139-x

Yang, S., Zhang, Z., Chen, W., Liang, C., Li, X., Liu, Z., et al. (2023). Fine-mapping and transcriptome analysis of the photosensitive leaf-yellowing gene CaLY1 in pepper (Capsicum annuum L.). *Hortic. Plant J.* 9, 122–132. doi: 10.1016/j.hpj.2022.06.007

Yuan, M., Xu, M. Y., Yuan, S., Chen, Y. E., Du, J. B., Xu, F., et al. (2010a). Light regulation to chlorophyll synthesis and plastid development of the chlorophyll-less golden-leaf privet. *J. Integr. Plant Biol.* 52, 809–816. doi: 10.1111/j.1744-7909.2010.00979.x

Yuan, M., Yuan, S., Zhang, Z.-W., Xu, F., Chen, Y.-E., Du, J.-B., et al. (2010b). Putative mutation mechanism and light responses of a protochlorophyllide oxidoreductase-less barley mutant NYB. *Plant Cell Physiol.* 51, 1361–1371. doi: 10.1093/pcp/pcq097

Zhang, H., Li, J., Yoo, J.-H., Yoo, S.-C., Cho, S.-H., Koh, H.-J., et al. (2006). Rice Chlorina-1 and Chlorina-9 encode ChlD and ChlI subunits of Mg-chelatase, a key enzyme for chlorophyll synthesis and chloroplast development. *Plant Mol. Biol.* 62, 325–337. doi: 10.1007/s11103-006-9024-z

Zhang, H., Liu, L., Cai, M., Zhu, S., Zhao, J., Zheng, T., et al. (2015). A point mutation of magnesium chelatase OsCHLI gene dampens the interaction between CHLI and CHLD subunits in rice. *Plant Mol. Biol. Rep.* 33, 1975–1987. doi: 10.1007/s11105-015-0889-3

Zhang, L., Zhang, S., Dai, Y., Wang, S., Wang, C., Li, F., et al. (2022). Mapping and validation of brGOLDEN: A dominant gene regulating carotenoid accumulation in brassica rapa. *Int. J. Mol. Sci.* 23, 12442. doi: 10.3390/ijms232012442

Zhao, Y., Huang, S., Wang, N., Zhang, Y., Ren, J., Zhao, Y., et al. (2022). Identification of a biomass unaffected pale green mutant gene in Chinese cabbage (Brassica rapa L. ssp. pekinensis). *Sci. Rep.* 12, 7731. doi: 10.1038/s41598-022-11825-1

Zhao, H., Yu, L., Huai, Z., Wang, X., and Ding, G. (2014). Mapping and candidate gene identification defining BnChd1-1, a locus involved in chlorophyll biosynthesis in Brassica napus. *Acta Physiologiae Plantarum* 36, 859–870. doi: 10.1007/s11738-013-1464-x

Zhou, P., Peng, J., Zeng, M., Wu, L., Fan, Y., and Zeng, L. (2021). Virus-induced gene silencing (VIGS) in Chinese narcissus and its use in functional analysis of NtMYB3. *Hortic. Plant J.* 7, 565–572. doi: 10.1016/j.hpj.2021.04.009

frontiers | Frontiers in Plant Science

TYPE Original Research
PUBLISHED 10 October 2024
DOI 10.3389/fpls.2024.1465905

OPEN ACCESS

EDITED BY
Xiangshu Dong,
Yunnan University, China

REVIEWED BY
Wei She,
Hunan Agricultural University, China
Qinglin Tang,
Southwest University, China

*CORRESPONDENCE
Xia An
anxia@zaas.ac.cn

RECEIVED 17 July 2024
ACCEPTED 12 September 2024
PUBLISHED 10 October 2024

CITATION
Li S, Ji Q, An X, Chen C, Luo X, Liu T and Zou L (2024) Genome-wide analysis of WRKY gene family and the dynamic responses of key WRKY genes involved in cadmium stress in *Brassica juncea*.
Front. Plant Sci. 15:1465905.
doi: 10.3389/fpls.2024.1465905

Genome-wide analysis of WRKY gene family and the dynamic responses of key WRKY genes involved in cadmium stress in *Brassica juncea*

Shaocui Li, Qingqing Ji, Xia An*, Changli Chen, Xiahong Luo, Tingting Liu and Lina Zou

Zhejiang Xiaoshan Institute of Cotton & Bast Fiber Crops, Zhejiang Institute of Landscape Plants and Flowers, Zhejiang Academy of Agricultural Sciences, Hangzhou, China

The WRKY transcription factors comprise one of the most extensive gene families and serve as pivotal regulators of plant responses to heavy metal stress. They contribute significantly to maintaining plant growth and development by enhancing plant tolerance. However, research on the role of WRKY genes in response to cadmium (Cd) stress in mustard is minimal. In this study, we conducted a genome-wide analysis of the mustard WRKY gene family using bioinformatics. The results revealed that 291 WRKY putative genes (*BjuWRKY*s) were identified in the mustard genome. These genes were categorized into seven subgroups (I, IIa-e and III) through phylogenetic analysis, with differences in motif composition between each subgroup. Homology analysis indicated that 31.62% of the genes originated from tandem duplication events. Promoter analysis revealed an abundance of abiotic stress-related elements and hormone-related elements within the *BjuWRKY* genes. Transcriptome analysis demonstrated that most *BjuWRKY* genes exhibited differential expression patterns at different Cd treatment stages in mustard. Furthermore, 10 *BjuWRKY* genes were confirmed to respond to Cd stress through the construction of a BjuWRKY protein interaction network, prediction of hub genes, and real-time fluorescence quantitative PCR analysis, indicating their potential involvement in Cd stress. Our findings provide a comprehensive insight into the WRKY gene family in mustard and establish a foundation for further studies of the functional roles of *BjuWRKY* genes in Cd stress response.

KEYWORDS

cadmium, *Brassica juncea*, WRKY gene family, gene expression, cadmium stress

1 Introduction

Heavy metals constitute a pervasive class of pollutants that have garnered global attention (Kamal et al., 2023). Among them, cadmium (Cd) stands out as one of the most common harmful heavy metals and is extremely toxic. As agriculture and industry continue to expand and development, Cd spreads rapidly in ecosystems through processes such as mining, industrial emissions and pesticide use (Li et al., 2021). Despite being non-essential elements without a known biological function in living organisms, they can still be absorbed and utilized by plants through their natural ion uptake channels (Liu et al., 2019). In addition, Cd has high hydrophilicity and mobility and is easily taken up by plants from the soil (Wei et al., 2024). Excessive levels of Cd prevent plant uptake and transfer of nutrients and water, resulting in reduced seedling growth rate and root activity (Yang et al., 2022). Cadmium that enters the plant through soil contamination can accumulate within the plant tissues and ultimately end up in the human body along the food chain (Li S. et al., 2023; Liu et al., 2017).

Transcription factors contain numerous phosphorylation sites, which serve as key regulators of cellular responses to heavy metal stress by controlling the expression of downstream genes (Li et al., 2022). Furthermore, they are also central components of the regulatory network for heavy metal detoxification and tolerance. Many transcription factors intimately related to heavy metal detoxification and resistance pathway have been identified in plants. Among them, transcription factors such as basic leucine zipper (bZIP) (Han et al., 2021), basic helix-loop-helix (bHLH) (Yao et al., 2018), myeloblastosis (MYB) (Agarwal et al., 2020), and ethylene response transcription factor (ERF) (Lin et al., 2017) have been shown to play important roles in the regulation of heavy metal stress in plants.

The WRKY family, comprising one of the largest families of transcription factors in plants and plays a pivotal role in various biological processes, including growth, development and stress response, particularly in the context of heavy metal toxicity and resistance (Hu et al., 2021; Li et al., 2022; Wani et al., 2021). WRKY protein belongs to plant specific transcription factors, named for its N-terminus containing a special distinctive seven-amino-acid conserved sequence WRKYGOK (Xiong et al., 2024). Additionally, the WRKY transcription factor possesses a highly conserved WRKY structural domain, which comprises about 60 amino acids at the N-terminus, and a novel zinc finger motif C2H2 (C–X4–5–C–X22–23–H–X–H) or C2HC (C–X7–C–X23–H–X– C) at their C-terminus (Xie et al., 2018). WRKY proteins induce or repress the expression of their downstream genes by specifically binding to the W-box [TGACC (A/T)] at the promoter site (Qin et al., 2022; Zentgraf et al., 2010). Based on the number of WRKY structural domains and the type of zinc finger motif, WRKY proteins can be categorized into three classes: proteins containing two WRKY structural domains belong to class I, while proteins with only one WRKY structural domain belong to classes II and III. Members of classes I and II have C2H2 zinc finger-like motifs, whereas class III WRKY proteins contain C2HC zinc finger-like motifs (Eulgem et al., 2000).

Numerous evidences indicate that WRKY transcription factors play crucial roles in plant growth, development, and hormone regulation. A previous comparative transcriptomic study on cotton somatic embryogenesis revealed that 4.8% of the gene coding for WRKY transcription factors were detected during this process. Further research has demonstrated that *GhWRKY15* not only participates in the regulation of rhizome development but also enhances resistance to viral and fungal infections in tobacco when overexpressed (Sun et al., 2018; Yu et al., 2012). In another study, Xiong et al. (2024) identified 89 *Pisum sativum* WRKY genes and found that hormone response elements (ABA\ MeJA\GA SA\IAA) were present in several *Pisum sativum* WRKY genes. Expression patterns varied across different tissues and fruit developmental stages, as well as in response to hormone treatments. It was speculated that the *PsWRKYs* regulate *Pisum sativum* growth and development through hormone-mediated signaling pathways (Xiong et al., 2024). Additionally, overexpression of *TaWRKY75-A* and *ZmWRKY79* in *Arabidopsis thaliana* has been shown to improves plant survival under drought stress by regulating ABA biosynthesis (Gulzar et al., 2021; Ye et al., 2021).

In addition, WRKY transcription factors have been shown to play an equally important role in abiotic stress response. Qin et al. (2022) identified 113 WRKY genes from the apple genome GDDH13, among which *MdWRKY70L* was co-induced by drought and salt stress. Its overexpression in transgenic tobacco plants enhanced stress tolerance to both drought and salt. *GbWRKY1* is another WRKY transcription factor that plays a crucial role in the regulation of phosphate starvation, participating in the regulation of phosphate homeostasis, as well as the distribution and mobilization of phosphate. Overexpression of *GbWRKY1* in *Arabidopsis* can reduce phosphorus deficiency symptoms, accumulate high levels of total phosphorus, increase lateral root development. and enhance phosphatase activity (Xu et al., 2012). In *Liriodendron chinense*, the expression patterns of several WRKY genes (e.g., *LchiWRKY33*, *LchiWRKY25*, and *LchiWRKY18*) were analyzed, and found that they may play functional roles in regulating the response of trees to cold, heat, or drought stress (Wu et al., 2022). Additionally, WRKY genes can enhance plant Cd tolerance or maintain metal ion homeostasis by regulating downstream functional genes. For instance, *AtWRKY12* negatively regulates Cd tolerance in *A. thaliana* by directly binding to the W-box of the *GSH1* promoter and repressing the expression of genes related to phytochelatin synthesis (Han et al., 2019). On the other hand, *AtWRKY13* enhances plant Cd tolerance by directly upregulating the ABC transporter PDR8 to promote the production of D-cysteine desulfurization enzyme and hydrogen sulfide in *Arabidopsis* (Zhang et al., 2020).

Brassica juncea L. is an annual herbaceous plant widely cultivated in China. It exhibits a wide variety of species, most of which are characterized by high biomass, rapid growth, high tolerance, and other distinctive features, allowing for multiple cultivation each year (Chen L. et al., 2020). Previous studies have shown that *B. juncea* has the potential to tolerate and accumulate heavy metals and is a good candidate for phytoremediation in heavy metal contaminated soils (Du et al., 2020). Specifically, the maximum Cd accumulation potential of *B. juncea* shoots has been reported to be over 400 $\mu g\ g^{-1}$, indicating its

potential as a promising genotype for remediation of Cd-contaminated soils (Szczygłowska et al., 2011). Several genes related to heavy metal accumulation and tolerance have been identified in *B. juncea*. For instance, mustard *HMA2* and *HMA4* have been reported to play an important role in Zn detoxification and chelation at subcellular level (Meraklı and Memon, 2023). BjCET1 is a metal ion transporter protein that enhances the heavy metal tolerance in yeast cells when heterologous expressed, reducing the accumulation of Cd or zinc. Moreover, constitutive expression of *BjCET1* rescues the heavy metal tolerance capacity of transgenic tobacco plants (Han et al., 2022). Furthermore, chain-specific transcriptome sequencing and miRNA sequencing were employed to conduct genome-wide identification and characterization of miRNAs and their target genes in *B. juncea* leaves and roots exposed to Cd stress. The results revealed that bra-miR172b-3p is a potential cadmium-specific resistance suppressor that may be negatively regulated in *ATCCS* (copper chaperone for superoxide dismutase) under Cd stress. These findings contribute to deeper understanding of the regulatory network of Cd-responsive miRNAs in *B. juncea* (Liu et al., 2021).

In this study, we systematically identified and characterized a comprehensive repertoire of 291 WRKY transcription factor genes within the *B. juncea* genome. Subsequently, we conducted a thorough examination of their structural features, conserved motifs, cis-regulatory elements, and inferred their evolutionary relationships through phylogenetic analysis. Employing an integrated approach combining RNA sequencing (RNA-seq) and quantitative reverse transcription polymerase chain reaction (qRT-PCR), we carefully elucidated the expression patterns of these WRKY genes under Cd stress. Moreover, we explored the functional importance of key hub genes that orchestrate plant responses to Cd stress. The findings from this study provide a strong foundation for future research aimed at elucidating the functional roles of *BjuWRKY* genes in mediating plant resilience to Cd stress.

2 Materials and methods

2.1 Identification of WRKY genes in *Brassica juncea*

The *A. thaliana* (TAIR_V10. 1) and *B. juncea* genomic data related to this study were obtained from BRAD (http://brassicadb.cn) (Chen et al., 2022; Yang et al., 2021). All potential BjuWrky proteins were systematically identified and retrieved using the Hidden Markov Model (HMM) search with the hmmsearch software and default parameter settings. The strict criterion for inclusion was that each protein must contain the characteristic WRKY structural domain (accession number PF03106) (Mistry et al., 2013; Tang et al., 2021). Also, we used the Conserved Structural Domain Database (CDD; https://www.ncbi.nlm.nih.gov/Structure/cdd/wrpsb.cgi) and SMART (https://smart.embl-heidelberg.de/) to independently verify the presence and integrity of conserved WRKY structural domains in the identified sequences. Subsequently, molecular weights and theoretical isoelectric points (pIs) of the amino acid sequences were calculated using the ExPASy (https://web.expasy.org/). In addition, the PSORT (http://psort1.hgc.jp/form.html) was applied to infer the possible subcellular localization of these proteins. Finally, all identified sequences were systematically named according to their respective chromosomal locations to ensure clarity and consistency of nomenclature throughout the study.

2.2 Phylogenetic tree construction and conserved motifs identification

To elucidate the evolutionary relationships between *B. juncea* and *A. thaliana* WRKY transcription factors, a phylogenetic tree was meticulously constructed. Initially, multiple sequence alignment of the identified WRKY proteins was performed using ClustalW software with default parameter settings to ensure optimal alignment accuracy and consistency. This alignment served as the basis for subsequent phylogenetic inference. The Neighbor-Joining (NJ) method, implemented in the MEGA7.0 software package, was utilized for constructing the phylogenetic tree (Kumar et al., 2016). To enhance the robustness and reliability of the branching patterns, a bootstrap analysis with 1000 replicates was performed. The phylogenetic tree was visualized using iTOL (https://itol.embl.de/).

2.3 Gene structure, conserved motif, and promoter analysis

The structural information of the WRKY gene, including introns, exons, and untranslated regions, was downloaded from BRAD and analyzed using TBtools (Chen C. et al., 2020). The conserved motifs present within the full-length sequences of the identified WRKY proteins were systematically characterized using the online Multiple Em for Motif Elicitation (MEME) suite (http://meme-suite.org/), with the default program setting, where the maximum number of motif was 10 (Bailey et al., 2009).

To gain insights into the regulatory mechanisms governing the expression of *BjWRKY* genes, a 2000 base pair (bp) region immediately upstream of the translational start codon "ATG" was retrieved from the *B. juncea* genome database for each identified gene. These promoter sequences were subjected to analysis using the PlantCARE database. To facilitate the interpretation and visualization of these complex datasets, the TBtools software was employed.

2.4 Chromosomal location and duplication analysis

Chromosomal localization information for each *BjuWRKY* gene was obtained from BRAD, and gene localization visualization with TBtools was used to construct chromosomal localization maps for all *BjuWRKYs* (Chen C. et al., 2020). Gene duplication events of *BjuWRKY* genes were analyzed by WGDI (v0.6.1) software (Sun et al., 2022) and visualized by shinyCircos. Each of the duplicated *BjuWRKY* gene pairs was aligned using the ParaAT 2.0 with MUSCLE (v3.8.31) as multiple sequence aligner (Edgar, 2004; Zhang et al., 2012). The number of nonsynonymous

(Ka) and synonymous (Ks) substitutions per duplicate *BjuWRKY* gene was calculated using KaKs_Calculator 3.0 (Zhang, 2022).

2.5 Plant materials and Cd stress treatments

The leaf mustard "137", selected and cultivated by the Zhejiang Academy of Agricultural Sciences, was utilized as the test material. The seeds were germinated on wet filter paper at 26°C. The germinated seedlings were then cultured in a growth chamber at 14 h/10 h (day/night) cycle for 7 d at 26°C. Subsequently, the seedlings were transplanted to one-half Hogan's nutrient solution for hydroponic cultivation, with the culture solution being changed every 5 days. 21 days, uniformly sized seedlings were selected for 100 µmol Cd stress treatment. Roots, stems, and leaves were sampled at 0 d, 1 d, and 4 d after Cd stress treatment, respectively. All samples were collected in three biological replicates.

2.6 *BjuWRKY* expression profiles in response to Cd stress and qRT-PCR expression analysis

Total RNA was isolated and converted into cDNA using TRIzol Reagent (Invitrogen, Waltham, MA, USA) and PrimeScript™ RT Master Mix (TaKaRa), respectively. The transcript levels were quantified using SYBR Green Premix Ex Taq II (TaKaRa) on a 7300 Real-Time PCR (Applied Biosystems, Carlsbad, CA, USA). Three independent experiments were performed, with three biological replicates per treatment.

To normalize gene expression levels, the $2^{-\Delta\Delta Ct}$ method was calculated. The *TIP41*(tonoplastic intrinsic protein 41) gene was used as the reference (Zheng et al., 2022). Primers used are listed in Supplementary Table S1.

The transcriptome of roots, stems and leaves of mustard at three time points under Cd stress was analyzed using RNA-seq. In this study, twenty-seven RNA libraries were generated, including three control libraries and twenty-four treatment libraries, to investigate the effect of treatment on gene expression. Raw reads were analyzed using FastQC (https://www.bioinformatics.babraham.ac.uk/projects/fastqc/) prior to assembly. Cutadapt software was used to remove low quality reads, including those with sequencing adapters, sequencing primers and nucleotides with mass fractions below 20. All downstream analyses were based on high quality clean data. The raw sequence data was submitted to the NCBI database under the registration number PRJNA1133808. The expression values were calculated by log2 (FPKM) and normalized via Z-score normalization. An expression profile heatmap was generated using the heatmap package in R (4.0.2).

2.7 Gene ontology annotation analysis and hub genes identified

For GO annotation analysis of all identified WRKY protein sequences, Blast2GO v3.0.11 (https://www.blast2go.com) and OmicsBox software were utilized (Conesa and Gotz, 2008). Based on the *Arabidopsis* correlation model, a functional protein association network was constructed in the STRING program (https://string-db.org/) with a confidence parameter of 0.4 and an interaction number of 5. The network was further visualized and analyzed using Cytoscape version 3.10.2.0.

The Cytoscape plugin cytoHubba offers various topological algorithms for ranking nodes base on their correlation to the network topology. We chose to use the Maximum Cluster Centrality (MCC) algorithm, which is based on identifying interconnections between genes and the maximum number of cliques to which a node may be affiliated (Chin et al., 2014; Liu et al., 2022). The Cytohubba plugin in Cytoscape was used to determine hub genes in the target module.

3 Results

3.1 Identification and characterization of WRKY transcription factors in *Brassica juncea*

The BjuWRKY proteins were searched and characterized from the BRAD database using Hidden Markov Models (HMM), and the identified candidate sequences were examined using CDD, Pfam, and SMART to confirm the WRKY structural domains (e-value < $1e^{-5}$). A total of 291 WRKY family members were finally identified from the *B. juncea* genome (Supplementary Table S2). The BjuWRKY family genes were sequentially named from *BjuWRKY1-BjuWRKY291* based on their location on the chromosome. The length of these genes ranged from 348bp (*BjWRKY31*)-3285bp (*BjWRKY157*), and the corresponding molecular weights of the proteins were between 13323.75 and 121396.56 Da (Dalton), and the isoelectric points (pI) ranged from 4.82-9.92. The subcellular localization of BjuWRKY proteins was predicted using the PSORT tool. Most of the BjuWRKY proteins localized in the nucleus. A few proteins, such as BjuWRKY91, BjuWRKY164, BjuWRKY201, and BjuWRKY283 localized in the chloroplasts. BjuWRKY101, BjuWRKY174 and BjuWRKY196 are localized in the cell membrane, while BjuWRKY167 was localized in both the nucleus and chloroplasts. Except for five proteins (BjuWRKY101, BjuWRKY167, BjuWRKY196, BjuWRKY201, and BjuWRKY234), the other BjuWRKY proteins had no transmembrane structures, indicating that they are not membrane proteins (Supplementary Table S3).

3.2 Phylogenetic analysis of *BjuWRKY* genes

To further explore the classification of subgroups of *BjuWRKY* genes and to elucidate the evolutionary relationship between *AtWRKY* and *BjuWRKY* genes, we constructed a phylogenetic tree using the maximum likelihood method (Figure 1). The phylogenetic tree showed that 291 *BjuWRKY*s were categorized into three

10.3389/fpls.2024.1465905

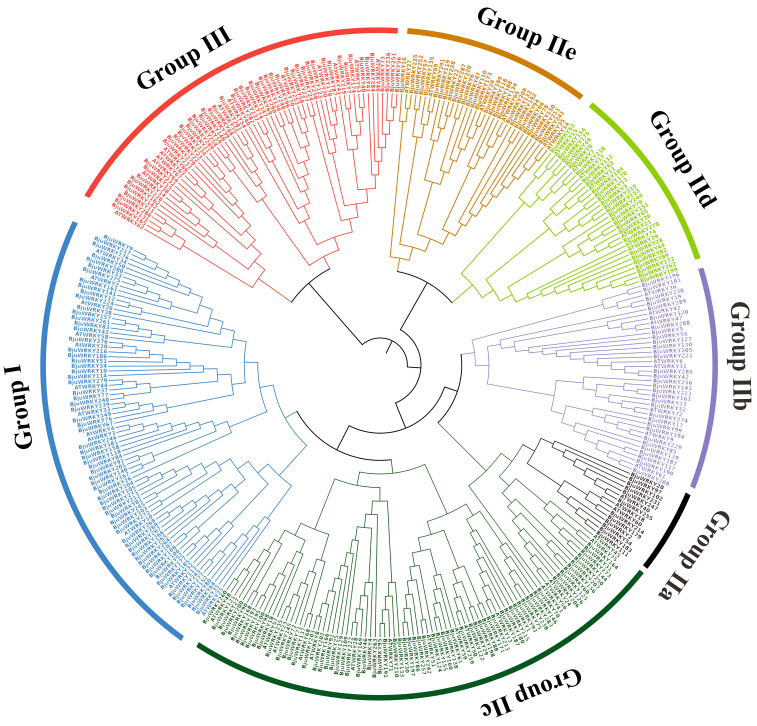

FIGURE 1
Phylogenetic relationships among the WRKY genes from *B. juncea* and *Arabidopsis*. The phylogenetic tree was constructed on the basis of the alignment of *B. juncea* and *Arabidopsis* WRKY proteins according to the maximum-likelihood method, with 1,000 bootstrap replicates.

subgroups: group I, II, and III. The group II contained the most WRKYs with 65.98%, while group I and III contained 47 and 52 WRKYs, respectively. Groups II-a, -b, and -c were clustered together with group I, whereas groups II-d and -e were more closely related to group III. In addition, WRKY proteins in group II could be further divided into five subgroups (IIa, IIb, IIc, IId, and IIe) containing 12, 32, 94, 27, and 27 members, respectively (as shown in Supplementary Table S3). The classification results for these members are similar to those obtained for *Arabidopsis* Within the three groups, the abundance of WRKY proteins varies between Arabidopsis and mustard, potentially attributable to processes of gene expansion or loss. It is evident that in subgroup IIa, both branches contain one or two AtWRKY proteins, and the number of BjuWRKY proteins in each branch of these branches increases to six, indicating the potential expansion of the BjuWRKY family in this subgroup.

3.3 Conserved motifs and gene structures of WRKY family in *B. juncea*

To further elucidate the structural features of conservation and diversification of BjuWRKY proteins, all BjuWRKY proteins were subjected to motif analysis using MEME. Details regarding the 10 putative motifs are provided in Supplementary Table S4. A total of 10 different motifs were identified, and the conserved motifs contained 20-50 amino acids. The number of conserved motifs for each BjuWRKY protein was 3 ~ 7 (Figure 2B). The motif2 and motif3 were present in all of the BjuWRKYs.

To further understand the gene structure of *BjuWRKY*s, we analyzed the introns and exons of *BjuWRKY* genes using the annotation information. The number of introns in the family of *BjuWRKY*s ranged from 1 to 15. Seventeen genes contained only one intron, and 146 (0.18%) and 59 (20.28%) genes contained two and three introns, respectively. Four or more introns were detected in 69 genes (Figure 2C). Combined with the gene structure and conserved protein motif analysis of BjuWRKY members, we found that members of the same subfamily have similar gene structures and conserved motif distributions among themselves, whereas different subfamilies have greater variations, suggesting that there is conservatism and similar functions within the same subfamily.

3.4 Analysis of cis-elements in the promoters of the *BjuWRKY* genes

To gain a deeper understanding of the function and regulatory mechanism of *BjuWRKY* genes, and to elucidate the role of cis-acting elements in *BjuWRKY*. The upstream 2000 bp sequence of each *BjuWRKY* gene was selected as the promoter sequence. The cis-acting elements in these promoter sequences were analyzed using PlantCARE and visualized using TBtools (Supplementary Figure S1). The identified cis-acting elements were categorized into four classes: stress-responsive, light-responsive, plant development-related, and phytohormone-responsive. Plant stress-responsive cis-acting elements included low-temperature-responsive (LTR), defense- and stress-responsive (TC-rich), drought-inducible (MBS), and trauma-

10.3389/fpls.2024.1465905

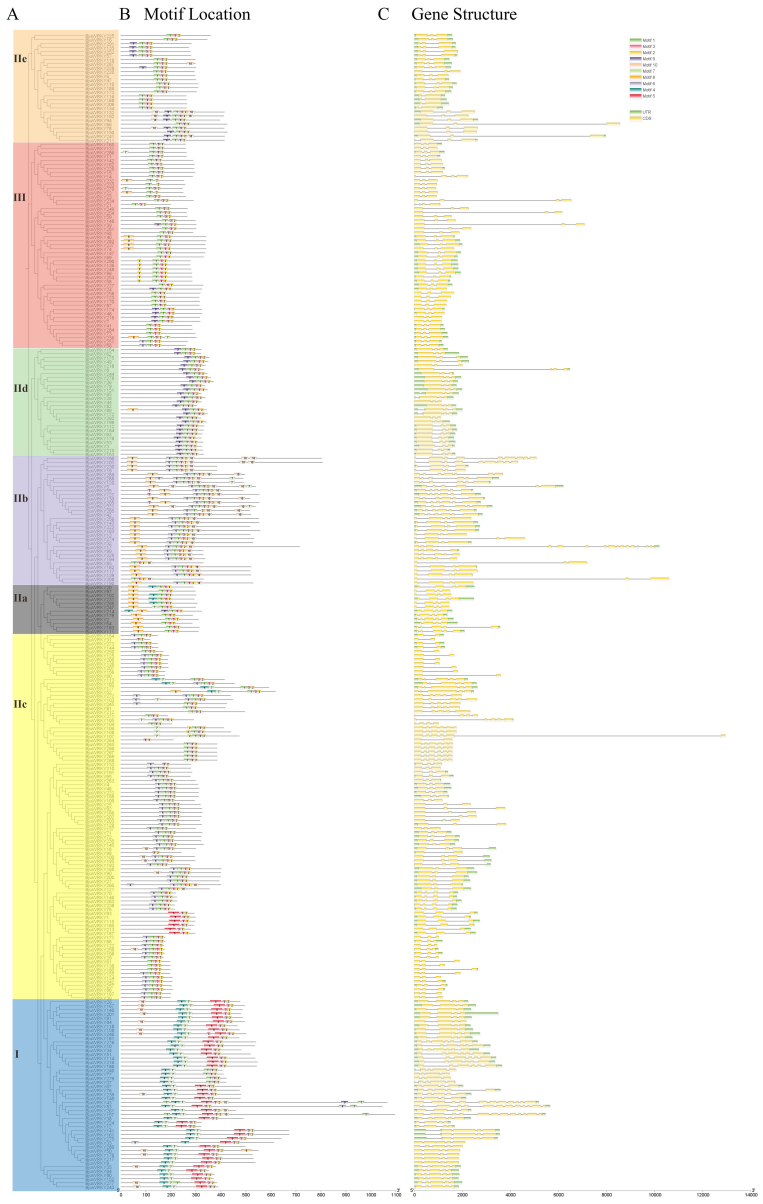

FIGURE 2
Phylogenetic relationships, motif compositions, and gene structures of *BjuWRKY* genes in *B. juncea*. **(A)** Phylogenetic analysis of *B. juncea* WRKY family members. **(B)** All conserved motifs in the WRKY proteins were identified using the MEME program. Different motifs are highlighted with different colored boxes (numbered 1–10). **(C)** Gene structures. Exons and 5′/3′ untranslated regions are indicated by green and yellow bars, respectively, whereas gray lines represent introns.

responsive (WUN-motif); and phytohormone-responsive cis-acting elements, including abscisic acid-responsive (ABRE), growth hormone-responsive (AuxRR-core and TGAelement), gibberellin-responsive elements (GARE-motif, P-box, and TATC-box), MeJA-responsive (CGTCA-motif and TGACGmotif), and salicylic acid-responsive (TCA-element and SARE) were widely present in the promoter region. Among these elements, ABA- and MeJA-related elements (ABRE, CGTCA-motif, and TGACG-motif) accounted for the largest portion, whereas SARE elements were found only in the promoter regions of *BjuWRKY38*, *BjuWRKY46*, *BjuWRKY47*, and *BjuWRKY169*, and *BjuWRKY280*, suggesting that these five genes may play a role in the SA signaling pathway. Other elements related to development and light response, such as GT1-motif and CAT-box were also found in the promoters of several WRKY genes (Figure 3).

3.5 Chromosomal locations and collinearity analysis of *BjuWRKY* genes

Based on the annotation information of the *B. juncea* genome, we mapped the distribution of genes on chromosomes. The Figure 4 shows that 291 genes were unevenly distributed on 18 chromosomes, with the number of genes distributed on chromosomes of subgenomes A and B was almost the same. The

10.3389/fpls.2024.1465905

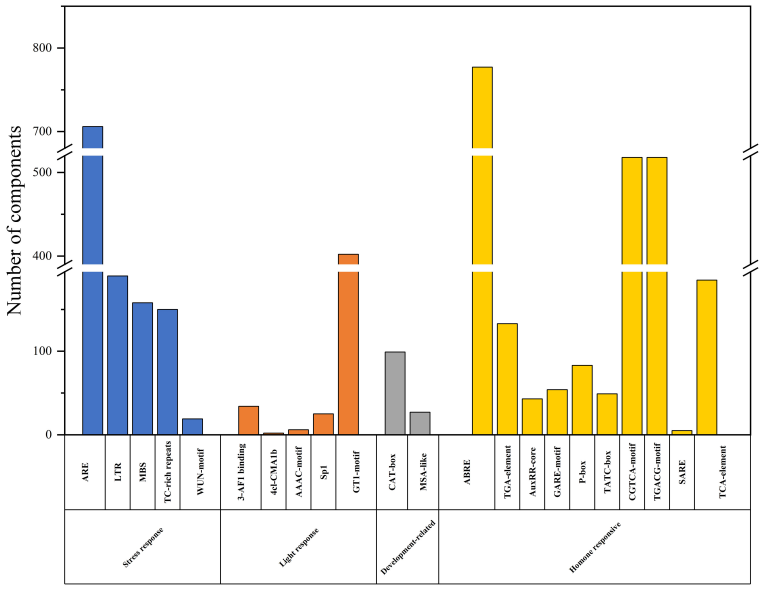

FIGURE 3
Cis-regulatory elements analysis in the promoter region of *BjuWRKY* genes. Cis-acting elements are divided into four categories based on functional annotation: stress response, light response, development-related, hormone responsive cis-acting elements.

highest number of genes was found in ChrA03 (25), followed by ChrB02, ChrA09 and ChrB05 with 23, 22 and 22 genes, respectively. The lowest number of individual genes were ChrA10, ChrA07 and ChrA01, ChrA06.

We also analyzed the replication events of the *BjuWRKY* gene. Gene duplication plays an important role in the amplification of gene families and their subsequent evolution. When two or more genes are located within a 200 kb chromosomal region, they are considered to be the result of tandem duplication events (Holub, 2001). In *BjuWRKY*, about 31.62% (92 out of 291) of the genes were found to have originated from tandem duplication events. The set of 39 tandemly duplicated *BjuWRKY*s contained 2-6 *BjuWRKY* genes. Specifically, the set of 29 tandemly duplicated *BjuWRKY*s contained 2 members, the set of 8 tandemly duplicated *BjuWRKY*s contained 3 members, and 4 and 6 members were involved in the set of 1 tandemly duplicated *BjuWRKY* (Supplementary Table S5), respectively. In addition to tandem duplication events, we observed that *BjuWRKY* genes are involved in segmental duplication, which indicates gene transfer and a change in the chromosome set (Figure 5). In addition, only about 2% of the *BjuWRKY* genes had ka/ks ratios exceeding 0.5 (Supplementary Figure S2), indicating that members of the *BjuWRKY* family are mainly under purifying selection.

3.6 *BjuWRKY* expression profiles under Cd stress conditions

To investigate the expression pattern of *BjuWRKY* genes in mustard under Cd stress, we obtained RNA-seq data from different organs of mustard. The dynamic expression patterns of 291 genes after Cd treatment were analyzed (Supplementary Table S6). The roots, stems and leaves were collected at 0 d, 1 d and 4 d of Cd treatment. The differential expression patterns of all genes were analyzed and grouped into 3 clusters (I, II, III) (Figure 6). Cluster I contained 75 *BjuWRKY* genes, cluster II 73 *BjuWRKY* genes, and cluster III 143 *BjuWRKY* genes. In roots, genes in cluster I showed different degrees of up-regulated expression at various time points after Cd treatment; in stems, most of them were up-regulated after 1 d of treatment and down-regulated for 4 d of treatment. In addition, most of the genes showed up-regulated expression in leaves, especially at 1 d of treatment. In contrast, most members of cluster II had the highest expression in roots, especially in leaves treated with Cd for 1 d. Only 13 genes did not show up-regulated expression. In cluster III, most of the genes in roots and stems showed an up-regulated trend.

3.7 Functional annotation and interaction network analysis of BjuWRKY proteins

To better characterize the function of *BjuWRKY* genes, we performed GO annotation and enrichment analyses based on the categories of biological process (BP), molecular function (MF), and cellular component (CC); these terms contribute to our comprehension of the gene's function at the molecular level (Figure 7). The GO-BP results predicted a large number (17) of significantly enriched terms. The most common and useful terms are cellular response to hydrogen peroxide (GO:0070301), regulation of phenylpropanoid metabolic process (GO: 2000762), cellular response to heat (GO: 0034605), defense response (GO: 0006952), response to hydrogen peroxide cellular response to stimuli (GO: 0042542), etc. GO-CC enrichment analyses revealed 9 high enrichments for nucleus (GO: 0005634), intracellular

10.3389/fpls.2024.1465905

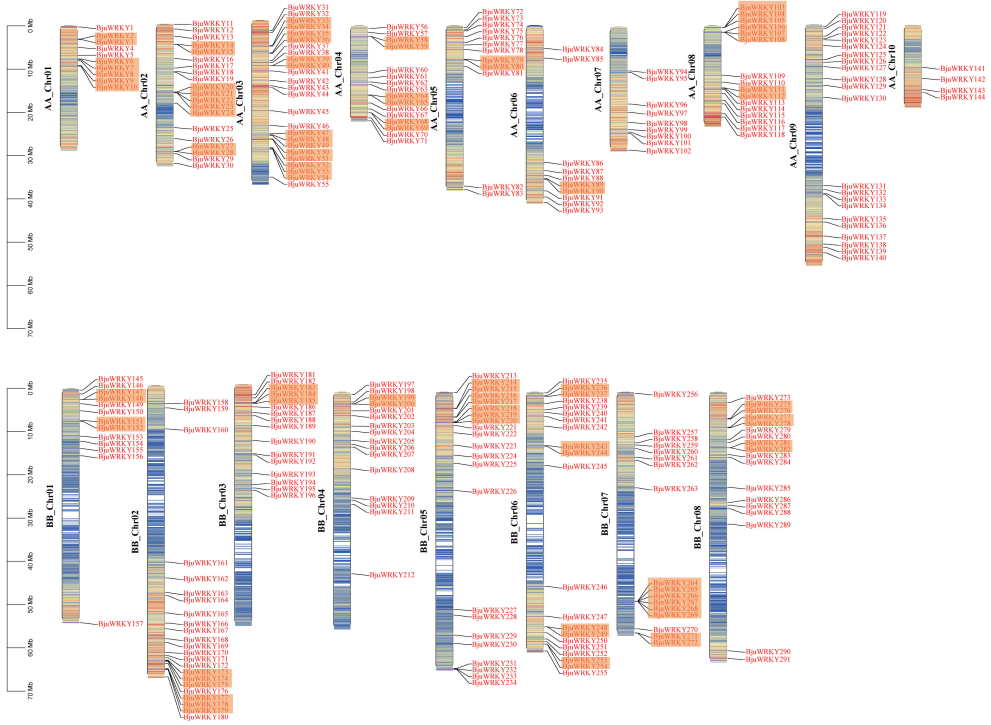

FIGURE 4
Distribution of the 291 *BjuWRKY* genes in the *B. juncea* genome. The colored columns represent chromosomes with the gene names shown on the right. Chromosome numbers are listed on the left, while chromosome sizes are indicated on the left side of the figure. The length of each chromosome on the left was estimated in mega base (Mb). The orange shadow represents tandem repeat genes.

membrane-bounded organelle (GO: 0043231), membrane-bounded organelle (GO: 0043227), intracellular organelle (GO: 0043229), organelle (GO: 0043226). The GO-MF enrichment detected 11 highly enriched terms, which included DNA binding (GO: 0003677), calmodulin binding (GO: 00905516), transcription factor activity (GO:0003700), transcription regulator activity (GO:0140110), and transcription regulatory region nucleic acid binding (GO: 0001067), etc. Overall, GO enrichment analysis confirmed the functional role of the *BjuWRKY* genes in cellular, molecular, and biological processes related to antioxidant enzymes, subcellular localization, and stress response. The Cytoscape plugin cytoHubba (Maximum Cluster Centrality (MCC) algorithm) was applied to identify 10 hub genes (Figure 8). Annotation of the 10 hub genes showed that they are mainly involved in stress response and specific binding (Supplementary Table S7).

3.8 Analysis of the expression pattern of key WRKY genes in different tissues under Cd stress

The hub genes in the protein-protein interaction network were selected for expression level validation (Figure 9). The results revealed that most of the genes were induced to be up-regulated for expression by Cd stress. Except for *BjuWRKY208*, the remaining *BjuWRKY* key genes were significantly up-regulated in roots at 1d and 4 d of Cd stress. Only the *BjuWRKY280* gene did not show a trend of increased and then decreased expression in roots after Cd stress. In stems, only *BjuWRKY290*, *BjuWRKY280*, and *BjuWRKY255* showed a gradual increase in expression after Cd stress, while the remaining genes displayed an increase followed by a decrease in expression trend. It is noteworthy that the *BjuWRKY215* gene was not induced to be expressed in stems treated with Cd for 1 d and 4 d. Notably, *BjuWRKY287* and *BjuWRKY215* were not induced to be expressed by Cd in leaves. In addition, *BjuWRKY205* and *BjuWRKY284* were significantly up-regulated for expression by Cd at 1 d and were not induced at 4 d. The opposite trend was observed for *BjuWRKY280*, whose expression was not induced by Cd treatment at 1 d and was significantly up-regulated by Cd treatment at 4 d.

Furthermore, we performed a correlation analysis between the RNA-seq and qRT-PCR results for ten selected genes. A correlation heatmap was established using the Sperman correlation method. The expression patterns of these genes exhibit a fundamental consistency with the transcriptome results, demonstrating a high correlation and thus indicating the reliability of the transcriptome data (Supplementary Figure S3).

4 Discussion

The *B. juncea* known for its widespread cultivation as a vegetable and oilseed worldwide, exhibits rapid growth and high biomass production (Kang et al., 2021; Singh et al., 2021). Its ability

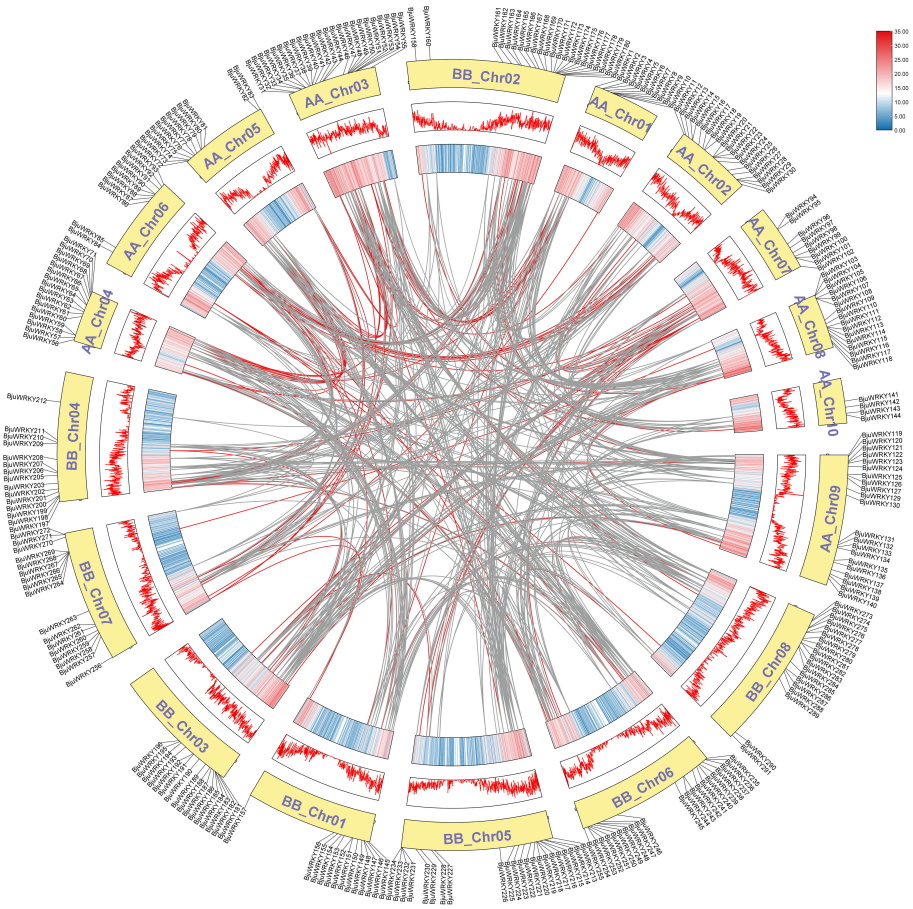

FIGURE 5
Synteny analysis of WRKY genes. Chromosomes were represented by yellow boxes with the gene names surrounding the boxes. Box with red line and colored box represents gene density. Segmental duplication gene pairs of *B. juncea* WRKY genes are linked by red lines. Gray lines indicate syntenic blocks in the *B. juncea* genome.

to tolerate and accumulate Cd confers a significant advantage in phytoremediation applications, allowing it to remediate soil while maintaining economic benefits (D'Alessandro et al., 2013; Li L. et al., 2023). Although multiple gene families related to *B. juncea* development and abiotic stresses have been reported (Khuman et al., 2024; Li et al., 2020; Verma et al., 2023), relatively few studies have been focused on heavy metal tolerance or sensitivity genes in *B. juncea*. The mechanisms of transport, uptake, and tolerance to Cd in *B. juncea* remain incompletely understood. Given that transcription factors of the *WRKY* family play pivotal roles in plant defense responses and secondary metabolism, studying the *BjuWRKY* family is crucial for elucidating the response mechanism of *B. juncea* to environmental factors, particularly heavy metal stress.

Transcription factors are essential in controlling plant development and stress responses. The WRKY transcription factors are not only in higher plants but also in other eukaryotes (Zhang and Wang, 2005). The publication of the genomes for *BjuWRKY* and its parents has enabled the identification of gene families associated with heavy metal response at the genome-wide level (Kang et al., 2021). In this study, we conducted a genome-wide analysis of the *B. juncea* WRKY transcription factor family and explored its potential functions under Cd stress. In the intricate plant evolution, gene expansion events emerge as pivotal forces driving the number of gene families, thereby contributing to the diversity and complexity of plant genomes (Xie et al., 2022). under this underground, we identified 291 WRKY genes in the *B. juncea* genome, significantly more than in *A. thaliana* (74) and *Oryza sativa* (109) (Eulgem and Somssich, 2007; Sahebi et al., 2018). The large number of genes may be attributed to duplication events during genome evolution. Related studies suggest that tandem and segmental duplication events are the primary drivers of WRKY evolution in plants, closely related to the expansion of gene functions and environmental adaptation (Chang and Duda, 2012). According to our statistics, 74 pairs of tandem duplicates and 274 pairs of segmental duplicates are present in the *B. juncea*

10.3389/fpls.2024.1465905

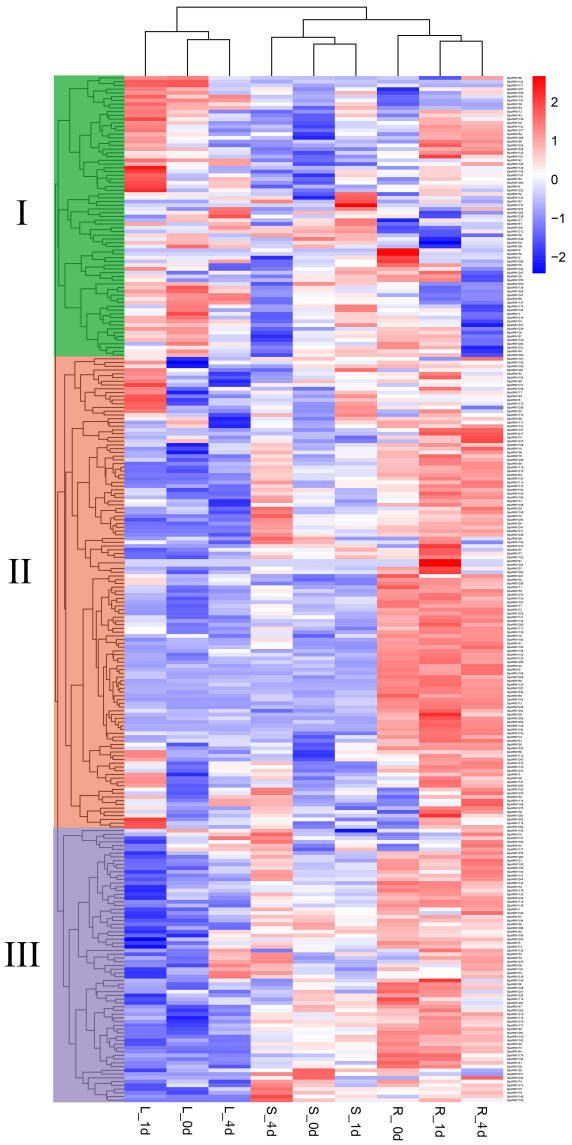

FIGURE 6
Expression analysis of *BjuWRKY* genes in several organs. The 0d, 1d, and 4d tags indicate the time-points when the samples were harvested. In the expression bar, the red color shows high, and the blue color shows low, expression levels. The expression heat map was created using FPKM values.

gene family, with a Ka/Ks ratio less than 0.5, indicating that the genes have experienced repetitive events and strong purifying selection pressures during the evolutionary process. Similar to typical WRKY family proteins in other species, the 291 WRKY genes were classified into groups I, IIa, IIb, IIc, IId, IIe, and III (Yang et al., 2023). The amino acid sequences of the WRKY proteins are highly conserved (Supplementary Figures S1–S3), with proteins in the same group sharing the same protein motifs. For instance, motifs 2 and 3 are present in all *BjuWRKYs*, and motifs 4,5,7 occur together in group I.

The expression pattern of WRKY gene in different tissues provides valuable insights into their functionality. Using transcriptome data, our analysis revealed that the expression of WRKY family genes varied in different tissues (Figure 6). The expression patterns of WRKY genes in various tissues and under abiotic stresses have been reported for several species. For instance, EjWRKY17 has been shown to enhance drought tolerance in transgenic *A. thaliana* (Wang et al., 2021). Similarly, overexpression of *AtWRKY30* significantly elevated resistance to salt stress in *A. thaliana* (Scarpeci et al., 2013). Furthermore, overexpression of *GmWRKY142* in *A. thaliana* and soybean hairy roots leads to decrease Cd uptake and positively regulate Cd tolerance (Cai et al., 2020).

The promoter region of the *BjuWRKY* gene contains various hormone and stress response elements, with some elements such as

10.3389/fpls.2024.1465905

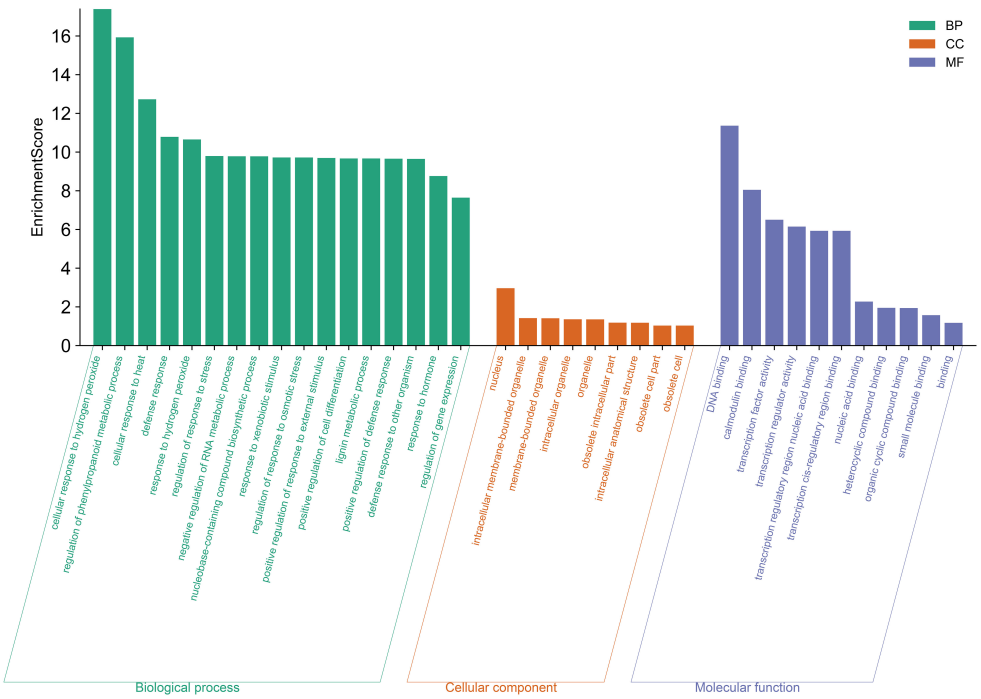

FIGURE 7
GO and functional annotation of BjuWRKY.

ARE, GTI-motif, ABRE, CGTCA-motif, and TGACG-motif exceeding 400 occurrences. This suggests that these genes may play important roles in response to stress, hormones, light, and developmental processes. In addition, GO enrichment analysis demonstrated that the molecular functions of *BjuWRKY* are primarily involved in stress- and defense-related processes. The highest number of genes was found in cellular component processes, which is consistent with our results on the subcellular

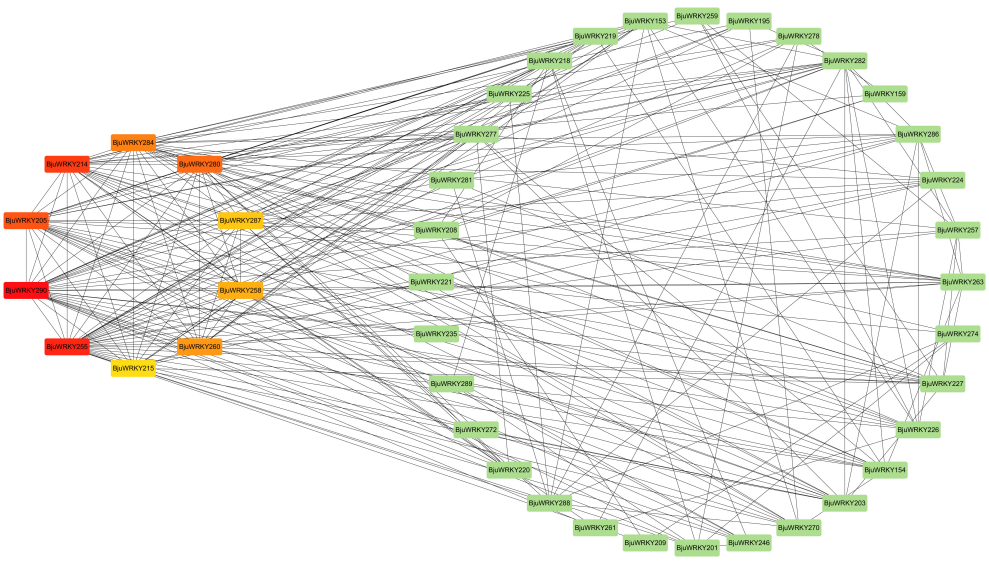

FIGURE 8
Interaction network of BjuWRKY factors in *B. juncea* according to orthologs in *Arabidopsis*.

10.3389/fpls.2024.1465905

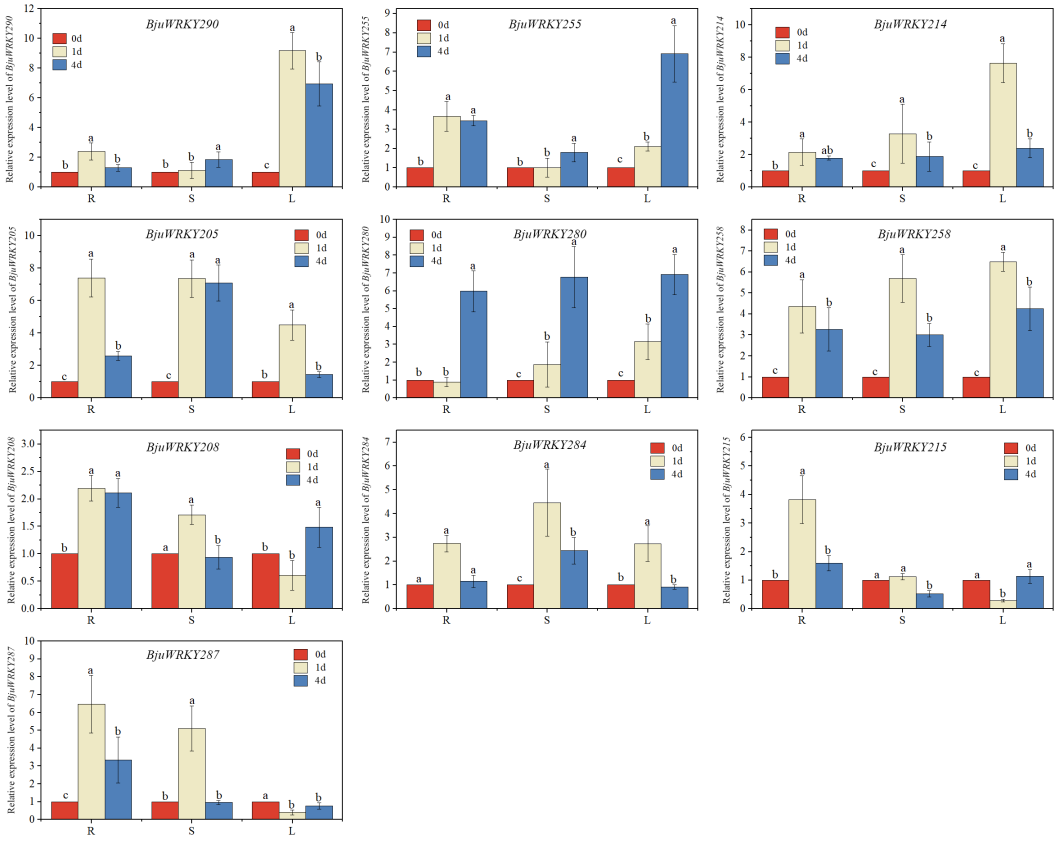

FIGURE 9
qRT-PCR verification of the Cd stress response of 10 *BjuWRKY*s. Expression analysis of *BjuWRKY*s under Cd stress conditions, determined by qRT-PCR. (n=3, $p < 0.05$). Different letters above bars indicate significant differences.

localization of BjuWRKY proteins. Based on the characterization of transcription factors, BjuWRKY proteins were significantly enriched in DNA binding, calmodulin binding, and transcription activity functions during molecular function processes.

Using String and Cytohubba plugin, we identified 10 hub genes, all of which were functionally annotated. In addition, WRKY TFs recognize and bind to the TTGAC(C/T) W-box in the promoter regions of target genes (Takeda, 2021). WRKY TFs can bind not only upstream promoters but also to upstream promoters of other genes regulated by WRKY TFs (Brand et al., 2013; Yang et al., 2023). Thus, it is speculated that in this network, the five hub genes annotated as "Interacts specifically with the W box". It is speculated that in this network, they may regulate plant tolerance more by working together with target genes.

5 Conclusion

In this study, a comprehensive analysis of the WRKY gene family in mustard (*Brassica juncea*) was conducted, identifying a total of 291 WRKY family genes and elucidating their evolutionary relationships. These genes were systematically classified into three main groups, with group II further subdivided into five distinct subgroups based on their phylogenetic affinities. Each group member exhibited a conserved gene structure and motif composition, underscoring their evolutionary relatedness. A thorough examination of the basic features, gene structures, conserved motifs, and cis-regulatory elements of these *BjuWRKY* genes was performed, offering a foundational framework for understanding the *BjuWRKY* gene family. To investigate the expression patterns of *BjuWRKY* genes, RNA-seq and RT-qPCR analyses were employed. The results revealed that 10 selected *BjuWRKY* genes displayed tissue-specific expression profiles and were significantly influenced by Cd stress. These findings suggest that these genes may play crucial roles in modulating mustard's response to Cd stress. To sum up, the study provides a solid foundation for further functional characterization of *BjuWRKY* genes implicated in stress resistance mechanisms in B. juncea, thereby advancing our understanding of the molecular basis of stress tolerance in this important crop species.

Data availability statement

The data presented in the study are deposited in the National Center for Biotechnology Information Sequence Read Archive repository, accession number PRJNA1133808. The names of the repository/repositories and accession number(s) can be found in the article/Supplementary Material.

Author contributions

SL: Conceptualization, Data curation, Software, Writing – original draft. QJ: Data curation, Software, Writing – original draft. XA: Conceptualization, Data curation, Formal analysis, Funding acquisition, Resources, Supervision, Writing – original draft. CC: Formal analysis, Methodology, Writing – review & editing. XL: Formal analysis, Investigation, Writing – review & editing. TL: Data curation, Resources, Writing – review & editing. LZ: Data curation, Investigation, Writing – review & editing.

Funding

The author(s) declare that no financial support was received for the research, authorship, and/or publication of this article.

Conflict of interest

The authors declare that the research was conducted in the absence of any commercial or financial relationships that could be construed as a potential conflict of interest.

Publisher's note

Supplementary material

The Supplementary Material for this article can be found online at: https://www.frontiersin.org/articles/10.3389/fpls.2024.1465905/full#supplementary-material

References

Agarwal, P., Mitra, M., Banerjee, S., and Roy, S. (2020). MYB4 transcription factor, a member of R2R3-subfamily of MYB domain protein, regulates cadmium tolerance via enhanced protection against oxidative damage and increases expression of PCS1 and MT1C in *Arabidopsis*. *Plant Sci.* 297, 110501. doi: 10.1016/j.plantsci.2020.110501

Bailey, T. L., Boden, M., Buske, F. A., Frith, M., Grant, C. E., Clementi, L., et al. (2009). MEME SUITE: tools for motif discovery and searching. *Nucleic Acids Res.* 37, W202–W208. doi: 10.1093/nar/gkp335

Brand, L. H., Fischer, N. M., Harter, K., Kohlbacher, O., and Wanke, D. (2013). Elucidating the evolutionary conserved DNA-binding specificities of WRKY transcription factors by molecular dynamics and in *vitro* binding assays. *Nucleic Acids Res.* 41, 9764–9778. doi: 10.1093/nar/gkt732

Cai, Z., Xian, P., Wang, H., Lin, R., Lian, T., Cheng, Y., et al. (2020). Transcription factor *GmWRKY142* confers cadmium resistance by up-regulating the cadmium tolerance 1-like genes. *Front. Plant Sci.* 11, 724. doi: 10.3389/fpls.2020.00724

Chang, D., and Duda, T. J. (2012). Extensive and continuous duplication facilitates rapid evolution and diversification of gene families. *Mol. Biol. Evol.* 29, 2019–2029. doi: 10.1093/molbev/mss068

Chen, C., Chen, H., Zhang, Y., Thomas, H. R., Frank, M. H., He, Y., et al. (2020). TBtools: an integrative toolkit developed for interactive analyses of big biological data. *Mol. Plant* 13, 1194–1202. doi: 10.1016/j.molp.2020.06.009

Chen, H., Wang, T., He, X., Cai, X., Lin, R., Liang, J., et al. (2022). BRAD V3.0: an upgraded Brassicaceae database. *Nucleic Acids Res.* 50, D1432–D1441. doi: 10.1093/nar/gkab1057

Chen, L., Long, C., Wang, D., and Yang, J. (2020). Phytoremediation of cadmium (Cd) and uranium (U) contaminated soils by *Brassica juncea* L. enhanced with exogenous application of plant growth regulators. *Chemosphere* 242, 125112. doi: 10.1016/j.chemosphere.2019.125112

Chin, C. H., Chen, S. H., Wu, H. H., Ho, C. W., Ko, M. T., and Lin, C. Y. (2014). cytoHubba: identifying hub objects and sub-networks from complex interactome. *BMC Syst. Biol.* 8 Suppl 4, S11. doi: 10.1186/1752-0509-8-S4-S11

Conesa, A., and Gotz, S. (2008). Blast2GO: A comprehensive suite for functional analysis in plant genomics. *Int. J. Plant Genomics* 2008, 619832. doi: 10.1155/2008/619832

D'Alessandro, A., Taamalli, M., Gevi, F., Timperio, A. M., Zolla, L., and Ghnaya, T. (2013). Cadmium stress responses in Brassica juncea: hints from proteomics and metabolomics. *J. Proteome Res.* 12, 4979–4997. doi: 10.1021/pr400793e

Du, J., Guo, Z., Li, R., Ali, A., Guo, D., Lahori, A. H., et al. (2020). Screening of Chinese mustard (*Brassica juncea* L.) cultivars for the phytoremediation of Cd and Zn based on the plant physiological mechanisms. *Environ. pollut.* 261, 114213. doi: 10.1016/j.envpol.2020.114213

Edgar, R. C. (2004). MUSCLE: multiple sequence alignment with high accuracy and high throughput. *Nucleic Acids Res.* 32, 1792–1797. doi: 10.1093/nar/gkh340

Eulgem, T., Rushton, P. J., Robatzek, S., and Somssich, I. E. (2000). The WRKY superfamily of plant transcription factors. *Trends Plant Sci.* 5, 199–206. doi: 10.1016/S1360-1385(00)01600-9

Eulgem, T., and Somssich, I. E. (2007). Networks of WRKY transcription factors in defense signaling. *Curr. Opin. Plant Biol.* 10, 366–371. doi: 10.1016/j.pbi.2007.04.020

Gulzar, F., Fu, J., Zhu, C., Yan, J., Li, X., Meraj, T. A., et al. (2021). Maize WRKY transcription factor *ZmWRKY79* positively regulates drought tolerance through elevating ABA biosynthesis. *Int. J. Mol. Sci.* 22, 10080. doi: 10.3390/ijms221810080

Han, Y., Fan, T., Zhu, X., Wu, X., Ouyang, J., Jiang, L., et al. (2019). WRKY12 represses GSH1 expression to negatively regulate cadmium tolerance in Arabidopsis. *Plant Mol. Biol.* 99, 149–159. doi: 10.1007/s11103-018-0809-7

Han, Y., Hou, Z., He, Q., Zhang, X., Yan, K., Han, R., et al. (2021). Genome-wide characterization and expression analysis of bZIP gene family under abiotic stress in *Glycyrrhiza uralensis*. *Front. Genet.* 12, 754237. doi: 10.3389/fgene.2021.754237

Han, L., Wu, X., Zhang, X., Hou, K., Zhang, H., and Shen, C. (2022). Identification and functional analysis of cation-efflux transporter 1 from *Brassica juncea* L. *BMC Plant Biol.* 22, 174. doi: 10.1186/s12870-022-03569-x

Holub, E. B. (2001). The arms race is ancient history in Arabidopsis, the wildflower. *Nat. Rev. Genet.* 2, 516–527. doi: 10.1038/35080508

Hu, W., Ren, Q., Chen, Y., Xu, G., and Qian, Y. (2021). Genome-wide identification and analysis of WRKY gene family in maize provide insights into regulatory network in response to abiotic stresses. *BMC Plant Biol.* 21, 427. doi: 10.1186/s12870-021-03206-z

Kamal, M. A., Perveen, K., Khan, F., Sayyed, R. Z., Hock, O. G., Bhatt, S. C., et al. (2023). Effect of different levels of EDTA on phytoextraction of heavy metal and growth of Brassica juncea L. *Front. Microbiol.* 14, 1228117. doi: 10.3389/fmicb.2023.1228117

Kang, L., Qian, L., Zheng, M., Chen, L., Chen, H., Yang, L., et al. (2021). Genomic insights into the origin, domestication and diversification of Brassica juncea. *Nat. Genet.* 53, 1392–1402. doi: 10.1038/s41588-021-00922-y

Khuman, A., Yadav, V., and Chaudhary, B. (2024). Evolutionary dynamics of the cytoskeletal profilin gene family in *Brassica juncea* L. reveal its roles in silique development and stress resilience. *Int. J. Biol. Macromol.* 266, 131247. doi: 10.1016/j.ijbiomac.2024.131247

Kumar, S., Stecher, G., and Tamura, K. (2016). MEGA7: molecular evolutionary genetics analysis version 7.0 for bigger datasets. *Mol. Biol. Evol.* 33, 1870–1874. doi: 10.1093/molbev/msw054

Li, S., Han, X., Lu, Z., Qiu, W., Yu, M., Li, H., et al. (2022). MAPK cascades and transcriptional factors: regulation of heavy metal tolerance in plants. *Int. J. Mol. Sci.* 23, 4463. doi: 10.3390/ijms23084463

Li, G., Shah, A. A., Khan, W. U., Yasin, N. A., Ahmad, A., Abbas, M., et al. (2021). Hydrogen sulfide mitigates cadmium induced toxicity in *Brassica rapa* by modulating physiochemical attributes, osmolyte metabolism and antioxidative machinery. *Chemosphere* 263, 127999. doi: 10.1016/j.chemosphere.2020.127999

Li, L., Wang, S., Wu, S., Rao, S., Li, L., Cheng, S., et al. (2023). Morphological and physiological indicators and transcriptome analyses reveal the mechanism ofselenium multilevel mitigation of cadmium damage in *Brassica juncea*. *Plants-Basel* 12, 1583. doi: 10.3390/plants12081583

Li, M., Xie, F., Li, Y., Gong, L., Luo, Y., Zhang, Y., et al. (2020). Genome-wide analysis of the heat shock transcription factor gene family in *Brassica juncea*: Structure, evolution, and expression profiles. *DNA Cell Biol.* 39, 1990–2004. doi: 10.1089/dna.2020.5922

Li, S., Zhuo, R., Yu, M., Lin, X., Xu, J., Qiu, W., et al. (2023). A novel gene *SpCTP3* from the hyperaccumulator *Sedum plumbizincicola* redistributes cadmium and increases its accumulation in transgenic Populus× canescens. *Front. Plant Sci.* 14, 1111789. doi: 10.3389/fpls.2023.1111789

Lin, T., Yang, W., Lu, W., Wang, Y., and Qi, X. (2017). Transcription factors *PvERF15* and *PvMTF-1* form a cadmium stress transcriptional pathway. *Plant Physiol.* 173, 1565. doi: 10.1104/pp.16.01729

Liu, M., He, X., Feng, T., Zhuo, R., Qiu, W., Han, X., et al. (2019). cDNA library for mining functional genes in *Sedum alfredii* Hance related to cadmium tolerance and characterization of the roles of a novel *SaCTP2* gene in enhancing cadmium hyperaccumulation. *Environ. Sci. Technol.* 53, 10926–10940. doi: 10.1021/acs.est.9b03237

Liu, Z., Li, X., Li, J., Zhao, H., Deng, X., Su, Y., et al. (2022). Identification of gene modules and hub genes associated with *Sporisorium scitamineum* infection using weighted gene co-expression network analysis. *J. Fungi* 8, 852. doi: 10.3390/jof8080852

Liu, L., Yin, H., Liu, Y., Shen, L., Yang, X., Zhang, D., et al. (2021). Analysis of cadmium-stress-induced microRNAs and their targets reveals bra-miR172b-3p as a potential Cd^{2+}-specific resistance factor in Brassica juncea. *Processes* 9, 1099. doi: 10.3390/pr9071099

Liu, H., Zhao, H., Wu, L., Liu, A., Zhao, F. J., and Xu, W. (2017). Heavy metal ATPase 3 (HMA3) confers cadmium hypertolerance on the cadmium/zinc hyperaccumulator *Sedum plumbizincicola*. *New Phytol.* 215, 687–698. doi: 10.1111/nph.2017.215.issue-2

Meraklı, N., and Memon, A. (2023). Gene Expression of metal transporting P-Type ATPases HMA2 and HMA4 in *Brassica juncea* L. grown at different Zn levels. *Russian J. Plant Physiol.* 70, 34. doi: 10.1134/S102144372260283X

Mistry, J., Finn, R. D., Eddy, S. R., Bateman, A., and Punta, M. (2013). Challenges in homology search: HMMER3 and convergent evolution of coiled-coil regions. *Nucleic Acids Res.* 41, e121. doi: 10.1093/nar/gkt263

Qin, Y., Yu, H., Cheng, S., Liu, Z., Yu, C., Zhang, X., et al. (2022). Genome-wide analysis of the WRKY gene family in Malus domestica and the role of *MdWRKY70L* in response to drought and salt stresses. *Genes* 13, 1068. doi: 10.3390/genes13061068

Sahebi, M., Hanafi, M. M., Rafii, M. Y., Mahmud, T., Azizi, P., Osman, M., et al. (2018). Improvement of drought tolerance in rice (*Oryza sativa* L.): genetics, genomic tools, and the WRKY gene family. *BioMed. Res. Int.* 2018, 3158474. doi: 10.1155/2018/3158474

Scarpeci, T. E., Zanor, M. I., Mueller-Roeber, B., and Valle, E. M. (2013). Overexpression of *AtWRKY30* enhances abiotic stress tolerance during early growth stages in Arabidopsis thaliana. *Plant Mol. Biol.* 83, 265–277. doi: 10.1007/s11103-013-0090-8

Singh, K. P., Kumari, P., and Rai, P. K. (2021). Current status of the disease-resistant gene(s)/QTLs, and strategies for improvement in brassica juncea. *Front. Plant Sci.* 12, 617405. doi: 10.3389/fpls.2021.617405

Sun, P., Jiao, B., Yang, Y., Shan, L., Li, T., Li, X., et al. (2022). WGDI: A user-friendly toolkit for evolutionary analyses of whole-genome duplications and ancestral karyotypes. *Mol. Plant* 15, 1841–1851. doi: 10.1016/j.molp.2022.10.018

Sun, R., Tian, R., Ma, D., Wang, S., and Liu, C. (2018). Comparative transcriptome study provides insights into acquisition of embryogenic ability in upland cotton during somatic embryogenesis. *J. Cotton Res.* 1, 1–13. doi: 10.1186/s42397-018-0010-1

Szczygłowska, M., Piekarska, A., Konieczka, P., and Namieśnik, J. (2011). Use of brassica plants in the phytoremediation and biofumigation processes. *Int. J. Mol. Sci.* 12, 7760–7771. doi: 10.3390/ijms12117760

Takeda, J. (2021). Molecular mechanisms of UVR8-mediated photomorphogenesis derived from revaluation of action spectra. *Photochem. Photobiol.* 97, 903–910. doi: 10.1111/php.13459

Tang, Y., Guo, J., Zhang, T., Bai, S., He, K., and Wang, Z. (2021). Genome-wide analysis of WRKY gene family and the dynamic responses of key WRKY genes involved in *Ostrinia furnacalis* attack in Zea mays. *Int. J. Mol. Sci.* 22, 13045. doi: 10.3390/ijms222313045

Verma, D., Kaushal, N., Balhara, R., and Singh, K. (2023). Genome-wide analysis of catalase gene family reveal insights into abiotic stress response mechanism in *Brassica juncea* and *B. rapa*. *Plant Sci.* 330, 111620. doi: 10.1016/j.plantsci.2023.111620

Wang, D., Chen, Q., Chen, W., Liu, X., Xia, Y., Guo, Q., et al. (2021). A WRKY transcription factor, ejWRKY17, from eriobotrya japonica enhances drought tolerance in transgenic arabidopsis. *Int. J. Mol. Sci.* 22, 5539. doi: 10.3390/ijms22115593

Wani, S. H., Anand, S., Singh, B., Bohra, A., and Joshi, R. (2021). WRKY transcription factors and plant defense responses: latest discoveries and future prospects. *Plant Cell Rep.* 40, 1071–1085. doi: 10.1007/s00299-021-02691-8

Wei, X., Geng, M., Yuan, J., Zhan, J., Liu, L., Chen, Y., et al. (2024). GhRCD1 promotes cotton tolerance to cadmium by regulating the GhbHLH12-GhMYB44-GhHMA1 transcriptional cascade. *Plant Biotechnol. J.* 7, 1–20. doi: 10.1111/pbi.14301

Wu, W., Zhu, S., Xu, L., Zhu, L., Wang, D., Liu, Y., et al. (2022). Genome-wide identification of the Liriodendron chinense WRKY gene family and its diverse roles in response to multiple abiotic stress. *BMC Plant Biol.* 22, 25. doi: 10.1186/s12870-021-03371-1

Xie, T., Chen, C., Li, C., Liu, J., Liu, C., and He, Y. (2018). Genome-wide investigation of WRKY gene family in pineapple: evolution and expression profiles during development and stress. *BMC Genomics* 19, 490. doi: 10.1186/s12864-018-4880-x

Xie, M., Zhao, C., Song, M., Xiang, Y., and Tong, C. (2022). Genome-wide identification and comparative analysis of *CLE* family in rapeseed and its diploid progenitors. *Front. Plant Sci.* 13, 998082. doi: 10.3389/fpls.2022.998082

Xiong, R., Peng, Z., Zhou, H., Xue, G., He, A., Yao, X., et al. (2024). Genome-wide identification, structural characterization and gene expression analysis of the WRKY transcription factor family in pea (*Pisum sativum* L.). *BMC Plant Biol.* 24, 113. doi: 10.1186/s12870-024-04774-6

Xu, L., Jin, L., Long, L., Liu, L., He, X., Gao, W., et al. (2012). Overexpression of *GbWRKY1* positively regulates the Pi starvation response by alteration of auxin sensitivity in Arabidopsis. *Plant Cell Rep.* 31, 2177–2188. doi: 10.1007/s00299-012-1328-7

Yang, R., Huang, T., Song, W., An, Z., Lai, Z., and Liu, S. (2023). Identification of WRKY gene family members in amaranth based on a transcriptome database and functional analysis of AtrWRKY42-2 in betalain metabolism. *Front. Plant Sci.* 14, 1300522. doi: 10.3389/fpls.2023.1300522

Yang, L., Li, N., Kang, Y., Liu, J., Wang, Y., Sun, H., et al. (2022). Selenium alleviates toxicity in *Amaranthus hypochondriacus* by modulating the synthesis of thiol compounds and the subcellular distribution of cadmium. *Chemosphere* 291, 133108. doi: 10.1016/j.chemosphere.2021.133108

Yang, J., Wang, J., Li, Z., Li, X., He, Z., Zhang, L., et al. (2021). Genomic signatures of vegetable and oilseed allopolyploid Brassica juncea and genetic loci controlling the accumulation of glucosinolates. *Plant Biotechnol. J.* 19, 2619–2628. doi: 10.1111/pbi.v19.12

Yao, X., Cai, Y., Yu, D., and Liang, G. (2018). bHLH104 confers tolerance to cadmium stress in *Arabidopsis thaliana*. *J. Integr. Plant Biol.* 60, 69–80. doi: 10.1111/jipb.12658

Ye, H., Qiao, L., Guo, H., Guo, L., Ren, F., Bai, J., et al. (2021). Genome-wide identification of wheat WRKY gene family reveals that taWRKY75-A is referred to drought and salt resistances. *Front. Plant Sci.* 12, 663118. doi: 10.3389/fpls.2021.663118

Yu, F., Huaxia, Y., Lu, W., Wu, C., Cao, X., and Guo, X. (2012). GhWRKY15, a member of the WRKY transcription factor family identified from cotton (*Gossypium hirsutum* L.), is involved in disease resistance and plant development. *BMC Plant Biol.* 12, 1–18. doi: 10.1186/1471-2229-12-144

Zentgraf, U., Laun, T., and Miao, Y. (2010). The complex regulation of WRKY53 during leaf senescence of Arabidopsis thaliana. *Eur. J. Cell Biol.* 89, 133–137. doi: 10.1016/j.ejcb.2009.10.014

Zhang, Z. (2022). KaKs_Calculator 3.0: Calculating selective pressure on coding and non-coding sequences. *Genomics Proteomics Bioinf.* 20, 536–540. doi: 10.1016/j.gpb.2021.12.002

Zhang, Q., Cai, W., Ji, T. T., Ye, L., Lu, Y. T., and Yuan, T. T. (2020). WRKY13 enhances cadmium tolerance by promoting D-CYSTEINE DESULFHYDRASE and hydrogen sulfide production. *Plant Physiol.* 183, 345–357. doi: 10.1104/pp.19.01504

Zhang, Y., and Wang, L. (2005). The WRKY transcription factor superfamily: its origin in eukaryotes and expansion in plants. *BMC Evol. Biol.* 5, 1. doi: 10.1186/1471-2148-5-1

Zhang, Z., Xiao, J., Wu, J., Zhang, H., Liu, G., Wang, X., et al. (2012). ParaAT: a parallel tool for constructing multiple protein-coding DNA alignments. *Biochem. Biophys. Res. Commun.* 419, 779–781. doi: 10.1016/j.bbrc.2012.02.101

Zheng, J., Li, H., Guo, Z., Zhuang, X., Huang, W., Mao, C., et al. (2022). Comprehensive identification and expression profiling of the VQ motif-containing gene family in *Brassica juncea*. *Biology-Basel* 11, 1814. doi: 10.3390/biology11121814

frontiers | Frontiers in Plant Science

TYPE Original Research
PUBLISHED 17 October 2024
DOI 10.3389/fpls.2024.1467006

OPEN ACCESS

EDITED BY
Xiangshu Dong,
Yunnan University, China

REVIEWED BY
Xiaonan Li,
Shenyang Agricultural University, China
Wei Liu,
Fujian Agriculture and Forestry University, China
Yinbo Ma,
Yangzhou University, China

*CORRESPONDENCE
Shuxin Xuan
yyxsx@hebau.edu.cn
Jianjun Zhao
jjz1971@aliyun.com

RECEIVED 19 July 2024
ACCEPTED 23 September 2024
PUBLISHED 17 October 2024

CITATION
Li J, Fan M, Zhang X, Yang L, Hou G, Yang L, Li N, Xuan S and Zhao J (2024) Integratedly analyzed quantitative proteomics with transcriptomics to discover key genes via *fg-1* non-heading mutant in the early heading stage of Chinese cabbage.
Front. Plant Sci. 15:1467006.
doi: 10.3389/fpls.2024.1467006

Integratedly analyzed quantitative proteomics with transcriptomics to discover key genes via *fg-1* non-heading mutant in the early heading stage of Chinese cabbage

Jingrui Li, Mi Fan, Xiaomeng Zhang, Liling Yang, Guangguang Hou, Lei Yang, Na Li, Shuxin Xuan* and Jianjun Zhao*

Collaborative Innovation Center of Vegetable Industry in Hebei, Hebei Key Laboratory of Vegetable Germplasm Innovation and Utilization, College of Horticulture, Hebei Agricultural University, Baoding, Hebei, China

Leaf heading is an important agronomic trait of Chinese cabbage, which directly affects its yield. Leaf heading formation in Chinese cabbage is controlled by its internal genotype and external environmental factors, the underlying mechanism of which remains poorly understood. To discover the leaf heading formation mechanism more deeply, this study analyzed the correlation between proteomic and transcriptomic data in the leaf heading formation mutant *fg-1* generated by EMS. iTRAQ-based quantitative proteomics techniques were performed to identify the protein expression profiles during the key periods of the early heading stage in the section of the soft leaf apical region (section a) and the whole leaf basal region (section d). We first identified 1,246 differentially expressed proteins (DEPs) in section a and 1,055 DEPs in section d. Notably, transcriptome–proteome integrated analysis revealed that 207 and 278 genes showed consistent trends at the genes' and proteins' expression levels in section a and section d, respectively. KEGG analyses showed that the phenylpropanoid biosynthesis pathway was enriched in both sections a and d. Furthermore, 86 TFs exhibited co-upregulation or co-downregulation, and seven out of 86 were involved in plant hormone synthesis and signal transduction pathways. This indicates that they are potentially related to the leaf heading formation in Chinese cabbage. Taken together, we have identified several key early-heading-formation-related factors via integration analysis of the transcriptomics and proteomics data. This provides sufficient gene resources to discover the molecular mechanism of leaf heading formation.

KEYWORDS

***Brassica rapa*, leaf heading, *fg-1* EMS mutant, quantitative proteomics techniques, integration analysis**

1 Introduction

Chinese cabbage (*Brassica rapa* ssp. *pekinensis*) is an important leafy vegetable crop with a leafy head that provides abundant mineral nutrients, crude fiber, and vitamins for human diet, is a popular vegetable in East Asia, particularly in China, Korea, and Japan, and has become a worldwide vegetable crop (Ramchiary et al., 2011; Park et al., 2020). The leafy head is an essential agronomic trait to evaluate the yield and quality of Chinese cabbage. The life cycle of Chinese cabbage undergoes nine stages: germination, seedling, rosette, folding, heading, post-heading, bolting, flowering, and podding (Yu et al., 2000; Wang et al., 2011). After the rosette stage, the edges of new leaves curl inward, the leaf angle decreases, and the leafy head forms (Li et al., 2019b). Heading formation is an extremely complex biological process in many leafy vegetables such as lettuce and cabbage. Numerous researchers have attempted to elucidate the molecular mechanisms of leaf heading formation related to morphology and genetics (Tabusam et al., 2022; Cheng et al., 2016; Yu et al., 2020; Alemán-Báez et al., 2022).

The basis of leafy head formation is leaf development. Currently, research on the leaf development mechanism of the model plant *Arabidopsis* is the most in-depth. Leaf-polarity-related genes have been identified, and the regulatory network is relatively clear (Ali et al., 2020). The related research results have laid the foundation for the study of leafy head development in Chinese cabbage. Chinese cabbage, also a member of the Brassicaceae family, has curled leaves and forms leafy heads with different embracing models, which is a specific trait for some *Brassica* species but not for *Arabidopsis* species. Moreover, the Chinese cabbage genome has undergone a triploid replication process, so the molecular regulatory mechanism of leaf development, especially leafy head development, is much more complex than that of *Arabidopsis* (Wang et al., 2011). The He Yuke Laboratory of the Chinese Academy of Sciences was the first to confirm at the molecular level that plant auxin genes are involved in regulating the formation of Chinese cabbage leaf heading (He et al., 2000; Yu et al., 2000, 2013). The whole-genome sequence analysis of Chinese cabbage chiifu401 identified the organ morphology and development-related genes (including auxin synthesis, transport, signal transduction, etc.) that may affect leaf heading development (Wang et al., 2011; Cheng et al., 2016). Using used 199 Chinese cabbage (*B. rapa*) with leaf heading and 119 cabbage (*B. oleracea*) non-heading genotypes as materials to reveal leaf heading development by genomic resequencing showed that leaf heading development is related to hormone and dorsoventrality-related genes as well as small-molecule-RNA (miRNA) gene.

It is generally believed that transcriptional profiling provides an overview of the potential functions of genes (Zhang et al., 2017). At the transcriptional level, the mechanism of leafy head formation has been preliminarily analyzed (Wang et al., 2012; Sun et al., 2019). However, most biological functions are carried out by proteins, and detecting changes in protein expression is thus more valuable than detecting changes in gene expression. Quantitative proteomics techniques, isobaric tags for relative absolute quantitation (iTRAQ)/tandem mass tag (TMT), have been used to analyze biological processes (Li et al., 2022; Liu et al., 2023) and leafy head formation (Zhang et al., 2016). Although transcriptomic and proteomic analyses are independent, a gene can control the generation of several proteins, and the synthesis of a protein may also involve the transcription of multiple genes. Therefore, gene transcription or protein translation alone cannot fully reflect the regulatory network of gene expression during plant development. In recent years, the integration of transcriptomics and proteomics has gradually become an important strategy to study the mechanisms of biological processes and the responses to various abiotic and biological stresses (Zhang et al., 2018; Ding et al., 2020). However, few studies have analyzed leafy head formation through a method integrating transcriptomics and proteomics (Zhang et al., 2016).

Leafy head formation, a quantitative trait additively controlled by low-dominance effects, is a complex biological process affected by many factors such as hormones, temperature, light, and so on (Ito and Kato, 1957; Tanaka et al., 2009). Exogenous GA_3 treatment leads to the non-heading mutant plant phenotype restored to the heading of the wild type of Chinese cabbage (Gao et al., 2020), and low temperature induced leaf heading formation (Zhang et al., 2016). Notably, former studies verified that the leafy-head-formation-related genes normally used different heading types of natural population materials, but their genetic backgrounds are too complex to identify the key genes efficiently. Besides that, most of the studies identify the related genes at the transcriptional level, which cannot fully refer to the real regulated functions of proteins. Therefore, in the present study, we selected flat growth mutant (*fg-1*), which was obtained from the EMS mutant library constructed in our laboratory (Lu et al., 2016b). Integratedly analyzed quantitative proteomic data obtained using the iTRAQ-based quantitative proteomics with transcriptome data previously obtained by RNA-Seq (Li et al., 2019a) was used to identify the candidate pathways and genes related to leaf heading formation in *fg-1*-mutant Chinese cabbage at the early leaf heading stage.

Leafy head formation is a complex biological process affected by many factors. Research showed that leaf heading formation in Chinese cabbage is a quantitative trait controlled additively by low-dominance effects that can be affected by auxin concentration, temperature, light intensity, and the ratio of carbohydrate to nitrogen among other factors (Ito and Kato, 1957; Tanaka et al., 2009). However, other research showed that the leaf heading trait is controlled by a pair of recessive alleles (Li et al., 2019a; Gao et al., 2020). Nowadays, an increasing number of studies have shown that plant hormones play important roles in leafy head formation (Gao et al., 2017; Gu et al., 2017; Yue et al., 2022). To identify the genes related to leafy head formation, former studies normally used Chinese cabbage of different heading types as materials, but the genetic backgrounds of the materials were not consistent. Besides that, most studies mainly focused on transcriptomic analysis but not proteomic analysis, in which genes-to-transcripts cannot fully explain the systemical function of proteins *in vivo*. Using transcriptomics and proteomics integrating analysis would be a more efficient assay to study leaf heading formation. Therefore, in the present study, we integratedly analyzed quantitative proteomic data obtained using the iTRAQ-based quantitative proteomics with transcriptome data previously obtained by RNA-Seq (Li et al., 2019a) to identify the candidate pathways and genes related to leaf heading formation in *fg-1*-mutant Chinese cabbage at the early leaf heading

stage, which was obtained from the EMS mutant library constructed in our laboratory and exhibited flat growth (Lu et al., 2016b). These results provided abundant candidate genes and key pathways and contributed deeper insights into the underlying molecular mechanisms of leaf heading formation.

2 Materials and methods

2.1 Plant materials

fg-1-mutant and WT lines were used as the experimental materials for the proteomic analysis of the mutant trait. The WT and *fg-1*-mutant seeds were sown on 50-hole trays in the plastic tunnel on the experimental farm at Hebei Agricultural University in Baoding (115.47 E, 38.87 N), China. Grown for 25 days, the seedlings were planted in soil in the greenhouse. Afterward, routine management was carried out. At 55 days after planting, proteome sampling was conducted, and three biological replicates were used for analysis. All leaf samples were frozen in liquid nitrogen to extract RNA immediately or stored at -80°C.

2.2 Protein extraction, iTRAQ labeling, and LC–MS/MS analysis

Extraction of protein from the sample was done by grinding, cracking, precipitation, washing, and redissolving according to a previous method (Zeng et al., 2018), and the protein concentration was determined by using a BCA kit (Beyotime Biotechnology) according to the manufacturer's instructions. The proteins were then subjected to trypsin digestion and labeled with the iTRAQ 8-plex kits (Applied Biosystems) according to the manufacturer's instructions. The tryptic peptides were fractionated by high-pH reverse-phase HPLC using an Agilent 300Extend C18 column.

LC–MS/MS analysis was performed on an EASY-nLC 1000 UPLC system. The peptides were subjected to NSI source followed by tandem mass spectrometry (MS/MS) in a Q ExactiveTM Plus instrument (Thermo) coupled online to the UPLC system.

2.3 Protein identification and quantification

The resulting MS/MS data were processed using the MaxQuant search engine (v.1.5.2.8). Tandem mass spectra were searched against the http://brassicadb.org/brad/database concatenated with the reverse decoy database. The FDR for protein identification and peptide spectrum match identification is set to 1%. Proteins with fold change >1.2 and p-value <0.05 in the two samples were considered as significant DEPs.

2.4 Bioinformatics methods

The Gene Ontology (GO) annotation proteome was derived from the UniProt-GOA database (www.http://www.ebi.ac.uk/GOA/). The Kyoto Encyclopedia of Genes and Genomes (KEGG) (http://www.genome.jp/kegg/) database was used for the annotation of protein pathways. The identified protein domain functional descriptions were annotated with InterProScan (a sequence analysis application) based on the protein sequence alignment method, and the InterPro domain database (http://www.ebi.ac.uk/interpro/) was used. The following criteria were used to determine the significant enrichment of GO terms, KEGG pathways, and protein domains: 1.2-fold change and a p-value ≤0.05.

2.5 Analysis of the correlations between the proteomic and transcriptomic results

The transcriptomic data used in this study were obtained from a previous study (Li et al., 2019a). By comparing the quantitative results of transcriptome and proteome, the genes that were quantified at both transcriptome and proteome levels were found. The correlation analysis was performed with R (version 3.5.1), and scatter plots were drawn based on the changes in the transcriptomic and proteomic results. When log2 FC >0 and the verified p-value <0.05, it is a significantly differentially expressed upregulated transcript; when log2 FC <0 and the verified p-value <0.05, it is a significantly differentially expressed downregulated transcript. When the ratio is greater than 1.2 and the p-value is less than 0.05, it indicates significant differential expression of upregulated proteins. When the ratio is less than 1/1.2 and the p-value is less than 0.05, it indicates significant differential expression of downregulated proteins. Through the above-mentioned criteria screening, significantly differentially expressed transcripts and proteins were obtained in each comparison group. The DEGs and DEPs were separately counted, and Venn diagrams were generated according to the results. The significant enrichment of GO terms and KEGG pathways was performed on the co-upregulated and co-downregulated transcripts separately.

3 Results

3.1 DEPs' identification of *fg-1* mutant and WT in the early heading stage

The flat growth mutant (*fg-1*) of the M6 generation was obtained from the mutant library of Chinese cabbage, which was previously developed by EMS treatment of seeds from the inbred wild-type (WT) line (Lu et al., 2016b). The *fg-1* mutant has flat leaves during growth before the heading stage and trends to exhibit heading at the heading stage, and WT exhibits an outward-curling heading pattern. Throughout the entire growth period of Chinese cabbage, the mutant and wild type are significantly different, especially in the early stage of heading. The leaf apical region of wild-type Chinese cabbage begins to embrace inward, and the leaf angle (the angle between the blade and the center) becomes smaller to form the leaf heading, while the mutant leaves continued with their flat growth until the harvest period (Figure 1A). Our previous study showed that the phenotypic traits of F1 plants were similar to

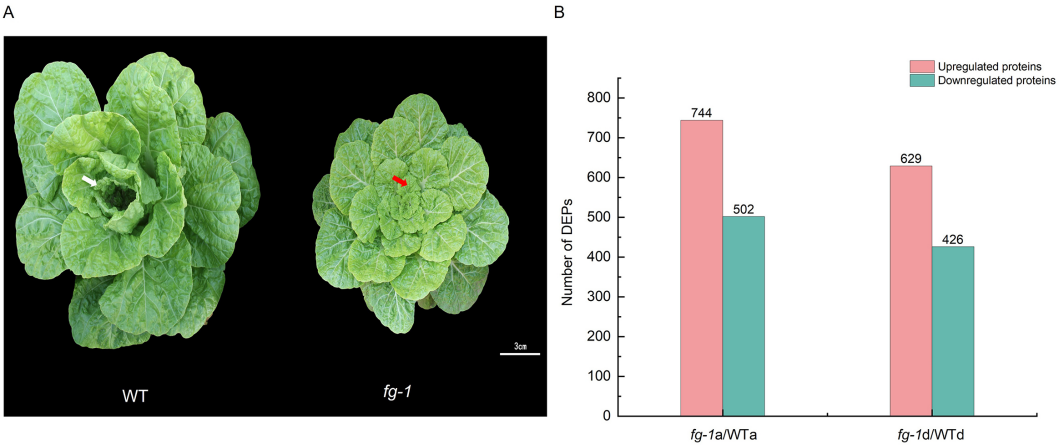

FIGURE 1
DEPs' identification of *fg-1* mutant and WT in the early heading stage of Chinese cabbage. Wild type and mutant of Chinese cabbage growing for 55 days in the early heading stage **(A)** and differentially expressed proteins (DEPs) **(B)**. The white arrow indicates the curling leaf in WT, and the red arrow indicates the flat leaf in *fg-1* in the early heading stage. Scale bar = 3 cm.

the wild type, and the segregation ratio of the F2 plants' traits conformed to the 3:1 ratio. The genetic analysis shows that the mutant trait is controlled by a pair of recessive alleles, while it is unknown which gene regulates leafy head (Li et al., 2019a).

To verify the key regulatory factors of leafy head formation, the proteome assays were first performed in the *fg-1* mutant and WT. In the early heading stage of *fg-1* mutant and WT (55 days after planting), the 16th leaf from the exterior of the leafy head was sampled at two positions—apical to the leaf (a) and basal to the leaf (d)—for proteome analysis (Supplementary Figure S1). After merging the data from three biological replicates, a total of 266,694 spectra were generated by iTRAQ of WT and *fg-1* Chinese cabbage leaves. Furthermore, 70,739 out of 266,694 spectra matched to known spectra, which identified 28,081 unique peptides and 7,287 proteins (Supplementary Table S1). Further analysis showed that the lengths of the peptides were mainly distributed in seven to 20 amino acids (Supplementary Figure S2A), and the primary mass error of the peptides was within 10 ppm (Supplementary Figure S2B). Besides that, the protein mass showed that the molecular weight of the protein was negatively correlated with the coverage (Supplementary Figure S2C). Next, we identified differentially expressed protein (DEP) species by exhibiting a fold change >1.2 and p-value <0.05. As the results have shown, a total of 1,246 DEPs (744 with increased levels and 502 with decreased levels) and 1,055 DEPs (629 with increased levels and 426 with decreased levels) were identified in section a and section d, respectively (Figure 1B). These indicate that the growth defects of the *fg-1* mutant result in numerous DEPs, which might be involved in leafy head formation in the early stage.

3.2 DEPs' functional characterization of *fg-1* mutant and WT in the early heading stage

To further characterize the features of DEPs on biological processes (BP), molecular functions (CC), and cellular composition (MF), GO enrichment analyses were conducted. Most of the upregulated DEPs were involved in photosynthetic-related BP and CC GO terms, such as "photosynthetic electron transport chain" and "photosynthetic membrane" in section a (Figure 2A); downregulated DEPs were involved in "protein transport", "mitochondrial inner membrane", and "electron carrier activity" in section d (Figure 2B). Upregulated DEPs were involved in "cell redox homeostasis", "organelle part", and "structural molecule activity" in section d (Figure 2C), and downregulated DEPs were involved in "disaccharide metabolic process", "cell periphery", and "protein domain specific binding" in section d (Figure 2D). These results suggested that "regulation of photosynthesis", "organic acid catabolic process", "protein transport", and "cell redox homeostasis" may play important roles in leaf heading formation.

To further investigate the function of DEPs, we analyzed KEGG pathway enrichment in some specific biological processes. There were 860 DEPs in section a of the mutant and WT, the upregulated DEPs were enriched with nine KEGG pathways, and downregulated DEPs were enriched with two KEGG pathways (Figures 3A, B). There were 650 DEPs in section d of the mutant and WT, the upregulated DEPs were enriched with seven KEGG pathways, and downregulated DEPs were enriched with three KEGG pathways (Figures 3C, D). Among the enrichment KEGG, phenylpropanoid biosynthesis (brp00940) was not only enriched in one comparison, which may play a key role in leaf heading formation.

3.3 Verified DEPs' and DEGs' association of *fg-1* mutant and WT in the early heading stage

To study the association of proteomic and previous transcriptomic data (Li et al., 2019a), integrated analysis was performed. In section a, 7,669 mRNAs and 1,246 proteins were subjected to integrative analysis, and 272 of these were identified in both transcriptomic and proteomic

10.3389/fpls.2024.1467006

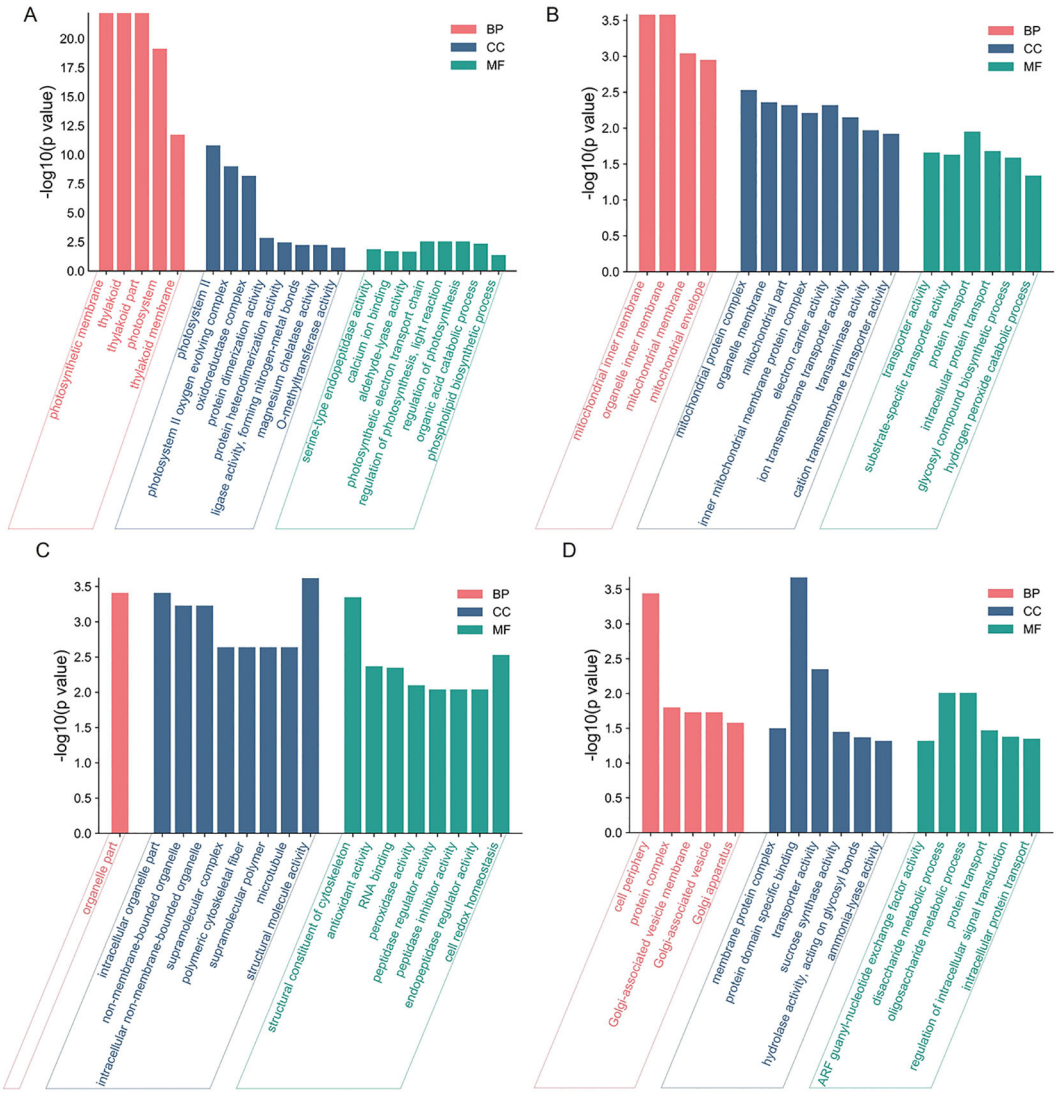

FIGURE 2
GO enrichment of DEPs in *fg-1* and WT. GO enrichment analysis of upregulated DEPs **(A)** and downregulated DEPs **(B)** in section a and upregulated DEPs **(C)** and downregulated DEPs **(D)** in section d. The DEPs were assigned to the three GO categories: biological processes (BP), cell components (CC), and molecular functions (MF). The X-axis represents the GO functional classification, and the Y-axis shows -log10 (*p*-value) enriched for each term.

analyses (Figure 4A). In section d, 4,823 mRNAs and 1,055 proteins were subjected to integrative analysis, and 304 of these were included in both the transcriptomic and proteomic results (Figure 4B). Additionally, the changes in expression at the transcript (log2 ratio of transcript) and protein (log2 ratio of protein) levels were analyzed via scatter plots. The data revealed correlations in section a (Pearson correlation coefficient, $r = 0.40$) (Supplementary Figure S3A) and in section d (Pearson correlation coefficient, r = 0.37) (Supplementary Figure S3B). Moreover, in section a, a total of 207 candidates' protein and transcript expression levels exhibited the same up- and downregulated trends (93 upregulated and 114 downregulated) (Figures 4A, B). In section d, a total of 278 candidates' protein and transcript expression levels exhibited the same up- and downregulated trends (150 upregulated and 128 downregulated) (Figures 4C, D).

Next, we integratedly analyzed GO and KEGG enrichment to explore the specific biological functions of these differentially expressed proteins and transcripts. In the GO enrichment analysis, upregulated candidates in section a were annotated to 18 GO terms (Figure 5A), including regulation of photosynthesis, light reaction, thylakoid membrane, calcium ion binding, and so on. The downregulated candidates in section a were annotated to 22 GO terms; among them, cell wall polysaccharide metabolic process, electron carrier activity, and extracellular region were the most enrichment GO terms in BP, CC, and MF, respectively (Figure 5B). In addition, the upregulated candidates in section d were annotated to 16 GO terms, including cell redox homeostasis, organelle part, structural molecule activity, and so on (Figure 5C), and the downregulated candidates in section d were annotated to 20 GO

10.3389/fpls.2024.1467006

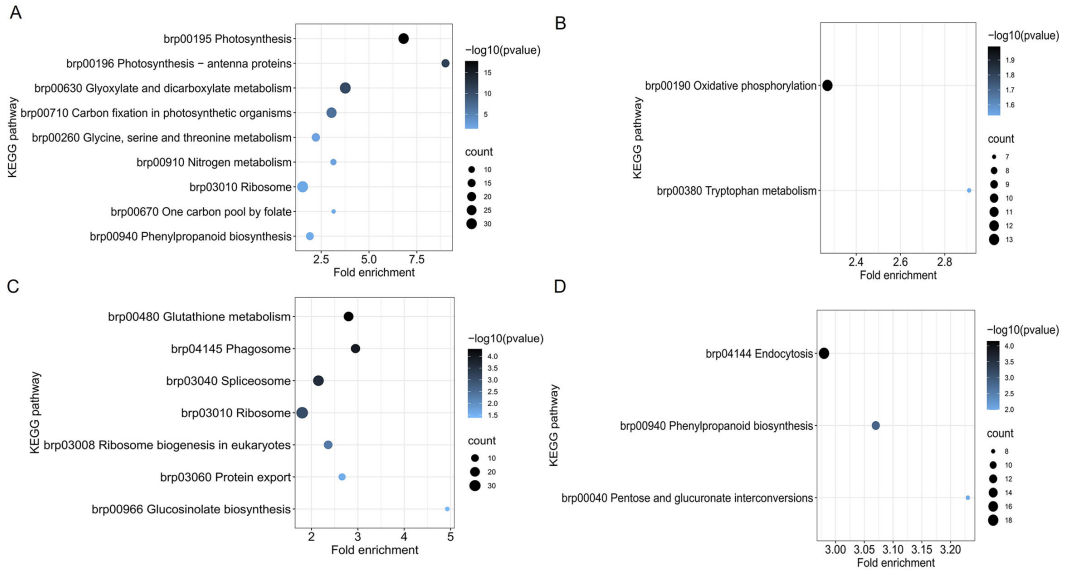

FIGURE 3
KEGG pathway enrichment of DEPs in *fg-1* and WT. KEGG pathway analysis of upregulated expressed proteins **(A)** and downregulated proteins **(B)** in section a and upregulated expressed proteins **(C)** and downregulated proteins **(D)** in section d. The vertical axis represents the pathway, and the horizontal axis represents the fold enrichment. The circle color indicates the significance of the enrichment with a -log10 (*p*-value), and the circle size represents the number of differential proteins in the pathway.

terms, including disaccharide metabolic process, cell periphery, protein domain specific binding, and so on (Figure 5D). Some of the GO terms were related to photosynthesis.

The upregulated transcripts and proteins were annotated to 11 KEGG pathways in section a and seven KEGG pathways in section d (Figures 6A, 7B). Among them, phenylpropanoid biosynthesis (brp00940) and biosynthesis of secondary metabolites (brp01110) were enrichment pathways in sections a and d. The downregulated transcripts and proteins were annotated to five KEGG pathways in section a, including isoquinoline alkaloid biosynthesis (brp00950) (Figure 6C), and six KEGG pathways in section d, including phenylpropanoid biosynthesis (brp00940) (Figure 6D). The

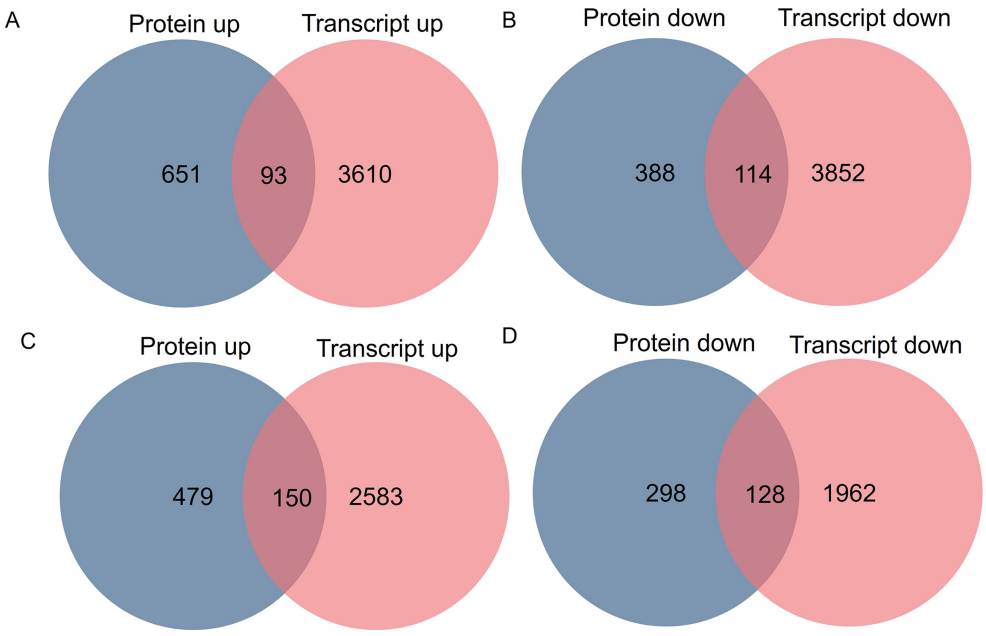

FIGURE 4
Comparative analysis of differentially expressed proteins and transcripts in *fg-1* mutant and WT. Venn diagram of upregulated genes and proteins **(A)** and downregulated genes and proteins **(B)** in section a and upregulated genes and proteins **(C)** and downregulated genes and proteins **(D)** in section d.

10.3389/fpls.2024.1467006

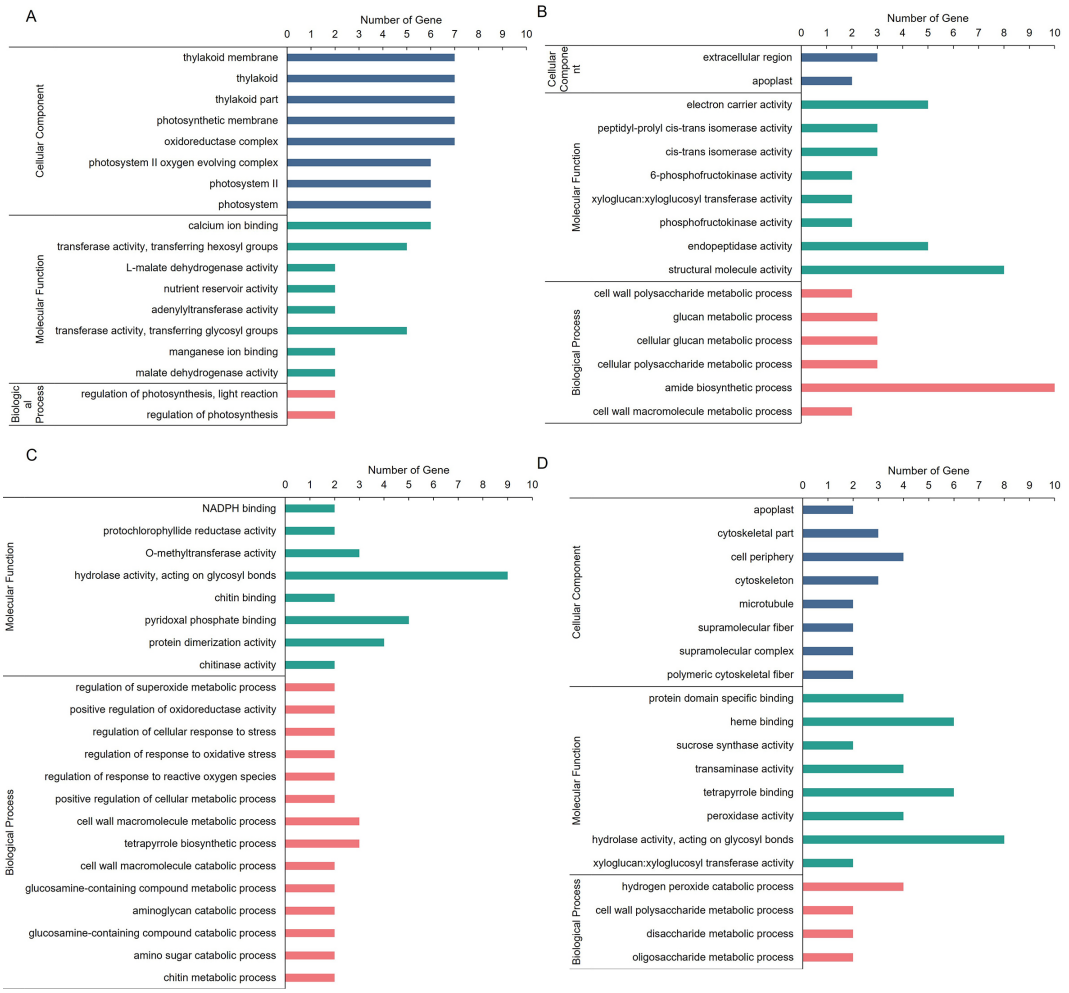

FIGURE 5
GO enrichment of DEPs in *fg-1* and WT. GO enrichment analysis of co-upregulated genes **(A)** and co-downregulated genes **(B)** in section a and co-upregulated genes **(C)** and co-downregulated genes **(D)** in section d. The DEPs were assigned to the three GO categories: biological processes (BP), cell components (CC), and molecular functions (MF). The X-axis represents the GO functional classification, and the Y-axis shows the gene numbers enriched for each term.

KEGG enrichment analysis showed that phenylpropanoid biosynthesis and biosynthesis of secondary metabolite pathway were enrichment in both sections a and d of upregulated transcripts and proteins. The pathway may be important in leaf heading formation.

3.4 Gene of transcription factor analysis of *fg-1* mutant and WT

Numerous studies have shown that transcription factors (TFs) are involved in regulating the leaf development of Chinese cabbage. Thus, we next performed an additional transcriptional enrichment analysis to identify key TFs. As the results showed, 86 TFs were exhibited to be co-upregulated and co-downregulated, in which 19 TFs' transcripts/proteins were co-upregulated and 38 TFs' transcripts/proteins were co-downregulated in section a (Figure 7A) and 19 TFs' transcripts/proteins were co-upregulated and 10 TFs' transcripts/proteins were co-downregulated in section d (Figure 7B). Among these, *UDPGT* (*UDP-glucosyltransferase*) has the highest number with four TF candidates, *RRM-1* and *Pkinase* have three TF members, nine transcription factors have two TFs candidates, and most of the TFs have one member only. *UDPGT* was the key regulator involved in zetin biosynthesis pathway, and *Pkinase* was the key regulator involved in signal transduction pathway. These indicates that hormone synthesis and signal transduction might play an important role in leaf heading formation in Chinese cabbage.

3.5 Identification of key genes and validation of gene expression levels

To further explore potential factors that regulate leaf heading formation, we analyzed the genes related to hormone synthesis and signal transduction pathways in proteomic and transcriptomic data.

10.3389/fpls.2024.1467006

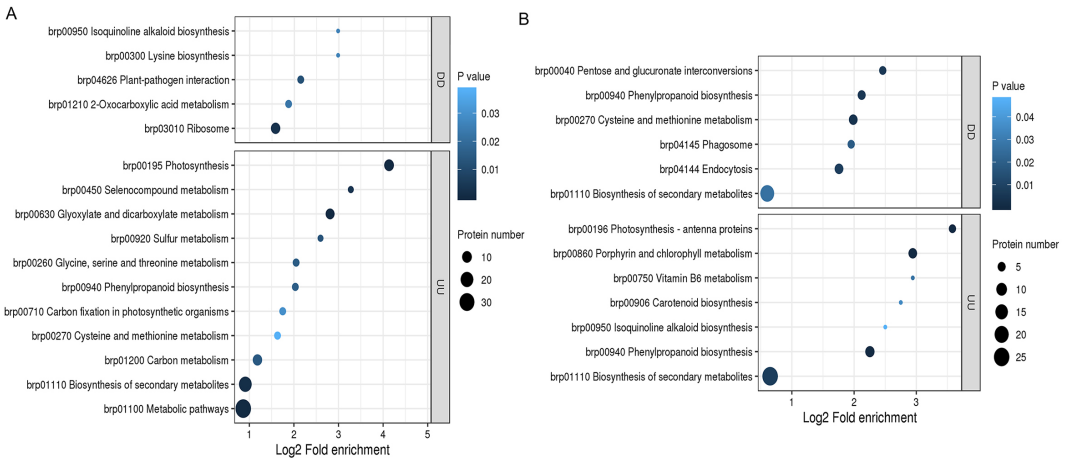

FIGURE 6
KEGG pathway enrichment of co-regulated genes in *fg-1* and WT. KEGG pathway enrichment analysis of co-regulation in section a **(A)** and section d **(B)**. DD indicates co-downregulation of genes, and UU indicates co-upregulation of genes. The horizontal axis represents the log2-transformed fold enrichment, the vertical axis represents the functional classification, the bubble size indicates the number of proteins, and the bubble color represents the enrichment significance (*p*-value).

The analysis discovered that there were 16 genes in the plant hormone synthesis and signal transduction pathways (Table 1). In section a, there were six genes that were co-regulated, including *UGT73C* (*UDP-glucosyltransferase 73C*), *metB* (*cystathionine gamma-synthase*), *GOT1* (*aspartate aminotransferase, cytoplasmic*), *TAT* (*tyrosine aminotransferase*), *SIMKK* (*mitogen-activated protein kinase kinase*), and *PR1* (*pathogenesis-related protein 1*). Among these genes, except *metB* that was co-upregulated, the other genes were co-downregulated. In section d, there are 10 genes that were co-regulated, including *ZEP* (*zeaxanthin epoxidase*), two *ACO* (*1-aminocyclopropane-1-carboxylic acid oxidase*), *TAT* (tyrosine aminotransferase), *LOX2S* (*lipoxygenase2S*), *PYR/PYL* (*pyrabactin resistance 1*), *GH3* (*Gretchen Hagen 3*), *NPR1* (*non-expresser of pathogenesis-related 1*), and two *TCH4* (xyloglucosyl transferase TCH4). Among these genes, *TAT*, *LOX2S*, and *GH3* were co-upregulated, and the other genes were co-downregulated.

4 Discussion

4.1 Identifying the key factors of plant development by iTRAQ

Proteins are the final executors of most cellular functions. Therefore, proteomics may be an effective strategy to identify the proteins or pathways that are responsible for plant development (Nogueira et al., 2012; Feng et al., 2018). The quantitative proteomics techniques have been used to analyze the ethylene-induced adventitious rooting process, and this proteomic analysis

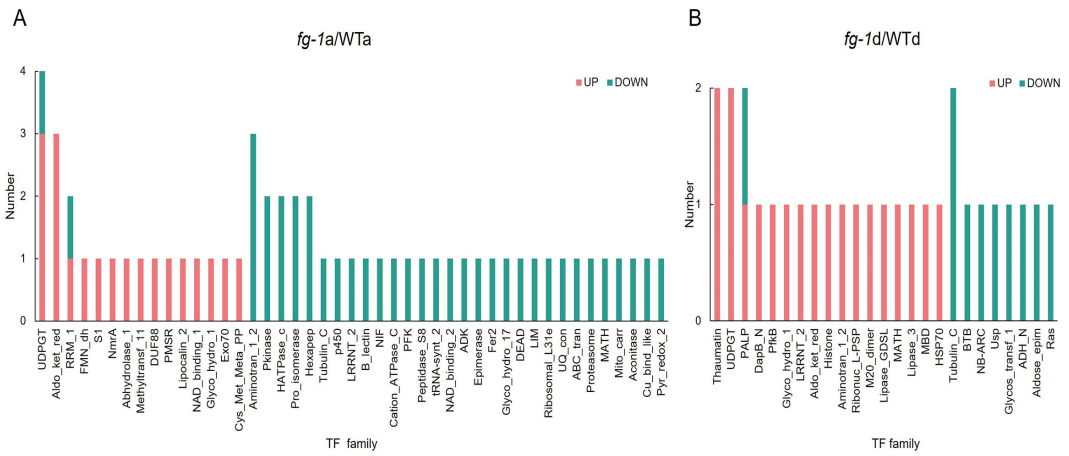

FIGURE 7
TF enrichment of *fg-1* mutant and WT. TF analysis in section a **(A)** and section d **(B)**. The x-axis represents the TF amounts, and the y-axis represents the classification. Orange represents co-upregulated factor, and blue represents co-downregulated TFs.

10.3389/fpls.2024.1467006

TABLE 1 Differentially expressed genes related to hormone synthesis and signal transduction pathways in *fg-1* and WT.

Section	Gene ID	Gene name	KEGG pathway	Hormone-related	Up/Down	TF family
Section a	Bra017224	UGT73C	Zeatin biosynthesis	Cytokinine	Down	UDPGT
	Bra039144	metB	Cysteine and methionine metabolism	Ethylene	Up	Cys_Met_Meta_PP
	Bra006103	GOT1	Cysteine and methionine metabolism	Ethylene	Down	Aminotran_1_2
			Phenylalanine metabolism	Salicylic acid		
	Bra007610	TAT	Cysteine and methionine metabolism	Ethylene	Down	Aminotran_1_2
			Phenylalanine metabolism	Salicylic acid		
	Bra014295	SIMKK	Plant hormone signal transduction	Ethylene	Down	Pkinase
	Bra013123	PR1	Plant hormone signal transduction	Salicylic acid	Down	–
Section d	Bra037130	ZEP	Carotenoid biosynthesis	Abscisic acid	Down	–
	Bra003687	ACO	Cysteine and methionine metabolism	Ethylene	Down	–
	Bra031090	ACO	Cysteine and methionine metabolism	Ethylene	Down	–
	Bra024204	TAT	Cysteine and methionine metabolism	Ethylene	Up	Aminotran_1_2
			Phenylalanine metabolism	Salicylic acid		
	Bra003526	LOX2S	α-Linolenic acid metabolism	Jasmonic acid	Up	–
	Bra021032	PYR/PYL	Plant hormone signal transduction	Abscisic acid	Down	–
	Bra006196	GH3	Plant hormone signal transduction	Auxin	Up	–
	Bra016938	NPR1	Plant hormone signal transduction	Salicylic acid	Down	BTB
	Bra024089	TCH4.1	Plant hormone signal transduction	Brassinosteroid	Down	–
	Bra011179	TCH4.2	Plant hormone signal transduction	Brassinosteroid	Down	–

identified 24 DEPs related to adventitious root development. The enzyme SAMS (S-adenosylmethionine synthase), which is upstream of ethylene synthesis, is directly involved in adventitious root development in cucumber (Lyu et al., 2021). The proteomic profile of K326 and Honghua Dajinyuan (HD) tobacco leaves has been found to vary among the four growth stages, and the galactose metabolism and glycosphingolipid biosynthesis-globo series pathways were significantly enriched in HD at the rosette growth stage, indicating that these genes may be correlated with tobacco mosaic disease (Chen et al., 2019). However, few proteomic studies of Chinese cabbage have explored the mechanism of leaf heading formation. Leaf heading is an important economic and breeding trait of Chinese cabbage. The molecular mechanisms involved in leaf heading formation remain unclear. Early leaf heading is the key stage for leaf heading formation, and *BcpLH*, one of the key genes to regulated leaf heading formation, was cloned in the early leaf heading stage (Zhang et al., 2016, 2022; Yu et al., 2000). Our study profiled the different sections and expression patterns of proteins involved in leaf heading formation in the early heading stage via the quantitative proteomics method. The analysis identified 1,246 DEPs in section a, 1,055 DEPs in section d, and 301 DEPs in both sections a and d. The upregulated DEPs were

enriched with nine KEGG pathways, and the downregulated DEPs were enriched with two KEGG pathways in section a. The upregulated DEPs were enriched with seven KEGG pathways, and the downregulated DEPs were enriched with three KEGG pathways. Phenylpropanoid biosynthesis is the enrichment in section d.

4.2 Key pathways are correlated with leaf heading formation

Both transcriptomic and proteomic data are important to understand the molecular processes involved in plant development (Galindo González et al., 2012; Haider and Pal, 2013; Wang et al., 2016). An analysis integrating proteomic and transcriptomic data to identify proteins and genes related to pepper genetic male sterility identified 52 DEGs/DEPs at both the proteomic and transcriptomic levels, and these DEPs and DEGs are involved in pollen exine formation, pollen wall assembly, pollen development, and phenylpropanoid biosynthesis (Cheng et al., 2019). An analysis of *Arabidopsis* seed development revealed that the proportion of genes with no correlation or even negative correlation between their protein and transcription levels increased during development, and the enriched pathways at different developmental stages differed. In the early developmental stage of *Arabidopsis* seeds, RNA processing and translation were enriched, and in the later developmental stage, photosynthesis, energy production, and metabolic processes were enriched (Mergner et al., 2020). Integrated analyses of *ask1*-mutant and wild-type *Arabidopsis* floral organs at the protein and transcription levels revealed the regulation of transcription regulators, kinases, peptidases, and ribosomal proteins, with implications for possible mechanisms of ASK1-E3 functions in floral development (Lu et al., 2016a). In our study, a total of 207 proteins exhibited the same expression patterns as did their transcripts in section a, and 278 transcripts and proteins exhibited the same trends in section d. In the KEGG enrichment analysis, the upregulated transcripts and proteins in section a were annotated to 11 KEGG pathways, including photosynthesis, and the downregulated transcripts and proteins were annotated to five KEGG pathways, including isoquinoline alkaloid biosynthesis. In section d, the upregulated transcripts and proteins were annotated to seven KEGG pathways, including photosynthesis-antenna proteins and phenylpropanoid biosynthesis, and the downregulated transcripts and proteins were annotated to six KEGG pathways, including phenylpropanoid biosynthesis. Pathways of photosynthesis-antenna proteins and phenylpropanoid may be related to leaf heading. Phenylpropanoid biosynthesis is one of the most important KEGG pathways in plants, including phenylalanine metabolism, which plays an important role in plant development and may be related to leaf heading (Dong and Lin, 2021). In BrAN3-silencing plants of Chinese cabbage, which stimulated leafy head formation at the early stage, DEGs are also enriched in the biosynthesis pathway of photosynthesis-antenna proteins and phenylpropanoid (Yu et al., 2019). These pathways play an important role in plant development and responding to phytohormones signals (Han et al., 2022; Li et al., 2023); therefore, these pathways may regulate Chinese cabbage leaf heading formation through phytohormone pathway regulation.

4.3 Plant hormone pathways are correlated with leaf heading formation

Phytohormones participate in various processes of plant development (Zhao et al., 2021) and also play important roles in leaf heading formation. Based on RNA-Seq analysis and the crosstalk ability of various phytohormones, five phytohormones (auxin, ethylene, ABA, JA, and GA) were candidates for leafy head formation in Chinese cabbage (Li et al., 2019b). DEGs involved in auxin, ethylene, GA, JA, ABA, BR, CK, and SA signaling pathways play either positive or negative roles in leafy head formation in Chinese cabbage (Yu et al., 2019). The transition leaves of leafy head showed the enrichment of transcripts associated with protein kinases, auxin, and BR pathways and the light-responsive pathway (Wang et al., 2012). Because phytohormones affected leafy head formation, we analyzed the genes with common changes in proteomics and transcriptome of *fg-1* compared with the wild type. We found, in section a, that there are five genes in auxin and ethylene biosynthesis pathway and the JA and ABA signal transduction pathway showed a common change, and in section d, there are eight genes in the JA and ABA biosynthesis pathway, auxin, BA, and SA signal transduction pathway. ABA biosynthesis and signal transduction pathway showed a common change. To clarify the specific role of phytohormones in leaf heading development, it is necessary to further analyze the key genes related to phytohormone biosynthesis and signal transduction.

4.4 Key gene affected leaf heading formation

TFs and environmental response genes were believed to play an important role in leaf heading formation in Chinese cabbage (Li et al., 2019b; Wang et al., 2012; Tabusam et al., 2022). In lettuce, loss-of-function of *SAWTOOTH 1* (a kind of TFs) downregulates many adaxial development-related genes but upregulates abaxial development-related genes to control leaf heading formation (An et al., 2022). In Chinese cabbage, *PCF transcription factor4* (*BrpTCP4*) genes modulate the head shape. *CIN-Like TCPs* regulated by temperature dynamics controlled the leaves' morphological changes in *Arabidopsis* (Malinowski et al., 2011). H^+-ATPase is affected by environmental stress, which leads to the flat-leaf morphology of *B. rapa* (Zhang et al., 2020). Reports showed that light interacts with auxin during leaf elongation (Fellner et al., 2003). In our study, 86 TFs were exhibited to be co-upregulated and co-downregulated in *fg-1* and WT. Among these, *UDPGT* has four TF candidates, which was one of the genes in the zetin biosynthesis

pathway. Besides that, we also found that some of the co-regulated genes were related to photosynthesis, such as *LHCB1* (light-harvesting complex II chlorophyll a/b binding protein 6), *LHCB5*, and *LHCB6*. These indicates that these TFs and light-related genes might regulate leaf heading formation in the early stage, and it needs to be further addressed in the future.

The genes of hormone synthesis and transduction pathway play an important role in leaf heading formation in Chinese cabbage (Li et al., 2019b). Many hormone-related *BrARF3.1* have been reported to affect leaf heading formation (Liang et al., 2016). A screening of the EMS-induced mutant library of Chinese cabbage found that the *GA* biosynthesis-related gene *BrKS1* is involved in leafy head formation (Gao et al., 2020). Both *BrKAO2* and *BrCPS1*, which are involved in the *GA* biosynthetic pathway, have been proven to be responsible for leafy head formation in Chinese cabbage (Gao et al., 2022; Huang et al., 2022), whereas, in this study, we did not find the *GA* biosynthesis-related gene. In this study, 16 genes were found to be involved in plant hormone synthesis and signal transduction pathways by integratedly analyzing quantitative proteomics and transcriptome. Among the 16 genes, in *PYR/PYL*s and *GH3*, the expression level was reported to be altered in the heading and non-heading Chinese cabbage (Li et al., 2019b). Increasing *GH3s* expression levels by overexpression of *OsARF19* (*AUXIN RESPENSE FACTOR19*) in rice reduces IAA content and increases the leaf angle (Zhang et al., 2015). Transcripts of *BcpLH* gene were increased when plants were sprayed with IAA (Yu et al., 2000). In the present study, GH3 transcript and protein co-upregulated in *fg-1*, based on our previous research, and IAA content decreased in *fg-1* (Li et al., 2019b)—maybe *GH3* plays an important role to regulate leafy head formation in Chinese cabbage. The remaining genes are rarely reported to be directly related to leaf heading and require further research.

5 Conclusion

The aim of our study was to discover the mechanism of leaf heading formation in Chinese cabbage in the early heading stage. We integratedly analyzed quantitative proteomics with transcriptomics to discover key related genes. A total of 207 and 278 genes were shown to be co-upregulated or co-downregulated in section a and section d, respectively. Based on KEGG analyses, we found that the phenylpropanoid biosynthesis pathway was enriched in both sections a and d. In addition, we further confirmed 86 TFs that were exhibited to be co-upregulated or co-downregulated, and seven out of 86 were involved in plant hormone synthesis and signal transduction pathways. In summary, we have discovered several key early heading-formation-related factors via integratedly analyzing quantitative proteomics with transcriptomics data. This provides potential gene resources for further research on the molecular mechanism of leaf heading formation.

Data availability statement

The authors acknowledge that the data presented in this study must be deposited and made publicly available in an acceptable repository, prior to publication. Frontiers cannot accept a article that does not adhere to our open data policies.

Author contributions

JL: Data curation, Writing – original draft. MF: Formal analysis, Writing – original draft. XZ: Supervision, Writing – original draft. LiY: Formal analysis, Writing – original draft. GH: Formal analysis, Writing – original draft. LeY: Validation, Writing – review & editing. NL: Writing – review & editing. SX: Supervision, Writing – review & editing. JZ: Supervision, Writing – review & editing.

Funding

The author(s) declare financial support was received for the research, authorship, and/or publication of this article.This research was funded by the National Natural Science Foundation of China (32172589), the Natural Science Foundation of Hebei (C2024204246).

Conflict of interest

The authors declare that the research was conducted in the absence of any commercial or financial relationships that could be construed as a potential conflict of interest.

Publisher's note

Supplementary material

The Supplementary Material for this article can be found online at: https://www.frontiersin.org/articles/10.3389/fpls.2024.1467006/full#supplementary-material

References

Alemán-Báez, J., Qin, J., Cai, C., Zou, C., Bucher, J., Paulo, M.-J., et al. (2022). Genetic dissection of morphological variation in rosette leaves and leafy heads in cabbage (*Brassica oleracea* var. *capitata*). *Theor. Appl. Genet.* 135, 3611–3628. doi: 10.1007/s00122-022-04205-w

Ali, S., Khan, N., and Xie, L. (2020). Molecular and hormonal regulation of leaf morphogenesis in arabidopsis. *Int. J. Mol. Sci.* 21, 5132. doi: 10.3390/ijms21145132

An, G., Yu, C., Yan, C., Wang, M., Zhang, W., Jia, Y., et al. (2022). Loss-of-function of *SAWTOOTH 1* affects leaf dorsiventrality genes to promote leafy heads in lettuce. *Plant Cell* 34, 4329–4347. doi: 10.1093/plcell/koac234

Chen, M., Yan, G., Wang, X., Huang, Z., Shao, X., Wu, D., et al. (2019). Investigating the proteomic expression profile of tobacco (*Nicotiana tabacum)* leaves during four growth stages using the iTRAQ method. *Anal. Bioanal. Chem.* 411, 403–411. doi: 10.1007/s00216-018-1453-4

Cheng, F., Sun, R., Hou, X., Zheng, H., Zhang, F., Zhang, Y., et al. (2016). Subgenome parallel selection is associated with morphotype diversification and convergent crop domestication in *Brassica rapa* and *Brassica oleracea*. *Nat. Genet.* 48, 1218–1224. doi: 10.1038/ng.3634

Cheng, Q., Li, T., Ai, Y., Lu, Q., Wang, Y., Sun, L., et al. (2019). Complementary transcriptomic and proteomic analysis reveals a complex network regulating pollen abortion in *GMS* (*msc-1*) pepper (*Capsicum annuum* L.*). Int. J. Mol. Sci.* 20, 1789. doi: 10.3390/ijms20071789

Ding, H., Mo, S., Qian, Y., Yuan, G., Wu, X., and Ge, C. (2020). Integrated proteome and transcriptome analyses revealed key factors involved in tomato (*Solanum lycopersicum*) under high temperature stress. *Food Energy Secur.* 9, e239. doi: 10.1002/fes3.239

Dong, N., and Lin, H. (2021). Contribution of phenylpropanoid metabolism to plant development and plant–environment interactions. *J. Integr. Plant Biol.* 63, 180–209. doi: 10.1111/jipb.13054

Fellner, M., Horton, L. A., Cocke, A. E., Stephens, N. R., Ford, D. E., and Van Volkenburgh, E. (2003). Light interacts with auxin during leaf elongation and leaf angle development in young corn seedlings. *Planta* 216, 366–376. doi: 10.1007/s00425-002-0881-7

Feng, D., Wang, Y., Lu, T., Zhang, Z., and Han, X. (2018). Proteomics analysis reveals marker proteins for minor vein initiation in rice leaf. *Funct. Integr. Genomics* 18, 581–591. doi: 10.1007/s10142-018-0612-1

Galindo González, L. M., El Kayal, W., Ju, C. J.-T., Allen, C. C. G., King-Jones, S., and Cooke, J. E. K. (2012). Integrated transcriptomic and proteomic profiling of white spruce stems during the transition from active growth to dormancy. *Plant Cell Environ.* 35, 682–701. doi: 10.1111/j.1365-3040.2011.02444.x

Gao, L., Lyu, S., Tang, J., Zhou, D., Bonnema, G., Xiao, D., et al. (2017). Genome-wide analysis of auxin transport genes identifies the hormone responsive patterns associated with leafy head formation in Chinese cabbage. *Sci. Rep.* 7, 42229. doi: 10.1038/srep42229

Gao, Y., Huang, S., Qu, G., Fu, W., Zhang, M., Liu, Z., et al. (2020). The mutation of ent-kaurene synthase, a key enzyme involved in gibberellin biosynthesis, confers a non-heading phenotype to Chinese cabbage (*Brassica rapa* L.ssp. *pekinensis). Hortic. Res.* 7, 178. doi: 10.1038/s41438-020-00399-6

Gao, Y., Qu, G., Huang, S., Liu, Z., Fu, W., Zhang, M., et al. (2022). *BrCPS1* function in leafy head formation was verified by two allelic mutations in Chinese cabbage (*Brassica rapa* L.ssp. *pekinensis*). *Front. Plant Sci.* 13. doi: 10.3389/fpls.2022.889798

Gu, A., Meng, C., Chen, Y., Wei, L., Dong, H., Lu, Y., et al. (2017). Coupling Seq-BSA and RNA-Seq analyses reveal the molecular pathway and genes associated with heading type in Chinese cabbage. *Front. Genet.* 8. doi: 10.3389/fgene.2017.00176

Haider, S., and Pal, R. (2013). Integrated analysis of transcriptomic and proteomic data. *Curr. Genomics* 14, 91–110. doi: 10.2174/1389202911314020003

Han, Y., Yang, R., Zhang, X., Wang, Q., Wang, B., Zheng, X., et al. (2022). Brassinosteroid accelerates wound healing of potato tubers by activation of reactive oxygen metabolism and phenylpropanoid metabolism. *Foods* 11, 906. doi: 10.3390/foods11070906

He, Y. K., Xue, W. X., Sun, Y. D., Yu, X. H., and Liu, P. L. (2000). Leafy head formation of the progenies of transgenic plants of Chinese cabbage with exogenous auxin genes. *Cell Res.* 10, 151–160. doi: 10.1038/sj.cr.7290044

Huang, S., Gao, Y., Xue, M., Xu, J., Liao, R., Shang, S., et al. (2022). *BrKAO2* mutations disrupt leafy head formation in Chinese cabbage (*Brassica rapa L.* ssp. *pekinensis). Theor. Appl.Genet.* 135, 2453–2468. doi: 10.1007/s00122-022-04126-8

Ito, H., and Kato, T. (1957). Studies on the head formation of Chinese cabbage. Histological and physiological studies of head formation. *J.Japan.soc.hort.sci.* 26, 154–162. doi: 10.2503/jjshs.26.154

Li, H., He, X., Gao, Y., Liu, W., Song, J., and Zhang, J. (2023). Integrative analysis of transcriptome, proteome, and phosphoproteome reveals potential roles of photosynthesis antenna proteins in response to brassinosteroids signaling in maize. *Plants* 12, 1290. doi: 10.3390/plants12061290

Li, R., Hou, Z., Gao, L., Xiao, D., Hou, X., Zhang, C., et al. (2019b). Conjunctive analyses of BSA-Seq and BSR-Seq to reveal the molecular pathway of leafy head formation in Chinese cabbage. *Plants* 8, 603. doi: 10.3390/plants8120603

Li, J., Yang, R., Jiang, Y., Sun, S., Li, J., Gu, H., et al. (2022). Comparative proteomic analysis by isobaric tags for the relative and absolute quantification reveals the responses of tobacco (*Nicotiana tabacum* L.) roots to different soil types. *Front. Plant Sci.* 13. doi: 10.3389/fpls.2022.847388

Li, J., Zhang, X., Lu, Y., Feng, D., Gu, A., Wang, S., et al. (2019a). Characterization of non-heading mutation in heading Chinese cabbage (*Brassica rapa* L.ssp. *pekinensis*). *Front. Plant Sci.* 10. doi: 10.3389/fpls.2019.00112

Liang, J., Liu, B., Wu, J., Cheng, F., and Wang, X. (2016). Genetic variation and divergence of genes involved in leaf adaxial-abaxial polarity establishment in *Brassica rapa*. *Front. Plant Sci.* 7. doi: 10.3389/fpls.2016.00094

Liu, S., Rao, J., Zhu, J., Li, G., Li, F., Zhang, H., et al. (2023). Integrated physiological, metabolite and proteomic analysis reveal the glyphosate stress response mechanism in tea plant (*Camellia sinensis*). *J. Hazard. Mater.* 454, 131419. doi: 10.1016/j.jhazmat.2023.131419

Lu, Y., Dai, S., Gu, A., Liu, M., Wang, Y., Luo, S., et al. (2016b). Microspore induced doubled haploids production from ethyl methanesulfonate (EMS) moaked flower buds is an efficient strategy for mutagenesis in Chinese cabbage. *Front. Plant Sci.* 7. doi: 10.3389/fpls.2016.01780

Lu, D., Ni, W., Stanley, B. A., and Ma, H. (2016a). Proteomics and transcriptomics analyses of Arabidopsis floral buds uncover important functions of ARABIDOPSIS *SKP1-LIKE1*. *BMC Plant Biol.* 16, 61. doi: 10.1186/s12870-015-0571-9

Lyu, J., Wu, Y., Jin, X., Tang, Z., Liao, W., Dawuda, M. M., et al. (2021). Proteomic analysis reveals key proteins involved in ethylene-induced adventitious root development in cucumber (*Cucumis sativus* L.). *PeerJ* 9, e10887. doi: 10.7717/peerj.10887

Malinowski, R., Kasprzewska, A., and Fleming, A. J. (2011). Targeted manipulation of leaf form via local growth repression. *Plant J.* 66, 941–952. doi: 10.1111/j.1365-313X.2011.04559.x

Mergner, J., Frejno, M., Messerer, M., Lang, D., Samaras, P., Wilhelm, M., et al. (2020). Proteomic and transcriptomic profiling of aerial organ development in Arabidopsis. *Sci. Data* 7, 334. doi: 10.1038/s41597-020-00678-w

Nogueira, F. C. S., Palmisano, G., Schwämmle, V., Campos, F. A. P., Larsen, M. R., Domont, G. B., et al. (2012). Performance of isobaric and isotopic labeling in quantitative plant proteomics. *J. Proteome Res.* 11, 3046–3052. doi: 10.1021/pr300192f

Park, C. H., Park, S.-Y., Park, Y. J., Kim, J. K., and Park, S. U. (2020). Metabolite profiling and comparative analysis of secondary metabolites in Chinese cabbage, radish, and hybrid *xBrassicoraphanus*. *J. Agric. Food Chem.* 68, 13711–13719. doi: 10.1021/acs.jafc.0c04897

Ramchiary, N., Nguyen, V. D., Li, X., Hong, C. P., Dhandapani, V., Choi, S. R., et al. (2011). Genic microsatellite markers in *Brassica rapa*: development, characterization, mapping, and their utility in other cultivated and wild brassica relatives. *DNA Res.* 18, 305–320. doi: 10.1093/dnares/dsr017

Sun, X., Basnet, R. K., Yan, Z., Bucher, J., Cai, C., Zhao, J., et al. (2019). Genome-wide transcriptome analysis reveals molecular pathways involved in leafy head formation of Chinese cabbage (*Brassica rapa*). *Hortic. Res.* 6, 130. doi: 10.1038/s41438-019-0212-9

Tabusam, J., Liu, M., Luo, L., Zulfiqar, S., Shen, S., Ma, W., et al. (2022). Physiological control and genetic basis of leaf curvature and heading in *Brassica rapa* L. *J. Adv. Res.* 53, 49–59. doi: 10.1016/j.jare.2022.12.010

Tanaka, N., Niikura, S., and Takeda, K. (2009). Inheritance of cabbage head formation in crosses of cabbage x ornamental cabbage and cabbage x kale. *Plant Breed.* 128, 471–477. doi: 10.1111/j.1439-0523.2008.01572.x

Wang, H., Lan, P., and Shen, R. F. (2016). Integration of transcriptomic and proteomic analysis towards understanding the systems biology of root hairs. *Proteomics* 16, 877–893. doi: 10.1002/pmic.201500265

Wang, F., Li, L., Li, H., Liu, L., Zhang, Y., Gao, J., et al. (2012). Transcriptome analysis of rosette and folding leaves in Chinese cabbage using high-throughput RNA sequencing. *Genomics* 99, 299–307. doi: 10.1016/j.ygeno.2012.02.005

Wang, X., Wang, H., Wang, J., Sun, R., Wu, J., Liu, S., et al. (2011). The genome of the mesopolyploid crop species *Brassica rapa*. *Nat. Genet.* 43, 1035–1039. doi: 10.1038/ng.919

Yu, J., Gao, L., Liu, W., Song, L., Xiao, D., Liu, T., et al. (2019). Transcription coactivator *ANGUSTIFOLIA3 (AN3)* regulates leafy head formation in Chinese cabbage. *Front. Plant Sci.* 10. doi: 10.3389/fpls.2019.00520

Yu, X., Peng, J., Feng, X., Yang, S., Zheng, Z., Tang, X., et al. (2000). Cloning and structural and expressional characterization of *BcpLH* gene preferentially expressed in folding leaf of Chinese cabbage. *Sci. China C. Life Sci.* 43, 321–329. doi: 10.1007/BF02879292

Yu, X., Wang, H., Zhong, W., Bai, J., Liu, P., and He, Y. (2013). QTL mapping of leafy heads by genome resequencing in the *RIL* population of *Brassica rapa*. *PLoS. One* 8, e76059. doi: 10.1371/journal.pone.0076059

Yu, C., Yan, C., Liu, Y., Liu, Y., Jia, Y., Lavelle, D., et al. (2020). Upregulation of a *KN1* homolog by transposon insertion promotes leafy head development in lettuce. *Proc. Natl. Acad. Sci. U.S.A.* 117, 33668–33678. doi: 10.1073/pnas.2019698117

Yue, X., Su, T., Xin, X., Li, P., Wang, W., Yu, Y., et al. (2022). The adaxial/abaxial patterning of auxin and auxin gene in leaf veins functions in leafy head formation of Chinese cabbage. *Front. Plant Sci.* 13. doi: 10.3389/fpls.2022.918112

Zeng, X., Xu, Y., Jiang, J., Zhang, F., Ma, L., Wu, D., et al. (2018). iTRAQ-Based comparative proteomic analysis of the roots of two winter turnip rapes (*Brassica rapa* L.) with different freezing-tolerance. *Int. J. Mol. Sci.* 19, 4077. doi: 10.3390/ijms19124077

Zhang, M., Huang, S., Gao, Y., Fu, W., Qu, G., Zhao, Y., et al. (2020). Fine mapping of a leaf flattening gene Bralcm through BSR-Seq in Chinese cabbage (Brassica rapa L. ssp. pekinensis). *Sci. Rep.* 10, 13924. doi: 10.1038/s41598-020-70975-2

Zhang, L., Su, W., Tao, R., Zhang, W., Chen, J., Wu, P., et al. (2017). RNA sequencing provides insights into the evolution of lettuce and the regulation of flavonoid biosynthesis. *Nat. Commun.* 8, 2264. doi: 10.1038/s41467-017-02445-9

Zhang, S., Wang, S., Xu, Y., Yu, C., Shen, C., Qian, Q., et al. (2015). The auxin response factor, *OsARF19*, controls rice leaf angles through positively regulating *OsGH 3-5* and *OsBRI 1*. *Plant Cell Environ.* 38, 638–654. doi: 10.1111/pce.12397

Zhang, C. W., Wei, Y. P., Xiao, D., Gao, L. W., Lyu, S. W., Hou, X. L., et al. (2016). Transcriptomic and proteomic analyses provide new insights into the regulation mechanism of low-temperature-induced leafy head formation in Chinese cabbage. *J. Proteomics* 144, 1–10. doi: 10.1016/j.jprot.2016.05.022

Zhang, K., Yang, Y., Wu, J., Liang, J., Chen, S., Zhang, L., et al. (2022). A cluster of transcripts identifies a transition stage initiating leafy head growth in heading morphotypes of *Brassica*. *Plant J.* 110, 688–706. doi: 10.1111/tpj.15695

Zhang, C., Yu, D., Ke, F., Zhu, M., Xu, J., and Zhang, M. (2018). Seedless mutant "Wuzi Ougan" (*Citrus suavissima Hort. ex Tanaka* 'seedless') and the wild type were compared by iTRAQ-based quantitative proteomics and integratedly analyzed with transcriptome to improve understanding of male sterility. *BMC Genet.* 19, 1–17. doi: 10.1186/s12863-018-0693-9

Zhao, B., Liu, Q., Wang, B., and Yuan, F. (2021). Roles of phytohormones and their signaling pathways in leaf development and stress responses. *J. Agric. Food Chem.* 69, 3566–3584. doi: 10.1021/acs.jafc.0c07908

frontiers | Frontiers in Plant Science

TYPE Original Research
PUBLISHED 20 January 2025
DOI 10.3389/fpls.2024.1518962

OPEN ACCESS

EDITED BY
Xiangshu Dong,
Yunnan University, China

REVIEWED BY
Zhansheng Li,
Chinese Academy of Agricultural Sciences, China
Hui Zhang,
Chinese Academy of Agricultural Sciences (CAAS), China
Yinbo Ma,
Yangzhou University, China

*CORRESPONDENCE
Xiaonan Li
gracesleexn83@syau.edu.cn
Zhongyun Piao
zypiao@syau.edu.cn

†These authors have contributed equally to this work

RECEIVED 29 October 2024
ACCEPTED 26 December 2024
PUBLISHED 20 January 2025

CITATION
Zhang Y, Jiang M, Sun S, Zhan Z, Li X and Piao Z (2025) Chinese cabbage orphan gene *BR3* confers bolting resistance to *Arabidopsis* through the gibberellin pathway. *Front. Plant Sci.* 15:1518962. doi: 10.3389/fpls.2024.1518962

Chinese cabbage orphan gene *BR3* confers bolting resistance to *Arabidopsis* through the gibberellin pathway

Yuting Zhang[1†], Mingliang Jiang[2†], Shurui Sun[1], Zongxiang Zhan[1], Xiaonan Li[1*] and Zhongyun Piao[1*]

[1]Molecular Biology of Vegetable Laboratory, College of Horticulture, Shenyang Agricultural University, Shenyang, China, [2]School of Agriculture, Jilin Agricultural Science and Technology University, Jilin, China

Premature bolting reduces the yield and quality of Chinese cabbage, making bolting resistance gene identification crucial for breeding superior and stable varieties. In this study, we identified an orphan gene *BOLTING RESISTANCE 3* (*BR3*) that positively regulates bolting resistance in *Arabidopsis thaliana*. The expression of *BR3* was developmentally regulated and occurred during the seedling and flowering stages. The BR3 protein was localized to both the plasma membrane and nucleus. *Arabidopsis BR3* overexpressing (*BR3*OE) plants exhibited delayed bolting and flowering times, an increased number of rosette leaves, reduced plant height, and fewer siliques under long-day (LD) conditions. Key flowering genes were significantly downregulated in *BR3*OE plants. *BR3*OE plants similarly exhibited delayed bolting and flowering times, and an increased number of rosette leaves under short-day (SD) conditions. *BR3*OE plants showed no significant phenotypic differences after vernalization treatment. *BR3*OE and WT plants exhibited early flowering after GA_3 treatment, and bolting and flowering time remained delayed in *BR3*OE plants compared with WT plants. Key *DELLA* genes *BrRGA1* and *BrRGL3* exhibited a co-expression pattern consistent with *BR3* gene in Chinese cabbage, which suggested that *BrRGA1* and *BrRGL3* genes may directly or indirectly regulated by *BR3* gene. *BR3* gene increased bolting resistance perhaps by upregulating the expression of *DELLA* genes in the GA pathway. This study provides new theoretical insights for addressing premature bolting in Chinese cabbage and offers novel approaches for breeding bolting-resistant varieties.

KEYWORDS

Chinese cabbage, orphan gene, *BR3*, bolting resistance, *Arabidopsis*, GA pathway

1 Introduction

Orphan genes (*OGs*) are widely present in every species and have no significant sequence similarity to known genes (Li and Wurtele, 2014; Rdelsperger et al., 2019; Jiang et al., 2022). Numerous plant genomes have been rapidly decoded with the sequencing technology advancements, which provided a solid foundation for identifying *OGs*. A number of *OGs* have been identified in diverse species. For instance, there are 1324 *OGs* in the genome of *Arabidopsis* and 529 in the genome of *B. rapa* (Lin et al., 2010; Jiang et al., 2018). These genes lack recognizable functional domains, motifs, or structures, posing significant challenges for functional characterization of *OGs*. However, previous studies have shown that *OGs* play crucial roles in biotic and abiotic stress responses (Luhua et al., 2008; Jiang et al., 2018; Qi et al., 2018; Li et al., 2019; Jiang et al., 2020a; Wang et al., 2021; Tanvir et al., 2022), metabolism regulation (Li and Wurtele, 2014; Li et al., 2015; Jones et al., 2016; Jiang et al., 2020b; Wang et al., 2024), and species-specific trait formation (Hanada et al., 2008; Cui et al., 2015; Ni et al., 2017; O'Conner and Li, 2020; Jiang et al., 2023; Zu et al., 2024). The functions of *OGs* in plant growth and development recently garnered increasing attention. The interaction of *Arabidopsis* ICE1 (INDUCER OF CBF EXPRESSION 1) and IDD14 (INDETERMINATE DOMAIN 14) activates the transcription of *OGs* to regulate lipid metabolism in pollen, thus promoting pollen development and viability (Luo et al., 2024). Additionally, a novel *OG*, *Bolting Resistance 1* (*BR1*), has been identified as a bolting resistance regulator in *B. rapa*, specifically delay flowering through vernalization and photoperiod pathways (Jiang et al., 2023). *OG Bolting Resistance 2* (*BR2*) that regulates bolting resistance through the vernalization pathway, and its *Arabidopsis* overexpression upregulated flowering repressor *FLC* and downregulated key floral integrators (Zu et al., 2024). These findings highlight the vital roles of Chinese cabbage *OGs* in bolting resistance, although the exact mechanisms remain unclear.

Flowering time is a crucial agronomic trait of plant growth and development that is influenced by external environmental signals (e.g., photoperiod, temperature, and vernalization) and internal factors (e.g., autonomous pathways, age, and GA) (Pieper et al., 2020). Hormones, particularly GAs, are involved in cell division, elongation, and the transition from seed germination to flowering (Macmillan and Takahashi, 1968; Teotia and Tang, 2015). GAs, a class of diterpenoid plant hormones, promote flowering upon appropriate exogenous application (Hedden, 2020; Zhang et al., 2020). Defects in GA biosynthesis and signaling pathways often lead to aberrant flowering phenotypes, such as in GA-deficient mutant *ga1-3*, which does not flower under SD conditions (Wilson et al., 1992). Conversely, *SPINDLY* (*SPY*) is a negative regulator of the GA signaling pathway, and the enhancement of GA signaling in *spy* mutants leads to early flowering in *Arabidopsis* (Silverstone et al., 2006). As central GA signaling components, DELLA proteins inhibit flowering by interacting with the BRM-NF-YC functional module (Zhang et al., 2023). DELLA proteins delay flowering by repressing the expression of flowering-promoting factors, such as *SOC1* and *LFY*. When GA signaling is enhanced, DELLA proteins are degraded, thereby relieving the repression of these genes (Achard and Genschik, 2008). Transcription factor *WRKY75* regulates the GA signaling pathway by interacting with DELLA proteins, thus influencing flowering time and the photoperiod response in *A. thaliana* (Zhang et al., 2017). Recent research has shown that several regulatory factors influence GA signaling through distinct mechanisms, including *C-TERMINAL DOMAIN PHOSPHATASE-LIKE3* (*CPL3*), *Basic helix-loop-helix 4* (*MdbHLH4*), *D2-Hydroxyglutarate Dehydroase* (*GhD2HGDH*), and *KNOTTED-like homeobox 15* (*MdKNOX15*). Although the role of GA signaling in flowering time regulation has been widely studied, its precise molecular mechanisms remain to be elucidated.

In this study, a novel *B. rapa OG BR3* was identified. The expression patterns and subcellular localization of *BR3* were determined. Flowering time and other related traits of *A. thaliana BR3*OE plants were analyzed under LD, SD, vernalization, and GA_3 treatments. Additionally, the expression patterns of key flowering-related genes were determined using qRT-PCR analysis. This study evaluated the specific pathway through which *BR3* regulates flowering, providing new insights into the function of *OGs* and offering a novel approach for breeding bolting-resistant Chinese cabbage varieties.

2 Materials and methods

2.1 Plant materials and cultivation

The plant materials used in this study were Chinese cabbage inbred line 'GT-24', wild-type *A. thaliana* (WT), T_3 generation of *BR3*-overexpressing *Arabidopsis* plants ('*BR3*OE'), and cultivated *Nicotiana benthamiana*. The cultivation methods followed those described in a previous study (Jiang et al., 2023).

2.2 *BR3* sequence analysis, vector construction, and plant transformation

The *BR3* sequence was analyzed as previously described (Jiang et al., 2023). The *BR3* sequence was amplified from 'Chiifu' and inserted into the EcoRI and XhoI restriction sites of pBinGlyRed3-35S vector which contains the hygromycin resistance gene. The recombinant vector pBinGlyRed3-35S-BR3 was introduced into *Agrobacterium tumefaciens* GV3101 competent cell using the freeze-thaw method. For the heterologous transformation of Chinese cabbage *BR3* into *Arabidopsis*, the methods were based on those used in previous studies (Jiang et al., 2018; Li et al., 2021; Jiang et al., 2023). The primer pairs used in this study are listed in Supplementary Table S1.

2.3 Photoperiod, vernalization, and GA_3 treatments

Plants were cultivated under LD (16-h light/8-h dark photoperiod) or SD (16-h dark/8-h light photoperiod) conditions

at approximately 22°C with 65% humidity. For vernalization treatment, germinated WT and *BR3*OE seeds were grown at 4°C for 4 weeks. For GA_3 treatment, WT and *BR3*OE *Arabidopsis* plants were sprayed with 20 μM GA_3 solution twice per week until flowering. In control groups of WT and *Arabidopsis BR3*OE plants, an equivalent amount of distilled water was sprayed. Phenotypic investigations were conducted following a previous study (Jiang et al., 2023). At least 15 plants were used for each experiment. After the cotyledons of Chinese cabbage 'GT-24' were fully expanded, 500 mg/L GA_3 was sprayed, and samples were collected 12 h after spraying, with a total of six applications. As a control, 'GT-24' was treated with an equal volume of distilled water.

2.4 Histochemical GUS assay and subcellular localization analyses

Histochemical GUS staining was performed as previously described (Li et al., 2021). Subcellular localization of the BR3 protein was performed according to the previous method (Jiang et al., 2023). After 24 h of incubation in the dark post-injection, samples were transferred to light conditions for continued incubation. Fluorescence signals were observed 48–72 h post-injection using a laser confocal microscope (Leica SP8, Germany) at excitation wavelengths.

2.5 Total RNA isolated, first-strand cDNA synthesis, and qRT-PCR

Total RNA isolated, first-strand cDNA synthesis, and qRT-PCR were conducted according to the methods described in previous studies (Jiang et al., 2018, 2023). The primers used for qRT-PCR analysis are listed in Supplementary Table S1.

2.6 Statistical analysis

Statistical analysis using Student's *t*-test or one-way ANOVA was performed using SPSS software (v26). Data are presented as the mean ± standard deviation (SD). Graphs were generated using GraphPad Prism software (v9.2).

3 Results

3.1 Sequence analysis of *BR3*

The *BR3* (*BraA07003496*) gene sequence was 347 bp and contained two exons and one intron located on the chromosome A07 of Chinese cabbage, encoding 76 amino acids (Supplementary Figure S1). A search in the NCBI-CDD conserved domain database showed that BR3 did not have any domains. BR3 was not predicted to function as a transcription factor based on the Plant Transcription Factor Database (TFDB). The Group-based Prediction System (GPS) showed that the BR3 protein lacked kinase activity. No signal peptides, cleavage sites, or transmembrane regions were identified. Structural prediction showed that BR3 consisted of α-helices, extended strands, and random coils, with random coils accounting for 42.11% of the structure. These findings suggest that *BR3* is a novel gene with an unknown function, warranting further investigation to elucidate its role.

3.2 *BR3* expression patterns in Chinese cabbage

To investigate the role of *BR3* gene expression during Chinese cabbage development, qRT-PCR analysis was performed on leaves at 2, 4, 6, 8, 10, and 12 days after the emergence of the first true leaf. The gene expression of *BR3* showed notably higher expression levels on days 6 and 8, suggesting that *BR3* gene expression persisted throughout the seedling growth phase (Figure 1A). Additionally, at 4 days after flowering, *BR3* expression was detected in the stem, leaf, flower, and flower buds, with the highest expression observed in the flowers (Figure 1B). This suggests that *BR3* may directly or indirectly involved in bolting resistance in Chinese cabbage.

3.3 *BR3* gene promoter expression analysis and subcellular localization of BR3 protein

To determine the spatiotemporal specificity of *BR3* gene expression, GUS staining was performed on the flower buds, leaves, and roots of *BR3* transgenic *Arabidopsis* plants. WT leaves were used as a negative control (Figures 2A–C). As shown in Figures 2D–F, significant blue staining was observed in the flower buds, leaves, and roots, indicating that the *BR3* gene in *Arabidopsis* is regulated and expressed in these tissues after flowering. To better understand the mechanisms by which the BR3 protein functions within the cell, subcellular localization analysis was conducted. The 35S::BR3::GFP plasmid was introduced into *N. benthamiana* leaves via *Agrobacterium tumefaciens* injection, and fluorescence was observed under a confocal microscope to determine the localization of the BR3 protein. The distribution of fluorescent signals from the transiently expressed fusion protein reveled that BR3 was localized in both the nucleus and plasma membrane (Figures 2G–L). These findings provide a foundation for unraveling the flowering regulatory mechanisms of *BR3*.

3.4 Delayed flowering of *BR3*OE is independent of photoperiod

To determine whether the late flowering phenotype of *BR3*OE was related to the photoperiod pathway, the flowering times of WT and *BR3*OE plants were recorded under LD and SD conditions.

*BR3*OE and WT plant phenotypes under LD conditions are shown in Figures 3A–C. The bolting time of *BR3*OE plants was 8.66

10.3389/fpls.2024.1518962

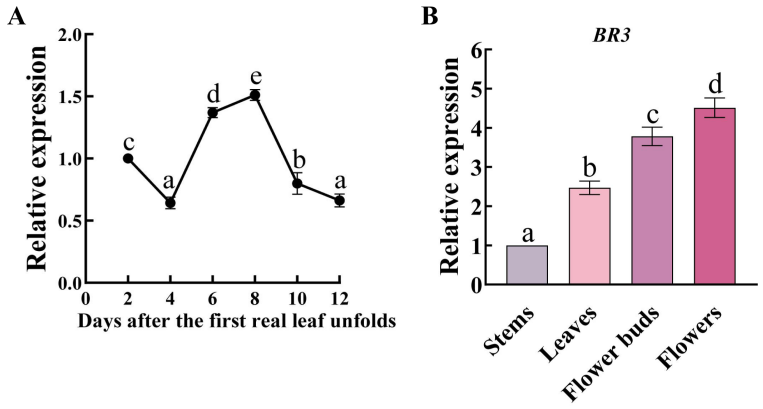

FIGURE 1
Expression patterns of the *BR3* gene in Chinese cabbage. **(A)** *BR3* gene expression during vegetative stage in Chinese cabbage. The samples of Chinese cabbage 'GT-24' cultured under LD conditions were collected from the aboveground parts of the Chinese cabbage at 2, 4, 6, 8, 10, and 12 days after the emergence of the first true leaf. **(B)** *BR3* gene expression during the reproductive stage of Chinese cabbage. The samples were collected from different tissues of the aboveground parts of 'GT-24' at 4 days after flowering. There were three biological and three technical replications. Data are presented as the mean ± SD (one-way ANOVA, $p < 0.05$). Different lowercase letters represent significant differences in gene expression between different development stages or tissues.

days later than that of WT (Figure 3D). In *BR3*OE plants, flowering time was delayed by 8.53 days (Figure 3E), and plant height decreased by 6.92 cm (Figure 3F). Concomitantly, the number of rosette leaves increased by 3.2 (Figure 3G), and the number of siliques was reduced by 9.47 (Figure 3H). Moreover, the phenotype of another *BR3*OE#2 line (Supplementary Figure S2) is consistent with that shown in the Figure 3C. Then, the expression levels of key flowering genes *AtFT*, *AtSOC1*, and *AtLFY* were measured using qRT-PCR. As shown in Figures 3I–K, the expression levels of *AtFT*, *AtSOC1*, and *AtLFY* were significantly downregulated in *BR3*OE plants compared with WT. These results suggest that *BR3* delays flowering in *Arabidopsis* by repressing the expression of *AtFT*, *AtSOC1*, and *AtLFY*.

The growth phenotypes of *BR3*OE and WT plants under SD conditions are shown in Figure 4A. The bolting time was delayed by 34.87 days (Figure 4B), and the flowering time of *BR3*OE plants was delayed by 35.27 days compared with that of WT plants (Figure 4C). The plant height was reduced by 2.21 cm (Figure 4D), and the number of rosette leaves increased by 3.53 (Figure 4E). *BR3* gene overexpression led to a late-flowering phenotype under both LD and SD conditions, suggesting that delayed flowering in *BR3*OE is not influenced by the photoperiod. Additionally, the increased number of rosette leaves in *BR3*OE plants at the time of flowering suggests that *BR3* promotes biomass accumulation, enhancing vegetative growth and inhibiting reproductive growth in *Arabidopsis*. These results indicate that *BR3* regulates bolting resistance independent of the photoperiod.

3.5 *BR3* delays flowering independent of the vernalization pathway

The bolting and flowering times of WT were advanced by 4.33 and 4.4 days, respectively, after vernalization treatment (Figures 5A, B). Additionally, compared with the non-treated group, plant height increased by 2.8 cm, and the number of rosette leaves was reduced by 3.2 (Figures 5C, D). However, in vernalized *BR3*OE plants, there were no significant differences in bolting time, flowering time, or number of rosette leaves (Figures 5D, E). These results indicate that vernalization promotes early flowering in WT but not in *BR3*OE plants, suggesting that the *BR3* gene delays flowering independently of the vernalization pathway and may function through other pathways.

3.6 *BR3*OE is responsive to the GA pathway

After treatment with GA_3, the bolting and flowering times of WT were advanced by 4.47 and 4.13 days, respectively, compared with the non-treated control group (Figures 6A, B). Plant height increased by 1.98 cm, and the number of rosette leaves decreased by 3.47 (Figures 6C, D). After GA_3 treatment, the bolting and flowering times of *BR3*OE plants were advanced by 5 and 4.73 days, respectively (Figure 6E), compared with non-treated plants, and the number of rosette leaves was reduced by 2.67 (Figure 6D). Exogenous GA_3 application promoted flowering in *BR3*OE plants, which displayed a phenotype similar to WT (Figure 6A), suggesting that the *BR3* gene influences flowering gene pathways in response to GA, leading to delayed flowering. DELLA proteins are key transcription factors in the GA signaling pathway. The *B. rapa* genome contains five DELLA subfamily members: *BrRGL1*, *BrRGL2*, *BrRGL3*, *BrRGA1*, and *BrRGA2*. The expression patterns of the five *DELLA* genes and the *BR3* gene in Chinese cabbage were analyzed using qRT-PCR. The expression of the *BrRGA2*, *BrRGL1*, and *BrRGL2* genes significantly decreased after the fifth sampling point. With the increase in the time and frequency of GA_3 treatments, the expression of the *BrRGA1* and *BrRGL3* genes significantly increased after the fifth sampling, with a consistent increase in *BR3* expression (Figure 7).

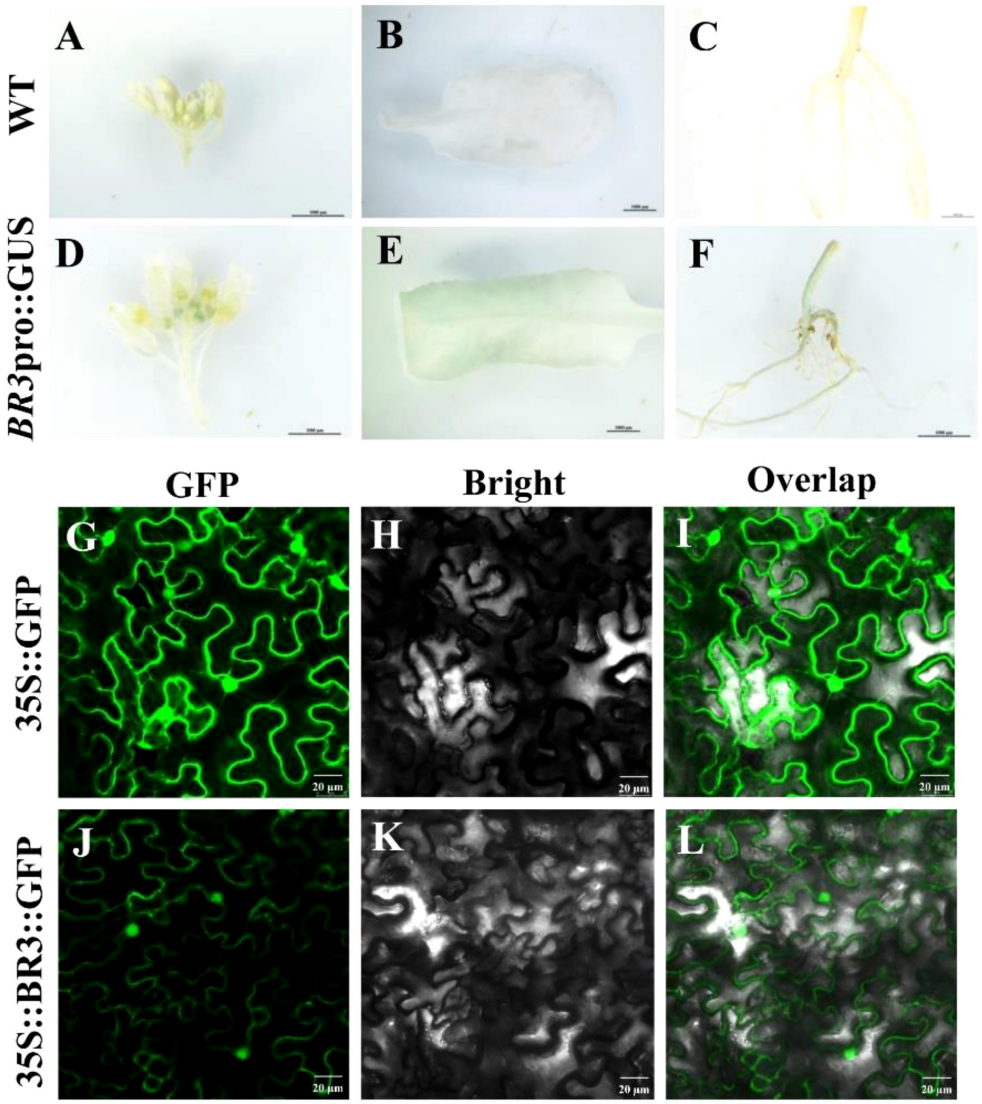

FIGURE 2
Expression analysis of *BR3* gene promoter and subcellular localization of BR3. **(A-F)** Expression analysis of promoter fusion with GUS. Scale bar: 1000 μm. Subcellular localization of BR3 protein. **(G-I)** 35S::GFP plasmid positive controls and **(J-L)** 35S::BR3::GFP localization in *N. benthamiana*. **(G, J)** GFP fluorescence channels. **(H, K)** Bright field. **(I, L)** Merge field. A Leica confocal microscope was used to collect images at 48 h after agro-infiltration. Control GFP localization was evident throughout these cells. Scale bar: 20 mm.

4 Discussion

OGs are unique genes in plant genomes that regulate species-specific development, metabolism, and stress responses, enabling plants to adapt to specific environments, optimize metabolic pathways, and enhance stress resistance. Although the function of most *OGs* remains unknown, these genes are ubiquitously present in all species (Jiang et al., 2020b), highlighting the biological significance of the function and mechanisms of *BrOGs*. Previous studies have screened and identified *OGs* in *B. rapa* and thoroughly analyzed *BrOGs* sequence characteristics and expression patterns (Jiang et al., 2018). This study identified a novel *OG*, *BR3*, which positively regulated bolting tolerance in *Arabidopsis*, which further confirming the relationship between *OGs* and species-specific trait formation. Sequence analysis showed that *BR3* with an unknown function that localized to both the cell membrane and nucleus, and key flowering genes were downregulated in *BR3*OE plants. Similarly, *BR1* overexpression downregulates key flowering integrators, such as *AtSOC1*, *AtLFY*, and *AtFUL* (Jiang et al., 2023). Additionally, *BR2* was found to be a positive regulator of bolting resistance through the vernalization pathway that localizes in the cell membrane, and in vernalized Chinese cabbage *BR2*OE, *BrVIN3.b* and *BrFRI* are downregulated, while *BrFLC5* is upregulated, with key flowering factors, such as *BrSOC1s*, *BrLFYs*, and *BrFTs*, downregulated (Zu et al., 2024). These studies strongly support the findings of this study. *BR3*OE exhibited a bolting-resistant phenotype, and exogenous application of GA_3 promoted flowering. Therefore, *BR3* might delay flowering by acting on key genes in the GA pathway.

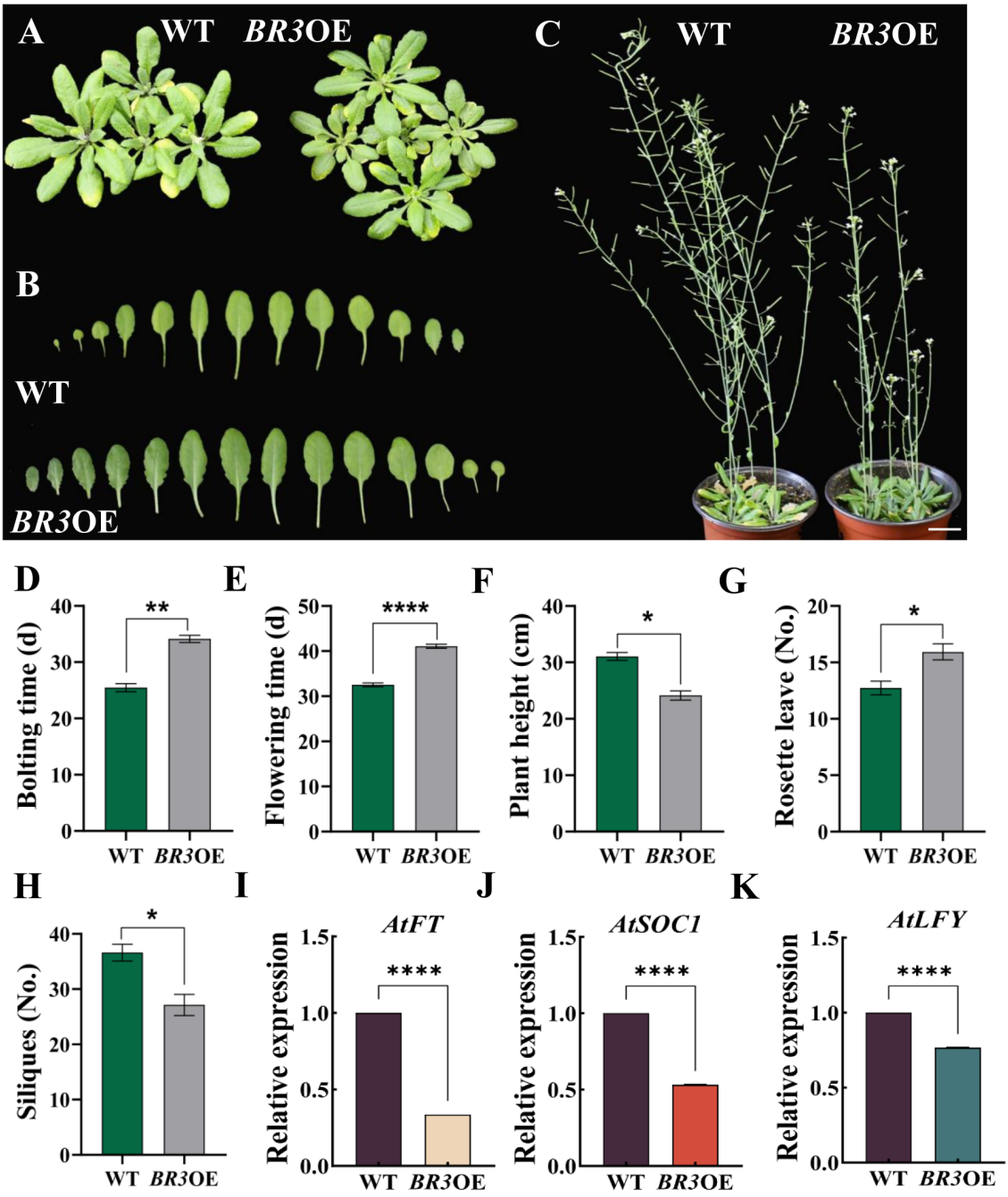

FIGURE 3
Phenotypes of WT and *BR3*OE under LD conditions and expression of key flowering genes. **(A)** Plant phenotypes of WT and *BR3*OE at 28 days. **(B)** Individual leaves of WT and *BR3*OE at 28 days. **(C)** Plant height of WT and *BR3*OE at 53 days. The scale bars are 2 cm. **(D)** Bolting time, **(E)** flowering time, **(F)** plant height, **(G)** number of rosette leaves, and **(H)** number of siliques of WT and *BR3*OE under LD conditions. **(I-K)** Expression of key flowering genes. Data are presented as the mean ± SD (Student's *t*-test, **p* < 0.05, ***p* < 0.01, and *****p* < 0.0001).

The differences in subcellular localization and promoter-induced expression indicate distinct *OGs* that regulate bolting resistance through different pathways.

In this study, *BR3* overexpression resulted in a delayed flowering phenotype under LD conditions (Figures 3C, E). Moreover, *BR3*OE plants showed significantly reduced expression of the *AtFT*, *AtSOC1*, and *AtLFY* genes compared with WT plants (Figures 3I–K). *AtFT* acts as a central integrator of environmental and endogenous signals that is translated into protein in the leaves and transported to the shoot apical meristem, where it upregulates *AtSOC1* expression (Corbesier et al., 2007). *SOC1* acts as a flowering integrator, coordinating other signaling pathways, such as photoperiod and temperature pathways, to regulate flowering time (Blazquez et al., 1998; Moon et al., 2003; Gregis et al., 2009;

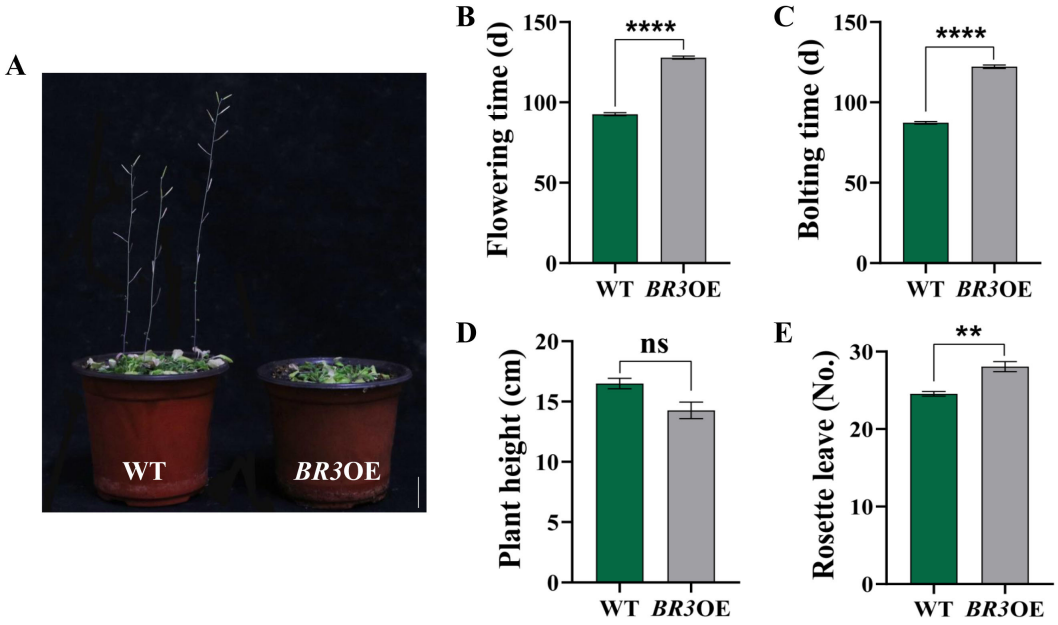

FIGURE 4
Phenotypes of WT and *BR3*OE plants under SD. **(A)** Phenotypes of WT and *BR3*OE at 120 days. The scale bars are 2 cm. **(B)** Bolting time, **(C)** flowering time, **(D)** plant height, and **(E)** number of rosette leaves of WT and *BR3*OE plants. Data are presented as the mean ± SD (Student's *t*-test, $^{**}p < 0.01$, and $^{****}p < 0.0001$).

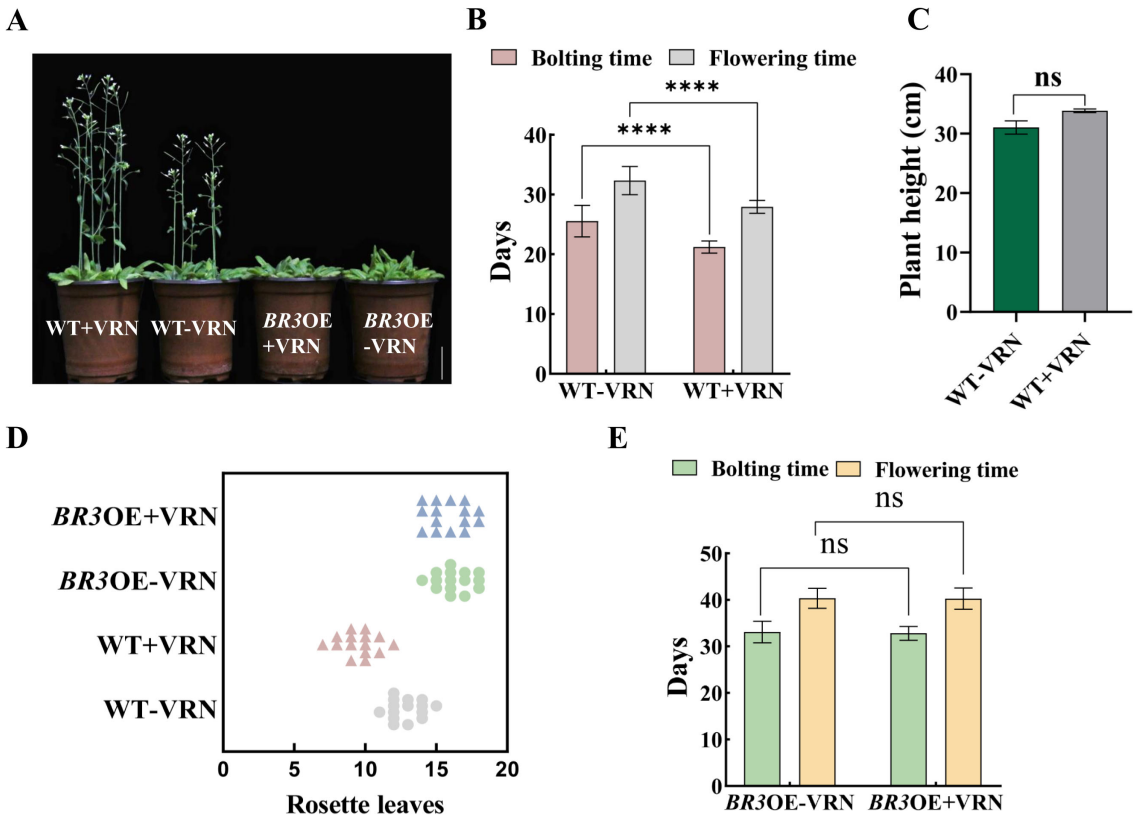

FIGURE 5
Agronomic traits in WT and *BR3*OE plants after vernalization treatment. **(A)** Phenotypes of WT and *BR3*OE control plants and plants treated with vernalization at 36 days. The scale bars are 2 cm. **(B)** Bolting and flowering time, **(C)** plant height, and **(D)** number of rosette leaves of vernalized and non-vernalized *Arabidopsis* WT plants. **(E)** Bolting and flowering time of vernalized and non-vernalized *Arabidopsis BR3*OE plants. +VRN, With vernalization treatment. -VRN, Without vernalization treatment. Data are presented as the mean ± SD; ns indicates not significant (Student's *t*-test, $^{****}p < 0.0001$).

10.3389/fpls.2024.1518962

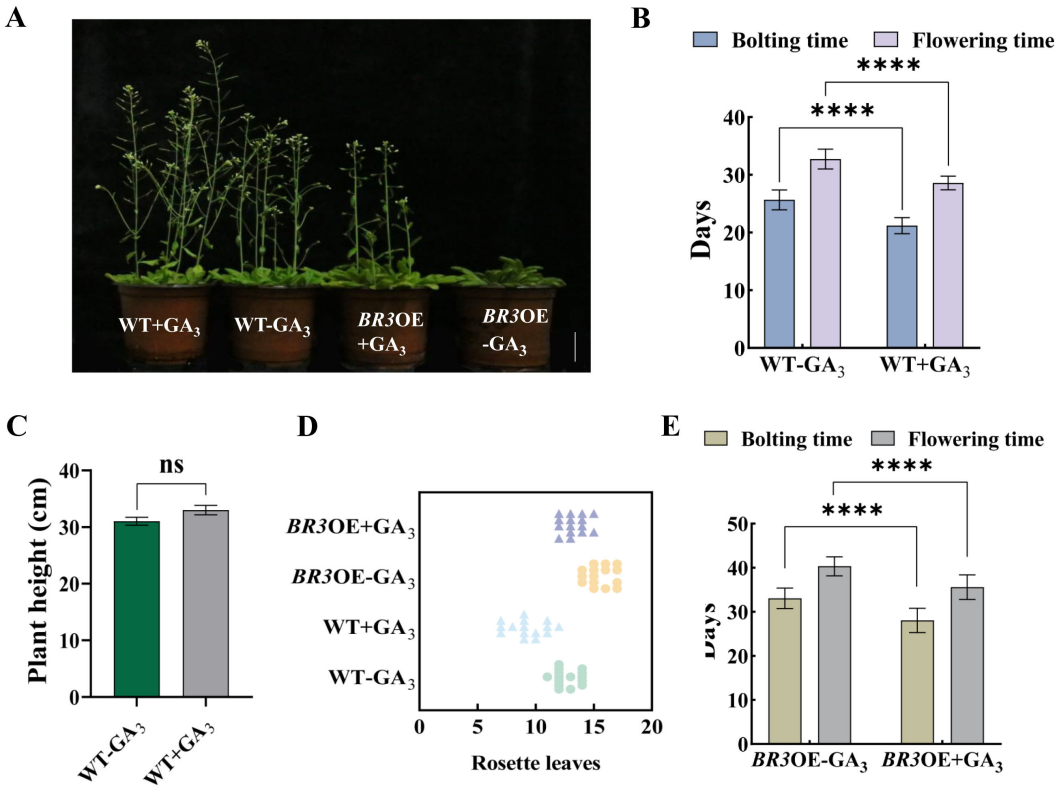

FIGURE 6
Agronomic traits in WT and *BR3*OE plants treated with GA_3. **(A)** Phenotypes of WT and *BR3*OE control plants and plants treated with GA_3 at 36 days. The scale bars are 2 cm. **(B)** Bolting and flowering time and **(C)** plant height of WT plants after GA_3 treatment. **(D)** Number of rosette leaves in WT and *BR3*OE plants treated with GA_3. **(E)** Bolting and flowering times of *BR3*OE plants treated with GA_3. $+GA_3$, With vernalization treatment. $-GA_3$, Without vernalization treatment. Data are presented as the mean ± SD (Student's *t*-test, ****$p < 0.0001$).

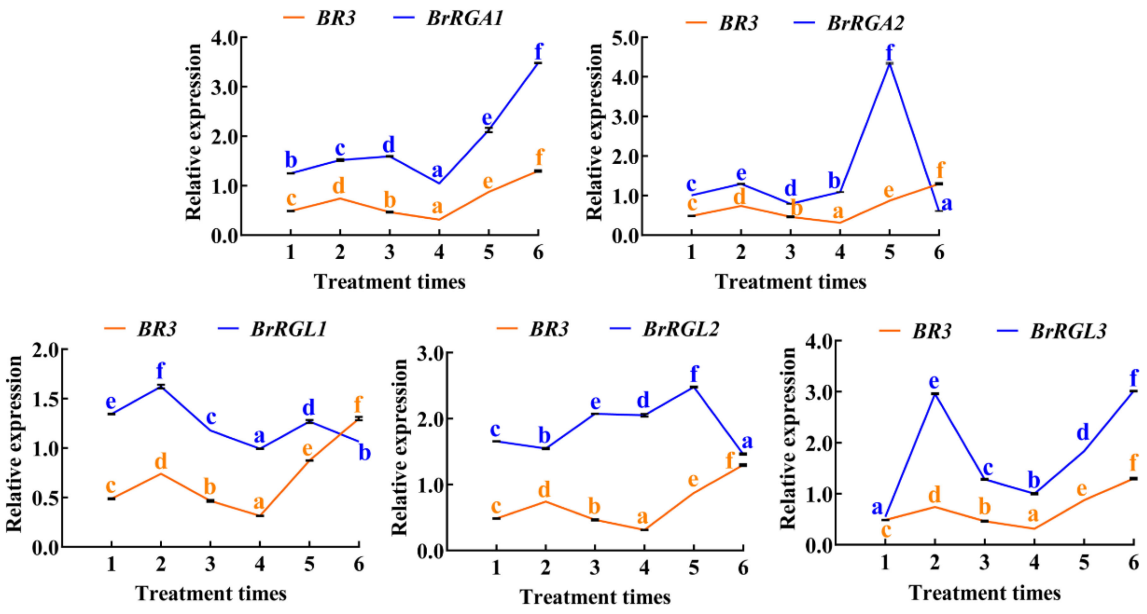

FIGURE 7
Expression analysis of *BR3* and *DELLA* genes in Chinese cabbage after GA_3 treatment. *RGA1, REPRESSOR of GA1*; *RGA2, REPRESSOR of GA2*; *RGL1, RGA-LIKE PROTEIN 3*; *RGL2, RGA-LIKE PROTEIN 2*; and *RGL3, RGA-LIKE PROTEIN 3*. The blue and yellow solid lines represent qRT-PCR results of the *DELLA* and *BR3* genes of Chinese cabbage 'GT-24', respectively. Data are presented as the mean ± SD (one-way ANOVA, $p < 0.05$). Different lowercase letters represent significant differences in gene expression between different treatment times.

Liu et al., 2009; Fornara et al., 2010). *LFY* is a key flowering activator whose high expression promotes floral organ formation. Additionally, *SOC1* enhances *LFY* expression by binding to its promoter region (Weigel et al., 1992). Exogenous GA_3 application significantly enhances *SOC1* expression in *Arabidopsis*, thereby shortening flowering time (Wang et al., 2022). Furthermore, GA influences flowering timing by directly affecting the expression of flowering regulatory genes such as *LFY* and *SOC1* (Mutasa-Göttgens and Hedden, 2009). Simultaneously, *FT* may also influence GA metabolism by regulating key enzymes, such as GA2 oxidase 8-3 (GA2ox8-3). *FT* overexpression under LD conditions reduces *GA2ox8-3*expression (Miskolczi et al., 2019). Under SD conditions, endogenous GA levels increase significantly before flowering, promoting flowering by inducing FT in the leaves and *SOC1* in the shoot apex (Fukazawa et al., 2021). GA promotes flowering by upregulating *FT* transcription under LD conditions (Hisamatsu and King, 2008; Porri et al., 2012). This suggests that *BR3* may inhibit bolting and flowering in *Arabidopsis* through the GA pathway.

In this study, among *Arabidopsis BR3*OE plants subjected to photoperiod, vernalization, and GA_3 treatments, only GA_3-treated plants exhibited early flowering (Figure 6). *BR3*OE exhibited a late bolting phenotypes, and GA_3 treatment promoted bolting and flowering. However, despite GA_3 treatment, bolting and flowering occurred later in *BR3*OE than in WT plants (Figures 6A, B, E). DELLA proteins are negative regulators of the GA signaling pathway and inhibit the expression of flowering-related genes by interfering with transcription factor activities. When GA levels increase, DELLA protein degradation alleviates this repression, promoting flowering gene expression (Achard et al., 2003; Sun and Gubler, 2004). Studies have shown that BrARGL1, a key DELLA protein in Chinese cabbage, suppresses bolting when overexpressed, resulting in significantly reduced expression of GA-regulated proteins (BraGASA6), flowering-related genes (*BraSOC1*, *BraLFY*), expansin proteins (BraEXPA11), and xyloglucan endotransglucosylases (BraXTH3). Conversely, *rgl1* mutants show the opposite phenotype. *BRARGL1* inhibits transcriptional activation of *BRASOC1* on *BRAXTH3* and *BRALFY* genes; however, GA_3 enhances transcriptional activation of *BraSOC1*, indicating that the *BraRGL1-BraSOC1* module regulates bolting and flowering in Chinese cabbage through the GA signaling pathway (Wang et al., 2023). The expression of *BrRGA2*, *BrRGL1*, and *BrRGL2* decreased with increased GA_3 application, potentially due to their degradation. The expression levels of *BrRGA1* and *BrRGL3* were consistent with *BR3*, suggesting that increased *BR3* expression promotes the of *BrRGA1* and *BrRGL3* expression (Figure 7). *BR3* increases bolting resistance by increasing the expression of *DELLA* genes in the GA pathway.

Premature bolting is a primary limiting factor for spring-sown Chinese cabbage and cultivation in high-altitude, cold regions, leading to reduced yield and quality and causing significant economic losses. Therefore, identifying bolting resistance genes and developing bolting-resistant varieties are critical for ensuring a year-round balanced supply and stable production. In this study, *Arabidopsis BR3*OE exhibited bolting resistance. After GA_3 treatment, bolting and flowering were promoted but occurred later than in GA_3-treated WT, suggesting that *BR3* may regulate bolting through the GA pathway. However, the proteins interacting with BR3 in Chinese cabbage, the transcription factors regulating its expression, and the molecular mechanisms by which the *BR3* gene controls bolting resistance in Chinese cabbage remain unclear. Addressing these topics will provide a theoretical basis for elucidating the molecular mechanism of bolting resistance and offer new insights and gene resources for breeding bolting-resistant Chinese cabbage varieties.

5 Conclusions

In this study, a newly identified *OG*, *BR3*, positively regulated bolting resistance, supporting the role of *OGs* in controlling species-specific trait formation. The *BR3* gene was highly expressed in flower buds and flowers, and the BR3 protein was localized in the nucleus and cell membrane. *BR3*OE exhibited a bolting-resistant phenotype and suppressed the expression of key flowering genes. Exogenous GA_3 treatment and qRT-PCR analysis of the *DELLA* gene suggest that *BR3* functions as a novel flowering time regulator through the gibberellin pathway. This study provides new insights into the breeding of bolting-resistant Chinese cabbage varieties and provides a theoretical foundation for further research on bolting resistance mechanisms in Chinese cabbage.

Data availability statement

The original contributions presented in the study are included in the article/Supplementary Material. Further inquiries can be directed to the corresponding authors.

Author contributions

YZ: Writing – review & editing, Conceptualization, Data curation, Methodology, Visualization, Writing – original draft. MJ: Formal analysis, Funding acquisition, Resources, Visualization, Writing – original draft, Writing – review & editing. SS: Methodology, Writing – review & editing. ZZ: Data curation, Project administration, Writing – review & editing. XL: Formal analysis, Funding acquisition, Methodology, Supervision, Validation, Writing – review & editing. ZP: Formal analysis, Funding acquisition, Resources, Supervision, Visualization, Writing – review & editing.

Funding

The author(s) declare financial support was received for the research, authorship, and/or publication of this article. This work was supported by the National Natural Science Foundation of China (32302568), the China Agriculture Research System of MOF and MARA (CARS-12), and the National Natural Science Foundation of China (32272715).

Conflict of interest

The authors declare that the research was conducted in the absence of any commercial or financial relationships that could be construed as a potential conflict of interest.

Generative AI statement

The author(s) declare that no Generative AI was used in the creation of this manuscript.

Publisher's note

All claims expressed in this article are solely those of the authors and do not necessarily represent those of their affiliated organizations, or those of the publisher, the editors and the reviewers. Any product that may be evaluated in this article, or claim that may be made by its manufacturer, is not guaranteed or endorsed by the publisher.

Supplementary material

The Supplementary Material for this article can be found online at: https://www.frontiersin.org/articles/10.3389/fpls.2024.1518962/full#supplementary-material

SUPPLEMENTARY FIGURE 1
Gene structure analysis of *BR3* revealed exons and intron.

SUPPLEMENTARY FIGURE 2
Phenotypes of WT and additional *BR3*OE#2 lines under LD conditions.

References

Achard, P., and Genschik, P. (2008). Releasing the brakes of plant growth: How GAs shutdown DELLA proteins. *J. Exp. Bot.* 60, 1085–1092. doi: 10.1093/jxb/ern301

Achard, P., Vriezen, W. H., van der Straeten, D., and Harberd, N. P. (2003). Ethylene regulates arabidopsis development *via* the modulation of DELLA protein growth repressor function. *Plant Cell* 15, 2816–2825. doi: 10.1105/tpc.015685

Blazquez, M. A., Green, R., Nilsson, O., Sussman, M. R., and Weigel, D. (1998). Gibberellins promote flowering of *Arabidopsis* by activating the *LEAFY* promoter. *Plant Cell* 10, 791–800. doi: 10.1105/tpc.10.5.791

Corbesier, L., Vincent, C., Jang, S., Fornara, F., Fan, Q., Searle, I., et al. (2007). FT protein movement contributes to long-distance signaling in floral induction of *Arabidopsis*. *Science* 316, 1030–1033. doi: 10.1126/science.1141752

Cui, X., Lv, Y., Chen, M., Nikoloski, Z., Twell, D., and Zhang, D. (2015). Young genes out of the male: an insight from evolutionary age analysis of the pollen transcriptome. *Mol. Plant* 8, 935–945. doi: 10.1016/j.molp.2014.12.008

Fornara, F., de Montaigu, A., and Coupland, G. (2010). SnapShot: control of flowering in *Arabidopsis*. *Cell* 141, 550–550. doi: 10.1016/j.cell.2010.04.024

Fukazawa, J., Ohashi, Y., Takahashi, R., Nakai, K., and Takahashi, Y. (2021). DELLA degradation by gibberellin promotes flowering *via* GAF1-TPR-dependent repression of floral repressors in Arabidopsis. *Plant Cell* 33, 2258–2272. doi: 10.1093/plcell/koab102

Gregis, V., Sessa, A., Dorca-Fornell, C., and Kater, M. M. (2009). The *Arabidopsis* floral meristem identity genes *AP1*, *AGL24* and *SVP* directly repress class B and C floral homeotic genes. *Plant J.* 60, 626–637. doi: 10.1111/j.1365-313x.2009.03985.x

Hanada, K., Zou, C., Lehti-Shiu, M. D., Shinozaki, K., and Shiu, S. H. (2008). Importance of lineage-specific expansion of plant tandem duplicates in the adaptive response to environmental stimuli. *Plant Physiol.* 142, 993–1003. doi: 10.1104/pp.108.122457

Hedden, P. (2020). The current status of research on gibberellin biosynthesis. *Plant Cell Physiol.* 61, 1832–1849. doi: 10.1093/pcp/pcaa092

Hisamatsu, T., and King, R. W. (2008). The nature of floral signals in *Arabidopsis*. II. Roles for *FLOWERING LOCUS T* (*FT*) and gibberellin. *J. Exp. Bot.* 59, 3821–3829. doi: 10.1093/jxb/ern232

Jiang, M., Dong, X., Lang, H., Pang, W., Zhan, Z., Li, X., et al. (2018). Mining of *Brassica*-specific genes (*BSGs*) and their induction in different developmental stages and under *Plasmodiophora brassicae* stress in *Brassica rapa*. *Int. J. Mol. Sci.* 19, 2064. doi: 10.3390/ijms19072064

Jiang, C., Hei, R., Yang, Y., Zhang, S., Wang, Q., Wang, W., et al. (2020a). An orphan protein of *Fusarium graminearum* modulates host immunity by mediating proteasomal degradation of *TaSnRK1α*. *Nat. Commun.* 11, 4382. doi: 10.1038/s41467-020-18240-y

Jiang, M., Li, X., Dong, X., Zu, Y., Zhan, Z., Piao, Z., et al. (2022). Research advances and prospects of orphan genes in plants. *Front. Plant Sci.* 13. doi: 10.3389/fpls.2022.947129

Jiang, M., Zhan, Z., Li, H., Dong, X., Cheng, F., and Piao, Z. (2020b). *Brassica rapa* orphan genes largely affect soluble sugar metabolism. *Hortic. Res.* 7, 181. doi: 10.1038/s41438-020-00403-z

Jiang, M., Zhang, Y., Yang, X., Li, X., and Lang, H. (2023). *Brassica rapa* orphan gene *BR1* delays flowering time in *Arabidopsis*. *Front. Plant Sci.* 14. doi: 10.3389/fpls.2023.1135684

Jones, D. C., Zheng, W., Huang, S., Du, C., Zhao, X., Yennamalli, R. M., et al. (2016). A clade-specific *Arabidopsis* gene connects primary metabolism and senscence. *Front. Plant Sci.* 7. doi: 10.3389/fpls.2016.00983

Li, X., Li, H., Zhao, Y., Zong, P., Zhan, Z., and Piao, Z. (2021). Establishment of a simple and efficient *Agrobacterium*-mediated genetic transformation system to Chinese Cabbage (*Brassica rapa* L. ssp. pekinensis). *Hortic. Plant J.* 7, 117–128. doi: 10.1016/j.hpj.2021.01.006

Li, G., Wu, X., Hu, Y., Muoz-Amatriaín, M., Luo, J., Zhou, W., et al. (2019). Orphan genes are involved in drought adaptations and ecoclimatic-oriented selections in domesticated cowpea. *J. Exp. Bot.* 70, 3101–3110. doi: 10.1093/jxb/erz145

Li, L., and Wurtele, E. S. (2014). The *QQS* orphan gene of *Arabidopsis* modulates carbon and nitrogen allocation in soybean. *Plant Biotechnol. J.* 13, 177–187. doi: 10.1111/pbi.12238

Li, L., Zheng, W., Yanbing, Z., Ye, H., and Tang, B. (2015). QQS orphan gene regulates carbon and nitrogen partitioning across species *via NF-YC* interactions. *Proc. Natl. Acad. Sci. U.S.A.* 112, 14734–14739. doi: 10.1073/pnas.1514670112

Lin, H., Moghe, G., Ouyang, S., Iezzoni, A., Shiu, S. H., Gu, X., et al. (2010). Comparative analyses reveal distinct sets of lineage-specific genes within *Arabidopsis thaliana*. *BMC Evol. Biol.* 10, 1–14. doi: 10.1186/1471-2148-10-41

Liu, C., Xi, W., Shen, L., Tan, C., and Yu, H. (2009). Regulation of floral patterning by flowering time genes. *Dev. Cell* 16, 711–722. doi: 10.1016/j.devcel.2009.03.011

Luhua, S., Ciftci-Yilmaz, S., Harper, J., Cushman, J., and Mittler, R. (2008). Enhanced tolerance to oxidative stress in transgenic *Arabidopsis* plants expressing proteins of unknown function. *Plant Physiol.* 148, 280–292. doi: 10.1104/pp.108.124875

Luo, L., Zheng, Y., Li, X., Chen, Q., Yang, D., Gu, Z., et al. (2024). ICE1 interacts with IDD14 to transcriptionally activate *QQS* to increase pollen germination and viability. *J. Integr. Plant Biol.* 66, 1801–1819. doi: 10.1111/jipb.13725

Macmillan, J., and Takahashi, N. (1968). Proposed procedure for the allocation of trivial names to the gibberellins. *Nature* 217, 170–171. doi: 10.1038/217170a0

Miskolczi, P., Singh, R. K., Tylewicz, S., Azeez, A., Maurya, J. P., Tarkowská, D., et al. (2019). Long-range mobile signals mediate seasonal control of shoot growth. *Proc. Natl. Acad. Sci. U.S.A.* 116, 10852–10857. doi: 10.1073/pnas.1902199116

Moon, J., Suh, S. S., Lee, H., Choi, K. R., and Lee, I. (2003). The *SOC1* MADS-box gene integrates vernalization and gibberellin signals for flowering in *Arabidopsis*. *Plant J.* 35, 613–623. doi: 10.1046/j.1365-313x.2003.01833.x

Mutasa-Göttgens, E., and Hedden, P. (2009). Gibberellin as a factor in floral regulatory networks. *J. Exp. Bot.* 60, 1979–1989. doi: 10.1093/jxb/erp040

Ni, F., Qi, J., Hao, Q., Lyu, B., Luo, M.-C., Wang, Y., et al. (2017). Wheat *Ms2* encodes for an orphan protein that confers male sterility in grass species. *Nat. Commun.* 8, 15121. doi: 10.1038/ncomms15121

O'Conner, S., and Li, L. (2020). Mitochondrial fostering: the mitochondrial genome may play a role in plant orphan gene evolution. *Front. Plant Sci.* 11. doi: 10.3389/fpls.2020.600117

Pieper, R., Tomé, F., Pankin, A., and Korff, M. V. (2020). *FLOWERING LOCUS T4* (*HvFT4*) delays flowering and decreases floret fertility in barley. *J. Exp. Bot.* 72, 107–121. doi: 10.1093/jxb/eraa466

Porri, A., Torti, S., Romera-Branchat, M., and Coupland, G. (2012). Spatially distinct regulatory roles for gibberellins in the promotion of flowering of *Arabidopsis* under long photoperiods. *Development* 139, 2198–2209. doi: 10.1242/dev.077164

Qi, M., Zheng, W., Zhao, X., Hohenstein, J. D., Kandel, Y., O'Conner, S., et al. (2018). *QQS* orphan gene and its interactor *NF-YC4* reduce susceptibility to pathogens and pests. *Plant Biotechnol. J.* 17, 252–263. doi: 10.1111/pbi.12961

Rdelsperger, C., Prabh, N., and Sommer, R. J. (2019). New gene origin and deep taxon phylogenomics: opportunities and challenges. *Trends Genet.* 35, 914–922. doi: 10.1016/j.tig.2019.08.007

Silverstone, A. L., Tseng, T.-S., Swain, S. M., Dill, A., Jeong, S. Y., Olszewski, N. E., et al. (2006). Functional analysis of *SPINDLY* in gibberellin signaling in *Arabidopsis*. *Plant Physiol.* 143, 987–1000. doi: 10.1104/pp.106.091025

Sun, T.-P., and Gubler, F. (2004). Molecular mechanism of gibberellin signaling in plants. *Annu. Rev. Plant Biol.* 55, 197–223. doi: 10.1146/annurev.arplant.55.031903.141753

Tanvir, R., Ping, W., Sun, J., Cain, M., Li, X., and Li, L. (2022). *AtQQS* orphan gene and *NtNF-YC4* boost protein accumulation and pest resistance in tobacco (*Nicotiana tabacum*). *Plant Sci.* 317, 111198. doi: 10.1016/j.plantsci.2022.111198

Teotia, S., and Tang, G. (2015). To bloom or not to bloom: role of microRNAs in plant flowering. *Mol. Plant* 8, 359–377. doi: 10.1016/j.molp.2014.12.018

Wang, C., Chen, S., Feng, A., Su, J., Wang, W., Feng, J., et al. (2021). *Xa7*, A small orphan gene harboring promoter trap for *AvrXa7*, leads to the durable resistance to *Xanthomonasoryzae* pv. Oryzae. *Rice* 14, 48. doi: 10.1186/s12284-021-00490-z

Wang, Y., Huang, X., Huang, X., Su, W., Hao, Y., Liu, H., et al. (2022). *BcSOC1* promotes bolting and stem elongation in flowering Chinese cabbage. *Int. J. Mol. Sci.* 23, 3459. doi: 10.3390/ijms23073459

Wang, L., O'Conner, S., Tanvir, R., Zheng, W., Cothron, S., Towery, K., et al. (2024). CRISPR/Cas9-based editing of *NF-YC4* promoters yields high-protein rice and soybean. *New Phytol.* doi: 10.1111/nph.20141

Wang, Y., Song, S., Hao, Y., Chen, C., Ou, X., He, B., et al. (2023). Role of *BraRGL1* in regulation of *Brassica rapa* bolting and flowering. *Hortic. Res.* 10, uhad119. doi: 10.1093/hr/uhad119

Weigel, D., Alvarez, J., Smyth, D. R., Yanofsky, M. F., and Meyerowitz, E. M. (1992). *LEAFY* controls floral meristem identity in *Arabidopsis*. *Cell* 69, 843–859. doi: 10.1016/0092-8674(92)90295-n

Wilson, R. N., Heckman, J. W., and Somerville, C. R. (1992). Gibberellin is required for flowering in *Arabidopsis thaliana* under short days. *Plant Physiol.* 100, 403–408. doi: 10.1104/pp.100.1.403

Zhang, L., Chen, L., and Yu, D. (2017). Transcription factor WRKY75 interacts with DELLA proteins to affect flowering. *Plant Physiol.* 176, 790–803. doi: 10.1104/pp.17.00657

Zhang, X., He, L., Zhao, B., Zhou, S., and Chen, J. (2020). *Dwarf and Increased Branching 1* controls plant height and axillary bud outgrowth in *Medicago truncatula*. *J. Exp. Bot.* 71, 6355–6365. doi: 10.1093/jxb/eraa364

Zhang, C., Jian, M., Li, W., Yao, X., Tan, C., Qian, Q., et al. (2023). Gibberellin signaling modulates flowering via the *DELLA–BRAHMA–NF-YC* module in *Arabidopsis*. *Plant Cell* 35, 3470–3484. doi: 10.1093/plcell/koad166

Zu, Y., Jiang, M., Zhan, Z., Li, X., and Piao, Z. (2024). Orphan gene *BR2* positively regulates bolting resistance through the vernalization pathway in Chinese cabbage. *Hortic. Res.* 11, uhae216. doi: 10.1093/hr/uhae216

frontiers | Frontiers in Plant Science

TYPE Original Research
PUBLISHED 22 January 2025
DOI 10.3389/fpls.2025.1532449

OPEN ACCESS

EDITED BY
Xiangshu Dong,
Yunnan University, China

REVIEWED BY
Tongkun Liu,
Nanjing Agricultural University, China
Ke Huang,
Hunan Agricultural University, China

*CORRESPONDENCE
Xiaonan Li
gracesleexn@163.com
Zhongyun Piao
zypiao@syau.edu.cn

†These authors have contributed equally to this work

RECEIVED 22 November 2024
ACCEPTED 07 January 2025
PUBLISHED 22 January 2025

CITATION
Jiang M, Zhan Z, Li X and Piao Z (2025) Construction and evaluation of *Brassica rapa* orphan genes overexpression library. *Front. Plant Sci.* 16:1532449. doi: 10.3389/fpls.2025.1532449

Construction and evaluation of *Brassica rapa* orphan genes overexpression library

Mingliang Jiang[1,2†], Zongxiang Zhan[1†], Xiaonan Li[1*] and Zhongyun Piao[1*]

[1]Molecular Biology of Vegetable Laboratory, College of Horticulture, Shenyang Agricultural University, Shenyang, China, [2]School of Agriculture, Jilin Agricultural Science and Technology University, Jilin, China

Orphan genes (*OGs*) are crucial for species-specific characteristics and stress responses and are restricted to a specific taxon. However, their functions within particular species are poorly understood. Previous research identified *OGs* in *Brassica rapa* (*BrOGs*). In this study, the *BrOGs* overexpression (BrOGsOE) library in *Arabidopsis thaliana* was constructed. Approximately 128 unknown functional *BrOGs* were selected from Chinese cabbage and were overexpressed. The analysis focused on the phenotypes of leaf morphology and flowering time against phenotypic differences between Chinese cabbage and *Arabidopsis*. Interestingly, 72.66% of the transgenic lines showed distinctive phenotypic changes. Chinese cabbage-specific features, including curved, hairy, upward or downward-curving leaves, serrated margins, and multiple leaves, were observed in the BrOGsOE lines. The *BrOGs* overexpression library was associated with numerous variations in flowering time, particularly delayed flowering. This suggested that the delayed flowering time caused by *BrOGs* may be associated with resistance to bolting seem in Chinese cabbage. Furthermore, the results of stress treatment of 24 BrOGsOE lines with no apparent significant phenotypes suggested that a number of *BrOGs* have both general and specific functions against environmental and pathogenic stress. The findings of this study provide a comprehensive overview of the roles of *BrOGs*, emphasizing their significance as a resource for identifying positive genes associated with species-specific characteristics and stress responses and offering a solid foundation for the functional analysis of *BrOGs*.

KEYWORDS

***Brassica rapa*, orphan genes, overexpression library, construction, evaluation**

1 Introduction

Orphan genes (*OGs*), known as species-specific genes, are characterized by their lack of detectable resemblance to other proteins and are prevalent across nearly all organisms (Jiang et al., 2022; Moreyra et al., 2023). They arise within a single species or a taxonomically confined gene family formed by expressing unique open reading frames

(ORF). They are present throughout evolutionary history (Liu et al., 2023). These *OGs* provide organisms with a reservoir of genetic components that enable rapid responses to altering selection pressures, serving as a disruptive factor in evolution and playing a vital role in adaptation to novel biological niches (Li et al., 2022). These genes have been found and described in several plants, including *A. thaliana* (Lin et al., 2010), *Populus trichocarpa* (Lin et al., 2013), *Citrus sinensis* (Xu et al., 2015), and *B. rapa* (Jiang et al., 2018). The results of these investigations provide references for the comprehensive analysis of *OGs*.

Considering the challenges in examining *OGs* due to their lack of comparability with proteins from other lineages (Kimmel et al., 2023), specific studies on the functions of *OGs* provide key basic references. These genes are frequently associated with responses to stress, particular characteristics of the species, the regulation of specialized genes, and fundamental metabolic processes (Jiang et al., 2022). Several *B. rapa OGs* (*BrOGs*) have been found to be essential for soluble sugar metabolism, with *B. rapa OG 1* (*BrOG1*) apparently regulating this process in a sucrose synthase (SUS)-dependent manner (Jiang et al., 2020). Other *BrOGs*, such as *BOLTING RESISTANCE 1* (*BR1*), have been shown to influence flowering time in *Arabidopsis*, potentially functioning *via* vernalization and photoperiodic pathways (Jiang et al., 2023). A second *OG* found from *B. rapa*, termed *BOLTING RESISTANCE 2* (*BR2*), positively modulates bolting resistance in both *Arabidopsis* and Chinese cabbage, potentially functioning through the vernalization pathway (Zu et al., 2024). Knockouts of the *Zea* genus-specific micropeptide microRPG1 encoded by the *qKDR1 REGULATED PEPTIDE GENE* (*RPG*) locus induces a faster kernel dehydration rate (KDR) in maize (Yu et al., 2024). A bean orphan protein MRE-binding transcription factor 1 (PvMTF-1) is related to a metal-responsive element involved in cadmium resistance in transgenic tobacco (*Nicotiana tabacum*) through activation of tryptophan biosynthesis (Sun et al., 2015). *Physcomitrium patens OG ABA-responsive drought tolerance* (*PpARDT*) imparts drought tolerance in terrestrial plants, possibly by promoting the ABA response, thereby elucidating the functions of *OG* in affecting lineage-specific adaptation, probably through the recruitment of pre-existing pathway components (Dong et al., 2022). The *Arabidopsis OG QQS* has been confirmed as a regulator of carbon and nitrogen partitioning in various species through interactions with Nuclear Factor Y subunit C (NF-YC), as well as influencing both stress responses and pollen germination and viability (Li and Wurtele, 2015; Li et al., 2015; Fakhar et al., 2023; Luo et al., 2024). Recently, CRISPR/Cas9-based editing of *NF-YC4* promoters to increase rice and soybean protein yields has shown that NF-YC4 interacts with QQS, paving the way for improved crop productivity and nutritional value (Wang et al., 2024). *Populus trichocarpa OG BOOSTER* (*BSTR*) has been found to impact photosynthesis, and overexpression of *BSTR* improved biomass gains in poplar and *Arabidopsis* (Feyissa et al., 2024). However, the functions of *BrOGs* are not well identified.

The genomes of *B. rapa* and the closely associated *A. thaliana* have been invaluable resources for studying genomic evolution. *B. rapa* is planted extensively throughout the world due to its highly varied morphological characteristics, which have significant economic and breeding value. These characteristics include the leafy heads of Chinese cabbage, the oversized organs of turnip, and the broad axillary branching of Pak-choi (Song et al., 2014). After the emergence of *Arabidopsis*, the *B. rapa* genome underwent diversification approximately 12.4 to 13.4 million years ago (Yang et al., 2006; Liu et al., 2014; Waminal et al., 2016). The reasons underlying the evolution of varieties with large phenotypic differences within such a relatively short period are not fully understood, and the mechanisms associated with the speciation and morphological diversification of *B. rapa* in response to both natural and artificial selection require further investigation. Various *BrOGs* were identified and characterized in a previous study (Jiang et al., 2018). However, further research is needed into the potential contributions of these newly emerged *BrOGs* to the complex morphological characteristics of *B. rapa*, together with their possible associations with species-specific adaptation and stress responses.

This study constructed and characterized an overexpression library of *BrOGs* in *A. thaliana* to enable the enhancement of *BrOG* functions and the discovery of genes. The phenotypes of the BrOGsOE lines were then examined. As *OGs* are frequently associated with various forms of stress (Jiang et al., 2022), BrOGsOE lines that were not associated with distinctive phenotypic variations were challenged with biotic and abiotic stressors. The findings of this study provide a detailed analysis of the roles of *BrOGs* in species-specific characteristics and responses to stress.

2 Materials and methods

2.1 Plant materials and growth conditions

The *A. thaliana* ecotype Col-0 (WT) and the transformed lines were allowed to grow in a long-day (LD) environment (16 h light/8 h dark cycles) under cool white fluorescent light at 22°C with 65-70% humidity. To identify *BrOGs* at DNA and expression levels in BrOGsOE plants, seedlings of the WT and BrOGsOE lines from 9 individuals (three biological replicates with three plants per replicate) were obtained for DNA and RNA extraction after two weeks of growth.

2.2 Plant vector constructions, transformation, and *Arabidopsis* BrOGsOE lines selection

According to the previous study, procedures for plant vector constructions, transformation, and *Arabidopsis* BrOGsOE lines selection were performed as described previously (Jiang et al., 2020). Homozygous BrOGsOE lines were identified *via* the DsRed protein in seeds using a combination of red fluorescent protein excitation light and filter. The sequences of the forward and reverse primers used for the vector constructs are provided in Supplementary Table S1.

2.3 Characterization of transgenic lines

For the characterization of BrOGsOE lines, flowering time, rosette radius, silique length, seed number, stem height, leaf shape, and fertility were measured as per the previously established protocols (Jiang et al., 2020). A total of 15 plants of every BrOGsOE line or WT were examined.

2.4 Pathogen inoculations and quantification

For pathogen stress treatment, 4-5-week-old WT and BrOGsOE lines were hand-infiltrated with *Pseudomonas syringae* pv. *tomato* DC3000 (*Pst* DC3000) bacterial suspensions (OD_{600} = 0.0002 in 10 mM $MgCl_2$), and the bacterial load was quantified at 3 dpi. *Pst* DC3000 was cultured as previously described (Nomura et al., 2012). Images were captured at 3 dpi. Three biological replicates were scored with at least 12 plants per replicate.

2.5 Salt- and heat-stress treatment

Seeds of WT and T_2 homozygous BrOGsOE lines were surface-sterilized with bleach, washed 5 times with sterile water, and seeded on 1/2 MS medium containing 1/2 Murashige and Skoog Basal Medium with Vitamins (PhytoTech, KS, US) and 0.8% (w/v) agar. Control plates were incubated in the dark for 3 days at 4°C and then grown at 22°C under LD conditions. For salt treatment, seeds of the WT and BrOGsOE plants were cultured on 1/2 MS agar medium plates and grown at 4°C for 3 days with either 0 or 150 mM NaCl. Images were captured after 9 days of incubation at 22°C. For heat stress, the plates were kept at 4°C for 3 days, followed by incubation at 22°C for 30 h with a further incubation at 45°C for 2 h, recovered and allowed to grow at 22°C for 6 days before imaging. The survival rates after salt and heat stress were calculated from the number of seedlings with green, expanded cotyledons; three biological replicates were scored with 16 to 18 plants per replicate.

2.6 DNA and RNA isolation, cDNA synthesis, PCR, semi-quantitative RT-PCR and qRT-PCR

All DNA and RNA extractions, cDNA synthesis, PCR, RT-PCR, and qRT-PCR were performed as described previously (Jiang et al., 2018). The *AtACTIN2* (*AT3G18780*) gene was used as the housekeeping gene for semi-quantitative RT-PCR to verify the BrOGsOE transgenic lines (Lu et al., 2012). The *AtPP2AA3* (*At1G13320*) gene was used as the internal control for qRT-PCR analysis of *A. thaliana Pathogenesis-related gene 1* (*AtPR1*) after *Pst* DC3000 treatment (Huot et al., 2017). Gene expression was calculated using the $2^{-\Delta\Delta Ct}$ method (Livak and Schmittgen, 2001). The experiment was carried out in three biological sets. The sequences of all the forward and reverse primers are provided in Supplementary Table S1.

2.7 Statistical analysis

Data were analyzed with SPSS v19.0 software using Student's *t*-test or one-way ANOVA followed by individual comparisons with Duncan's multiple range test. GraphPad Prism v8.0.2 and TBtools-II v2.119 (Chen et al., 2023) software were used for illustrations.

3 Results

3.1 Phenotypic variations between Chinese cabbage and *A. thaliana*

Plants controlled by developmental genetic programming show species-specific features. Despite the close relationship between *A. thaliana* and Chinese cabbage, substantial variation is seen in different phenotypic characteristics, including leaf morphology, leaf size, and flowering phenotype. Heading Chinese cabbage possesses a leafy head characterized by very inwardly curled blades at the shoot apex, and the leafy head consists of multiple heading leaves that typically curve inwards after the rosette stage (Ren et al., 2018). The multiple leaves with serrated margins and downward or upward curves contrast sharply with the relatively fewer and flat leaves of *A. thaliana* (Figure 1). In the life cycles of flowering plants, the primary developmental transition is from vegetative to reproductive growth (Domagalska et al., 2007). Chinese cabbage is a late-flowering plant that requires several weeks of exposure to low temperatures (a process known as vernalization) to induce flowering, whereas *Arabidopsis* displays only a small vernalization response (Sheldon et al., 2000; Yuan et al., 2009).

Collectively, the study into the leaf morphology and flowering phenotype of Chinese cabbage holds considerable importance for breeding. However, within a short evolutionary timeframe, the phenotypes of Chinese cabbage and *Arabidopsis*, have diverged markedly, suggesting that *BrOGs*, as newly evolved genes, may play a significant role in phenotypic regulation. Due to the limited data available on *BrOGs* function, bioinformatics analysis is an effective means of acquiring more information. This led to the development of a transgenic library of *BrOGs*.

3.2 Construction of the *BrOGs* overexpression library and phenotypic observations

For a better understanding of *BrOGs* functions, a *BrOGs* overexpression library was constructed in *Arabidopsis*. One hundred and twenty-eight unknown functional Chinese cabbage *BrOGs* were successfully transformed into *Arabidopsis* by floral dip transformation with random selection, including 43 *BrOGs* that were successfully transformed in previous studies (Jiang et al., 2020) and have been summarized and analyzed in this article. These 128 *BrOGs* were identified in a previous study (Jiang et al., 2018). The expression of the *BrOGs* was regulated by the Cauliflower Mosaic Virus 35S (CaMV35S) promoter (Supplementary Figure S1). The addition of the *DsRed* gene regulated by the CaMV35S promoter

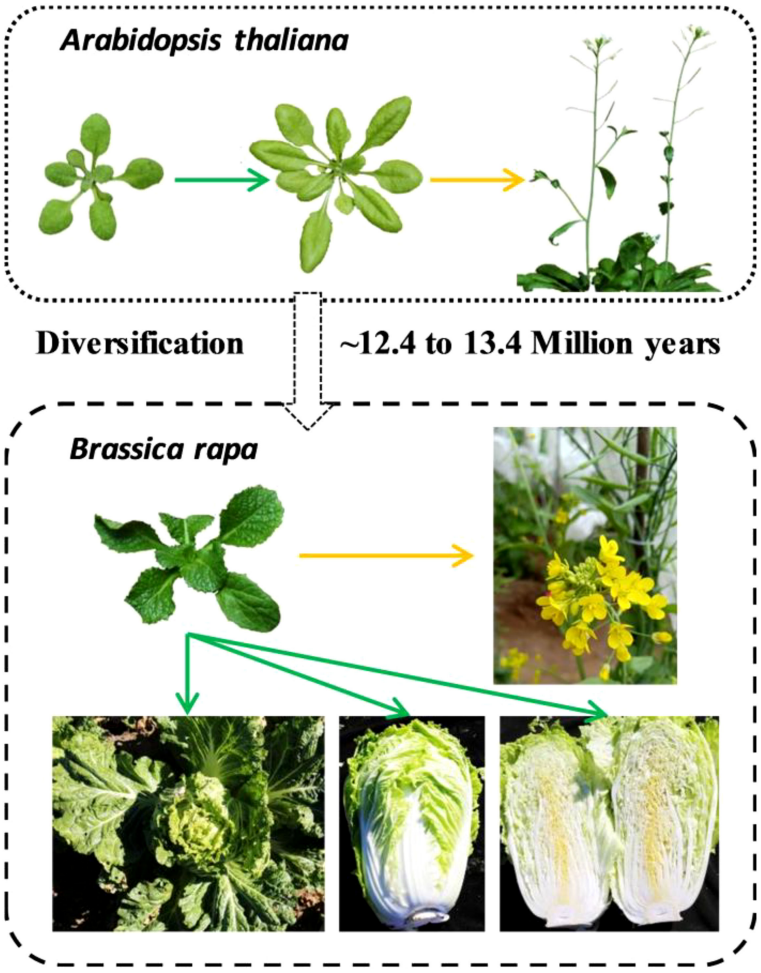

FIGURE 1
Comparison of evolutionary relationships and phenotypic differences between Chinese cabbage and *A. thaliana*. Chinese cabbage has wavy margins, serrated blades with uneven surfaces, and downward or upward-curved leaves, in contrast to the flat leaves of *A. thaliana*. Chinese cabbage requires several weeks of exposure to cold (vernalization) to induce flowering, whereas *Arabidopsis* displays only a small vernalization response. The green arrow represents vegetative growth, and the yellow arrow represents reproductive growth.

enhances the accessibility and efficiency of screening transgenic plants (Zhang et al., 2013). After the floral dip transformation, the T_2 homozygous seeds derived from various self-pollinated T_1 transgenic seed lines were identified *via* the *DsRed* gene. To further confirm the correctness of the BrOGsOE plants, 10 BrOGsOE plants and WT were randomly selected for verification at DNA and expression levels. Both genomic and CDS sequences were successfully amplified in the BrOGsOE lines (Supplementary Figure S2) and there were no target strips in the WT. Furthermore, target bands were sequenced, confirming the accuracy of the *BrOGs* sequences. The study then, considering the specific phenotypes of Chinese cabbage compared to *A. thaliana* (Figure 1), focused on the characteristics of leaf shape and flowering time.

Phenotypic changes in the BrOGsOE lines were investigated, focusing specifically on leaf morphology, flowering time, and other characteristics. The following traits were specifically analyzed during the vegetative and reproductive stages: flowering duration, stem height, rosette radius, leaf shape and color, silique length, and seed number. Stable homozygous T_2 transgenic plants were used for observation. A total of 93 BrOGsOE lines with phenotype variations were obtained, accounting for 72.66%, and no phenotypic variation was found in the remaining 35 BrOGsOE lines (27.34%) (Figure 2).

The delayed flowering phenotype was relatively common in the transgenic library, comprising approximately 49% of the samples. The early flowering phenotype was represented by 9% of the samples, and approximately 42% of the transgenic plants exhibited no discernible difference in flowering time (Figures 2, 3). The results of the investigation of representative extremely significant phenotypes of BrOGsOE lines are shown in Supplementary Table S2. Notably, 49% of the BrOGsOE lines showed a delayed flowering phenotype, with some lines showing various other phenotypes, including reduced or increased rosette radius, increased or decreased stem height, variations in leaf shape, decreased silique length, fewer seed numbers, and yellow leaf color. For example, BrOG72OE, BrOG76OE, and BrOG105OE all showed delayed flowering. The leaves of these transgenic plants were characterized by more uneven leaf surfaces and greater serration of the leaf edges relative to the WT. The BrOG126OE transgenic plants exhibited the delayed flowering phenotype accompanied by a reduced

10.3389/fpls.2025.1532449

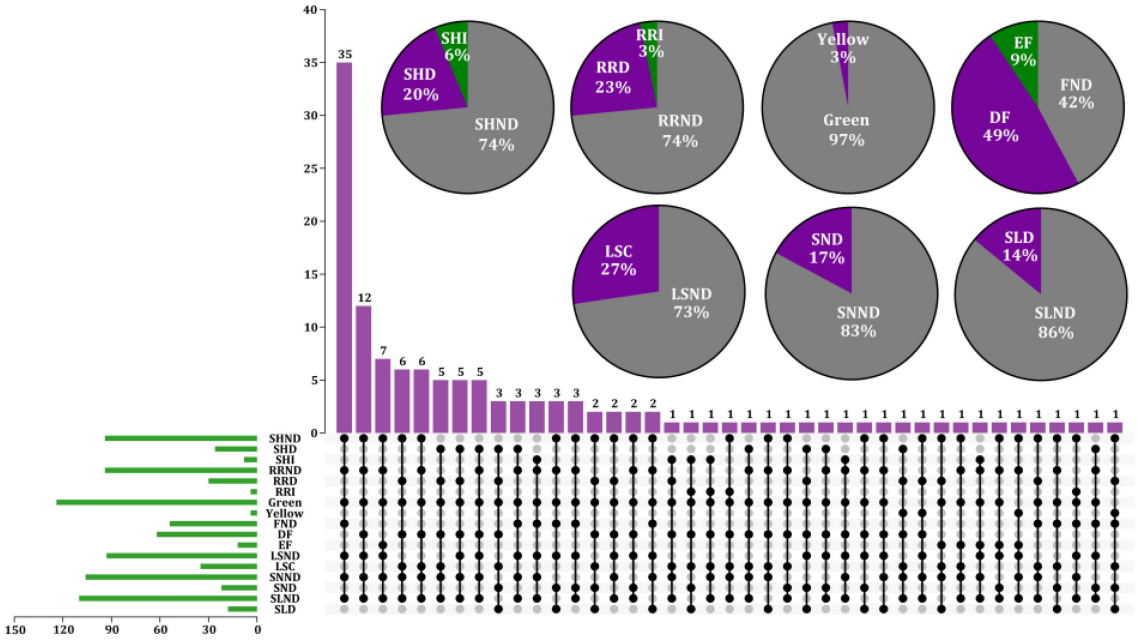

FIGURE 2
Characterization of different transgenic line types and phenotype analysis of 128 BrOGsOE lines. Different BSGsOE lines showed both unique and shared phenotypes. The purple column represents the summary of the various phenotypes of different transgenic plants. The gray solid circle indicates that the transgenic plant has no corresponding phenotype. The green column in the lower left corner depicts the total number of transgenic plants respective to phenotype. The pie charts in the upper right corner show the percentage of single phenotypes, including stem height, rosette radius, leaf color, flowering time, leaf shape, seed number, and silique length. SHND indicates stem height no difference when compared with WT; SHD and SHI indicate stem height decrease and increase, respectively; RRND indicates rosette radius no difference; RRD and RRI indicate rosette radius decrease and increase, respectively; Leaf color is represented by Green and Yellow; FND indicates no difference in flowering time; DF and EF indicate delayed and early flowering, respectively; LSND indicates leaf shape no difference; LSC indicates leaf shape change; SNND indicates seed number no difference; SND indicates seed number decrease; SLND indicates silique length no difference; SLD indicates silique length decrease.

rosette radius and a significant increase in rosette leaves. The percentage of the delayed flowering type was markedly higher than that of the early flowering type, and delayed flowering was accompanied by additional phenotypic features.

The phenotypes of the BrOG7OE transgenic plants included an upward-curled leaf and an increase in leaf hair (Figure 3A). BrOG78OE displayed a delayed flowering phenotype, lower rosette radius, and curled leaves (Figure 3B). BrOG88OE also showed a delayed flowering phenotype, together with reduced stem height, a shortened silique length, and fewer seeds per silique (Figure 3C). Moreover, 35 *Arabidopsis* lines were identified that showed visible changes in leaf shape, including BrOG13OE and BrOG37OE. This suggests a clear correlation between the leaf shape of these *Arabidopsis* lines and the specific leaf characteristics of Chinese cabbage.

3.3 Screening of pathogen stress-response BrOGsOE lines

Specific *OGs* have been found to be crucial for responses to biotic and abiotic stressors (Fakhar et al., 2023). In the current overexpression library, 27.34% of the BrOGsOE lines showed no phenotypic differences relative to WT (Figure 2). These 35 transgenic lines were hypothesized to respond to biotic or abiotic stressors. Thus, 24 of the 35 BrOGsOE lines with no significant phenotypic differences were selected for challenge with a pathogen (*Pst* DC3000). Most BrOGsOE lines showed disease symptoms similar to those of the WT at 3 days post-inoculation (dpi) after *Pst* DC3000 infection. However, BrOG36OE, BrOG49OE, and BrOG51OE developed disease symptoms that were either milder or less severe than those of the WT (Figures 4A–D). This suggests that the bacterial load in BrOGsOE lines was less than that in WT plants (Figure 4E). The transcription levels of the salicylic acid (SA) signaling pathway marker gene *AtPR1* were compared between WT and BrOGsOE plants at the time of *Pst* DC3000 infection, as SA-mediated response is essential for protecting *Arabidopsis* against *Pst* DC3000. Significantly higher levels of *AtPR1* transcripts were observed in infected BrOGsOE plants at 3 dpi compared to the infected WT plants (Figure 4F), seen in lower bacterial growth and fewer disease symptoms in the BrOGsOE lines. These findings indicated that immunity could be induced in *Arabidopsis* by *BrOGs*, which in turn enhanced the durability of the innate immune system through the maintenance of defense mechanisms.

3.4 Screening of salt stress-response BrOGsOE lines

Salt stress is an important abiotic stress that can markedly restrict the productivity of plants (Qin et al., 2017). To define the

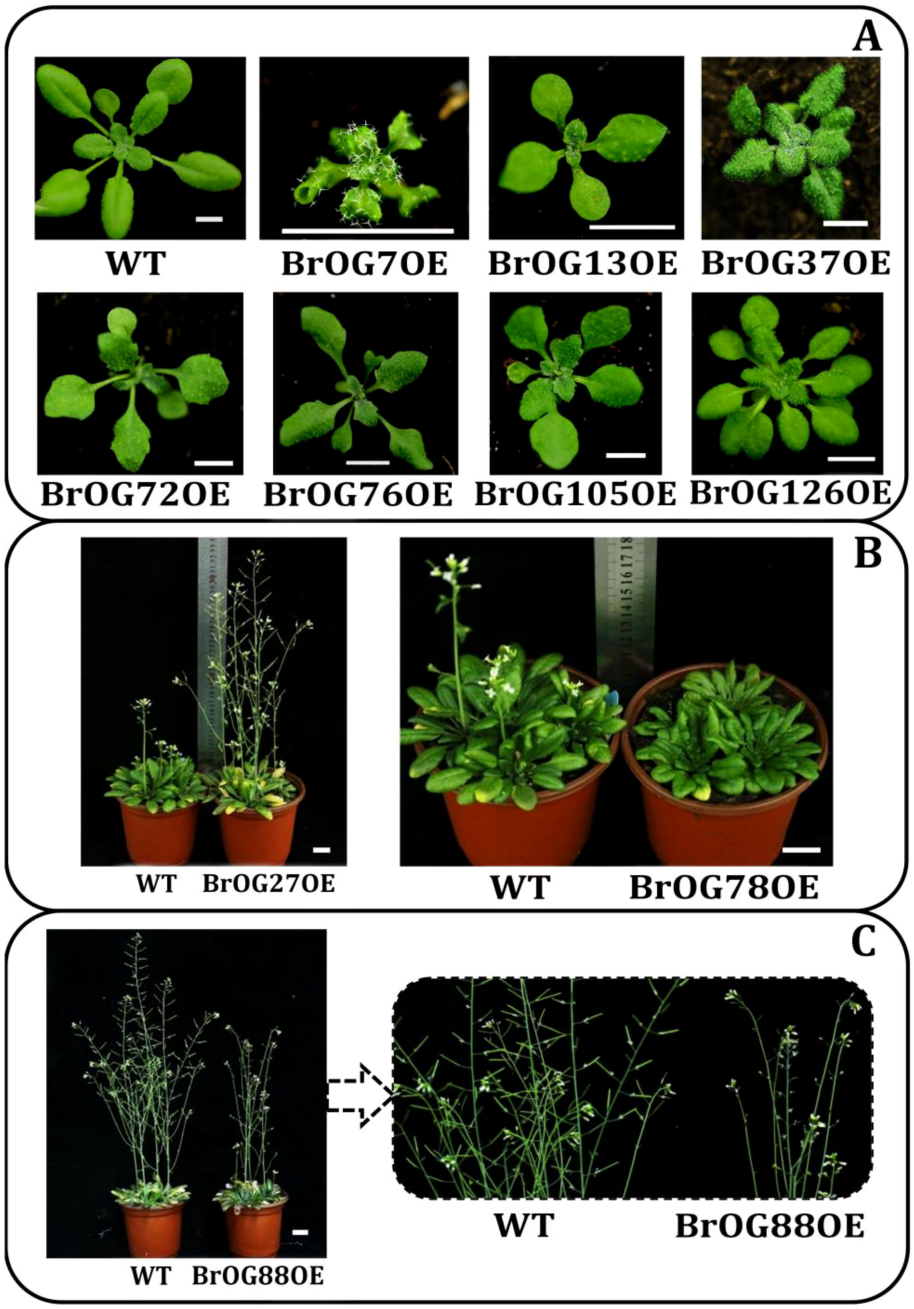

FIGURE 3
Visible transgenic lines appearing in phenotypes of *BrOGs* over-expression (OE) *Arabidopsis* lines. WT indicates *A. thaliana* Col-0. These phenotypes are represented in the T_2 generations. Representative individuals are shown at **(A)** 22 days (Bar = 0.5 cm), **(B)** 33 days, and **(C)** 45 days of growth (Bar = 2 cm).

functions of *BrOGs* in response to salt stress, WT and BrOGsOE seeds were cultivated on 1/2 MS medium plates containing 0 or 150 mM NaCl. It was observed that many seedlings appeared bleached and dead after growth on 1/2 MS medium with 150 mM NaCl, in contrast to 1/2 MS medium without NaCl. The survival rate of most BrOGsOE lines was similar (12 BrOGsOE lines) or more sensitive (5 BrOGsOE lines) to that of WT seedlings (Supplementary Figure S3). A total of 7 BrOGsOE lines displayed enhanced tolerance to salt stress when compared to WT, such as BrOG33OE, BrOG53OE, and BrOG116OE, which possessed the highest survival rates (Figure 5; Supplementary Figure S3). The current analysis clearly showed that *BrOGs* were positively or negatively involved in the salt stress response, indicating the vital roles of *BrOGs* in plant adaptation to salt stress.

3.5 Screening of heat stress-response BrOGsOE lines

Heat stress has a significant impact on agricultural crop productivity, and is especially relevant in current conditions of climate change (Weng et al., 2014). Transgenic lines and WT seeds

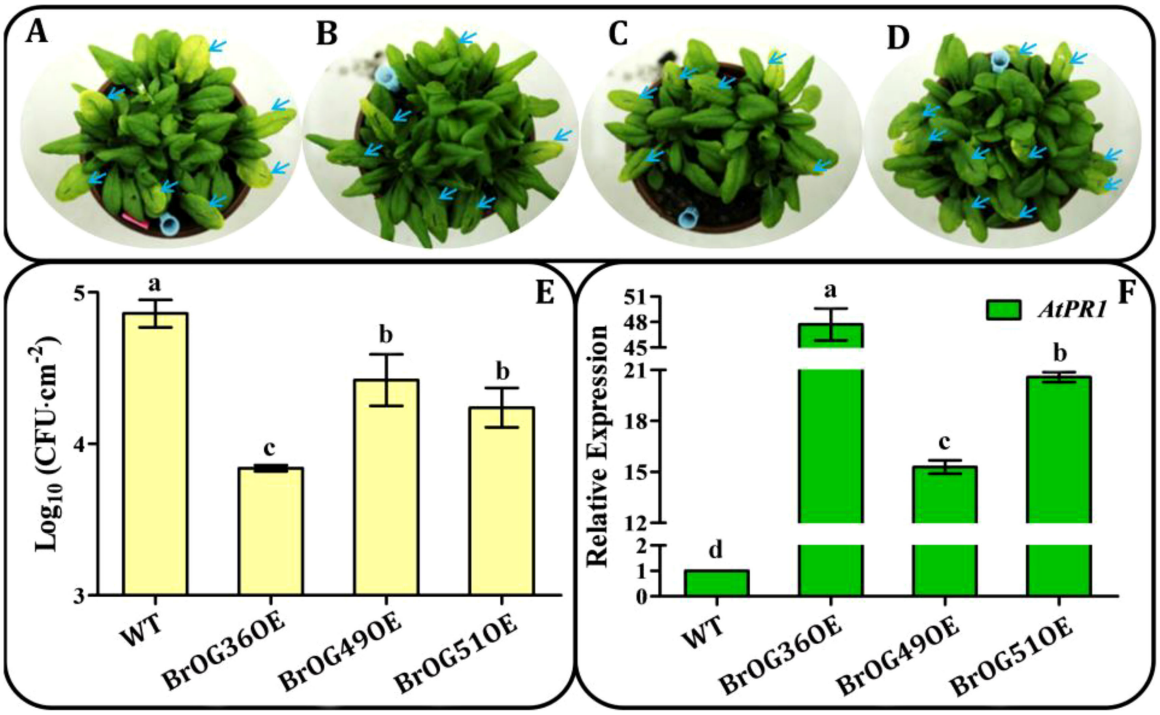

FIGURE 4
Growth of *P. syringae* pv. *tomato* (*Pst*) DC3000 on WT and BrOGsOE lines at 3 dpi. **(A-D)** WT, BrOG36OE, BrOG49OE, and BrOG51OE lines inoculated with *Pst* DC3000 (OD_{600} = 0.0002) at 3 dpi. **(E)** Bacterial growth in WT and BrOGsOE lines inoculated with *Pst* DC3000. Quantification of colony-forming units (CFUs) at 3 dpi. **(F)** *Pst* DC3000-induced *AtPR1* expression was analyzed at 3 dpi by qRT-PCR. *AtPP2AA3* gene was used as the internal reference. Different letters represent significant variances ($p < 0.05$) shown by one-way ANOVA with Duncan's multiple-range test. All data are shown as mean ± SE of three biological replicates.

were cultivated on plates at 4°C for 3 days followed by 22°C for 30 h. The seeds were then heated for 2 h at 45°C and kept at 22°C for 7 days. No significant differences in the heat stress-response were observed between the 11 BrOGsOE lines and the WT (Supplementary Figure S4). Importantly, the survival rates of the remaining 13 BrOGsOE lines were all markedly decreased under heat stress treatment (Figure 6; Supplementary Figure S4). The BrOG30OE, BrOG33OE, and BrOG127OE lines were the most sensitive to heat stress (Figure 6). These findings suggested that these transgenic lines reduced their basal heat stress tolerance.

4 Discussion

The application of genetically modified plants, especially transgenic lines, is considered an ideal way to explore gene

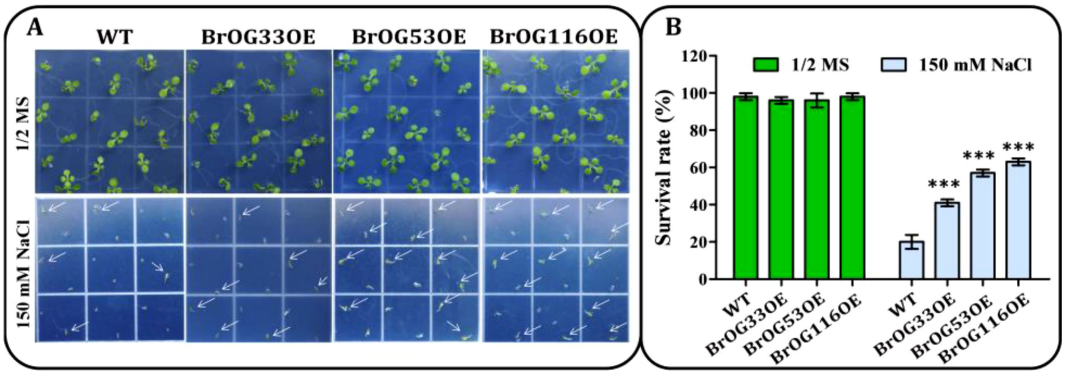

FIGURE 5
Salt stress resistant BrOGsOE lines. **(A)** Phenotypes associated with salt stress. Seeds of the WT and BrOGsOE lines were cultivated on 1/2 MS agar medium enriched with 0 or 150 mM NaCl, then placed at 4°C for 3 d Images were captured at 9 d after incubation at 22°C. **(B)** Survival rates. Asterisk (***) indicate a significant difference ($p < 0.001$) from the WT, shown by Student's *t*-test. All data are shown as mean ± SE of three biological replicates; at least 16 seedlings were scored for each replicate/genotype.

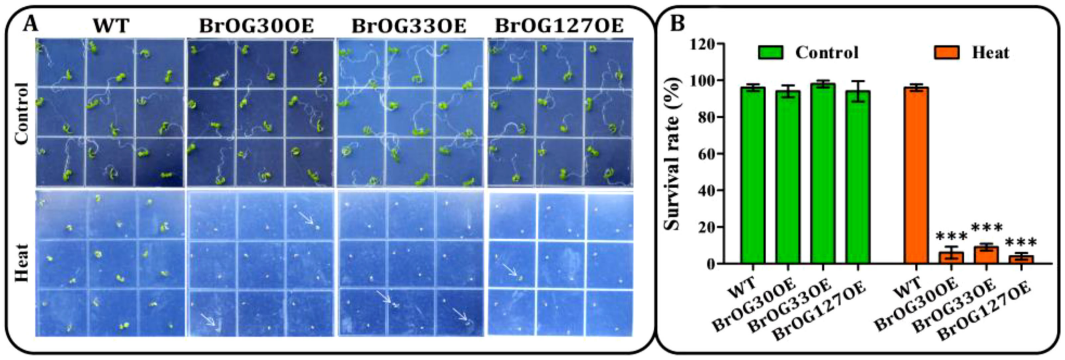

FIGURE 6
BrOGsOE lines sensitive to basal heat stress. **(A)** Heat stress phenotypes. Seedlings were incubated for 3 days at 4°C followed by 22°C for 30 h, then heated at 45°C for 2 h and recovered and allowed to grow at 22°C for 6 d before imaging. Untreated plants cultured at 22°C were depicted as controls. **(B)** Survival rates. Asterisk (***) indicate significant difference ($p < 0.001$) from the WT by Student's *t*-test. All data are shown as mean ± SE of three biological replicates; at least 16 seedlings were scored for each replicate/genotype.

function. Recent developments in biotechnology have significantly reduced the generation times of these plants. The present study established an overexpression library for *Arabidopsis* using 128 *BrOGs* from Chinese cabbage. This led to the successful generation of visible transgenic lines through the overexpression of *BrOGs* in *Arabidopsis*. These genes show no sequence similarities with *Arabidopsis* genes, thus providing a solid basis for assessing the function of *BrOGs* (Jiang et al., 2018). Similarly, previous study assembled a cotton-FOX-*Arabidopsis* library that contained 6,830 transgenic lines of *Arabidopsis* resources enabling the identification of gene functions in cotton (Li et al., 2020). Moreover, approximately 6,000 transgenic *Arabidopsis* lines were generated using the iFOX-Hunting system, revealing a substantial percentage of lines with complete *B. napus* transgene insertions and facilitating basic insights into the high-throughput analysis of gene functions in *B. napus* (Ling et al., 2018). Thus, the *Arabidopsis BrOGs* overexpression library not only served as a platform for exploring the unknown functions of *BrOGs* but also provided the plant materials needed to examine the mechanism of action of such genes.

In terms of the phenotypic variation between Chinese cabbage and *A. thaliana*, this study focused primarily on two traits, namely, leaf shape and flowering time. According to the results, 72.66% of the transgenic lines in the T_2 generation showed marked phenotypic differences (Figure 2). To further confirm the phenotypic variations caused by transgene expression, the *BrOGs* in BrOGsOE lines were evaluated at the DNA and expression levels. Variations in leaf morphology, including wavy leaves, serrated margins, hairy leaves, upward or downward-curved leaves, and multiple leaves, demonstrated a clear relevance between these *Arabidopsis* transgenic lines and Chinese cabbage-specific leaf traits. This suggests that *BrOGs* could be associated with the specific leaf characteristics of Chinese cabbage. Moreover, 49% of the transgenic lines showed delayed flowering, with several of the BrOGsOE lines sharing this trait with other types. A recent study demonstrated that the overexpression of *BrOG37* (*BOLTING RESISTANCE 2*, *BR2*) delayed flowering in Chinese cabbage, and further investigation showed that *BR2* positively regulates bolting resistance *via* the vernalization pathway (Zu et al., 2024). These results, therefore, support the hypothesis that *OGs* may have similar functions in different plant species. Flowering time regulation could be influenced by various signaling pathways, and the phenomenon of delayed flowering time could lead to additional phenotype variations that have been reported in many *Arabidopsis* lines (Griffiths et al., 2006; Domagalska et al., 2007). Furthermore, Chinese cabbage usually requires vernalization and photoperiodism to promote flowering and bolting (Elers and Wiebe, 1984). This study predicted that *BrOGs* associated with delayed flowering may negatively regulate flowering in Chinese cabbage, making it resistant to bolting, and thus contributing significantly to the understanding of the mechanism controlling flowering control in preventing Chinese cabbage from flowering prematurely. The results indicated that *BrOGs* are effective genetic resources for elucidating the complex genetic mechanisms underlying variations in morphological characteristics, such as leaves and flowering time, in Chinese cabbage. Moreover, such *BrOGs* may also act as critical factors in the evolution of specific traits in Chinese cabbage. The mechanisms underlying delayed or early flowering, changes in leaf shape, and increased leaf numbers warrant further research.

Orphan genes have been found to possess crucial roles in biotic interactions and environmental responses in various plants (Jiang et al., 2022). *Pst* DC3000 infects hundreds of taxonomically diverse plant species, and the potential to cause disease in *A. thaliana* rendered it a suitable model for investigating plant-pathogen interactions (Thilmony et al., 2006; Nomura et al., 2012). In this study, 3 of 24 transgenic lines were resistant to *Pst* DC3000 infection and showed higher expression of *AtPR1* and fewer bacteria compared with the WT plants. Similarly, the Brassicaceae-specific gene, *Enhancer of Vascular Wilt Resistance 1* (*EWR1*), has been shown to provide resistance against vascular wilt pathogens (Yadeta et al., 2014). Moreover, *Triticum aestivum Fusarium Resistance Orphan Gene* (*TaFROG*) provides resistance against the mycotoxigenic fungus *Fusarium graminearum* (Perochon et al., 2015). The rice tribe-specific gene *Oryza sativa defense-responsive gene 10* (*OsDR10*) acts as a negative regulator in resistance to bacterial blight disease (Xiao et al., 2009), and the

Arabidopsis OG QQS is down-regulated in response to *Pst* DC3000 infection (Arendsee et al., 2014). These results indicated that *BrOGs* have been recruited to regulate responses to biotic stresses. Future research should explore further specificity of resistance mechanisms and functions of *BrOGs* against various pathogens, such as *Plasmodiophora brassicae*, which may provide a source to identify novel resistance-associated genes in crops.

Several factors, such as soil salinity and high temperature, negatively impact crop productivity (Weng et al., 2014; Qin et al., 2017). Among the *BrOGs* overexpression lines, 50% were insensitive to salt stress, 20.83% showed sensitive phenotypes, and 29.17% revealed increased tolerance. Similarly, a recent study reported that approximately 70% of *A. thaliana* knockout mutants corresponded to genes of unknown function associated with unaltered phenotypes under salt stress. In comparison, 6.65% showed tolerance, and 16.52% showed sensitivity to salt stress (Luhua et al., 2013). Cross-stress analysis of stress-response mutants further indicated that some *BrOGs* display specific functions under certain stress conditions. For example, the BrOG36OE lines were resistant to *Pst* DC3000 infection, while the BrOG6OE lines were tolerant to salt stress, suggesting that these *BrOGs* may be involved in specific signal transduction pathways or networks associated with specific stress responses. These findings are consistent with those of a previous study showing that genes of unknown function are species-specific and give rise to different cellular networks (Luhua et al., 2008). Several transgenic lines (BrOG33OE, BrOG53OE, and BrOG116OE) were tolerant to salt stress but sensitive to both *Pst* DC3000 infection and heat stress. Similar reports have shown that transgenic *Arabidopsis* expresses unknown functional proteins that enhance tolerance to oxidative stress without increased tolerance to osmotic, salinity, heat, or cold stresses (Luhua et al., 2008). Interestingly, the transgenic lines (BrOG49OE and BrOG51OE) that displayed tolerance to *Pst* DC3000 were also tolerant to salt stress. Furthermore, transgenic lines (BrOG25OE, BrOG30OE, and BrOG59OE) that showed sensitivity to *Pst* DC3000 infection were also observed to be sensitive to salt and heat stress, suggesting that these genes may play crucial roles in various stress responses. Previous findings showed the genes of unknown function in *Arabidopsis* could have generalized functions against stress by the activation of multiple acclimation mechanisms (Luhua et al., 2013). *BrOGs* can thus play both general and specific roles in response to pathogen invasion and environmental perturbations, and further research on *BrOGs*' functions can provide new insights into mechanisms underlying plant responses to biotic and abiotic stressors.

5 Conclusions

In this study, a *BrOGs* overexpression library was constructed and comprehensively evaluated in *A. thaliana*. Significant relationships were observed between the phenotypes of these BrOGsOE lines and the specific traits of Chinese cabbage. The proportion of the delayed flowering type was much higher than that of the early flowering type, and additional phenotypes frequently accompanied delayed flowering. Various *BrOGs* have both general and specific functions against environmental and pathogenic stresses. These findings reveal the roles of *BrOGs* in the formation of species-specific traits and responses to stress, providing an important reference for the subsequent analysis of the mechanism of action of *BrOGs*.

Data availability statement

The original contributions presented in the study are included in the article/Supplementary Material. Further inquiries can be directed to the corresponding authors.

Author contributions

MJ: Data curation, Formal analysis, Funding acquisition, Investigation, Resources, Visualization, Writing – original draft, Writing – review & editing. ZZ: Data curation, Methodology, Project administration, Resources, Writing – review & editing. XL: Formal analysis, Funding acquisition, Methodology, Supervision, Validation, Writing – review & editing. ZP: Formal analysis, Resources, Supervision, Visualization, Writing – review & editing.

Funding

The author(s) declare financial support was received for the research, authorship, and/or publication of this article. This work was supported by the National Natural Science Foundation of China (Grant No. 32302568), the China Agriculture Research System of MOF and MARA (Grant No. CARS-12), and the National Natural Science Foundation of China (Grant No. 32272715).

Conflict of interest

The authors declare that the research was conducted in the absence of any commercial or financial relationships that could be construed as a potential conflict of interest.

Generative AI statement

The author(s) declare that no Generative AI was used in the creation of this manuscript.

Publisher's note

Supplementary material

The Supplementary Material for this article can be found online at: https://www.frontiersin.org/articles/10.3389/fpls.2025.1532449/full#supplementary-material

SUPPLEMENTARY FIGURE 1
Schematic diagram of CaMV35S::DsRed expression vector. LB indicates left border, RB indicates right border, and MCS represents multiple cloning sites.

SUPPLEMENTARY FIGURE 2
Confirmation of *BrOGs* gene expression in BrOGsOE lines. **(A)** PCR analysis of the *BrOGs* in WT and BrOGsOE plants at the DNA level. **(B)** Analysis of *BrOGs* expression by semi-quantitative RT-PCR in BrOGsOE lines. GSPs indicated *BrOGs* gene-specific primers, and *AtActin2* represented the *Arabidopsis ACTIN2* gene primers.

SUPPLEMENTARY FIGURE 3
The survival rates of WT plants and BrOGsOE lines in response to salt stress. Significant differences (***$p < 0.001$; **$p < 0.01$; *$p < 0.05$) relative to the WT by Student's *t*-test. All data are shown as mean ± SE of three biological replicates; at least 16 seedlings were scored for each replicate/genotype.

SUPPLEMENTARY FIGURE 4
The survival rates of WT plants and BrOGsOE lines in response to basal heat stress. Significant differences (***$p < 0.001$; **$p < 0.01$; *$p < 0.05$) relative to the WT by Student's *t*-test. All data are shown as mean ± SE of three biological replicates; at least 16 seedlings were scored for each replicate/genotype.

References

Arendsee, Z. W., Li, L., and Wurtele, E. S. (2014). Coming of age: orphan genes in plants. *Trends Plant Sci.* 19, 698–708. doi: 10.1016/j.tplants.2014.07.003

Chen, C., Wu, Y., Li, J., Wang, X., Zeng, Z., Xu, J., et al. (2023). TBtools-II: A "one for all, all for one" bioinformatics platform for biological big-data mining. *Mol. Plant* 16, 1733–1742. doi: 10.1016/j.molp.2023.09.010

Domagalska, M. A., Schomburg, F. M., Amasino, R. M., Vierstra, R. D., Nagy, F., and Davis, S. J. (2007). Attenuation of brassinosteroid signaling enhances *FLC* expression and delays flowering. *Development* 134, 2841–2850. doi: 10.1242/dev.02866

Dong, X.-M., Pu, X.-J., Zhou, S.-Z., Li, P., Luo, T., Chen, Z.-X., et al. (2022). Orphan gene *PpARDT* positively involved in drought tolerance potentially by enhancing ABA response in *Physcomitrium* (*Physcomitrella*) *patens*. *Plant Sci.* 319, 111222. doi: 10.1016/j.plantsci.2022.111222

Elers, B., and Wiebe, H. J. (1984). Flower formation of Chinese cabbage. I. Response to vernalization and photoperiods. *Sci. Hortic.* 22, 219–231. doi: 10.1016/0304-4238(84)90055-4

Fakhar, A. Z., Liu, J., Pajerowska-Mukhtar, K. M., and Mukhtar, M. S. (2023). The ORFans' tale: new insights in plant biology. *Trends Plant Sci.* 28, 1379–1390. doi: 10.1016/j.tplants.2023.06.011

Feyissa, B. A., de Becker, E. M., Salesse-Smith, C. E., Zhang, J., Yates, T. B., Xie, M., et al. (2024). An orphan gene *BOOSTER* enhances photosynthetic efficiency and plant productivity. *Dev. Cell.* doi: 10.1016/j.devcel.2024.11.002

Griffiths, J., Murase, K., Rieu, I., Zentella, R., Zhang, Z. L., Powers, S. J., et al. (2006). Genetic characterization and functional analysis of the GID1 gibberellin receptors in *Arabidopsis*. *Plant Cell* 18, 3399–3414. doi: 10.1105/tpc.106.047415

Huot, B., Castroverde, C. D. M., Velasquez, A. C., Hubbard, E., Pulman, J. A., Yao, J., et al. (2017). Dual impact of elevated temperature on plant defence and bacterial virulence in *Arabidopsis*. *Nat. Commun.* 8, 1808. doi: 10.1038/s41467-017-01674-2

Jiang, M., Dong, X., Lang, H., Pang, W., Zhan, Z., Li, X., et al. (2018). Mining of *Brassica*-specific genes (*BSGs*) and their induction in different developmental stages and under *Plasmodiophora brassicae* stress in *Brassica rapa*. *Int. J. Mol. Sci.* 19, 2064. doi: 10.3390/ijms19072064

Jiang, M., Li, X., Dong, X., Zu, Y., Zhan, Z., Piao, Z., et al. (2022). Research advances and prospects of orphan genes in plants. *Front. Plant Sci.* 13. doi: 10.3389/fpls.2022.947129

Jiang, M., Zhan, Z., Li, H., Dong, X., Cheng, F., and Piao, Z. (2020). *Brassica rapa* orphan genes largely affect soluble sugar metabolism. *Hortic. Res.* 7, 181. doi: 10.1038/s41438-020-00403-z

Jiang, M., Zhang, Y., Yang, X., Li, X., and Lang, H. (2023). *Brassica rapa* orphan gene *BR1* delays flowering time in *Arabidopsis*. *Front. Plant Sci.* 14. doi: 10.3389/fpls.2023.1135684

Kimmel, J., Schmitt, M., Sinner, A., Jansen, P., Mainye, S., Ramón-Zamorano, G., et al. (2023). Gene-by-gene screen of the unknown proteins encoded on *Plasmodium falciparum* chromosome 3. *Cell Syst.* 14, 9–23.e27. doi: 10.1016/j.cels.2022.12.001

Li, S., Chen, H., Hou, Z., Li, Y., Yang, C., Wang, D., et al. (2020). Screening of abiotic stress-responsive cotton genes using a cotton full-length cDNA overexpressing *Arabidopsis* library. *J. Integr. Plant Biol.* 62, 998–1016. doi: 10.1111/jipb.12861

Li, J., Singh, U., Bhandary, P., Campbell, J., Arendsee, Z., Seetharam, A. S., et al. (2022). Foster thy young: enhanced prediction of orphan genes in assembled genomes. *Nucleic Acids Res.* 50, e37. doi: 10.1093/nar/gkab1238

Li, L., and Wurtele, E. S. (2015). The *QQS* orphan gene of *Arabidopsis* modulates carbon and nitrogen allocation in soybean. *Plant Biotechnol. J.* 13, 177–187. doi: 10.1111/pbi.12238

Li, L., Zheng, W., Zhu, Y., Ye, H., Tang, B., Arendsee, Z. W., et al. (2015). *QQS* orphan gene regulates carbon and nitrogen partitioning across species via NF-YC interactions. *Proc. Natl. Acad. Sci. U. S. A.* 112, 14734–14739. doi: 10.1073/pnas.1514670112

Lin, W.-L., Cai, B., and Cheng, Z.-M. (2013). Identification and characterization of lineage-specific genes in *Populus trichocarpa*. *Plant Cell Tiss. Organ Cult.* 116, 217–225. doi: 10.1007/s11240-013-0397-9

Lin, H., Moghe, G., Ouyang, S., Iezzoni, A., Shiu, S. H., Gu, X., et al. (2010). Comparative analyses reveal distinct sets of lineage-specific genes within *Arabidopsis thaliana*. *BMC Evol. Biol.* 10, 41. doi: 10.1186/1471-2148-10-41

Ling, J., Li, R., Nwafor, C. C., Cheng, J., Li, M., Xu, Q., et al. (2018). Development of iFOX-hunting as a functional genomic tool and demonstration of its use to identify early senescence-related genes in the polyploid *Brassica napus*. *Plant Biotechnol. J.* 16, 591–602. doi: 10.1111/pbi.12799

Liu, S., Liu, Y., Yang, X., Tong, C., Edwards, D., Parkin, I. A. P., et al. (2014). The *Brassica oleracea* genome reveals the asymmetrical evolution of polyploid genomes. *Nat. Commun.* 5, 3930. doi: 10.1038/ncomms4930

Liu, J., Yuan, R., Shao, W., Wang, J., Silman, I., and Sussman, J. L. (2023). Do "Newly Born" orphan proteins resemble "Never Born" proteins? A study using three deep learning algorithms. *Proteins* 91, 1097–1115. doi: 10.1002/prot.26496

Livak, K. J., and Schmittgen, T. D. (2001). Analysis of relative gene expression data using real-time quantitative PCR and the $2^{-\Delta\Delta CT}$ method. *Methods* 25, 402–408. doi: 10.1006/meth.2001.1262

Lu, S. X., Webb, C. J., Knowles, S. M., Kim, S. H., Wang, Z., and Tobin, E. M. (2012). *CCA1* and *ELF3* Interact in the control of hypocotyl length and flowering time in *Arabidopsis*. *Plant Physiol.* 158, 1079–1088. doi: 10.1104/pp.111.189670

Luhua, S., Ciftci-Yilmaz, S., Harper, J., Cushman, J., and Mittler, R. (2008). Enhanced tolerance to oxidative stress in transgenic Arabidopsis plants expressing proteins of unknown function. *Plant Physiol.* 148, 280–292. doi: 10.1104/pp.108.124875

Luhua, S., Hegie, A., Suzuki, N., Shulaev, E., Luo, X., Cenariu, D., et al. (2013). Linking genes of unknown function with abiotic stress responses by high-throughput phenotype screening. *Physiol. Plant* 148, 322–333. doi: 10.1111/ppl.12013

Luo, L., Zheng, Y., Li, X., Chen, Q., Yang, D., Gu, Z., et al. (2024). ICE1 interacts with IDD14 to transcriptionally activate *QQS* to increase pollen germination and viability. *J. Integr. Plant Biol.* 66, 1801–1819. doi: 10.1111/jipb.13725

Moreyra, N. N., Almeida, F. C., Allan, C., Frankel, N., Matzkin, L. M., and Hasson, E. (2023). Phylogenomics provides insights into the evolution of cactophily and host plant shifts in *Drosophila*. *Mol. Phylogenet. Evol.* 178, 107653. doi: 10.1016/j.ympev.2022.107653

Nomura, H., Komori, T., Uemura, S., Kanda, Y., Shimotani, K., Nakai, K., et al. (2012). Chloroplast-mediated activation of plant immune signalling in *Arabidopsis*. *Nat. Commun.* 3, 926. doi: 10.1038/ncomms1926

Perochon, A., Jianguang, J., Kahla, A., Arunachalam, C., Scofield, S. R., Bowden, S., et al. (2015). *TaFROG* encodes a Pooideae orphan protein that interacts with snrk1 and enhances resistance to the mycotoxigenic fungus *Fusarium graminearum*. *Plant Physiol.* 169, 2895–2906. doi: 10.1104/pp.15.01056

Qin, T., Zhao, H., Cui, P., Albesher, N., and Xiong, L. (2017). A nucleus-localized long non-coding rna enhances drought and salt stress tolerance. *Plant Physiol.* 175, 1321–1336. doi: 10.1104/pp.17.00574

Ren, W., Wang, H., Bai, J., Wu, F., and He, Y. (2018). Association of microRNAs with types of leaf curvature in *Brassica rapa*. *Front. Plant Sci.* 9. doi: 10.3389/fpls.2018.00073

Sheldon, C. C., Rouse, Dt., Finnegan, E. J., Peacock, W. J., and Dennis, E. S. (2000). The molecular basis of vernalization: the central role of *FLOWERING LOCUS C* (*FLC*). *Proc. Natl. Acad. Sci. U. S. A.* 97, 3753–3758. doi: 10.1073/pnas.97.7.3753

Song, X., Li, Y., Liu, T., Duan, W., Huang, Z., Wang, L., et al. (2014). Genes associated with agronomic traits in non-heading Chinese cabbage identified by expression profiling. *BMC Plant Biol.* 14, 71. doi: 10.1186/1471-2229-14-71

Sun, N., Liu, M., Zhang, W., Yang, W., Bei, X., Ma, H., et al. (2015). Bean metal-responsive element-binding transcription factor confers cadmium resistance in tobacco. *Plant Physiol.* 167, 1136–1148. doi: 10.1104/pp.114.253096

Thilmony, R., Underwood, W., and He, S. Y. (2006). Genome-wide transcriptional analysis of the *Arabidopsis thaliana* interaction with the plant pathogen *Pseudomonas syringae* pv. tomato DC3000 and the human pathogen *Escherichia coli* O157:H7. *Plant J.* 46, 34–53. doi: 10.1111/j.1365-313X.2006.02725.x

Waminal, N. E., Perumal, S., Lee, J., Kim, H. H., and Yang, T.-J. (2016). Repeat evolution in *Brassica rapa* (AA), *B. oleracea* (CC), and *B. napus* (AACC) genomes. *Plant Breed. Biotech.* 4, 107–122. doi: 10.9787/pbb.2016.4.2.107

Wang, L., O'Conner, S., Tanvir, R., Zheng, W., Cothron, S., Towery, K., et al. (2024). CRISPR/Cas9-based editing of NF-YC4 promoters yields high-protein rice and soybean. *New Phytol*. doi: 10.1111/nph.20141

Weng, M., Yang, Y., Feng, H., Pan, Z., Shen, W. H., Zhu, Y., et al. (2014). Histone chaperone *ASF1* is involved in gene transcription activation in response to heat stress in *Arabidopsis thaliana*. *Plant Cell Environ.* 37, 2128–2138. doi: 10.1111/pce.12299

Xiao, W., Liu, H., Li, Y., Li, X., Xu, C., Long, M., et al. (2009). A rice gene of *de novo* origin negatively regulates pathogen-induced defense response. *PloS One* 4, e4603. doi: 10.1371/journal.pone.0004603

Xu, Y., Wu, G., Hao, B., Chen, L., Deng, X., and Xu, Q. (2015). Identification, characterization and expression analysis of lineage-specific genes within sweet orange (*Citrus sinensis*). *BMC Genomics* 16, 995. doi: 10.1186/s12864-015-2211-z

Yadeta, K. A., Valkenburg, D.-J., Hanemian, M., Marco, Y., and Thomma, B. P. H. J. (2014). The Brassicaceae-specific *EWR1* gene provides resistance to vascular wilt pathogens. *PloS One* 9, e88230. doi: 10.1371/journal.pone.0088230

Yang, T.-J., Kim, J. S., Kwon, S.-J., Lim, K.-B., Choi, B.-S., Kim, J.-A., et al. (2006). Sequence-level analysis of the diploidization process in the triplicated *FLOWERING LOCUS C* region of *Brassica rapa*. *Plant Cell* 18, 1339–1347. doi: 10.1105/tpc.105.040535

Yu, Y., Li, W., Liu, Y., Liu, Y., Zhang, Q., Ouyang, Y., et al. (2024). A *Zea* genus-specific micropeptide controls kernel dehydration in maize. *Cell* 188, 1–16. doi: 10.1016/j.cell.2024.10.030

Yuan, Y. X., Wu, J., Sun, R. F., Zhang, X. W., Xu, D. H., Bonnema, G., et al. (2009). A naturally occurring splicing site mutation in the *Brassica rapa FLC1* gene is associated with variation in flowering time. *J. Exp. Bot.* 60, 1299–1308. doi: 10.1093/jxb/erp010

Zhang, C., Iskandarov, U., Klotz, E. T., Stevens, R. L., Cahoon, R. E., Nazarenus, T. J., et al. (2013). A thraustochytrid diacylglycerol acyltransferase 2 with broad substrate specificity strongly increases oleic acid content in engineered *Arabidopsis thaliana* seeds. *J. Exp. Bot.* 64, 3189–3200. doi: 10.1093/jxb/ert156

Zu, Y., Jiang, M., Zhan, Z., Li, X., and Piao, Z. (2024). Orphan gene *BR2* positively regulates bolting resistance through the vernalization pathway in Chinese cabbage. *Hortic. Res.* 11, uhae216. doi: 10.1093/hr/uhae216

frontiers | Frontiers in Plant Science

TYPE Original Research
PUBLISHED 09 May 2025
DOI 10.3389/fpls.2025.1507338

OPEN ACCESS

EDITED BY
Yoonkang Hur,
Chungnam National University,
Republic of Korea

REVIEWED BY
Kaushal Pratap Singh,
Directorate of Rapeseed Mustard Research (DRMR), India
Shrushti Joshi,
Savitribai Phule Pune University, India

*CORRESPONDENCE
Fady Mohareb
f.mohareb@cranfield.ac.uk

RECEIVED 07 October 2024
ACCEPTED 01 April 2025
PUBLISHED 09 May 2025

CITATION
Kourani M, Anastasiadi M, Hammond JP and Mohareb F (2025) Prolonged heat stress in *Brassica napus* during flowering negatively impacts yield and alters glucosinolate and sugars metabolism. *Front. Plant Sci.* 16:1507338. doi: 10.3389/fpls.2025.1507338

Prolonged heat stress in *Brassica napus* during flowering negatively impacts yield and alters glucosinolate and sugars metabolism

Mariam Kourani[1], Maria Anastasiadi[1], John P. Hammond[2] and Fady Mohareb[1*]

[1]The Bioinformatics Group, Centre for Soil, Agrifood and Biosciences (SABS), Cranfield University, Cranfield, United Kingdom, [2]School of Agriculture, Policy and Development, University of Reading, Reading, United Kingdom

Oilseed rape (*Brassica napus*), one of the most important sources of vegetable oil worldwide, is adversely impacted by heatwave-induced temperature stress especially during its yield-determining reproductive stages. However, the underlying molecular and biochemical mechanisms are still poorly understood. In this study, we investigated the transcriptomic and metabolomic responses to heat stress in *B. napus* plants exposed to a gradual increase in temperature reaching 30°C in the day and 24°C at night for a period of 6 days. High-performance liquid chromatography (HPLC) and liquid chromatography–mass spectrometry (LC-MS) was used to quantify the content of carbohydrates and glucosinolates, respectively. Results showed that heat stress reduced yield and altered oil composition. Heat stress also increased the content of carbohydrate (glucose, fructose, and sucrose) and aliphatic glucosinolates (gluconapin and progoitrin) in the leaves but decreased the content of the indolic glucosinolate (glucobrassicin). RNA-Seq analysis of flower buds showed a total of 1,892, 3,253, and 4,553 differentially expressed genes at 0, 1, and 2 days after treatment (DAT) and 4,165 and 1,713 at 1 and 7 days of recovery (DOR), respectively. Heat treatment resulted in downregulation of genes involved in respiratory metabolism, namely, glycolysis, pentose phosphate pathway, citrate cycle, and oxidative phosphorylation especially after 48 h of heat stress. Other downregulated genes mapped to sugar transporters, nitrogen transport and storage, cell wall modification, and methylation. In contrast, upregulated genes mapped to small heat shock proteins (sHSP20) and other heat shock factors that play important roles in thermotolerance. Furthermore, two genes were chosen from the pathways involved in the heat stress response to further examine their expression using real-time RT-qPCR. The global transcriptome profiling, integrated with the metabolic analysis in the study, shed the light on key genes and metabolic pathways impacted and responded to abiotic stresses exhibited as a result of exposure to heat waves during flowering. DEGs and metabolites

identified through this study could serve as important biomarkers for breeding programs to select cultivars with stronger resistance to heat. In particular, these biomarkers can form targets for various crop breeding and improvement techniques such as marker-assisted selection.

KEYWORDS

***Brassica napus*, oilseed rape, heat stress, RNA-seq, HPLC, LC-MS, simple sugars, glucosinolates**

1 Introduction

Over the last decade, climate change has led to more extreme climatic events, impacting crop productivity and threatening global food security (Ismaili et al., 2015; Lamaoui et al., 2018). These extreme events include periods of high temperature stress in the form of heatwaves (Goel et al., 2023), broadly defined as periods of excessively high temperature as compared to the local climate (Dikšaitytė et al., 2019). Previous studies have shown that heat stress can be detrimental during reproduction development due to the damage caused to plant organs and cellular structures (Hedhly, 2011; Hinojosa et al., 2019; Goel et al., 2023). During reproduction, high temperature can induce irreversible structural and physiological changes in both male and female floral organs, leading to premature senescence (Lohani et al., 2020; Jagadish et al., 2021). High temperature stress can also decrease chlorophyll synthesis and disrupt photosynthesis and respiration, further reducing the yield potential of crop plants (Hasanuzzaman et al., 2014; Zandalinas et al., 2016). Thus, understanding the impact of heatwaves on crops and particularly during reproductive stages is essential to the development of varieties that can withstand these periods of elevated temperatures.

Traditionally, most heat stress experiments involve a heat shock, where plants are subjected to a high temperature within a very short time (10–15°C above their optimal temperature, from several minutes to a few hours) (Wahid et al., 2007). As a result, plant responses to heat shock have been well studied (Huang et al., 2019; Wang et al., 2020), but relatively little information exists on the responses to heatwaves, especially at the transcriptomic and metabolomic levels (Jin et al., 2011; Glaubitz et al., 2017).

In plants, heat shock reduces photosynthesis and respiratory metabolism and increases antioxidant activity (Huang et al., 2019; Wang et al., 2020). Heat shock also negatively affects plant growth and productivity (Ismaili et al., 2015). While these experiments revealed the regulatory mechanisms in response to sudden heat stress (Seth et al., 2021; Ikram et al., 2022; Li et al., 2022), they do not fully represent the impact of temperature changes in the field during heatwave conditions. As a result, several studies employed prolonged warming experiments to study heat stress (Jin et al., 2011; Way and Yamori, 2014; Glaubitz et al., 2017). In *Arabidopsis*, studies showed that plants exhibit different response patterns to prolonged warming (7 days) as compared to heat shocks (Jin et al., 2011; Wang et al., 2020). While prolonged warming led to a reduction in stomatal conductance, heat shock increased transpiration. Under both heat shock and prolonged heat stress, there was an induction of antioxidant enzymes in *Arabidopsis*; however, these were significantly higher under the heat shock treatment compared to the prolonged heat treatment (Wang et al., 2020).

Oilseed rape (*Brassica napus* L.) is the second largest source of oilseed after soybean and the third largest source of vegetable oil worldwide (USDA, 2025). Cultivation and breeding practices have resulted in numerous genetically diverse lines with strong agronomic and adaptation traits (Sun et al., 2017). As a result, *B. napus* is widely cultivated around the world for food, biofuel, and animal feed (Namazkar et al., 2016). Like other major temperate field crops, *B. napus* can be extremely sensitive to high temperature stress, especially if it occurs during flowering or seed development, threatening yields and quality (Angadi et al., 2000; Koscielny et al., 2018; Kourani et al., 2022). Studies in different *Brassica* species have found negative relationships between heat stress and seed yield and quality (Yu et al., 2014). For example, under elevated temperature scenarios, four *B. napus* cultivars experienced a significant reduction in seed biomass, resulting in a 58% decrease in the oil yield and 77% decrease in the essential fatty acid C18:3-ω3 (Namazkar et al., 2016). Heat stress also reduced oil seed content and impaired carbohydrate incorporation into triacylglycerols in *B. napus* (Huang et al., 2019). Additionally, impairment of chlorophyll biosynthesis and disruption of the biochemical reactions of photosystems were exhibited in 10-day-old *B. napus* seedlings subjected to 38°C (Hasanuzzaman et al., 2014). This was manifested through a significant reduction in chlorophyll and leaf relative water content and through an inefficient antioxidant defence system (Hasanuzzaman et al., 2014). Despite the significant advances that these studies have made in understanding the effect of heat stress on different *Brassica* species, most of the research have focused on the seedling stage or grain filling. However, the impact of heatwaves on the transcriptomics and metabolomics of *B. napus*, particularly during its yield determining reproductive stages, is still poorly understood (Kourani et al., 2022).

The aim of this study was therefore to investigate the transcriptomic and metabolomic responses to heat stress in *B.*

napus during flowering stage under simulated field conditions. To achieve this, a heat treatment experiment simulating heatwave episode of *B. napus* cv. Westar was conducted in a controlled environment. Global transcriptome profiling using RNA-Seq was employed to identify differentially expressed genes in flower buds of heat stressed plants (30°C/24°C day/night for a period of 6 days). This was complemented with HPLC and LC-MS analyses to detect changes in sugars and glucosinolates (GLS) concentration in leaves in response to the heat treatment. Therefore, this study aims to provide insights into the impact of a future warmer climate on the important oil crop species *B. napus* during its reproductive stages.

2 Materials and methods

2.1 Plant materials and physiological parameters

Seeds of spring oilseed rape (*Brassica napus* L., cv. Westar) were surface-sterilised and sown into seed trays filled with a seed potting mix (Clover Peat, Dungannon, Northern Ireland). Trays were then placed in polyethylene tunnels for 4 weeks at the Crops and Environment Laboratory, University of Reading, to germinate. Twenty-eight days after sowing (DAS), the plants were transplanted into 3-L pots containing a peat based potting mix (Clover Peat).

At green bud stage (38 DAS), the plants were moved to two controlled environment chambers [Fitotron, Weiss Technik (UK) Ltd], for a period of 1 week to adjust to the new environment before the start of the heat experiment. Each cabinet contained 16 plants and was maintained under control conditions of 20°C/14°C day/night and a photoperiod of 16/8-h light/dark.

2.2 Heatwave experimental design

Since the flowering stage of winter-sown *B. napus* occurs during May in the UK, an analysis of daily weather temperatures during this developmentally crucial period was carried out using the UK Meteorological (Met) Office weather data obtained from the Met office (n.d.) and from WeatherOnline (n.d.) platforms. The data showed an increase in the frequency of high temperature fluctuations during May, ranging between 26°C and 28°C over several days (Supplementary Figure S1). Given the continuous rise in global temperature, it is expected that future heatwaves would increase in severity and duration (Seneviratne et al., 2012). Based on these data, the current study temperature simulates a heat stress event through a temperature increase to 30°C/24°C day/night for a period of 6 days and 20°C/14°C day/night for control. Forty-five DAS, the temperature in one cabinet was kept under control conditions (20°C/14°C) and denoted as control cabinet, while the second cabinet was set to a gradual increase in temperature and denoted as heat treatment (HT) cabinet. To mimic a heatwave, the temperature in the HT cabinet was increased gradually from 20°C to 30°C between 9:00 and 12:00 in three steps: 20°C at 9:00 h, 24°C at 10:00 h, 28°C at 11:00 h, and 30°C at 12:00 h. The temperature was held at 30°C until 22:00 h (Supplementary Figure S2B), before it was dropped gradually and maintained at 24°C until 8:00 of the next day (Supplementary Figure S2B). This cycle of gradual increase (day) and decrease (night) of temperature was held for 5 days (Supplementary Figure S2C). On the sixth day of treatment, the temperature was gradually decreased to 20°C/14°C day/night cycle (Supplementary Figure S2D) and held for a recovery period of 7 days (Supplementary Figure S2E). During heat treatment, the plants were frequently irrigated to avoid drought.

2.3 Sample preparation for transcriptomic analysis

Five biological replicates from each treatment condition were collected at days 0, 1, 2, 6, and 12 of the experiment. Each replicate was made up of three individual plants. Three flower buds were collected per plant (nine buds per replicate). All samples were immediately snap frozen in liquid nitrogen before they were stored at −80°C. Bud samples were ground into fine powder using pestle and mortar, with the frequent addition of liquid nitrogen to stop enzymatic reactions. The ground material was then stored at −80°C until RNA extraction.

2.4 RNA extraction and sequencing

Total RNA from bud samples was extracted using the Spectrum™ Plant Total RNA Kit (Sigma-Aldrich Dorest, UK) in accordance with the manufacturer's protocol and treated with genomic DNAse using DNASE 70-On Column DNase I Digestion set (Sigma-Aldrich) to eliminate DNA contamination. RNA quantification was estimated on both NanoDrop 2000 (Thermo Scientific) and Qubit 2.0 fluorometer (Invitrogen, USA), and its quality was evaluated on 1% (w/v) denaturing formaldehyde agarose gel (MOPS). Samples were shipped over dry ice to Novogene Europe, where sequencing was performed on the Illumina Novaseq™ 6,000 (PE150) platform.

2.5 Differential expression and cluster analysis

Raw sequence reads were assessed for quality using FastQC tools (v0.11.5) (Andrews, 2012). The mean sequence lengths were 150 bp, and the mean sequence GC content was 43%. The mean quality scores in each base position were higher than 36, and the mean quality scores per sequence were 36. As a result, sequence trimming was not necessary.

STAR software (v2.7.10a) was used to map the clean reads to the *B. napus* cv. Westar v0 reference genome (Song et al., 2020), and the percentage of aligned reads was calculated by using the flagstat command from samtools on each alignment file generated by STAR aligner (Supplementary Figure S3). To estimate transcript

abundance, RNA-Seq by Expectation-Maximisation (RSEM) software (v1.2.18) was used in three steps to prepare the reference, calculate expression, and generate the count matrices. First, rsem-prepare-reference script was used with "–gff3" option to extract reference sequences from the genome and "—star" option to build STAR indices. Next, rsem-calculate-expression script was used with "–paired-end" option to align input reads against the reference transcriptome with STAR and calculated expression values using the alignments. Finally, rsem-generate-data-matrix script was used to generate the count matrices from expression results files.

For differential expression analysis, DESeq2 (v1.41.10) was used in R environment (Love et al., 2014) with default parameters. A pre-filtering step was performed to keep transcripts that have a minimum count of 10 reads in a minimum of four samples. To identify transcripts that were significantly differentially expressed, the two conditions (heat stress versus control) were contrasted in pairwise comparisons. Thresholds of $|\log2(\text{foldchange})| \geq 0.5$ and adjusted p-value < 0.05 (using the Benjamini and Hochberg method) were considered to identify significantly differentially expressed transcripts between the two treatment conditions.

Significant DEGs in each contrast were further analysed using K-mean clustering based on the kmeans() function in R (distance: Euclidean), with log2FC as the input.

2.6 Gene Ontology and KEGG pathway enrichment analysis of DEGs

Gene Ontology (GO) and Kyoto Encyclopedia of Genes and Genomes (KEGG) enrichment analyses were conducted on the DEGs using OmicsBox (BioBam Bioinformatics, 2019). The significantly enriched GO terms and biological pathways in HT samples as compared to control at different timepoints were identified to determine heat-stress-related functions and pathways. The analysis was carried out using Fisher exact statistical test with FDR adjustment cutoff <0.05. The background dataset consisted of all *B. napus* cv. Westar identifiers present in the assembly's annotation file (Song et al., 2020).

2.7 Validation of RNA-seq results by real-time quantitative PCR

Sucrose Synthase 5 (SS5) and Heat Shock Protein 20 (HSP20) were chosen from the pathways that were involved in the heat stress response to further examine their expression in real time using real-time quantitative PCR (RT-qPCR). Five timepoints were chosen for each gene to represent the time course of the experiment. SS5 and HSP20 were not analysed at 1 day after treatment (DAT), as they exhibited similar expression profile at 0 and 1 DAT; therefore, one timepoint was selected (Supplementary Table S2).

Total RNA used for transcriptomic sequencing was used for cDNA synthesis. First, cDNA was synthesised from 1 µg total RNA by Invi trogen SuperScript IV VILO Master Mix kit according to the manufacturer's instructions (Thermo Fisher Scientific). The RT-qPCR reaction volume was 20 µL consisting of 3 µL cDNA, 10 µL SYBR Premix Ex Taq II (Takara, China), 1 µL (200 nM final concentration) of 4 µM of each primer (forward and reverse, Supplementary Table S3), and 5 µL RNAse-free water. Three technical and three biological replicates for each sample were measured with the following protocol: 50°C for 2 min, 95°C for 2 min, followed by 40 cycles of 95°C for 3 s, 60°C for 30 s, followed by dissociation curve analysis ramping from 60°C to 95°C with a ramp rate of 0.3°C s^{-1} on an ABI StepOne Plus RT-qPCR platform (Applied Biosystems, USA). BnaActin was used as housekeeping gene to normalise the data. The relative expression level of all selected genes at each timepoint was calculated using the $2^{-\Delta\Delta CT}$ method of the StepOne software (v2.2.2).

2.8 Sample preparation for metabolomic analysis

Five biological replicates from each treatment condition were collected at days 0, 1, 2, 5, 6, 8, and 12 of the heat treatment experiment. Each replicate was made up of three youngest fully expanded leaves collected from three plants. All leaf samples were immediately snap frozen in liquid nitrogen before being stored at −80°C until further analysis. Frozen leaf samples were freeze-dried for 5 days, then ground into a fine powder using a Precellys 24 lysis and homogenisation (Stretton Scientific, Alfreton, UK) and stored at −40°C in sealed sample bags until extraction and analysis.

2.9 Glucosinolates extraction and analysis

GLS extraction was carried out as per the protocol of Bell et al. (2015) as follows: 40 mg of ground leaf powder was heated in a dry block at 75°C for 2 min. This step was done as a precautionary measure to inactivate as much myrosinase enzyme as possible before extraction (Pasini et al., 2012). Afterwards, 1 mL of preheated (70% v/v) methanol (70°C) was added to each sample and placed in a water bath for 20 min at 70°C. Samples were then centrifuged for 5 min (6,000 rpm at 18°C) to collect the loose material into a pellet. The supernatant was then transferred into fresh labelled Eppendorf tube and stored at −80°C until further analysis. Before LC-MS analysis, the samples were filtered using 0.25-µm filter discs, diluted in 50% methanol at a 1:4 ratio (dilution factor =5) and spiked with 100 µL of the internal standard Sinigrin (100 ng mL^{-1}). The GLS content was analysed by SCIEX QTRAP 6500+ LC-MS.

For LC separation, a Waters Acquity BEH C18 column (particle size, 1.7 µ, 2.1 × 50 mm) with a Security VanGuard system from Waters (UK) was used. The mobile phase consisted of water with 0.1% formic acid (A) and methanol with 0.1% formic acid (B). The gradient started at 5% B and was raised to 90% B in 3.5 min, held at 90% B for 0.5 min and re-equilibrated at 5% B for 1 min. The total time of the gradient program was 5 min. The flowrate was 0.4 mL min^{-1} with a column temperature of 60°C. A 1-µL aliquot of sample was injected for analysis.

The LC system was interfaced with a SCIEX QTRAP 6500+ mass spectrometer equipped with an IonDrive Turbo V ion source. Multiquant software was used to control sample acquisition and data analysis. The QTRAP 6500+ mass spectrometer was tuned and calibrated according to the manufacturer's recommendations. For quantification, an external standard calibration curve was prepared using a series of standard samples containing the following GLS: Gluconapin (GNA), Progoitrin (PRO) and Glucobrassicin (GBS), with concentrations of 1,000, 500, 250, 100, 50, 10, and 1 ng mL^{-1}. Two-way mixed ANOVA in R was performed at 0.05 significance level to calculate the significance variation in concentration under heat treatment as compared to control.

2.10 Sugars content extraction and analysis

The extraction of soluble sugars (glucose, fructose, and sucrose) was performed as follows: 50 mg of ground leaf powder was extracted with 1 mL of 62.5% methanol/37.5% HPLC-grade water (v/v) at 55°C over a period of 15 min in a shaking water bath and vortexed every 5 min. Afterwards, the samples were allowed to cool for 2 min and then centrifuged at 13,000 rpm for 10 min and filtered using 0.25-µm filter discs. The supernatant was then transferred to a clean labelled Eppendorf tube and stored at −80°C until further analysis. Before HPLC analysis, the samples were diluted in HPLC-grade water in a 1:2 ratio (dilution factor = 3). Chromatographic separation of sugars content was performed using HPLC (Agilent 1260, Infinity Series) equipped with an Evaporative Light Scattering Detector (ELSD) system and an Asahipak NH2P-50 4E column (250 × 4.6 mm; Shodex, Tokyo, Japan) in an isocratic elution mode. The mobile phase consisted of 75% acetonitrile/25% water at a flowrate of 1 mL min^{-1}, a column temperature of 40°C, and an injection volume of 20 µL. The analysis had a total run time of 25 min. For quantification, an external standard calibration curve was prepared using a series of standard samples containing glucose, fructose, and sucrose with the concentrations: 0.025, 0.05, 0.1, 0.5, and 1 mg mL^{-1}.

2.11 Near-infrared spectroscopy scanning

Following the treatments, the plants were allowed to complete their lifecycle, and total aboveground biomass and seed yields were collected from individual plants. Seed samples were scanned with a DA 7250 NIR analyser (PerkinElmer, Beaconsfield, UK). The seed samples were scanned for moisture, oil, and protein content and for fatty acid composition of the oil.

2.12 Statistical analysis

Two-way mixed ANOVA was performed at 0.05 significance level to calculate the statistically significant differences between the means of sugars and glucosinolate concentration under heat treatment as compared to control. For a significant two-way interaction between treatment and timepoint, the following analysis were conducted: the simple main effects of treatment on sugars concentration were examined at each timepoint, using Bonferroni-adjusted p-values for multiple comparisons. This was followed by pairwise comparisons between treatment levels (heat stress vs. control) at each timepoint to determine whether the mean sugars concentrations differed significantly between heat stress and control. In addition, near-infrared spectroscopy (NIRS) data were analysed for the investigated components using a t-test. All statistical analysis was performed using R.

3 Results

3.1 Prolonged heat exposure reduced yield and altered *B. napus* oil composition

Heat treatment significantly altered plant growth and appearance, with visible physiological changes on the flowers and buds (Figure 1). At 5 DAT, flowers displayed smaller and paler petals compared to plants growing under control conditions. At 3

FIGURE 1
B. napus flowers and buds at 5 DAT and 3 DOR, respectively.

days of recovery (DOR), many buds suffered from abscission, appeared brown, and shrunken in size on plants subjected to the heat treatment. At maturity, heat-treated plants exhibited less total biomass and total seed weight relative to control plants (Supplementary Figure S4). In terms of oil quality, heat treatment significantly decreased linoleic acid, linolenic acid, and palmitic acid concentration but increased oleic acid and stearic acid concentration in seeds compared to control plants (Supplementary Figure S5).

3.2 Differential gene expression identifies distinct patterns of expression in *B. napus* under heat stress and recovery

Libraries were constructed and sequenced on the Illumina NovaSeq platform. An average of 47 million reads were generated per sample after low-quality reads were filtered out (Supplementary Table S1). Following this cleaning step, approximately 90%–95.49% total reads per sample were mapped to the *B. napus* cv. Westar v0 reference genome (Supplementary Figure S3) (Song et al., 2020). Principle component analysis (PCA) was used to analyse the samples that drove the group separation (Supplementary Figure S7). PC1 and PC2 captured 48.9% and 8.2% of the total variance of the samples, respectively. The analysis showed that both control and treatment samples clustered near each other at 7 DOR, which demonstrated that heat-treated plants might have started to return to normal after 7 days of recovery.

To understand the effect of heat stress on gene expression in *B. napus*, differentially expressed genes (DEGs) were identified in a pairwise comparison between heat treatment and control conditions at five timepoints during and after heat treatment. A total of 1,892, 3,253, 4,553, 4,165, and 1,713 genes were differentially expressed at days 0, 1, and 2 DAT and 1 and 7 DOR, respectively (Supplementary Figure S8). Analysis of the top differentially expressed genes after 24 h of heat treatment revealed that eight transcripts with logFC ranging between 4.4 and 10.8 mapped to small heat shock proteins (sHSP20), in addition to transcripts mapped to other heat shock factors such as Elongation Factor 1-beta 1-like and Chaperone Protein ClpB1 (Supplementary Table S7). On the other hand, top downregulated genes featured transcripts mapped to sugars transporters, nitrogen transport and storage, cell wall modification, and methylation (Supplementary Table S8). Similarly, after 48 h of heat treatment, many of the identified transcripts remained among the top DE, both up- and downregulated, highlighting the significant effect of heat stress on the functions performed by these enzymes and proteins.

To identify trends in the expression of genes across the time course of the experiment, K-means clustering was applied to 9,933 DE genes with logFC ≥ 0.5. The algorithm randomly assigned each gene into one of the clusters based on the Euclidean distance between the gene and the cluster mean. Six distinctive clusters based on expression changes across the five timepoints were identified (Figure 2). Interestingly, clusters 1 and 3 (475 and 607 genes), showed opposite expression patterns towards the end of the heat treatment and the start of the recovery phase. In cluster 1, the expression profile of genes decreased at 1 DOR (HS6vsC6), before returning to normal levels at 7 DOR (HS12vsC12), while in cluster 3, a sharp increase in expression was observed at 1 DOR (HS6vsC6), which returned to normal levels at 7 DOR (HS12vsC12).

In clusters 2 and 5 (3,470 and 1,333 genes), genes were downregulated along the course of the experiment but more pronounced during the heat treatment phase especially in cluster 5, which exhibited a greater decrease in expression. Both clusters 4 and 6 (398 and 3,518 genes) showed increased expression during the treatment before it started to decline towards the end, reaching normal levels at 7 DOR (HS12vsC12) (Figure 2).

3.3 Validation of RNA-seq data by quantitative real-time PCR

To verify the reliability of RNA sequencing results, two genes with diverse expression profiles, including upregulated or downregulated at different timepoints of the experiment, were selected for real-time qPCR to measure expression levels. As a result, Heat Shock Protein 20 (HSP20) and Sucrose Synthase 5 (SS5), exhibited similar expression profiles between RT-qPCR and RNA-seq data (Supplementary Figure S9, Supplementary Table S4), with correlation coefficients of r=0.86 and r=0.68, respectively.

3.4 Functional annotation of DEGs identifies key pathways responding to heat treatment and recovery

Gene Ontology (GO) enrichment analysis of the DEGs was performed to identify enriched GO terms. Terms such as “binding,” “catalytic activity,” “metabolic process,” “hydrolase activity,” and “ion binding” were among the predominant enriched terms at all timepoints with more transcripts mapped to these terms during heat treatment than during recovery (Supplementary Figures S10-S14). Oxidoreductase, hydrolase, and transferase were among the top identified enzymes (Supplementary Figure S15). These results suggest that high temperature activates several metabolic processes through the expression of numerous enzymes involved in alleviating the impact of heat stress not only during the stress period but also during recovery.

Based on Kyoto Encyclopedia of Genes and Genomes (KEGG) enrichment analysis (Kanehisa and Goto, 2000), pathways in the respiratory metabolism, namely, glycolysis and pentose phosphate pathway were enriched in all heat treatment comparisons at all timepoints, while citrate cycle and oxidative phosphorylation were enriched at 2 DAT and 1 DOR, respectively (Supplementary Figures S16-S19). Other related pathways were also enriched along the course of the treatment and during recovery period, and these include one carbon pool by folate (enriched at 1 and 2 DAT and 1 DOR), carbon fixation in photosynthetic organisms, cysteine and methionine metabolism (enriched at 1 and 2 DAT), glycerolipid and tryptophan metabolism (enriched at 2 DAT), fatty acid

10.3389/fpls.2025.1507338

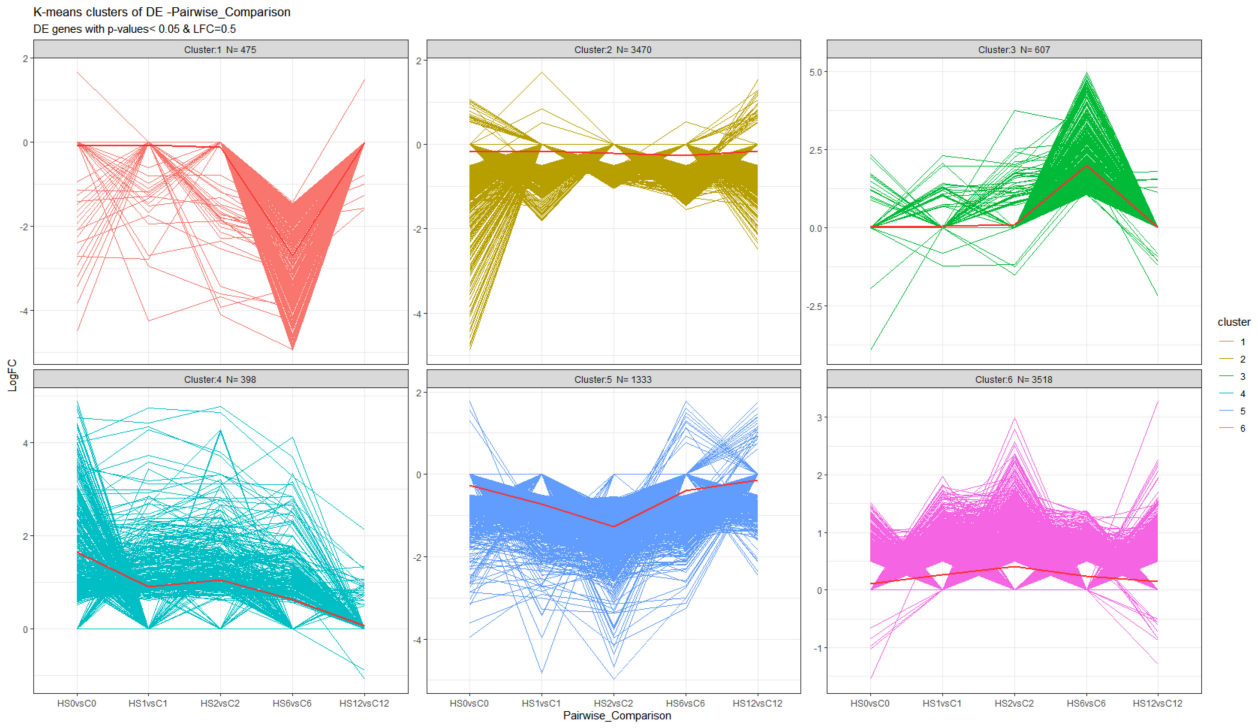

FIGURE 2
K-means cluster analysis of differential expressed genes in *B. napus* during and after heat treatment. K-means clustering was applied to 9,933 DE genes with logFC ≥ 0.5 using the "kmeans" function in R package "stats" (v. 3.2.2), where k represents a pre-specified number of clusters. Six groups of genes were classified, with N the number of genes in each cluster, and the solid red lines in each cluster indicate mean changes in DEG expression.

biosynthesis and pyruvate metabolism (enriched at 1 DOR), and fructose and mannose metabolism (enriched at 7 DOR). In the present study, most of the genes involved in these pathways were responsive to high temperature stress, with their expression declining with the onset of heat treatment, especially after 48 h (Supplementary Figures S20-S27).

3.4.1 Heat treatment downregulated the transcript levels of most aliphatic and indolic GLSs synthetic genes

Analysis of the aliphatic GLS synthetic and regulatory genes showed that heat treatment had a significant effect on the expression of 18 genes at 2 DAT (Figure 3). A total of 13 genes encoding different GLS synthetic genes including different UDP glycosyltransferases and glutathione S-transferases were downregulated, while five genes encoding GLS-related transcription factors were upregulated. At 1 DOR, which marks 24 h of recovery, nine genes that were not differentially expressed under heat treatment were found upregulated. These genes include different cytochrome P450 genes, transcription factors, branched-chain aminotransferase 4.2, and isopropylmalate dehydrogenase 2.

Analysis of the indolic GLS synthetic and regulatory genes showed that heat treatment altered the expression of 16 and 23 out of 44 genes at 1 and 2 DAT, respectively (Figure 4). These genes include sulfotransferases, cytochrome P450 genes, UDP glycosyltransferases, glutathione S-transferases, and transcription factors. After 1 week recovery (7 DOR), most of the differentially expressed genes identified during heat treatment were no longer differentially expressed. This is similar to what was seen with the aliphatic GLS encoding genes. Interestingly, one transcript encoding UDP glycosyltransferase 74E2-like remained downregulated after 1 week of recovery.

3.4.2 Heat treatment downregulated the transcript levels of most sulphur assimilation and transport genes

Analysis of the genes encoding sulphur assimilation and transport during heat treatment showed that 20 transcripts were downregulated in response to heat at either 1 or 2 DAT or both (Figure 5). One transcript encoding sulphate transporter was upregulated at 1 and 2 DAT, while two transcripts encoding adenylyl sulphate kinase was upregulated at 2 DAT only. Interestingly, after the end of heat treatment, only five transcripts remained downregulated at 1 DOR, and two transcripts encoding adenylyl sulphate kinase and ATP sulfurylase were upregulated at 7 DOR.

3.4.3 Metabolic analysis revealed altered leaf concentration of aliphatic and indolic GLS in response to heat treatment

Given the changes observed in the abundance of transcripts associated with GLS metabolism and sulphur assimilation and transport, the concentration of two aliphatic GLS progoitrin

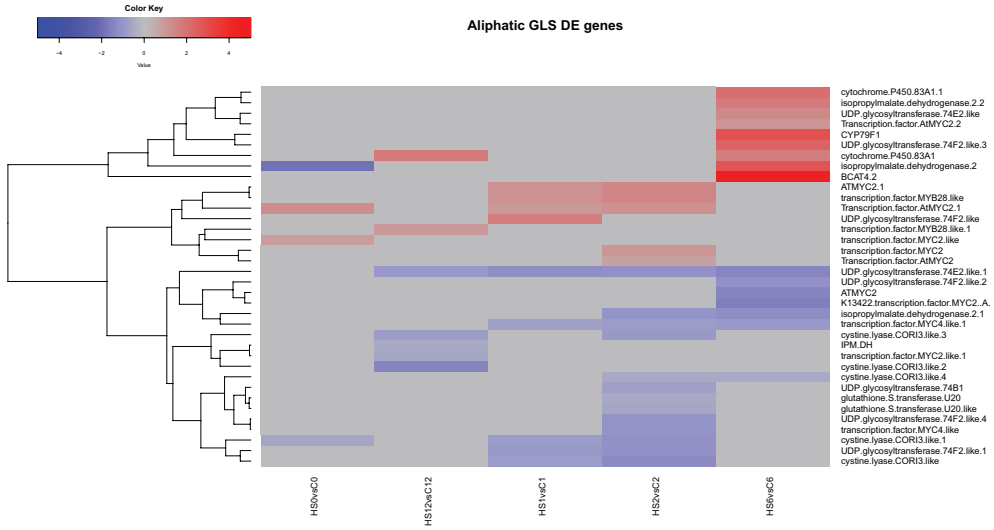

FIGURE 3
Heatmap showing differential expression of genes involved in the regulation or biosynthesis of aliphatic glucosinolates (GLS) in *Brassica napus*. A total of 13 genes encoding different GLS synthetic genes including different UDP glycosyltransferases and glutathione S-transferases were downregulated, while five genes encoding GLS-related transcription factors were upregulated at 2 DAT.

(PRO) and gluconapin (GNA), and one indole GLS glucobrassicin (GBS) were quantified using LC-MS. Their role in response to different abiotic stress factors has been previously reported (Ljubej et al., 2021; Jasper et al., 2020). Two-way mixed ANOVA pairwise comparisons showed a gradual increase in both PRO and GNA concentration in response to heat (Figures 6, 7). This increase was significant at 2 DAT. After 5 days of the heat treatment, the concentration of GLS started to decline but remained higher in heat-treated plants than in the leaves of control plants. In contrast, the concentration GBS decreased in response to heat treatment (Figure 8). During recovery, the concentration of GBS continued to decrease with the difference being significant at 1 and 3 DOR. After 1 week of recovery, GBS concentration in heat-treated plants remained lower than that of the control.

3.4.4 Heat treatment downregulated the transcript levels of most sugar transporter genes

To investigate the effect of heat stress on sugars transport and metabolism, analyses of genes encoding the SWEET and ERD6-like sugars transporters were undertaken. Compared to the control plants, heat stress significantly altered the expression of 21 SWEET genes with logFC ranged between −5 and 5 (Figure 9). These genes belonged to the phylogenetic clades II and III. Members of these clades predominantly transport hexose and sucrose, respectively. Nine of these transcripts were downregulated at 2 DAT, while two were upregulated. Interestingly, out of the 13 genes that were DE at 1 DOR, five upregulated genes were not DE during heat stress (were not affected by heat treatment) and became upregulated after the removal of stress (Figure 9).

Analysis of genes encoding the tonoplastic glucose symporters showed that 11 transcripts mapped to different ERD6-like genes (Figure 10). At 2 DAT, five were downregulated and two were upregulated.

In addition, one transcript mapping to a facilitated glucose transporter member 8-like showed a LogFC of −9.2 at 1 DAT and transcripts encoding sucrose transporters (SUCs) were found upregulated at 1 DAT and 1 DOR (Supplementary Figure S28). In addition to their significant role in phloem loading and unloading, these transporters are also involved in sugars influx into the cytosol. Furthermore, the present results showed that the expression of transcripts mapping to the sucrose-synthesizing enzyme, sucrose phosphate synthase (SPS) increased during heat treatment (Supplementary Table S5), while the expression of sucrose catalysing enzymes, namely, sucrose synthase and cell wall invertase significantly decreased (Supplementary Table S6).

3.4.5 Metabolic analysis revealed an increase in leaf concentration of sugars in response to heat treatment

To investigate the effect of heat stress on the sugar concentration in the leaves of *B. napus*, the concentration of fructose, glucose, and sucrose were quantified using high-performance liquid chromatography. Under control growth conditions, leaf fructose, glucose, and sucrose concentration increased slowly as the plants grew (Figures 11–13). In contrast, in the heat-treated plants, the leaf concentration of individual sugars increased. Two-way mixed ANOVA pairwise comparisons showed that the change in sugar concentration was significant during both heat treatment and recovery for glucose and fructose.

After the removal of heat stress, the leaf concentration of sucrose in the treated plants decreased gradually until it reached a lower concentration than that of the control plants at 3 DOR. In

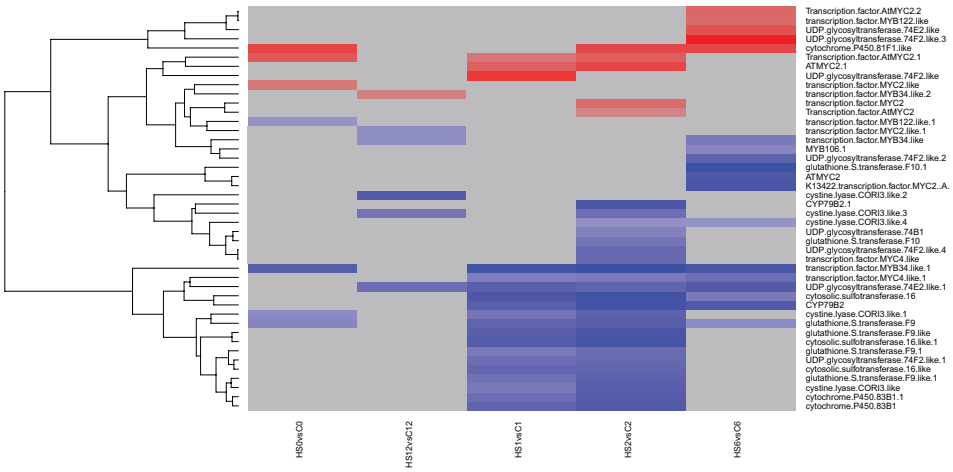

FIGURE 4
Heatmap showing differential expression of genes involved in the regulation or biosynthesis of indolic glucosinolates (GLS) in *Brassica napus*. A total of 16 and 23 out of 44 genes encoding different sulfotransferases, cytochrome P450 genes, UDP glycosyltransferases, glutathione S-transferases, and transcription factors were downregulated at 1 and 2 DAT, respectively.

contrast, fructose and glucose concentration showed a slight decrease initially before they increased again significantly at 3 DOR. After 7 days of recovery, the content of fructose, glucose, and sucrose dropped substantially, reaching lower concentration than that of the control plants.

4 Discussion

To investigate the effect of prolonged high temperatures (heatwaves) on the growth and adaptability of *B. napus*, especially during its yield-determining reproductive stages, heat treatment experiment was designed in a way that mimic field temperature fluctuations. In the present study, *B. napus* plants were exposed to a gradual increase in temperature for a 6-day period, and samples were collected at different timepoints during treatment and recovery. The results showed a prevailing effect on the plants both physiologically and metabolically. Heat treatment negatively impacted seed weight and total plant biomass (Supplementary Figure S4), consistent with similar negative impacts documented in *B. napus* and in other plants such as *Arabidopsis* and wheat (Aksouh-Harradj et al., 2006; Zhang et al., 2017; Bheemanahalli et al., 2019). Bheemanahalli et al. (2019) reported a significant decrease in seed number (23%) and seed weight (34.6%) upon heat stress during flowering. Similarly, *Arabidopsis* plants exposed to heat stress at the bolting stage exhibited a reduction in silique length and increased sterility (Zhang et al., 2017). This suggests that heat stress during flowering irreversibly damages vital processes leading to reduced productivity. NIRS showed significant effects of heat treatment on fatty acid concentrations in seeds in response to heat (Supplementary Figure S5). Several studies have observed heat-induced alterations in lipid composition (Namazkar et al., 2016; Zhou et al., 2018; Zoong Lwe et al., 2021). For example, *B. napus* exposed to elevated temperature and CO_2 levels showed a 77% reduction in linolenic acid content. Heat stress also significantly decreased other polyunsaturated fatty acids (Namazkar et al., 2016), highlighting the broader impact of heat on the plant's lipid profile. Moreover, high night temperatures in *B. napus* have led to the overexpression of genes involved in fatty acid catabolism (Zhou et al., 2018). Different heat-tolerant and susceptible genotypes further displayed distinct heat-induced changes in lipid content (Narayanan et al., 2016, 2020), highlighting genotype-specific responses to heat stress. Because lipids and proteins are the major constituents of biological membranes, maintaining cellular homeostasis depends mainly on the dynamic nature of lipid composition (Zheng et al., 2011). This suggests an essential role of cellular membrane lipid remodelling under high temperature stress. Additionally, under periods of reduced carbon availability in plants, the conversion of lipids to organic acids provides an additional source of energy, thus contributing to the plants' acclimation process (Yuenyong et al., 2019).

At the metabolomic level, heat treatment significantly altered the level of GLS and sugars and led to the differential expression of many genes involved in their synthesis, metabolism, and transport. Our study also demonstrated an increase of glucose, fructose, and sucrose concentration in leaf in during heat stress, with level slowly reaching, similar or slightly less levels to their control counterpart upon removal and recovery from the stressor. GLS and sugars are among the major secondary metabolites naturally occurring in *Brassica* species (Ayaz et al., 2006; Rao et al., 2021). Their primary site of synthesis occurs mainly in the leaves, from where they are transported to other parts of the plant (Pacheco-Sangerman et al., 2023; Ren et al., 2022). While reports on the sugar content of leaves are common (Ren et al., 2022; Zafar et al., 2022; Dellero et al., 2024), GLS have been thoroughly investigated in seeds (Wang et al., 2019; Tang et al., 2023; Jhingan et al., 2023), with fewer studies focusing on their presence in leaves (Rhee et al., 2020).

In this study, the levels of GLS and sugars were extracted and quantified from *B. napus* leaves, and their roles in heat stress response were investigated.

10.3389/fpls.2025.1507338

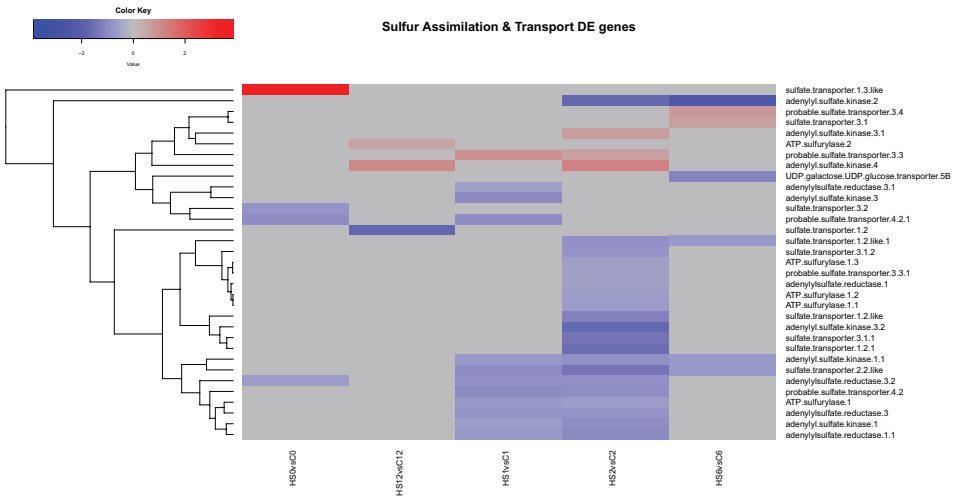

FIGURE 5
Heatmap showing differential expression of genes involved in the assimilation and transport of sulphur in *Brassica napus*. A total of 20 transcripts were downregulated in response to heat at either 1 or 2 DAT or both.

4.1 Heat stress resulted in differential expression of many genes involved in multiple functional and metabolic processes especially at 2 DAT

In this study, comparative transcriptome analysis between heat treatment and control identified 9,933 significantly differentially expressed transcripts ($|\log2(\text{foldchange})| \geq 0.5$, FDR $\leq$ 0.05) (Supplementary Figure S8A) with a balanced proportion of up- and downregulated genes in contrast HS0vsC0 (0 DAT), and more downregulated than upregulated genes in the rest of the contrasts were identified. This suggests that the impact of heat treatment on the plant's transcriptome after 24 h of heat stress, resulted in downregulation of many genes involved in multiple functional and metabolic processes such as glycolysis, PPP, citrate cycle, and oxidative phosphorylation. In contrast, HS12vsC12 (7 DOR), although the

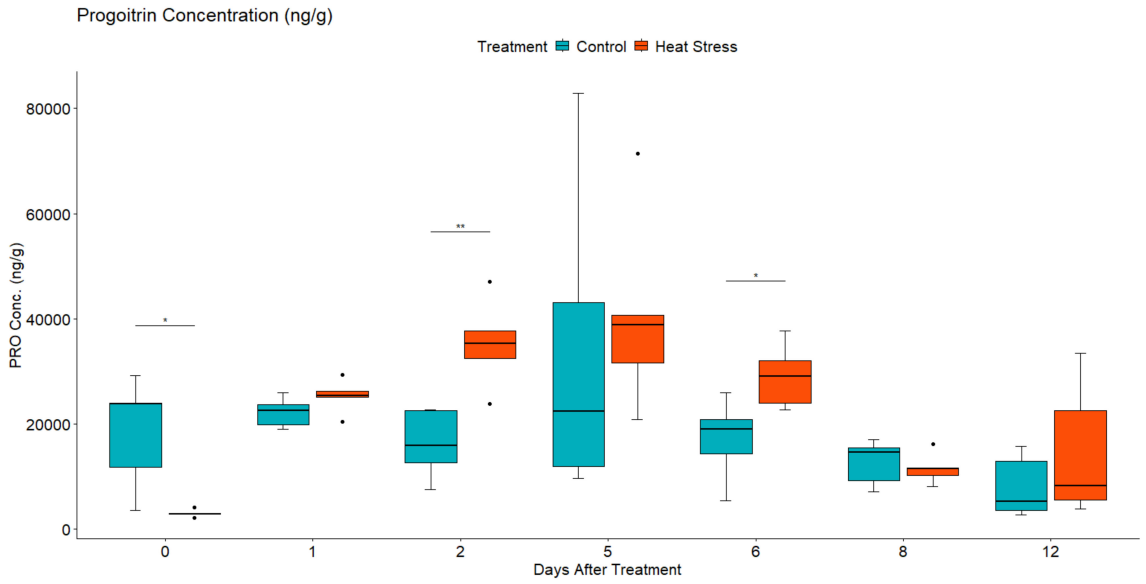

FIGURE 6
Leaf progroitin (PRO) concentration in ng/g of dry weight (DW) in *Brassica napus* plants subjected to heat treatment (30°C/24°C day/night) at 0–5 DAT (red) or maintained under control temperatures (20°C/14°C day/night) at all timepoints (blue). GLS concentrations were quantified using LC-MS. Data were analysed using two-way mixed ANOVA pairwise comparisons. Each box plot represents data from five replicates, showing the median (horizontal bar), 25th and 75th percentiles (the box), and the min and max values (whiskers), with outliers as dots. Significant differences between heat-treated and control plants at each timepoint are denoted by (*) for p-value $\leq$ 0.05 or (**) for p-value $\leq$ 0.01. Heat treatment significantly increased leaf concentration of aliphatic GLS Progoitrin.

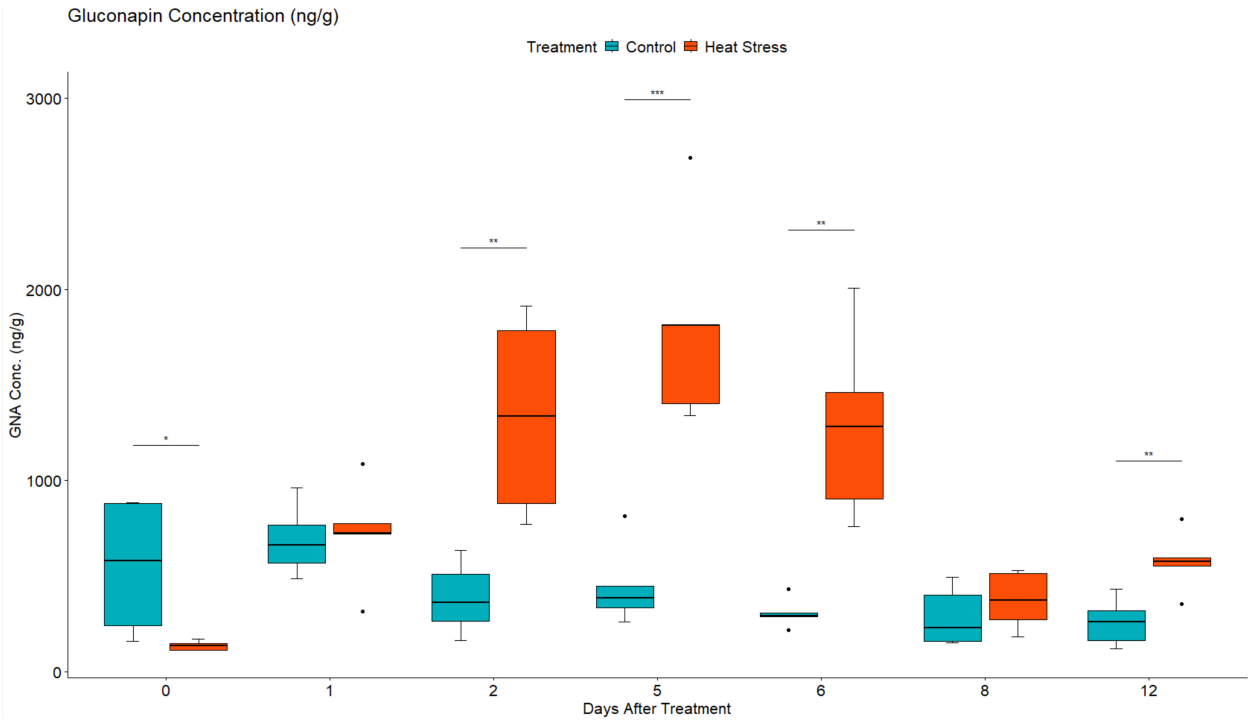

FIGURE 7
Leaf gluconapin (GNA) concentration in ng/g of dry weight (DW) in *Brassica napus* plants subjected to heat treatment (30°C/24°C day/night) at 0–5 DAT (red) or maintained under control temperatures (20°C/14°C day/night) at all timepoints (blue). GLS concentrations were quantified using LC-MS. Data were analysed using two-way mixed ANOVA pairwise comparisons. Each box plot represents data from five replicates, showing the median (horizontal bar), 25th and 75th percentiles (the box), and the min and max values (whiskers), with outliers as dots. Significant differences between heat-treated and control plants at each timepoint are denoted by (*) for p-value ≤ 0.05 or (**) for p-value ≤ 0.01 or (***) for p-value ≤ 0.001. Heat treatment significantly increased leaf concentration of aliphatic GLS gluconapin.

proportion of downregulated genes was higher than the upregulated ones, the total number of DEG decreased dramatically as the plant started to restore its metabolic functions after 7 days of recovery.

Differential expression analysis showed that some of the genes encoding sugar transporters, nitrogen transport and storage, cell wall modification, and methylation were downregulated (Supplementary Tables S8, S10). In contrast, several genes mapping to small heat shock proteins (sHSP), other heat shock transcription factors, methylation, and redox balance-related genes were upregulated (Supplementary Tables S7, S9). Among the top DE transcripts were several transcripts that mapped to HSPs and other HSFs. Notably, members of the sHSP family, also known as the HSP20 family proteins, such as HSP17.6, HSP22, and HSP23.6, showed high expression levels throughout the heat treatment, with expression reaching a log2FC of 11 at 2 DAT. This protein family is the most abundantly produced in plants in response to heat stress, and their role in plant responses to various abiotic stresses has been established (Sun et al., 2020). Other studies also reported the involvement of HSFs in different biotic and abiotic stress (Mishra et al., 2002, 2019; Chowdhary et al., 2023). In *A. thaliana*, thermoprotection tests demonstrated the role of HSFA6b in thermotolerance acquisition (Huang et al., 2016). Moreover, Giorno et al. (2009) showed that HsfA2 and Hsp17-CII are induced under high temperature in tomato, which are responsible for activating protection mechanisms during heat stress.

4.2 DEGs showed enrichment of pathways related to respiratory metabolism

The analysis of KEGG-enriched pathways revealed the main underlying biochemical pathways altered in *B. napus* in response to heat stress (Supplementary Figures S16-S19). In accordance with other reports (Estravis-Barcala et al., 2021; Li et al., 2022), DEGs showed an enrichment of pathways related to respiratory metabolism, namely, glycolysis, citrate cycle, oxidative phosphorylation, and pentose phosphate pathway (PPP). At 2 DAT, the impact of heat stress on glycolysis was manifested by the downregulation of the key enzymes phosphoglucomutase, aldose 1-epimerase, hexokinase, glucose-6-phosphate isomerase, and 6-phosphofructokinase (Supplementary Figure S21). Moreover, most of the citrate cycle genes were also downregulated at 2 DAT (Supplementary Figure S22). In the electron transport chain (ETC), gene expression analysis showed that most of the involved genes were downregulated under heat treatment, except for succinate dehydrogenase (SDH), which was upregulated (Supplementary Figure S23). In mitochondrial metabolism, SDH also known as complex II, plays a central role in the citrate cycle and ETC (Huang and Millar, 2013). Additionally, SDH is thought to impact different components of the plant stress response, including stomatal conductance and ROS scavenging (Huang et al., 2019).

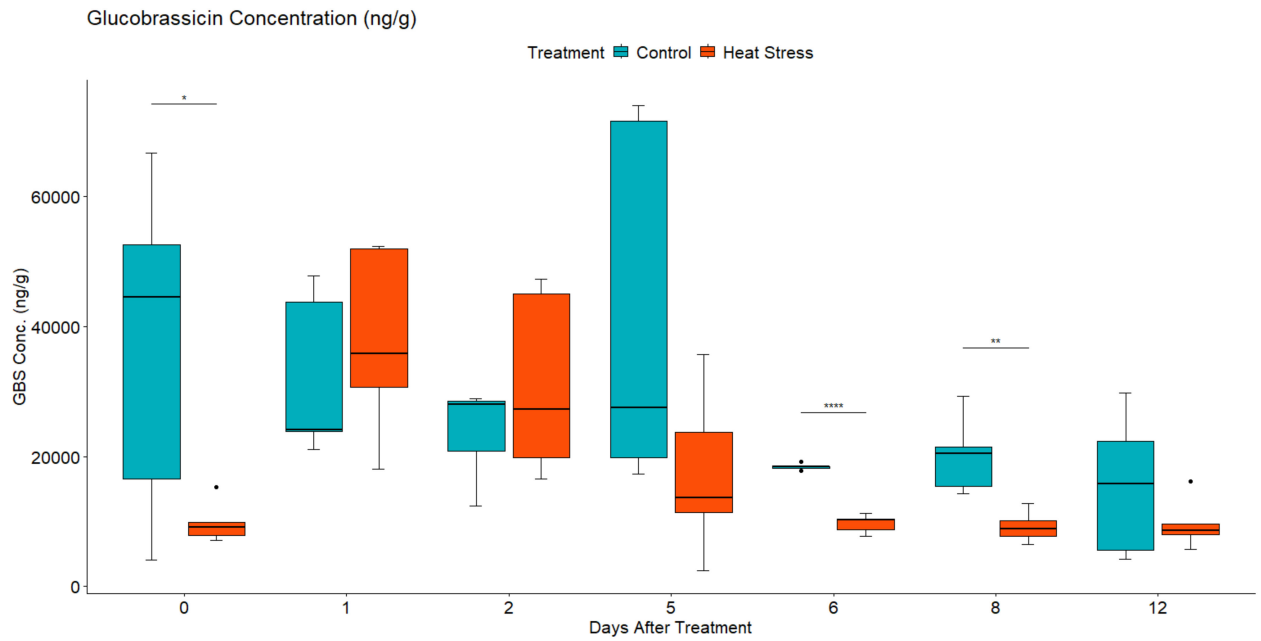

FIGURE 8
Leaf glucobrassicin (GBS) concentration in ng/g of dry weight (DW) in *Brassica napus* plants subjected to heat treatment (30°C/24°C day/night) at 0–5 DAT (red) or maintained under control temperatures (20°C/14°C day/night) at all timepoints (blue). GLS concentrations were quantified using LC-MS. Data were analysed using two-way mixed ANOVA pairwise comparisons. Each box plot represents data from five replicates, showing the median (horizontal bar), 25th and 75th percentiles (the box), and the min and max values (whiskers), with outliers as dots. Significant differences between heat-treated and control plants at each timepoint are denoted by (*) for p-value ≤ 0.05 or (**) for p-value ≤ 0.01 or (****) for p-value ≤ 0.0001. Heat treatment significantly decreased leaf concentration of the indolic GLS glucobrassicin.

Although respiratory pathways have been found to have potential roles in adaptive response to abiotic stress, mainly through reducing the production of ROS (Van Dongen et al., 2011), under extreme conditions such as severe or prolonged heat stress, respiratory enzymes are deactivated, and proteins are denatured leading to culminating of ROS and a total breakdown of mitochondrial respiration (Scafaro et al., 2021). This negatively impacts oxygen and carbon fluxes and eventually leads to more severe yield penalty (Rasmusson et al., 2020). In line with this, results from heat stress experiment on seagrass showed that high midday temperature stress of 40°C was associated with significant decrease in biomass (George et al., 2018). Likewise, Impa et al. (2019) found that under high night temperature, wheat tolerant cultivar exhibited smaller reductions in biomass and lower rates of both net photosynthesis and respiration compared to other wheat cultivars (Impa et al., 2019).

In the PPP, the oxidative phase (OPPP) was mainly affected at 1 DAT, and this was indicated by the differential expression of glucose-6-phosphate dehydrogenase (G6PDH) and 6-phosphogluconate dehydrogenase (6PGDH) enzymes (Supplementary Figure S24). G6PDH and 6PGDH are the key enzymes in the OPPP. They catalyse the first and third steps of the pathway, respectively (Long et al., 2016), and have been reported to be associated with the response to various abiotic stresses in plants (Gong et al., 2012). Esposito (2016) reported the involvement of the OPPP in the early response to abiotic stress factors, forming a true metabolic sensor to oxidative stress. At 2 DAT, most of the oxidative and non-oxidative phase enzymes were downregulated, including transketolase (TK), transaldolase, and phosphofructokinase enzymes (Supplementary Figure S25). TK has a central role in primary metabolism, where the products of the involved reactions produce the precursors for nucleic acids biosynthesis, aromatic amino acids, and vitamins (Bi et al., 2013). Bi et al. (2013) showed that the cucumber TK gene (*CsTK*) was sensitive to temperature and light (Bi et al., 2013, 2019). Likewise, the transaldolase gene was found to be involved in the regulation of expression of genes involved in the ABA signalling pathway and the enzymes responsive to ROS (Rong et al., 2021). The results of this study add further evidence to the involvement of the PPP enzymes in the heat stress response in *B. napus*.

4.3 Heat stress altered GLS metabolism during treatment

At the transcriptomic level, heat treatment differentially affected the expression of GLS synthesis and regulatory genes (Figures 3, 4). Several genes encoding different UDP glycosyltransferases and glutathione S-transferases appeared downregulated, while others encoding GLS-related transcription factors were upregulated, suggesting that these genes might have participated at different stages of the stress response.

The influence of heat stress on individual GLS was further evaluated through metabolomic analysis of two aliphatic GLS

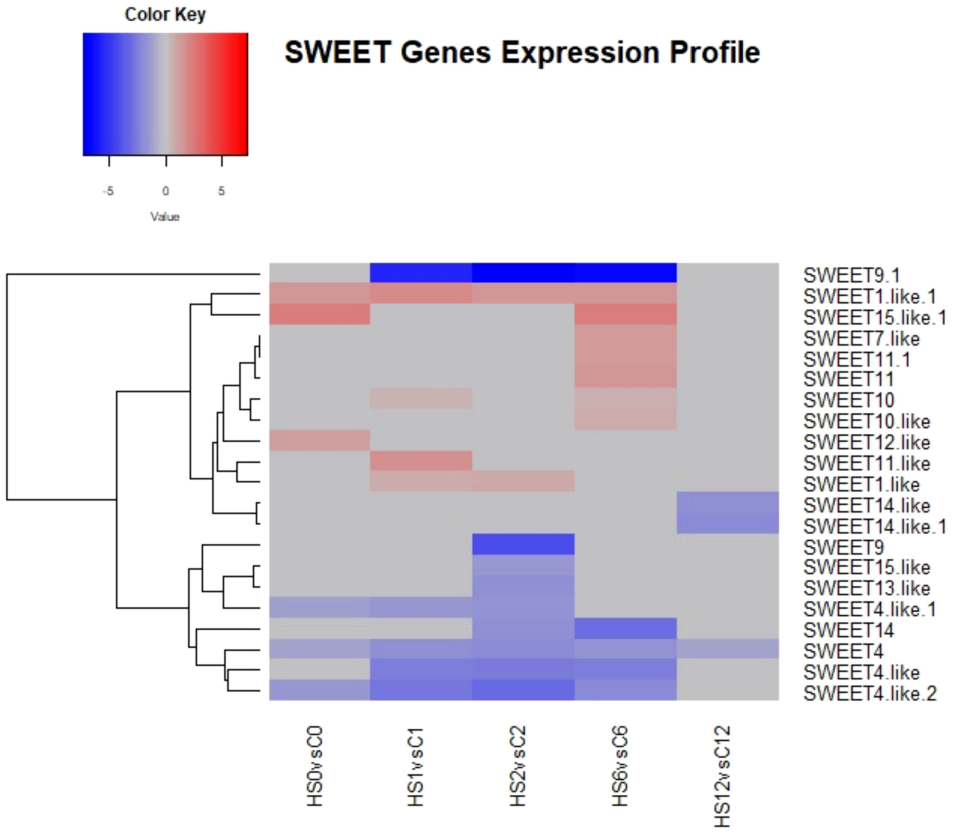

FIGURE 9
Heatmap showing differential expression of SWEET genes involved in sugar transport in *Brassica napus*. Heat stress significantly altered the expression of 21 SWEET genes with logFC ranged between −5 and 5.

[progoitrin (PRO) and gluconapin (GNA)] and one indolic GLS [glucobrassicin (GBS)]. The role of these GLS in response to different abiotic stress factors has been previously reported (Jasper et al., 2020; Ljubej et al., 2021). In the current study, the concentration of PRO and GNA significantly increased in response to heat stress before it started to decline at 5 DAT (Figures 6, 7). This decline could have resulted from membrane damage caused by prolonged exposure to heat, leading to GLS degradation. In addition, the removal of heat stress after 5 DAT could also be another factor for the decline in GLS content. In addition to its primary role in response to plant pathogen interaction (Hopkins et al., 2009; Touw et al., 2020), GLS accumulation in response to heat stress has also been previously reported (Valente Pereira et al., 2002; Martínez-Ballesta et al., 2013; Jasper et al., 2020). When plants are stressed, growth is reduced, and carbon utilisation is predominantly diverted towards the production of secondary metabolites. As part of the plant defence mechanism, GLS play important role as osmoprotective compounds (Martínez-Ballesta et al., 2013), where their concentration increases in response to stress, providing protection against oxidative damage. At 30°C/15°C (day/night) temperature regime, *Brassica oleracea* seedlings had significantly higher GLS concentration than plants cultivated at lower temperatures (22°C/15°C and 18°C/12°C) (Valente Pereira et al., 2002). Similarly, an *Arabidopsis* GLS mutant experienced a remarkable decline in growth and development and was found to be less heat tolerant than wild-type plants upon exposure to high temperature (Ludwig-Müller et al., 2000).

In contrast, indolic glucosinolate GBS showed a downward trend where concentration decreased gradually in response to heat (Figure 8). Similar results have been found where GBS concentration was reduced in response to heat treatment (Bohinc and Trdan, 2012). In addition, during short-term high-temperature stress, the transcript level of the indolic glucosinolates synthetic genes was predominantly downregulated (Rao et al., 2021). Several studies reported that indole GLS are much more sensitive to heat treatment (Bones and Rossiter, 2006; Bohinc and Trdan, 2012) and can demonstrate more thermal degradation than aliphatic GLS at lower temperatures (Orlemans et al., 2006).

The results of our study indicate that the concentration of GLS in the leaves of *B. napus* is influenced by high-temperature stress, which was previously reported in other *Brassica* species (Rask et al., 2000; Bohinc and Trdan, 2012). It also shows that different groups of GLS (aliphatic versus indolic) differ in their response to heat stress. As reported by Ljubej et al. (2021), the different accumulation trends of these groups could correspond to different protective mechanisms driven by individual GLS with diverse chemical structures and bioactivities (Ljubej et al., 2021). These

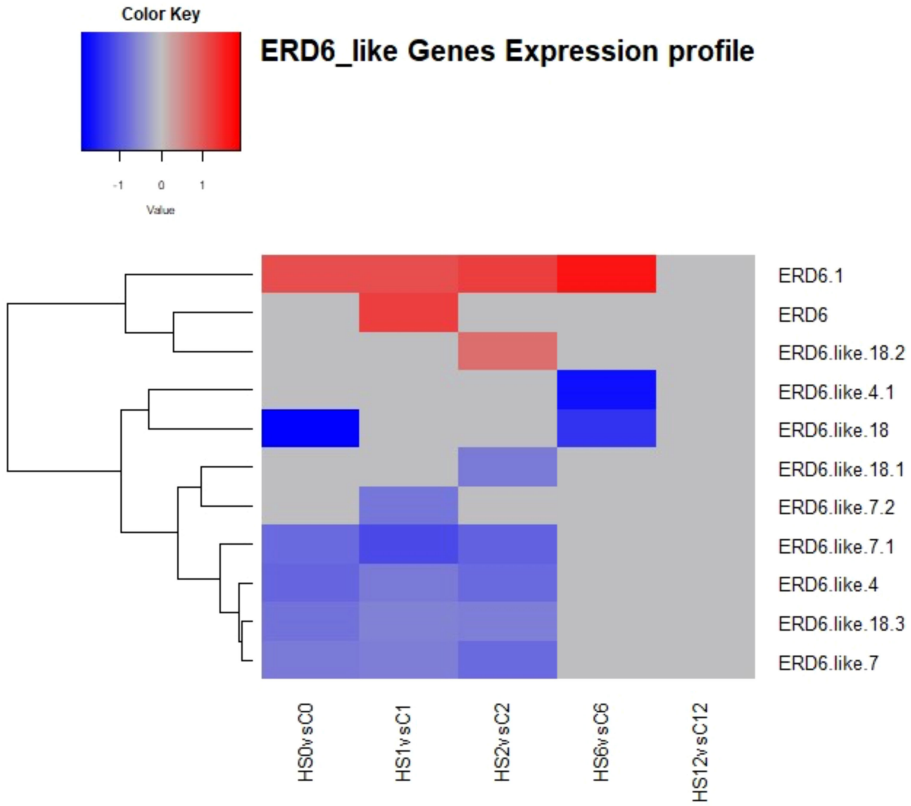

FIGURE 10
Heatmap showing differential expression of ERD-6 like genes involved in sugars transport in *Brassica napus*. At 2 DAT, five transcripts were downregulated, and two transcripts were upregulated.

mechanisms may prioritise energy towards aliphatic GLS production, which are known to play crucial roles in ROS mitigation (Martínez-Ballesta et al., 2013). Additionally, the reduced availability of GLS precursors, such as nitrogen and sulphur, under stressful conditions may influence the allocation of GLS across plant tissues. In response, plants might break down their GLS and utilise the released sulphur to support primary metabolic processes, such as protein synthesis, within specific organs (Brown et al., 2003; Martínez-Ballesta et al., 2013). This plasticity highlights GLS players in balancing stress resilience and adaptation. By selectively modifying GLS content, plants can fine-tune their responses to stress, meeting immediate defence demands while ensuring long-term survival and reproductive success.

4.4 Heat stress altered the expression of sulphur assimilation and transport genes

In the current study, the transcript levels of sulphur assimilation and transport genes were significantly downregulated especially at 2 DAT (Figure 5). This included several adenylyl sulphate kinases and reductases, ATP sulphurylase (ATPS), and sulphate transporter genes. These genes are important for the activation, catalysis, and transport of sulphur compounds (Capaldi et al., 2015). Moreover, enrichment pathway analysis showed that cysteine and methionine metabolism pathway was among the top significantly enriched pathways at 1 and 2 DAT (Supplementary Figures S16, S17). In this pathway, 11 transcripts mapping to S-adenosylmethionine synthetase and 11 transcripts mapping to homocysteine S-methyltransferases were downregulated (Supplementary Figure S20). These enzymes are among the key enzymes that control the methionine pool (Capaldi et al., 2015). Given that GLS compounds are rich in sulphur, assimilation of sulphur is closely associated with GLS biosynthesis. Cysteine, which is the terminal metabolite in sulphur assimilation, acts as a sulphur donor for methionine, a precursor for aliphatic GLS. This renders cysteine an important intersection point between sulphur assimilation and GLS biosynthesis (Rao et al., 2021). Such proximity between sulphur and these amino acids makes cysteine and methionine metabolism pathway directly related to GLS biosynthesis.

4.5 Heat stress altered sugar metabolism during treatment and recovery periods

In the present study, heat treatment altered carbohydrate concentration as the amounts of glucose, fructose, and sucrose increased with heat treatment (Figures 11-13). At the transcriptional level, the starch hydrolysing enzyme alpha-amylase was induced. Conversely, the starch-synthesizing enzymes such as

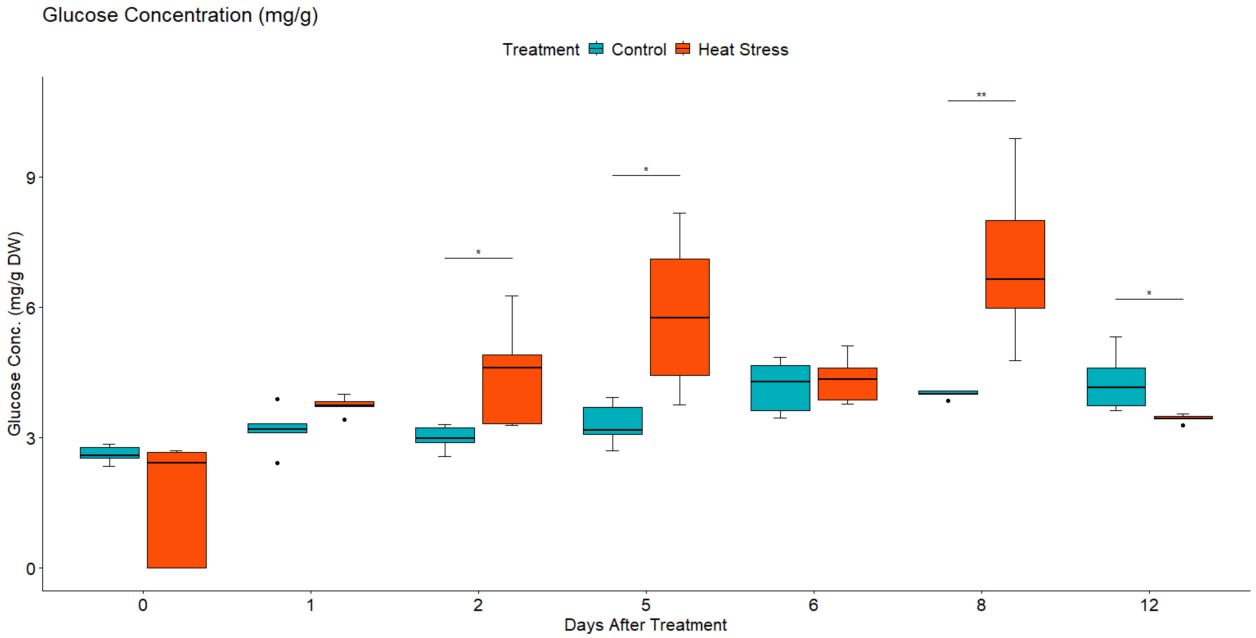

FIGURE 11
Leaf glucose concentration in mg/g of dry weight (DW) in *Brassica napus* plants subjected to heat treatment (30°C/24°C day/night) at 0–5 DAT (red) or maintained under control temperatures (20°C/14°C day/night) at all timepoints (blue). Concentration was quantified using HPLC. Data were analysed using two-way mixed ANOVA pairwise comparisons. Each box plot represents data from five replicates, showing the median (horizontal bar), 25th and 75th percentiles (the box), and the min and max values (whiskers), with outliers as dots. Significant differences between heat-treated and control plants at each timepoint are denoted by (*) for p-value ≤ 0.05 or (**) for p-value ≤ 0.01. Heat treatment significantly increased leaf concentration of glucose.

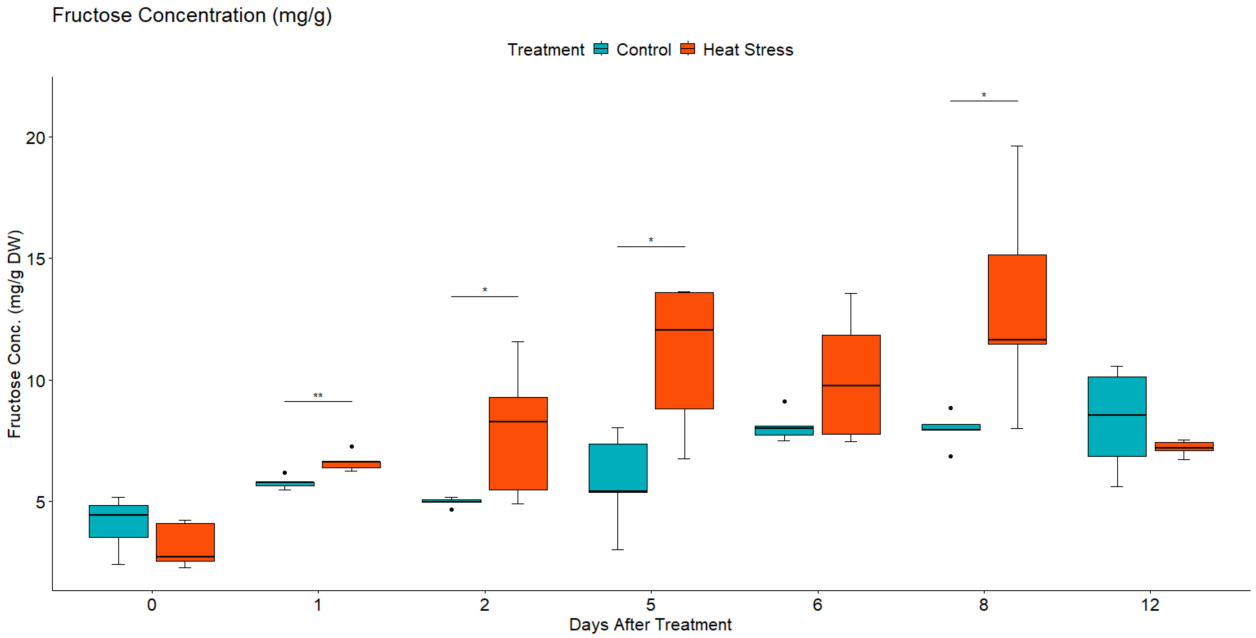

FIGURE 12
Leaf fructose concentration in mg/g of dry weight (DW) in *Brassica napus* plants subjected to heat treatment (30°C/24°C day/night) at 0–5 DAT (red) or maintained under control temperatures (20°C/14°C day/night) at all timepoints (blue). Concentration was quantified using HPLC. Data were analysed using two-way mixed ANOVA pairwise comparisons. Each box plot represents data from five replicates, showing the median (horizontal bar), 25th and 75th percentiles (the box), and the min and max values (whiskers), with outliers as dots. Significant differences between heat-treated and control plants at each timepoint are denoted by (*) for p-value ≤ 0.05 or (**) for p-value ≤ 0.01. Heat treatment significantly increased leaf concentration of fructose.

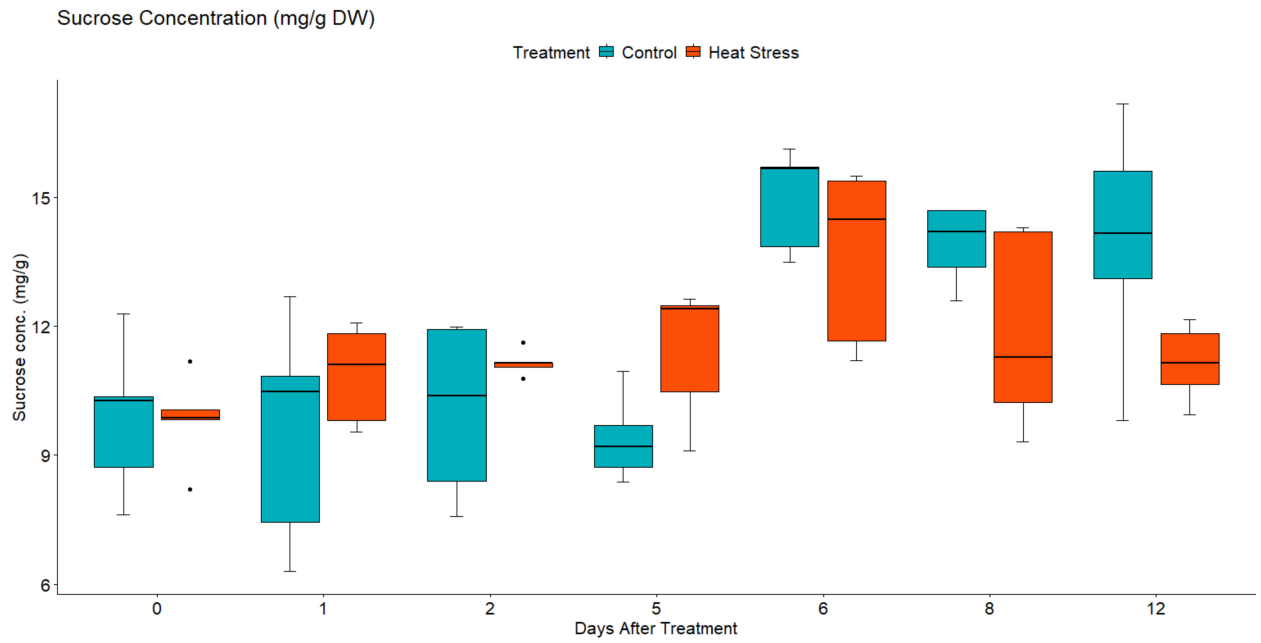

FIGURE 13
Leaf sucrose concentration in mg/g of dry weight (DW) in *Brassica napus* plants subjected to heat treatment (30°C/24°C day/night) at timepoints 0–5 (red) or maintained under control temperatures (20°C/14°C day/night) at all timepoints (blue). Concentration was quantified using HPLC. Data were analysed using two-way mixed ANOVA pairwise comparisons. Each box plot represents data from five replicates, showing the median (horizontal bar), 25th and 75th percentiles (the box) and the min and max values (whiskers), with outliers as dots.

phosphoglucomutase (PGM), AGPase, and hexokinase were inhibited (Supplementary Figure S21, S27). Likewise, heat induced the upregulation of sucrose-synthesizing enzymes and the downregulation of sucrose-hydrolysing enzymes such as cell wall invertase and sucrose synthase (Supplementary Tables S5, S6). These results suggest that heat-induced starch hydrolysis and promoted sucrose synthesis. Furthermore, heat stress downregulated many sugars transporters such as SWEET and ERD6-like (Figures 9, 10) and led to sugar accumulation in the leaves. Several studies have shown that various environmental stresses significantly impact sugar metabolism and transport in plants (Xalxo et al., 2020; Mathan et al., 2020). For instance, drought and salinity stress have been reported to increase sucrose content in both leaf and root tissues of rice (Mathan et al., 2020). Similarly, heat-stressed moth bean seedlings exhibited a notable accumulation of total sugars and proline across different genotypes (Harsh et al., 2016).

Heat stress not only impairs carbohydrate assimilation but also reduces sugar export from leaves (Julius et al., 2017). Marias et al. (2017) observed increased glucose and fructose levels in the leaves of *Coffea arabica* under heat stress. In maize, high temperatures decreased the 13C export rate from ear leaves, leading to enhanced growth of vegetative parts but reduced grain yield (Suwa et al., 2010). It is proposed that SWEET transporters efflux sucrose into the phloem apoplast, while SUT transporters import sucrose into the sieve element-companion cell complex (Osorio et al., 2014). During heat stress, leaves are the first tissues to sense and suffer from heat damage, and they utilise sugars to scavenge reactive oxygen species (ROS) and alleviate oxidative stress. Additionally, sugars serve as an energy source in high-respiration environments, helping maintain cell–water balance and membrane integrity through osmotic adjustments (Burke, 2007). Given the critical role of sugars in stress responses, the findings of this study, combined with previous observations, suggest that heat stress inhibits sugars export by SWEETs and/or its import by SUTs in heat-stressed leaves, resulting in sugars accumulation. Thereby, maintaining leaf sugar content through reducing source to sink export is considered a tolerance strategy (Kaushal et al., 2013). It is also worth noting that the decrease in sink demand due to growth limitation could also contribute to the accumulation of sugars in the source leaves under stressful conditions (Hummel et al., 2010; Lemoine et al., 2013).

5 Conclusion

Through a comprehensive transcriptomic and metabolomic analysis, this study brings evidence for the effect of high temperature stress and, in particular, heatwaves on different functional and metabolic pathways, highlighting its role in the plant stress defence system. More specifically, our results indicated that heat treatment:

1. inhibited important metabolic pathways such as respiratory metabolism, namely, glycolysis, pentose phosphate pathway, citrate cycle, and oxidative phosphorylation especially after 48 h of heat treatment;
2. reduced yield and plant biomass and altered seed composition;

3. altered sugar and glucosinolate levels in leaves;
4. induced the expression of 9,933 genes, which were differentially regulated during heat treatment and recovery. Most of the top up- and downregulated genes involved in key biological processes such as heat shock proteins, cellular processes regulation, transcription factors, cell wall remodelling, sugar and secondary metabolites transport, and metabolism.

Altogether, this study is an attempt to tackle the question of how plants face and adapt to heat stress and to provide insights into the impact of a future warmer climate on plants especially during reproductive stages. At the transcriptomic level, the key DEGs identified in this study could serve as important biomarkers that can be utilised by breeding programs to select cultivars with stronger resistance to heat. In particular, the identified genes could be further characterised and used as genetic markers for marker assisted selection, where plant breeders could select plant performance based on the composition of these genetic biomarkers rather than through waiting for the plants' phenotypic performance, thus accelerating traditional crop breeding for stress tolerance traits. In addition, the identified genes could form a target for genome editing techniques such as the clustered regularly interspaced short palindromic repeat (CRISPR)/CRISPR-associated protein 9 (Cas9), an approach that has already been explored in crop improvement programs especially for rapid development of abiotic stress-tolerant crops (Zafar et al., 2020). This can be applied by modifying sensitive or negatively regulating genes and activating positively regulated genes involved in stress response pathways to enhance the plant's ability to withstand stress (Kumar et al., 2023). Finally, this study represents an important step towards developing an understanding of the heat stress response and tolerance mechanisms, a knowledge that could be transferred to other plants.

Data availability statement

The datasets presented in this study can be found in online repositories. The names of the repository/repositories and accession number(s) can be found below: https://www.ncbi.nlm.nih.gov/, SUB14296957.

Author contributions

MK: Data curation, Formal analysis, Validation, Visualization, Writing – original draft. MA: Funding acquisition, Investigation, Project administration, Supervision, Writing – review & editing. JH: Conceptualization, Data curation, Funding acquisition, Investigation, Methodology, Project administration, Resources, Software, Supervision, Validation, Writing – review & editing. FM: Conceptualization, Funding acquisition, Investigation, Project administration, Resources, Supervision, Writing – review & editing.

Funding

The author(s) declare that financial support was received for the research and/or publication of this article. This project was supported by the UKRI-BBSRC project "Evaluating epigenetic and transcriptomic adaptations to climate change in *Brasicca napus* (oilseed rape)"—Project reference: 2451341. This work was supported by the UK Research and Innovation (UKRI) - [Grant Reference No. 2451341].

Acknowledgments

We thank Dr. Luke Bell from the University of Reading (School of Agriculture, Policy & Development) for providing the reference standards for glucosinolates and Monika Jodkowska from Cranfield University (Plant Science Laboratory) for developing the method for the LC-MS experiment.

Conflict of interest

The authors declare that the research was conducted in the absence of any commercial or financial relationships that could be construed as a potential conflict of interest.

Generative AI statement

The author(s) declare that no Generative AI was used in the creation of this manuscript.

Publisher's note

Supplementary material

The Supplementary Material for this article can be found online at: https://www.frontiersin.org/articles/10.3389/fpls.2025.1507338/full#supplementary-material

References

Aksouh-Harradj, N., Campbell, L., and Mailer, R. (2006). Canola response to high and moderately high temperature stresses during seed maturation. *Can. J. Plant Sci.* 86, 967–980. doi: 10.4141/P05-130

Andrews, S. (2012). *FastQC: a quality control tool for high throughput sequence data*. Available online at: http://www.bioinformatics.babraham.ac.uk/projects/fastqc (Accessed October 01, 2024).

Angadi, S. V., Cutforth, H. W., Miller, P. R., McConkey, B. G., Entz, M. H., Brandt, S. A., et al. (2000). Response of three Brassica species to high temperature stress during reproductive growth. *Can. J. Plant Sci.* 80, 693–701. doi: 10.4141/P99-152

(2019). *OmicsBox – Bioinformatics Made Easy, BioBam Bioinformatics*. Available online at: https://www.biobam.com/omicsbox (Accessed October 10, 2024).

Ayaz, F. A., Glew, R. H., Millson, M., Huang, H. S., Chuang, L. T., Sanz, C., et al. (2006). Nutrient contents of kale (*Brassica oleraceae* L. var. acephala DC.). *Food Chem.* 96, 572–579. doi: 10.1016/j.foodchem.2005.03.011

Bell, L., Oruna-Concha, M. J., and Wagstaff, C. (2015). Identification and quantification of glucosinolate and flavonol compounds in rocket salad (*Eruca sativa*, *Eruca vesicaria* and *Diplotaxis tenuifolia)* by LC–MS: Highlighting the potential for improving nutritional value of rocket crops. *Food Chem.* 172, 852–861. doi: 10.1016/j.foodchem.2014.09.116

Bheemanahalli, R., Sunoj, V. S. J., Saripalli, G., Prasad, P. V. V., Balyan, H. S., Gupta, P. K., et al. (2019). Quantifying the impact of heat stress on pollen germination, seed set, and grain filling in spring wheat. *Crop Sci.* 59, 684–696. doi: 10.2135/cropsci2018.05.0292

Bi, H., Li, F., Wang, H., and Ai, X. (2019). Overexpression of transketolase gene promotes chilling tolerance by increasing the activities of photosynthetic enzymes, alleviating oxidative damage and stabilizing cell structure in *Cucumis sativus* L. *Physiologia Plantarum* 167, 502–515. doi: 10.1111/ppl.12903

Bi, H., Wang, M., Dong, X., and Ai, X. (2013). Cloning and expression analysis of transketolase gene in Cucumis sativus L. *Plant Physiol. Biochem.* 70, 512–521. doi: 10.1016/j.plaphy.2013.06.017

Bohinc, T., and Trdan, S. (2012). Environmental factors affecting the glucosinolate content in Brassicaceae. *J. Food Agric. Environ.* 10, 357–360.

Bones, A. M., and Rossiter, J. T. (2006). The enzymic and chemically induced decomposition of glucosinolates. *Phytochemistry* 67, 1053–1067. doi: 10.1016/j.phytochem.2006.02.024

Brown, P. D., Tokuhisa, J. G., Reichelt, M., and Gershenzon, J. (2003). Variation of glucosinolate accumulation among different organs and developmental stages of *Arabidopsis thaliana*. *Phytochemistry* 62, 471–481. doi: 10.1016/S0031-9422(02)00549-6

Burke, J. J. (2007). Evaluation of source leaf responses to water-deficit stresses in cotton using a novel stress bioassay. *Plant Physiol.* 143, 108121. doi: 10.1104/pp.106.087783

Capaldi, F. R., Gratão, P. L., Reis, A. R., Lima, L. W., and Azevedo, R. A.. (2015). Sulfur Metabolism and Stress Defense Responses in Plants. *Tropical Plant Biology.* 8(3–4), 60–73. doi: 10.1007/s12042-015-9152-1

Chowdhary, A. A., Mishra, S., Mehrotra, S., Upadhyay, S. K., Bagal, D., and Srivastava, V. (2023). Plant transcription factors: An overview of their role in plant life. In S. K. Upadhyay (Ed.) *Plant Transcription Factors*, 3–20. doi: 10.1016/b978-0-323-90613-5.00003-0

Dellero, Y., Berardocco, S., and Bouchereau, A. (2024). U-13C-glucose incorporation into source leaves of *Brassica napus* highlights light-dependent regulations of metabolic fluxes within central carbon metabolism. *J. Plant Physiol.* 292, 154162. doi: 10.1016/j.jplph.2023.154162

Dikšaitytė, A., Viršilė, A., Žaltauskaitė, J., Januškaitienė, I., and Juozapaitienė, G. (2019). Growth and photosynthetic responses in *Brassica napus* differ during stress and recovery periods when exposed to combined heat, drought and elevated CO_2. *Plant Physiol. Biochem.* 142, 59–72. doi: 10.1016/j.plaphy.2019.06.026

Esposito, S. (2016). Nitrogen assimilation, abiotic stress and glucose 6-phosphate dehydrogenase: The full circle of reductants. *Plants (Basel Switzerland)* 5, 24. doi: 10.3390/plants5020024

Estravis-Barcala, M., Heer, K., Marchelli, P., Ziegenhagen, B., Arana, M. V., and Bellora, N. (2021). Deciphering the transcriptomic regulation of heat stress responses in *Nothofagus pumilio*. *PloS One* 16, e0246615. doi: 10.1371/journal.pone.0246615

George, R., Gullström, M., Mangora, M. M., Mtolera, M. S. P., and Björk, M. (2018). High midday temperature stress has stronger effects on biomass than on photosynthesis: A mesocosm experiment on four tropical seagrass species. *Ecol. Evol.* 8, 4508–4517. doi: 10.1002/ece3.3952

Giorno, F., Wolters-Arts, M., Grillo, S., Scharf, K.-D., Vriezen, W. H., and Mariani, C. (2009). Developmental and heat stress-regulated expression of HsfA2 and small heat shock proteins in tomato anthers. *J. Exp. Bot.* 61, 453–462. doi: 10.1093/jxb/erp316

Glaubitz, U., Li, X., Schaedel, S., Erban, A., Sulpice, R., Kopka, J., et al. (2017). Integrated analysis of rice transcriptomic and metabolomic responses to elevated night temperatures identifies sensitivity- and tolerance-related profiles. *Plant Cell Environ.* 40, 121–137. doi: 10.1111/pce.12850

Goel, K., Kundu, P., Sharma, P., and Zinta, G. (2023). Thermosensitivity of pollen: a molecular perspective. *Plant Cell Rep.* 42, 843–857. doi: 10.1007/s00299-023-03003-y

Gong, H., Chen, G., Li, F., Wang, X., Hu, Y., and Bi, Y. (2012). Involvement of G6PDH in heat stress tolerance in the calli from *Przewalskia tangutica* and *Nicotiana tabacum*. *Biol. plantarum* 56, 422–430. doi: 10.1007/s10535-012-0072-8

Harsh, A., Sharma, Y. K., Joshi, U., Rampuria, S., Singh, G., Kumar, S., et al. (2016). Effect of short-term heat stress on total sugars, proline and some antioxidant enzymes in moth bean (*Vigna aconitifolia*). *Ann. Agric. Sci.* 61, 57–64. doi: 10.1016/j.aoas.2016.02.001

Hasanuzzaman, M., Nahar, K., Alam, M. M., and Fujita, M. (2014). Modulation of antioxidant machinery and the methylglyoxal detoxification system in selenium-supplemented *Brassica napus* seedlings confers tolerance to high temperature stress. *Biol. Trace Element Res.* 161, 297–307. doi: 10.1007/s12011-014-0120-7

Hedhly, A. (2011). Sensitivity of flowering plant gametophytes to temperature fluctuations. *Environ. Exp. Bot.* 74, 9–16. doi: 10.1016/j.envexpbot.2011.03.016

Hinojosa, L., Matanguihan, J. B., and Murphy, K. M. (2019). Effect of high temperature on pollen morphology, plant growth and seed yield in quinoa (*Chenopodium quinoa* Willd.). *J. Agron. Crop Sci.* 205, 33–45. doi: 10.1111/jac.2019.205.issue-1

Hopkins, R. J., Van Dam, N. M., and Van Loon, J. J. (2009). Role of glucosinolates in insect-plant relationships and multitrophic interactions. *Annu. Rev. Entomol.* 54, 57–83. doi: 10.1146/annurev.ento.54.110807.090623

Huang, R., Liu, Z., Xing, M., Yang, Y., Wu, X., Liu, H., et al. (2019). Heat stress suppresses *Brassica napus* seed oil accumulation by inhibition of photosynthesis and BnWRI1 pathway. *Plant Cell Physiol.* 60, 1457–1470. doi: 10.1093/pcp/pcz052

Huang, S., and Millar, A. H. (2013). Succinate dehydrogenase: the complex roles of a simple enzyme. *Curr. Opin. Plant Biol.* 16, 344–349. doi: 10.1016/j.pbi.2013.02.007

Huang, Y. C., Niu, C. Y., Yang, C. R., and Jinn, T. L. (2016). The heat stress factor HSFA6b connects ABA signalling and ABA-mediated heat responses. *Plant Physiol.* 172, 1182–1199. doi: 10.1104/pp.16.00860

Hummel, I., Pantin, F., Sulpice, R., Piques, M., Rolland, G., Dauzat, M., et al. (2010). Arabidopsis plants acclimate to water deficit at low cost through changes of carbon usage: an integrated perspective using growth, metabolite, enzyme, and gene expression analysis. *Plant Physiol.* 154, 357–372. doi: 10.1104/pp.110.157008

Ikram, M., Chen, J., Xia, Y., Li, R., Siddique, K. H. M., and Guo, P. (2022). Comprehensive transcriptome analysis reveals heat-responsive genes in flowering Chinese cabbage (*Brassica campestris* L. ssp. chinensis) using RNA sequencing. *Front. Plant Sci.* 13. doi: 10.3389/fpls.2022.1077920

Impa, S. M., Sunoj, V. S. J., Krassovskaya, I., Bheemanahalli, R., Obata, T., and Jagadish, S. V. K. (2019). Carbon balance and source-sink metabolic changes in winter wheat exposed to high night-time temperature. *Plant Cell Environ.* 42, 1233–1246. doi: 10.1111/pce.13488

Ismaili, A., Salavati, A., and Mohammadi, P. P. (2015). A comparative proteomic analysis of responses to high-temperature stress in hypocotyl of canola (*Brassica napus* L.). *Protein Pept. Lett.* 22, 285–299. doi: 10.2174/0929866521666141124102755

Jagadish, S. K., Way, D. A., and Sharkey, T. D. (2021). Plant heat stress: concepts directing future research. *Plant Cell Environ.* 44, 1992–2005. doi: 10.1111/pce.14050

Jasper, J., Wagstaff, C., and Bell, L. (2020). Growth temperature influences postharvest glucosinolate concentrations and hydrolysis product formation in first and second cuts of rocket salad. *Postharvest Biol. Technol.* 163, 111157. doi: 10.1016/j.postharvbio.2020.111157

Jhingan, S., Harloff, H. J., Abbadi, A., Welsch, C., Blümel, M., Tasdemir, D., et al. (2023). Reduced glucosinolate content in oilseed rape (*Brassica napus* L.) by random mutagenesis of *BnMYB28* and *BnCYP79F1* genes. *Sci. Rep.* 13, 2344. doi: 10.1038/s41598-023-28661-6

Jin, B., Li, W., Jing, W., Jiang, K. Z., Yang, W., Jiang, X. X., et al. (2011). The effect of experimental warming on leaf functional traits, leaf structure and leaf biochemistry in *Arabidopsis thaliana*. *BMC Plant Biol.* 11, 35. doi: 10.1186/1471-2229-11-35

Julius, B. T., Leach, K. A., Tran, T. M., Mertz, R. A., and Braun, D. M. (2017). Sugar transporters in plants: new insights and discoveries. *Plant Cell Physiol.* 58, 1442–1460. doi: 10.1093/pcp/pcx090

Kanehisa, M., and Goto, S. (2000). KEGG: Kyoto encyclopedia of genes and genomes. *Nucleic Acids Res.* 28, 27–30. doi: 10.1093/nar/28.1.27

Kaushal, N., Awasthi, R., Gupta, K., Gaur, P., Siddique, K. H. M., and Nayyar, H. (2013). Heat-stress-induced reproductive failures in chickpea (*Cicer arietinum*) are associated with impaired sucrose metabolism in leaves and anthers. *Funct. Plant Biol.* 40, 1334–1349. doi: 10.1071/FP13082

Koscielny, C. B., Hazebroek, J., and Duncan, R. W. (2018). Phenotypic and metabolic variation among spring *Brassica napus* genotypes during heat stress. *Crop Pasture Sci.* 69, 284–295. doi: 10.1071/CP17259

Kourani, M., Mohareb, F., Rezwan, F. I., Anastasiadi, M., and Hammond, J. P. (2022). Genetic and physiological responses to heat stress in *Brassica napus*. *Front. Plant Sci.* 13. doi: 10.3389/fpls.2022.832147

Kumar, M., Prusty, M. R., Pandey, M. K., Singh, P. K., Bohra, A., Guo, B., et al. (2023). Application of CRISPR/Cas9-mediated gene editing for abiotic stress management in crop plants. *Front. Plant Sci.* 14). doi: 10.3389/fpls.2023.1157678

Lamaoui, M., Jemo, M., Datla, R., and Bekkaoui, F. (2018). Heat and drought stresses in crops and approaches for their mitigation. *Front. Chem.* 6. doi: 10.3389/fchem.2018.00026

Lemoine, R., La Camera, S., Atanassova, R., Dédaldéchamp, F., Allario, T., Pourtau, N., et al. (2013). Source-to-sink transport of sugar and regulation by environmental factors. *Front. Plant Sci.* 24. doi: 10.3389/fpls.2013.00272

Li, M., Li, J., Zhang, R., Lin, Y., Xiong, A., Tan, G., et al. (2022). Combined analysis of the metabolome and transcriptome to explore heat stress responses and adaptation mechanisms in celery (*Apium graveolens* L.). *Int. J. Mol. Sci.* 23, 3367. doi: 10.3390/ijms23063367

Ljubej, V., Radojčić,, Redovniković, I., Salopek-Sondi, B., Smolko, A., Roje, S., et al. (2021). Chilling and freezing temperature stress differently influence glucosinolates content in *Brassica oleracea* var. *acephala*. *Plants (Basel)* 10, 1305. doi: 10.3390/plants10071305

Lohani, N., Singh, M. B., and Bhalla, P. L. (2020). High temperature susceptibility of sexual reproduction in crop plants. *J. Exp. Bot.* 71, 555–568. doi: 10.1093/jxb/erz426

Long, X., He, B., Fang, Y., and Tang, C. (2016). Identification and characterization of the glucose-6-phosphate dehydrogenase gene family in the para rubber tree, *Hevea brasiliensis*. *Front. Plant Sci.* 7. doi: 10.3389/fpls.2016.00215

Love, M. I., Huber, W., and Anders, S. (2014). Moderated estimation of fold change and dispersion for RNA-seq data with DESeq2. *Genome Biol.* 15, 550. doi: 10.1186/s13059-014-0550-8

Marias, D., Meinzer, F. C., and Still, C. (2017). Impacts of leaf age and heat stress duration on photosynthetic gas exchange and foliar nonstructural carbohydrates in *Coffea arabica*. *Ecol. Evol.* 7, 1297–1310. doi: 10.1002/ece3.2017.7.issue-4

Martínez-Ballesta, M., del, C., Moreno, D. A., and Carvajal, M. (2013). The physiological importance of glucosinolates on plant response to abiotic stress in Brassica. *Int. J. Mol. Sci.* 14, 11607–11625. doi: 10.3390/ijms140611607

Mathan, J., Singh, A., and Ranjan, A. (2020). Sucrose transport in response to drought and salt stress involves ABA-mediated induction of OsSWEET13 and OsSWEET15 in rice. *Physiologia Plantarum* 171, 620–637. doi: 10.1111/ppl.13210

Met Office *UK temperature, rainfall and sunshine time series*. Available online at: https://www.metoffice.gov.uk/research/climate/maps-and-data/uk-temperature-rainfall-and-sunshine-time-series (Accessed January 10, 2023).

Mishra, S., Chowdhary, A. A., Mehrotra, S., and Srivastava, V. (2019). Function of plant heat shock transcription factors in abiotic stress. In S. K. Upadhyay (Ed.), *Energy Environ. Sustainability*, 113–126. doi: 10.1007/978-981-15-0690-1_6

Mishra, S. K., Tripp, J., Winkelhaus, S., Tschiersch, B., Theres, K., Nover, L., et al. (2002). In the complex family of heat stress transcription factors, HsfA1 has a unique role as master regulator of thermotolerance in tomato. *Genes Dev.* 16, 1555–1567. doi: 10.1101/gad.228802

Müller, J. L., Krishna, P., and Foreiter, C. (2000). A glucosinolate mutant of *Arabidopsis* is thermosensitive and defective in cytosolic Hsp90 expression after heat stress. *Plant Physiol.* 123, 949–958. doi: 10.1104/pp.123.3.949

Namazkar, S., Stockmarr, A., Frenck, G., Egsgaard, H., Terkelsen, T., Mikkelsen, T., et al. (2016). Concurrent elevation of CO_2, O_3 and temperature severely affects oil quality and quantity in rapeseed. *J. Exp. Bot.* 67, 4117–4125. doi: 10.1093/jxb/erw180

Narayanan, S., Tamura, P. J., Roth, M. R., Prasad, P. V. V., and Welti, R. (2016). Wheat leaf lipids during heat stress: I. High day and night temperatures result in major lipid alterations. *Plant Cell Environ.* 39, 787–803. doi: 10.1111/pce.12649

Narayanan, S., Zoong-Lwe, Z. S., Gandhi, N., Welti, R., Fallen, B., Smith, J. R., et al. (2020). Comparative lipidomic analysis reveals heat stress responses of two soybean genotypes differing in temperature sensitivity. *Plants* 9, 457. doi: 10.3390/plants9040457

Orlemans, K., Barrett, D. M., Bosch Suades, C., Verkerk, R., and Dekker, M. (2006). Thermal degradation of glucosinolates in red cabbage. *Food Chem.* 95, 19–29. doi: 10.1016/j.foodchem.2004.12.013

Osorio, S., Ruan, Y. L., and Fernie, A. R. (2014). An update on source-to-sink carbon partitioning in tomato. *Front. Plant Sci.* 5. doi: 10.3389/fpls.2014.00516

Pacheco-Sangerman, F., Gómez-Merino, F. C., PeraltaSánchez, M., Alcántar-González, G., and Trejo-Téllez, L. I. (2023). Glucosinolates: Structure, classification, biosynthesis and functions in higher plants. *Agro Productividad* 16 (4), 107–114. doi: 10.32854/agrop.v16i3.2567

Pasini, F., Verardo, V., Caboni, M. F., and D'Antuono, L. F. (2012). Determination of glucosinolates and phenolic compounds in rocket salad by HPLC-DAD-MS: Evaluation of *Eruca sativa Mill.* And *Diplotaxis tenuifolia* L. genetic resources. *Food Chem.* 133, 1025–1033. doi: 10.1016/j.foodchem.2012.01.021

Rao, S.-Q., Chen, X.-Q., Wang, K.-H., Zhu, Z.-J., Yang, J., and Zhu, B. (2021). Effect of short-term high temperature on the accumulation of glucosinolates in *Brassica rapa*. *Plant Physiol. Biochem.* 161, 222–233. doi: 10.1016/j.plaphy.2021.02.013

Rask, L., Andréasson, E., Ekbom, B., Eriksson, S., Pontoppidan, B., and Meijer, J. (2000). Myrosinase: gene family evolution and herbivore defense in Brassicaceae. *Plant Mol. Biol.* 42, 93–113. doi: 10.1023/A:1006380021658

Rasmusson, L. M., Buapet, P., George, R., Gullström, M., Gunnarsson, P. C. B., and Björk, M. (2020). Effects of temperature and hypoxia on respiration, photorespiration, and photosynthesis of seagrass leaves from contrasting temperature regimes. J. Norkko (Ed.), ICES. *J. Marine Sci.* 77, 2056–2065. doi: 10.1093/icesjms/fsaa093

Ren, Y., Zhu, J., Zhang, H., Lin, B., Hao, P., and Hua, S. (2022). Leaf Carbohydrate Metabolism Variation Caused by Late Planting in Rapeseed (*Brassica napus* L.) at Reproductive Stage. *Plants* 11, 1696. doi: 10.3390/plants11131696

Rhee, J.-H., Choi, S., Lee, J.-E., Hur, O.-S., Ro, N.-Y., Hwang, A.-J., et al. (2020). Glucosinolate content in brassica genetic resources and their distribution pattern within and between inner, middle, and outer leaves. *Plants* 9, 1421. doi: 10.3390/plants9111421

Rong, Y., Li, T., Liu, X., Shi, S., Wang, X., and Tu, P. (2021). A transaldolase from Aquilaria Sinensis involves in ABA-mediated seed germination and root growth. doi: 10.21203/rs.3.rs-234062/v1

Scafaro, A. P., Fan, Y., Posch, B. C., Garcia, A., Coast, O., and Atkin, O. K. (2021). Responses of leaf respiration to heatwaves. *Plant Cell Environ.* 44, 2090–2101. doi: 10.1111/pce.14018

Seneviratne, S. I., Nicholls, N., Easterling, D.Goodess C., Kanae, S., Kossin, J., et al. (2012). "Changes in climate extremes and their impacts on the natural physical environment," in *Managing the Risks of Extreme Events and Disasters to Advance Climate Change Adaptation*. Ed. C. B. Field, et al (Cambridge University Press, Cambridge, UK, and New York, NY, USA), 109–230. A Special Report of Working Groups I and II of the Intergovernmental Panel on Climate Change (IPCC).

Seth, R., Maritim, T. K., Parmar, R., and Sharma, R. K. (2021). Underpinning the molecular programming attributing heat stress associated thermotolerance in tea (*Camellia sinensis* (L.) O. Kuntze). *Hortic. Res.* 8. doi: 10.1038/s41438-021-00532-z

Song, J. M., Guan, Z., Hu, J., Guo, C., Yang, Z., Wang, S., et al. (2020). Eight high-quality genomes reveal pan-genome architecture and ecotype differentiation of *Brassica napus*. *Nat. Plants* 6, 34–45. doi: 10.1038/s41477-019-0577-7

Sun, F., Fan, G., Hu, Q., Zhou, Y., Guan, M., Tong, C., et al. (2017). The high quality genome of *Brassica napus* cultivar 'ZS11' reveals the introgression history in semi-winter morphotype. *Plant J.* 92, 452–468. doi: 10.1111/tpj.13669

Sun, X., Zhu, J., Li, X., Li, Z., Han, L., and Luo, H. (2020). AsHSP26.8a, a creeping bentgrass small heat shock protein integrates different signaling pathways to modulate plant abiotic stress response. *BMC Plant Biol.* 20, 184. doi: 10.1186/s12870-020-02369-5

Suwa, R., Hakata, H., Hara, H., El-Shemy, H. A., Adu-Gyamfi, J. J., Nguyen, N. T., et al. (2010). High temperature effects on photosynthate partitioning and sugar metabolism during ear expansion in maize (Zea mays L.) genotypes. *Plant Physiol. Biochem.* 48, 124–130. doi: 10.1016/j.plaphy.2009.12.010

Tang, Y., Zhang, G., Jiang, X., Shen, S., Guan, M., Tang, Y., et al. (2023). Genome-wide association study of glucosinolate metabolites (mGWAS) in *Brassica napus* L. *Plants* 12, 639. doi: 10.3390/plants12030639

Touw, A. J., Verdecia Mogena, A., Maedicke, A., Sontowski, R., van Dam, N. M., and Tsunoda, T. (2020). Both biosynthesis and transport are involved in glucosinolate accumulation during root-herbivory in *Brassica rapa*. *Front. Plant Sci.* 10. doi: 10.3389/fpls.2019.01653

USDA. (2025). Oilseeds: World markets and trade. United States Department of Agriculture, Foreign Agricultural Service. https://apps.fas.usda.gov/psdonline/circulars/oilseeds.pdf

Valente Pereira, F. M. V., Rosa, E., Fahey, J. W., Stephenson, K. K., Carvalho, R., and Aires, A. (2002). Influence of temperature and ontogeny on the Levels of glucosinolates in broccoli (*Brassica oleracea* Var. italica) sprouts and their effect on the induction of mammalian phase 2 enzymes. *J. Agric. Food Chem.* 50, 6239–6244. doi: 10.1021/jf020309x

Van Dongen, J. T., Gupta, K. J., Ramírez-Aguilar, S. J., Araújo, W. L., Nunes-Nesi, A., and Fernie, A. R. (2011). Regulation of respiration in plants: A role for alternative metabolic pathways. *J. Plant Physiol.* 168, 1434–1443. doi: 10.1016/j.jplph.2010.11.004

Wahid, A., Gelani, S., Ashraf, M., and Foolad, M. R. (2007). Heat tolerance in plants: An overview. *Environ. Exp. Bot.* 61, 199–223. doi: 10.1016/j.envexpbot.2007.05.011

Wang, L., Ma, K. B., Lu, Z. G., Ren, S. X., Jiang, H. R., Cui, J. W., et al. (2020). Differential physiological, transcriptomic and metabolomic responses of Arabidopsis leaves under prolonged warming and heat shock. *BMC Plant Biol.* 20. doi: 10.1186/s12870-020-2292-y

Wang, J., Yu, H., Zhao, Z., Sheng, X., Shen, Y., and Gu, H. (2019). Natural Variation of Glucosinolates and Their Breakdown Products in Broccoli (*Brassica oleracea* var. italica) Seeds. *J. Agric. Food Chem.* 67, 12528–12537. doi: 10.1021/acs.jafc.9b06533

Way, D. A., and Yamori, W. (2014). Thermal acclimation of photosynthesis: On the importance of adjusting our definitions and accounting for thermal acclimation of respiration. *Photosynthesis Res.* 119, 89–100. doi: 10.1007/s11120-013-9873-7

WeatherOnline *Max temperature London - Observations 05.2017 interval: 02 Weeks | United Kingdom Weather History*. Available online at: https://www.weatheronline.co.uk/weather/maps/city (Accessed January 10, 2023).

Xalxo, R., Yadu, B., Chandra, J., Chandrakar, V., and Keshavkant, S. (2020). Alteration in carbohydrate metabolism modulates thermotolerance of plant under heat stress. In S. H. Wani, S. S. Wani and A. S. A. Bhat (Eds.), *Heat Stress Tolerance Plants*, 77–115. doi: 10.1002/9781119432401.ch5

Yu, E., Fan, C., Yang, Q., Li, X., Wan, B., Dong, Y., et al. (2014). Identification of heat responsive genes in *Brassica napus* siliques at the seed-filling stage through transcriptional profiling. *PloS One* 9, e101914. doi: 10.1371/journal.pone.0101914

Yuenyong, W., Sirikantaramas, S., Qu, L. J., and Buaboocha, T. (2019). Isocitrate lyase plays important roles in plant salt tolerance. *BMC Plant Biol.* 19, 472. doi: 10.1186/s12870-019-2086-2

Zafar, I., Hussain, A. I., Fatima, T., Abdullah Alnasser, S. M., and Ahmad, A. (2022). Inter-varietal variation in phenolic profile, sugar contents, antioxidant, anti-proliferative and antibacterial activities of selected brassica species. *Appl. Sci.* 12, 5811. doi: 10.3390/app12125811

Zafar, S. A., Zaidi, S. S. E. A., Gaba, Y., Singla-Pareek, S. L., Dhankher, O. P., Li, X., et al. (2020). Engineering abiotic stress tolerance via CRISPR/Cas-mediated genome editing. *J. Exp. Bot.* 71, 470–479. doi: 10.1093/jxb/erz476

Zandalinas, S. I., Rivero, R. M., Martínez, V., Gómez-Cadenas, A., and Arbona, V. (2016). Tolerance of citrus plants to the combination of high temperatures and drought is associated to the increase in transpiration modulated by a reduction in abscisic acid levels. *BMC Plant Biol.* 16, 1–16. doi: 10.1186/s12870-016-0791-7

Zhang, S. S., Yang, H., Ding, L., Song, Z. T., Ma, H., Chang, F., et al. (2017). Tissue-specific transcriptomics reveals an important role of the unfolded protein response in maintaining fertility upon heat stress in Arabidopsis. *Plant Cell* 29, 1007–1023. doi: 10.1105/tpc.16.00916

Zheng, G., Tian, B., Zhang, F., Tao, F., and Li, W. (2011). Plant adaptation to frequent alterations between high and low temperatures: Remodelling of membrane lipids and maintenance of unsaturation levels. *Plant Cell Environ.* 34, 1431–1442. doi: 10.1111/j.1365-3040.2011.02341.x

Zhou, L., Yan, T., Chen, X., Li, Z., Wu, D., Hua, S., et al. (2018). Effect of high night temperature on storage lipids and transcriptome changes in developing seeds of oilseed rape. *J. Exp. Bot.* 69, 1721–1733. doi: 10.1093/jxb/ery004

Zoong Lwe, Z., Sah, S., Persaud, L., Li, J., Gao, W., Reddy, K. R., et al. (2021). Alterations in the leaf lipidome of Brassica carinata under high-temperature stress. *BMC Plant Biol.* 21, 404. doi: 10.1186/s12870-021-03189-x

frontiers | Frontiers in Plant Science

TYPE Original Research
PUBLISHED 09 May 2025
DOI 10.3389/fpls.2025.1513353

OPEN ACCESS

EDITED BY
Xiaodong Yang,
Yangzhou University, China

REVIEWED BY
Md Mostofa Uddin Helal,
Shanxi Agricultural University, China
Kaushal Pratap Singh,
Directorate of Rapeseed Mustard Research (DRMR), India

*CORRESPONDENCE
Eva Heinrich
eva.heinrich@agr.uni-goettingen.de

RECEIVED 18 October 2024
ACCEPTED 27 March 2025
PUBLISHED 09 May 2025

CITATION
Heinrich E, Schierholt A and Möllers C (2025) QTL mapping of flowering time in *Brassica napus*: a study on the interplay between temperature and day length after vernalization. *Front. Plant Sci.* 16:1513353. doi: 10.3389/fpls.2025.1513353

QTL mapping of flowering time in *Brassica napus*: a study on the interplay between temperature and day length after vernalization

Eva Heinrich[1]*, Antje Schierholt[2] and Christian Möllers[1]

[1]Department of Crop Sciences, Division of Crop Plant Genetics, Georg-August-University Göttingen, Göttingen, Germany, [2]Department of Crop Sciences, Division of Plant Breeding Methodology, Georg-August University Göttingen, Göttingen, Germany

Flowering is a critical life stage for plants, and the regulation of flowering is heavily influenced by environmental factors and is genetically very complex. In oilseed rape (*Brassica napus* L.), a major oil crop, yield is heavily dependent on successful flowering. Until now, the influences of day length and temperature on flowering time have mostly been studied in spring-type rape, although they also affect flowering in winter oilseed rape after vernalization, and changing climate conditions alter springtime temperatures. In this study, a doubled haploid population derived from a cross between a winter and a spring-type oilseed rape was examined for the effect of cool and warm temperatures (11°C and 22°C) in combination with long and short days (8/16-h light) on flowering time after vernalization. Quantitative trait locus (QTL) analysis revealed major QTLs for flowering time in two homologous regions on chromosomes C06 and A07, which were found to interact epistatically. It was found that temperature can either delay or promote flowering depending on day length and genotype, highlighting the complex interplay between these factors. Our study provides new insights into the genetic basis of flowering time regulation in *B. napus*, especially after vernalization, and highlights the importance of considering the interplay between temperature and day length in breeding programs for this crop, particularly in the context of climate change.

KEYWORDS

epistasis, genetic variation, circadian rhythm, photoperiod, gene homology, winter rape, epigenetic, vernalization

1 Introduction

Flowering time is regulated in a complex network with different pathways that interact with each other and are well studied in *Arabidopsis thaliana* (Blümel et al., 2015; Quiroz et al., 2021). The internal and external signals are thereby controlling the autonomous and gibberellin pathways, as well as the vernalization, temperature, and day length pathways. Most of the environmental cues are sensed in the leaves and lead to the expression of *FLOWERING LOCUS T* (*FT*) through signaling cascades. The FT protein travels to the apical meristem and initiates the generative phase (Jaeger et al., 2013). Oilseed rape (*Brassica napus* L.) is closely related to *Arabidopsis*. However, a genome triplication occurred in the evolution of the genus *Brassica*, and the hybridization of *Brassica rapa* and *Brassica oleracea* led to the allopolyploid species *B. napus* with the A and C subgenomes (Chalhoub et al., 2014). Therefore, genes occur with a high copy number variation, including flowering time genes, which makes flowering time regulation in the *B. napus* complex (Schiessl et al., 2017; Schiessl, 2020).

Vernalization is the initiation of flowering through a prolonged cold period. In crop plants, the requirement of a vernalization period to initiate flowering separates winter crops from spring crops; therefore, the vernalization pathway is well studied in *B. napus* (Ferreira et al., 1995; Raman et al., 2016; Richter and Möllers, 2018; Schiessl et al., 2019).

Studies in *Arabidopsis* have shown the complexity of the molecular mechanisms for the regulatory pathways of day length and temperature. The influence of day length is often regulated over the inner circadian clock with the central regulator CONSTANS, a direct FT activator (Takagi et al., 2023). They are known to interact with each other, as well as with the plant age and the gibberellin pathway, making this one of the most complex pathways for flowering (Song et al., 2013; Kim and Sung, 2014; Blümel et al., 2015). Even though this is the case, many studies on the influence of temperature on flowering have been done without considering other abiotic factors like day length (Schiessl, 2020; Jiang, 2023). In particular, the effect of temperature and day length after vernalization is not studied in *B. napus*. Like *Arabidopsis* (Amasino and Michaels, 2010), oilseed rape is a long-day plant, for which longer day length and higher temperature generally lead to earlier flowering (Major, 1980; King and Kondra, 1986; Mendham and Salisbury, 1995; Nanda et al., 1996; Robertson et al., 2002; Nelson et al., 2014). So far, quantitative trait locus (QTL) mapping studies identified chromosomes A02, A03, A10, C03, C04, C05, and C09 as carrying photoperiod-sensitive genes (Robert et al., 1998; Axelsson et al., 2001; Cai et al., 2008; Luo et al., 2014; Rahman et al., 2018). However, most of the molecular markers used at that time do not allow identification of their physical positions on current reference genomes (Chalhoub et al., 2014; Sun et al., 2017; Lee et al., 2020).

For the effect of temperature, only very few studies have been done, all of them on spring-type rapeseed. Abelenda et al. (2023) studied the difference in flowering time between 21°C and 28°C in different spring-type cultivars. Most cultivars delayed flowering time under the higher temperature, but one genotype accelerated flowering and showed different *FT* expression. Salisbury and Green (1991) reported interactions between temperature and day length on flowering time in spring genotypes of European, Canadian, and Australian origins. In a Canadian spring oilseed rape doubled haploid (DH) population, Rahman et al. (2018) detected QTLs for flowering time for different day lengths and temperature regimes. In *B. rapa*, Xiao et al. (2019) mapped flowering time QTLs for responses to ambient temperature and photoperiod on nearly all chromosomes.

In conclusion, all these studies have shown genotypic differences in response to day length and temperature regarding flowering time regulation. However, the majority of those studies in *B. napus* were done on spring types or the effect of different temperatures during or before vernalization in winter types. Even though rising temperatures during winter and early spring caused by climate change are evident in areas of winter oilseed rape cultivation, the reaction of flowering time in winter oilseed rape to temperature and its interaction with day length has been understudied. Therefore, the objectives of the present work were to test the impact of day length and temperature on flowering time in fully vernalized plants of the DH population DH4079 × Express617 and to assess the interaction between temperature and day length. To achieve these objectives, plants vernalized for 9 weeks were grown under four different controlled conditions with combinations of short and long days (8 and 16 h) and at two temperature regimes (11°C and 22°C) to determine days to flowering. A single-nucleotide polymorphism (SNP) marker-based linkage map was used to map QTLs and identify candidate genes.

2 Methods

2.1 Plant material

The inbred line 617 from the winter oilseed rape cultivar Express (Norddeutsche Pflanzenzucht Hans-Georg Lembke KG, Holtsee, Germany) and the doubled haploid line DH4079 (Ferrie, 2003) from the Swedish spring-type cultivar Topas were crossed to generate F1 seeds. A DH population consisting of 184 lines was developed from clonally propagated F1 plants as described by Valdés et al. (2018).

2.2 Day length and temperature experiment

The effect of day length and temperature on the flowering time of fully vernalized plants was determined in a split–split plot design with two-factor levels in temperature (11°C and 22°C) and two-factor levels in day length (8 and 16 h) with five replications. Seeds of 184 DH lines, the parental genotypes, and the F1 were sown in two 96 multi-pot trays (Quickpot 96, HerkuPlast Kubern GmbH, Ering, Germany) with a total size of 335 × 515 mm in four duplicates. Single pots had a size of 38 × 38 × 78 mm and were

filled with soil (Fruhstorfer Erde type T25, HAWITA Gruppe GmbH, Vechta, Germany) and cultivated for 3 to 4 weeks in the greenhouse until the two- to three-leaf developmental stages (BBCH 12 to 13; Lancashire et al., 1991). Then, the multi-pot trays were transferred to a vernalization chamber adjusted to 4°C–5°C and 8 h cool white light (Schuch Typ 164/12 L96C 82W) for 9 weeks. After vernalization, the plants were transferred to two growth chambers with different temperatures, which were divided with sheets impervious to light to allow treatment with different day lengths. Therefore, the conditions consisted of 4 day length and temperature combinations of 8 h/11°C (SD11), 8 h/22°C (SD22), 16 h/11°C (LD11), and 16 h/22°C (LD22). For testing the effect of day lengths and temperatures, the positions of the genotypes on the multi-pot trays were randomized in each replication and condition. Growth chambers were equipped with Philips MASTER Green Power CG T 400 W, providing light intensities of 110–120 $\mu mol \cdot m^{-2} \cdot s^{-1}$. Plants were watered and fertilized on a regular basis and treated with fungicides and insecticides, when necessary. Days to flowering (DTF) was recorded starting from the day of transfer to the climate chamber. Replications were terminated at day 135. Genotypes that did not flower at day 135 but showed buds were recorded with a value of 150 DTF, and if they did not show buds, they were recorded with a value of 165 DTF. The means over all replications of each condition were used to calculate differences in days to flowering. Differences between DTF under short and long days at the same temperature (SD-LD11 and SD-LD22) and between low and high temperatures under the same day length (11-22LD and 11-22SD) were calculated. A full list of phenotypic data is available in Supplementary Table S1.

2.3 Statistical analysis

PLABSTAT 3A software (Utz, 2011) was used to calculate the analysis of variance and heritabilities. The ANOVA for day length and temperature experiment was performed using the model for a split–split plot design: $Y_{ijkl} = \mu + r_i + t_j + r_i t_j + d_k + t_j d_k + r_i t_j d_k + g_l + g_l t_j + g_l d_k + g_l t_j d_k + g_l t_j d_k r_i$, where Y_{ijkl} is the trait value of the genotype l in the day length condition k and the temperature condition j in replication i; μ is the general mean; t_j and r_i are the effects of temperature j and replication i, respectively; and $r_i t_j$ is the interaction between the ith replication and jth temperature, which is treated as the first stratum error. The effect of the kth day length is d_k, and $t_j d_k$ is the interaction between the jth temperature and kth day length, $r_i t_j d_k$ is the second stratum error (interactions between the ith replication, jth temperature, and kth day length; g_l is the effect of the lth genotype; $g_l t_j$, $g_l d_k$, and $g_l t_j d_k$ are the interactions between the lth genotype with the jth temperature and kth day length, while $g_l t_j d_k r_i$ is the third stratum error term. The factors genotypes and replications were taken as random. Broad-sense heritabilities were calculated using the formula $H^2 = \sigma_g^2 / (\sigma_g^2 + \sigma_{gtde}^2 / T)$, with coefficient T = 20 as the product of all factor levels.

Other statistical analyses were performed in R (R. Core Team, 2019). Figures of the descriptive statistics were created in R using the package ggplot2 (Wickham, 2016; R. Core Team, 2019). A Tukey's test was used to test significant differences ($p \leq 0.01$) between subgroups in figures with a box plot.

2.4 QTL analysis

A previously published full marker map consisting of 21,583 markers distributed over 19 linkage groups was used to develop a bin map of 1,883 markers (Valdés et al., 2018). Mean values over the five replications were used in QTL mapping for all traits. QTL mapping was performed using the WinQTL Cartographer software version 2.5 (Wang et al., 2012), and the composite interval mapping (CIM) algorithm was employed with the following specifications: independent logarithm of odds (LOD) significance thresholds ($\alpha = 0.05$) were estimated for each trait by 1,000 permutation tests. Model 6 was employed; the forward and backward stepwise regression method was used to set cofactors. The genome was scanned at 1-cM intervals, and the window size was set to 10 cM. The 95% confidence interval for each QTL was determined by one LOD drop from the peak position. Additive effects, as well as the percentage of phenotypic variance explained by a QTL, were determined. A positive additive effect of a QTL is an additive effect by the allele of the winter oilseed rape parent Express617. To test epistasis, a multiple-interval mapping method was used. QTLs found in CIM were used as input and the BIC-M0 model with 1-cM walk speed and 10-cM window size. Additive × additive effects were significant with a LOD score of 2.4.

SNP marker sequences were provided by Isobel Parkin (AAFC, Saskatoon, SK, Canada), aligned using the BLAST algorithm against the reference genome sequence of "Express617" (Lee et al., 2020) by use of the Galaxy BLASTn-short algorithm (Cock et al., 2015), and used to create a physical map. Figures of the maps were drawn using MapChart (Voorrips, 2002). Gene annotation was provided by Schilbert et al. (2021).

3 Results

3.1 Quantifying the effect of day length and temperature on flowering time of fully vernalized plants

According to the analysis of variance, DTF is predominantly influenced by the effect of day length (Table 1). The size of the variance components for the effect of day length was almost 20 times that of the temperature and more than two times that of the genotype. The size of the variance components for the temperature × day length interaction was 1.5 times that of the effects of temperature. DTF showed a high broad-sense heritability of $H^2 = 95\%$. Short-day (SD) conditions (8-h light) delayed the mean DTF in the DH population, as well as for the parents and F1, but also increased the range (Table 2).

The mean of the DH lines showed an earlier flowering time due to higher temperatures under long-day (LD) conditions (16-h light) from 52 days at 11°C to 35 days at 22°C. The range increased under 22°C and SD conditions (Table 2, Figure 1). Under SD conditions,

10.3389/fpls.2025.1513353

TABLE 1 Components of variance and broad-sense heritability (H^2) for days to flowering for the DH population DH4079 × Express617 (n = 184) at two different temperatures T (11°C and 22°C) and two different day length conditions D (8 h and 16 h) after full vernalization treatment.

Source	Degrees of freedom	Components of variance	
Replication (R)	4	36.1	*
Temperature (T)	1	34.9	**
Day length (D)	1	656.9	***
Genotype (G)	183	244.9	***
R × T	4	17.2	**
D × T	1	53.4	***
R × D × T	14	9.3	***
T × G	183	30.1	***
D × G	183	91.2	***
D × T × G	183	12.1	**
R × D × T × G	2,641	236.8	
H^2 (%)		95	

* p ≤ 0.10, ** p ≤ 0.05, and *** p ≤ 0.01.

the means for DTF under the two temperature regimes were no longer significantly different (Table 2, Figure 1). In all conditions, the winter oilseed rape parent Express617 flowered later than the spring-type parent DH4079, and the F1 showed an intermediate phenotype but had values slightly closer to those of the spring-type parent (Figure 1).

The effect of day length differences on DTF in the DH population, calculated by subtracting DTF under LD from DTF under SD, had in a temperature of 22°C a population mean of SD-LD22 = 43 days and in 11°C only SD-LD11 = 29 days (Table 2). However, under both temperatures, the range was extensive from −4 up to 100 days of difference in flowering time. In the winter oilseed rape parent Express617, the effects of day length differences were SD-LD11 = 32 days and SD-LD22 = 60 days, while the effects in the spring-type parent DH4079 were lower and similar in both temperatures (SD-LD11 = 15 and SD-LD22 = 16 days).

The effect of temperature differences, calculated by subtracting DTF at 22°C from 11°C at the respective day lengths, showed under LD a population mean of 11-22LD = 17 days and under SD a mean of 11-22SD = 3 days differences in flowering (Table 2). The values for this effect of temperature differences on the DH lines ranged between −20 and 44 days under the long-day conditions (11-22LD) and between −44 and 40 days under the short-day conditions (11-22SD). This range showed the ability of warmer temperatures to either accelerate or delay DTF compared to cool temperatures, depending on the genotype and in interaction with the day length conditions. Under LD conditions, the effect of temperature differences on the spring-type parent DH4079 was 11-22LD = 21 days, with an acceleration of flowering through warmer temperatures. In the winter-type parent Express617, the value was lower with 11-22LD = 14 days, and the F1 showed an intermediate phenotype. Under SD, the warmer temperature led to a delayed flowering time in Express617 with 11-22SD = −15 days, while still accelerating in the F1 (11-22SD = 12 days) and DH4079 (11-22SD = 19 days, Table 2, Figure 1). For DH4079, the effects of temperature differences showed similar values with 11-22LD = 21 days and 11-22SD = 19 days as the effects of day length differences, indicating no interaction between temperature and day length in this parental genotype (Table 2).

3.2 Identification of major genomic regions with clusters of QTL

The QTL analysis (Table 3) revealed between four and seven QTLs for each trait, which when summed up could explain between

TABLE 2 Descriptive statistics for days to flowering of vernalized plants of the DH4079 × Express617 DH population grown under four different conditions, with different temperatures (11°C and 22°C) and different day lengths: short day (SD; 8 h) and long day (LD; 16 h).

	DH lines (n = 184)				Parental genotypes				
Condition	Min	Max	Median	Mean	DH4079	F1	Express617	LSD 5%	H^2 [%]
LD 11°C	34	89	51	52	38	49	72	9.9	84
LD 22°C	17	105	31	35	17	30	58	13.4	87
SD 11°C	42	153	78	80	52	75	103	15.8	90
SD 22°C	28	165	74	78	33	63	118	29.8	86
Effect of day length differences on DTF									
SD-LD 11°C	−4	66	26	29	15	26	32		
SD-LD 22°C	7	100	40	43	16	34	60		
Effect of temperature differences on DTF									
11-22°C LD	−20	44	18	17	21	19	14		
11-22°C SD	−44	40	5	3	19	12	−15		

Effects of temperature and day length differences on DTF were calculated for each genotype.
LSD 5%, least significant difference; DTF, days to flowering.

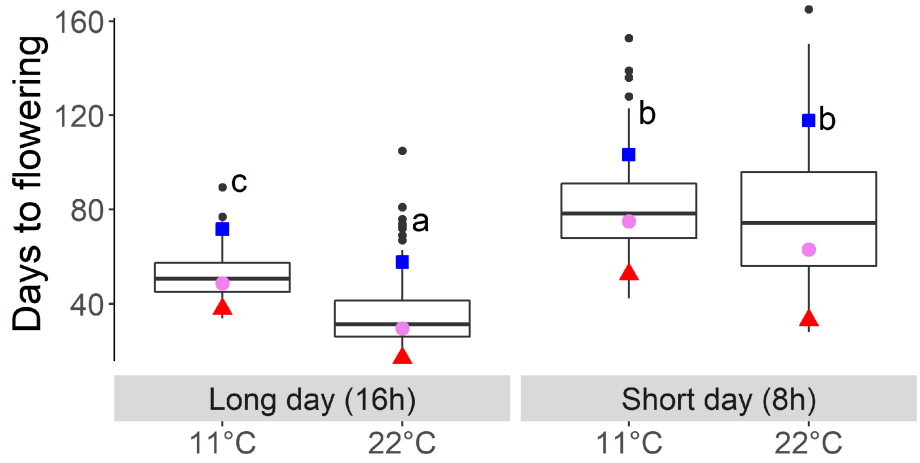

FIGURE 1
Days to flowering of the fully vernalized DH population growing under different temperatures (11°C and 22°C) and day length (short- and long-day) conditions. Letters indicate significantly different subgroups ($p \leq 0.01$) tested with Tukey's test. Winter oilseed rape parent Express617 is indicated with blue square, spring-type parent DH4079 indicated with red triangle, and F1 indicated with violet circle.

TR^2 = 38.6% and 65.2% of the phenotypic variance of the respective trait (Table 3). Most QTLs for days to flowering showed a positive effect, except for QTLs on A05 (LD22-3) and C06 (LD22-7, SD11-5, SD11-6, and SD22-5), indicating that the delay of flowering was caused mainly by Express617 alleles (Table 3). Certain regions of the genome showed an accumulation of QTLs. The major QTLs were forming clusters on chromosomes A07 and C06 (Figures 2, 3).

3.2.1 QTLs on chromosome A07

On the linkage group A07, two QTL clusters were identified (Figure 2). At the beginning of the genetic map between 0 and 9.9 cM, four QTLs were located, three of which are related to flowering under short days (SD11-2, SD22-2, SD-LD11-1, and LD11-2). The major QTLs of both traits regarding DTF under SD conditions collocated here; QTL SD11-2 at 0 cM explained R^2 = 24.9% of the variance with an additive effect of 10.3 days, and QTL SD22-2 at 0 cM explained R^2 = 28.1% with an additive effect of a = 17.6 days. The second-largest QTL LD11-2 for the trait DTF under 11°C and LD was positioned at 0 cM with an explained variance of R^2 = 9.5% and an additive effect of a = 2.9 days. Since the peaks for those three QTLs were located at 0 cM, the real QTLs may be located outside of the genetic map. The major QTL for the effect of day length differences at 11°C, SD-LD11-1, was located on A07 at 7.2 cM with an explained variance of R^2 = 30.1% and an additive effect of a = 7.6 days. For all four QTLs, the Express617 allele delayed flowering. Between 24.5 and 30.9 cM on the same chromosome A07, three QTLs formed a second cluster; two major QTLs for the temperature differences were mapped here, even though the confidence intervals did not overlap (Figure 2), and one QTL for day length differences at 22°C was mapped. For temperature differences under LD, the largest QTL 11-22LD-2 at 30.4 cM explained a phenotypic variance of R^2 = 18.7% and an additive effect of a = −3.7 days. For temperature differences under SD, the largest QTL 11-22SD-2 mapped at 26.8 cM and explained R^2 = 15.2% of the phenotypic variance with an additive effect of a = −6.7 days. Their additive effects were negative, meaning that the Express617 allele made this effect smaller by either delaying DTF at 22°C or accelerating DTF under 11°C. The second-largest QTL for day length differences at 22°C (SD-LD22-1) was located on A07 at 27.8 cM, falling into the confidence interval of 11-22SD-2 (Figure 2), and explained R^2 = 9.3% of the phenotypic variance (a = 8.1 days).

3.2.2 QTLs on chromosome C06

At the beginning of C06 from 0 to 6.7 cM, a QTL cluster for DTF in SD was located (Figure 3). The second-largest QTL for DTF in warm SD conditions, SD22-5, was located on C06 at 0 cM (R^2 = 14.4%, a = −12.7 days). It had overlapping confidence intervals with the third largest QTL for DTF in cool SD conditions, SD11-5 (R^2 = 11.3%, a = −6.9 days), and the second-largest QTL for the effect of day length difference under 11°C, SD-LD11-4 (R^2 = 16.6%, a = −5.6 days), which were both collocated on C06 at 2 cM.

On the same chromosome C06 between 18.8 and 39.1 cM, a QTL cluster with four QTLs regarding the reaction of DTF to day length and temperature was located. The effects of temperature difference under SD and LD were both mapped with their second-largest QTL in this cluster, although they showed no overlapping confidence intervals. QTL 11-22LD-5 on C06 at 21.6 cM explained R^2 = 14.7% of the variance with a positive additive effect of a = 3.3 days. QTL 11-22SD-4 on C06 at 27.3 cM explained R^2 = 11.9% of the variance with a positive additive effect of a = 6.0 days. The effect of day length differences at 22°C had its major QTL SD-LD22-4 on C06 at 28.3 cM with R^2 = 18.1% explained variance and an additive effect of a = −9.9 days, meaning the DH4079 allele at this position delayed flowering under SD. The DTF under SD and 11°C mapped with the minor QTL SD11-6 at 29.3 cM and an explained variance of R^2 = 3.2% and a = −3.7 days. The three QTLs 11-22SD-4, SD-LD22-4, and SD11-6 had overlapping confidence intervals.

TABLE 3 Quantitative trait loci mapped for DTF under different temperature and day length conditions, the effects of temperature, and the effects of day length in the DH4079 × Express617 population.

QTL_name	Chr.	Position [cM]	CI [cM][a]			Marker flanking CI left	Marker flanking CI right	LOD	Additive	R^2 [%][b]	TR^2 [%][c]
Long day at 11°C											
LD11-1	A02	54.4	53.6	–	56	Bn-A01-p16630613	Bn-A02-p8549867	16.0	4.4	23.1	46.4
LD11-2	A07	0.0	0	–	4.6	Bn-scaff_24104_1-p344071	Bn-A07-p21478337	7.4	2.9	9.5	
LD11-3	C02	5.6	3.3	–	7.2	Bn-A02-p1705187	Bn-scaff_15714_1-p3087640	6.3	2.7	7.9	
LD11-4	C02	62.6	58.3	–	65.2	Bn-scaff_23546_1-p103326	Bn-scaff_16449_1-p318325	4.7	2.2	5.9	
Long day at 22°C											
LD22-1	A02	30.3	26.2	–	33.5	Bn-A02-p24449690	Bn-A02-p21930156	10.3	5.2	13.5	64.5
LD22-2	A02	54.4	51.81	–	56.91	Bn-A02-p11713324	Bn-A02-p8057234	4.4	3.8	4.9	
LD22-3	A05	8.7	4.9	–	16.9	Bn-A05-p917769	Bn-A05-p2254100	3.5	−2.7	3.9	
LD22-4	A07	18.0	15.1	–	23.2	Bn-A07-p21271213	Bn-A07-p19912379	11.9	5.7	16.2	
LD22-5	C02	5.6	3.8	–	6.7	Bn-scaff_17752_1-p128342	Bn-scaff_22970_1-p213807	7.2	4.4	9.1	
LD22-6	C02	73.4	71.1	–	77.2	Bn-scaff_15712_2-p104622	Bn-scaff_17109_4-p101748	5.4	3.6	6.7	
LD22-7	C06	14.8	10.8	–	18.5	Bn-A07-p20999615	Bn-A07-p20251365	7.2	−4.6	10.1	
Short day at 11°C											
SD11-1	A02	21.5	21	–	23.6	Bn-A02-p24844291	Bn-A02-p24708197	4.0	4.1	5.0	63.0
SD11-2	A07	0.0	0	–	2.4	Bn-scaff_24104_1-p344071	Bn-A07-p21995054	17.5	10.3	24.9	
SD11-3	C02	3.5	1.5	–	6.7	Bn-A02-p1705187	Bn-scaff_22970_1-p213807	11.0	7.4	14.5	
SD11-4	C02	66.2	65.2	–	69.3	Bn-scaff_16449_1-p318325	Bn-scaff_15712_6-p470292	3.4	3.8	4.2	
SD11-5	C06	2.0	0	–	4.6	Bn-A07-p22140320	Bn-A07-p21587819	8.4	−6.9	11.3	
SD11-6	C06	29.3	27.4	–	39.1	Bn-scaff_15763_1-p1492117	Bn-scaff_16903_1-p230137	2.8	−3.7	3.2	
Short day at 22°C											
SD22-1	A02	52.3	50.3	–	55.9	Bn-A02-p12449263	Bn-A02-p8549867	3.1	5.5	3.4	65.2
SD22-2	A07	0.0	0	–	1.6	Bn-scaff_24104_1-p344071	Bn-A07-p21995054	19.2	17.6	28.1	
SD22-3	C02	11.7	8.2	–	14.2	Bn-scaff_15714_1-p2978071	Bn-scaff_15714_1-p2481342	9.0	10.6	11.7	
SD22-4	C02	73.4	64.21	–	78.01	Bn-scaff_16298_1-p102179	Bn-scaff_17109_1-p1144887	6.1	8.2	7.5	
SD22-5	C06	0.0	0	–	2	Bn-A07-p22140320	Bn-A07-p21587819	11.0	−12.7	14.4	

(Continued)

10.3389/fpls.2025.1513353

TABLE 3 Continued

QTL_name	Chr.	Position [cM]	CI [cM][a]			Marker flanking CI left	Marker flanking CI right	LOD	Additive	R^2 [%][b]	TR^2 [%][c]
Effect of day length under 11°C (calculated difference between SD11 and LD11)											
SD-LD11-1	A07	7.2	7.2	–	9.9	Bn-A07-p21478337	Bn-A07-p21271213	18.2	7.6	30.1	60.6
SD-LD11-2	C02	12.3	12.2	–	14.7	Bn-scaff_15714_1-p2978071	Bn-scaff_15714_1-p2481342	7.0	4.2	10.0	
SD-LD11-3	C03	0.5	0	–	1	Bn-scaff_16614_1-p1995086	Bn-scaff_16614_1-p1467715	2.9	2.9	3.9	
SD-LD11-4	C06	2.0	0	–	6.7	Bn-A07-p22140320	Bn-A07-p21354084	10.9	−5.6	16.6	
Effect of day length under 22°C (calculated difference between SD22 and LD22)											
SD-LD22-1	A07	27.8	27.3	–	28.8	Bn-A07-p18985169	Bn-A07-p17930992	6.2	8.1	9.3	38.6
SD-LD22-2	C02	11.7	7.2	–	16.1	Bn-scaff_22970_1-p213807	Bn-A02-p2776634	4.4	5.8	6.7	
SD-LD22-3	C02	80.6	75.41	–	90.31	Bn-scaff_17088_1-p12134	Bn-scaff_17623_1-p119334	3.1	4.5	4.5	
SD-LD22-4	C06	28.3	26.5	–	31.4	Bn-A07-p17598687	Bn-scaff_18206_3-p49133	11.2	−9.9	18.1	
Effect of temperature under LD (calculated difference between LD11 and LD22)											
11-22LD-1	A05	13.8	9.6	–	17.3	Bn-A05-p1347246	Bn-A05-p2254100	4.0	2.1	6.9	51.5
11-22LD-2	A07	30.4	29.6	–	30.9	Bn-A07-p17930992	Bn-A07-p13247613	10.3	−3.7	18.7	
11-22LD-3	C01	40.7	39.1	–	42.6	Bn-scaff_19193_1-p725427	Bn-scaff_17731_1-p166950	2.9	−1.8	4.8	
11-22LD-4	C02	74.4	74.2	–	77.3	Bn-scaff_22144_1-p193415	Bn-scaff_17109_4-p101748	3.7	−2.0	6.2	
11-22LD-5	C06	21.6	18.8	–	23.7	Bn-A07-p20251365	Bn-A07-p19093712	8.3	3.3	14.7	
Effect of temperature under SD (calculated difference between SD11 and SD22)											
11-22SD-1	A05	7.2	4.1	–	8.2	Bn-A05-p761283	Bn-A05-p1335771	4.1	4.3	6.9	39.7
11-22SD-2	A07	26.8	24.5	–	29.3	Bn-A07-p19912379	Bn-A07-p17930992	8.5	−6.7	15.2	
11-22SD-3	C02	76.5	69.81	–	79.51	Bn-scaff_15712_6-p662107	Bn-scaff_17109_1-p859844	3.4	−3.9	5.7	
11-22SD-4	C06	27.3	25.2	–	28.3	Bn-A07-p18947073	Bn-A07-p12876226	6.9	6.0	11.9	

DTF, days to flowering; QTL, quantitative trait locus.
[a]95% confidence interval.
[b]Explained phenotypic variance of the QTL.
[c]Phenotypic variance explained by all QTLs of the trait.

10.3389/fpls.2025.1513353

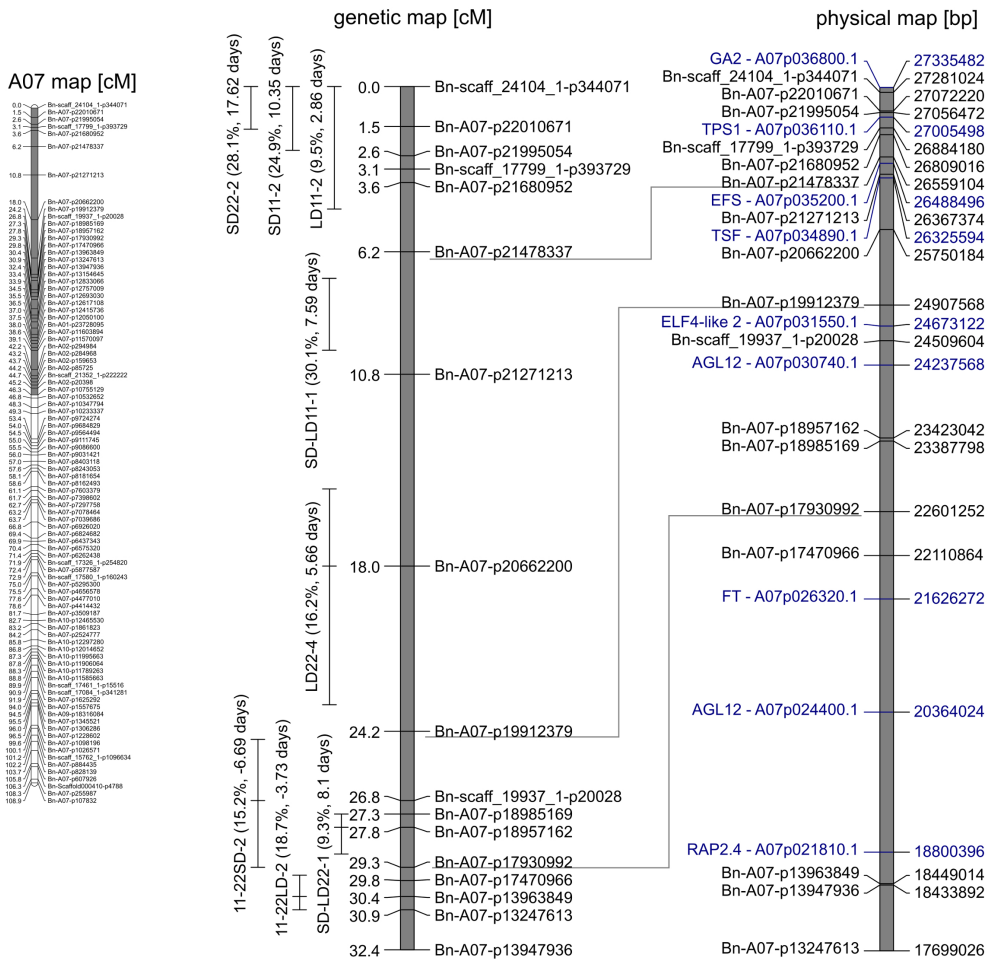

FIGURE 2
Gray marked in genetic map of A07 (left) is the section enhanced on the right. Genetic (middle) map depicts the quantitative trait loci (QTLs) clustering on A07. QTLs are given with peak and 95% confidence interval. The phenotypic variance explained (in percent) and additive effect (in days) of the QTL are shown in brackets. In the corresponding physical (left) map, candidate genes (blue) and the respective gene ID in the reference genome of "Express617" are shown.

Interestingly, the Express617 allele accelerated flowering under short days and warm temperatures in both clusters, contrary to the cluster on A07.

3.2.3 Epistatic effects between QTLs on A07 and C06

Seven traits showed a QTL on both A07 and C06. For six of these traits, additive × additive epistatic effects were found between QTLs on chromosomes A07 and C06. The epistatic effect between QTL SD11-2 on A07 and QTL SD11-5 on C06 with an effect of a × a = −7.0 was the strongest epistatic effect in this study (Table 4). When grouping the DH population by the alleles of two markers located near the short day-sensitive clusters, one on A07 (Bn-A07-p21478337, 6.2 cM) and one on C06 (Bn-A07-p21354084, 7.7 cM), the epistatic effect can be observed in the phenotype (Figures 4, 5). Tukey's test between the four haplotype groups showed no significant difference between the two groups that shared the DH4079 allele on A07 ($A_{DH}C_{DH}$ and $A_{DH}C_{Exp}$) under any condition. Therefore, the DH allele on A07 masked the allelic effect on C06. Except for cool long-day conditions at 11°C, the allele combination $A_{Exp}C_{DH}$ resulted in a late flowering group of genotypes.

3.3 Presentation of known flowering time genes in the QTL regions on A07 and C06

The cluster for DTF under short days at the beginning of the genetic map of A07 consisted of three QTLs (SD11-2, SD22-2, and LD11-2). Since the peaks for those three QTLs were located at 0 cM, the real QTLs may be located outside of the genetic map. Two possible candidate genes were located in this genomic region: *GA REQUIRING 2* (*GA2*) was located outside of the genetic map, and *TREHALOSE-6-PHOSPHATE SYNTHASE 1* (*TPS1*) was located between two markers in the confidence interval of QTL LD11-2 (Figure 2). As a possible candidate gene, *EARLY FLOWERING IN SHORT DAYS* (*EFS*) was identified for the QTL for the effect of day length differences at 11°C, SD-LD11-1, at 7.2 cM (Figure 2).

10.3389/fpls.2025.1513353

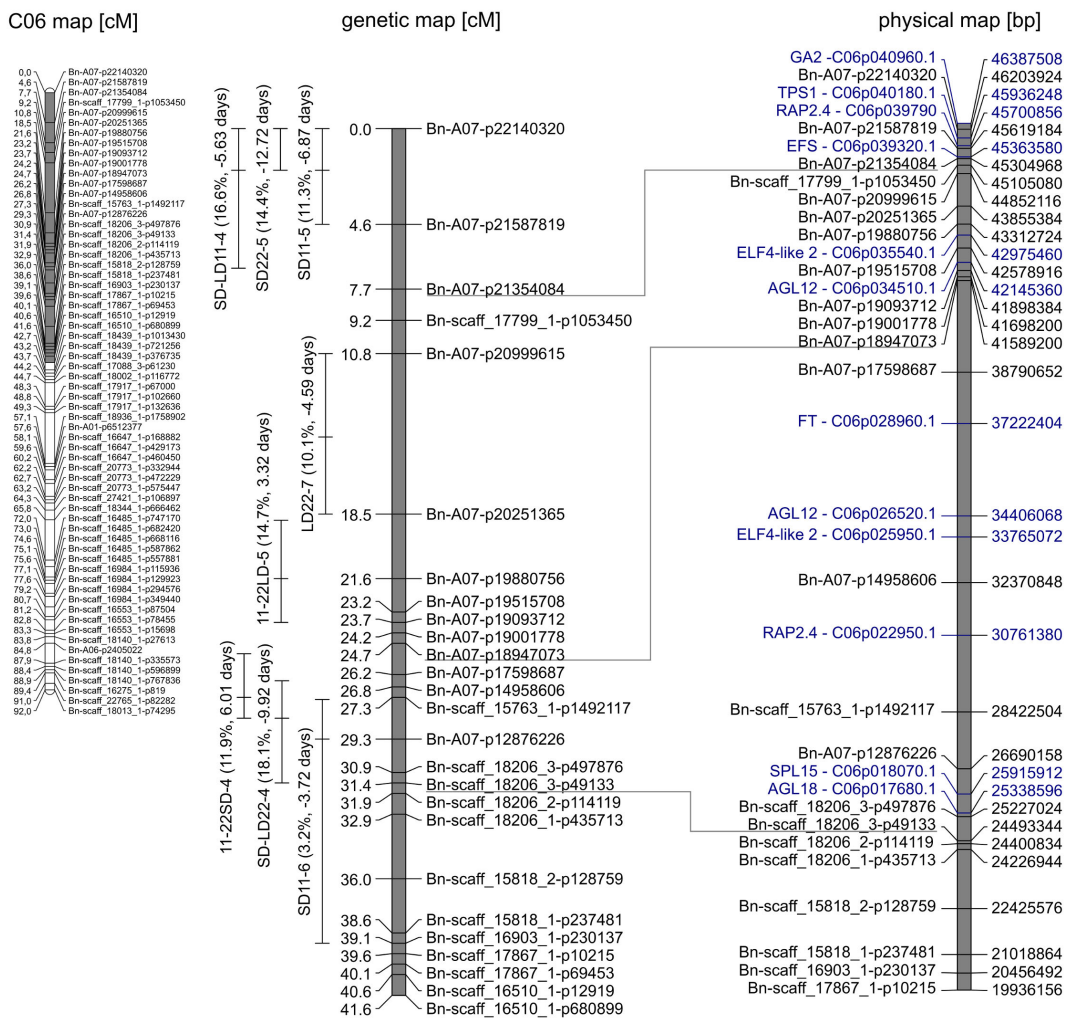

FIGURE 3
Gray marked in genetic map of C06 (left) is the section enhanced on the right. Genetic (middle) map depicts the quantitative trait loci (QTLs) clustering on C06. QTLs are given with peak and 95% confidence interval. The phenotypic variance explained (in percent) and additive effect (in days) of the QTL are shown in brackets. In the corresponding physical (right) map, candidate genes (blue) and the respective gene ID in the reference genome of "Express617" are shown.

The second QTL cluster formed between 24.5 and 30.9 cM on chromosome A07. Here, two major QTLs for the temperature differences were mapped (11-22SD-2 and 11-22LD-2), as well as one QTL for day length differences at 22°C (SD-LD22-1). No known flowering time gene could be found for the confidence interval of SD-LD22-1. With regard to the QTL for temperature difference, the confidence interval of QTL 11-22SD-2 covered a genomic region with *AGAMOUS-LIKE 12* (*AGL12*) and *EARLY FLOWERING4-like 2* (*ELF4-like2*) homologs. The confidence interval of QTL 11-22LD-2 included copies of *FLOWERING LOCUS T* (*FT*), *AGL12*, and *RELATED TO AP2 4* (*RAP2.4*) as possible candidate genes (Figure 2).

At the beginning of C06, the QTL cluster for DTF in SD was located from 0 to 6.7 cM (Figure 3). The peak of SD22-5 and the confidence intervals of all three reached the end of the genetic map, which means that genes located outside the genetic map should be considered; therefore, *GA2* is another possible candidate gene (Figure 3) similar to the cluster on A07. Homologs of *TPS1* and *RAP2.4* were identified as candidate genes for QTLs SD22-5, SD11-5, and SD-LD11-4; *EFS* was identified as an additional possible candidate gene for SD-LD11-4 (Figure 3). On chromosome C06 between 18.8 and 39.1 cM, a QTL cluster with four QTLs regarding the reaction of DTF to day length and temperature was located. For QTLs 11-22SD-4 and SD-LD22-4, *FT*, *AGL12*, *ELF4-like2*, and *RAP2.4* were identified as possible candidate genes. The genes *SPL15* and *AGL18* are possible candidate genes for SD-LD22-4 and SD11-6.

The physical maps of A07 and C06 show many homologs of the same genes in between them, and QTLs of the same trait are often located near homologous genes on A07 and C06 (Figures 2, 3). According to Chalhoub et al. (2014), these regions are homoeologous in the reference genome Darmor-*bzh*. Our results indicate that the homology between the chromosomes is also true

for the used reference genome Express617 (Lee et al., 2020) and our population.

4 Discussion

4.1 Short days delay flowering after vernalization

The aim of this study was to close a research gap in quantifying the effect of temperature and day length after vernalization on DTF, especially in material with a genetic background in both spring- and winter-type oilseed rape. Plants were vernalized for 9 weeks and grown in two different day length conditions (8 and 16 h) as well as two different temperature conditions (11°C and 22°C). With regard to day length, it was confirmed that short-day conditions delay flowering time. The genetic analysis showed that QTLs of the same trait mapped on homoeologous regions on A07 and C06, which, therefore, resulted in similar candidate genes and epistatic effects.

Previous studies in *Arabidopsis* and *Brassica* have shown that these long-day plants show a late flowering genotype under SD conditions. In *Brassica* species, a change of day length between 12 and 14 h showed the biggest response (King and Kondra, 1986; Nanda et al., 1996). Later flowering genotypes showed stronger responses to photoperiod than early flowering genotypes (King and Kondra, 1986; Robertson et al., 2002). The DH population of this study also showed a strong delay of DTF under SD conditions after the vernalization requirement was fulfilled, even to the point where some genotypes did not even start flowering at the end of the experiment (Figure 1). However, genetic variation in the amount of delay was observed as shown by the calculation of the effects of day length (SD-LD11°C and SD-LD22°C) and the range of DTF (Table 2, Figures 1, 5). The delay of flowering under short days was observed in both parental genotypes (Table 2; Figure 1). The QTL analysis revealed two important genomic regions, where several QTLs for DTF under SD conditions and the effects of day length differences formed clusters. The clusters were located on homoeologous regions on A07 and C06, which means that they were orthologous in the two ancestral species of *B. napus*: *B. rapa* and *B. oleracea* (Chalhoub et al., 2014). The cluster on chromosome A07 was located between 0 and 9.9 cM, where QTLs for DTF under short day (SD22-2 and SD11-2) collocated and a QTL for the effect of day length differences at 11°C SD-LD11-1 was located nearby (Figure 2). The cluster at the beginning of the genetic map of C06 was located between 0 and 6.7 cM, where the confidence interval of QTL SD22-5 overlapped with that of QTLs SD11-5 and SD-LD11-4 (Figure 3). However, the direction of the additive effect was different between the clusters on A07 and C06. For the QTL on A07, the winter oilseed rape Express617 allele delayed flowering in short-day conditions. In contrast to that, the additive effect was negative for the QTL on C06 with the spring-type DH4079 allele delaying flowering in short days. Additionally, epistatic effects were recorded between the respective QTLs (Table 4). The DH alleles on A07 masked the allelic effect on C06, as the group with the $A_{DH}C_{DH}$ haplotype and the group with the $A_{DH}C_{Exp}$ haplotype showed no significant difference in their means according to Tukey's test (Figures 4, 5). The allele combination $A_{Exp}C_{DH}$ resulted in the largest delay in flowering under short days and also warm long-day conditions (Figure 4), as can be seen especially in the effect of day length differences, where this allele combination was always significantly different from the others (Figure 5). In both homologous genomic regions, copies of the flowering time candidate genes *GA2*, *EFS*, and *TPS1* were located. In *A. thaliana*, TPS1 is the protein responsible for the synthesis of trehalose-6-phosphate (T6P), a sugar signal. TPS1 is necessary for the expression of *FT* and other flowering-inducing genes (Wahl et al., 2013). However, there is no current knowledge about the influence of *TPS1* on flowering through the day length pathways. The protein GA2 is part of the gibberellin synthesis (Berardini et al., 2015). Gibberellin (GA) is a phytohormone that activates flowering but is also involved in many other developmental and stress pathways. Variations in the gene *GA2* would, therefore, influence more phenotypic traits than flowering time. EFS is known in *Arabidopsis* as an *FLC* activator (recruited by the *PAF1*-like complex), meaning its activity delays flowering (Kim et al., 2005). Kim et al. (2005) showed that a mutation in *EFS* accelerates flowering time under short days more than *fri* or *flc* mutations with an active *EFS*. Thus, there is an *FLC*-independent effect of *EFS* on flowering time under short days, whose mechanism is not yet known.

Previous QTL studies in *B. napus* did not present photosensitive QTLs on A07 and C06 but on several other parts of the genome on chromosomes A02, A03, A10, C03, C04, C05, and C09 (Robert et al., 1998; Axelsson et al., 2001; Cai et al., 2008; Luo et al., 2014; Rahman et al., 2018). Therefore, the homoeologous regions on A07 and C06 are novel discoveries for day length-dependent flowering time regulation. This is not surprising considering the complexity of the flowering time regulation. Furthermore, DH4079 contributed an allele on A07, which masked the effect of the C06 alleles (Table 3; Figure 4). The C06 DH4079 allele could only delay flowering in the absence of the A07 DH4079 allele (Figure 4); hence, the C06 DH4079 allele is masked in the parent. In conclusion, epistatic effects should not be ignored, especially in a plant with a complex genome like *B. napus*, where several homolog copies of a gene exist. Further research is needed to reveal the complexity of flowering time regulation found in *B. napus* and in these two homolog regions.

4.2 The effect of temperature on flowering time is dependent on day length and genotype

We calculated the effect of temperature on DTF by subtracting DTF at 22°C from DTF at 11°C (11°–22°C); a positive value stands for earlier flowering at warmer temperatures and a negative number for later flowering. Surprisingly, higher temperatures could either delay or accelerate flowering, depending on the genotype (Table 2). While most plant species react with earlier flowering to higher temperatures due to warmer temperatures, it has been shown that high temperatures can also delay flowering (Fitter and Fitter, 2002; Jiang, 2023), something also observed in *B. napus* (Abelenda et al., 2023).

10.3389/fpls.2025.1513353

TABLE 4 Epistatic effects between QTLs (see Table 3) for days to flowering (DTF) under different day length and temperature conditions, as well as for the effect of day length and temperature in the DH4079 × Express617 population.

1st QTL	Chr.	Pos. [cM]	Interaction with	"2nd QTL"	Chr.	Pos. [cM]	Additive × additive effect
LD22-2	A02	54.4	×	LD22-4	A07	18.0	1.8
LD22-1	A02	30.3	×	LD22-5	C02	5.6	2.2
LD11-1	A02	54.4	×	LD11-4	C02	62.6	0.5
LD22-1	A02	30.3	×	LD22-7	C06	14.8	−3.1
LD22-4	A07	18.0	×	LD22-5	C02	5.6	1.7
11-22LD-2	A07	30.4	×	11-22LD-4	C02	74.4	−2.3
SD22-2	**A07**	**0.0**	×	**SD22-5**	**C06**	**0.0**	−5.2
SD11-2	**A07**	**0.0**	×	**SD11-5**	**C06**	**2.0**	−7.0
SD-LD11-1	**A07**	**7.2**	×	**SD-LD11-4**	**C06**	**2.0**	−3.9
LD22-4	**A07**	**18.0**	×	**LD22-7**	**C06**	**14.8**	−2.1
SD-LD22-1	**A07**	**27.8**	×	**SD-LD22-4**	**C06**	**28.3**	−4.5
11-22LD-2	**A07**	**30.4**	×	**11-22LD-5**	**C06**	**21.6**	1.6
SD11-3	C02	3.5	×	SD11-6	C06	29.3	−2.1
LD22-5	C02	5.6	×	LD22-7	C06	14.8	−2.3
11-22LD-4	C02	74.4	×	11-22LD-5	C06	21.6	1.8

QTL, quantitative trait locus; LD, long day; SD, short day.
Epistatic interactions between QTL cluster on A07 and C06 marked in bold.

The ANOVA showed that the effect of temperature on DTF was much smaller than the effect of the interaction between temperature and day length (Table 1). In the phenotypic analysis, DH4079 as a Swedish spring type showed a reaction to temperature that was independent of day length and vice versa (Table 2), so when sown in spring, the cultivar can react to warm temperatures without a negative interaction with day length. In contrast, German winter oilseed rape Express617 reacted differently to warmer temperatures depending on the day length; under LD, the flowering was 14 days earlier at 22°C, but under SD warmer temperatures, the flowering was delayed by 15 days. This is the first study to show how important it is to research the combined effect of day length and temperature after vernalization in winter oilseed rape. It should be noted, that in this experiment, the temperatures were constant and did not change between night and day. Other conditions may have led to different results since thermosensing is discussed to vary between day and night (Xiao et al., 2013; Hayes et al., 2021).

We found that in our QTL analysis, homoeologous regions on the linkage groups C06 and A07 responsible for the regulation of flowering time with QTL clusters for traits related to flowering depended on temperature and day length (Table 3, Figures 2, 3). The cluster on A07 between 24.5 cM and 30.9 cM was comprised of QTLs 11-22LD-2, 11-22SD-2, and SD-LD22-1 (Figure 2). The cluster on C06 between 18.8 and 39.1 cM was comprised of QTLs 11-22LD-4, 11-22SD-5, SD-LD22-4, and SD11-6 (Figure 3). On A07, it was the Express617 allele and, on C06, the DH4079 allele that delayed DTF at 22°C or under short days. The two homoeologous clusters showed epistatic effects between QTLs 11-22LD2 and 11-22LD-5 (a × a = 1.6), SD-LD22-1 and SD-LD22-4 (a × a = −4.5), and LD22-4 and LD22-7 (a × a = −2.1). QTLs 11-22SD-2 and 11-22SD-4 showed no epistasis. In each of those genomic regions, homologous copies of the flowering regulator genes *ELF4-LIKE 2*, *AGL12*, *RAP2.4*, and *FT* were located. No details about the function of *ELF4-LIKE 2* are known yet. In *Arabidopsis*, *ELF4-LIKE 2* could not rescue *elf4* mutants (Lin et al., 2019), which does not exclude another function in flowering time regulation. In *Arabidopsis*, *AGL12* has been shown to positively regulate flowering specifically in the apical meristem due to long-day conditions or independently due to higher temperatures (Tapia-López et al., 2008; Rodríguez-Bolaños et al., 2023). However, vernalization has been reported to negate the influence of *AGL12* (Tapia-López et al., 2008), and in our experiment, vernalization was applied. Transcription factor RAP2.4 is involved in many plant developmental processes. Its transcription is induced by abiotic stress, including heat stress, and is reduced by light, and overexpression has been shown to result in earlier flowering time in *Arabidopsis* (Lin et al., 2008). A temperature-dependent activity of the FT protein was shown, as low temperatures reduce the function of FT in *Arabidopsis* (Teper-Bamnolker and Samach, 2005). Under warm short-day conditions, PIF4 is positively regulating *FT* by binding to the promotor and activating transcription (Kumar et al., 2012). Changes in the promotor region of *FT* could cause genotype-specific differences in the regulation of flowering time by other transcription factors. For *B.*

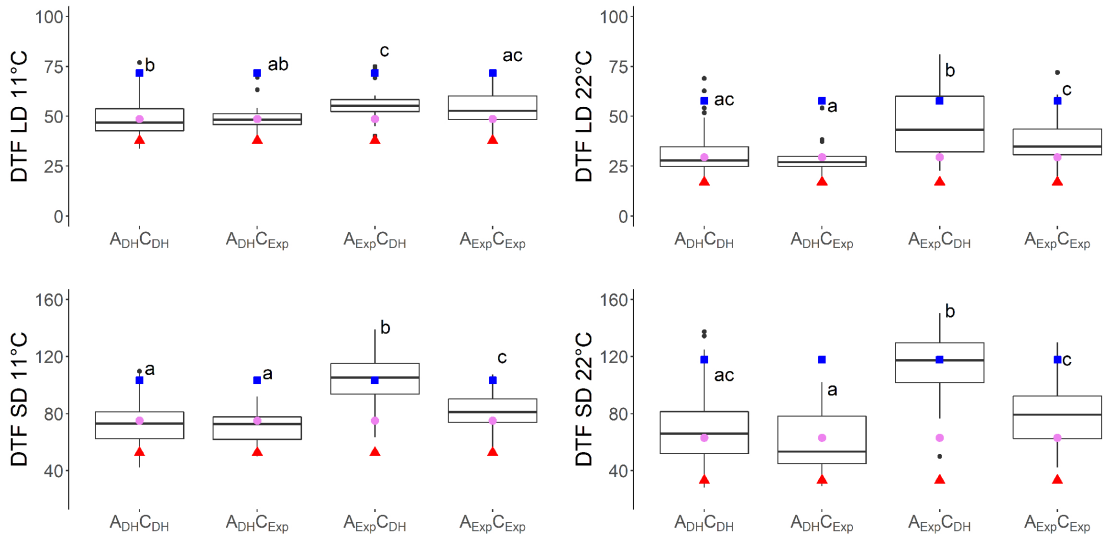

FIGURE 4
Days to flowering (DTF) in different temperatures (11°C and 22°C) and day length [short day (SD) and long day (LD)] conditions of vernalized DH population divided by alleles of two SNP markers: Bn-A07-p21478337 on A07 at 6.2 cM, indicated by A, and Bn-A07-p21354084 on C06 at 7.7 cM, indicated by C. Subscript "DH" indicates parental DH4079 allele, and subscript "Exp" indicates parental Express617 allele. Letters indicate significantly different subgroups ($p \leq 0.01$) tested with Tukey's test within conditions. Phenotypic values of Express617 (blue square), F1 (pink circle), and DH4079 (red triangle) are given.

napus, differences in *FT* expression have been shown in spring-type cultivars between 21°C and 28°C (Abelenda et al., 2023) for *FT* homologs A02, A07, and C06. Ghanbari (2016) found *FT* on C06 as the candidate gene for a flowering time QTL in an autumn sown field trial of the DH population of Sansibar × Oase, two winter oilseed rape genotypes, thus influencing flowering time in spring after full vernalization. It can be concluded that there is a genotype-specific interaction between temperature and day length. When sown in the field in autumn, winter oilseed rape should not induce flowering on warm winter days, while spring types may induce flowering earlier if warm temperatures permit it. Due to the different regulations of *FT* through temperature under short days, *FT* is a viable candidate gene, already supported by other studies on chromosomes A07 and C06 (Abelenda et al., 2023; Ghanbari, 2016).

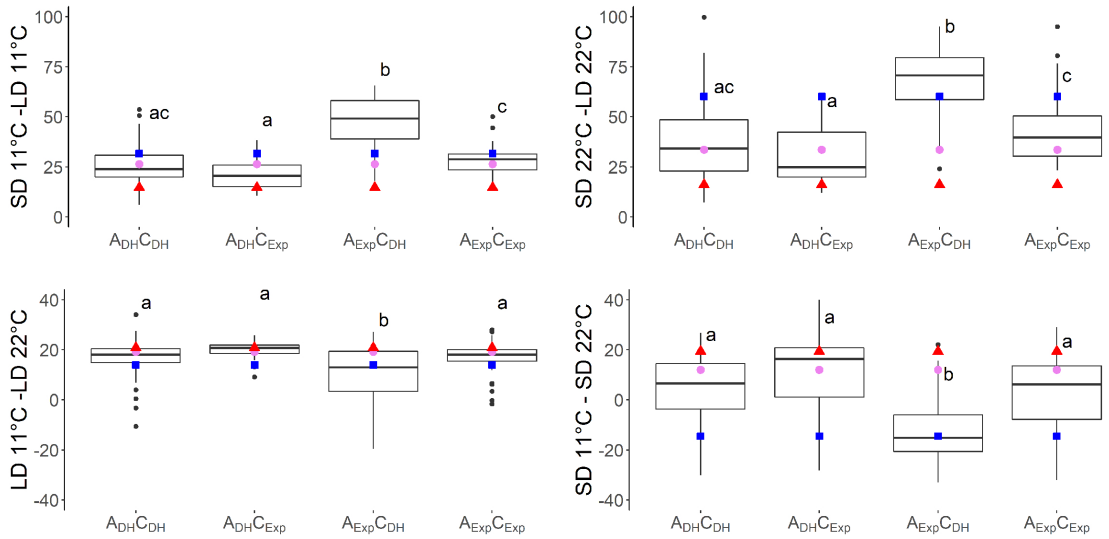

FIGURE 5
Effects of temperature and day length calculated by subtracting days to flowering (DTF) in different temperatures (11°C minus 22°C) and day length [short day (SD) minus long day (LD)] conditions of vernalized DH population divided by alleles of two SNP markers: Bn-A07-p21478337 on A07 at 6.2 cM, indicated by A, and Bn-A07-p21354084 on C06 at 7.7 cM, indicated by C. Subscript "DH" indicates parental DH4079 allele, and subscript "Exp" indicates parental Express617 allele. Letters indicate significantly different subgroups ($p \leq 0.01$) tested with Tukey's test within conditions. Phenotypic values of Express617 (blue square), F1 (pink circle), and DH4079 (red triangle) are given.

4.3 Outlook: more research on the effect of changing climate conditions in spring on winter rapeseed is needed

In conclusion, day length had an immense influence on flowering time in the DH4079 × Express617 population, and novel QTL regions were discovered on chromosomes A07 and C06. The gene *EFS*, which represses flowering under short days, was identified as a viable candidate gene. The influence of temperature × day length interactions on flowering time after vernalization is less studied for rapeseed, although with pending climate change, this may become an issue when warm spring temperatures shift to earlier months when the days are shorter. We found that the effects for temperature and day length interactions are greater than just the temperature effect and suggest that these two important abiotic factors should not be studied independently. The effect of temperature under short days is also genotype-specific, and the combination of higher temperatures and short-day conditions can either delay or accelerate flowering time.

Both parental genotypes had alleles, which suppressed flowering under short days and warm temperatures, but on different loci. On C06, the alleles derived from the spring-type parent DH4079 were responsible for this effect, while on A07, the alleles from the winter-type parent Express617 were responsible. In the presence of the DH4079 allele on A07, the effects of the alleles on C06 were masked, and the delay in flowering time through short-day conditions was not expressed. The QTLs on C06 and A07 were located in homoeologous regions and resulted consequently in the same candidate genes. This genetic diversity is a valuable basis for breeding *B. napus* to counter the environmental effects of climate change.

Data availability statement

The original contributions presented in the study are included in the article/Supplementary Material. Further inquiries can be directed to the corresponding author.

Author contributions

EH: Writing – original draft, Writing – review & editing, Conceptualization, Data curation, Formal analysis, Investigation, Methodology, Project administration, Validation. AS: Methodology, Supervision, Writing – review & editing. CM: Methodology, Supervision, Writing – review & editing, Conceptualization, Funding acquisition, Investigation, Project administration, Resources, Validation.

Funding

The author(s) declare that financial support was received for the research and/or publication of this article. This research was funded by the DFG (Deutsche Forschungsgemeinschaft) in the Priority Program 1530 "Flowering Time Control: from natural variation to crop improvement", Project number 270184074.

Acknowledgments

We acknowledge support by the Open Access Publication Funds of the Göttingen University.

Conflict of interest

The authors declare that the research was conducted in the absence of any commercial or financial relationships that could be construed as a potential conflict of interest.

Generative AI statement

The author(s) declare that Generative AI was used in the creation of this manuscript. For editing the abstract and the title, Chat-AI (Meta LLaMA 3.1 8B Instruct) provided by the GWDG (Gesellschaft für wissenschaftliche Datenverarbeitung mbH Göttingen) was utilized with the prompts provided by the Generative AI as included in the Supplementary File S2.

Publisher's note

Supplementary material

The Supplementary Material for this article can be found online at: https://www.frontiersin.org/articles/10.3389/fpls.2025.1513353/full#supplementary-material

SUPPLEMENTARY FILE S2
Chat log with Chat-AI to improve the abstract and title.

References

Abelenda, J. A., Trabanco, N., Del Olmo, I., Pozas, J., Del Martín-Trillo, M. M., Gómez-Garrido, J., et al. (2023). High ambient temperature impacts on flowering time in Brassica napus through both H2A.Z-dependent and independent mechanisms. *Plant Cell Environ.* 46, 1427–1441. doi: 10.1111/pce.14526

Amasino, R. M., and Michaels, S. D. (2010). The timing of flowering. *Plant Physiol.* 154, 516–520. doi: 10.1104/pp.110.161653

Axelsson, T., Shavorskaya, O., and Lagercrantz, U. (2001). Multiple flowering time QTLs within several Brassica species could be the result of duplicated copies of one ancestral gene. *Genome* 44, 856–864. doi: 10.1139/g01-082

Berardini, T. Z., Reiser, L., Li, D., Mezheritsky, Y., Muller, R., Strait, E., et al. (2015). The Arabidopsis information resource: Making and mining the "gold standard" annotated reference plant genome. *Genesis* 53, 474–485. doi: 10.1002/dvg.22877

Blümel, M., Dally, N., and Jung, C. (2015). Flowering time regulation in crops—what did we learn from Arabidopsis? *Curr. Opin. Biotechnol.* 32, 121–129. doi: 10.1016/j.copbio.2014.11.023

Cai, C. C., Tu, J. X., Fu, T. D., and Chen, B. Y. (2008). The genetic basis of flowering time and photoperiod sensitivity in rapeseed Brassica napus L. *Russ J. Genet.* 44, 326–333. doi: 10.1134/S1022795408030137

Chalhoub, B., Denoeud, F., Liu, S., Parkin, I. A. P., Tang, H., Wang, X., et al. (2014). Plant genetics. Early allopolyploid evolution in the post-Neolithic Brassica napus oilseed genome. *Science* 345, 950–953. doi: 10.1126/science.1253435

Cock, P. J. A., Chilton, J. M., Grüning, B., Johnson, J. E., and Soranzo, N. (2015). NCBI BLAST+ integrated into Galaxy. *Gigascience* 4, 39. doi: 10.1186/s13742-015-0080-7

Ferreira, M. E., Satagopan, J., Yandell, B. S., Williams, P. H., and Osborn, T. C. (1995). Mapping loci controlling vernalization requirement and flowering time in Brassica napus. *Theor. Appl. Genet.* 90, 727–732. doi: 10.1007/BF00222140

Ferrie, A. (2003). "Microspore culture of Brassica species," in *Doubled Haploid Production in Crop Plants*. Eds. M. Maluszynski, K. J. Kasha, B. P. Forster and I. Szarejko (Springer Netherlands, Dordrecht), 205–215.

Fitter, A. H., and Fitter, R. S. R. (2002). Rapid changes in flowering time in British plants. *Science* 296, 1689–1691. doi: 10.1126/science.1071617

Ghanbari, M. (2016). Inheritance and genetic variation of shoot elongation before winter in oilseed rape (Brassica napus L.). Georg-August-University, Göttingen. Plant breeding.

Hayes, S., Schachtschabel, J., Mishkind, M., Munnik, T., and Arisz, S. A. (2021). Hot topic: Thermosensing in plants. *Plant Cell Environ.* 44, 2018–2033. doi: 10.1111/pce.13979

Jaeger, K. E., Pullen, N., Lamzin, S., Morris, R. J., and Wigge, P. A. (2013). Interlocking feedback loops govern the dynamic behavior of the floral transition in Arabidopsis. *Plant Cell* 25, 820–833. doi: 10.1105/tpc.113.109355

Jiang, D. (2023). Complex regulation of flowering by high temperatures. *Plant Cell Environ.* 46, 1423–1426. doi: 10.1111/pce.14574

Kim, S. Y., He, Y., Jacob, Y., Noh, Y.-S., Michaels, S., and Amasino, R. (2005). Establishment of the vernalization-responsive, winter-annual habit in Arabidopsis requires a putative histone H3 methyl transferase. *Plant Cell* 17, 3301–3310. doi: 10.1105/tpc.105.034645

Kim, D.-H., and Sung, S. (2014). Genetic and epigenetic mechanisms underlying vernalization. *Arabidopsis Book* 12, e0171. doi: 10.1199/tab.0171

King, J. R., and Kondra, Z. P. (1986). Photoperiod response of spring oilseed rape (Brassica napus L. and B. campestris L.). *Field Crops Res.* 13, 367–373. doi: 10.1016/0378-4290(86)90037-7

Kumar, S. V., Lucyshyn, D., Jaeger, K. E., Alós, E., Alvey, E., Harberd, N. P., et al. (2012). Transcription factor PIF4 controls the thermosensory activation of flowering. *Nature* 484, 242–245. doi: 10.1038/nature10928

Lancashire, P. D., Bleiholder, H., van Boom, T., Langelüddeke, P., Stauss, R., Weber, E., et al. (1991). A uniform decimal code for growth stages of crops and weeds. *Ann. Appl. Biol.* 119, 561–601. doi: 10.1111/j.1744-7348.1991.tb04895.x

Lee, H., Chawla, H. S., Obermeier, C., Dreyer, F., Abbadi, A., and Snowdon, R. (2020). Chromosome-scale assembly of winter oilseed rape brassica napus. *Front. Plant Sci.* 11. doi: 10.3389/fpls.2020.00496

Lin, R.-C., Park, H.-J., and Wang, H.-Y. (2008). Role of Arabidopsis RAP2.4 in regulating light- and ethylene-mediated developmental processes and drought stress tolerance. *Mol. Plant* 1, 42–57. doi: 10.1093/mp/ssm004

Lin, K., Zhao, H., Gan, S., and Li, G. (2019). Arabidopsis ELF4-like proteins EFL1 and EFL3 influence flowering time. *Gene* 700, 131–138. doi: 10.1016/j.gene.2019.03.047

Luo, Y. X., Luo, C. Y., Du, D. Z., Fu, Z., Yao, Y. M., Xu, C. C., et al. (2014). Quantitative trait analysis of flowering time in spring rapeseed (B. napus L.). *Euphytica* 200, 321–335. doi: 10.1007/s10681-014-1140-2

Major, D. J. (1980). Photoperiod response characteristics controlling flowering of nine crop species. *Can. J. Plant Sci.* 60, 777–784. doi: 10.4141/cjps80-115

Mendham, N. J., and Salisbury, P. A. (1995). "Physiology: crop development, growth and yield," in *Brassica oilseeds: production and utilization*. Eds. D. Kimber and D. I. McGregor (CAB International, Wallingford), 11–64.

Nanda, R., Bhargava, S. C., Tomar, D., and Rawson, H. M. (1996). Phenological development of Brassica campestris, B. juncea, B. napus and B. carinata grown in controlled environments and from 14 sowing dates in the field. *Field Crops Res.* 46, 93–103. doi: 10.1016/0378-4290(95)00090-9

Nelson, M. N., Rajasekaran, R., Smith, A., Chen, S., Beeck, C. P., Siddique, K. H. M., et al. (2014). Quantitative trait loci for thermal time to flowering and photoperiod responsiveness discovered in summer annual-type Brassica napus L. *PloS One* 9, e102611. doi: 10.1371/journal.pone.0102611

Quiroz, S., Yustis, J. C., Chávez-Hernández, E. C., Martínez, T., La Sanchez, M., d., P., et al. (2021). Beyond the genetic pathways, flowering regulation complexity in arabidopsis thaliana. *Int. J. Mol. Sci.* 22 (11), 5716. doi: 10.3390/ijms22115716

Rahman, H., Bennett, R. A., and Kebede, B. (2018). Molecular mapping of QTL alleles of Brassica oleracea affecting days to flowering and photosensitivity in spring Brassica napus. *PloS One* 13, e0189723. doi: 10.1371/journal.pone.0189723

Raman, H., Raman, R., Coombes, N., Song, J., Prangnell, R., Bandaranayake, C., et al. (2016). Genome-wide association analyses reveal complex genetic architecture underlying natural variation for flowering time in canola. *Plant Cell Environ.* 39, 1228–1239. doi: 10.1111/pce.12644

R. Core Team (2019). *R: A language and environment for statistical computing* (Vienna, Austria). Available at: https://www.R-project.org/.

Richter, J. C., and Möllers, C. (2018). Genetic variation for vernalization requirement of winter oilseed rape. *Acta Hortic.* 1202, 87–92. doi: 10.17660/ActaHortic.2018.1202.13

Robert, L. S., Robson, F., Sharpe, A., Lydiate, D., and Coupland, G. (1998). Conserved structure and function of the Arabidopsis flowering time gene CONSTANS in Brassica napus. *Plant Mol. Biol.* 37, 763–772. doi: 10.1023/a:1006064514311

Robertson, M. J., Asseng, S., Kirkegaard, J. A., Wratten, N., Holland, J. F., Watkinson, A. R., et al. (2002). Environmental and genotypic control of time to flowering in canola and Indian mustard. *Aust. J. Agric. Res.* 53, 793. doi: 10.1071/AR01182

Rodríguez-Bolaños, M., Martínez, T., Juárez, S., Quiroz, S., Domínguez, A., Garay-Arroyo, A., et al. (2023). XAANTAL1 reveals an additional level of flowering regulation in the shoot apical meristem in response to light and increased temperature in arabidopsis. *Int. J. Mol. Sci.* 24 (16), 12773. doi: 10.3390/ijms241612773

Salisbury, P. A., and Green, A. G. (1991). "Developmental responses in spring canola cultivars," in *GCIRC 1991 Congress*, 1769–1774.

Schiessl, S. (2020). Regulation and subfunctionalization of flowering time genes in the allotetraploid oil crop brassica napus. *Front. Plant Sci.* 11. doi: 10.3389/fpls.2020.605155

Schiessl, S., Huettel, B., Kuehn, D., Reinhardt, R., and Snowdon, R. (2017). Post-polyploidisation morphotype diversification associates with gene copy number variation. *Sci. Rep.* 7, 41845. doi: 10.1038/srep41845

Schiessl, S. V., Quezada-Martinez, D., Tebartz, E., Snowdon, R. J., and Qian, L. (2019). The vernalisation regulator FLOWERING LOCUS C is differentially expressed in biennial and annual Brassica napus. *Sci. Rep.* 9, 14911. doi: 10.1038/s41598-019-51212-x

Schilbert, H. M., Schöne, M., Baier, T., Busche, M., Viehöver, P., Weisshaar, B., et al. (2021). Characterization of the brassica napus flavonol synthase gene family reveals bifunctional flavonol synthases. *Front. Plant Sci.* 12. doi: 10.3389/fpls.2021.733762

Song, Y. H., Ito, S., and Imaizumi, T. (2013). Flowering time regulation: Photoperiod- and temperature-sensing in leaves. *Trends Plant Sci.* 18, 575–583. doi: 10.1016/j.tplants.2013.05.003

Sun, F., Fan, G., Hu, Q., Zhou, Y., Guan, M., Tong, C., et al. (2017). The high-quality genome of Brassica napus cultivar 'ZS11' reveals the introgression history in semi-winter morphotype. *Plant J.* 92, 452–468. doi: 10.1111/tpj.13669

Takagi, H., Hempton, A. K., and Imaizumi, T. (2023). Photoperiodic flowering in Arabidopsis: Multilayered regulatory mechanisms of CONSTANS and the florigen FLOWERING LOCUS T. *Plant Commun.* 4, 100552. doi: 10.1016/j.xplc.2023.100552

Tapia-López, R., García-Ponce, B., Dubrovsky, J. G., Garay-Arroyo, A., Pérez-Ruíz, R. V., Kim, S.-H., et al. (2008). An AGAMOUS-related MADS-box gene, XAL1 (AGL12), regulates root meristem cell proliferation and flowering transition in Arabidopsis. *Plant Physiol.* 146, 1182–1192. doi: 10.1104/pp.107.108647

Teper-Bamnolker, P., and Samach, A. (2005). The flowering integrator FT regulates SEPALLATA3 and FRUITFULL accumulation in Arabidopsis leaves. *Plant Cell* 17, 2661–2675. doi: 10.1105/tpc.105.035766

Utz, H. F. (2011). "PLABSTAT: Ein Computerprogramm zur statistischen Analyse von pflanzenzüchterischen Experimenten," in *Institute of Plant Breeding, Seed Science and Population Genetics* (Hohenheim: University of Hohenheim).

Valdés, A., Clemens, R., and Möllers, C. (2018). Mapping of quantitative trait loci for microspore embryogenesis-related traits in the oilseed rape doubled haploid population DH4069 × Express 617. *Mol. Breed.* 38, 73. doi: 10.1007/s11032-018-0822-1

Voorrips, R. E. (2002). MapChart: Software for the graphical presentation of linkage maps and QTLs. *J. Heredity*. 93, 77–78. doi: 10.1093/jhered/93.1.77

Wahl, V., Ponnu, J., Schlereth, A., Arrivault, S., Langenecker, T., Franke, A., et al. (2013). Regulation of flowering by trehalose-6-phosphate signaling in Arabidopsis thaliana. *Science* 339, 704–707. doi: 10.1126/science.1230406

Wang, S., Basten, C. J., and Zeng, Z.-B. (2012). *Windows QTL cartographer 2.5*. (Raleigh, NC: Department of Statistics, North Carolina State University).

Wickham, H. (2016). *ggplot2: Elegant Graphics for Data Analysis* (New York: Springer-Verlag).

Xiao, D., Shen, H.-R., Zhao, J.-J., Wei, Y.-P., Liu, D.-R., Hou, X.-L., et al. (2019). Genetic dissection of flowering time in Brassica rapa responses to temperature and photoperiod. *Plant Sci.* 280, 110–119. doi: 10.1016/j.plantsci.2018.10.027

Xiao, D., Zhao, J. J., Hou, X. L., Basnet, R. K., Carpio, D. P. D., Zhang, N. W., et al. (2013). The Brassica rapa FLC homologue FLC2 is a key regulator of flowering time, identified through transcriptional co-expression networks. *J. Exp. Bot.* 64, 4503–4516. doi: 10.1093/jxb/ert264

Frontiers in
Plant Science

Cultivates the science of plant biology and its applications

The most cited plant science journal, which advances our understanding of plant biology for sustainable food security, functional ecosystems and human health.

Discover the latest Research Topics

See more →

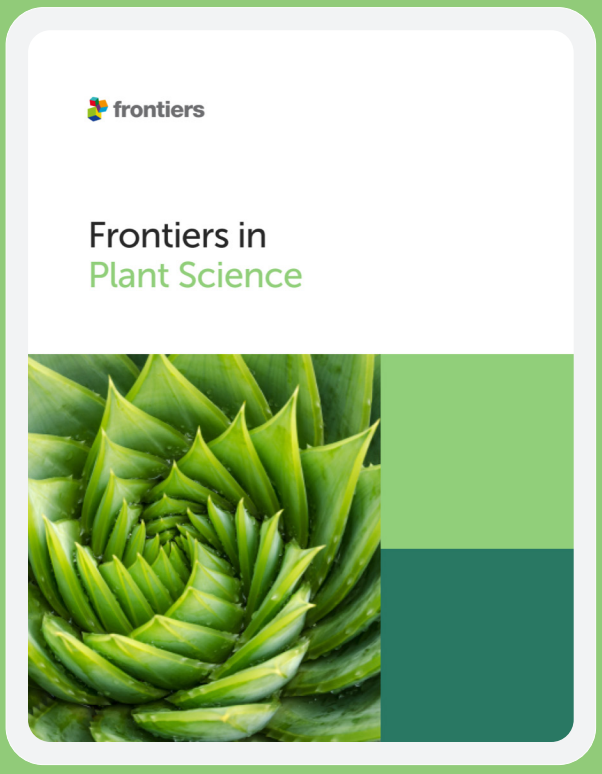

Frontiers

Avenue du Tribunal-Fédéral 34
1005 Lausanne, Switzerland
frontiersin.org

Contact us

+41 (0)21 510 17 00
frontiersin.org/about/contact